Carbon Paste Macrocycle Doped Composite Electrodes for the Selective Electrochemical Detection of Dopamine

A thesis submitted to the National University of Ireland in fulfilment of the requirements for the degree of

Doctor of Philosophy

By

Gama Theophile Gnahore

NUI MAYNOOTH

Ollscoil na hÉireann Má Nuad

Department of Chemistry,

Faculty of Science and Engineering,

National University of Ireland, Maynooth,

Maynooth,

Co. Kildare,

Ireland

February 2014

Research Supervisors: Dr. Trinidad Velasco-Torrijos and Dr. John Colleran

Head of Department: Dr. John Stephens

Table of Contents

Contents

Declaration

This is to certify that the material presented within this thesis has not been submitted previously for a Degree to this or any other University. All material presented, except where acknowledged and cited, is the original work of the author.

Gama Theophile Gnahore

February 2014

Dedication

Dedicated with love to my sister Christine Boyoro.

List of abbreviations

A	Ampere
AA	Ascorbic Acid
Ac_2O	Acetic Anhydride
aCSF	Artificial Cerebrospinal Fluid
AE	Auxiliary Electrode
br	Broad
CACE	Calix[4]arene crown-4 ether
$CaCl_2$	Calcium Chloride
CD	Cyclodextrin
$CDCl_3$	Deuterated chloroform
CD_3CN	Acetonitrile
CE	Counter Electrode
CH_2Cl_2	Dichloromethane
cm	Centimetre
CM-β-CD	Carboxymethyl beta-Cyclodextrin
cm^{-1}	Wavenumbers
CPE	Carbon Paste Electrode
CSF	Cerebrospinal Fluid
CuAAC	Copper (I)-catalysed azide-alkyne cycloaddition
CuI	Copper Iodide
CV	Cyclic Voltammetry
d	Doublet
DA	Dopamine
DAT	Dopamine Transporter
DC	Dopaminechrome
DCE	Dropping Carbon Electrode
dd	Doublet of doublets
DIEA	N,N-Diisopropyllethylamine
DME	Dropping Mercury Electrode
DMF	*N,N*-dimethylformamide
DMSO-d_6	Deuterated dimethyl sulphoxide
DOQ	Dopaminoquinone
DPV	Differential Pulse Voltammetry

D_2O	Deuterium Oxide
EDX	Energy Dispersive X-ray
E	Potential
E_f	Final Potential
E_i	Initial Potential
ESI	Electrochemical Impedance Spectroscopy
EtOAc	Ethyl Acetate
E_v	Vortex Potential
EtOH	Ethanol
Fc	Ferrocene
Fc-β-CD	Ferrocene beta-Cyclodextrin
g	Gram
GCE	Glassy Carbon Electrode
GNPs	Gold Nanoparticles
GO	Graphene Oxide
GPE	Graphene Paste Electrode
IR	Infrared
h	Hour
HCl	Hydrochloric acid
H_2SO_4	Sulfuric Acid
Hz	Hertz
I	Current
I_{Bg}	Background Current
I_{pa}	Anodic Peak Current
I_{pc}	Cathodic Peak Current
I_2	Iodine
J	Coupling Constant
K_a	Binding Constant
KBr	Potassium Bromide
KCl	Potassium Chloride
KOH	Potassium Hydroxide
KH_2PO	Potassium Dihydrogen Phosphate
K_2HPO	Potassium Hydrogen Phosphate
LCD	Leucodopaminechrome
L-DOPA	L-3,4-dihyroxyphenylalanine

LOD	Limit of Detection
LSV	Linear Sweep Voltammetry
M	Molar
m	Multiplet
MeOH	Methanol
$MgSO_4$	Magnesium Sulfate
MHz	Megahertz
mL	Millilitre
mmol	Millimole
MS	Mass Spectrometry
MWCNT	Multiwall Carbon Nanotubes
NaN_3	Sodium Azide
N_2	Nitrogen
NaCl	Sodium chloride
NaOH	Sodium Hydroxide
NMR	Nuclear Magnetic Resonance
O_2	(molecular) Oxygen
OAc	Acetoxy group
PBS	Phosphate Buffer Solution
pH	Logarithmic scale of concentration of hydronium ions ($-\log[H_3O^+]$)
Ph_3P	Triphenylphosphine
pK_a	Minus log of association constant K_a of a given solution ($-\log K_a$)
ppm	Parts Per Million
Pt	Platinum
R_{ct}	Charge Transfer Resistance
RDV	Rotating Disc Voltammetry
REF	Reference (electrode)
R^2	Correlation Coefficient
s	Singlet
S_b	Standard Deviation
SCE	Saturated Calomel Electrode
SEM	Scanning Electron Microscopy
S-β-CD	Sulfated beta-Cyclodextrin
t	Triplet
TFA	Trifluoroacetic acid

TLC	Tin Layer Chromatography
UV-Vis	Ultraviolet-visible
V	Volts
WE	Working Electrode
ΔE_p	Peak potential separation
$\Delta\delta$	Chemical shift change
μL	Microlitre
μS	Microsiemens
ν	Scan rate
$\nu^{1/2}$	Square roots of scan rate
ω	Angular Velocity
λ	Wavelength (nm)
°C	Degree Celsius
5-HT	Serotonin

List of electrodes modification designations

β-CDCPE	Neutral beta–Cyclodextrin modified carbon paste electrode
S-β-CDCPE	Sulfated beta–Cyclodextrin modified carbon paste electrode
CM-β-CDCPE	Carboxymethyl beta-Cyclodextrin modified carbon paste electrode
NCPE	Nafion modified carbon electrode
Fc-β-CDCPE	Ferrocene beta–Cyclodextrin complex modified carbon paste electrode
FcCPE	Ferrocene modified carbon paste electrode
S-β-CDGPE	Sulfated beta–Cyclodextrin modified graphene paste electrode
CPE/O	Carbon paste electrode with oxides layer
$CD_{6.6}$CPE	Heptakis 6-deoxy-6-(1-(4,5-dicarboxyl)-1,2,3-triazolyl)-beta-Cyclodextrin modified carbon paste electrode
$CD_{6.7}$CPE	Heptakis (6-(4-hydroxymethyl-1H-[1,2,3] triazol-1-yl)-6-deoxy)-beta-Cyclodextrin modified carbon paste electrode

Acknowledgements

First and foremost, I would like to thank my supervisors Dr. Trinidad Velasco-Torrijos and Dr. John Colleran. I am deeply indebted to both of you for your guidance and understanding. You have patiently and with full assistance led me throughout this academic achievement. The experience and knowledge I have gained is priceless and the teaching backgrounds−organic synthesis and electrochemistry−will definitely have a great impact in my future career. It was a great pleasure to have a chance to work with you. I am also thankful to the entire lecturers and the technicians from the chemistry department.

My sincere gratitude goes to the Dublin City Council for the financial support throughout the years.

To all the postgrads and postdocs, past and present, you've certainly made my time in Maynooth memorable. I would like to extend my thanks to Trini's past and present crew: Carol, Roisin, Lorna, Andrew and Jessica. I have certainly learnt from each of you and I cannot thank you enough. Further thanks are extended to Sam, my electrochemistry colleague.

To Brett (Ross), I'll never forget the instructions received via telephone to have the NMR machine run. You are a genius! I am very grateful to Conor for the help in using the SEM and to Adelaide for giving me some tips in writing a thesis. Haixin, thanks for your friendship. To all of you, postgrads and postdocs, I have not mentioned here, I really thank you. A special thank you to my mates from the chemistry football team: Finno (the man himself), Niall M. and John K. (competing to score the most goals), Noel (shouting who is back for us?), Ken (the leader with an amazing fitness). Chiggy (Chris, the warrior striker) and Jack (the talented midfield). These Friday games are special and I will miss them when I will leave Maynooth.

To my sisters and brothers in Côte d'Ivoire and France, you have all contributed to the success of my studies. I extend my special thanks to my cousin and friend Christian ('Golyze'), my younger brother Mahi, my sister Emilie, my cousin Nathalie, my uncle Dr Oupoh and my nephews Bradley and Leeroy for their continuous grateful encouragements. Thank you!

My appreciation also goes to my soul mate Cathy, my daughter Elisha and my son Aiden for their love and support. I love you very much. To my mum and dad, you have inspired me and made me the person I am today. Thank you for everything!

Finally, to my sister Christine, I have no words to describe your love and support. Thanks a million.

Merci Seigneur!

Abstract

The neurotransmitter dopamine (DA) has shown to play a very important role in the functioning of the central nervous system. Thus, the determination of DA is of great importance in the fields of neurochemistry and biomedical chemistry. In this thesis, a number of carbon paste electrodes modified with macrocycles for the electrochemical detection of DA is reported. The different macrocycles employed were based on cyclodextrin derivatives and consist of sulfated β-CD (S-β-CD), carboxymethyl β-CD (CM-β-CD), Ferrocene complex β-CD (Fc-β-CD), Heptakis 6-deoxy-6-(1-(4,5-dicarboxyl)-1,2,3-triazolyl)-β-CD ($CD_{6.6}$) and Heptakis (6-(4-hydroxymethyl-1H-[1, 2, 3] triazol-1-yl)-6-deoxy)-β-cyclodextrin ($CD_{6.7}$). The fabricated electrodes were characterized by using surface techniques and electrochemical methods such as energy dispersive X-ray (XRD), scanning electron microscopy (SEM), electrochemical impedance spectroscopy (ESI) and cyclic voltammetry (CV). The detection of DA at all modified electrodes (except for $CD_{6.7}$) resulted in an enhancement of the oxidation signal response over that of the bare electrode. High performance of the electrochemical detection of DA was obtained at S-β-CD modified CPE such as a wide concentration range (from 5×10^{-7} M to 5×10^{-4} M) and low detection limit (1.33×10^{-7} M). It was shown that the sensitivity of the developed sensor towards the detection of DA depends on the amount of S-β-CD incorporated within the paste. The optimum sensor architecture was made by impregnating 0.545 g S-β-CD in a carbon paste containing 0.71 g graphite and 200 μL silicone oil. In addition, graphite was replaced by graphene and the electrochemical behaviour of DA at the S-β-CD modified graphene electrode was investigated by DPV. The results showed that the S-β-CD modified graphene electrode exhibited excellent electrochemical oxidation of DA in phosphate buffer solution (pH 6.8) compared to the bare graphite paste electrode. $CD_{6.6}$ and $CD_{6.7}$ were synthesised in order to exhibit further increase in the signal responses of DA. The formation of inclusion complexes of $CD_{6.6}$ and $CD_{6.7}$ with DA was studied by ^{1}H-NMR spectroscopy. A 2:1 and 1:1 stoichiometry was obtained in the case of $CD_{6.6}$:DA and $CD_{6.7}$:DA, respectively. The bare GPE was modified with $CD_{6.6}$ and the electrode was miniaturised from macro to micro-size level. This configuration also was shown to improve the detection of DA (3×10^{-7} M).

This thesis also aimed to utilise these modified electrodes to enhance the selectivity for DA over two interferents, ascorbic acid (AA) and serotonin (5-HT). Improvements in the selectivity of DA were obtained at the S-β-CD modified GPE as AA was excluded

at the electrode surface. Moreover, the results showed that DA, AA and 5-HT in coexisting solutions can be simultaneously oxidised at significantly different potentials in the presence of S-β-CD modified CPE. The voltammetric response of the three compounds could be completely separated at the modified electrode using both cyclic voltammetry (CV) and differential pulse voltammetry (DPV) techniques at optimal conditions. DPV provided larger peak potential separations and higher response sensitivities of DA, AA, and 5-HT compared to CV.

1 Introduction and Literature Review

1.1 Carbon Paste as an Electrode Material

Carbon paste electrodes (CPEs) are composite electrodes because they result from the combination of two or more materials. They consist of a mixture of, at least, an electrically conducting carbon powder and an organic liquid (binder). They have been widely applied in electrochemistry due to their advantages: inexpensive, easy to prepare, easy to handle and low background currents. They possess an added advantage in that the surface can be renewed rapidly. The choice of carbon paste components (carbon powder and binder), their ratio of mixture, and the way in which the CPEs are prepared (homogenisation of the paste, packing of the paste in the electrode body, etc.) are important aspects that determine the properties, characteristics and behaviour of CPEs.

1.1.1 The Invention of Carbon Paste

The development of carbon paste is closely connected with classical dropping mercury electrode (DME). The linking point had appeared in the late 1950s, when Adams [1] and his students were testing a new "dropping carbon electrode" (DCE) as an alternative to the DME for anodic oxidations of organic compounds, where the mercury drop could not be used. Although this concept finally failed, a thicker mixture of softer consistency, carbon paste, was found to be capable of satisfactorily replacing the originally intended DCE configuration.

1.1.2 Carbon Powder (Graphite)

Powdered carbon (graphite), as the main carbon paste component of a CPE electrode, is an ideal material to use in electrochemical measurements. Typical carbon electrode materials generally obey criteria such as particle size in micrometres, uniform distribution of the particles, high chemical purity, and low adsorption capabilities. Naturally, the type and quality of graphite used, as well as the overall amount in the carbon paste mixture, are reflected in all typical properties of the respective mixture. The most often selected carbon powder is spectroscopic graphite with particles in the low micrometric scale (typically 5 – 20 μm).

1.1.3 Binder (pasting liquid)

Traditional carbon pastes contain a binder which mechanically links the individual graphite particles. However, beside this main function, the binder co-determines the properties of the carbon paste. Typical parameters required for binders are: (i) chemical

inertness and electro-inactivity, (ii) high viscosity and low volatility, (iii) minimal solubility in aqueous solutions and (iv) immiscibility with organic solvents.

The most popular binder used for preparation of carbon pastes are mineral (paraffin) oils such as Nujol. However, the spectrum of potentially applicable binders is relatively wide. Indeed, carbon pastes reported in the literature employ various types of binders including aliphatic and aromatic hydrocarbons and their halogenated derivatives, silicone oils and greases [1], and nearly solid silicone rubbers [2]. In contrast to ordinary pasting liquids, some binders capable of acting in some chemical processes have been used. This is the case of organic esters (organophosphate and dialkyl phthalate) [3] or ionic liquids [4]. Solidifying substances, such as Phenathrene [5] and paraffin wax [6] are types of binders that undergo a physical state transformation during carbon paste preparation. At known temperatures, such a substance occurs as a liquid which can be properly homogenised with graphite; when cooled down, it becomes compact and acts as a solid binder.

Because of the presence of lipophilic binder in common mixtures, carbon pastes have typically a hydrophobic surface which, in aqueous solution, repels hydrophilic species involved in the electrode transformations of a great number of redox systems. This effect can enhance specificity at CPEs which, in turn depends upon the carbon paste composition and the quality of graphite and binder components.

1.1.4 Modifying Carbon Pastes

A diversity of modification procedures applicable to the carbon paste electrode material is arguably the most important features of carbon pastes. According to literature reviews [7, 8], chemically modified carbon paste electrodes and carbon paste biosensors can be prepared by various ways.

Modification *in situ* is a simple and widely used approach applicable to the bare carbon paste, similarly as with other common electrodes [7-9]. In contrast to compact solid materials such as glassy carbon, pyrolytic graphite, platinum or gold, the hydrophobic surface of carbon paste mixtures may markedly enhance the entrapment of some lipophilic modifiers. Mechanical mixing of modifiers into the carbon paste bulk is another frequent way of modification which is done with substances in solid state. [10, 11]. This body of work will detail the mechanical binding of macrocyclic carbohydrate derivatives into carbon paste. Impregnated macrocycles promote interaction between the electrode and analyte through “supramolecular chemistry”, and can be termed ‘molecular recognition elements’. Dissolution in the binder is feasible with some ion

exchangers (such as Aliquat 336 [12], Amberlite LA-2 [13-15], Dowex 50W [16]), or other lipophilic compounds (trioctyl phosphine-oxide, TOPO [17] or fatty acids [18]). Impregnation of carbon powder can also be achieved by soaking graphite particles with a solution containing dissolved modifier. After evaporation of the solvent, carbon powder pre-treated in this way is then normally mixed and homogenized with the liquid binder chosen. This modification provides effective delivery of modifier into the carbon paste bulk.

Electrolytic activation (anodization / cathodization) can be classified as a specific type of modification [7, 19] feasible via electrode oxidation / reduction at certain potentials, which can give rise to hydrophilic functional groups at the carbon paste surface.

The use of additional membranes can be applied to carbon paste sensors in order to prevent undesirable interference in samples with more complex matrices [20-22]. The protective layer of choice for a bare carbon paste electrode can be either thick polycarbonate membrane used in combination with biosensors [23] and gas probes [24], or a thin film of ethanolic Nafion applied onto the surface of a chemically modified electrode [25].

1.1.5 Conductivity of Carbon Paste

The excellent conductivity of carbon paste is still one of the puzzling questions within the field of CPEs [26]. Some images of the carbon paste microstructure, taken by scanning electron - and optical microscopic observations [27-30], have revealed that carbon pastes represent mixtures with a rather unconsolidated structure in which the graphite particles are all covered with a very thin film of the non-conducting binder. Nevertheless, the individual graphite particles are apparently in some physical contact beneath the binder layer, which may explain a very low ohmic resistance of most carbon pastes [11]. A typical morphology for carbon paste is shown in Figure 1.1.

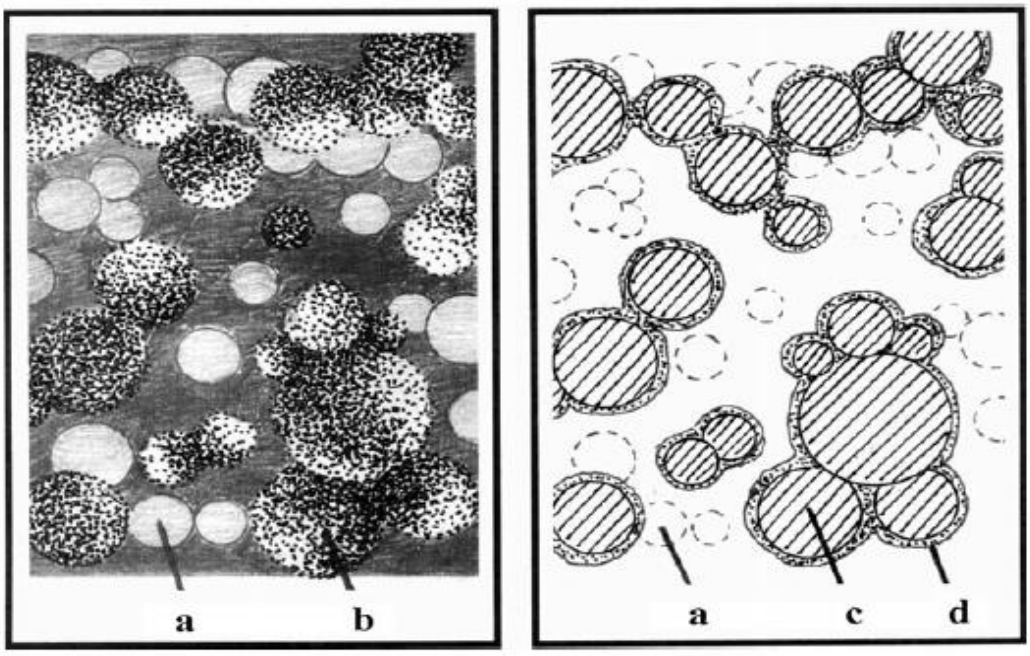

Figure 1.1: Microstructure of carbon paste with spherical particle (left) and the corresponding cross-section (right). a) carbon paste bulk revealing graphite particle coated with binder, b) the respective outer layer, c) graphite particle alone, d) thin film of binder [27].

1.2 Supramolecular Chemistry

The term "supramolecular chemistry" was introduced by Lehn to define the chemistry of "intermolecular bonds" [31, 32]. The "guest" molecule is held in the internal cavity of the "host" only by non-covalent forces [33]. The way from simple molecules to complex supramolecular structures implies the primary stage of molecular recognition, followed by self-reorganisation and generation of supramolecular architectures in the final stage [34]. Over the last three decades, supramolecular chemistry has gradually become a new independent interdisciplinary science, at the interface between biology, synthetic and physical chemistry [32, 35].

The cage-like organic molecules such as cyclodextrins, cryptands, calixarenes, cyclophanes, spherands and crown ethers, available with accessible internal cavities, can serve as host [36, 37] and fit well in the area of supramolecular chemistry. Among these macrocycles, cyclodextrins (CDs) are the most important and promising hosts because they are water-soluble natural products, inexpensive, commercially available, non-toxic and readily functionalised. The use of CDs as receptors or hosts in supramolecular chemistry has a variety of applications such as drug delivery [38-41], food industry [42, 43], solubilisation of environmental pollutants [44], molecular reactor

for the mediation of organic reactions [45], fluorescence [46] and electrochemical sensors [47-49].

1.2.1 Click Reaction as an Efficient Tool in Supramolecular Chemistry

Azides and alkynes display high mutual reactivity and they have been termed bioorthogonal because of their stability and inertness towards the functional groups typically found in biological systems [50].

Recent reports have dealt with the study and synthesis of rigid macrocycles using copper-catalysed azide-alkyne cycloaddition (CuAAC) click chemistry, and the characterization of their host-guest binding properties [51, 52]. A prototypical example is the highly preorganized, shape-persistent macrocycle displayed in Figure 1.2. The four triazole units are perfectly positioned for the recognition of a spherical anion such as chloride [53]. This example demonstrates that the use of CuAAC click chemistry not only allows the rapid, orthogonal and high yielding construction of macrocycles, but can also utilise triazoles as molecular recognition agents.

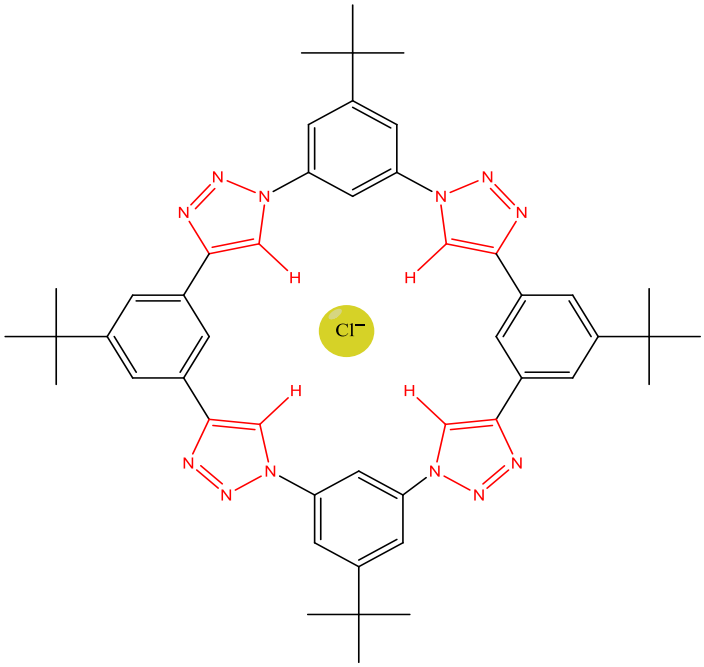

Figure 1.2: Triazole-containing macrocycle for the binding of chloride anion. In Red: triazole groups as the key functionalities responsible for binding.

1.3 Cyclodextrins (CDs)

1.3.1 History

CDs were first isolated in 1891 by Villiers, when he noted formation of a crystalline substance from a *Bacillus amylobacter* culture grown on starch [19, 20, 54]. He found the elemental composition to be $(C_6H_{10}O_5)_2 \bullet 3H_2O$, and named this compound "cellulostine". The first inclusion chemistry involving these "cellulostines" was observed by Schardinger, when the author noted that they formed complexes with iodine [54]. In 1904, Schardinger isolated a new organism capable of producing acetone and ethyl alcohol from sugar and starch-containing plant material [55]. In 1911, he described that this strain, called *Bacillus macerans*, also produces large amounts of crystalline dextrins from starch. Schardinger named his crystalline products 'crystallised dextrin α' and 'crystallised dextrin β' [55]. It took until 1935 before 'dextrin γ' was isolated. Several fractionation schemes for the production of CDs [56, 57] were also developed. At that time, the structures of these compounds were still uncertain, but in 1942 the structures of α and β-CD were determined by X-ray crystallography [58]. In 1948, the X-ray structure of γ-CD followed and it was recognised that CDs can form inclusion complexes.

In 1961, evidence for the existence of δ-, ζ-, ε- and even η-CD (9–12 residues) was provided. The main interest in CDs lies in their ability to form inclusion complexes with several compounds [59-62].

1.3.2 Structure and Physicochemical Properties

The most common types of CDs are α-CD, β-CD and γ-CD, referred to as first generation or parent CDs. α-CD, β-CD and γ-CD are composed of six, seven and eight α-(1,4)-linked glycosyl units, respectively [63]. The chemical structure of each CD is given in Figure 1.3.

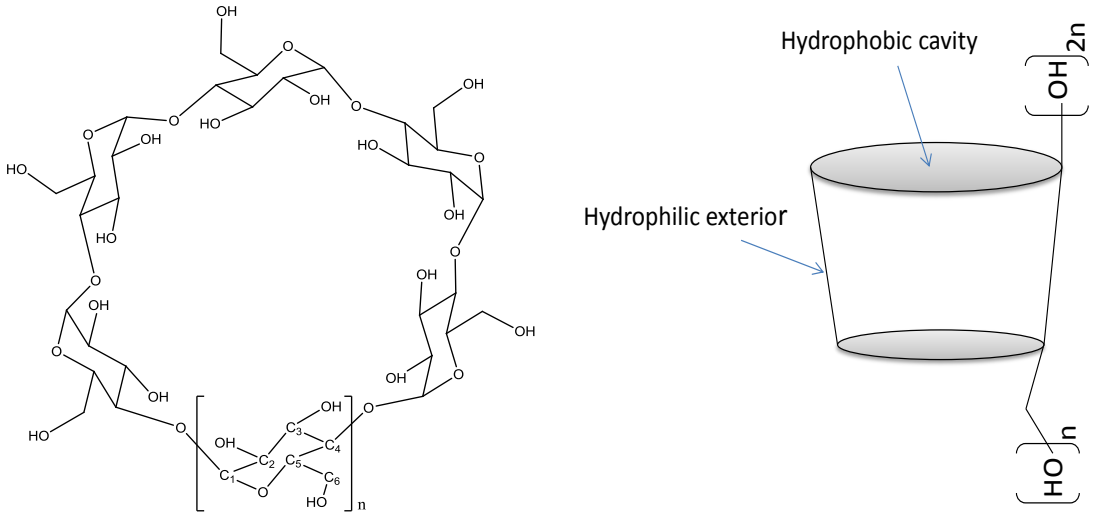

(a) (b)

Figure 1.3: Chemical structure of CDs, n = 1(α-CD), n = 2(β-CD), n = 3(γ-CD) (a) and toroid shape of CDs showing interior cavity, n = 6(α-CD), n = 7(β-CD), n = 8(γ-CD) (b).

CDs form "bucket-like" structures, thus they display a wide and narrow entrance. Both the narrow and wide cavity rim of CDs bears hydroxyl groups.

The macrocyclic ring is a conical cylinder, which is frequently characterized as a doughnut or wreath-shaped truncated cone. The cavity is lined with hydrogen atoms and glycosidic oxygen bridges. The nonbonding electron pairs of the glycosidic oxygen bridges are directed towards the cavity centre, producing a high electron density and lending to it a Lewis-base character [64]. Therefore, the exterior of the CD is hydrophilic, while the interior is hydrophobic in nature. Within the macrocycle, the hydroxyl group at C2 position from one glucopyranose ring and the hydroxyl group at C3 position from the adjacent ring can form a hydrogen bonding. Some general structural properties of CDs are presented in Table 1.1 [54].

Table 1.1: Cyclodextrin characteristics [54]

Properties	α-CD	β-CD	γ-CD
Number of glucopyranose units	6	7	8
Molecular weight (g / mol)	972	1135	1297
Solubility in water at 25°C (g / 100 mL)	14.5	1.85	23.2
Outer diameter (Å)	14.6	15.4	17.5
Cavity diameter (Å)	5.7	7.8	9.5
Height of torus (Å)	7.9	7.9	7.9
Approximate cavity volume ($Å^3$)	174	262	427

1.3.3 Cyclodextrin Inclusion Complexes

As mentioned earlier, the most important property of CDs is their ability to partially or fully complex a wide range of hydrophobic guest molecules into their cavity in the aqueous phase as shown in Scheme 1.1. Generally, in an aqueous solution, the CD cavity (slightly apolar) is occupied by water molecules, which is thermodynamically unfavourable (polar-apolar interaction). Therefore, water molecules inside the cavity have fewer tendencies to form hydrogen bonds in the same way as in solution which result in a higher enthalpy and higher energy. When hydrophobic guest molecules are incorporated into the cavity, the energy of the system is lowered by substituting these enthalpy-rich water molecules with those hydrophobic guest molecules to form the complex of CDs and guest molecules [65].

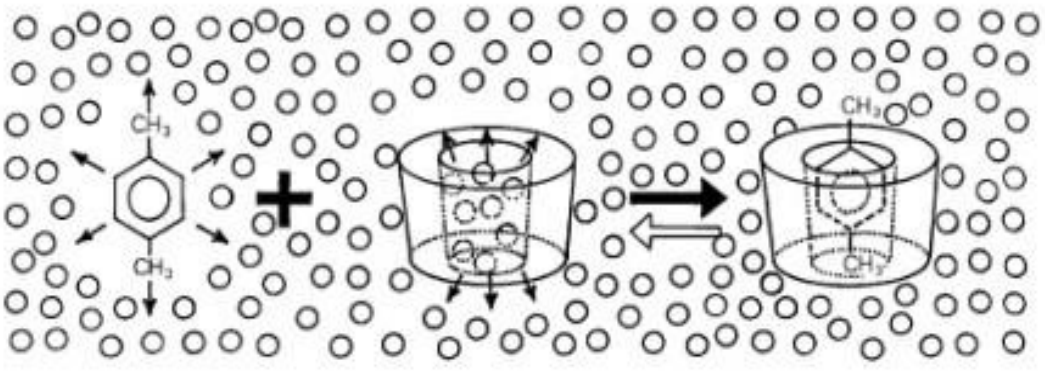

Scheme 1.1: Schematic illustration of inclusion complexation of p-xylene by CD [54].

Guest molecules may form inclusion complexes with different stoichiometries. Cyclodextrin:guest (CD:G) ratios may be 1:1, 2:1, 1:2, 2:2, etc [54, 66-69]. When an inclusion complex is formed in solution, equilibrium between the dissociated species and the associated complex is established. The measure of the strength between a guest complexation with CD is defined as K_a, the binding constant. The complexation (CD:G) can be described as shown in Equations 1.1, 1.2 and 1.3 for 1:1, 1:2 and 2:1 stoichiometry, respectively [70].

$$G + CD \leftrightharpoons G{-}CD \qquad \text{Equation 1.1}$$

$$G{-}CD + CD \leftrightharpoons G{-}CD_2 \qquad \text{Equation 1.2}$$

$$G{-}CD + G \leftrightharpoons G_2{-}CD \qquad \text{Equation 1.3}$$

These equilibria summarise the formation of CD:G 1:1, 1:2 or 2:1 complexes with the following association constants (shown in Equations 1.4, 1.5 and 1.6, respectively):

$$K_{1:1} = \frac{[G-CD]}{[G][CD]} \qquad \text{Equation 1.4}$$

$$K_{1:2} = \frac{[G-CD_2]}{[G-CD][CD]} \qquad \text{Equation 1.5}$$

$$K_{2:1} = \frac{[G_2-CD]}{[G-CD][G]} \qquad \text{Equation 1.6}$$

[G] and [CD] represent the concentrations of the dissociated guest and CD species, and [G–CD] is the inclusion complex concentration. In general, the formation of more complicated complexes G_m–CD_n can be described by the following equilibrium:

$$_mG + _nCD \leftrightharpoons G_m–CD_n \qquad \text{Equation 1.7}$$

An equation for the overall association constant $K_{m:n}$:

$$K_{m:n} = \frac{[G_m-CD_n]}{[G]_m[CD]_n} \qquad \text{Equation 1.8}$$

There is a variety of interactions considered important in the complexation process of CDs. The major driving forces are hydrophobic interactions which consist largely of London dispersion forces [71]. Other factors also believed to contribute to interaction include enthalpy-driven displacement of water molecules from the CD cavity (briefly discussed above); Van der Waals between CD and the guest; electrostatic, polar and ionic interactions [72, 73] including dipole-dipole and hydrogen-bonding. The understanding of these driving forces involved in the molecular recognition of CDs is fundamentally important, not only for CD chemistry but also for supramolecular chemistry as a whole.

1.3.4 Non-covalent Interactions

Non-covalent interactions are the driving force of supramolecular chemistry. As already mentioned, Lehn has defined supramolecular chemistry as "chemistry of the intermolecular bond" due to the crucial role of these interactions in holding supramolecular systems together. In this section the different common types of intermolecular forces, which can be facilitated by CDs structure, are briefly discussed.

1.3.4.1 Hydrogen Bonding

Hydrogen bonding involves donor-acceptor interactions between two atoms. One atom, X-H, will act as a proton donor, while another atom, Y, will act as a proton acceptor [74] resulting in the hydrogen bond X-H···Y. In general, the atom X should be sufficiently electronegative to withdraw electron density from the proton so that atom Y may donate electron density to the proton. Atom Y should have a lone pair or polarizable π electrons in order to act as a hydrogen bond acceptor. The strength of H-bonds can vary considerably in biological systems, ranging from 10-20 $kJmol^{-1}$[74].

1.3.4.2 Van der Waals Interactions

Van der Waals interactions refer to intermolecular interactions between molecules that have an instantaneous dipole and an induced dipole. They are typically very weak (2-4 $kJmol^{-1}$). These interactions are electrostatic in nature, although they are due normally to partial charges within a molecule rather than Coulombic interactions between ions. Instantaneous dipole-induced dipole interactions are also sometimes called London forces or dispersion forces [75]. Because electrons are constantly moving, the electron density is not homogenously distributed in a bond at a given instant of time, so that at one moment the electron density may be congregated more at one side of the molecule than the other, even if the molecule is non-polar. Van der Waals forces can be either attractive or repulsive, depending on the distance between the atoms involved [76-78]. The interaction can be attractive from a distance and become more attractive as the molecules approach each other, but as the molecules become very close together, the interactions become repulsive due to repulsion between the electron clouds of the two molecules.

1.3.4.3 The Hydrophobic Effect

The hydrophobic effect is the observed tendency of non-polar substances to aggregate in aqueous solution and exclude water molecules [79]. The name, literally meaning "water-fearing" describes the segregation and apparent repulsion between water and non-polar substances.

In terms of supramolecular chemistry, complexation of a nonpolar guest into the hydrophobic receptor site of a host molecule is favourable due to the release of water molecules from the host's receptor pocket, with a resulting increase in entropy [80]. Also, the complexation of a non-polar guest into a host's hydrophobic receptor may be enthalpically favourable, as the water that is released from the hosts receptor can then more readily form hydrogen bonds with other water molecules in the solvent [80].

1.3.4.4 The π-π Stacking Interactions

The π-π stacking interactions generally involve aromatic systems, whose planar rings contain delocalized π-electrons above and below the plane of the ring. The C–H bond is slightly polar ($C^{\delta-}$–$H^{\delta+}$), so that the outer edge of the aromatic group tends to be slightly electropositive while the π-electrons near the carbon atoms have a slight negative charge [81].

Two common arrangements between π-stacked aromatic rings are the edge-to-face and the offset face-to-face arrangements. In the edge-to-face arrangement, the slightly negatively charged π-electrons in one ring are attracted to the slightly positive hydrogen atoms on the edge (in the plane) of another ring, so that the two rings are arranged perpendicular to each other. With the offset face-to-face arrangement, the rings are parallel to each other but are offset from each other in order to allow oppositely charged regions of the molecules to align with each other [81].

1.3.4.5 Electrostatic Interactions

Electrostatic interactions are Coulombic (charge-based) interactions that result in an attraction between two oppositely charged molecules. These can generally include ion-ion, and ion-dipole interactions, as well as dipole-dipole interactions and permanent dipole-induced dipole interactions. The strength can vary, ranging from 5-15 $kJmol^{-1}$ [80, 82]. Electrostatic interactions, especially ion-ion, are often among the strongest non-covalent interactions available. Permanent dipole-dipole interactions involve interactions between molecules that have a permanent dipole, being partially negative at one end and partially positive at the other end. These molecules will interact so that the partially positive end of one molecule will attract the partially negative end of the other molecule. Permanent dipole-induced dipole interactions may occur when a molecule with a permanent dipole and a non-polar molecule approach each other.

1.3.5 Characterization of Inclusion Complexes

A number of techniques, including spectrophotometry and fluorescence spectroscopy, are commonly used to study the formation of host-guest complexes in supramolecular chemistry. The most direct evidence for the inclusion of a guest into a host cavity in solution is obtained by ^{1}H-NMR spectroscopy [83-85]. This technique relies on changes in the chemical shifts of protons' NMR signals of the guest and the host upon complexation. A complex between CDs and a guest can be characterised by the stoichiometry of the complex and its stability constant, K_a. The stoichiometry of the

complex can be determined with Job's plot, also called the method of continuous variation. In this method, experimentally observable spectral parameters (usually chemical shifts that are sensitive to complex formation) are followed upon varying host to guest ratios, where the sum of their concentration is kept constant. The differences in chemical shifts (Δδ) induced from complexation are plotted as a function of the mole fraction of the guest (or the host). The ratio of the molar fraction at the position of maximum indicates the stoichiometry of the complex. The changes in δ of certain protons of the guest upon addition of CD are numerically analysed to afford the binding constant (K_a) of the CD-guest complex. This is known as the NMR chemical shift titration method [86].

1.3.6 Cyclodextrin Derivatives

Numerous CD derivatives have been synthesized for a number of purposes, including, to increase aqueous solubility, to increase selectivity of a host/guest combination, or to control the release rate and bioavailability of a drug. The three natural CDs contain 18 (α), 21 (β), and 24 (γ) hydroxyl groups that can be chemically modified. Modification reactions with CDs are governed by two important issues, the nucleophilicity of the hydroxyl groups at the C2-, C3-, and C6-positions, and the ability of the CD to form an inclusion complex with the reagents used [87].

The primary hydroxyl groups at the C6-positions are the most nucleophilic and basic. Secondary hydroxyl groups at the C2-positions are the most acidic, while the hydroxyl groups at the C3-position are the most inaccessible [87, 88]. Electrophilic reagents will preferentially react with C6-positions, while very reactive reagents will attack all positions. Due to the differences in reactivity between the three types of hydroxyl groups, substitution reactions with cyclodextrins are not totally random, and in some cases can be controlled with success [54, 61, 88-90]. In cases where exact position and number of substituents are not important, water-soluble CD derivatives are easily achieved through the random modification of hydroxyl groups to hydroxylpropyl, sulfopropyl, carboxymethyl, or sulfate groups [54, 91, 92].

1.3.7 Application of Cyclodextrins

CDs are widely used in a variety of areas. In the food industry (generally the largest industry consumers of β-CD), CD as stabilizing or thickening agents could retain some aroma compounds in food matrices during thermal processes (cooking, pasteurization) [93]. CDs also have applications in the agro-industry through complex formations with

pesticides, herbicides, insect repellents [94, 95]. CDs can play a major role in environmental science in terms of solubilisation of organic contaminants, enrichment and removal of organic pollutants and heavy metals from soil, water and atmosphere [96-98]. β-CD can be incorporated onto textile by means of spraying, printing, padding, grafting, surface coating, impregnation, inkjet printing or via sol-gel [99-101].

In the pharmaceutical industry, in which often drugs are sparingly soluble in water, CDs are of vital importance. The conventional drug formulation systems are not enough to attain drug formulations without adverse effects and irritations. However, formulations involving CDs increase solubility, enhance stability, improve bioavailability, reduce dose and volatility of the so-called drugs and masking the unpleasant odours and bitter tastes [102]. CDs have also been subject of intensive electrochemical research including both their behaviour in homogeneous solutions and in thin films attached to the electrode surfaces [103-105]. They are employed in electrochemical sensing devices for the determination of selected analytes. The electrochemical measurements can prove the formation of CD complexes either from a decrease of the diffusion-limited currents resulting from a change of the diffusion coefficient or as a rather subtle shift of the redox potential [106, 107]. The latter effect is a safe criterion for the reversible redox systems [108], whereas the irreversible electron transfer reactions may bring complications due to the coupling of electron transfer kinetics to the subsequent chemical steps or due to the influence of the adsorptive inhibition of CDs accumulated at the electrode surface [109, 110].

1.4 Dopamine

Dopamine (DA), also called 3,4-dihydroxyphenylethylamine is a catecholamine. It consists of a benzene ring with two hydroxyl groups (catechol) connected to a primary amine through an aliphatic ethylene linker (Figure 1.4). At physiological pH values for human blood, DA and other catecholamines occur in their protonated form [111, 112] with protonation occurring at the terminal amino group of the alkylamine side chain. The conformational flexibility due to rotations about the C–N and the two C–C bonds of the ethylamine side chain of protonated DA is expected to be an important factor for molecular recognition phenomena in host–guest interactions.

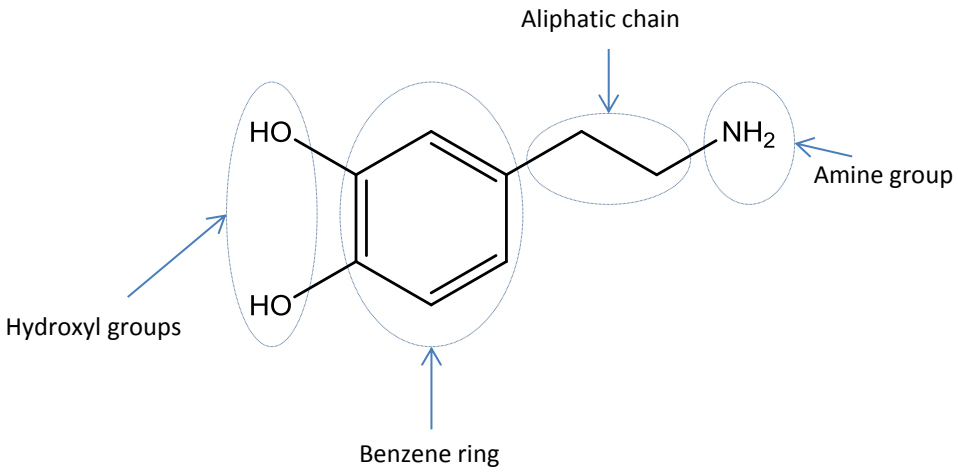

Figure 1.4: Chemical structure of DA.

1.4.1 Function and Biological Importance of DA

DA is an essential neurotransmitter in cerebral functions. Dysfunction in the dopaminergic transmission influences a variety of neurological and psychiatric disorders such as Parkinson's disease (deficit in the dopaminergic system) and schizophrenia (hyperactivity of dopaminergic system) [111]. In addition, DA plays an important role in motor control and "reward". It is related to addiction, and affects brain processes that control emotional response [112]. As a hormone in vesicles of the adrenal medulla, it regulates the heart beat rate and the blood pressure [112, 113].

DA is biosynthesized from tyrosine (a naturally occurring amino acid) in a two-step process taking place in dopaminergic neurons located in few discrete regions of the brain. Tyrosine is converted into L-Dopa by the enzyme tyrosine hydroxylase. L-Dopa can then be converted to DA, which subsequently can be converted to norepinephrine and finally epinephrine by a series of enzymes (Scheme 1.2 [114]).

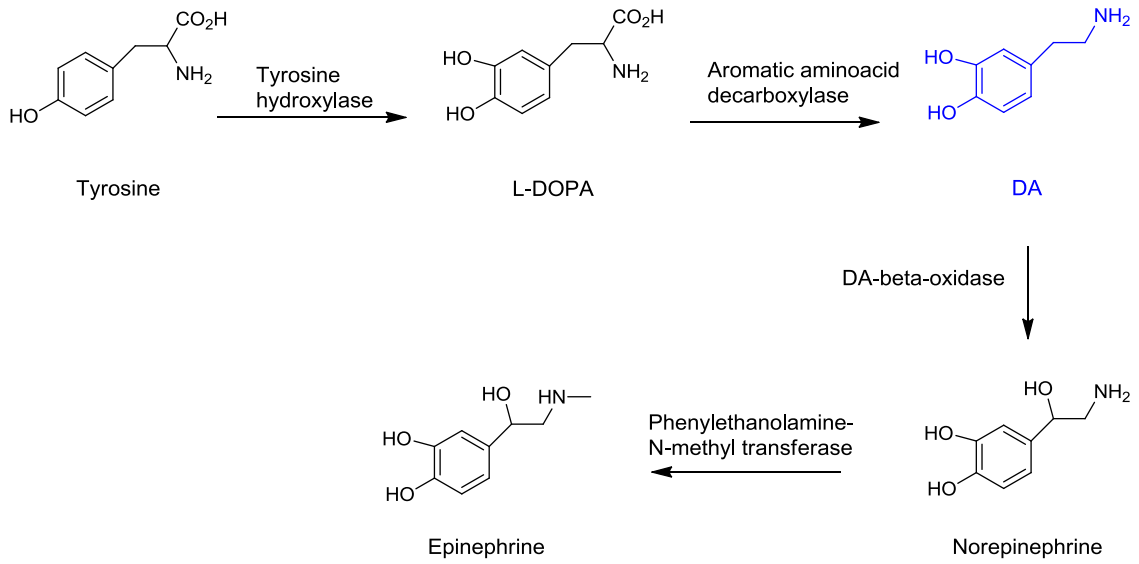

Scheme 1.2: The biosynthetic pathway of DA [114]

Figure 1.5 illustrates an example of a typical dopaminergic synapse [115]. DA is packaged into synaptic vesicles and, on nerve firing, is released into the synaptic space, where it can activate postsynaptic DA receptors as well as presynaptic DA auto-receptors. In this example, DA binds to the D1 and D2 postsynaptic receptors. D2 auto receptor would regulate the amount of DA released in the synapse, while the DA transporter (DAT) would control the reuptake of neurotransmitter from the extracellular space.

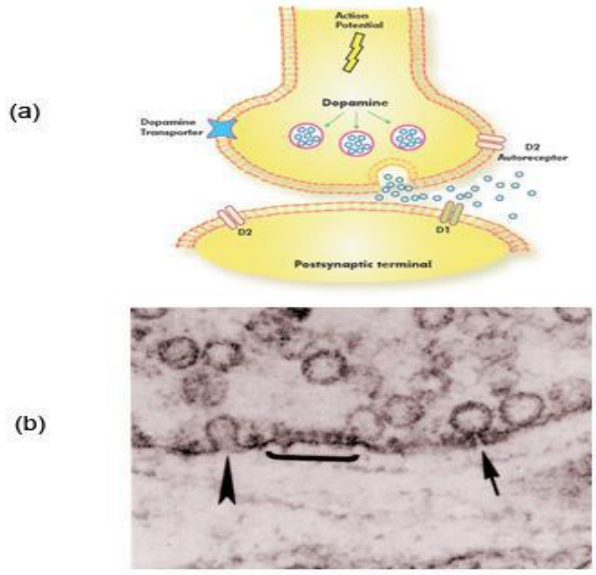

Figure 1.5: Synaptic Neurotransmission. Illustration of a generalized DA synapse (a). Synaptic exocytosis events (b). The arrows represent the secretion of neurotransmitters into the extracellular space. The active docking zone for neurotransmitter-containing vesicles is indicated by the bar [115].

1.4.2 Electrochemical Detection of DA

As mentioned above, DA plays a very important role in the functioning of the central nervous system, thus, fluctuations in levels of DA in the cerebrospinal fluid (CSF) are linked to many neurological disorders. The accurate quantification of DA becomes more and more important in clinical tests, serum and urine [116]. Therefore, it is essential to develop rapid and simple methods to detect it.

There has been considerable interest in developing new electrochemical methods to measure the concentration of this neurotransmitter in biological samples [117, 118]. A major problem of electrochemical detection of DA in real biological matrixes is the coexistence of many interfering compounds such as ascorbic acid (AA). AA usually coexists with DA in extracellular fluid at a high concentration level, nearly 10^3 times higher than DA [119, 120]. Moreover, DA and AA are oxidized at nearly the same potential at the electrode, which results in an overlapped voltammetric response. It is thus futile to discriminate DA from AA by electrochemical methods at a bare electrode. It is therefore very important to take into account both selectivity and sensitivity in the development of new voltammetric sensors for the determination of DA. Several works in the literature describe the development of new methodologies that employ chemically modified electrodes for the determination of DA in the presence of AA. The intensive use of chemically modified electrodes has gained much attention recently because of their interesting features for analytical use, such as good sensitivity, high selectivity, reproducibility, better stability and anti-fouling behaviour [121].

More specific chemically modified electrodes for electrochemical detection concern the use of CDs or their derivatives. A number of examples have been published in this regard. Chen *et al* [122] reported the use of GNPs/CDSH-Fc/nafion modified electrode for the detection of DA in the presence of AA. The sensor was fabricated by forming the inclusion complex between mono-6-thio-β-cyclodextrin (CD-SH) and ferrocene (Fc) functionalized gold nanoparticles (GNPs) films on a platinum electrode. The sensor provided a suitable environment to accelerate the electron transfer between DA and the electrode and also minimised leakage of the mediator during measurements. This resulted in the substantially enhanced stability and reproducibility of the modified electrode. At the same time, the presence of AA had no effect on the detection of DA. A linear calibration graph was obtained over the DA concentration range from 2×10^{-6} M to 5×10^{-5} M with a detection limit of 9×10^{-8} M.

Another sensor using β-CD as molecular receptor in the determination of DA has been developed by Alarcon-Angeles *et al* [123]. The authors utilised a combination of β-CD

and multiwall carbon nanotubes (MWCNT) drop-cast on a glassy carbon electrode. The integrated sensor showed improved analytical performance characteristics in catalytic oxidation of DA compared with non-modified electrode. The guest DA molecule was entrapped inside the cavity of immobilized β-CD. β-CD then acts as a mediator that ensures a better electrical contact between the GCE and the bulk DA solution. Moreover, the MWCNT adjacent to the β-CD enhances the electron transfer improving the overall electrochemical response of the DA. The detection of DA was obtained over the range from 1×10^{-5} to 8×10^{-5} M by amperometric method with a detection limit of 6.7×10^{-6} M.

On consideration of the aforementioned, the present research work aimed at designing a reliable method for the electrochemical detection of DA, in the presence of AA and 5-HT. Initially CPE modified with macrocyclic compounds such as sulfated β-cyclodextrin (S-β-CD), carboxymethyl β-CD (CM-β-CD) and Heptakis 6-deoxy-6-(1-(4,5-dicarboxyl)-1,2,3-triazolyl)-β-CD ($CD_{6.6}$) were fabricated as new type of electrodes for the sensitive electrochemical detection of DA in an aqueous solution. Also, it is proposed that the simultaneous determination of DA, AA and 5-HT is feasible using the S-β-CD modified CPE in phosphate buffer solution at pH 6.8. The proposed sensor has been applied to the determination of DA and AA in artificial cerebrospinal fluid (aCSF) with satisfactory results.

1.5 Objectives and Outline of Thesis

In this Ph.D. study, the feasibility of a number of chemically modified CPEs for electrochemical detection of DA and its interferents, (ascorbic acid, and serotonin), was investigated. Compared to noble metal electrodes, CPEs are endowed with many good qualities such as low background current, low cost, possibility to incorporate different substances during the paste preparation, easy preparation, simple renewal of their surface and possibilities of miniaturisation. These important advantages have made the use of carbon pastes a very important material in electrochemical analysis. The work presented herein describes carbon paste as a ‘support material’, which has been modified mainly with different cyclodextrin derivatives for selective and sensitive detection of DA. There is only limited number of reports on using cyclodextrin in the sensing of DA. Moreover, most cyclodextrins used are neutral β-CDs. Therefore, part of this study aims at synthesising cyclodextrin derivatives capable of enhancing the detection of DA.

The research content includes the description of electrochemical and analytical techniques employed throughout this study, which are detailed in Chapter 2. This chapter also gives the procedure for the synthesis of cyclodextrin derivatives and their characterisation by nuclear magnetic resonance (NMR), infrared (IR) and mass spectrometry. In addition, the experimental procedure for the preparation of graphene from graphite is given. Chapter 3 is concerned with the physical and electrochemical properties of chemically modified electrodes. Scanning electron microscope (SEM) was used to obtain information about the surface morphology of the modified electrodes.

In Chapter 4, the electrochemical performance of the chemically modified CPEs towards the detection of DA was examined. This also includes the mechanism (or mode of sensing) of DA electrochemical oxidation at each electrode and kinetics. Chapter 5 details the electrochemical study of DA in presence of interferents ascorbic acid and / or serotonin. The calibration curves and relevant limit of detection for DA (ascorbic acid and serotonin) are detailed. Chapter 6 presents a discussion of synthesised cyclodextrin derivatives and reports the complexation study of DA with the cyclodextrin derivatives. In this chapter, the use of microelectrodes in order to improve the sensitivity towards the detection of DA is also addressed. Each chapter comprises a separate introduction, results and discussion section while Chapter 7 provides a general conclusion of this thesis, possible applications and recommendations for future research.

1.6 References

1. Adams, R.N., *Carbon Paste Electrodes.* Analytical Chemistry, 1958. **30**(9): p. 1576-1576.

2. Pungor, E. and Szepesva,E., *Voltammetric Studies with Silicone Rubber-Based Graphite Electrodes.* Analytica Chimica Acta, 1968. **43**(2): p. 289-296.

3. Svancara, I. and Vytras, K., *Voltammetry with Carbon Paste Electrodes Containing Membrane Plasticizers Used for Pvc-Based Ion-Selective Electrodes.* Analytica Chimica Acta, 1993. **273**(1-2): p. 195-204.

4. Liu, H.T., et al., A*n ionic liquid-type carbon paste polyoxometalate-modified electrode and its properties.* Electrochemistry Communications, 2005. **7**(12): p. 1357-1363.

5. Diewald, W., et al., *Voltammetric Behaviour of Thallium(III) at a Solid Heterogeneous Carbon Electrode Using Ion-Pair Formation.* Analyst, 1994. **119**(2): p. 299-304.

6. Walcarius, A., Mariaulle, P., and Lamberts, L., *Zeolite-modified solid carbon paste electrodes.* Journal of Solid State Electrochemistry, 2003. **7**(10): p. 671-677.

7. Kalcher, K., *Chemically Modified Carbon Paste Electrodes in Voltammetric* A*nalysis.* Electroanalysis, 1990. **2**(6): p. 419-433.

8. Kalcher, K., et al., *Sensors Based on Carbon-Paste in Electrochemical* A*nalysis - a Review with Particular Emphasis on the Period 1990-1993.* Electroanalysis, 1995. **7**(1): p. 5-22.

9. Vytras, K. and Svancara, I., A*pplications of Carbon-Paste Electrodes in Electroanalysis.* Chemicke Listy, 1994. **88**(7): p. 412-422.

10. Ravichandran, K. and Baldwin, R.P., *Chemically Modified Carbon Paste Electrodes.* Journal of Electroanalytical Chemistry, 1981. **126**(1-3): p. 293-300.

11. Svancara, I. and Schachl, K., *Testing of unmodified carbon paste electrodes.* Chemicke Listy, 1999. **93**(8): p. 490-499.

12. Mojica, E.R.E., et al., *Lead detection using a pineapple bioelectrode.* Philippine Agricultural Scientist, 2006. **89**(2): p. 134-140.

13. Cai, X., et al., *Voltammetric Determination of Trace* A*mounts of Mercury with a Carbon Paste Electrode Modified with an* A*nion-Exchanger.* Fresenius Journal of Analytical Chemistry, 1993. **345**(1): p. 25-31.

14. Neuhold, C., et al., *Voltammetric Determination of Nitrate with a Modified Carbon-Paste Electrode.* Electroanalysis, 1994. **6**(3): p. 227-236.

15. Kalcher, K., *Voltammetric Behaviour of Hexachloroiridate(Iv) Solutions on Chemically Modified Carbon Paste Electrodes.* Fresenius Zeitschrift Fur Analytische Chemie, 1986. **324**(1): p. 47-51.

16. Svancara, I., et al., *Simple and rapid determination of iodide in table salt by stripping potentiometry at a carbon-paste electrode.* Analytical and Bioanalytical Chemistry, 2002. **372**(7-8): p. 795-800.

17. Kalcher, K., H. Greschonig, and Pietsch, R., *Extractive Preconcentration of Gold with Carbon Paste Electrodes Modified with Organophosphorous Compounds.* Fresenius Zeitschrift Fur Analytische Chemie, 1987. **327**(5-6): p. 513-517.

18. Elmaali, N.A., Ghandour, M.A., and J.M. Kauffmann, *Cephalosporin Antibiotics at Carbon-Paste and Modified Carbon-Paste Electrodes in Both Aqueous and Biological Media.* Bioelectrochemistry and Bioenergetics, 1995. **38**(1): p. 91-97.

19. French, D., *The Schardinger Dextrins.* Advances in Carbohydrate Chemistry, 1957. **12**: p. 189-280.

20. Stoddart, J.F., A *Century of Cyclodextrins - Foreword.* Carbohydrate Research, 1989. **192**: p. R12-R15.

21. Gorton, L., *Carbon-Paste Electrodes Modified with Enzymes, Tissues, and Cells.* Electroanalysis, 1995. **7**(1): p. 23-45.

22. Svancara, I., et al., *Carbon paste electrodes in modern electroanalysis.* Critical Reviews in Analytical Chemistry, 2001. **31**(4): p. 311-345.

23. Kuwana, T. and French, W.G., *Electrooxidation or Reduction of Organic Compounds into Aqueous Solutions Using Carbon Paste Electrode.* Analytical Chemistry, 1964. **36**(1): p. 241-242.

24. Suye, S.I., et al., *Mediated amperometric determination of ammonia with a methanol dehydrogenase from Pseudomonas sp AM-1 immobilized carbon paste electrode.* Biosensors & Bioelectronics, 1996. **11**(5): p. 529-534.

25. Gao, Z.Q., et al., *Differential Pulse Voltammetric Determination of Cobalt with a Perfluorinated Sulfonated Polymer-2,2-Bipyridyl Modified Carbon Paste Electrode.* Analytical Chemistry, 1991. **63**(10): p. 953-957.

26. Kalcher, K., et al., *The Encyclodepia of Sensors* 2006, Stevenson Ranch: American Scientific.

27. Svancara, I., et al., A *microscopic study on carbon paste electrodes.* Electroanalysis, 1996. **8**(1): p. 61-65.

28. Digua, K., Kauffmann, J.M., and Delplancke, J.L., *Surfactant Modified Carbon-Paste Electrode . Part 1. Electrochemical and Microscopic Characterization.* Electroanalysis, 1994. **6**(5-6): p. 451-458.

29. Metelka, R., Vytras, K., and Bobrowski, A., *Effect of the modification of mercuric oxide on the properties of mercury films at HgO-modified carbon paste electrodes.* Journal of Solid State Electrochemistry, 2000. **4**(6): p. 348-352.

30. Chadim, P., et al., *Gold-plated carbon paste electrodes for anodic stripping determination of arsenic.* Collection of Czechoslovak Chemical Communications, 2000. **65**(6): p. 1035-1046.

31. Lehn, J.M., *From Molecular to Supramolecular Chemistry - Science, Art and Industry.* Interdisciplinary Science Reviews, 1985. **10**(1): p. 72-85.

32. Lehn, J.M., *Cryptates - Inclusion Complexes of Macropolycyclic Receptor Molecules.* Pure and Applied Chemistry, 1978. **50**(9-10): p. 871-892.

33. Norgaard, K. and Bjornholm, T., *Supramolecular chemistry on water - towards self-assembling molecular electronic circuitry.* Chemical Communications, 2005(14): p. 1812-1823.

34. Rapis, E., *Self-organization and supramolecular chemistry of protein films from the nano- to the macroscale.* Technical Physics, 2004. **49**(4): p. 494-498.

35. Gulikkrzywicki, T., C. Fouquey, and J.M. Lehn, *Electron-Microscopic Study of Supramolecular Liquid-Crystalline Polymers Formed by Molecular-Recognition-Directed Self-Assembly from Complementary Chiral Components.* Proceedings of the National Academy of Sciences of the United States of America, 1993. **90**(1): p. 163-167.

36. Cram, D.J., *Molecular Container Compounds.* Nature, 1992. **356**(6364): p. 29-36.

37. Conn, M.M. and Rebek, J., *Self-assembling capsules.* Chemical Reviews, 1997. **97**(5): p. 1647-1668.

38. Scalia, S., Villani, S., and Casolari, A., *Inclusion complexation of the sunscreen agent 2-ethylhexyl-p-dimethylaminobenzoate with hydroxypropyl-beta-cyclodextrin: effect on photostability.* Journal of Pharmacy and Pharmacology, 1999. **51**(12): p. 1367-74.

39. Yang, T.Z., et al., *Cyclodextrins in nasal delivery of low-molecular-weight heparins: In vivo and in vitro studies.* Pharmaceutical Research, 2004. **21**(7): p. 1127-1136.

40. Ahn, H.J., et al., *Effects of cyclodextrin derivatives on bioavailability of ketoprofen.* Drug Development and Industrial Pharmacy, 1997. **23**(4): p. 397-401.

41. Li, P., Zhao, L.W., and Yalkowsky, S.H., *Combined effect of cosolvent and cyclodextrin on solubilization of nonpolar drugs.* Journal of Pharmaceutical Sciences, 1999. **88**(11): p. 1107-1111.

42. Szente, L. and Szejtli, J., *Cyclodextrins as food ingredients.* Trends in Food Science & Technology, 2004. **15**(3-4): p. 137-142.

43. Astray, G., et al., A *review on the use of cyclodextrins in foods.* Food Hydrocolloids, 2009. **23**(7): p. 1631-1640.

44. Carroll, K.C. and Brusseau, M.L., *Dissolution, cyclodextrin-enhanced solubilization, and mass removal of an ideal multicomponent organic liquid.* Journal of Contaminant Hydrology, 2009. **106**(1-2): p. 62-72.

45. Barr, L., et al., *Cyclodextrin molecular reactors.* Journal of Inclusion Phenomena and Macrocyclic Chemistry, 2004. **50**(1-2): p. 19-24.

46. Ogoshi, T. and Harada, A., *Chemical sensors based on cyclodextrin derivatives.* Sensors, 2008. **8**(8): p. 4961-4982.

47. Zhang, F.F., et al., A *novel sensor based on electropolymerization of beta-cyclodextrin and L-arginine on carbon paste electrode for determination of fluoroquinolones.* Analytica Chimica Acta, 2013. **770**: p. 53-61.

48. Li, W., et al., *Highly sensitive and reproducible cyclodextrin-modified gold electrodes for probing trace lead in blood.* Talanta, 2009. **78**(3): p. 717-722.

49. Wang, X.H., et al., *Synthesis of a beta-cyclodextrin derivate and its molecular recognition behavior on modified glassy carbon electrode by diazotization.* Tetrahedron, 2010. **66**(39): p. 7815-7820.

50. Itsuno, S., *Chiral polymer synthesis by means of repeated asymmetric reaction.* Progress in Polymer Science, 2005. **30**(5): p. 540-558.

51. Schulz, M. and Christoffers, J., *New macrocyclic bistriazolophanes with thioindigo chromophore.* Tetrahedron, 2013. **69**(2): p. 802-809.

52. Hradilova, L., et al., *Study of direct macrocycle formation via the cyclisation of propargyl 2-azidobenzoate.* Tetrahedron Letters, 2013. **54**(10): p. 1218-1221.

53. Li, Y.J. and Flood, A.H., *Pure C-H hydrogen bonding to chloride ions:* A *preorganized and rigid macrocyclic receptor.* Angewandte Chemie-International Edition, 2008. **47**(14): p. 2649-2652.

54. Szejtli, J., *Introduction and general overview of cyclodextrin chemistry.* Chemical Reviews, 1998. **98**(5): p. 1743-1753.

55. Eastburn, S.D. and Tao, B.Y., A*pplications of Modified Cyclodextrins.* Biotechnology Advances, 1994. **12**(2): p. 325-339.

56. Stella, V.J. and Rajewski, R.A., *Cyclodextrins: Their future in drug formulation and delivery.* Pharmaceutical Research, 1997. **14**(5): p. 556-567.

57. Matsuda, H. and Arima, H., *Cyclodextrins in transdermal and rectal delivery.* Advanced Drug Delivery Reviews, 1999. **36**(1): p. 81-99.

58. Buschmann, H.J. and Schollmeyer, E., A*pplications of cyclodextrins in cosmetic products:* A *review.* Journal of Cosmetic Science, 2002. **53**(3): p. 185-191.

59. Lu, X.N. and Chen, Y., *Chiral separation of amino acids derivatized with fluoresceine-5-isothiocyanate by capillary electrophoresis and laser-induced fluorescence detection using mixed selectors of beta-cyclodextrin and sodium taurocholate.* Journal of Chromatography A, 2002. **955**(1): p. 133-140.

60. Baudin, C., et al., *Inclusion of organic pollutants in cyclodextrins and derivatives.* International Journal of Environmental Analytical Chemistry, 2000. **77**(3): p. 233-242.

61. Kumar, R., et al., *Biotransformation of cholesterol using Lactobacillus bulgaricus in a glucose-controlled bioreactor.* Bioresource Technology, 2001. **78**(2): p. 209-211.

62. Koukiekolo, R., et al., *Mechanism of porcine pancreatic alpha-amylase - Inhibition of amylose and maltopentaose hydrolysis by alpha-, beta- and gamma-cyclodextrins.* European Journal of Biochemistry, 2001. **268**(3): p. 841-848.

63. Dass, C.R. and Jessup, W., A*polipoprotein* A-*I, cyclodextrins and liposomes as potential drugs for the reversal of atherosclerosis.* A *review.* Journal of Pharmacy and Pharmacology, 2000. **52**(7): p. 731-761.

64. Szejtli, J., *Past, present, and future of cyclodextrin research.* Pure and Applied Chemistry, 2004. **76**(10): p. 1825-1845.

65. Menard, F.A., M.G. Dedhiya, M.G., and Rhodes, C.T., *Physicochemical* A*spects of the Complexation of Some Drugs with Cyclodextrins.* Drug Development and Industrial Pharmacy, 1990. **16**(1): p. 91-113.

66. Breslow, R., et al., *Sequence selective binding of peptides by artificial receptors in aqueous solution.* Journal of the American Chemical Society, 1998. **120**(14): p. 3536-3537.

67. Bibby, D.C., Davies, N.M., and Tucker, I.G., *Preparation and characterization of beta-cyclodextrin and poly(acrylic acid) microspheres.* Journal of Microencapsulation, 1998. **15**(5): p. 629-637.

68. Davis, M.E., *Non-viral gene delivery systems.* Current Opinion in Biotechnology, 2002. **13**(2): p. 128-131.

69. Srichana, T., Suedee, R., and Reanmongkol, W., *Cyclodextrin as a potential drug carrier in salbutamol dry powder aerosols: the in-vitro deposition and toxicity studies of the complexes.* Respiratory Medicine, 2001. **95**(6): p. 513-519.

70. Connors, K.A., *The stability of cyclodextrin complexes in solution.* Chemical Reviews, 1997. **97**(5): p. 1325-1357.

71. Tabushi, I., Kuroda, Y., and Mizutani, T., *Functionalized Cyclodextrins as* A*rtificial Receptors - Guest Binding to Bisimidazolyl-Beta-Cyclodextrin.Zinc.* Tetrahedron, 1984. **40**(3): p. 545-552.

72. Bennaim, A. and Marcus, Y., *Solvation Thermodynamics of Nonionic Solutes.* Journal of Chemical Physics, 1984. **81**(4): p. 2016-2027.

73. Southall, N.T., Dill, K.A., and Haymet, A.D.J., A *view of the hydrophobic effect.* Journal of Physical Chemistry B, 2002. **106**(3): p. 521-533.

74. Liu, L. and Guo, Q.X., *The driving forces in the inclusion complexation of cyclodextrins.* Journal of Inclusion Phenomena and Macrocyclic Chemistry, 2002. **42**(1-2): p. 1-14.

75. Dappe, Y.J., Ortega, J., and Flores, F., *Weak Chemical Interaction and van der Waals Forces: A Combined Density Functional and Intermolecular Perturbation Theory - Application to Graphite and Graphitic Systems.* Atomic-Scale Modeling of Nanosystems and Nanostructured Materials, 2010. **795**: p. 45-79.

76. Buckingham, A.D., Del Bene, J.E., and McDowell, S.A.C., *The hydrogen bond.* Chemical Physics Letters, 2008. **463**(1-3): p. 1-10.

77. Murthy, P.S., *Molecular handshake: Recognition through weak noncovalent interactions.* Journal of Chemical Education, 2006. **83**(7): p. 1010-1013.

78. Leckband, D. and Israelachvili, J., *Intermolecular forces in biology.* Quarterly Reviews of Biophysics, 2001. **34**(2): p. 105-267.

79. Chandler, D., *Interfaces and the driving force of hydrophobic assembly.* Nature, 2005. **437**(7059): p. 640-647.

80. Beer, P.D., Gale, P.A., and David, K.S., *Supramolecular Chemistry*, in *Supramolecular Chemistry* 2003, Oxford Chemistry Primers: Oxford University Press: Oxford. p. 1-14.

81. Shinoda, K. and Fujihira, M., *Analysis of Solubility of Hydrocarbons in Water.* Bulletin of the Chemical Society of Japan, 1968. **41**(11): p. 2612-2615.

82. Steed, J.W., Turner, D.R., and Wallace, K.J., *Core Concepts in Supramolecular Chemistry* 2007, Chichester: John Wiley & Sons, Ltd.

83. Jadhav, G.S. and Vavia, P.R., *Physicochemical, in silico and in vivo evaluation of a danazol-beta-cyclodextrin complex.* International Journal of Pharmaceutics, 2008. **352**(1-2): p. 5-16.

84. Sinha, V.R., et al., *Complexation of celecoxib with beta-cyclodextrin: Characterization of the interaction in solution and in solid state.* Journal of Pharmaceutical Sciences, 2005. **94**(3): p. 676-687.

85. Franco, C., et al., *Studies on coumestrol/beta-cyclodextrin characterization.* International Journal of Pharmaceutics, 2009. **369**(1-2): p. 5-11.

86. Schneider, H.J., et al., *NMR studies of cyclodextrins and cyclodextrin complexes.* Chemical Reviews, 1998. **98**(5): p. 1755-1785.

87. Peroche, S. and Parrot-Lopez, H., *Novel fluorinated amphiphilic cyclodextrin derivatives: synthesis of mono-, di- and heptakis-(6-deoxy-6-perfluoroalkylthio)-beta-cyclodextrins.* Tetrahedron Letters, 2003. **44**(2): p. 241-245.

88. Tabushi, I., Shimokawa, K., and Fujita, K., *Specific Bifunctionalization on Cyclodextrin.* Tetrahedron Letters, 1977(18): p. 1527-1530.

89. Djedainipilard, F., et al., *Potential Formation of Intramolecular Inclusion Complexes in Peptido-Cyclodextrins as Evidenced by Nmr-Spectroscopy.* Journal of the Chemical Society-Perkin Transactions 2, 1995(4): p. 723-730.

90. Venema, F., Rowan, A.E., and Nolte, R.J.M., *Binding of porphyrins in cyclodextrin dimers.* Journal of the American Chemical Society, 1996. **118**(1): p. 257-258.

91. Nakagawa, T., et al., *The Stereoselective Synthesis of Cyclomaltopentaose - a Novel Cyclodextrin Homolog with Dp-5.* Tetrahedron Letters, 1994. **35**(12): p. 1921-1924.

92. Takahashi, Y. and Ogawa, T., *Glucan Synthesis .6. Total Synthesis of Cyclomaltohexaose.* Carbohydrate Research, 1987. **164**: p. 277-296.

93. Jouquand, C., Ducruet, V., and Giampaoli, P., *Partition coefficients of aroma compounds in polysaccharide solutions by the phase ratio variation method.* Food Chemistry, 2004. **85**(3): p. 467-474.

94. Singh, M., Sharma, R., and Banerjee, U.C., *Biotechnological applications of cyclodextrins.* Biotechnology Advances, 2002. **20**(5-6): p. 341-359.

95. Sanchez, F.J.M., et al., *Modeling of monolith-supported affinity chromatography.* Biotechnology Progress, 2004. **20**(3): p. 811-817.

96. Hirayama, F. and Uekama, K., *Cyclodextrin-based controlled drug release system.* Advanced Drug Delivery Reviews, 1999. **36**(1): p. 125-141.

97. Hashimoto, H., *Present status of industrial application of cyclodextrins in Japan.* Journal of Inclusion Phenomena and Macrocyclic Chemistry, 2002. **44**(1-4): p. 57-62.

98. Xia, Y.Y. and Wan, J.M., *Preparation and adsorption of novel cellulosic fibers modified by beta-cyclodextrin.* Polymers for Advanced Technologies, 2008. **19**(4): p. 270-275.

99. Voncina, B. and Le Marechal, A.M., *Grafting of cotton with beta-cyclodextrin via poly(carboxylic acid).* Journal of Applied Polymer Science, 2005. **96**(4): p. 1323-1328.

100. Martel, B., et al., *Polycarboxylic acids as crosslinking agents for grafting cyclodextrins onto cotton and wool fabrics: Study of the process parameters.* Journal of Applied Polymer Science, 2002. **83**(7): p. 1449-1456.

101. Martel, B., et al., *Capture and controlled release of fragrances by CD finished textiles.* Journal of Inclusion Phenomena and Macrocyclic Chemistry, 2002. **44**(1-4): p. 439-442.

102. Szejtli, J., *Utilization of cyclodextrins in industrial products and processes.* Journal of Materials Chemistry, 1997. **7**(4): p. 575-587.

103. Ferancova, A. and Labuda, J., *Cyclodextrins as electrode modifiers.* Fresenius Journal of Analytical Chemistry, 2001. **370**(1): p. 1-10.

104. Ferancova, A., et al., *Cyclodextrins as supramolecular complex agents in electroanalytical chemistry: Review 1995-2001.* Chemicke Listy, 2002. **96**(11): p. 856-862.

105. Bersier, P.M., et al., *Polarography of Penem Carbapenem* A*ntibiotics and the* A*zetidinone Intermediate.* Electroanalysis, 1990. **2**(5): p. 373-381.

106. Nuwer, M.J., Odea, J.J., and Osteryoung, J.G., *Kinetics and Thermodynamics of Inclusion of Para-Nitrophenolate with* A*lpha-Cyclodextrin Measured with Pulse Voltammetry.* Journal of Physical Chemistry, 1991. **95**(24): p. 10070-10076.

107. Taraszewska, J. and Piasecki, A.K., *Inclusion Complexes of Isomeric Chloronitrobenzenes with* A*lpha-Cyclodextrins and Beta-Cyclodextrins Studied by Polarography -* A*nalysis of the Possibilities of the Method.* Journal of Electroanalytical Chemistry, 1987. **226**(1-2): p. 137-146.

108. Strelets, V.V., et al., *Electrochemistry of Inclusion Complexes of Organometallics - Complexation of Ferrocene and* A*zaferrocene by Cyclodextrins.* Journal of Electroanalytical Chemistry, 1991. **310**(1-2): p. 179-186.

109. Goledzinowski, M., *The Influence of* A*lpha-Cyclodextrins, Beta-Cyclodextrins and Gamma-Cyclodextrins on the Kinetics of the Electrode-Reactions in 1 M* $NaClO_4$ *and 0.5 M* Na_2SO_4 A*queous-Solutions.* Journal of Electroanalytical Chemistry, 1989. **267**(1-2): p. 171-189.

110. Pospisil, L. and Svestka, M., *Growth of compact layers at the interface .3. Surface aggregation of alpha- and gamma-cyclodextrins in aqueous solutions of potassium fluoride.* Journal of Electroanalytical Chemistry, 1997. **426**(1-2): p. 47-53.

111. Nagy, P.I., Alagona, G., and Ghio, C., *Theoretical studies on the conformation of protonated dopamine in the gas phase and in aqueous solution.* Journal of the American Chemical Society, 1999. **121**(20): p. 4804-4815.

112. Solmajer, P., Kocjan, D., and Solmajer, T., *Conformational Study of Catecholamines in Solution.* Zeitschrift Fur Naturforschung C. Journal of Biosciences, 1983. **38**(9-10): p. 758-762.

113. Wang, X.Y., Jin, B.K., and Lin, X.Q., *In-situ FTIR spectroelectrochemical study of dopamine at a glassy carbon electrode in a neutral solution.* Analytical Sciences, 2002. **18**(8): p. 931-933.

114. Thompson, R.F., *The Brain:* A *Neuroscience Primer*. 2 ed. 1993: W. H. Freeman and Company.

115. Torritarelli, F., et al., *Temporal Coincidence between Synaptic Vesicle Fusion and Quantal Secretion of* A*cetylcholine.* Journal of Cell Biology, 1985. **101**(4): p. 1386-1399.

116. Wightman, R.M., May, L.J., and Michael, A.C., *Detection of Dopamine Dynamics in the Brain.* Analytical Chemistry, 1988. **60**(13): p. A769-779A.

117. Stamford, J.A., et al., *Fast Cyclic Voltammetry - Neurotransmitter Measurement in Real-Time and Real-Space.* Bioelectrochemistry and Bioenergetics, 1995. **38**(2): p. 289-296.

118. Davidson, C., et al., *Effect of cocaine, nomifensine, GBR 12909 and WIN 35428 on carbon fiber microelectrode sensitivity for voltammetric recording of dopamine.* Journal of Neuroscience Methods, 2000. **101**(1): p. 75-83.

119. Yogeswaran, U. and Chen, S.M., *Separation and concentration effect of f-MWCNTs on electrocatalytic responses of ascorbic acid, dopamine and uric acid at f-MWCNTs incorporated with poly (neutral red) composite films.* Electrochimica Acta, 2007. **52**(19): p. 5985-5996.

120. Nasri, Z. and Shams, E., A*pplication of silica gel as an effective modifier for the voltammetric determination of dopamine in the presence of ascorbic acid and uric acid.* Electrochimica Acta, 2009. **54**(28): p. 7416-7421.

121. Kawagoe, K.T. and Wightman, R.M., *Characterization of* A*mperometry for in-Vivo Measurement of Dopamine Dynamics in the Rat-Brain.* Talanta, 1994. **41**(6): p. 865-874.

122. Chen, M., et al., *Fabrication of GNPs/CDSH-Fc/nafion modified electrode for the detection of dopamine in the presence of ascorbic acid.* Materials Science & Engineering C-Materials for Biological Applications, 2011. **31**(7): p. 1271-1277.

123. Alarcon-Angeles, G., et al., *Enhanced host-guest electrochemical recognition of dopamine using cyclodextrin in the presence of carbon nanotubes.* Carbon, 2008. **46**(6):p.898-906.

2 Experimental Details

2.1 Introduction

This chapter outlines the experimental techniques and procedures carried out during this study. A description of all the chemicals, material composites and instrumentation employed in the experiments is given. The theoretical background of each experiment and related equations are also described. In addition, the methodology for the synthesis of cyclodextrin derivatives is provided.

2.2 Experimental Techniques

This section gives a brief overview of electrochemical / analytical techniques employed in this study. The techniques used throughout this study include cyclic voltammetry (CV), potentiostatic measurements, linear sweep voltammetry (LSV), differential pulse voltammetry (DPV), rotating disc voltammetry (RDV), ultraviolet–visible spectroscopy (UV-Vis), scanning electron microscopy (SEM) coupled with energy dispersive x-ray analysis (EDX), electrochemical impedance spectroscopy (ESI), infrared spectroscopy (IR), mass spectrometry and nuclear magnetic resonance (NMR).

2.2.1 Voltammetry

In this Ph.D. study, a number of techniques focused on current measurement (voltammetry), therefore, before the different voltammetry techniques used are discussed, it is imperative to understand the concept of the word voltammetry. Voltammetry is a category of electroanalytical methods used in analytical chemistry and various industrial processes. In voltammetry, information about an analyte is obtained by measuring the current as the potential is varied [1, 2]. Most experiments control the potential (Volts) of an electrode in contact with the analyte while measuring the resulting current (Amperes) [3].

2.2.2 Cyclic Voltammetry

Cyclic voltammetry (CV) is the most widely used electrochemical technique. The technique can be used to study electron transfer mechanisms in reactions, providing information on the reversibility, kinetics, and formal reduction and oxidation potentials of a system [3]. During the CV experiment, the solution is kept stationary in order to avoid movement of ions to the electrode surface by mechanical means. The initial applied potential, E_i, is swept to a vertex potential, E_v, where the scan is reversed and swept back to the final potential, E_f, which usually equals the original potential, E_i. This

process creates a cyclic effect and is typically repeated a number of times. The magnitude of the Faradaic current, I_{pa} (anodic peak current) or I_{pc} (cathodic peak current), is an indication of the rate at which electrons are being transferred between the redox species and the electrode.

A plot of applied potential versus current is used to depict the generated cyclic voltammogram. A typical voltammogram is shown in Figure 2.1. The scan shown starts at a slightly negative potential, –0.2 V, up to some positive switching value, +0.4 V, at which the scan is reversed back to the starting potential. The current is first observed to peak at E_{pa} = 0.169 V (with value I_{pa}) indicating that an oxidation is taking place and then drops due to depletion of the reducing species from the diffusion layer. During the return scan the process is reversed (reduction is now occurring) and a peak current is observed at E_{pc} = 0.142 V (with corresponding value, I_{pc}). The current is recorded as a function of the applied potential.

Unless otherwise stated, all peak currents were determined in the form $I_p - I_{Bg}$, where I_p is the observed peak current and I_{Bg} is the background current. As shown in Figure 2.1, the intersection of the two lines gives the I_{Bg}, and this is then subtracted from I_p to give the background corrected DA peak current (I_{pa}). This method of I_{pa} determination was also employed in differential pulse voltammetry (DPV) and rotating disc voltammetry (RDV) experiments.

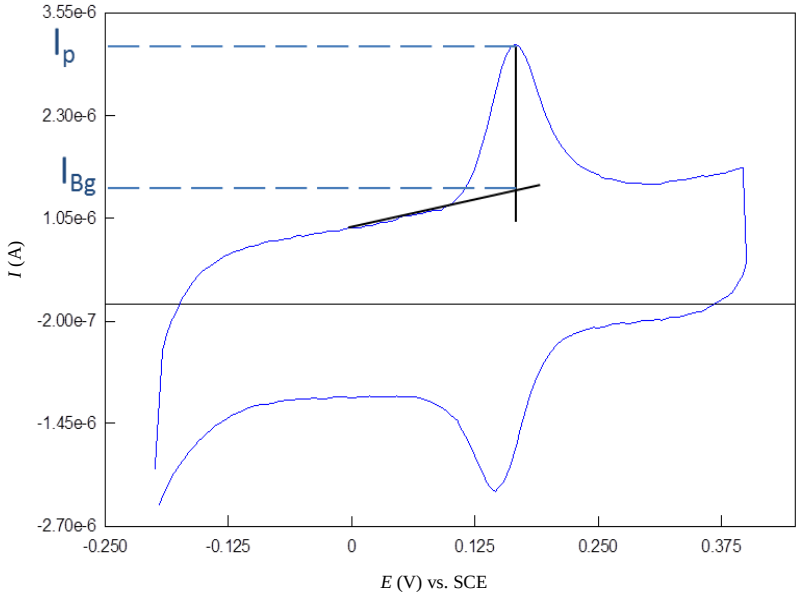

Figure 2.1: Typical current-potential profile of a cyclic voltammogram for a reversible redox species.

The CV technique was firstly used to characterise the prepared carbon paste materials. Secondly, it was used as an investigative tool to study the electrochemical behaviour of DA and 5-HT. Finally, the interfering compound AA on DA signal was analysed at different carbon paste material composites under CV.

2.2.3 Linear Sweep Voltammetry

Linear sweep voltammetry (LSV) is a voltammetric method where the current at a working electrode is measured while the potential between the working electrode and a reference electrode is swept linearly in time. Oxidation or reduction of species is registered as a peak or through in the current signal at the potential at which the species begins to be oxidized or reduced [3].

LSV was used as a preliminary technique to examine the electrochemical behaviour of bare CPE in the electrolyte solution (0.1 M PBS).

2.2.4 Differential Pulse Voltammetry

Differential pulse voltammetry (DPV) is one of the most suitable techniques to characterize electrochemical systems since it presents a peak-shaped response with the nonfaradaic contribution and the ohmic drop effect significantly reduced as compared to alternative procedures [3, 4]. Improved detection limits are achieved by eliminating the double layer capacitance so that the current recorded is totally faradaic [5]. The potential wave form for DPV, shown in Figure 2.2, consists of small pulses (of constant amplitude) superimposed upon a staircase wave form. The current is sampled twice in each pulse period (once before the pulse, and at the end of the pulse). The difference between these two current values is recorded and plotted as a function of the applied potential.

DPV was used to improve the detection limit of DA and investigate the voltammetric response of a ternary mixture containing DA, AA and 5-HT solution.

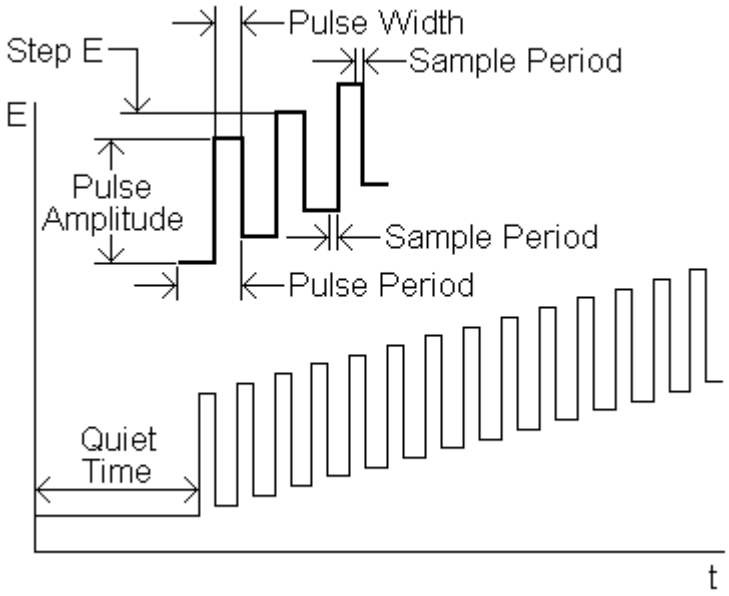

Figure 2.2: Schematic of differential pulse voltammetry technique, showing the step method applied and the parameter setting required.

2.2.5 Rotating Disc Voltammetry

A rotating disc electrode (RDE) is a hydrodynamic working electrode in a three electrode system [3]. RDE provides an efficient and reproducible mass transport, and hence the analytical measurement can be made with high sensitivity. The convective nature of the electrode results in very short response time. The detection limits of the electrode can be lowered via periodic changes in the rotation speed. The more useful descriptor of rotation rate is the angular velocity, ω (s^{-1}), where $\omega = 2\pi f$. Electrical connection is made to the electrode by means of a brush contact.

The RDE as shown in Figure 2.3 was constructed from carbon paste composite imbedded in a rod of an insulating material (Teflon). The paste was firmly packed into the cavity of the Teflon in order to provide sufficient coverage of the conical part of aluminium. The aluminium itself was attached to a motor which provided electrical contact to the paste.

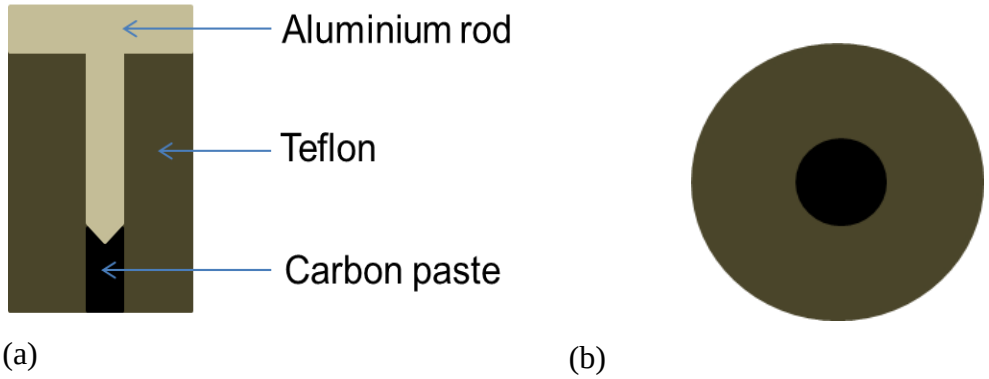

Figure 2.3: Schematic illustration of constructed electrode for Rotating disc voltammetry experiments. Side view (a) and bottom view (b).

During the experiment, the electrode was concentrically rotated in the solution, creating convection path flowing perpendicular to the electrode and then radially out from the surface as shown in Figure 2.4. This rapid mixing of the solution enables constant replenishment of the detected species to the electrode surface. A potential was applied relative to a SCE reference electrode while a platinum (Pt) wire served as an auxiliary electrode.

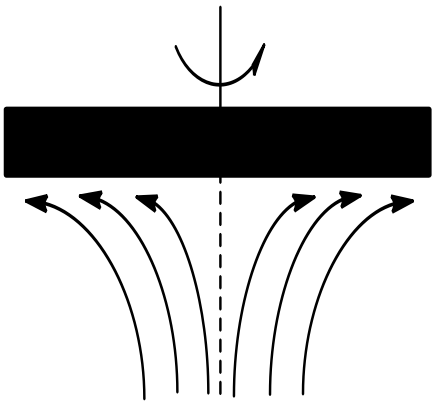

Figure 2.4: Flow profile at a rotating disc electrode.

In general, for the RDE, the limiting current, I_L, produced by oxidation or reduction of DA at the different electrode surface can be described by the Levich equation (Equation 2.1), where n is the number of electron transferred per molecule, F is the Faraday constant, A is the electrode surface area, C is the analyte concentration, D is the analyte diffusion coefficient, v is the kinematic viscosity of the solution and ω is the angular velocity of the rotating disk.

$$I_L = 0.62nFAC D^{2/3} v^{-1/6} \omega^{1/2} \qquad \text{Equation 2.1}$$

The current is measured as a function of the potential and the resulting voltammograms generally exhibit a sigmoid shaped wave as shown in Figure 2.5. A schematic representation of the set-up is shown in Figure 2.6 [6].

RDV was used to determine the heterogeneous rate constant for electron transfer between electrode surface and DA.

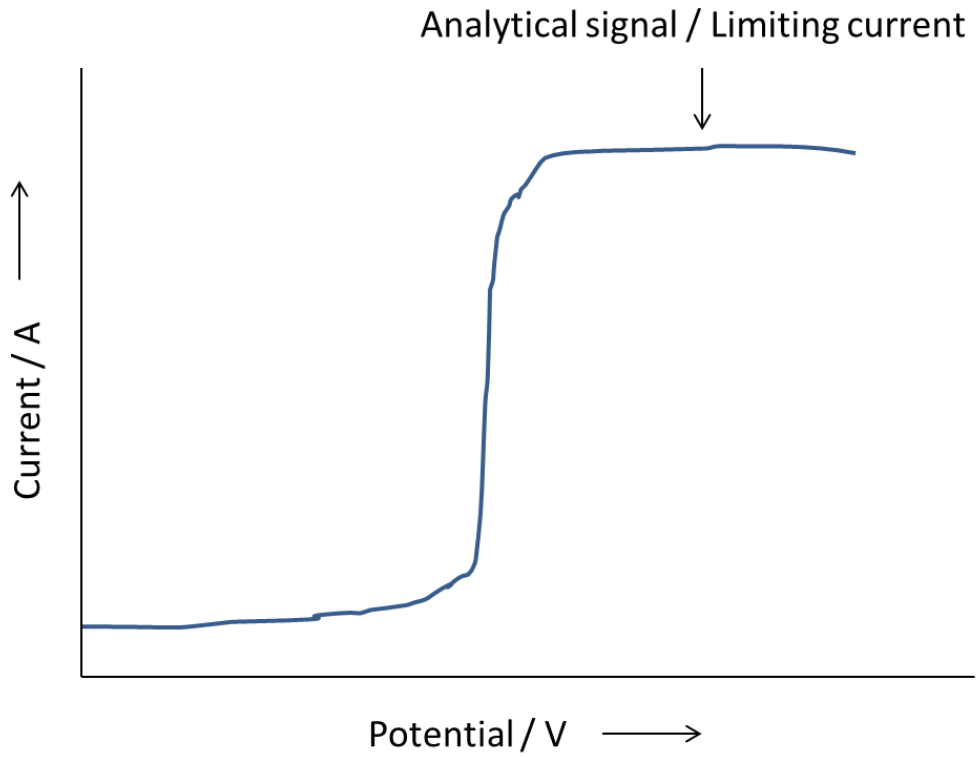

Figure 2.5: Typical rotation disc response.

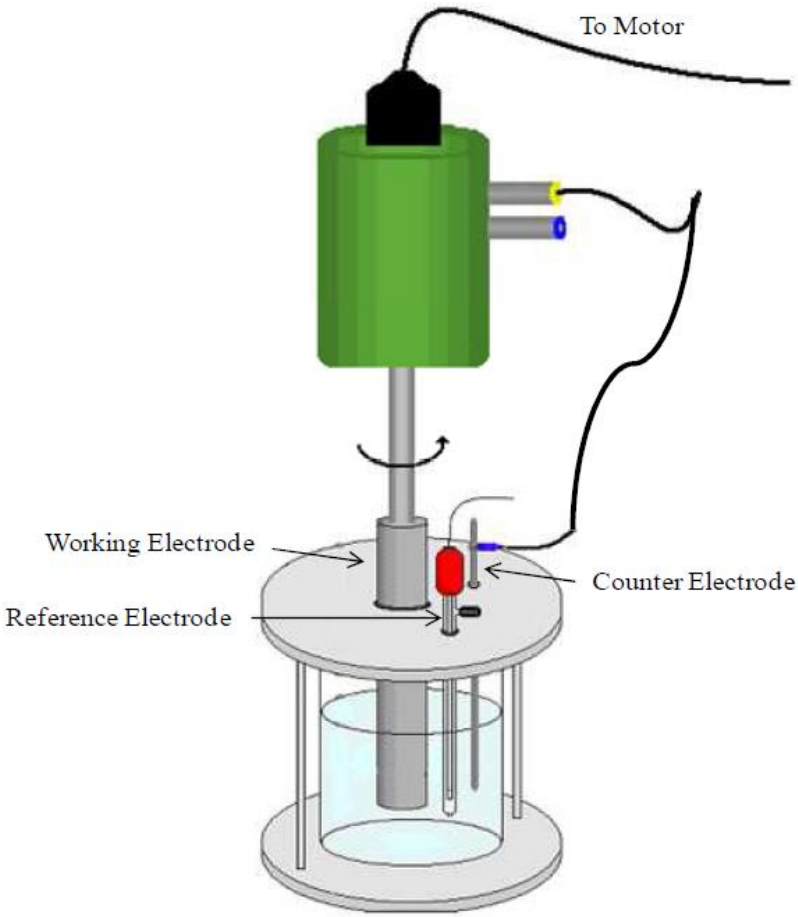

Figure 2.6: Schematic illustration of the rotation disc voltammetry set-up, with three-cell electrode system [6].

2.2.6 Microscopy and Spectroscopy Techniques

2.2.6.1 Microscopy

Microscopy is the technical field of using microscopes to view samples or objects. There are three well-known branches of microscopy: optical, electron and scanning probe microscopy. Optical and electron microscopy involve the diffraction, reflection, or refraction of electromagnetic radiation / electron beam interacting with the subject of study, and the subsequent collection of this scattered radiation in order to build up an image. This process may be carried out by wide-field irradiation of the sample (transmission electron microscopy) or by scanning of a fine beam over the sample (scanning electron microscopy). Scanning probe microscopy involves the interaction of a scanning probe with the surface or object of interest [7].

2.2.6.1.1 Optical microscopy

Optical microscope remains the fundamental tool for phase identification. The optical microscope magnifies an image by sending a beam of light through the object. The condenser lens focuses the light on the sample and the objective lens magnifies the beam, which contains the image, to the projector lens so the image can be viewed. Optical microscopy was employed to observe the surface of S-β-CD modified CPE after an electrochemical measurement in order to describe whether or not the paste was stable.

2.2.6.1.2 Scanning Electron Microscope (SEM)

Scanning electron microscope (SEM) is a powerful microscope that images the sample surface by scanning it with a high-energy beam of electrons in a faster scan pattern. The electrons interact with the atoms that make up the sample producing signals that contain information about the sample's surface topography, composition and other properties such as electrical conductivity [7]. Since the SEM is operated under high vacuum the specimens that can be studied must be compatible with high vacuum (~ 10-5 mbar). This means that liquids and materials containing water and other volatile components cannot be studied directly. Also fine powder samples need to be fixed firmly to a specimen holder substrate so that they will not contaminate the SEM specimen chamber. Non-conductive materials need to be attached to a conductive specimen holder and coated with a thin conductive film by sputtering or evaporation. Typical coating materials are Au, Pt, Pd, their alloys, as well as carbon. Applications include physical and chemical characterization of surfaces, microstructural analysis, corrosion damage, particle analysis and foreign materials.

SEM was employed for the characterisation of the carbon paste material composites. EDX was used for elemental analysis of the surface of carbon paste composite.

2.2.6.2 Spectroscopy

Spectroscopy is the study of the interaction between radiation and matter as a function of wavelength, frequency or energy which is usually in the form of photon of light and represented as $E = hv$ where h is the Planck constant [8]. A plot of the response as a function of wavelength - or more commonly frequency - is referred to as a spectrum.

2.2.6.2.1 Energy dispersive X-ray spectroscopy (EDX)

Energy dispersive X-ray spectroscopy (EDX) is an analytical technique used for the elemental analysis or chemical characterization of a sample. As a type of spectroscopy, it relies on the investigation of a sample through interactions between electromagnetic radiation and matter, analysing X-rays emitted by the matter in response to being hit with charged particles. The characterisation capabilities using EDX are due in large part to the fundamental principle that each element has a unique atomic structure allowing unique set of peaks on its X-ray spectrum [9-11]. All elements from atomic number 4 (Beryllium) to 92 (Uranium) can be detected in principle, though not all instruments are equipped for 'light' elements ($Z < 10$). Qualitative analysis involves the identification of the lines in the spectrum and is fairly straightforward owing to the simplicity of X-ray spectra. Quantitative analysis (determination of the concentrations of the elements present) entails measuring line intensities for each element in the sample and for the same elements in calibration Standards of known composition. By scanning the beam in a television-like raster and displaying the intensity of a selected X-ray line, element distribution images or 'maps' can be produced. Also, images produced by electrons collected from the sample reveal surface topography or mean atomic number differences according to the mode selected. As already mentioned, EDX was used to determine the elemental composition at the surface of the different carbon paste composites.

2.2.6.2.2 Infrared spectroscopy

Infrared (IR) spectroscopy is a well-known analytical technique which deals with the infrared region of the electromagnetic spectrum. It can be used to identify compounds or investigate sample composition. Infrared spectroscopy exploits the fact that molecules have specific frequencies at which they rotate or vibrate corresponding to discrete energy levels (vibrational modes). These resonant frequencies are determined by the shape of the molecular potential energy surfaces, the masses of the atoms and, by the associated vibronic coupling. Infrared spectroscopy is widely used in both research and industry as a simple and reliable technique for measurement, quality control and dynamic measurement.

In this study, IR was used for the characterisation of graphene and the synthesised macrocycles. As all compounds were in solid state, the method utilised to prepare the sample consisted of grinding a quantity of the compound with potassium bromide finely (to remove scattering effects from large crystals). The powder mixture was then pressed

in a mechanical press to form a translucent pellet through which the beam of the spectrometer can pass [12].

2.2.6.2.3 Ultraviolet-visible spectroscopy

Ultraviolet-visible spectroscopy (UV-Vis) involves the spectroscopy of photons in the UV-visible region. The absorption in the visible ranges directly affects the colour of the chemicals involved. In this region of the electromagnetic spectrum, molecules undergo electronic transitions. Absorption of photons of light measures transitions from the ground state to the excited state [12].

Molecules containing π-electrons or non-bonding electrons can absorb the energy in the form of ultraviolet or visible light to excite these electrons to higher anti-bonding molecular orbitals. The more easily excited the electrons, the longer the wavelength of light it can absorb.

This analytical technique can be used to determine the amount of substance present in a sample. This is because the absorbance is proportional to the concentration of the absorbing species given by the Beer-Lambert law, $A = \varepsilon\, l\, c$, where A is the absorbance, ε is the molar absorptivity, l is the path length and c is the concentration of the absorbing species. UV-Vis spectroscopy is routinely used in the quantitative determination of solutions of transition metal ions and highly conjugated organic compounds [13].

In this study, UV-Vis was employed for the characterisation of Fc-β-CD and graphene oxide.

2.2.6.2.4 Electrochemical Impedance Spectroscopy (EIS)

Electrochemical impedance spectroscopy (EIS) is a relatively new and powerful method of characterizing many of the electrical properties of materials and their interfaces with electronically conducting electrodes. It may be used to investigate the dynamics of bound or mobile charge in the bulk or interfacial regions of any kind of solid or liquid material: ionic, semiconducting, mixed electronic–ionic and even insulators (dielectrics) [14]. It is also used to explore the properties of porous electrodes, and for investigating passive surfaces [15]. EIS technique has been shown to be effective for probing the redox and structural features of a surface-confined species [16]. Other advantages include: (i) rapid acquisition of data such as ohmic resistance, capacitance, inductance, film conductivity, as well as charge or electron transfer at the electrode-film interface,

(ii) the ability to obtain accurate, reproducible measurement, and (iii) characterize interfacial properties in the absence of redox reactions. Impedance is measured by applying a sinusoidal potential V (t), of small amplitude to an electrochemical cell and measuring resultant sinusoidal current I (t), through the cell [17, 18]. The applied sinusoidal potential and current are represented as a function of time. These measurements are done over a suitable frequency range and the results can be related to the physical and chemical properties of the material [17, 18]. The relationship is shown in Equation 2.2:

$$Z = V(t) / I(t) \qquad \text{Equation 2.2}$$

where V (t) and I (t) are the sinusoidal applied voltage and sinusoidal current at time t, respectively. The sinusoidal applied voltage V (t) can be expressed as shown in Equation 2.3, where V_o is the maximum potential amplitude, ω is the radial frequency (in $rad.s^{-1}$) and can be related to frequency f (Hz) as $\omega = 2\pi f$.

$$V(t) = V_o \sin\omega t \qquad \text{Equation 2.3}$$

At the same frequency as the applied sinusoidal potential, the current response I (t) is also sinusoidal but with a shift in phase (Equation 2.4),

$$I(t) = I_o \sin(\omega+\theta) \qquad \text{Equation 2.4}$$

where I_o is the maximum current applied and θ is the phase shift by which the voltage lags the current [18]. Therefore, impedance is a vector quantity where the quantity Z = V (t) / I (t) represents the magnitude and θ represent the direction. The complex notation of impedance is shown in Equation 2.5.

$$Z = Z' + jZ'' \qquad \text{Equation 2.5}$$

where Z' and Z'' are the real and imaginary parts of the impedance respectively and j is a complex number [18]. If the real part is plotted on the X-axis and the imaginary part is plotted on the Y-axis of a chart, a Nyquist plot is obtained. The Nyquist plot has several advantages. The primary one is that the plot format makes it easy to see the effects of the ohmic resistance. At sufficiently high frequencies, it is easy to extrapolate the semicircle toward the left, down to the x axis to read the ohmic resistance. EIS data are commonly analysed by fitting to an equivalent electrical circuit model. Most of the circuit elements in the model are common electrical elements such as resistors, capacitors, and inductors. The electrochemical properties of graphene paste electrode (compared to that obtained at bare CPE) were examined using ESI.

2.2.6.2.5 Nuclear magnetic resonance (NMR) spectroscopy

Nuclear Magnetic Resonance (NMR) spectroscopy has become the dominant method of analysis for organic compounds [19], because in many cases it provides a way to determine an entire structure.

The NMR spectroscopy phenomenon is based on the fact that nuclei of atoms have magnetic properties that can be utilised to yield chemical information. In many atoms such as ^{1}H, ^{13}C, ^{31}P, ^{15}N, ^{19}F, the nucleus does possess an overall spin of ½. For spin ½ nuclei, the angular momentum can have two possible values: +½ or –½. Therefore, these nuclei align either with or against the applied magnetic field. Depending on the type of nucleus, there is a characteristic resonance frequency [20].

^{1}H-NMR is the most frequently used and can provide information on a wide variety of factors including the number of different hydrogens present in a molecule and the electronic environment of the different types of hydrogen.

In conjunction to an applied magnetic field, there is a local magnetic field surrounding the molecule. This is due to the electron clouds surrounding each atom. These local fields can then shield the molecule from the applied magnetic field [19]. As each atom of a molecule has a varying arrangement of electrons, the degree of shielding can differ. This is then translated onto a ^{1}H-NMR spectrum with a unique signal, known as a chemical shift (δ), measured in parts per million (ppm).

^{1}H-NMR spectra were typically recorded from 0 to 10 ppm. The greater the effect of shielding, the smaller the chemical shift, thus the closer the ^{1}H-NMR signal is to 0 ppm. Thus, a highly shielded molecule appears upfield on a ^{1}H-NMR spectrum. The reverse is the case for a poorly shielded molecule; it has a larger chemical shift and appears downfield on the spectrum.

In this study, NMR spectroscopy was used to characterise the synthesised cyclodextrin derivatives. In addition, ^{1}H-NMR was employed to investigate the complexation of these cyclodextrins with DA. This was achieved by monitoring the chemical environment of the individual DA protons which were most affected by complexation. The chemical shift of these protons were also used to evaluate the binding or association constant (K_a) and the stoichiometry of the complex.

2.3 The Electrochemical Cell Set-up

All electrochemical techniques were carried out using a conventional three-cell electrode system, as shown in Figure 2.7 [19]. This system consists of a working electrode (WE), a counter or auxiliary electrode (CE/AE) and a reference electrode (RE or REF). In this study, The REF was a saturated calomel electrode (SCE) and the CE consisted of a platinum (Pt) wire. The WE was mainly modified CPE. Some details on its construction are discussed in Chapter 3.

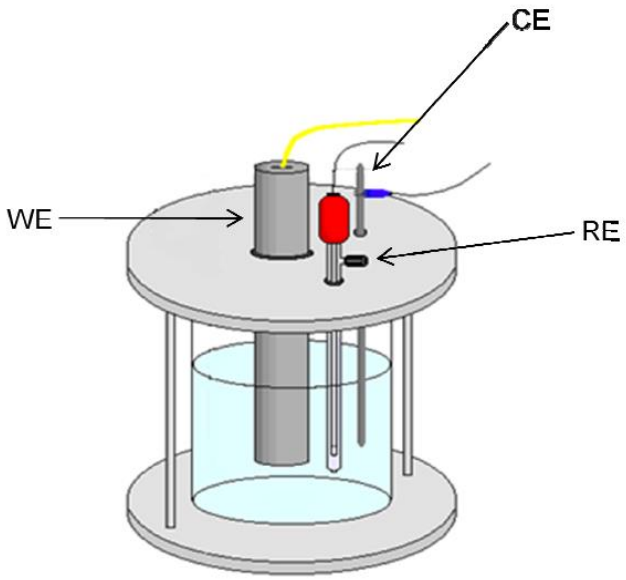

Figure 2.7: Schematic of the electrochemical cell used for electrochemical measurements [21].

The cell was then connected to a potentiostat and the results were recorded by a computer in the manner shown in Figure 2.8 [21]. In general, the potential is measured between the REF and the WE and the current is measured between the WE and the CE.

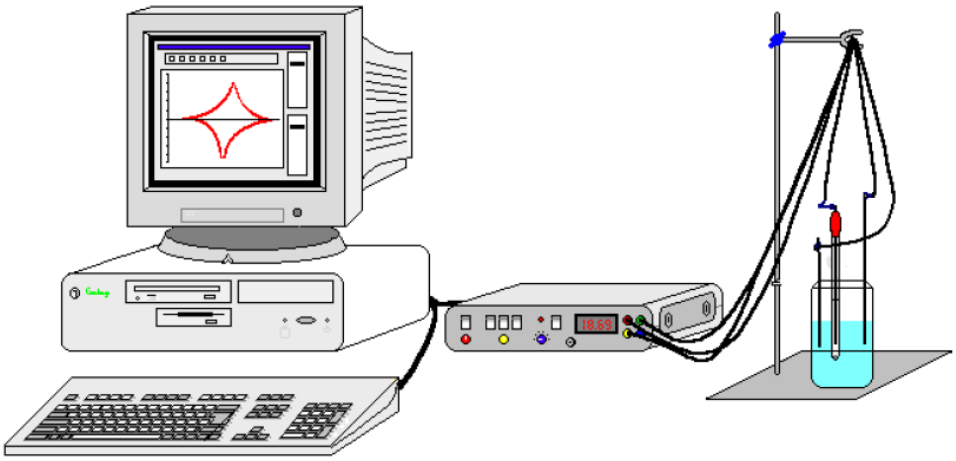

Figure 2.8: Experiment set-up of a potentiostat connected to a three-cell electrode and the data recorded using computer software [21].

2.4 Chemicals and Solutions

The chemicals used throughout this study were purchased from Sigma-Aldrich or its subsidiary company Fluka and used as received. The electrochemical electrolytes were prepared in milli Q water. In general, for electrochemical analysis, 0.1 M Phosphate Buffer Solution (PBS) was used as the supporting electrolyte. PBS was made of K_2HPO_4 and KH_2PO_4. KCl (0.1 M) was only used for comparative purposes. Artificial cerebrospinal fluid (aCSF) was used to simulate the salts concentration in the brain. All DA, AA or 5-HT solutions were prepared freshly before each experiment. In the event that a change in pH was required, it was adjusted accordingly with appropriate amount of an acidic or a basic solution using H_2SO_4 and NaOH respectively.

2.5 Instrumentation

Potentiostatic, Linear sweep voltammetry (LSV) and cyclic voltammetry (CV) were carried out using a Solartron potentiostat (Model SI 1285A). Differential pulse voltammetry (DPV) was carried out using a Chi440 potentiostat (Model 400). The software package for the Solartron potentiostat was Scribner Associates Corrware for Windows Version 2.2 and in the case of the CHi440 potentiostat, Chi440 software, Version 2.0.6 was employed. From each of these software packages, data were then transferred and further analysed using Scribner Associates CorrView Version 2.3a.

During the rotary disc voltammetry (RDV) experiments, the working electrode was rotated using the Princeton Applied Research Model 636 Ring-Disc Electrode System apparatus.

Electrochemical impedance spectroscopy (ESI) was carried out using a Solartron potentiostat (Model SI 1287) coupled to a Solartron frequency response analyser (Model 1255A). Further analysis was performed with Zplot (Version 2.1).

Scanning electron microscopy (SEM) was carried out on a Hitachi S-3200-N with a tungsten filament electron source, maximum magnification of 300,000x and a resolution 3.5 nm. This microscope was equipped with an Oxford Instrument INCAx-act EDX system with a silicon drift detector. The sample analysed were sputtered with a very thin gold film using an AGAR Automatic Sputter Coater in order to obtain a better resolution images.

The NMR spectroscopy experiments were carried out using a Shielded Bruker Avance AV 300 high performance digital NMR spectrometer complete with Bruker Avance 300 digital single bay AV NMR console, Ultrashield 300 MHz magnet and QNP 5 mm probe.

Mass spectroscopy was performed on an Agilent-LC 1200 Series coupled to a 6210 Agilent Time-Of-Flight (TOF) mass spectrometer equipped with an electrospray source both positive and negative (ESI +/–).

UV-Vis spectroscopy experiments were carried out on Varian Cary 50 UV-Vis spectrometer.

Conductivity measurements were performed using equipment Jenway 4510.

General analysis of data and plotting of graphs were performed in Sigmaplot 12.0. A linear regression equation is given as $f = y_0 + a*x$.

2.6 The Working Electrodes

Carbon paste electrode (CPE) is the main type of electrode used throughout this study. Details on its fabrication are given in Chapter 3. Glassy carbon electrode (GCE) was only used for comparative purposes.

2.6.1 Modification of Carbon Paste Electrodes

As mentioned in Chapter 1, CPEs can be modified using a number of methods and with different compounds [22, 23] to achieve the desired chemical, electrochemical, catalytic, photochemical or optical properties [24]. CPEs are useful to construct electrochemical sensors. They can be utilised in a large potential interval and offer several interesting possibilities when studying compounds that are soluble in aqueous media. In this study, various techniques were used to modify CPEs such as the composite, the dip coating and the drop-casting technique.

2.6.1.1 Composite technique

This process consisted of impregnating the carbon paste material with a chemical modifier. In this study, appropriate amount of the chemical modifier was added to the graphite (or graphene) prior to mixing. The modifiers employed based on this technique are sulfated β-cyclodextrin (S-β-CD), carboxymethyl β-cyclodextrin (CM-β-CD), neutral β-cyclodextrin (β-CD), Nafion, Heptakis6-deoxy-6-(1-(4,5-dicarboxyl)-1,2,3-triazolyl)-β-CD **6.6** ($CD_{6.6}$), Heptakis(6-(4-hydroxymethyl-1H-[1,2,3]triazol-1-yl)-6-deoxy)-β-cyclodextrin **6.7** ($CD_{6.7}$).

2.6.1.2 Dip Coating

It involves the immersion of the bare electrode in solution of a catalyst or a modifier for a period of time to allow for surface adsorption of the material. The electrode is later withdrawn and the solvent is allowed to dry [25, 26]. In this study, dip coating was carried out using nafion as modifier for electrochemical detection of DA.

2.6.1.3 Drop-Casting

The bare electrode is modified by placing a (or few) drop(s) of the catalyst or modifier on its surface and allowing the solvent to dry off [27, 28]. Nafion was drop-cast on bare CPE for electrochemical detection of DA.

2.6.2 Carbon Composite Microelectrodes

Carbon composite microelectrodes were prepared (courtesy of Dr Niall Finnerty) by trimming approximately 4.5 cm lengths of 200 µm coated Teflon-insulated silver wire (200 µm bare diameter, 270 µm coated diameter (8T), Advent Research Material, Suffolk, UK). The wire was carefully cut at both ends using a sharp scalpel to create an even disk surface. 3 mm of the wire was exposed by removing the Teflon from one end

of the wire and the Teflon was carefully pushed up the wire to create a 2mm cavity. The cavity was then packed with carbon composite by dipping the tip of the electrode into the paste. This process was repeated until the cavity was completely packed. A flat active surface at the tip of the electrode was obtained by gently tapping the electrode off a hard, flat surface. The 3 mm of exposed wire was soldered into a gold clip for electrical conductivity and rigidity. A schematic representation of the microelectrode is shown in Figure 2.9.

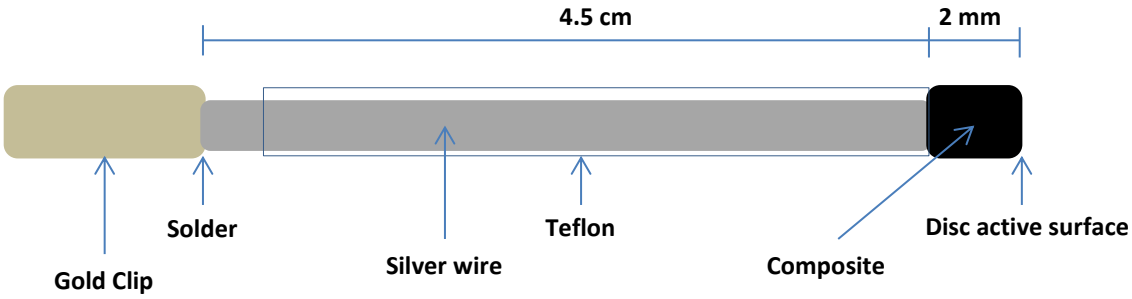

Figure 2.9: Schematic representation of a carbon paste microelectrode.

2.7 Synthesis of Cyclodextrin Derivatives

2.7.1 General Procedure and Instrumentation

All chemicals purchased were reagent grade and used without further purification unless stated otherwise. Toluene was distilled over Na wire and benzophenone. Anhydrous DMF and Pyr were purchased from Sigma Aldrich. Reactions were monitored with thin layer chromatography (TLC) on Merck Silica Gel F_{254} plates, using mixtures of Pet Ether/EtOAc unless otherwise stated. Detection was effected either by visualisation in UV light and/or charring in a mixture of 5% sulphuric acid-EtOH or phosphomomolybdic acid-EtOH. Evaporation under reduced pressure was always affected with the bath temperature kept below 40 ^{o}C.

NMR spectra were obtained on a Bruker Avance 300 MHz spectrometer operated at 300 MHz for ^{1}H NMR analysis and 75 MHz for ^{13}C analysis at 298 K. Proton and carbon signals were assigned with the aid of 2D NMR experiments (COSY) and DEPT experiments. Chemicals shifts for ^{1}H NMR acquired in $CDCl_3$ are reported in ppm relative to residual solvent proton (δ 7.26 ppm). Flash chromatography was performed according to the method of Still et al. with Merck Silica Gel 60, using adjusted mixtures of Pet Ether/EtOAc unless otherwise stated. High resolution mass spectra (HR-MS)

were performed on an Agilent-L 1200 Series coupled to a 6210 Agilent Time-of-Flight (TOF) mass spectrometer equipped with an both a positive and negative electrospray source. Infra-red spectra were obtained in the region 4000-400 cm^{-1} on a Nicolet Impact 400D spectrophotometer or using a Perkin Elmer 2000 FTIR spectrometer.

2.7.2 Synthesis of Heptakis(6-iodo-6-deoxy)-β-cyclodextrin (β-CD-I_7) 6.1 [29]

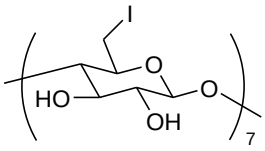

6.1

I_2 (10.9 g, 43 mmol) and Ph_3P (11.28 g, 43 mmol) were mixed in dry DMF (50 mL). The solution increased in temperature from room temperature to about 60˚C after addition was complete. Then, oven-dried β-cyclodextrin (2 g, 1.76 mmol) was added to the dark brown solution. The reaction mixture was stirred for 20 h at 90˚C under N_2 atmosphere. It was concentrated under reduced pressure to $^1/_3$ of its original volume and the pH was adjusted to 9-10 by addition of sodium methoxide (3 M, 13 mL), with simultaneously cooling on ice-water bath. The brown orange precipitate obtained was filtered, washed with excess methanol and dried under high vacuum to yield Heptakis(6-iodo-6-deoxy)-β-cyclodextrin (2.784 g, 83 %) as a light brown solid.

^{1}H-NMR (300 MHz, DMSO-d_6): δ = 3.15 – 3.54 (m, 21H, *Ha*-6, *H*-4 and *H*-2), 3.54 – 3.75 (m, 14H, *H*-3 and *H*-5), 3.81 (d, *J* = 9.3 Hz, 7H, *Hb*-6), 4.98 (br s, 7H, *H*-1), 5.72 – 6.47 (br s, 14H, O*H*-2 and O*H*-3).

IR (KBr, cm^{-1}): 3383 (O-H), 2915 (C-H), 1047 (C-O-C).

The data is in agreement with the literature values [29].

2.7.3 Synthesis of Heptakis(6-azido-6-deoxy)-β-cyclodextrin (β-CD-(N3)$_7$) 6.2 [29]

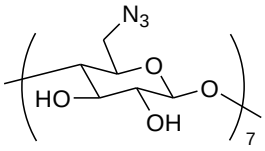

6.2

Compound **6.1** (1.416 g, 0.74 mmol) was dissolved in anhydrous DMF, followed by addition of NaN_3 (1.93 g, 29.7 mmol). The resulting suspension was stirred at 80˚C for 24 h under N_2 atmosphere. The suspension was then concentrated under reduced pressure to $^1/_3$ of its starting volume and washed with distilled water. After filtration, the residue was washed with water and dried under high vacuum to yield Heptakis(6-azido-6-deoxy)-β-cyclodextrin (0.6 g, 62 %) as a slight brown powder.

^{1}H-NMR (300 MHz, DMSO-d_6): δ = 3.19 – 3.47 (m, 14H, *H*-4 and *H*-2), 3.47 – 3.68 (m, 14H, *H*-3 and *H*-5), 3.68 – 3.94 (m, 14H, *H*-6), 4.91 (br s, 7H, *H*-1), 5.78 (br s, 7H, O*H*-3), 5.93 (br s, 7H, O*H*-2).

^{13}C-NMR (300 MHz, DMSO-d_6): δ = 51.82 (*C*-6), 70.28 (*C*-5), 71.95 (*C*-2), 72.54 (*C*-3), 83.14 (*C*-4), 101.99 (*C*-1).

IR (KBr, cm^{-1}): 3380 (O-H), 2927 (C-H), 2107 (N_3), 1049 (C-O-C).

The data is in agreement with the literature values [29].

2.7.4 Synthesis of Acetylated-per-azido-β cyclodextrin 6.3 [30]

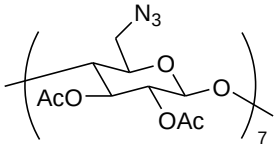

6.3

To a solution of β-CD-$(N_3)_7$ **6.2** (0.3 g, 0.23 mmol) in dry pyridine (6 mL), acetic anhydride (6 mL) was added. The mixture was stirred for 24 h at room temperature under N_2 atmosphere. Then, the mixture was concentrated and the residue was dissolved

in CH_2Cl_2 (10 mL) and washed with 0.1 N HCl solution (2 × 10 mL) followed by brine (2 × 10 mL) and water (2 × 10 mL). The organic layer was dried over $MgSO_4$ and concentrated to give a crude orange product. The crude product was purified by column chromatography (EtOAc / Pet. Ether 3:1). The proper fractions were collected and concentrated to give Acetylated-per-azido-β-cyclodextrin **6.3** (0.31 g, 70 %) as white solid.

^{1}H-NMR (300 MHz, DMSO-d_6): δ = 1.92 – 2.16 (s, 42H, COC*H*$_3$), 3.55 – 3.70 (m, 14H, *H*-6), 3.75 – 3.93 (m, 7H, *H*-4), 3.94 – 4.07 (m, 7H, *H*-5), 4.82 (dd, *J* = 3.0, 6.0 Hz, 7H, *H*-2), 5.10 (d, *J* = 3.0 Hz, 7H, *H*-1), 5.30 (t, *J* = 9.0 Hz, 7H, *H*-3).

^{13}C-NMR (300 MHz, DMSO-d_6): δ = 20.51 (CO*C*H$_3$), 50.78 (*C*-6), 69.68 (*C*-5), 69.82 (*C*-2), 76.85 (*C*-3), 96.29 (*C*-4), 169.32 (*C*-1), 170.00 (*C*OCH$_3$), 170.34 (*C*OCH$_3$).

ESI-MS (m/z): calculated for $(M+Na)^+$ $C_{70}H_{91}N_{21}O_{42}Na$: 1920.5602; Found: 1920.5502.

IR (KBr, cm^{-1}): 3631 (OH), 2942 (C-H), 2104 (N_3), 1742 (CO), 1375 (CH_3), 1025 (C-O-C).

The data is in agreement with the literature values [30].

2.7.5 Synthesis of Dimethyl Acetylenedicarboxylate 6.4 [31]

6.4

Acetylenedicarboxylic acid (1 g, 8.77 mmol) was dissolved in absolute methanol (3 mL) and concentrate H_2SO_4 (0.5 mL) was added to the solution. The flask was stoppered and the reaction mixture was allowed to stand with intermittent shaking for 72 h at room temperature during which a layer of ester separated. Then, the mixture was poured over crushed ice and extracted with two 5 mL portions of ether. The combined ether extract was dried over $CaCl_2$ and evaporated under reduced pressure to yield the title compound **6.4** (0.769 g, 62 %) as a clear, colourless liquid. It was used without further purification.

^{1}H-NMR (300 MHz, $CDCl_3$): δ = 3. 86 (s, 6H, CO_2CH_3)

The data is in agreement with the literature values [31].

2.7.6 Synthesis of Acetylated Heptakis-6-deoxy-6-(1-(4,5-dicarboxyl)-1,2,3-triazolyl)-β-CD 6.5 [32]

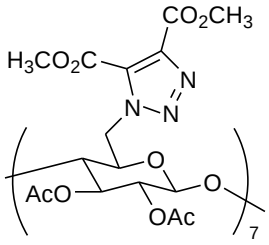

6.5

The acetylated azido compound **6.3** (0.235 g, 0.12 mmol) was dissolved in toluene (5 mL). Dimethyl Acetylenedicarboxylate (0.32 mL, 2.60 mmol) was added to the solution, which was refluxed for 17 h at 110˚C under argon atmosphere. The mixture was concentrated under reduced pressure, yielding a crude oil product. The crude product was purified by column chromatography (Toluene / Ethanol 9:1). The correct fractions were collected and concentrated to afford the title compound **6.5** (0.35 g, 85 %) as white solid.

^{1}H-NMR (300 MHz, CD_3CN): δ = 2. 01 (s, 21H, $COCH_3$), 2.12 (s, 21H, $COCH_3$), 3.55 – 3.67 (m, 7H, *H*-4), 3.82 (s, 21H, CO_2CH_3), 3.86 (s, 21H, CO_2CH_3), 4.42 – 4.62 (m, 14H, *H*-2 and *H*-5), 4.82 – 5.01 (m, 14H, *H*-6), 5.42 – 5.55 (m, 14H, *H*-1 and *H*-3).

^{13}C-NMR (300 MHz, DMSO-d_6): δ = 20.00 ($COCH_3$), 48.88 (*C*-6), 51.97, 53.08 (CO_2CH_3), 68.79, 69.48, 69.84 (*C*-2, *C*-3, *C*-5), 76.28 (*C*-4), 95.94 (*C*-1), 132.27, 139.09 (*C*C), 158.89, 160.10 ($COCH_3$), 169.37, 169.99 ($COCH_3$).

IR (KBr, cm^{-1}): 3464 (OH), 1747 (CO), 1372 (CH_3), 1049 (C-O-C).

The data is in agreement with the literature values [32].

2.7.7 Synthesis of Heptakis-6-deoxy-6-(1-(4,5-dicarboxyl)-1,2,3-triazolyl)-β-CD 6.6 [32]

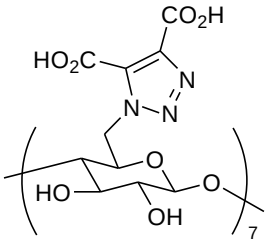

6.6

Compound **6.5** (0.1 g, 0.035 mmol) and KOH (0.108 g, 1.92 mmol) were mixed in dioxane-CH_3OH-H_2O (17:2:1). The mixture was allowed to stir at room temperature for 24 h. After this time, a white precipitate was formed all around the flask. The solvent was carefully decanted, and the crude product was triturated in ethanol (5 mL). The crude product was filtered, re-dissolved in water and acidified to pH 2 by a strong cation exchanger under H^+ form (Dowex 50W). The solution was concentrated and dried under high vacuum to yield the title compound **6.6** (0.55 g, 74 %) as a white solid.

^{1}H-NMR (300 MHz, D_2O): δ = 3.30 (t, 7H, *J* = 9.0 Hz, *H*-3), 3.35 – 3.45 (m, 7H, *H*-2), 3.83 (t, 7H, *J* = 9.0 Hz, *H*-4), 4.09 – 4.24 (m, 7H, *H*-5), 4.29 – 4.47 (m, 7H, *Ha*-6), 4.56 – 4.75 (m, 7H, *Hb*-6), 5.01 (d, *J* = 3.0 Hz, 7H, *H*-1).

^{13}C-NMR (300 MHz, D_2O): δ = 49.14 (*C*-6), 69.53, 71.65, 72.35 (*C*-2, *C*-3, *C*-5), 82.86 (*C*-4), 101.74 (*C*-1), 133.53, 139.37 (*C*C), 160.76, 163.23 (*C*O_2H).

The data is in agreement with the literature values [32].

2.7.8 Synthesis of Heptakis(6-(4-hydroxymethyl-1H-[1,2,3] triazol-1-yl)-6-deoxy)-β-cyclodextrin 6.7 [33]

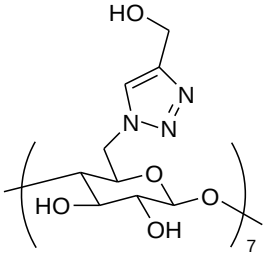

6.7

Azide **6.3** (0.5 g, 0.038 mmol) and CuI (0.36 g, 0.19 mmol) were dissolved in 50 % MeOH and DMF (1 mL) to which propargyl alcohol (15.8 µL, 0.27 mmol) and DIEA (33 µL, 0.19 mmol) were added by syringe and the mixture was stirred at rt for 24 h. The resulting green suspension was clarified using aqueous NH_4OH (30 %, 2mL), and Chelex 100 sodium form was added to the deep blue solution to complex copper ions. The solution was allowed to stir vigorously overnight, and the yellow supernatant obtained was concentrated to give the crude product which was triturated with absolute ethanol to yield the title compound **6.7** (0.13 g, 18 %) as a beige powder.

^{1}H-NMR (300 MHz, D_2O): δ = 3.35 (t, 7H, *J* = 9 Hz, *H*-4), 3.51 – 3.62 (m, 7H, *H*-2), 3.95 (t, 7H, *J* = 9 Hz, *H*-3), 4.06 – 4.46 (m, 35H, *H*-6, *H*-5 and C*H*$_2$OH), 5.07 (d, 7H, *H*-1), 7.85 (s, 7H, triazole *H*).

^{13}C-NMR (300 MHz, DMSO-d_6): δ = 49.29 (*C*OH, triazole), 54.59 (*C*-6), 69.65 (*C*-5), 71.72 (*C*-3), 72.44 (*C*-2), 82.50 (*C*-4), 101.51 (*C*-1), 124.11, 147.58 (*C*C).

ESI-MS (m/z): calculated for $(M+H)^+$ $C_{63}H_{91}N_{21}O_{35}H$: 1702.6144; Found: 1702.6118.

The data is in agreement with the literature values [33].

2.7.9 Synthesis of Heptakis(6-amino-6-deoxy)-β-cyclodextrin (β-CD-NH_2) 6.8 [34]

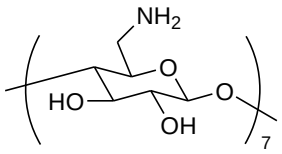

6.8

The azido compound **6.3** (0.5 g, 0.38 mmol) was dissolved in DMF (10 mL) and PPh_3 (1.58 g, 6.01 mmol) was added. The evolution of N_2 can be observed by the formation of bubbles in the reaction flask. After about 1 h, during which time the evolution of N_2 ceased, concentrated aqueous NH_3 (1.5 mL, approximately 35 %) was added dropwise to the solution. Shortly after the addition of the NH_3 solution was completed, the reaction mixture turned into an off-white suspension. It was stir at rt for 24 h, and the resulting suspension was concentrated under reduced pressure. The product was then precipitate by addition of EtOH (25 mL). The precipitate was washed with EtOH and

dried under high vacuum to yield the title compound **6.8** (0.38 g, 89 %) as a light brown solid.

To allow characterisation of **6.8** by NMR spectroscopy, the HCl salt form of **6.8** was prepared by suspending compound **6.8** in a small volume of H_2O followed by addition of dilute HCl until the pH had reached about 6. At this pH, a clear solution formed which gave a yellow glass when evaporated under reduced pressure.

^{1}H-NMR (300 MHz, D_2O): δ = 3.10 – 3.26 (m, 7H, *Ha*-6), 3.30 – 3.44 (m, 14H, *H*-2 and *H*-4), 3.45 – 3.67 (m, 7H, *H*-3), 3.91 (t, 7H, *J* = 9 Hz, *H*-5), 4.06 – 4.19 (m, 7H, *Hb*-6), 5.08 (d, *J* = 3 Hz, 7H, *H*-1).

^{13}C-NMR (300 MHz, D_2O): δ = 40.07 (*C*-6), 67.66, 71.45, 71.99 (*C*-2, *C*-3, *C*-5), 82.05 (*C*-4), 101.24 (*C*-1).

ESI-MS (m/z): calculated for $(M+H)^+$ $C_{42}H_{77}N_7O_{28}H$: 1128.4917; Found: 1128.4911.

IR (KBr, cm^{-1}): 3370 (OH and NH), 2942 (C-H), 1050 (C-O-C).

The data is in agreement with the literature values [34].

2.7.10 Synthesis of Ferrocene β-CD (Fc-β-CD) complex

Ferrocene (2 g, 10 mmol) and an excess of neutral β-CD (4 g, 3.53 mmol) were added into ethylene glycol (100 mL), followed by stirring at room temperature for 24 h. Then, the mixture was laid up motionlessly for more than 8 h so as to allow the inclusion reaction conducting completely. The solvent was carefully decanted and the precipitate was washed with distilled water (100 mL) to allow the insoluble complex separate from solution. After filtration, the precipitate was washed with THF (100 mL) to remove excess Ferrocene and distilled water (3 × 100 mL). Fc-β-CD inclusion complex was obtained as light yellow powder, and characterised by IR and UV-Vis spectroscopy.

Figure 2.10 shows the IR spectra of neutral β-CD and Fc-β-CD inclusion complex. The frequencies for β-CD observed at 3389.58 cm^{-1}, 2927.29 cm^{-1}, and 1157.63 cm^{-1} correspond to the symmetric and antisymmetric stretching of OH, CH_2, and C–C, respectively. Meanwhile the respective functional groups from Fc-β-CD inclusion complex were recorded at 3368.45 cm^{-1}, 2927.29 cm^{-1}, 1156.58 cm^{-1}. Table 2.1 shows the difference in frequencies between β-CD and the inclusion complex. The shift difference observed might be owing to the effect of Ferrocene included in the cavity of

β-CD. In addition, the absorption peak at 423 nm observed from the UV-Vis spectrum of Fc-β-CD inclusion complex (Figure 2.11) was assigned to the characteristic peak of ferrocene [35].

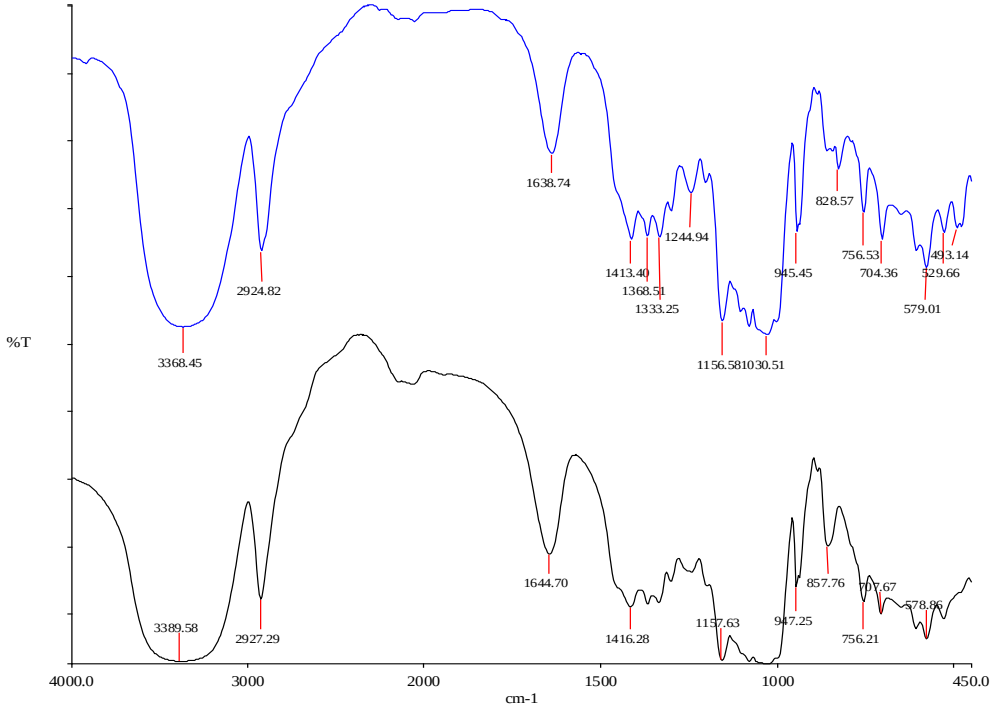

Figure 2.10: IR spectra of β-CD (−) and Fc-β-CD (−).

Table 2.1: Comparison between characteristic functional groups intensity of βCD and the inclusion complex

Functional groups	Wavenumber (cm^{-1})		Changes
	βCD	FcβCD inclusion complex	Δδ
ν[OH]	3389.58	3368.45	+21.13
ν[CH_2]	2927.29	2924.82	+2.47
ν[C−C]	1157.63	1156.58	+1.05

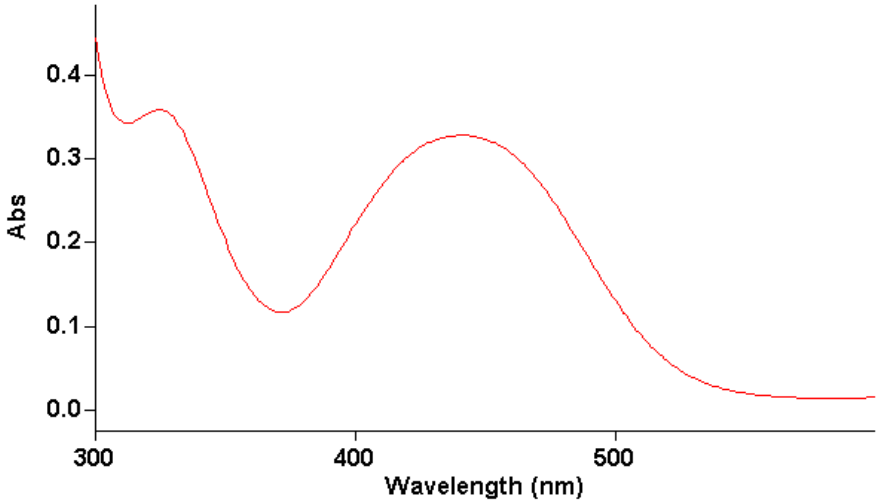

Figure 2.11: UV-Vis spectrum of Fc-β-CD

2.7.11 Synthesis of Graphene

Graphene was synthesised based on the Hummers method [36, 37].

(i) Oxidation of graphite

Graphite powder (4 g) was added to sulphuric acid (92 mL) and the mixture was stirred at room temperature for about 8 h. $KMnO_4$ (12 g, 0.076 mol) was added and the reaction mixture was stirred for 30 min while maintaining the temperature at 36˚C. The mixture was then heated at 80˚C in a water bath for 1 h, followed by addition of water (200 mL). The reaction temperature was increased to 95˚C for 30 min. Another portion of water (200 mL) and H_2O_2 were added. The mixture was then filtered while it was still hot. The cake obtained was washed with 5 % HCl and a large quantity of deionised water to give Graphite Oxide, which was re-dispersed in water by sonication for 1 h. The product was filtered through a Buchner funnel to give graphene oxide (GO) as a brown solid.

(ii) Reduction of Graphene Oxide (GO)

GO (100 mg) was loaded into a 250-mL round bottom flask and water (100 mL) was then added, yielding a dark brown dispersion. The dispersion was sonicated until no particulate matter was visible. Hydrazine hydrate (1 mL, 32.1 mmol) was then added and the solution heated in an oil bath at 95 ° C under a water cooled-condenser for 24 h over which the reduced GO precipitated out as a black solid. This product was isolated

by filtration over a Buchner funnel and washed copiously with water (5 × 100 mL), and dried over the funnel under a continuous air flow through the solid product cake.

(iii) Understanding chemical preparation of Graphene

GO shows good hydrophilicity and dispersibility in water because it contains a large number of hydrophilic functional groups, such as OH, COOH and epoxide (as demonstration through IR spectroscopy) introduced during oxidation process of graphite. Thus, hydrophilic GO is readily exfoliated in water [38]. Ideally, GO must be rigorously reduced after exfoliation to recover the desirable properties of graphene. GO can be chemically reduced with various reducing agents, such as hydrazine monohydrate [39-41] sodium borohydride [42, 43] hydroquinone [44] strongly alkaline [45] sulfur-containing compounds [46, 47] amines [48]. Among the reducing agents described above, hydrazine monohydrate is most widely used, mainly due to its strong reduction activity to eliminate most oxygen-containing functional groups of GO [41]. Hydrazine monohydrate was chosen in this study and its reaction with GO results in stable aggregate Graphene, insoluble in water as shown in Figure 2.12, whereas GO was well dispersed into water to form a stable dark brown suspension. This is evidence that most of the oxygen functional group have been removed during treatment of hydrazine monohydrate with GO. In addition, all attempts to disperse the as-prepared Graphene in organic solvents such a toluene, ether or chloroform failed. An illustration of the synthesis of Graphene is shown in Figure 2.13.

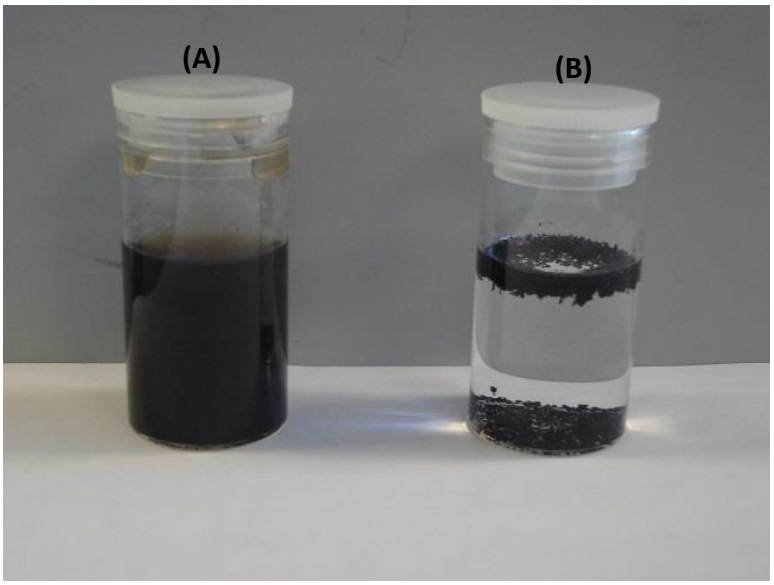

Figure 2.12: Photographic images of (A) Graphene Oxide and (B) reduced Graphene in water.

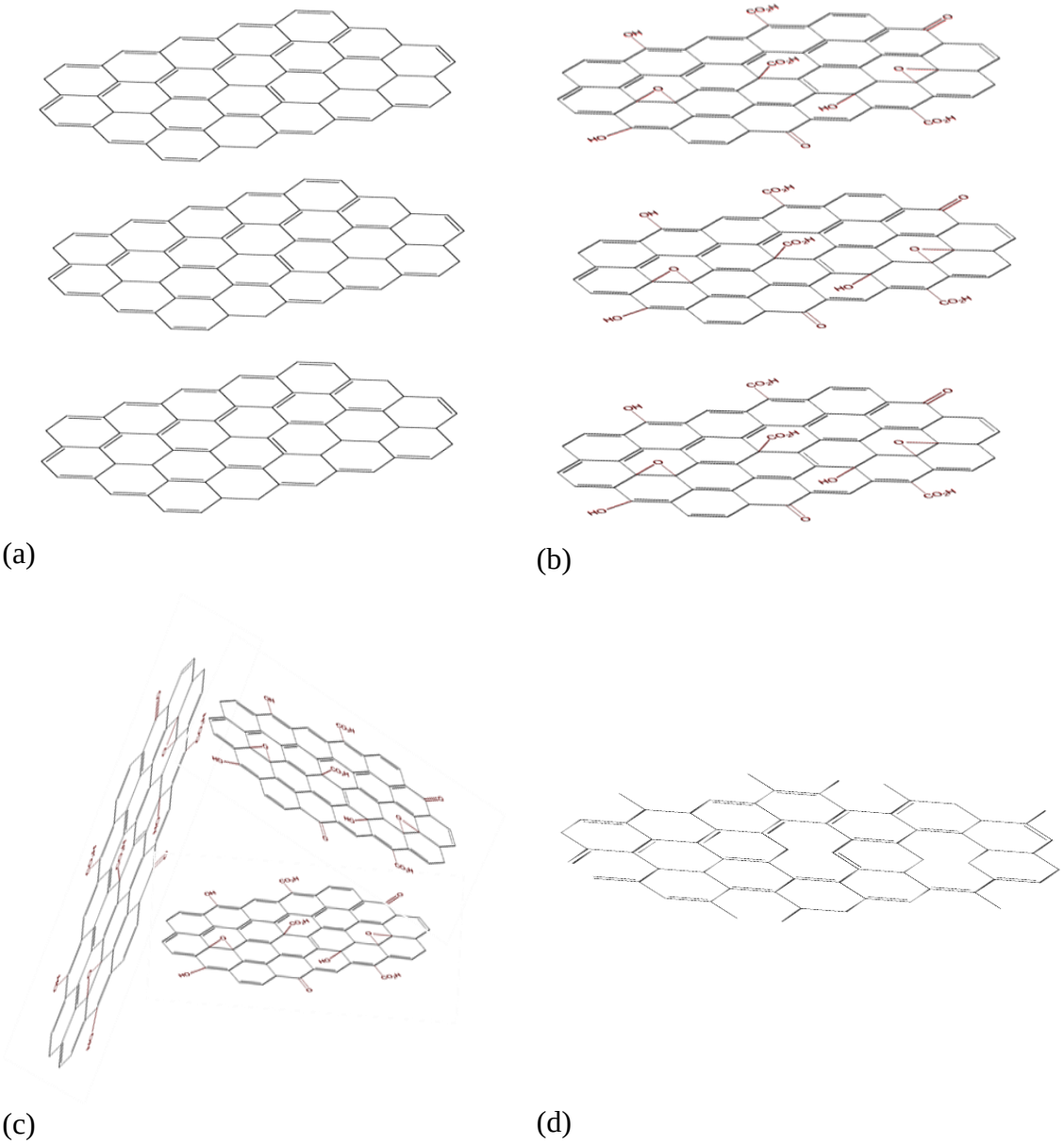

Figure 2.13: Schematic of the procedure followed for the production of graphene. (a) Graphite, the starting material. (b) Graphite Oxide obtained by oxidative treatment of graphite, (c) exfoliation of Graphite Oxide by ultra-sonication generating Graphene Oxide, (d) reduction of GO using hydrazine monohydrate to produce graphene.

(iv) Characterisation of graphene oxide and reduced graphene

Figure 2.14 shows IR spectra of graphene oxide and graphene. As observed, the presence of different oxygen functionalities in graphene oxide (Figure 2.14(a)) was confirmed at 3400 cm^{-1} (O–H stretching vibration), at 1720 cm^{-1} (stretching vibration from C=O), at 1620 cm^{-1} (skeletal vibrations from unoxidised graphitic domains), at 1220 cm^{-1} (C–OH stretching vibrations), and at 1060 cm^{-1} (C–O

stretching vibrations). This result is in agreement with the work reported by Xu *et al* [49]. The functional groups observed are responsible for the water solubility, making the dispersion of graphene oxide stable. In comparison, peaks due to oxygen functional groups are almost entirely removed in reduced graphene as shown in Figure 2.14(b).

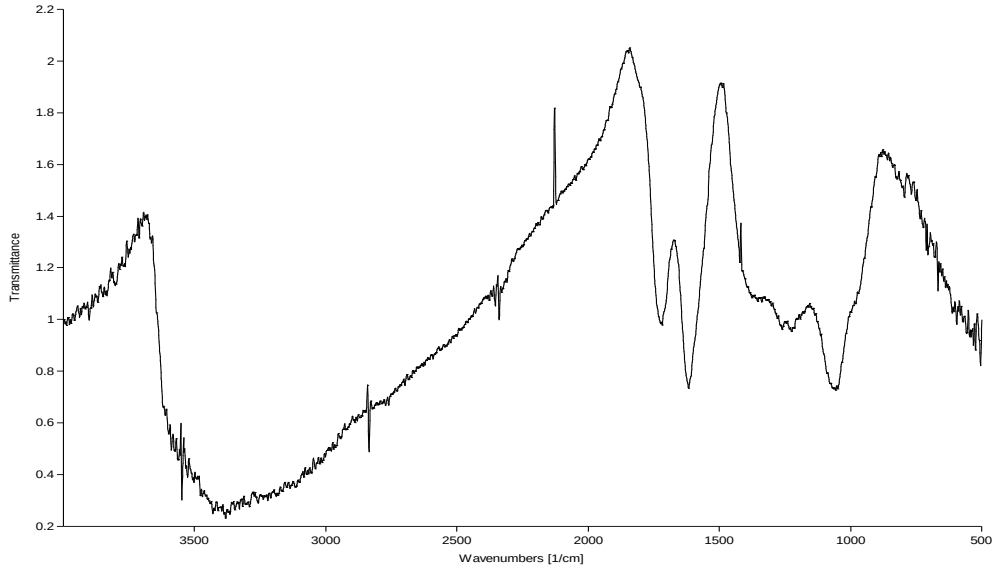

(a)

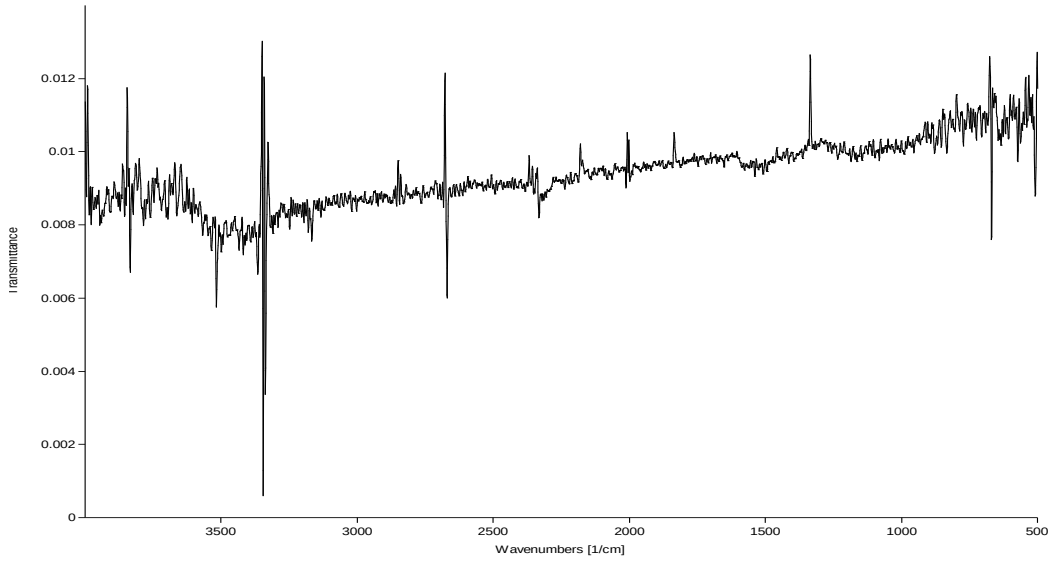

(b)

Figure 2.14: IR spectra of graphene oxide (a) and reduced graphene (b).

Graphene oxide was further characterised using UV-Vis spectroscopy. As shown in Figure 2.15, the spectrum of graphene oxide exhibits a maximum absorption peak about 230 nm, corresponding to π-π* transition of C–C bonds [41].

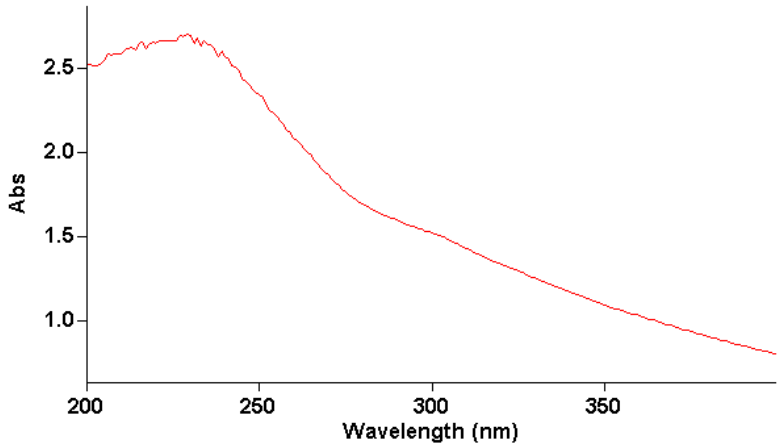

Figure 2.15: The UV-Vis absorption spectrum of graphene oxide.

As already mentioned, this second chapter includes the description of all electrochemical/analytical techniques employed in this thesis. It also gives the experimental procedures for the synthesis of graphene, cyclodextrin derivatives $CD_{6.6}$, $CD_{6.7}$ and Fc-β-CD. These materials, including commercially available compounds such as S-β-CD, CM-β-CD or nafion were used to fabricate the composite CPEs for the electrochemical detection of DA. It has to be noted that the different working electrodes were prepared mainly by mixing the modifiers into carbon paste. Before considering the electrochemical performance of the fabricated electrodes towards the sensing of DA, their characterisation was undertaken using surface techniques and electrochemical methods such as SEM, EDX, EIS, DPV, and CV, which is discussed in the following chapter.

2.8 References

1. Wang, J., A*nalytical Electrochemistry*. 2nd Ed., 1994, New York: VCH publishers Inc.

2. Peter, K., *Laboratory Techniques in Electroanalytical Chemistry*. 2nd Ed., 1984, New York and Basel: Marcel Dekker, INC.

3. Bard, A.J. and Faulkner, L.R., *Electrochemical Methods: Fundamentals and* A*pplications*. 2nd Ed., 2001, Hoboken NJ: John Wiley & Sons.

4. Lopez-Tenes, M., et al., *Study of an EE mechanism using double potential step techniques.* Journal of Electroanalytical Chemistry, 2002. **528**(1-2): p. 159-169.

5. Greef, R., et al., *Instrumental Methods in Electrochemistry* 1985: Southampton Electrochemistry / Ellis Horwood LTD.

6. Alcock, B., E., *Conducting Polymer Films Modified with Metal Particles and Varying Degrees of Hydrophobicity for applications in Electrocatalysis*, in *Chemistry* 2005, National University of Ireland, Maynooth: National University of Ireland, Maynooth.

7. Gervasi, C.A., et al., *Comparative cyclic voltammetry and SEM analysis of tin electrodes in citrate buffer solutions.* Journal of Electroanalytical Chemistry, 2007. **601**(1-2): p. 194-204.

8. Douglas, A., S., Stanley, C., R., and James, H., F., *Principles of instrumental analysis* 2007, Australia: Thomson Brooks/Cole.

9. Goldstein, J., et al., *Scanning Electron Microscopy and X-ray Microanalysis*. 3rd Ed., 2003: Springer.

10. Hudson, J.B., *Surface Science:* A*n Introduction* 1998, New York: John Wiley & Sons, Inc.

11. Jiang, X. and Wang, T., *Study on adsorption and reaction mechanism of preparation of TiO_2/SiO_2 by adsorption phase reactor technique.* Applied Surface Science, 2006. **252**(23): p. 8029-8035.

12. Harwood, L.M. and Moody, C.J., *Experimental organic chemistry: Principles and Practice*. 2nd Ed., 1989: Wiley-Blackwell.

13. Willard, H.H., et al., *Instrumental methods of analysis*. 7th Ed., 1988, California: Wadsworth Pub Co.

14. Barsoukov, E. and Mcdonald, J.R., *Impedance Spectroscopy: Theory, Experiment, and* A*pplications*. 2nd Ed., 2005, New Jersey: Wiley & sons Inc.

15. Macdonald, J.R. and Kenan, W.R., *Impedance Spectroscopy: Emphasizing Solid Materials and Systems*1987: Wiley.

16. Katz, E. and Wilner, I., *Ultrathin Electrochemical Chemo- and Biosensors: Technology and Performance*, 2004, New York: Springer-vrelag.

17. Shulga, O.V. and Palmer, C., *Detection of V-type nerve agent degradation products at electrodes modified by PPy/PQQ using $CaCl_2$ as supporting electrolyte.* Analytical and Bioanalytical Chemistry, 2006. **385**(6): p. 1116-1123.

18. Macdonald, J.R. and Barsoukov, E., *Impedance Spectroscopy*. 2nd Ed., 2005, New Jersey: John Wiley and Sons Inc.

19. McMurry, J., *Fundamentals of organic chemistry* 1986: Brooks/Cole Publishing Company.

20. Carey, F.A., *Organic Chemistry*. 4th Ed., 2000: McGraw-Hill Companies.

21. Harley, C.C., *the Formation of an Electrochemical Sensor for the Selective Detection of Dopamine*, in *Chemistry*, 2009, National University of Ireland, Maynooth: National University of Ireland, Maynooth.

22. Wrzosek, B. and Bukowska, J., *Molecular structure of 3-amino-5-mercapto-1,2,4-triazole self-assembled monolayers on Ag and Au surfaces.* Journal of Physical Chemistry C, 2007. **111**(46): p. 17397-17403.

23. Jia, W.Z., et al., *Electrocatalytic oxidation and reduction of H_2O_2 on vertically aligned Co_3O_4 nanowalls electrode: Toward H_2O_2 detection.* Journal of Electroanalytical Chemistry, 2009. **625**(1): p. 27-32.

24. Pontolio, J.O., et al., *Preparation and characterization of electrochemically modified electrodes containing the metal complexing moiety quinolin-8-ol anchored to the polymeric film.* Journal of Electroanalytical Chemistry, 2005. **584**(2): p. 124-130.

25. Abbaspour, A., Khajehzadeh, A., and Ghaffarinejad, A., *Electrocatalytic oxidation and determination of hydrazine on nickel hexacyanoferrate nanoparticles-modified carbon ceramic electrode.* Journal of Electroanalytical Chemistry, 2009. **631**(1-2): p. 52-57.

26. Yi, Q.F., et al., A *novel titanium-supported nickel electrocatalyst for cyclohexanol oxidation in alkaline solutions.* Journal of Electroanalytical Chemistry, 2007. **610**(2): p. 163-170.

27. Jafarian, M., et al., A *study of the electro-catalytic oxidation of methanol on a cobalt hydroxide modified glassy carbon electrode.* Electrochimica Acta, 2003. **48**(23): p. 3423-3429.

28. Weng, Y.C., Rick, J.F., and Chou, T.C., A *sputtered thin film of nanostructured Ni/Pt/Ti on Al_2O_3 substrate for ethanol sensing.* Biosensors & Bioelectronics, 2004. **20**(1): p. 41-51.

29. Chen, L., et al., *Synthesis and chromatographic properties of a novel chiral stationary phase derived from heptakis(6-azido-6-deoxy-2,3-di-O-phenylcarbamoylated)-beta-cyclodextrin immobilized onto amino-functionalized*

silica gel via multiple urea linkages. Journal of Chromatography A, 2002. **950**(1-2): p. 65-74.

30. Boger, J., Corcoran, R.J., and Lehn, J.M., *Cyclodextrin Chemistry - Selective Modification of* A*ll Primary Hydroxyl-Groups of* A*lpha-Cyclodextrins and Beta-Cyclodextrins.* Helvetica Chimica Acta, 1978. **61**(6): p. 2190-2218.

31. Benkeser, R.A., Hazdra, J.J., and Burrous, M.L., *Factors Influencing the Direction of Elimination in Ester Pyrolyses.* Journal of the American Chemical Society, 1959. **81**(20): p. 5374-5379.

32. RoehriStoeckel, C., Dangles, O., and Brouillard, R., A *simple synthesis of a highly water soluble symmetrical beta-cyclodextrin derivative.* Tetrahedron Letters, 1997. **38**(9): p. 1551-1554.

33. Kim, H.Y., et al., *Click synthesis of estradiol-cyclodextrin conjugates as cell compartment selective estrogens.* Bioorganic & Medicinal Chemistry, 2010. **18**(2): p. 809-821.

34. Ashton, P.R., et al., A*mino acid derivatives of beta-cyclodextrin.* Journal of Organic Chemistry, 1996. **61**(3): p. 903-908.

35. Chen, M., et al., *Fabrication of GNPs/CDSH-Fc/nafion modified electrode for the detection of dopamine in the presence of ascorbic acid.* Materials Science & Engineering C-Materials for Biological Applications, 2011. **31**(7): p. 1271-1277.

36. Rummeli, M.H., et al., *Graphene: Piecing it Together.* Advanced Materials, 2011. **23**(39): p. 4471-4490.

37. Hummers, W.S. and Offeman, R.E., *Preparation of Graphitic Oxide.* Journal of the American Chemical Society, 1958. **80**(6): p. 1339-1339.

38. Stankovich, S., et al., *Stable aqueous dispersions of graphitic nanoplatelets via the reduction of exfoliated graphite oxide in the presence of poly(sodium 4-styrene sulfonate).* Journal of Materials Chemistry, 2006. **16**(2): p. 155-158.

39. Tung, V.C., et al., *High-throughput solution processing of large-scale graphene.* Nature Nanotechnology, 2009. **4**(1): p. 25-29.

40. Compton, O.C., et al., *Electrically Conductive "*A*lkylated" Graphene Paper via Chemical Reduction of* A*mine-Functionalized Graphene Oxide Paper.* Advanced Materials, 2010. **22**(8): p. 892-896.

41. Li, D., et al., *Processable aqueous dispersions of graphene nanosheets.* Nature Nanotechnology, 2008. **3**(2): p. 101-105.

42. Shen, J.F., et al., *Fast and Facile Preparation of Graphene Oxide and Reduced Graphene Oxide Nanoplatelets.* Chemistry of Materials, 2009. **21**(15): p. 3514-3520.

43. Shin, H.J., et al., *Efficient Reduction of Graphite Oxide by Sodium Borohydrilde and Its Effect on Electrical Conductance.* Advanced Functional Materials, 2009. **19**(12): p. 1987-1992.

44. Wang, G.X., et al., *Facile synthesis and characterization of graphene nanosheets.* Journal of Physical Chemistry C, 2008. **112**(22): p. 8192-8195.

45. Fan, X.B., et al., *Deoxygenation of Exfoliated Graphite Oxide under* A*lkaline Conditions:* A *Green Route to Graphene Preparation.* Advanced Materials, 2008. **20**(23): p. 4490-4493.

46. Chen, W.F., Yan, L.F., and Bangal, P.R., *Chemical Reduction of Graphene Oxide to Graphene by Sulfur-Containing Compounds.* Journal of Physical Chemistry C, 2010. **114**(47): p. 19885-19890.

47. Zhou, T.N., et al., A *simple and efficient method to prepare graphene by reduction of graphite oxide with sodium hydrosulfite.* Nanotechnology, 2011. **22**(4).

48. Che, J.F., Shen, L.Y., and Xiao, Y.H., A *new approach to fabricate graphene nanosheets in organic medium: combination of reduction and dispersion.* Journal of Materials Chemistry, 2010. **20**(9): p. 1722-1727.

49. Xu, Y.X., et al., *Flexible graphene films via the filtration of water-soluble non covalent functionalized graphene sheets.* Journal of the American Chemical Society, 2008. **130**(18): p. 5856-5857.

3 Sensor Characterisation: A study of Electrochemical and physical properties of Carbon Paste Composites

3.1 Introduction

Since their invention in 1958, the use of CPEs has evolved and developed, particularly in the field of electrochemistry. In contrast to commercially available solid electrodes for which basic electrochemical characteristics are comparable for almost all products of renowned manufacturers, each carbon paste represents an individual material where the physico-chemical and electrochemical properties may markedly differ from case to case (regardless of the fact whether carbon pastes are hand-made in laboratories or purchased as ready-prepared mixtures) [1]. Electrochemical properties of various types of CPEs can then be predicted only approximately and a more detailed characterization requires appropriate testing measurements [1, 2]. Therefore newly prepared carbon pastes need to be tested and the procedures chosen for testing measurements should also reveal some specific characteristics of CPEs [2]; potential limits and background currents, investigations on the surface characteristics by means of reaction kinetics and reproducibility measurements [2].

Generally, the reasons for the characterisation of an electrode are to find an efficient electrode for a given purpose, or, to propose an optimal employment of an electrode. A number of authors have characterised CPEs. Adam *et al* [3, 4] have characterised CPEs with respect to their applicability in anodic and cathodic voltammetry. Farsang [5] studied the optimisation of the carbon paste composition via the chemical structure of the binder by observing the behaviour of several CPEs prepared from silicone oils with different molecular weight. Lindquist [6] carried out a systematic comparison of the properties of carbon pastes when investigating mainly the effect of binders with respect to their content in the paste mixture. Studies concerning detailed surface characterisation of various carbon pastes were published again by Adams *et al* [7].
Based on a combination of previous procedures [3, 4] with experimental approaches, a scheme illustrating a possible way to formulate the sequence of individual steps for testing CPEs is given in Figure 3.1 [8]. It worth noting that the scheme structure is general and it can therefore be adapted for any electrochemical technique.

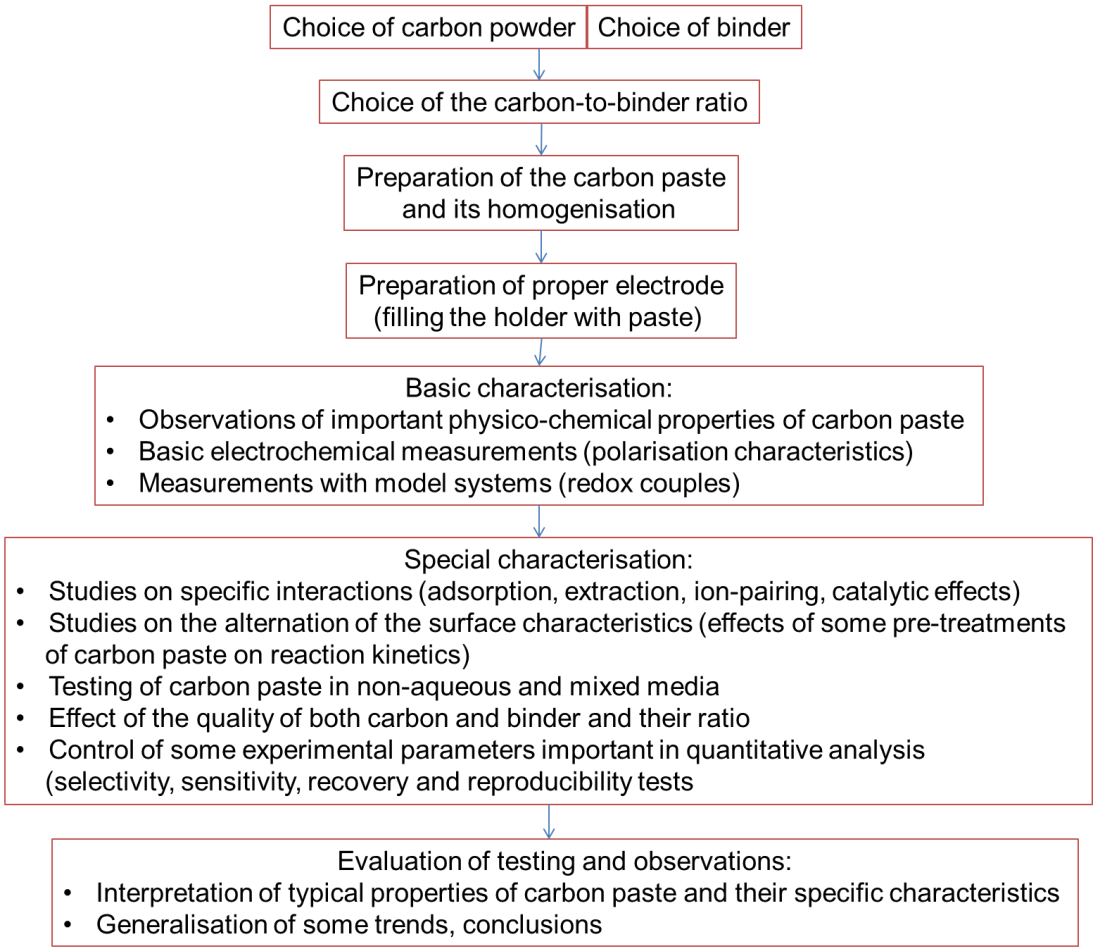

Figure 3.1: General scheme for testing CPEs [8].

In this chapter, the electrochemical characterisation of the carbon paste electrodes was carried out in a typical three electrode cell, with a saturated calomel electrode (SCE) used as a reference electrode. Different modified carbon paste electrodes were used as working electrodes and prepared with graphite powder, a suitable liquid binder (silicon oil) and a modifier. Moreover, the modification of carbon paste electrodes was performed on the surface or in the bulk paste. For instance, in nafion modified carbon paste electrode, 0.05% nafion 117 solution was drop-cast on the surface of a bare carbon paste electrode. In the case of sulfated β-cyclodextrin, carboxymethyl β-cyclodextrin or Ferrocene β-cyclodextrin complex, the modifier was mixed to the bulk carbon paste. The physical properties of these carbon paste electrodes were studied using a variety of techniques such as optical microscopy, scanning electron microscopy, energy dispersive X-ray spectroscopy and electrochemical impedance spectroscopy.

3.2 Results and discussion

3.2.1 Fabrication of Composite Carbon Paste Electrodes

The modified carbon paste electrode was prepared by thoroughly hand-mixing the desired amount of sulfated β-cyclodextrin (S-β-CD) with 0.71 g graphite powder (< 20 µm) and 200 µL silicon oil in an agate mortar for about 30 minutes to get a homogeneous S-β-CD modified carbon paste (S-β-CDCPE). To facilitate the homogeneity of the paste, both dry powders (graphite and sulfated β-cyclodextrin) were mixed within a vial before grinding. The resulting composite material was then packed into the end of Teflon (2 mm diameter) and electrical contact was made by means of copper rod. The Teflon was packed in small portions, each layer being compressed before adding the next. The surface was smoothened on a piece of weighing paper until a shiny appearance was obtained. The freshly made carbon electrodes were left unused for few hours to allow final homogenisation. This process of "self-homogenisation" has been reported in the literature [8]. All sensors: Carboxymethyl β-cyclodextrin modified CPE (CM-β-CDCPE), Neutral β-cyclodextrin modified CPE (β-CDCPE), Nafion modified CPE (NCPE), Heptakis 6-deoxy-6-(1-(4,5-dicarboxyl)-1,2,3-triazolyl)-β-CD 6.6 ($CD_{6.6}$CPE), Heptakis (6-(4-hydroxymethyl-1H-[1,2,3] triazol-1-yl)-6-deoxy)-β-cyclodextrin **6.7** ($CD_{6.7}$CPE). An illustration for the construction of the modified carbon paste electrode is shown in Figure 3.2. The unmodified CPEs were fabricated using the same process (without addition of a modifying agent).

A drop-cast method was also used to modify the CPE. This technique was related to the fabrication of Nafion and Ferrocene-β-cyclodextrin modified CPE. In this case, a drop (or few drops) of Nafion solution and Ferrocene- β-cyclodextrin (Fc-β-CD) suspension was placed, respectively, on the surface of a previously prepared (bare) carbon paste electrode and the solvent was allowed to evaporate.

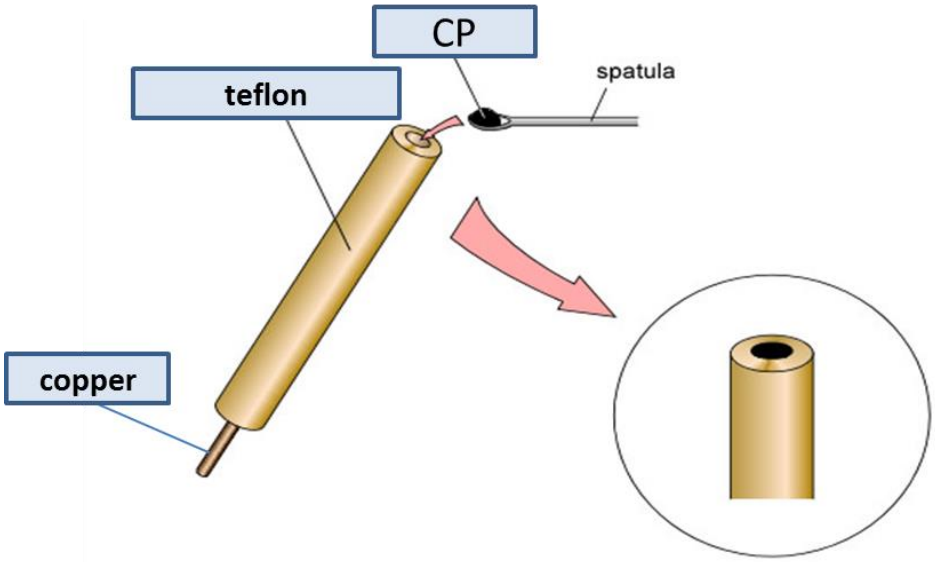

Figure 3.2: Schematic representation for preparation of carbon paste electrode.

3.2.2 Storage of Modified Carbon Paste (Electrodes)

Once prepared, the composite carbon paste was kept in a vial as shown in Figure 3.3. Carbon paste mixture may undergo significant changes in time. This feature ("ageing of carbon paste"), is characteristic for carbon pastes made from more volatile binders such as organo-phosphates [9]. Due to desiccation, these mixtures age more rapidly than ordinary carbon paste composites and have a shelf-life of two to three weeks only [2, 9]. Such undesirable behavior has confirmed assumptions that ageing of carbon paste is associated solely with the properties of the binders unless the modifying agent itself shows some stability issues overtime. Graphite (carbon) is very stable and ageing of CPE has not been reported previously. Silicon oil and Paraffin oil used in this study are two well-known and frequently used binders for the preparation of CPE. These non-conducting substances have minimal volatility, immiscible with aqueous solutions and exhibit a chemical and electrochemical inertness [4, 10]. Carbon paste composites made from such binders could be used for several months or few years. Such a long-term stability was demonstrated experimentally in a literature report [4], when a silicone oil made CPE employed for measurement at the beginning of 2001 was found usable in 2005 (after 4 years of storage). For storage of the unemployed electrodes, it is recommended to place them in a beaker with distilled water where the electrode end filled with paste is completely dipped into the waterline [2, 4].

In this study, all voltammetry measurements were obtained using ready-constructed electrodes; and thus, electrode storage in water was not an issue. However, it is

important to keep the vial of carbon paste closed when not in use. Like most forms of graphite it may absorb contaminants from the laboratory environment.

Figure 3.3: Photographic image of a composite carbon paste.

3.2.3 Electrochemical Characterisation of Composite Carbon Paste Electrodes

The electrochemical properties of composite CPEs were examined using cyclic voltammetry, linear sweep voltammetry, differential pulse voltammetry and electrochemical impedance spectroscopy. The purpose of the voltammetry experiments was to investigate the electrochemical properties of composite CPEs in supporting electrolyte (0.1 M PBS) and to some extent in DA solutions. Electrochemical impedance spectroscopy was used to study the charge transport processes occurring at surface of composite CPEs.

3.2.3.1 Electrochemical properties of composite CPEs in supporting electrolyte

The voltammetric behaviour of the carbon paste electrodes (modified and unmodified) was examined using cyclic voltammetry. When bare CPE or S-β-CDMCPE was run in 0.1 M PBS, an unexpected redox process was observed as shown in Figure 3.4. A distinct anodic peak observed at 0.058 V vs. SCE and a cathodic peak at 0.018 V vs. SCE. A characteristic of the redox peak shown is that it is variable in intensity, but most importantly, it occurs at redox potential close to that of DA.

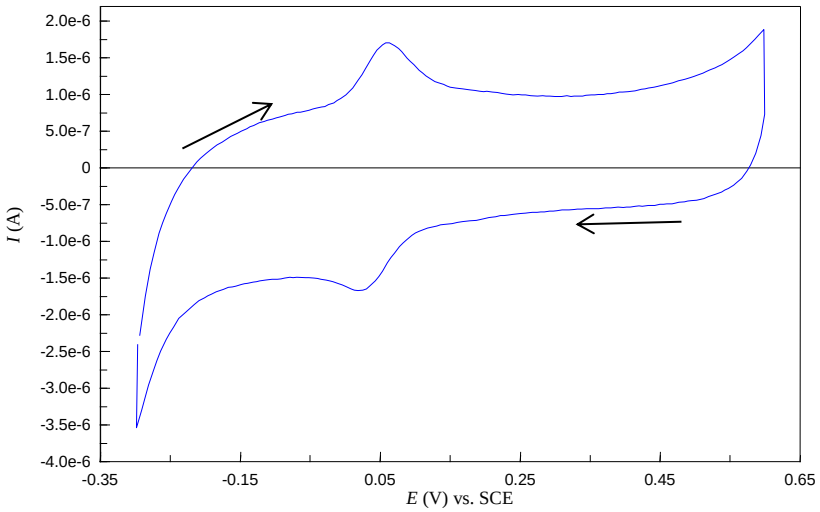

Figure 3.4: Cyclic voltammogram of S-β-CD (0.095g) modified CPE in PBS (0.1 M), pH 6.8; scan rate 50 mV / s.

There is no diminution in the peak size with cycle number as shown in Figure 3.5, which suggests that potential scanning does not remove species responsible for the redox peak from the electrode surface. A steady state is obtained after the fourth cycle. It was reported in the literature [11] that oxygen adsorbs onto the carbon electrode and the functional groups can form very stable oxide species.

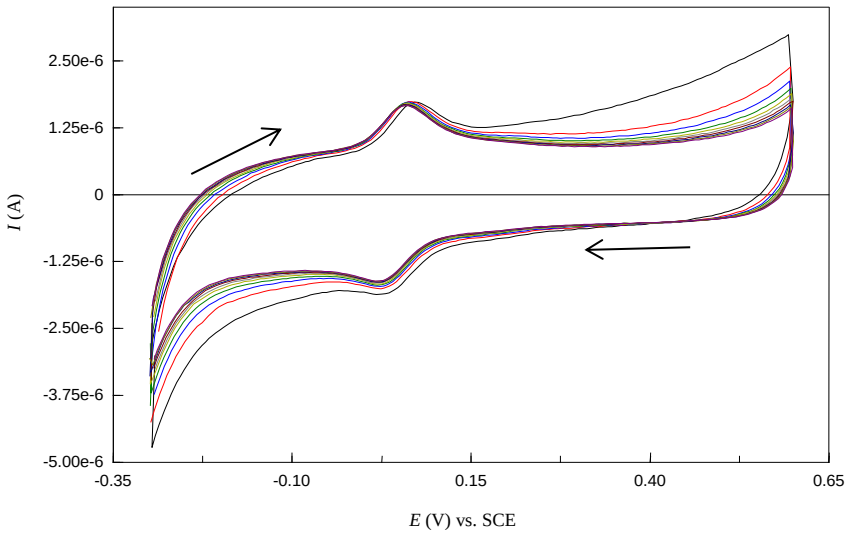

Figure 3.5: Cyclic voltammograms of S-β-CD (0.095g) modified CPE in PBS (0.1 M), pH 6.8, showing different cycle numbers; scan rate 50 mV / s.

Linear Sweep Voltammetry was also employed to confirm the presence of oxidation peak within the potential range studied (from –0.2 V to +0.6 V). This technique is used for recording voltammograms for primary diagnostic purposes due to its simplicity

although its sensitivity is rather poor as an analytical technique [12, 13]. However, when the electrode behaviour was examined in supporting electrolyte, an intense anodic wave at 0.068 V vs. SCE was clearly observed (Figure 3.6). This is evidence of some definite oxidation process occurring at the electrode surface.

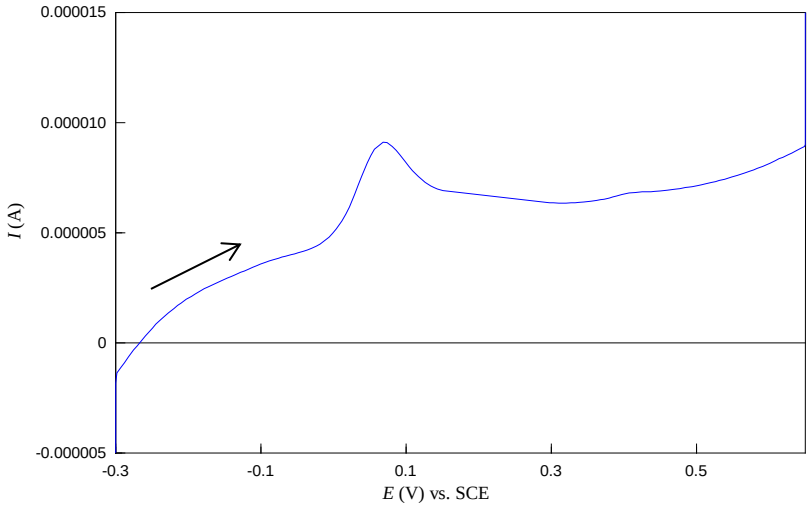

Figure 3.6: Linear sweep voltammetry for S-β-CD (0.095g) modified CPE in PBS (0.1 M), pH 6.8; scan rate 50 mV /s.

3.2.3.2 Removal of oxides from CPEs surfaces

Several attempts were made to remove the oxide redox peak in order to achieve featureless background currents for CPE. This consisted of varying the electrochemical window and scan rate, packing the carbon paste into the Teflon holder relatively tight to avoid considerable pockets of air within the paste, using different sources of polishing papers or changing the electrolytes (KCl or aCSF instead of PBS), conditioning the electrode or using deaerated PBS. None of these methods helped in the removal of the redox "pre-peak". Generally, oxides on carbon electrodes surfaces are removed with UHV heat treatment [14-16] or specific blocking of surface carbonyls. It has also been proposed that anodisation causes the removal of organic molecules from the carbon surface, rendering the electrode cleaner and therefore more accessible to solution species [7].

In this study, potentiostatic treatment was performed which consisted of applying a constant potential of +1 V vs. SCE to the working electrode and the current flowing through the circuit measured. The resulting voltammograms is displayed in Figure 3.7(a). The working electrode was then removed from the cell, a very thin layer of paste was extruded from the Teflon holder, and the electrode surface was polished. The

electrode was quickly transferred back into the PBS. Finally, a cyclic voltammetry was run which resulted in successful removal of oxide species from the electrode surface, with a lower background current as shown in Figure 3.7(b).

(a)

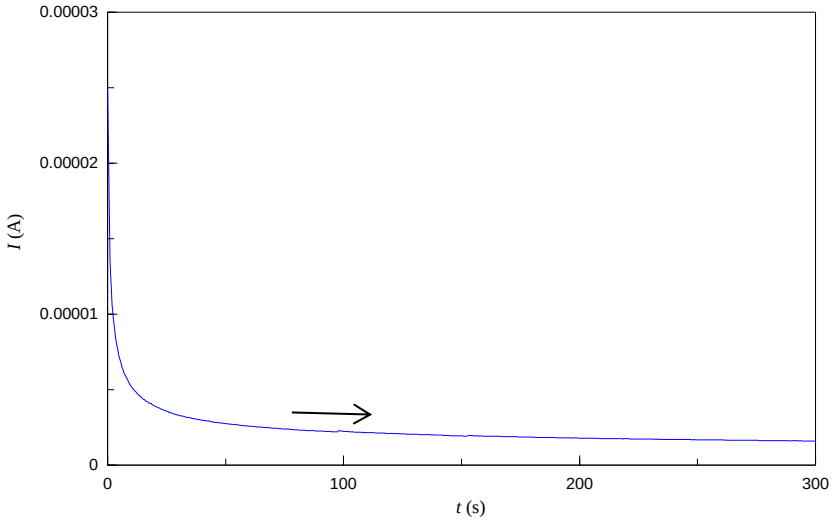

(b)

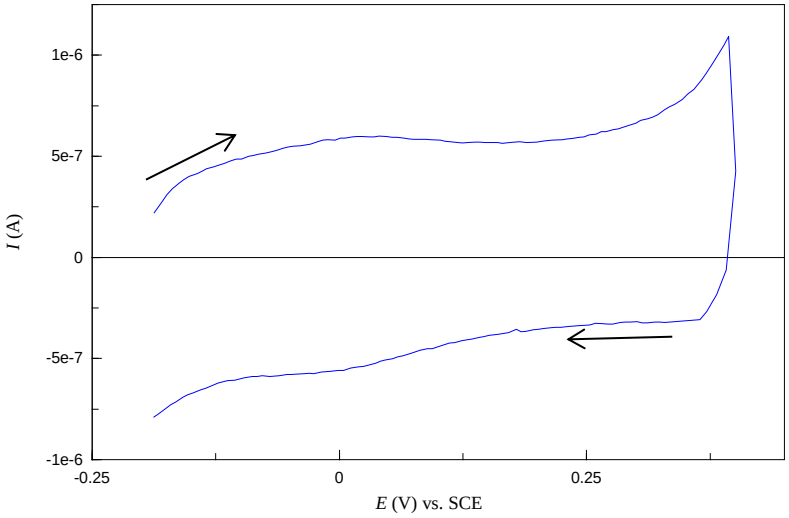

Figure 3.7: Potentiostatic measurement of S-β-CD (0.095g) modified CPE (a) and corresponding cyclic voltammograms (b), in PBS (0.1 M), pH 6.8; scan rate 50 mV / s.

3.2.3.3 Understanding surface structure of oxide electrodes

A literature search was carried out for a better understanding of the redox system observed. In fact, it is well known that interaction of oxygen-containing gases with carbon surfaces produces stable oxygen containing surface species [11]. The surface oxides form spontaneously on most carbon surfaces, and are unavoidable without special effort. It also has to be noted that for the preparation of the composite carbon pastes, grinding was conducted in air, therefore the combination of heat and surface energy could provide an environment favorable for oxidation of carbon by atmospheric

oxygen. The nature and formation of oxygen-containing functional groups on carbon have been studied extensively, and identified as carbonyls, phenolic OH, lactones, ethers, and carboxylates. On carbon surfaces, they are referred to collectively as "surface oxides" or merely "oxides" [17]. Examples of surface oxides that form at a graphitic edge are shown schematically in Figure 3.8. These functional groups are those encountered in traditional organic chemistry reactions. They are formed by chemisorption of oxygen on carbon surfaces. Chemisorption of oxygen on carbon surfaces depends on the surface structure, the availability of reactive sites, such as graphitic edge planes or defects, and also on the surface temperature.

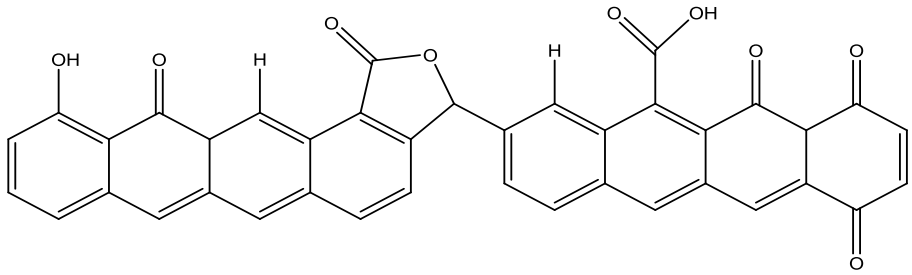

Figure 3.8: Schematic representation of structure of surface oxides configuration on graphite.

Two independent reaction mechanisms have been proposed for the oxidation of graphite surfaces: (1) reaction from the direct collisions of O_2 molecules with the reactive carbon sites (Eley-Rideal [ER] mechanism) and (2) the surface migration mechanism, for example, the reaction with the migrating oxygen molecules that are first adsorbed on nonreactive sites (Langmuir-Hinshelwood [LH] mechanism). The ER mechanism is initiated by the direct collision of the oxygen molecules with the graphitic defect sites. The reaction mechanism according to the LH formalism consists of two distinct steps: the physisorption of molecular oxygen on the graphitic basal surfaces, and the diffusion of these species to defect sites that subsequently results in the formation of carbon-oxygen surface functional groups. The graphite surface sites involved in these two steps are illustrated in Figure 3.9 as basal plane and edge plane, respectively.

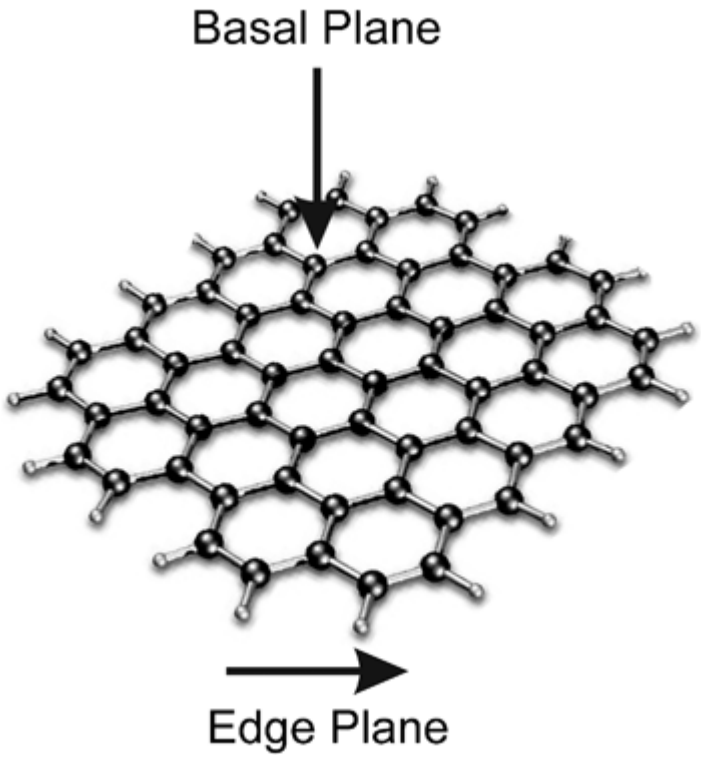

Figure 3.9: Schematic illustration of basal and edge plane in graphite: basal plane is part of electron rich. Edge planes are very reactive due to partial saturation of valences [18].

This interaction of molecular oxygen with a basal plane of graphite is physisorption in nature, without any charge-transfer. The second step of the oxidation reaction involves the surface diffusion of the physisorbed molecular oxygen to vacancies or edge sites, where it then undergoes a reduction to form species such as super peroxide O_2^-, or peroxide O_2^{2-} and finally makes stable covalent bonds with the carbon atoms.

The strong covalent sp^2 hybridized bonds within the carbon basal planes, and weak delocalized π-bonds between planes, result in the high affinity of oxygen to the unsaturated bonds of edge carbon atoms. Thus oxygen chemisorption occurs only on the edge planes [19].

As already mentioned, the multitude of functional groups formed on carbon surfaces is due to different reactivity of the two different types of edge sites (Figure 3.9), and the introduction of these functional groups on the carbon surfaces drastically alters the physico-chemical surface properties. Most importantly, these functional groups directly take part in surface reactions and therefore play a crucial role in heterogeneous oxidation catalysis. The ratio I_{pa} to I_{pc} of the redox activity which is equal to 0.89, from Figure 3.4, is not far away from unity, suggesting a fairly reversible process. From the

electrochemical standpoint, it is notable that the only known reversible oxygen gas electrode at room temperature involves carbon as the conducting substrate and requires the presence of HO^- and HO_2^- in solution. There is some evidence that the oxygen involved may be adsorbed as a peroxidic complex (C_yO_2) [20]. The electrode reaction is probably as follows:

$$(C_y) + O_2 \leftrightharpoons (C_yO_2) \qquad \text{Equation 3.1}$$

$$(C_yO_2) + H_2O + 2e^- \leftrightharpoons (C_y) + HO_2^- + HO^- \qquad \text{Equation 3.2}$$

The overall reaction rate is proportional to the concentration of (C_yO_2) formed.

3.2.3.4 Background (residual) current at CPEs

Background current represents probably one of the most important parameters of carbon pastes in voltammetry and related techniques. The level of the background current cannot be exactly defined; it strongly depends on the composition of the carbon paste as well as upon the type of measurement. Despite the presence of typically insulating binders of silicone oil type, common carbon paste mixtures exhibit a very low ohmic resistance. This phenomenon was firstly studied in detail by Beilby and Mather [21]. The graphite particles are practically covered with a very thin film of the binder. Nevertheless, the individual graphite particles are apparently in some physical contact beneath the binder layer, which may explain a very low ohmic resistance of most carbon pastes. One of the main advantages of carbon paste electrodes in electrochemical studies is their low background current, compared to solid graphite or noble metal electrodes. Such a low background current levels permits the electrochemical detection of very low concentrations of electroactive material at low current densities. The residual current of glassy carbon is fifteen times higher than that obtained using bare carbon paste electrode, as shown in Figure 3.10. GC and bare CPE background currents of 4.073×10^{-7} A and 2.793×10^{-8} A, respectively. Such a difference is in accordance with the literature report [22]. GC is a gas impermeable material which effectively combines the characteristics of carbon and glass. It is a hard solid prepared by heat-treatment at elevated temperature. Unlike GC, CPEs are softs and made by simple mixture of graphite with binder. The absolute magnitude of the background in CPEs is given by a variety of factors such as the quality of graphite used [7], the carbon-to-binder ratio and, to a certain extent, to the individual polarizability in the supporting medium. In this

example (Figure 3.10), the low background current is probably related to the hydrophobic nature of the binder. Although both electrodes belong to the same family (carbon based electrodes), the hydrophobic properties at the surface of the carbon paste electrode may promote a lower residual current. It has to be noted that this hydrophobicity can result in moderately reversible or totally irreversible behavior of numerous compounds and the redox couple at CPEs whereas the same substances measured at ordinary solid electrodes may exhibit a fair reversibility [7, 23]. This is why the oil-to-graphite ratio is significantly important.

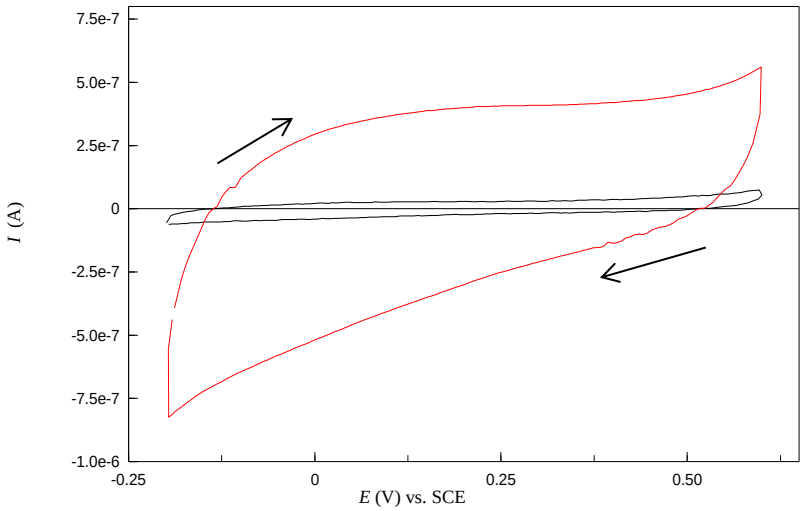

Figure 3.10: Cyclic voltammograms of bare GC electrode (—) and bare CPE (—) in 0.1 M PBS, pH 6.8; scan rate 50 mV / s.

3.2.3.5 Carbon-to-liquid ratio

It is quite a complicated task to choose a suitable carbon-to-binder ratio for the measurement of a specific analyte [11]. A more general recommendation is 1 g carbon powder for 0.3 mL binder. This figure appears to be optimal with respect to stability and electrochemical behavior [8]. For example, too "dry" as well as too liquid carbon paste can have some important consequences on the electrochemistry of the analyte studied. The surface of such pastes is usually not renewable or reproducible [24]. The determination of the optimum ratio of graphite to organic liquid is essentially an empirical process. Therefore, an evaluation of the ratio from test measurements was necessary in this study. Preliminary voltammetry tests on DA (5×10^{-5} M in 0.1 M PBS) were performed to determine a suitable graphite-to-silicon oil ratio. In this work, carbon paste was prepared using constant amount of graphite powder (0.71 g) and S-β-CD (0.095 g) while varying the concentration of silicon oil as shown in Table 3.1. Clearly,

there is an inverse relationship between the amount of silicon oil and dopamine peak current: DA peak currents decrease as oil concentration increase. Moreover, background currents increase as oil concentration decrease. In a fundamental study, Adam et al [7] concluded that the lesser content of oil in the paste the more rapid charge transfer (lesser irreversibly), the more lipophilic binder (via the increased alkyl chain of hydrocarbon like pasting liquid) the lower the rate constant and the slower the charge transfer. Lowering the quantity of binder in the paste has a positive effect on the electrochemical signal of dopamine, with 200 µL silicon oil found as the optimal value (Table 3.1). A lower oil quantity (than 200 µL) with respect to total powder weight (0.095 g S-β-CD + 0.71 g graphite) may result in loss of paste from the electrode due to inefficient binding. This effect is similar enough to the behaviour of the carbon paste electrode when applying a constant potential higher than 2.0 V vs. SCE or less than –1.5 V vs. SCE in order to remove oxide species from the electrode surface as demonstrated previously.

Table 3.1: Effect of silicon oil on DA peak current at S-β-CD (0.095g) modified CPE.

Oil amount (µL)	DA oxidation peak current (A)	Background current (A)
200	1.255×10^{-6}	5.643×10^{-7}
300	8.715×10^{-7}	4.919×10^{-7}
400	8.385×10^{-7}	4.050×10^{-7}
500	8.206×10^{-7}	2.736×10^{-7}
600	5.891×10^{-7}	1.569×10^{-7}

3.2.3.6 Electrochemical window dependence of DA peak current at untreated CPE

Differential pulse voltammetry (DPV) technique was employed to analyse the effect of electrochemical window on DA peak signal at CPE with oxide layer. In this experiment, the electrochemical window chosen was [–0.20 V to +0.27 V], which normally shows redox behaviour of oxide containing electrode around 0.00 V vs. SCE. As shown in Figure 3.11, when successive increasing concentrations of DA in the range of 5×10^{-7} M to 1.1×10^{-5} M were used in such a window, the corresponding peaks from 9×10^{-6} M to 1.1×10^{-5} M DA were the only concentrations clearly observed. DA could not efficiently be quantified below 9×10^{-6} M. This demonstrates the strong influence of oxides in the determination of relatively low concentrations of DA using the electrochemical window [–0.20 V to +0.27 V]. Given the reactivity of carbon surfaces

toward oxygen, it is difficult to maintain an oxide-free carbon surface in an aqueous electrochemical environment, particularly with DPV, which is a "pulse" technique as opposed to CV. A simple approach consisting of shortening the electrochemical window was employed to minimise the influence of oxide and enhance electrode sensitivity towards DA. This was discussed in detail in Chapter 4.

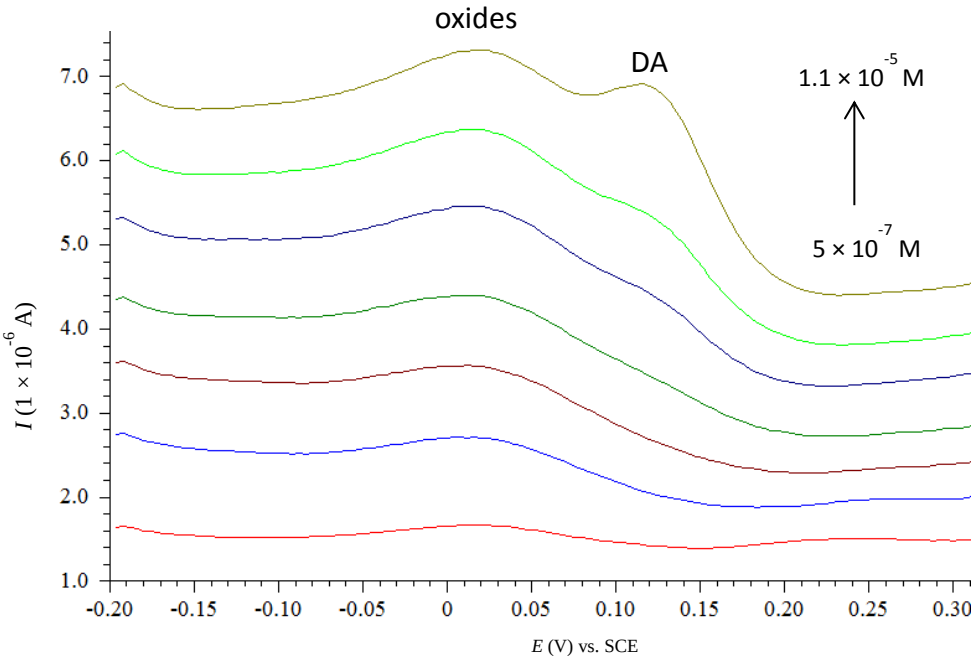

Figure 3.11: Differential pulse voltammograms of DA at S-β-CD (0.545g) modified CPE at different concentrations in 0.1 M PBS (pH 6.8): (—) 5 × 10^{-7} M, (—) 8 × 10^{-7} M, (—) 1 × 10^{-6} M, (—) 3 × 10^{-6} M, (—) 6 × 10^{-6} M, (—) 9 × 10^{-6} M and 1.1 × 10^{-5} M (—).

To further investigate the influence of oxides on DA peak current, the oxide covered electrode was run in 0.1 M PBS only, with 2 minutes accumulation time between each voltammogram without potentiostatic treatment of electrode or purging PBS with nitrogen gas, prior to measurement. The results are shown in Figure 3.12(a). It was observed that the oxide peak developed continuously with time. The corresponding graph in Figure 3.12(b) shows linearity between oxide peak current and time. Therefore only a relatively high concentration of DA could be detected. As opposed to CV, where an oxidation and reduction wave of oxides is observed, DPV only shows the anodic process. The pulsed waveform generated using DPV stimulates a pronounced oxide peak response and, thus, masks the DA signal.

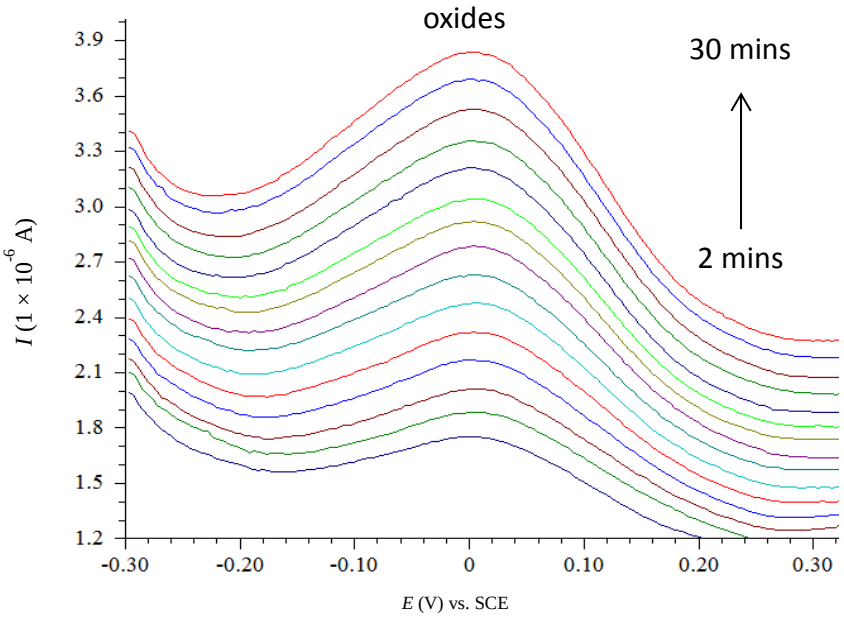

(a)

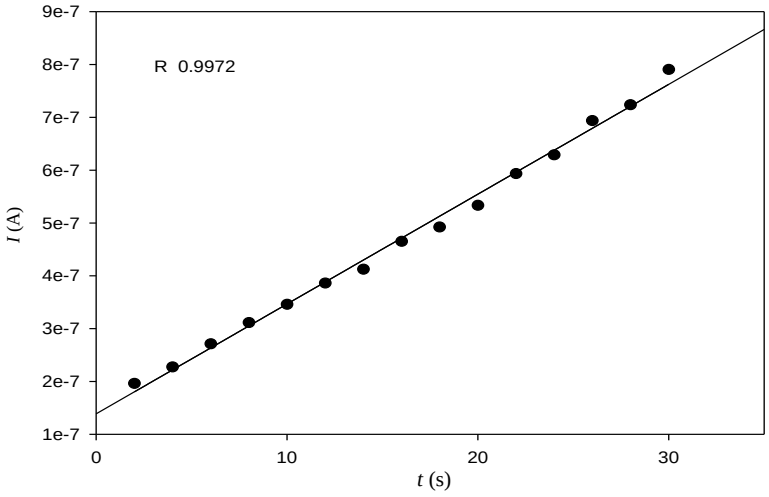

(b)

Figure 3.12: Differential pulse voltammograms of S-β-CD (0.545g) modified CPE recorded in 0.1 M PBS, pH 6.8 (a) and resulting graph of oxides peak current as a function of time (b).

3.2.3.7 Electrochemical Impedance Spectroscopy (EIS) Studies

Since the resistance for an electrode is one of the most important factors which affect electrochemical behaviour, the characterisation of electrode responses can give information about the interface and consequently the nature of the reaction between the analyte and the electrode. The property of electrode interface can be investigated by EIS [25, 26].

The EIS study was aimed at comparing the electrochemical behaviour of the synthesised graphene with that of graphite and glassy carbon. ESI experiments for bare graphene paste electrode (GPE), glassy carbon electrode (GCE) and carbon paste electrode (CPE)

made with graphite were carried out in 1×10^{-3} M $K_3[Fe(CN)_6]$ / $K_4[Fe(CN)_6]$ by applying an AC frequency range from 65000 to 0.1 Hz under a +0.2 V (vs. SCE) open circuit potential condition. Figure 3.13 shows the typical Nyquist plots for GPE, GCE and CPE. In the Nyquist plot (Z'' vs. Z'), the semi-circle part correspond to the electron transfer limiting process. Thus, the charge transfer resistance (R_{ct}) for the redox probe was measured as the diameter of the semi-circle [27]. Figure 3.13(a) indicates that the kinetics of the electrodes reaction with $K_3[Fe(CN)_6]$ / $K_4[Fe(CN)_6]$ depend considerably on the nature of electrode surface as it is clear that the impedance responses of GPE, CPE and GCE show great difference in R_{ct}. Compared with GCE, CPE has a much larger R_{ct} (50000 Ω), which indicates that GPE has much more rapid electron transfer ability in this aqueous system than CPE. Another factor that may contribute to the R_{ct} difference is the rough nature of the surface of the bare CPE (SEM images, Figure 3.15).

At bare GCE, in the Nyquist plot, both the semicircle and linear regions exist, but in case of GPE, the semicircle almost disappeared (R_{ct} ~ 2000 Ω) and only a clear linear region, attributed to a Warburg impedance, is observed (Figure 3.13(b)). As the semi-circle diameter of the impedance spectrum represents the charge transfer resistance which controls the electron-transfer kinetics of the redox probe at the electrode interface (R_{ct}), diminished or absence of semi-circle region indicates the dramatic decrease of R_{ct} at GPE, which is due to excellent conductivity of graphene.

Due to the presence of a binder (silicone oil), the GPE surface possesses a high hydrophobicity that may hinder the access of the probe analyte to the electrode surface. However, the experimental results suggest that the hydrophobic surface of GPE does not influence the kinetics of highly polar species such as $K_3[Fe(CN)_6]$ / $K_4[Fe(CN)_6]$. The presence of defects at the GPE may facilitate the electron transfer between the probe analyte and the electrode.

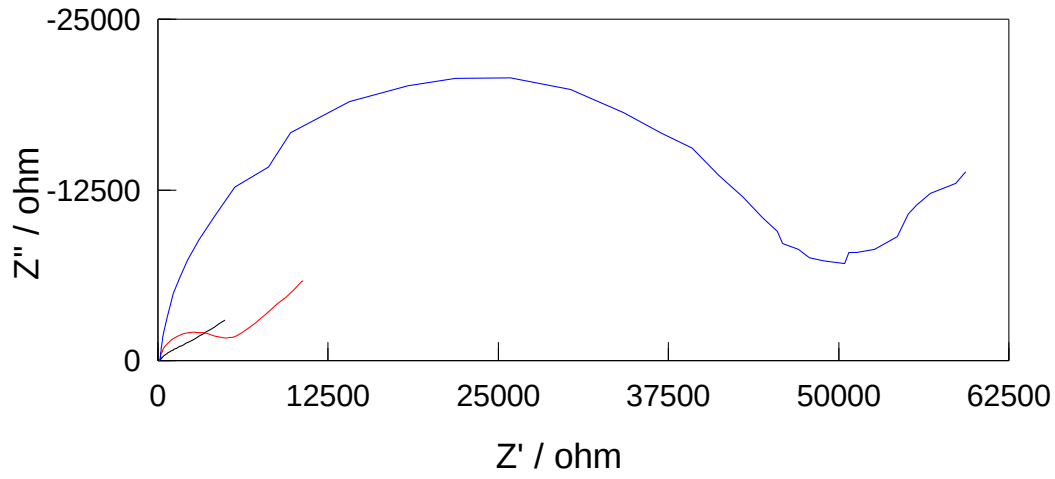

(a)

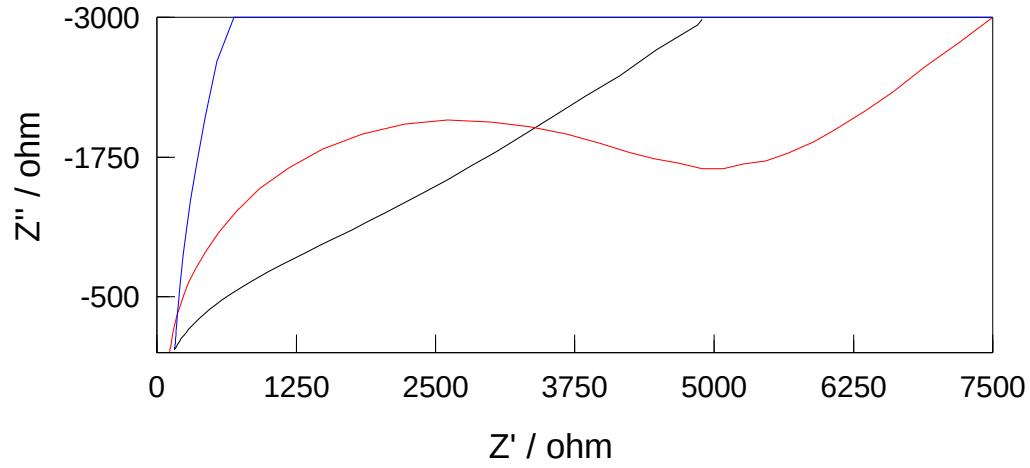

(b)

Figure 3.13: The electrochemical spectra of CPE (—), GCE (—) and GPE (—) (a). Enlarged spectra to observe clearly the response of GPE (b).

3.2.4 Physical characterization of CPEs

The optical microscopic image of a surface of a carbon paste modified electrode shows a remarkable stability after a potentiostatic measurement recorded at +1.00 V vs. SCE as shown in Figure 3.14(a). The composite material remained packed in the Teflon holder. In contrast, when 3.00 V vs. SCE was applied to the electrode in order to remove oxides from the electrode surface, the paste was extruded from the holder and spread all over the Teflon surface as shown in Figure 3.14(b).

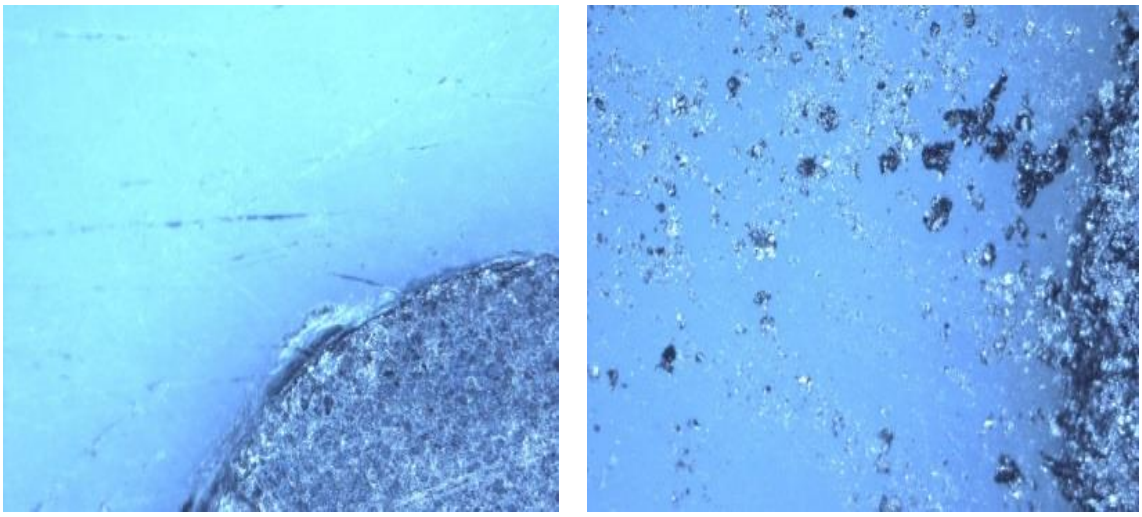

(a) (b)

Figure 3.14: Optical microscopic images of modified CPE after holding electrode at +1 V vs. SCE (a), and +3 V vs. SCE (a) for 5 minutes.

3.2.4.1 SEM of bare carbon (graphite) paste electrode

SEM was used to characterise the morphology of the bare and modified CPEs. It is obvious that the morphology of the investigated surfaces is different. Figure 3.15 represents the SEM image of the bare CPE, which shows conglomerations of flat graphite sheet domains over the whole surface.

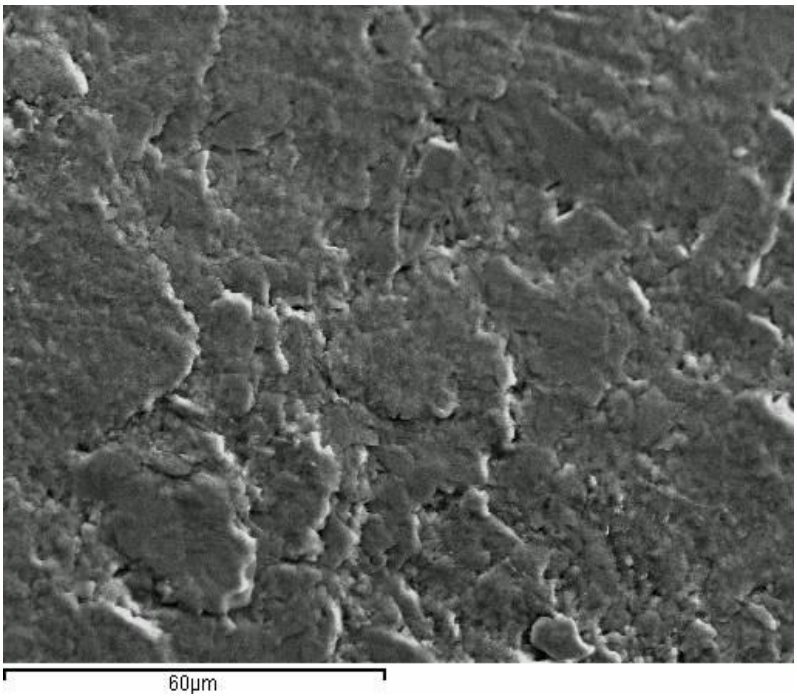

Figure 3.15: SEM micrograph of bare CPE.

3.2.4.2 SEM and EDX of sulfated β-cyclodextrin modified carbon paste electrode

Figure 3.16(a) shows the SEM image of the modified electrode when 0.545 g S-β-CD was added into the carbon paste. Despite the presence of oil binder (200 μL for 1.255 g total powder weight), non-uniform flakes are observed. It is important to emphasize here that it is possible to adjust the oil content in order to obtain a more compact paste without considerably affecting the electrochemical properties of the paste. What is interesting here is the stability of the S-β-CD modified electrode when 200 μL of silicon oil is used and the related electrochemical results. The electrochemical properties of the composite, evaluated by cyclic voltammetry, showed a reversible behaviour with respect to dopamine / dopamine-o-quinone. Leaching of the redox mediator, cyclodextrin, or the paste itself was not observed. A magnified SEM image (Figure 3.16(b)) shows several spots which may be related to S-β-CD and suggested a homogeneous distribution of S-β-CD throughout the paste.

For quantitative representation of the components into the S-β-CD modified carbon paste electrode, EDX was employed. The presence of C, O, Si, Na and S are shown in the spectrum Figure 3.16(c). It is worth mentioning that the strong peaks of Na and S are related to cyclodextrin. C comes from graphite. Si and O are part of silicon oil.

(a) (b)

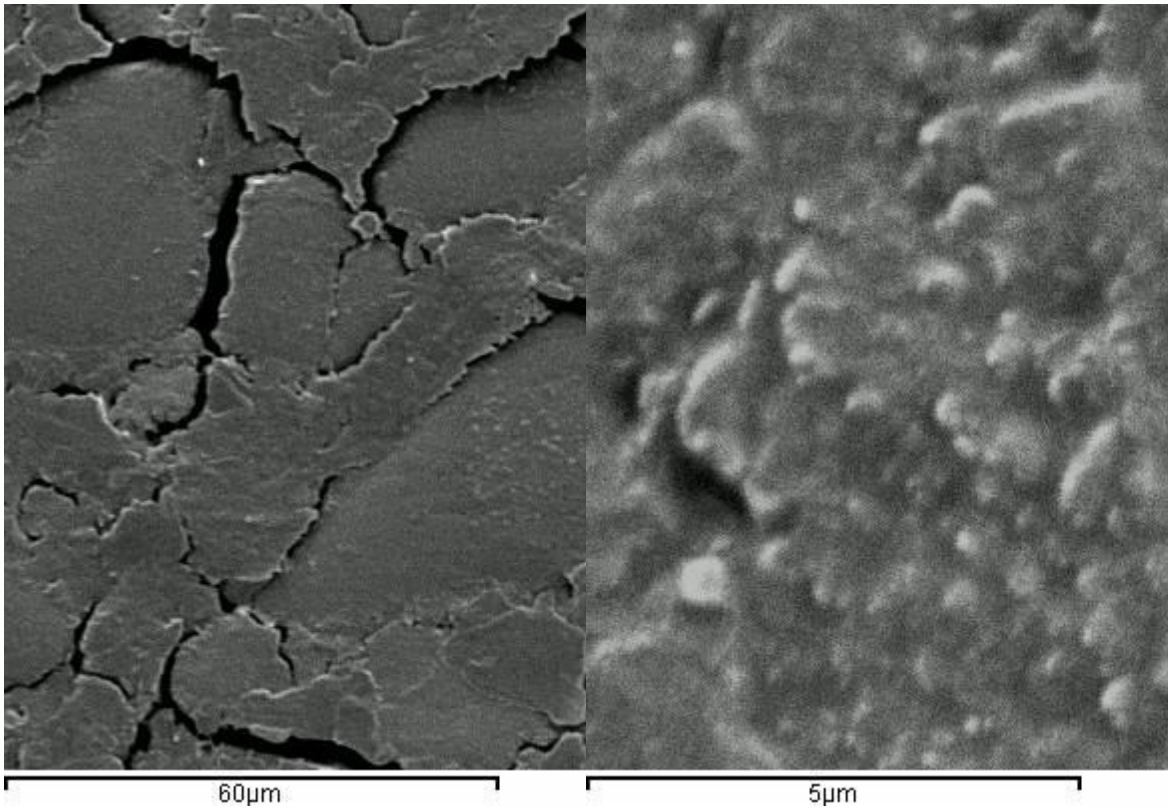

Figure 3.16: SEM micrograph of S-β-CD (0.545 g) modified CPE at 60 µm (a) and 5µm (b). Below, EDX spectrum of S-β-CD (0.545 g) modified CPE (c).

3.2.4.3 SEM and EDX of carboxymethyl β-cyclodextrin modified carbon paste electrode

The SEM image of carboxymethyl β-cyclodextrin modified carbon paste (CM-β-CDCPE) displayed in Figure 3.17(a) shows a rough surface morphology. Although, the same amount of cyclodextrin (0.545 g) was added into the paste, it is not obvious to distinguish the surface of CM-β-CDCPE from the surface of S-β-CDCPE. However, the difference between the two cyclodextrin modifiers are observed using EDX. Atomic composition analysis of the composite shows that carboxymethyl β-cyclodextrin

modified electrode does not contain S atom but also shows the Na element as shown in Figure 3.17(b). In fact, carboxymethyl β-cyclodextrin is in a sodium salt form.

(a)

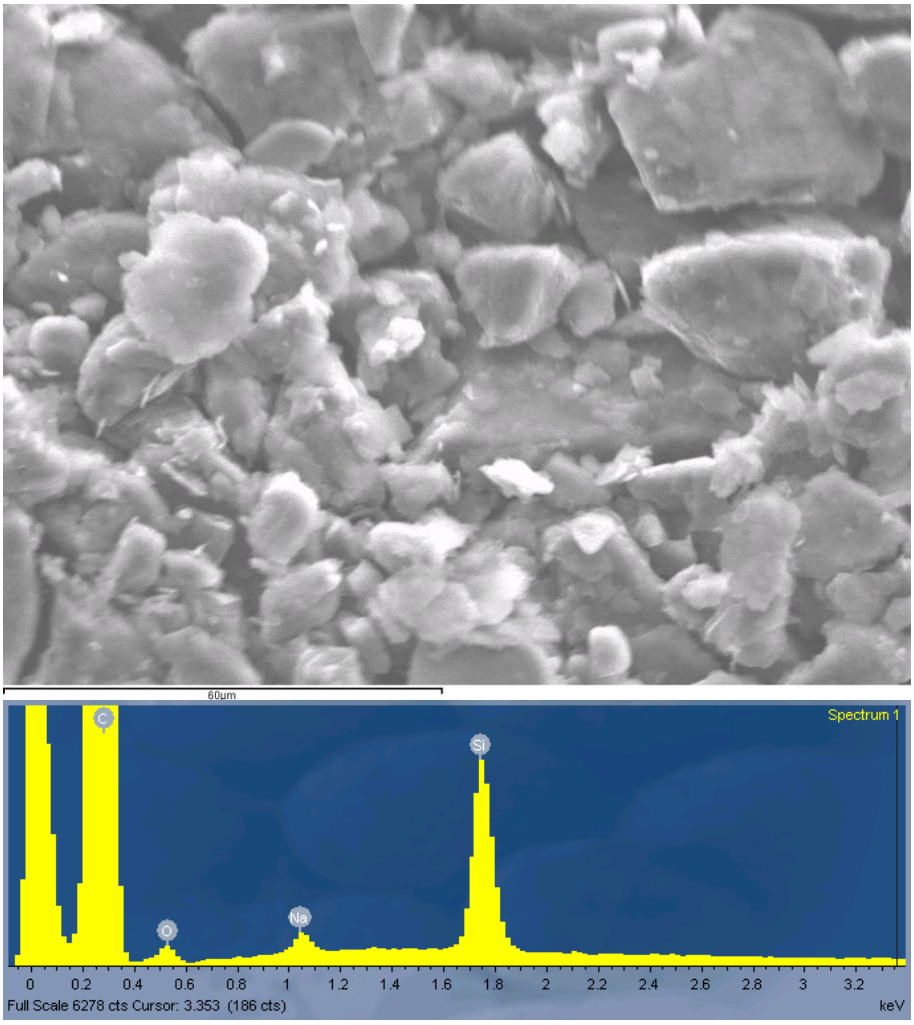

(b)

Figure 3.17: SEM micrograph (a) and EDX spectrum (b) of CM-β-CD (0.545g) modified CPE.

3.2.4.4 SEM and EDX of Ferrocene β-cyclodextrin modified carbon paste electrode

The SEM morphology of Fc-β-CD modified carbon paste electrode is shown in Figure 3.18(a). Several spots are found homogeneously distributed on the electrode surface, which are due to the presence of Fc-β-CD molecules. This also demonstrates that the modifier was perfectly dispersed in the paste. The relatively darker areas are related to the graphite conducting micro-structure. In addition, EDX spectrum shown in Figure 3.18(b) indicates the presence of iron.

(a)

(b)

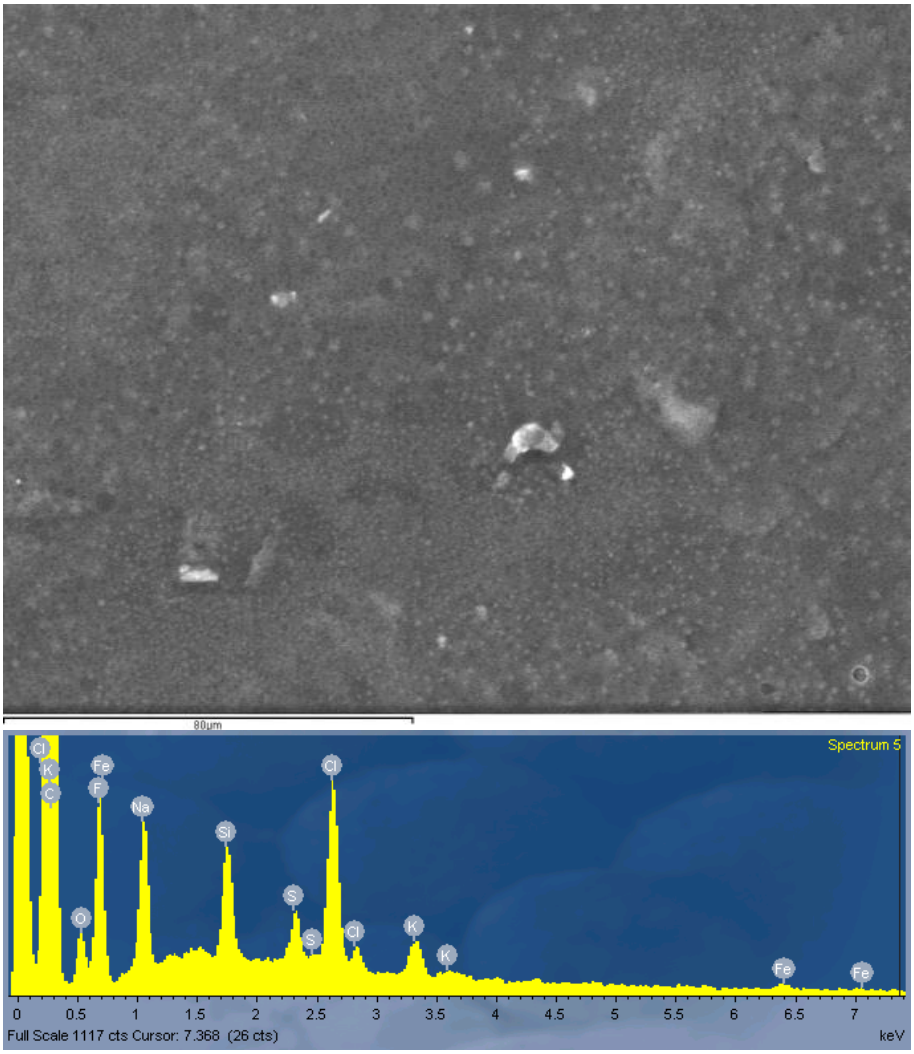

Figure 3.18: SEM micrograph (a) and EDX spectrum (b) of Fc-β-CD modified CPE.

3.2.4.5 SEM and EDX of graphene paste electrode

Compare with bare carbon paste electrode, graphene paste electrode displays a more compact, uniform and smoother surface as shown in Figure 3.19(a). This could effectively increase the apparent electroactive surface areas of the electrode and significantly improve the electrochemical performance on analyte. EDX image of graphene paste electrode in Figure 3.19 (b) shows the same elemental composition found in bare graphite paste electrode.

(a)

(b)

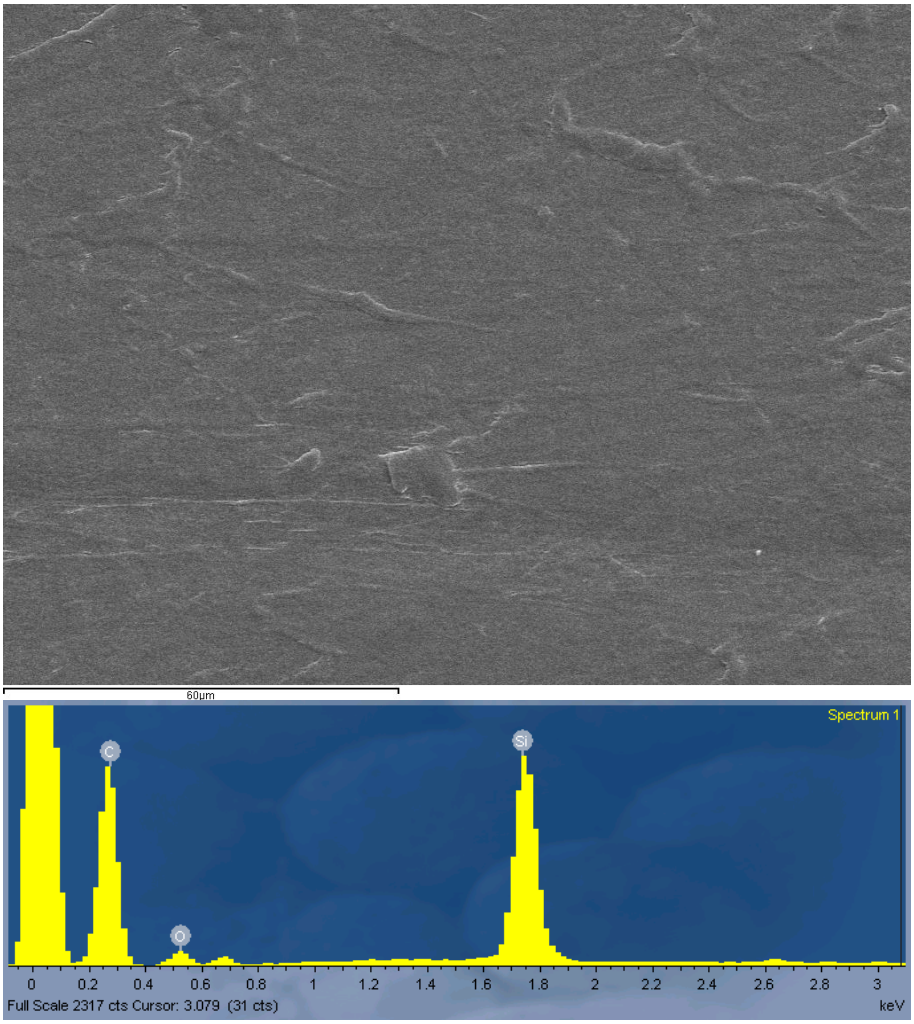

Figure 3.19: SEM micrograph (a) and EDX spectrum (b) of bare GPE.

3.2.4.6 SEM and EDX of sulfated β-cyclodextrin modified graphene paste electrodes

In Figure 3.20(a), it can be clearly seen that graphene containing S-β-CD aggregate and stack to multilayers with numerous edges. It is important to note that the surface of the modified graphene is smoother than corresponding modified graphite (S-β-CD). EDX spectrum shown in Figure 3.20(b) demonstrates that S-β-CD was well incorporated within the carbon paste.

(a)

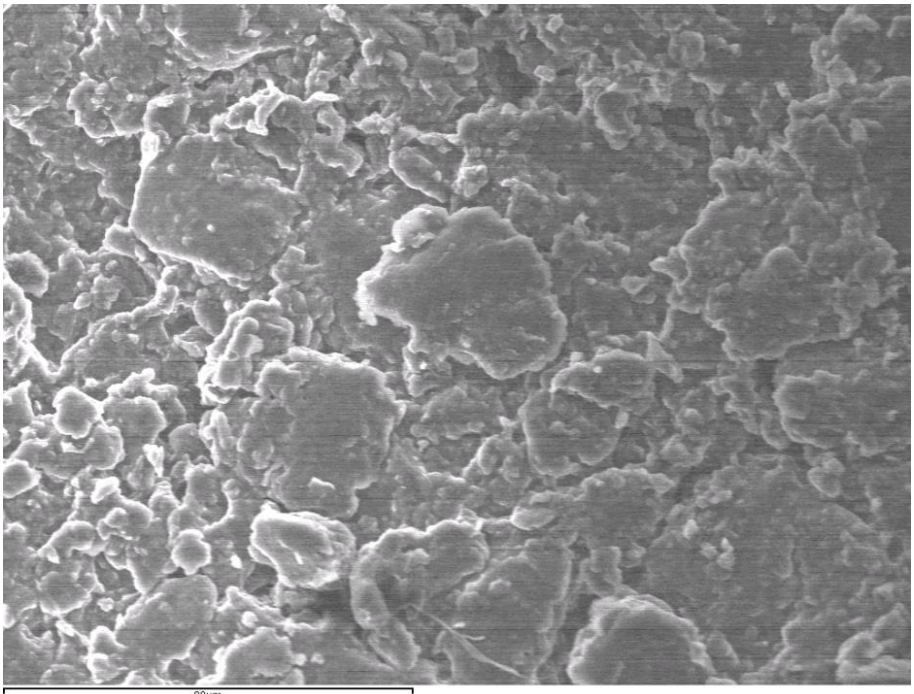

(b)

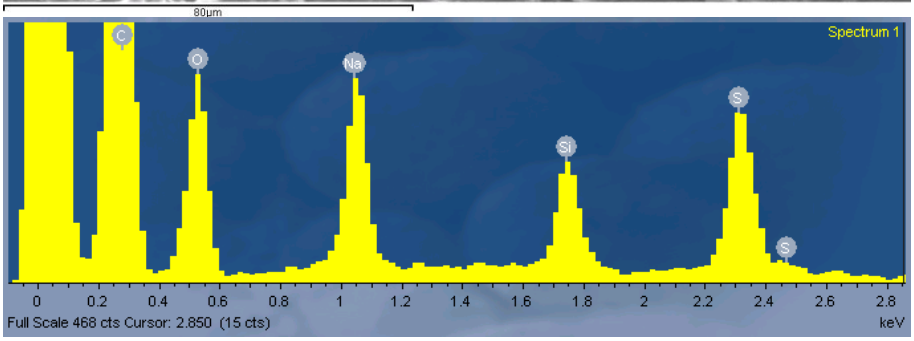

Figure 3.20: SEM micrograph (a) and EDX spectrum (b) of S-β-CD (0.545g) modified GPE.

3.2.4.7 SEM and EDX of nafion modified carbon paste electrode

Nafion is a commonly used ion-exchanger polymer with characteristics such as good film forming ability. While the surface of the bare CPE was found to have a slight roughness, it became smoother when the surface of the electrode was coated with nafion film as shown in Figure 3.21(a). Nafion itself has almost ideal properties to be a modifier. It is electrochemical inert, insoluble in water, and possesses hydrophobic character. Hence it mingles perfectly with the graphite, giving a uniform electrode surface. EDX spectrum of nafion modified carbon paste electrode displayed in Figure 3.21(b), shows trace amount of F and S atoms, which are some of fundamental elements forming the polymer. Nafion unique ionic properties are a result of incorporating perfluorovinyl ether groups terminated with sulfonate groups on tetrafluoroethylene (Teflon) backbone.

(a)

(b)

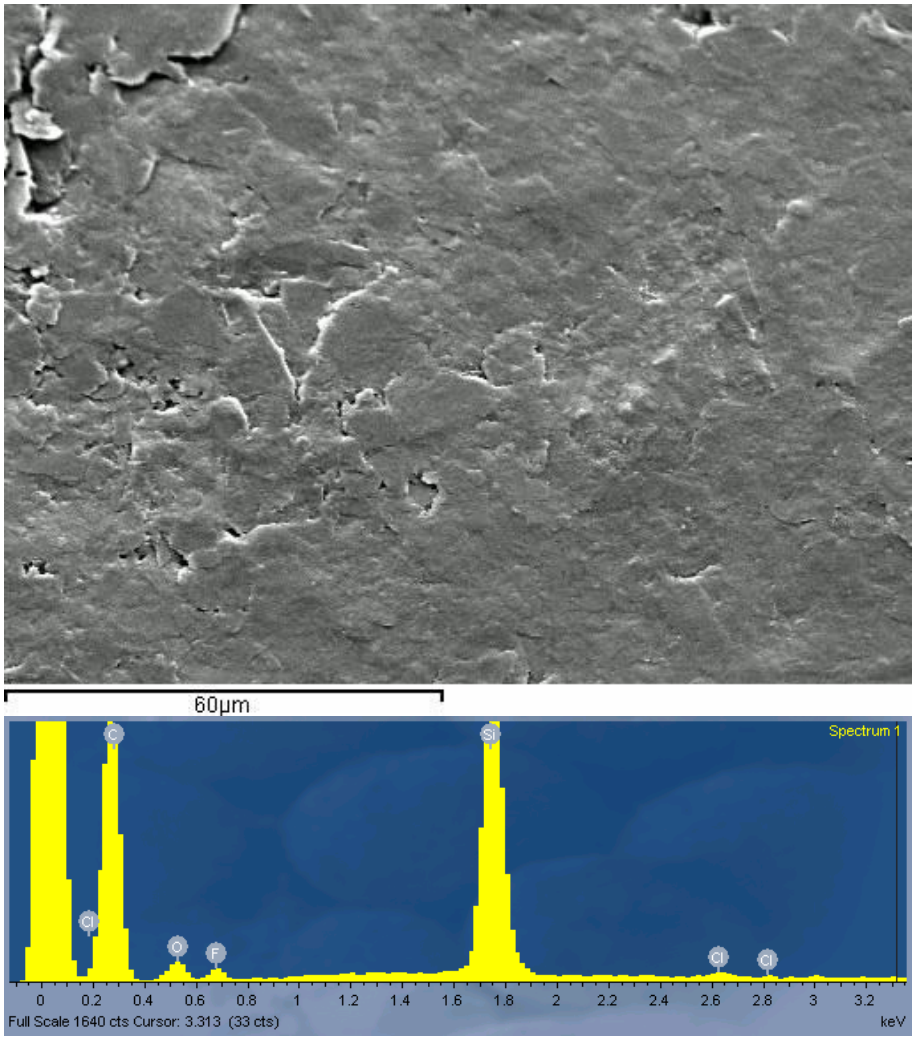

Figure 3.21: SEM micrograph (a) and EDX spectrum (b) of Nafion modified CPE.

As already mentioned, this chapter is concerned with the fabrication and characterisation of the modified electrodes. The following chapter focus on the electrochemical capabilities of the modified electrodes towards the sensing of DA.

3.3 References

1. Gorton, L., *Carbon-Paste Electrodes Modified with Enzymes, Tissues, and Cells.* Electroanalysis, 1995. **7**(1): p. 23-45.

2. Svancara, I. and Vytras, K., *Preparation and Properties of Carbon-Paste Electrodes.* Chemicke Listy, 1994. **88**(3): p. 138-146.

3. Olson, C. and Adams, R.N., *Carbon Paste Electrodes* A*pplication to* A*nodic Voltammetry.* Analytica Chimica Acta, 1960. **22**(6): p. 582-589.

4. Olson, C. and Adams, R.N., *Carbon Paste Electrodes* A*pplication to Cathodic Reductions and* A*nodic Stripping Voltammetry.* Analytica Chimica Acta, 1963. **29**(4): p. 358-363.

5. Farsang, G., *Voltammetric Properties and* A*nalytical Uses of Carbon Paste Electrodes Prepared with Silicone Oil.* Acta Chimica Academiae Scientarium Hungaricae, 1965. **45**(3): p. 163.

6. Lindquis.J, *Study of 7 Different Carbon Paste Electrodes.* Journal of Electroanalytical Chemistry, 1974. **52**(1): p. 37-46.

7. Rice, M.E., Galus, Z., and Adams, R.N., *Graphite Paste Electrodes - Effects of Paste Composition and Surface-States on Electron-Transfer Rates.* Journal of Electroanalytical Chemistry, 1983. **143**(1-2): p. 89-102.

8. Svancara, I. and Schachl, K., *Testing of unmodified carbon paste electrodes.* Chemicke Listy, 1999. **93**(8): p. 490-499.

9. Svancara, I. and Vytras, K., *Voltammetry with Carbon Paste Electrodes Containing Membrane Plasticizers Used for Pvc-Based Ion-Selective Electrodes.* Analytica Chimica Acta, 1993. **273**(1-2): p. 195-204.

10. Kalcher, K., *Chemically Modified Carbon Paste Electrodes in Voltammetric* A*nalysis.* Electroanalysis, 1990. **2**(6): p. 419-433.

11. Panzer, R.E. and P.J. Elving, P.J., *Nature of Surface Compounds and Reactions Observed on Graphite Electrodes.* Electrochimica Acta, 1975. **20**(9): p. 635-647.

12. Bard, A.J., Faulkner., L. R., *Electrochemical methods.* 2002.

13. Ye, B.X., Xia, P., and Lin, L., *Determination of the neurotransmitter-norepinephrine in the presence of ascorbic acid using carbon fiber microelectrodes activated by potentiostat.* Microchemical Journal, 2000. **64**(2): p. 125-130.

14. Chen, P.H. and McCreery, R.L., *Control of electron transfer kinetics at glassy carbon electrodes by specific surface modification.* Analytical Chemistry, 1996. **68**(22): p. 3958-3965.

15. Fagan, D.T., Hu, I.F., and Kuwana, T., *Vacuum Heat-Treatment for Activation of Glassy-Carbon Electrodes.* Analytical Chemistry, 1985. **57**(14): p. 2759-2763.

16. Marchon, B., et al., *Tpd and Xps Studies of O_2, CO_2, and H_2O Adsorption on Clean Polycrystalline Graphite.* Carbon, 1988. **26**(4): p. 507-514.

17. McCreery, R.L., *Advanced carbon electrode materials for molecular electrochemistry.* Chemical Reviews, 2008. **108**(7): p. 2646-2687.

18. Kampouris, D.K. and Banks, C.E., *Exploring the physicoelectrochemical properties of graphene.* Chemical Communications, 2010. **46**(47): p. 8986-8988.

19. Laine, N.R., Vastola, F.J., and Walker, P.L., *Importance of Active Surface Area in Carbon-Oxygen Reaction.* Journal of Physical Chemistry, 1963. **67**(10): p. 2030-2034.

20. Davies, M.O., et al., *The Oxygen Electrode .1. Isotopic Investigation of Electrode Mechanisms.* Journal of the Electrochemical Society, 1959. **106**(1): p. 56-61.

21. Beilby, A.L. and Mather, B.R., *Resistance Effects of 2 Types of Carbon Paste Electrodes.* Analytical Chemistry, 1965. **37**(6): p. 766-768.

22. Vanderlinden, W.E. and Dieker, J.W., *Glassy-Carbon as Electrode Material in Electroanalytical Chemistry.* Analytica Chimica Acta, 1980. **119**(1): p. 1-24.

23. Ravichandran, K. and Baldwin, R.P., *Enhanced Voltammetric Response by Electrochemical Pretreatment of Carbon Paste Electrodes.* Analytical Chemistry, 1984. **56**(9): p. 1744-1747.

24. Kalcher, K., et al., *Sensors Based on Carbon-Paste in Electrochemical Analysis - a Review with Particular Emphasis on the Period 1990-1993.* Electroanalysis, 1995. **7**(1): p. 5-22.

25. Macdonald, J.R. and Kenan, W.R., *Impedance Spectroscopy: Emphasizing Solid Materials and Systems*1987: Wiley.

26. Alfonta, L., Katz, E., and Willner, I., *Sensing of acetylcholine by a tricomponent-enzyme layered electrode using faradaic impedance spectroscopy, cyclic voltammetry, and microgravimetric quartz crystal microbalance transduction methods.* Analytical Chemistry, 2000. **72**(5): p. 927-935.

27. Hortholary, C. and Coudret, C., *An approach to long and unsubstituted molecular wires: Synthesis of redox-active, cationic phenylethynyl oligomers designed for self-assembled monolayers.* Journal of Organic Chemistry, 2003. **68**(6): p. 2167-2174.

4 Sensor application: Electrochemical Performance of the Composite Carbon Paste Electrodes Towards the Detection of DA

4.1 Introduction

Carbon paste electrodes (CPEs) have received special attention in electroanalysis due to their simplicity and rapid preparation [1-3]. They undoubtedly represent one of the most convenient materials for the preparation of modified electrodes. A modifier can be loaded onto the surface of the CPE, dissolved in a binder, or admixed mechanically to the paste during its homogenisation. In voltammetry, CPEs having a wider anodic potential range [4], with an ease of surface renewal and reproducible peak current measurement, have proven to be the most suitable electrode for a variety of analytes when compared to other metal or glassy carbon electrodes [4, 5]. Carbon materials are very useful components to study the electrochemical behaviour of several biomolecules. In bio-sensing, researchers are keen to develop materials capable of detecting neurotransmitters, enzymes, proteins, DNA, cells, tissues, and many others biological molecules. In the case of neurotransmitters, CPEs have been used to detect or characterize acetylcholine [6, 7], dopamine [8, 9], serotonin [10, 11], norepinephrine [12, 13] and nitric oxide [14].

These neurotransmitters are packaged into synaptic vesicles clustered beneath the membrane in the axon terminal, on the presynaptic side of a synapse. They are released and diffuse across the synaptic clefs, where they bind to specific receptors in the membrane on the postsynaptic side of the synapse.

As a catecholamine neurotransmitter, DA has a key physiological role in transmitting chemical signals from a neuron to a target cell across a synapse [15]. DA is linked to a number of neurological disorders such as Parkinson's disease (decrease level of DA) and schizophrenia. It is related to addiction, HIV infection [16-18] and affects brain processes that control emotional response. Monitoring DA levels *in vitro* or *in vivo* could provide valuable information on the efficacy of various treatments aiming at healing or controlling diseases. Therefore, electrodes that are capable of sensing DA, rapidly, accurately and reliably, are of great medical importance.

Various techniques such as fluorimetry, chemiluminescence, capillary electrophoresis, and ion chromatography [19-22] have been developed for detection of DA. Compared with these above approaches, an electrochemical method has received considerable interest. It is widely employed owing to its fast detection, simplicity, reproducibility, impressive cost-effectiveness, and potential for miniaturization [23-25]. Thus, electrochemistry is a powerful method for monitoring DA, both *in vitro* and *in vivo*. In order to facilitate the detection of DA, a modifier is needed, more specifically a chemical that would catalyse its chemical transformation.

Researchers have developed different types of electrodes for DA measurement based on the modification of gold, glassy carbon, diamond or carbon nanotubes. The DA sensors developed in this Ph.D. thesis are mainly based on the modification of CPE with different cyclodextrin derivatives such as Sulfated β-cyclodextrin, Carboxymethyl β-cyclodextrin or Ferrocene β-cyclodextrin complex. Electrochemical studies were performed using SCE as auxiliary electrode and PBS as supporting electrolyte. Electrochemical techniques such cyclic voltammetry and differential pulse voltammetry were employed to determine qualitative characteristics of DA. In general, the results have demonstrated that modified CPEs are better than bare CPE as biosensor electrode materials for the detection of DA.

4.2 Results and discussion

4.2.1 Bare CPE

Carbon paste based-sensors utilised in this study are made primarily from a mixture of graphite powder and a binder such as silicone oil and are commonly referred to as CPEs. The details for the preparation of CPE were described in Chapter 3. The electrochemical study of bare CPE towards the redox process of DA in aqueous media is presented.

4.2.1.1 DA electrochemical redox process at bare CPE

The voltammetric behaviour of DA at the bare carbon (graphite) paste electrode (CPE) was examined using cyclic voltammetry. Figure 4.1 shows typical cyclic voltammogram of 5×10^{-5} M DA solution in 0.1 M PBS (pH 6.8) using the potential range [–0.2 V; +0.6 V]. The cyclic voltammogram is characterized by the appearance of distinct anodic peak at +0.225 V and a cathodic peak at +0.092 V vs. SCE. The separation in peak potential between the anodic peak potential and the cathodic peak potential, ΔE_p, was 0.133 V, and the ratio of redox peak currents (I_{pa} / I_{pc}) was 1.20. The oxidation and reduction peak current are 2.25×10^{-7} and 1.88×10^{-7} A, respectively, and represent typical current responses for 5×10^{-5} M DA at bare CPE. These results are characteristic of a quasi-reversible electrode process [26]. The anodic peak can be ascribed to the oxidation of DA to dopaminoquinone (DOQ) and the coupled cathodic peak to the reduction of DOQ back to DA [27].

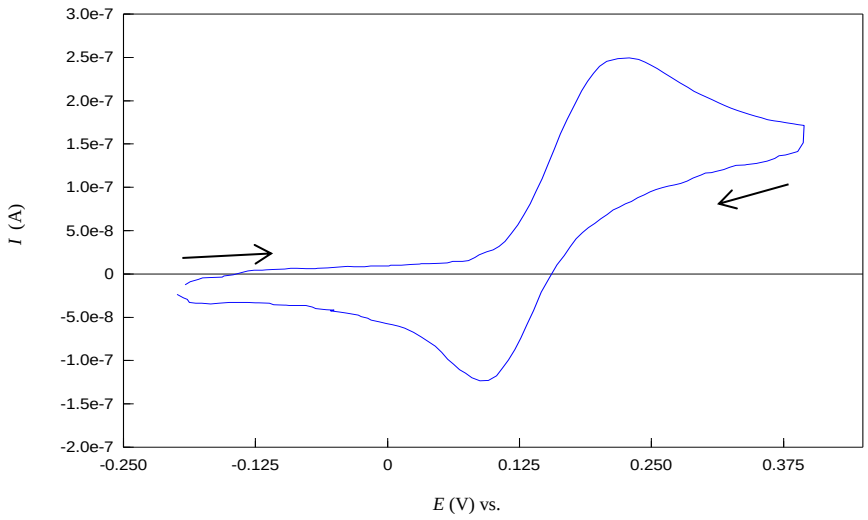

Figure 4.1: Cyclic voltammograms of DA (5×10^{-5} M) at bare CPE in 0.1 M PBS (pH 6.8); scan rate: 50 mV / s.

4.2.1.2 Effect of scan rate on DA peak current

As shown in Figure 4.2, the effect of scan rate on DA oxidation at bare CPE was investigated by cyclic voltammetry. At scan rates in the range of 10 to 100 mV / s, the oxidative peak current of the bare CPE in DA solution increases linearly with the scan rate. Further analysis of the data reveals DA redox behaviour is under both diffusion and adsorption control. The graph of current I_p vs. scan rate (ν) and square root of scan rate ($\nu^{1/2}$) were plotted and are displayed in Figure 4.3. In the range of 10 to 100 mV / s, the anodic peak current is proportional to ν and $\nu^{1/2}$ with correlation coefficients 0.9979 and 0.9688, respectively. It is more likely that the charge transfer is under a partially adsorption control process at the first three highest scan rates (100, 80 and 60 mV / s). E_{pa} for these specific scan rates is constant as shown in Table 4.1. This indicates a quasi-reversible nature of the electrode reaction. The lower scan rate (40, 20 and 10 mV / s) seemed to show a more diffusion-controlled process. With exception of the highest scan rate employed, the peak potential for DA oxidation shifted slightly to a more positive potentials with increasing of the scan rate. Similarly the reduction peak E_{pc} values shifted anodically to a more negative potential with increasing scan rate as displayed in Table 4.1.

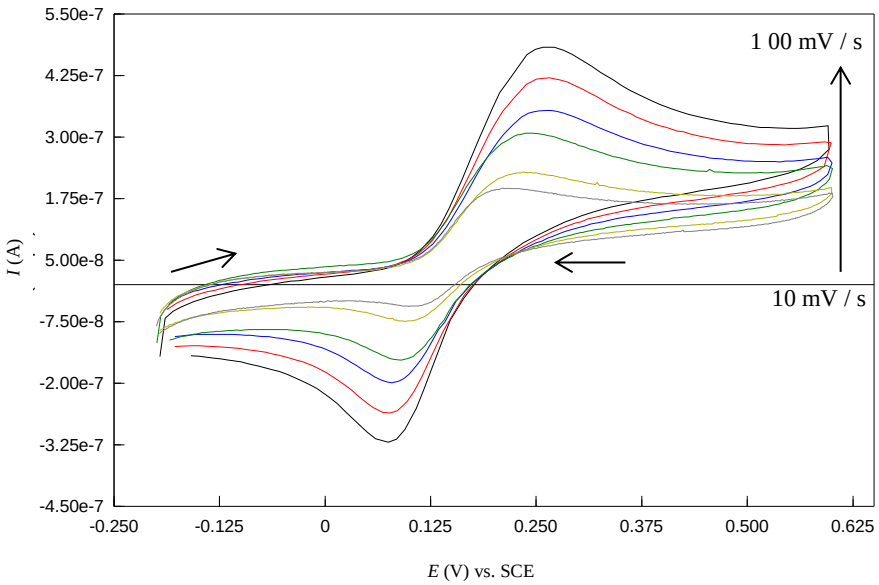

Figure 4.2: Cyclic voltammograms for the effect of variation of scan rates of DA (5×10^{-5} M) at bare CPE from 100 to 10 mV / s, in 0.1 M PBS (pH 6.8).

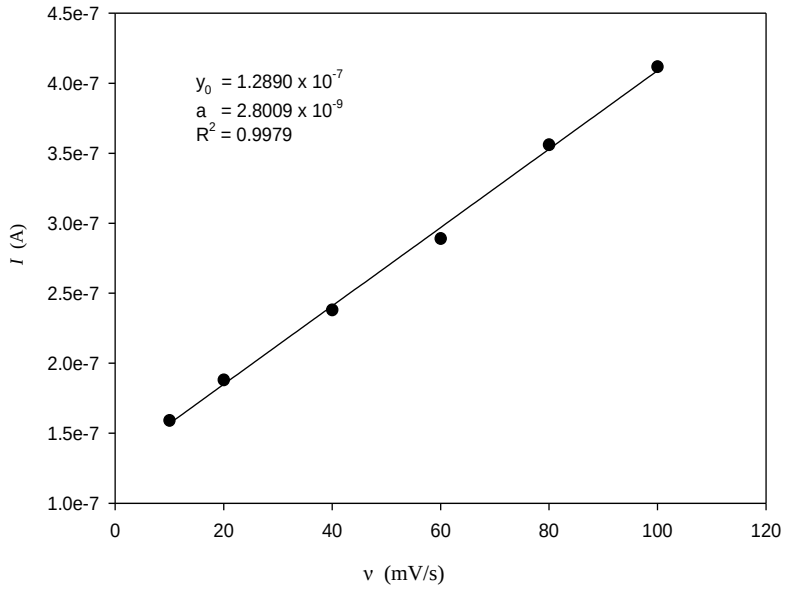

(a)

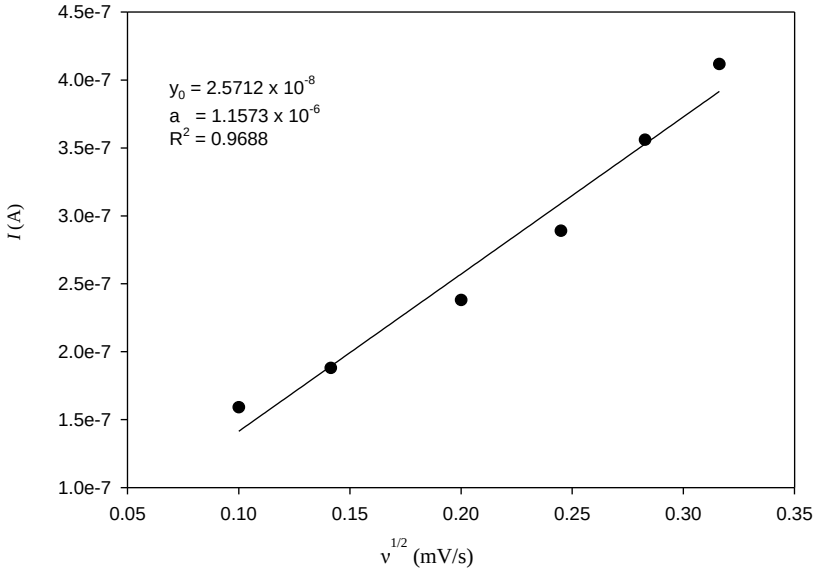

(b)

Figure 4.3: The variation of oxidation peak current for DA (5×10^{-5} M) at bare CPE as a function of (a) scan rate, and (b) square root of scan rate. Supporting electrolyte 0.1 M PBS (pH 6.8).

Table 4.1: Effect of scan rate on peak potential recorded at bare CPE.

Scan Rate (mV / s)	Oxidation Peak Potential (V)
100	0.26
80	0.26
60	0.26
40	0.24
20	0.23
10	0.20

The diagnosis of an adsorption-controlled oxidation of DA at the bare CPE is more difficult to rationalise but we infer that the nature of the electrode surface plays an important role in the electron transfer process. In aqueous solution, the hydrophobic surface of CPE repels hydrophilic species [28]. Although DA has a hydrophobic moiety (benzene ring), it is essentially a hydrophilic molecule. A diffusion-controlled process of DA at bare CPE was reported experimentally [29]. On the other hand, the apparent accumulation of DA at bare CPE remains unclear. Only few sources quote that the hydrophobic layer of binder at the carbon paste surface may promote the adsorption of some molecules, particularly lipophilic compounds [30].Therefore, it was assumed that a weak adsorption of DA to the bare CPE surface is possible through a π–π interaction of the benzene moiety with graphite. Further supporting that two regime processes occurred at the bare CPE, the log of oxidation peak currents was plotted against the log of scan rate. A linear relationship was obtained (as shown in Figure 4.4) with a slope of 0.506. This value, comprised in the range from 0.5 to 1 indicated that the electron transfer at bare CPE is simultaneously under a diffusion and adsorption process according to Laviron [31].

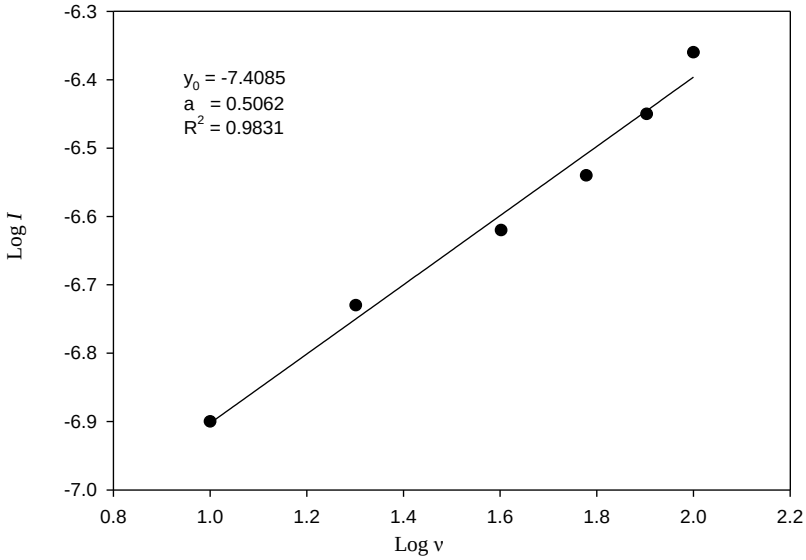

Figure 4.4: The variation of logarithm of oxidation peak current for DA (5×10^{-5} M) at bare CPE as a function logarithm of scan rate. Supporting electrolyte 0.1 M PBS (pH 6.8).

4.2.2 S-β-CD Modified CPE

In order to enhance the electrochemical response of DA at bare CPE, S-β-CD was used as a molecular recognition element. Like most cyclodextrin derivatives, S-β-CD can form host-guest inclusion complexes with a wide range of suitably sized guest molecules. This charged cyclodextrin derivative is electro-inactive, and as part of the electrode, it has the ability to sense DA via electrostatic interaction and inclusion complex formation. In this thesis, S-β-CD was used as the main type of modifier, and it has been demonstrated that S-β-CD modified CPE effectively enhanced DA signal.

4.2.2.1 DA electrochemical redox process at S-β-CD modified CPE

The S-β-CD modified CPE exhibited excellent electroanalytical response towards the oxidation of DA. This was demonstrated by comparing the electrochemical behaviour of DA at bare CPE with a modified electrode prepared with an optimal amount of S-β-CD (0.545 g). The cyclic voltammograms of 5×10^{-5} M DA in a 0.1 M PBS at S-β-CD modified CPE is shown in Figure 4.5. The oxidation peak potential occurs at +0.172 V and the reduction peak potential at 0.153 V, respectively, giving a peak potential separation (ΔE_p) of +0.019 V. The oxidation and reduction peak currents were 2.44×10^{-6} and 2.45×10^{-6} A, respectively, yielding an I_{pa} / I_{pc} ratio of unity. In addition, the oxidation peak potential of DA shifts in the negative direction at S-β-CD modified CPE when compared to bare CPE. These results indicate that the S-β-CD modified electrode is able to accelerate the rate of DA electron transfer. It was shown previously that the

oxidation peak current of DA at bare CPE was 2.25 × 10^{-7} A. This tremendous enhancement (>10 times) of the DA oxidation signal at the modified electrode is attributed to the chemical properties of S-β-CD. The effect of S-β-CD on the performance of the modified electrode is discussed in details in section 4.2.2.5.

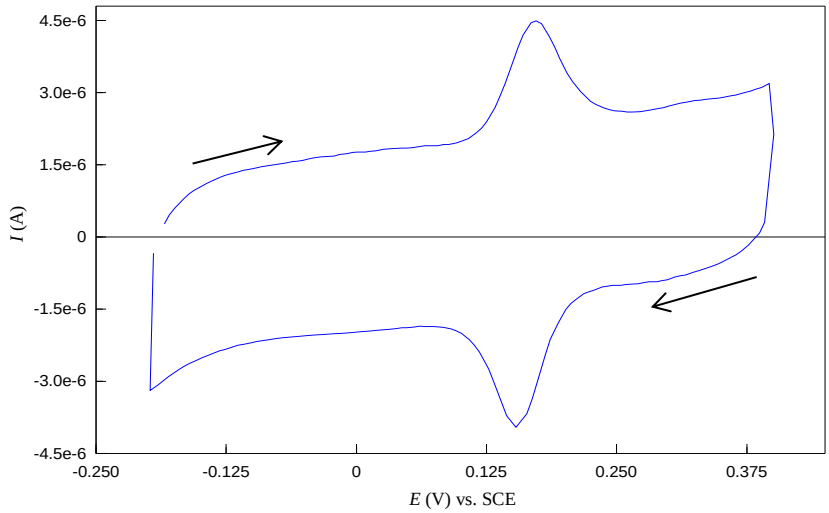

Figure 4.5: Cyclic voltammograms of 5 × 10^{-5} M DA at S-β-CD modified CPE, in 0.1 M PBS (pH 6.8); scan rate: 50 mV / s.

4.2.2.2 Mechanism of DA electrochemical oxidation

There is some confusion in the literature about the mechanism by which the electrochemical oxidation of DA occurs. To get a better understanding, cyclic voltammetry of DA solutions was performed at S-β-CD modified CPE using a relatively wide electrochemical window [–0.4 V; +0.4 V]. Four different concentrations of DA (5 × 10^{-5}, 1 × 10^{-4}, 5 × 10^{-4} and 1 × 10^{-3} M) were investigated in 0.1 M PBS at pH 6.8. As displayed in Figure 4.6, two pair of redox peaks are observed and can be ascribed to the electron transfer-chemical reaction-electron transfer (ECE) mechanism [32, 33]. The reaction system is represented in Scheme 4.1. The first step of DA oxidation (step E) involves two electron transfer and generation of DOQ. DOQ as a Michael acceptor undergoes nucleophilic attack [33]. This intramolecular proton transfer leads to the formation of leucodopaminechrome (step C) as shown in Equation 4.2. Leucodopaminechrome, in turn, is oxidised further via another two electron transfer to dopaminochrome (second step E).

From Figure 4.6, the pair of redox peaks observed at the positive potentials corresponds to the redox process described in Equation 4.1, whereas the pair of redox peaks observed at the negative potentials relates to Equation 4.3. The peak currents are

considerably smaller for this second redox couple. The peak currents increase as the concentration of DA rises, as expected. Since the pK_a of DA is 8.9 [34], below this pH value DA exists mainly in its protonated form and shows weak nucleophilic activity for intramolecular 1,4-Michael addition. However, in a solution of pH 6.8 the amount of unprotonated DOQ is sufficient for the cyclization reaction to occur. The product obtained (leucodopaminechrome) is next reversibly oxidized to dopaminechrome which manifests as a small redox pair. Similar result at a glassy carbon electrode modified electrode was obtained experimentally [35]. Although, a detailed mechanism for the electrochemical oxidation of DA was described above, DA detection is often simplified by using a potential window that encompasses the redox region for the DA / DOQ. Therefore, an electrochemical window excluding redox couple Leucodopaminechrome (LC) / Dopaminechrome (DC) is chosen throughout this study (unless otherwise mentioned).

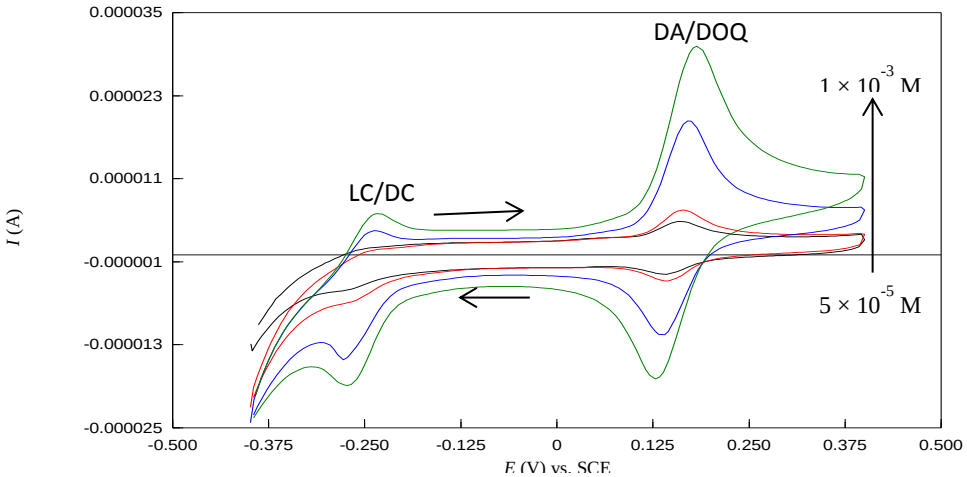

Figure 4.6: Cyclic voltammograms obtained for different concentrations of DA (5×10^{-5}, 1×10^{-4}, 5×10^{-4} and 1×10^{-3} M) at S-β-CD modified CPE in 0.1 M PBS; scan rate: 50 mV / s.

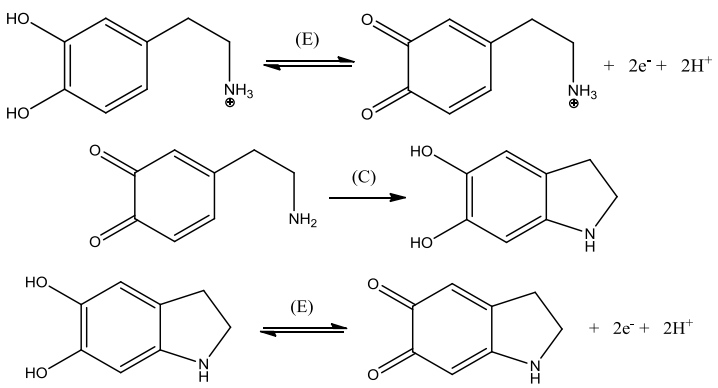

Scheme 4.1: Proposed DA reaction at S-β-CD modified CPE in 0.1 M PBS at pH 6.8.

To generate further support that an ECE mechanism correctly describes the electrochemical redox process of DA, the first five voltammogrammetric cycles for a 5 × 10^{-4} M DA solution are shown in Figure 4.7(a). The oxidation of Leucodopaminechrome (LDC) to Dopaminechrome (DC) was observed only after the first cycle as shown in Figure 4.7(b) (highlighted oxidation wave of LDC / DC from Figure 4.7(a)). This is consistent with the mechanism outlined in Scheme 4.1.

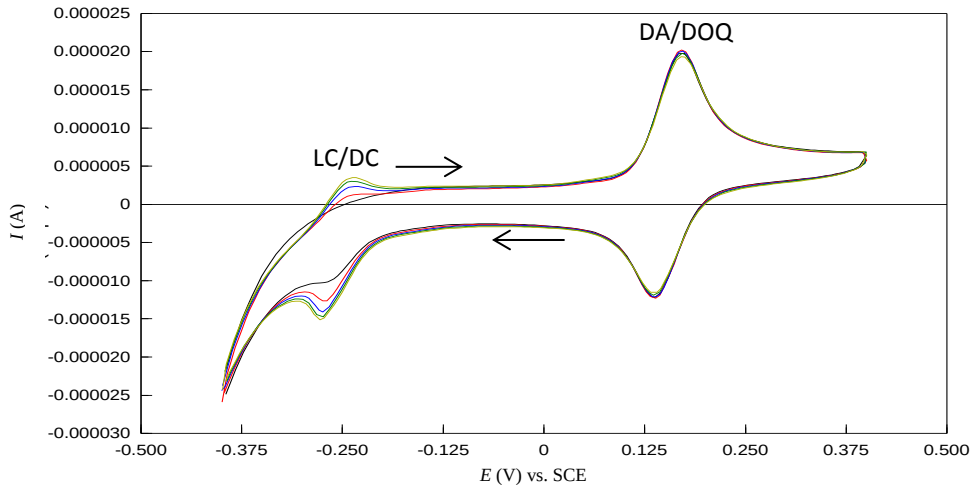

(a)

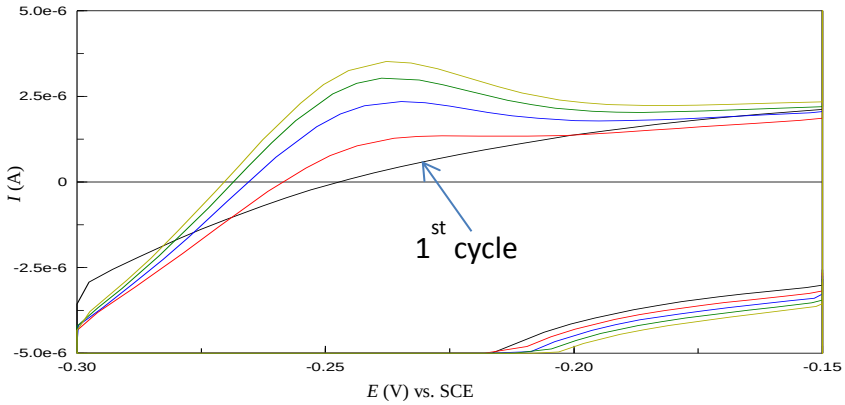

(b)

Figure 4.7: Cyclic voltammograms of 5 × 10^{-5} M DA at S-β-CD modified CPE (a), highlighted oxidation peaks of LC to DC (b), in 0.1 M PBS (pH 6.8); scan rate: 50 mV / s.

4.2.2.3 Effect of scan rate on peak current

The effect of potential scan rate on the peak current of DA oxidation at S-β-CD modified CPE was investigated under similar experimental conditions described in Chapter 3 (for bare CPE). Figure 4.8(a) illustrates the effect of scan rate on DA oxidation at the modified electrode by cyclic voltammetry. It was found that the anodic

peak current in 5 × 10^{-5} M DA solution increased linearly with the scan rate (Figure 4.8(b)) in the range of 10 to 80 V vs. SCE, suggesting the oxidation of DA is under adsorption-control at the modified electrode. Unlike bare CPE, the peak potential remains constant with increasing scan rate, which is characteristic of reversible redox process for an adsorbed species at a modified electrode. It has to be noted that the background current increased considerably as the scan rate increased. This is probably caused by mass transport of supporting electrolyte (0.1 M PBS) from the bulk to the double layer region, and non-faradaic current increase from the double layer which undergoes charging and discharging processes during the electron (and chemical) transfer.

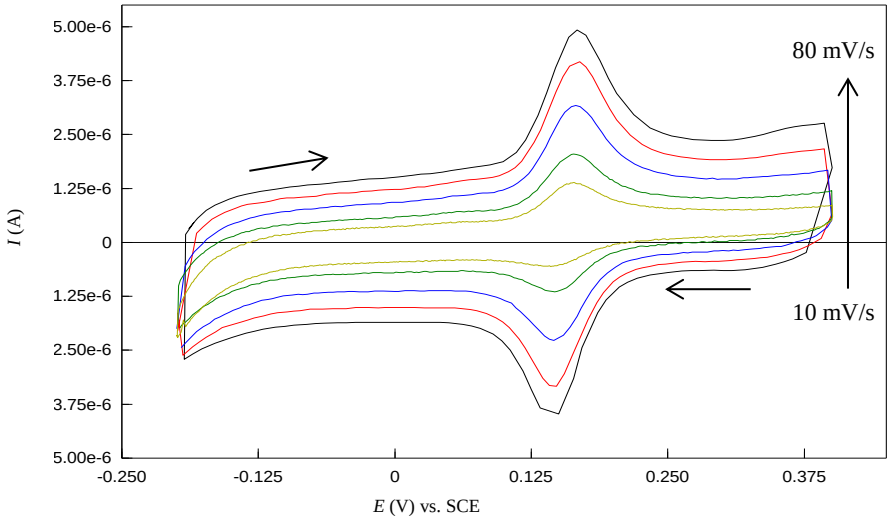

(a)

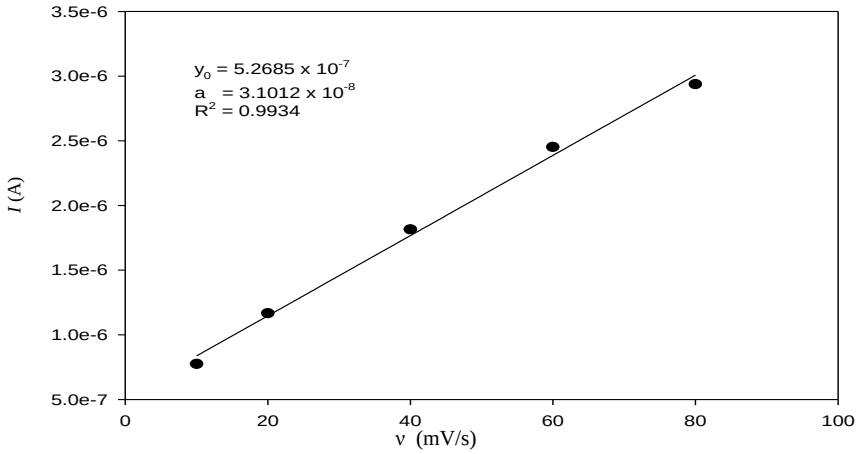

(b)

Figure 4.8: Cyclic voltammograms for the effect of variation of scan rates of DA (5 × 10^{-5} M) at S-β-CD modified CPE from 10 to 80 mV / s (a) and corresponding variation of oxidation peak current as a function of scan rate (b). Supporting electrolyte 0.1 M PBS (pH 6.8).

4.2.2.4 DA adsorption characteristics of bare CPE and S-β-CD modified CPE

To demonstrate further the adsorption ability of S-β-CD modified CPE, a preconcentration experiment was performed by immersing bare CPE and S-β-CD modified CPE separately in 5×10^{-5} M DA solutions for five minutes. After rinsing both electrodes with distilled water, cyclic voltammograms were recorded in a fresh PBS. The resulting voltammograms are shown in Figure 4.9. No DA signal was obtained at bare CPE, while DA redox peaks were clearly observed at S-β-CD modified CPE. This proves that DA is significantly adsorbed onto the surface of the modified electrode due to the presence of S-β-CD, possibly through host-guest or ionic interactions. It is worth mentioning that the modified electrode, here, contains the optimal amount of S-β-CD (0.545 g) in terms of DA detection. Thus, the value of the peak current is highly dependent on the concentration of S-β-CD within the paste, and the optimisation process is detailed in Section 4.2.2.5. The voltammogram traces chosen for comparison (in Figure 4.9) are the first cycles obtained from the unmodified and S-β-CD modified electrodes. The oxidation peak current in the case of S-β-CD modified CPE was 2.21×10^{-6} A. Interestingly, ΔE_p for this first cycle is 0.027 V (vs. SCE), confirming the reversibility of electron transfer process at the modified electrode. It has to be noted that with successive cycling, a reduction and subsequent disappearance of the redox peaks is observed at the modified electrode.

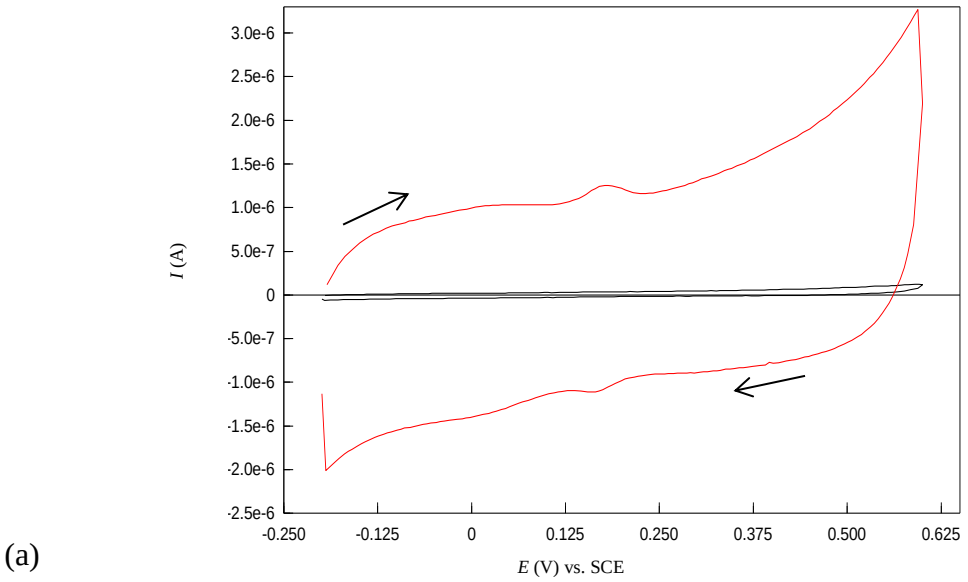

(a)

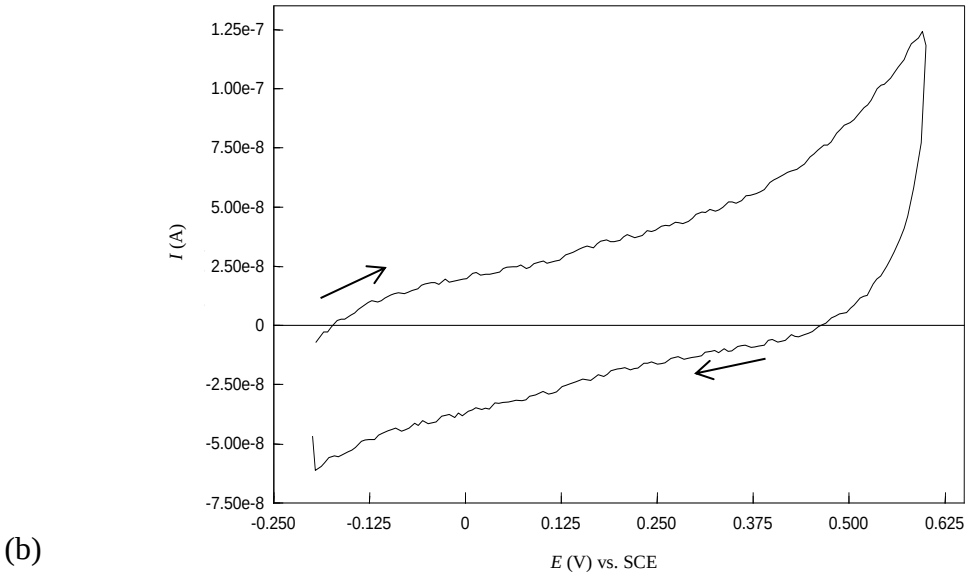

(b)

Figure 4.9: Cyclic voltammograms of S-β-CD modified CPE (—) and bare CPE (—) in 0.1 M PBS (a), after both electrodes were dipped in DA (5 × 10^{-5} M) for 5 minutes. Highlighted cyclic voltammogram of bare CPE (b); scan rate 50 mV / s.

4.2.2.5 Effect of amount of S-β-CD on DA oxidation peak current

One of the most effective parameters in modified electrodes performance is the composition. The effect of the amount of S-β-CD on DA oxidation peak current was investigated using cyclic voltammetry. In this study, a number of S-β-CD modified CPE was prepared with different ratio of S-β-CD. Typically, S-β-CD was varied from 0.145 g to 0.895 g in increments of 0.05 g. It should be noted that mass of graphite was kept constant while the amount of silicone oil was also varied (carbon paste ratios are given in Table 4.2). The experiments were carried out in triplicate and an average value of DA oxidation peak currents was recorded. As shown in Figure 4.10, the oxidative peak

current of DA increased remarkably by increasing the amount of S-β-CD from 0.145 g to 0.495 g. An apparent steady state current response for DA oxidation is then obtained from 0.495 g to 0.695 g. However, the oxidation peak current of DA decreased greatly when the amount of S-β-CD exceeded 0.695 g. These experimental results suggest that an amount of S-β-CD, lower than 0.495 g is not sufficient to promote an optimum oxidation peak current of DA, and a higher amount than 0.695 g can inhibit the electrical conductivity of carbon paste. The range from 0.495 to 0.695 g was considered to be the optimal amount for detection of DA. Consequently, 0.545 g of S-β-CD was chosen to modify the carbon paste for electrochemical detection of DA.

Table 4.2: The effect of S-β-CD on DA oxidation peak current. The composition of S-β-CD modified CPE was made by varying the amount of S-β-CD and silicone oil while keeping the amount of graphite constant.

Graphite (g)	Silicone oil (µL)	S-β-CD (g)	DA oxidation peak current (A)
0.71	136	0.145	1.4751×10^{-6}
0.71	144	0.195	1.4796×10^{-6}
0.71	152	0.245	1.5100×10^{-6}
0.71	160	0.295	1.5892×10^{-6}
0.71	168	0.345	1.5760×10^{-6}
0.71	176	0.395	1.6771×10^{-6}
0.71	184	0.445	1.8276×10^{-6}
0.71	192	0.495	2.3676×10^{-6}
0.71	200	0.545	2.4006×10^{-6}
0.71	208	0.595	2.3478×10^{-6}
0.71	216	0.645	2.3408×10^{-6}
0.71	224	0.695	2.2988×10^{-6}
0.71	232	0.745	1.9841×10^{-6}
0.71	240	0.795	1.7911×10^{-6}
0.71	248	0.845	1.5876×10^{-6}
0.71	256	0.895	1.5917×10^{-6}

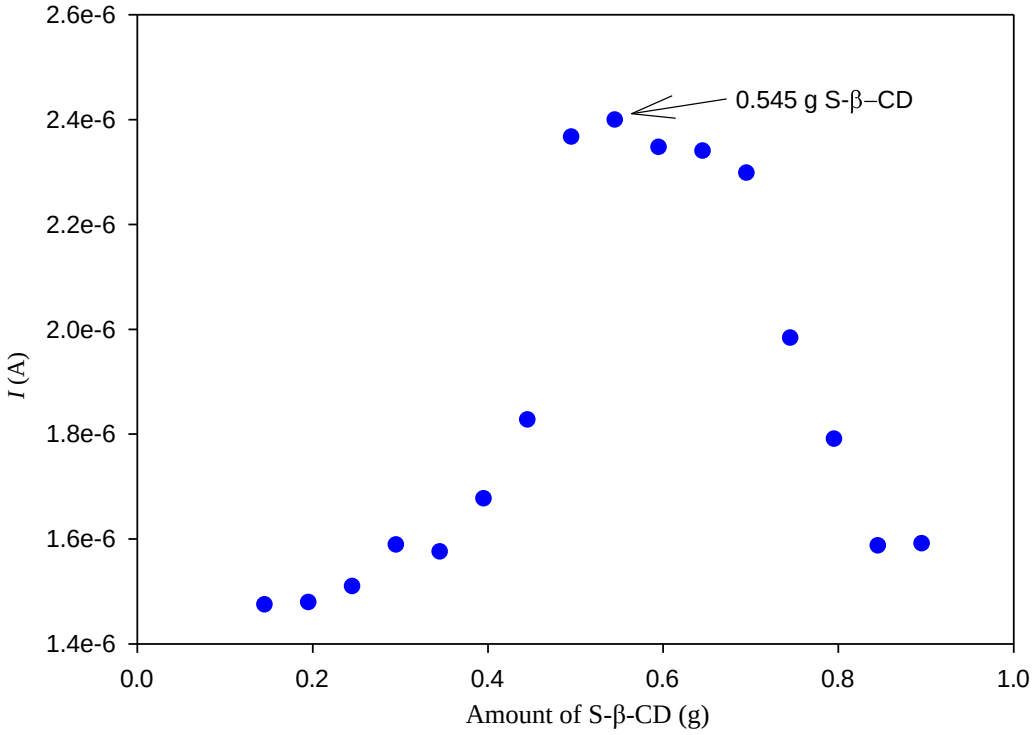

Figure 4.10: Effect of the amount of S-β-CD on DA oxidative peak current.

4.2.2.6 Mode of sensing of DA at S-β-CD modified CPE

The mode of sensing of S-β-CD modified CPE was considered from two perspectives. Firstly, the adsorption test conducted previously, shows that DA interacts with S-β-CD at the electrode / solution interface. The highly electronegative sulfate groups are expected to promote strong electrostatic attraction with the positively charged DA molecule at pH 6.8. This may also help to facilitate the inclusion of protonated DA in the cavity of cyclodextrin, thus, promoting sensor selectivity. The supramolecular interaction processes may justify the observed increase in the DA oxidation peak current. The (increased) affinity facilitates an enhancement in the rate of electron transfer at the electrode / solution interface. Secondly, previous studies carried out in our laboratory [36-38], suggest that DA forms an inclusion complex with S-β-CD in solution. These studies based on NMR and UV-Vis spectroscopy give an insight into the mode of sensing of DA at polypyrrole sulfated β-cyclodextrin modified glassy carbon electrode. The effect of S-β-CD on the peak intensity was also examined using the more sensitive technique DPV. It was demonstrated that S-β-CD modified CPE exhibit remarkable enhancement effects on the oxidation peak currents of DA. The voltammograms were recorded using the potential range, 0.00 – 0.25 V vs. SCE, in 5 ×

10^{-5} M DA, with 0.1 M PBS as supporting electrolyte at bare CPE and S-β-CD modified CPE. Another important parameter to be considered is that DPV was performed after 2 minutes accumulation time at both the modified and bare electrodes. As shown in Figure 4.11, oxidation peaks were observed at 0.132 V and 0.136 V vs. SCE, for bare CPE and S-β-CD modified CPE, respectively, corresponding to the oxidation of DA to DOQ. A peak current enhancement, nearly 10 fold, at S-β-CD modified CPE (6.14×10^{-6} A) compared to bare CPE (6.53×10^{-7} A) was observed. Thus the results confirm that the presence of S-β-CD improved the sensitivity of the carbon paste for the electrochemical detection of DA.

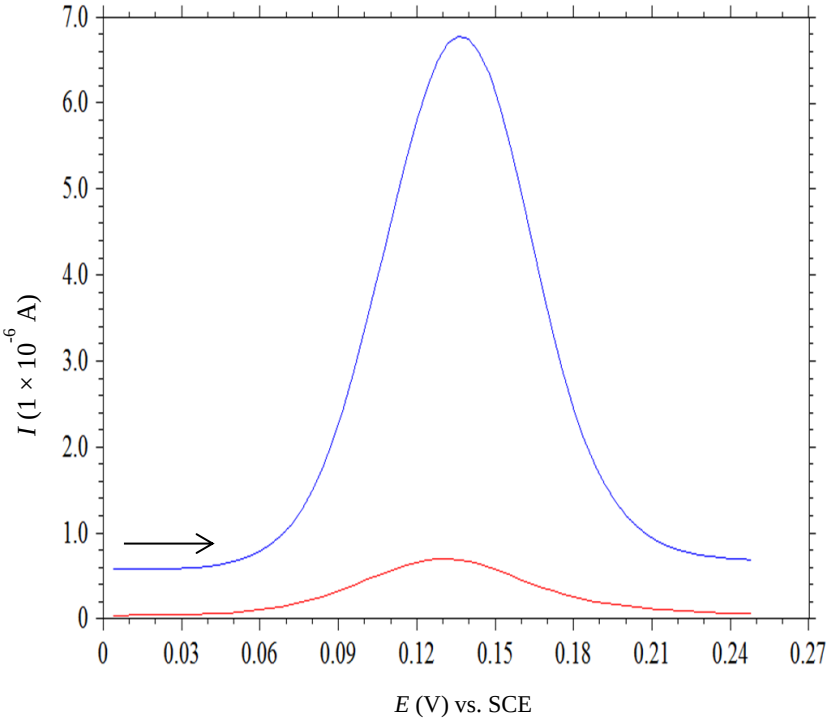

Figure 4.11: Differential Pulse Voltammograms of DA (5×10^{-5} M) at S-β-CD modified CPE (—) and bare CPE (—) in 0.1 M PBS, pH 6.8.

When the solution pH was equal to 6.8, the $–OSO_3Na$ group of cyclodextrin is likely to dissociate leaving a negative charge group $–OSO_3^-$ (pK_a of $–OSO_3H$ is about 1.6 [41]). Under these conditions, the $–NH_2$ group on DA could obtain a proton and form the cation of DA (pK_a = 8.9). Therefore, the negative charge group $–OSO_3^-$ on the surface of S-β-CD modified CPE has a great (electrostatic) affinity to the DA positive ions, promoting the oxidation of DA in the neutral buffer solution (pH 6.8). An illustration of such a mode of DA sensing is shown in Scheme 4.2.

A higher voltammetric background current at the S-β-CD modified CPE compared to bare CPE was also observed. As already mentioned, this large background current could be caused by the complex charging current at the modified electrode / electrolyte interface compared to the non-modified electrode.

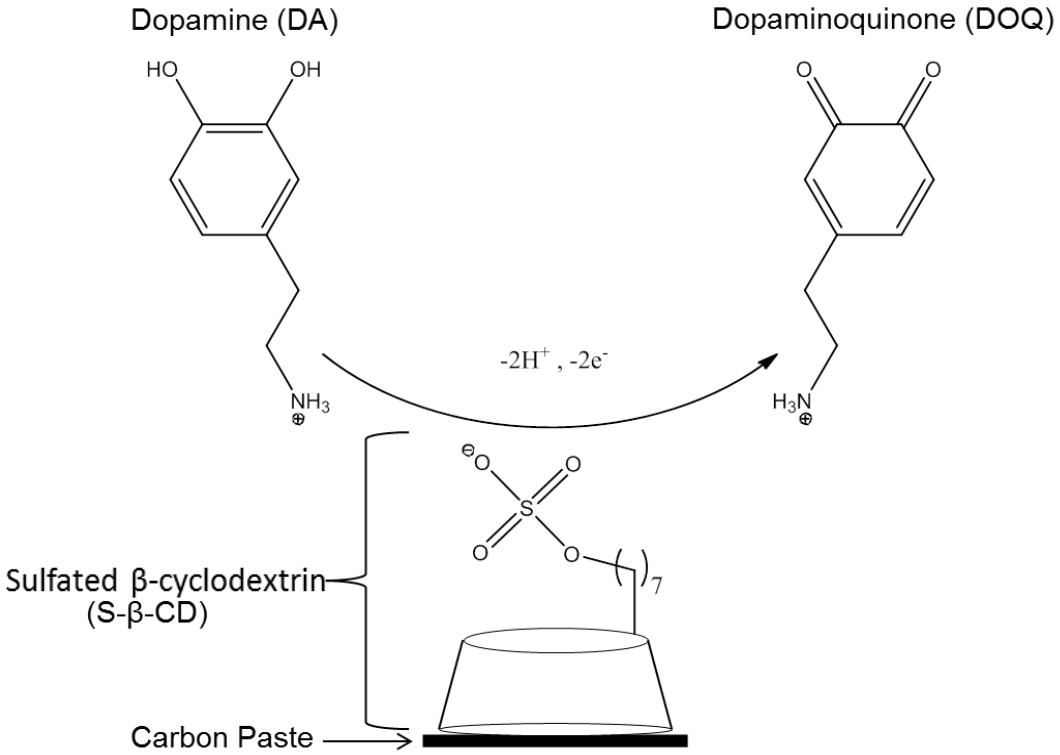

Scheme 4.2: Schematic representation of the DA oxidation process at S-β-CD modified CPE.

4.2.3 Electrode Pre-treatment

It is important to condition the electrodes before detection of DA. Among several methods, cyclic voltammetric sweeping from –0.2 to +0.4 V in PBS prior to DA detection was chosen for bare CPE. As can be seen from Figure 4.12(a), when bare CPE was run directly in DA solution, steady-state oxidation currents were not observed. Particularly, DA oxidation signal decreases as cycle numbers increase. However, when using pre-treated electrodes, a stable DA response was obtained on continuous cycling (steady state). This is characterised by overlapping DA redox peak obtained after 1st cycle (Figure 4.12(b)). In the case of S-β-CD modified CPE, voltammograms obtained when electrode was run directly in DA solution is characterised by unstable, increasing cycles as shown in Figure 4.13(a). Stable cycles are obtained when the modified electrode was placed in DA solution at least five minutes before cyclic voltammograms

were recorded (Figure 4.13(b)). These simple pre-treatment methods were used throughout the thesis unless otherwise stated.

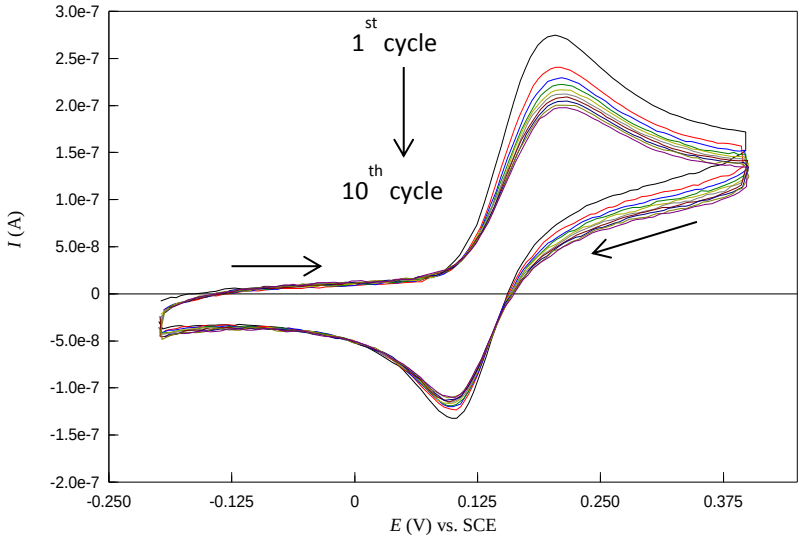

(a)

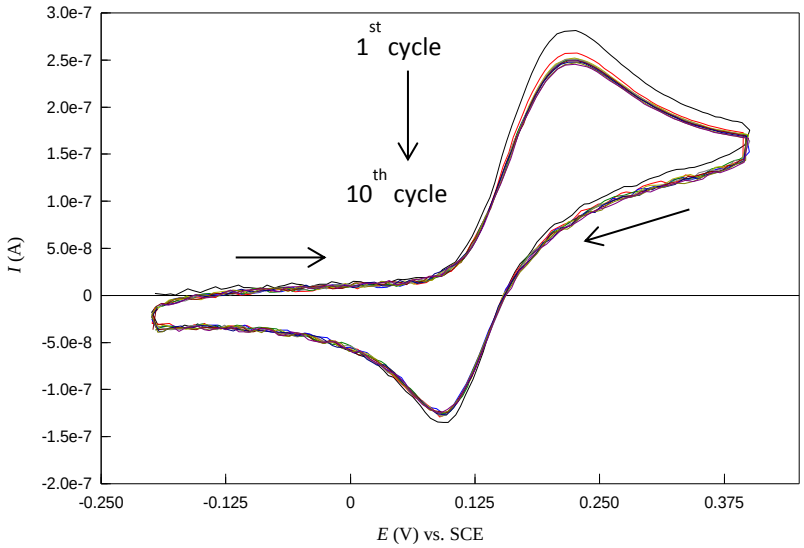

(b)

Figure 4.12: Cyclic voltammetry of DA (5 x10^{-5} M) at bare CPE, (a) electrode placed directly in DA solution, (b) electrode run in PBS prior DA solution.

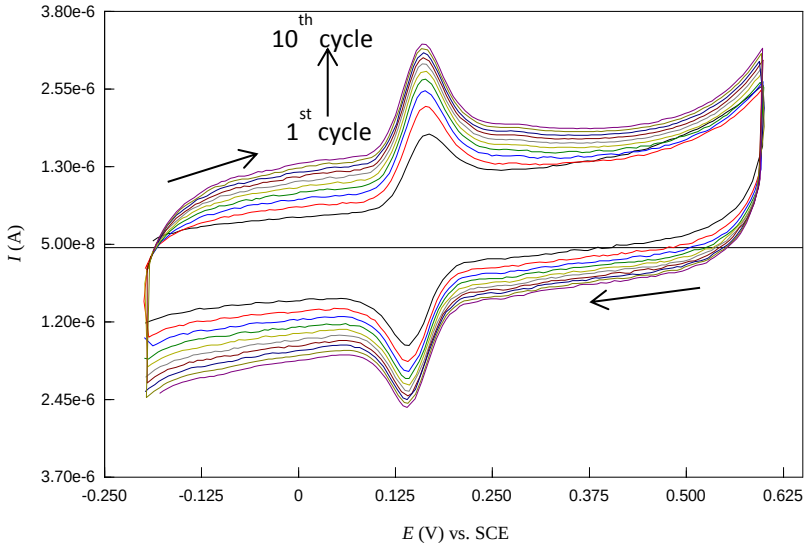

(a)

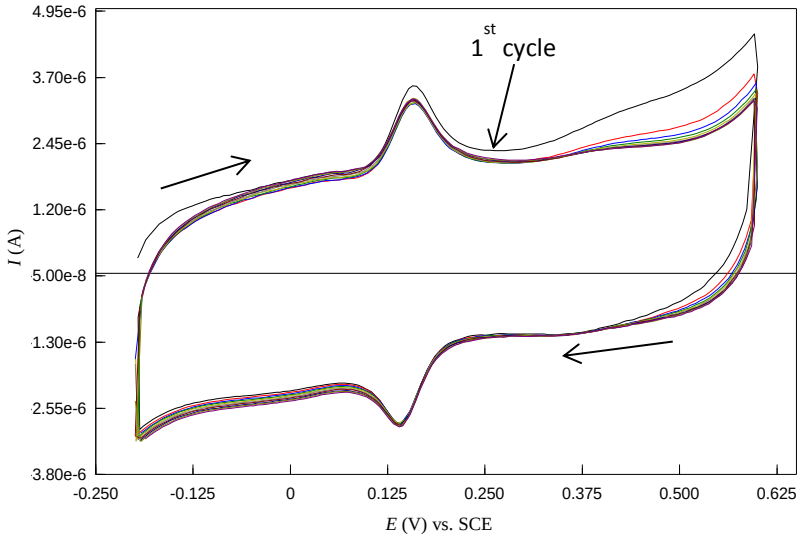

(b)

Figure 4.13: Cyclic voltammetry of DA (5 x10^{-5} M) at bare S-β-CD modified CPE, (a) electrode placed directly in DA solution, (b) electrode run in PBS prior DA solution.

4.2.4 DA Electrochemical Redox Process at Carbon Paste Electrode with Oxide Layer

A considerable attention is being given to the study of oxide materials because of their pronounced influence on the catalytic, ion-exchange, adsorption, and other properties of carbon materials. Although, oxide species was removed from the electrode surface to avoid potential interference with DA, their effect at the surface of electrodes on the electrochemical behaviour of DA appears interesting. In fact, it was found that oxides have a positive effect on the redox properties of DA when a relatively high concentration (of DA) is used. For instance, an oxide containing electrode showed a

better oxidation peak current for 5×10^{-5} M DA compared with corresponding electrode free oxide.

4.2.4.1 DA response at oxide / S-β-CD modified CPE and oxide / bare CPE

Cyclic voltammograms at oxide containing and oxide free S-β-CD modified CPE were recorded in 5×10^{-5} M DA solution as displayed in Figure 4.14. As can be seen, the peak potential separation of 0.016 V vs. SCE and a peak current increase (1.50×10^{-6} A) were observed at oxide / S-β-CD modified CPE, showing that the electron transfer rate is possible and even enhanced at oxide / S-β-CD containing electrode. ΔE_p and I_{pa} for DA at oxide free S-β-CD modified CPE being respectively 0.016 V vs. SCE and 8.44×10^{-7} A. So, based on ΔE_p, the rate of electron transfer rate is the same in both cases. However, DA signal is much more improved at oxide containing S-β-CD modified CPE due to some interactions between DA and oxides at the modified electrode surface. It is important to mention that the modified electrode in both cases contain the same relatively small amount of S-β-CD (0.095 g). Therefore, the difference between the intensity of DA signal is clearly dependent on the presence of oxide species.

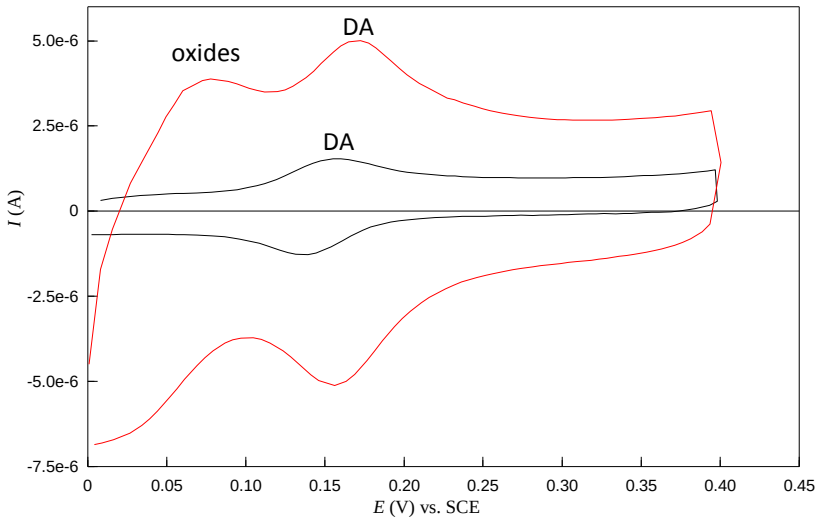

Figure 4.14: Cyclic voltammetry of DA (5×10^{-6} M) at oxide covered S-β-CD modified CPE (—) and oxide free S-β-CD modified CPE (—). Supporting electrolyte PBS (0.1 M); scan rate 50 mV / s.

The availability of DA near or on the electrode surface may have been increased by the presence of oxide functional groups. Although, functional groups forming the oxides have been discussed in Chapter 3, the categorisation of redox systems (included DA) according to their sensitivity to surface oxide naturally leads to questions about electron

transfer mechanisms. A variety of possible mechanisms have been identified for carbon surfaces including, but not limited to, (1) outer sphere [40], (2) bridging by either a ligand or a surface group [41, 42], (3) redox mediation [43, 44], (4) adsorption to surface sites [45], (5) electrostatic effects [46] and (6) proton and electron transfer [47]. Although, the mechanism must involve some interactions between surface electrode and the redox systems, and based on the diversity of surface oxides, the nature of the specific interactions is not obvious. In the case of DA, the enhancement of peak current at S-β-CD modified CPE may result from a combination of both S-β-CD and oxides ability to interact with DA molecules. The inclusion complex formed between DA and S-β-CD and a probable electrostatic interaction or bonding sites of surface oxides may permit enhancement of DA signal. The redox behaviour of DA at oxide / bare CPE (without S-β-CD) was also examined. Figure 4.15(a) shows the voltammograms at oxide free and CPE with oxide layer, run in 5×10^{-5} M DA in the potential range [0.0 V, +0.6 V] vs. SCE at 50 mV / s. Two main observations can be made. Firstly, clear oxidation and reduction peaks for DA located at 0.154 V and 0.125 V vs. SCE, respectively, were observed yielding a ΔE_p value of 0.029 V. When the same concentration of DA and electrochemical window were considered for oxide free bare CPE, and a ΔE_p value of 0.208 V vs. SCE was obtained (Figure 4.15(b)). Next, the residual current was considerably increased at oxide covered electrode, due to the presence of oxide species at the electrode surface. These observations suggest that the presence of oxides at the CPE surface helps to promote electron transfer and / or charging processes at the electrode / solution interface. The issue with oxide-containing electrodes arise when lower DA concentrations are used. From the voltammograms presented, oxidation peak current of oxide and DA are very close, therefore DA signal is masked by the oxide peak when relatively smaller DA concentration is used. This is discussed in detail in Chapter 5.

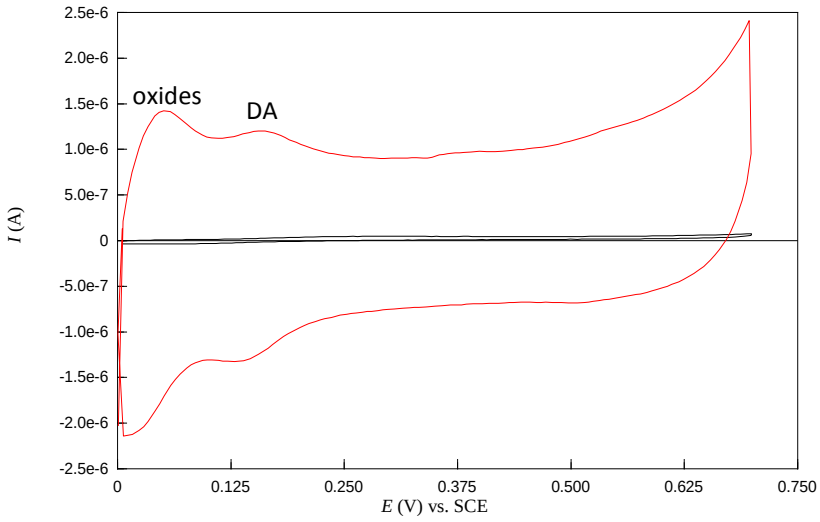

(a)

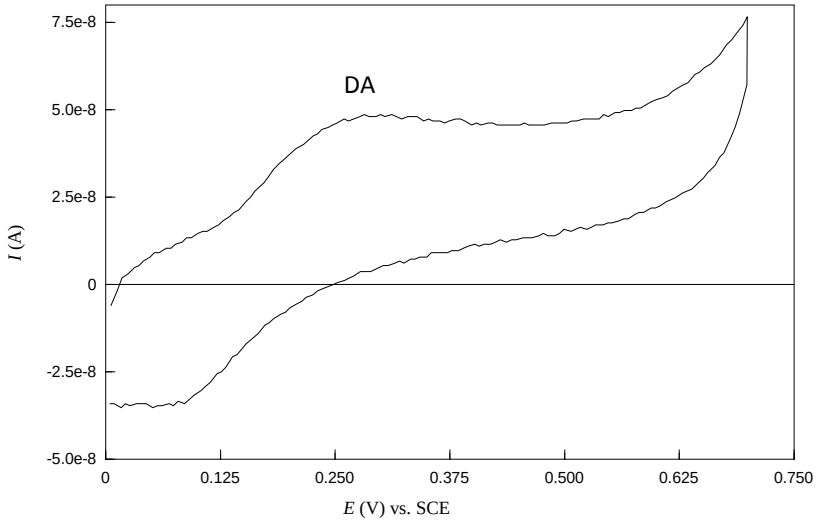

(b)

Figure 4.15: Cyclic voltammetry of DA (5×10^{-5} M) at CPE with oxide layer (—) and bare CPE (—) (a), highlighted voltammogram at bare CPE (b).
Supporting electrolyte PBS (0.1 M); scan rate 50 mV / s.

4.2.4.2 Reproducibility at oxide / S-β-CD modified CPE

Oxides species at the electrode surface can affect reproducibility of DA oxidation, and an investigation was carried out using cyclic voltammetry [48]. In order to investigate reproducibility of voltammograms at oxide containing electrodes, data (n = 3) were recorded in 5×10^{-5} M DA (pH 6.8) at 50 mV / s. Each voltammogram was obtained using a fresh CPE surface. As shown in Figure 4.16(a), the voltammograms were not reproducible under these conditions. Electrode preparation is particularly important for achieving reproducible electrochemical behaviour. Even the most common preparation

procedures, such as polishing, significantly modified the surface structure and this can have dramatic effects on reactivity. After exploring several parameters, it was found that accumulation time slightly improved reproducibility of voltammograms, although DA response was not really reproducible. Figure 4.16(b) shows that cyclic voltammograms of 5×10^{-5} M DA at oxide containing S-β-CD modified CPE almost overlap, when electrode is allowed to stand in DA solution for 2 minutes before recording the voltammograms. Difficulties in efficient reproducibility probably arise from the type and distribution of oxide functional groups at electrode surface. Although, the importance of particular surface oxides to electrode kinetics at carbon electrodes is well recognized [49], their surface coverage is hard to control. The type of carbon material, its pre-treatment, exposure to air or electrolyte, can all affect the total oxide coverage on a particular carbon surface.

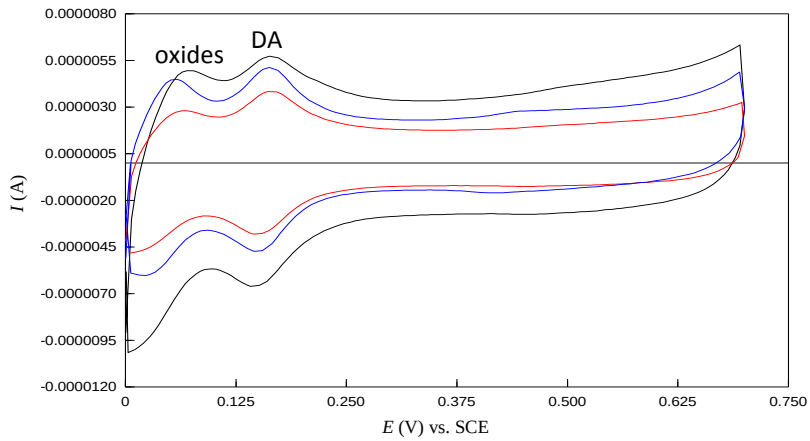

(a)

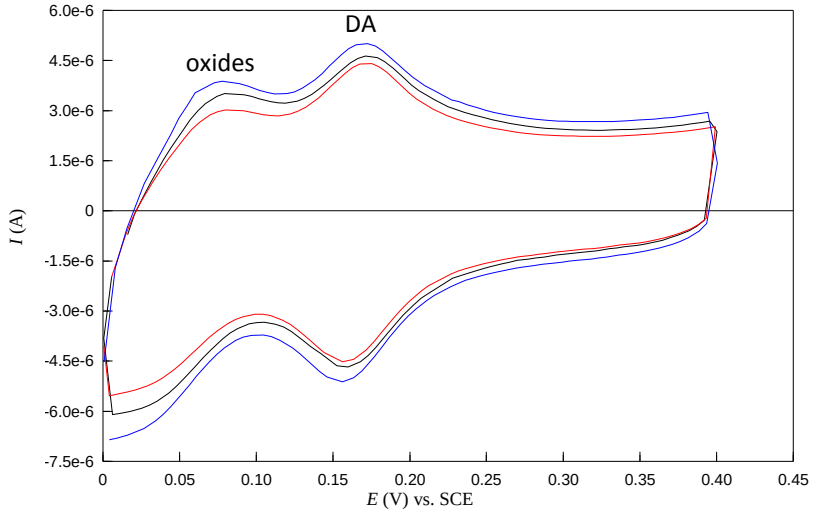

(b)

Figure 4.16: Cyclic voltammetry of DA (5×10^{-5} M) at oxide containing S-β-CD modified CPE, (a) with 2 seconds accumulation time, (b) 120 seconds accumulation time. Supporting electrolyte PBS (0.1 M); scan rate 50 mV / s.

4.2.4.3 Effect of scan rate on DA response at oxide containing S-β-CD modified CPE

The influence of scan rate on DA oxidation at oxide containing S-β-CD modified CPE was investigated by cyclic voltammetry (Figure 4.17(a)). The oxidative peak current of 5×10^{-5} M DA solution increases linearly with scan rates in the range of 10 to 80 V vs. SCE. It was therefore assumed that the electrode reaction of DA at oxide containing S-β-CD modified CPE was typically of an adsorption controlled process. In addition, the positive oxidation peak potential E_{pa} (0.173 V) is constant with increase of the scan rate. This indicates the reversible nature of the oxide containing S-β-CD modified CPE reaction. The enhancement on the remarkable adsorption characteristics of oxide containing electrodes may be probed by interaction of specific oxide functional groups such as carboxylate with protonated DA or some interactions such as hydrogen bonding. It is known that DA oxidation is significantly slower at diamond than glassy carbon electrodes, most likely because of adsorption effects [50]. DA can be catalysed by hydrogen bonding of surface carbonyls to adsorb DA molecules, and diamond does not provide necessary adsorption sites unless specifically treated.

(a)

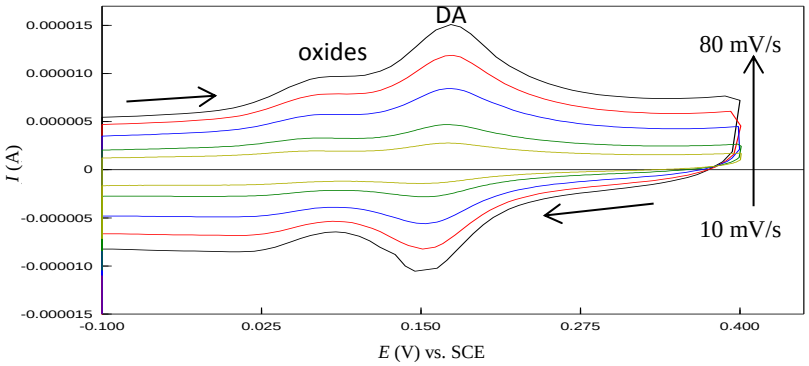

(b)

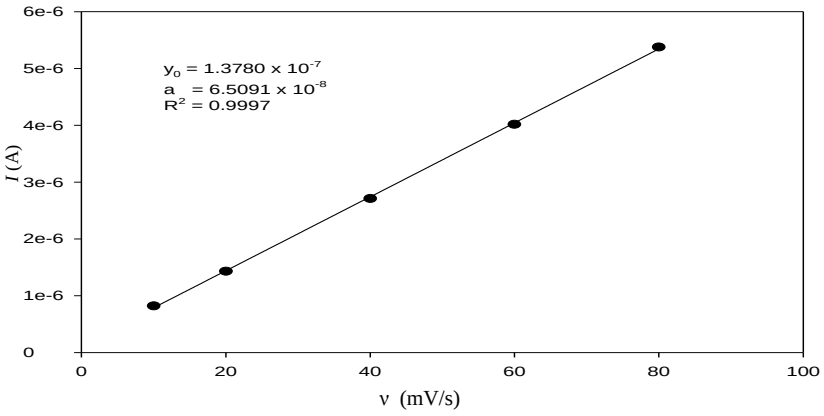

Figure 4.17: Cyclic voltammograms for the effect of variation of scan rates of DA (5×10^{-5} M) at oxide containing S-β-CD modified CPE from 10 to 80 mV / s (a) and corresponding variation of oxidation peak current as a function of scan rate (b). Supporting electrolyte 0.1 M PBS (pH 6.8).

4.2.4.4 Potentiostatic removal of DA species from electrode surface

One of the main advantages of CPEs is the comfortable renewal of their surface. This is done in few seconds by wiping off the used surface layer on a weighing paper to obtain a fresh surface. Although, this characteristic method of CPE was mostly used in this thesis, another way of regenerating the CPE surface was also examined. Firstly, a background current was obtained, using S-β-CD modified CPE (Figure 4.18(a)). Then, the electrode was placed in 5×10^{-5} M DA solution for 2 minutes and the peak current recorded to be 6.12×10^{-6} A as shown in Figure 4.18(b). The electrode was removed from the DA solution, rinsed thoroughly with distilled water, and immersed in the supporting electrolyte solution. The resulting voltammograms (in Figure 4.18(c)) shows an intense peak (9.23×10^{-7} A) corresponding to oxidation of adsorbed species at the electrode surface. The electrode was subjected to potentiostatic treatment (Figure 4.18(d)) by holding it at +1.0 V vs. SCE in the blank PBS for one minute to give a fresh electrode surface which is displayed in Figure 4.18(e). Finally the 'cleaned' electrode was immersed back in the initial DA solution for 2 seconds before the voltammograms recorded. The I_{pa} value obtained was 6.03×10^{-6} A as shown in Figure 4.18(f). This value is close to that obtained with a fresh CPE surface, confirming an alternative way to obtain a 'new' surface. This cleaning process not only allows the oxidation products of DA to exclude away from the electrode surface, but strongly suggests that S-β-CD molecules at the surface of the electrode are active after removal of DA species. The turnover characteristics of S-β-CD in the paste enable repeated interaction between S-β-CD and DA molecules to produce peak current intensities similar in magnitude to those obtained before potentiostatic treatment. It has to be noted this experiment was done in triplicate and gave an acceptable mean ratio of 0.998 between DA I_{pa} values before and after potentiostaic treatment as shown in Table 4.3.

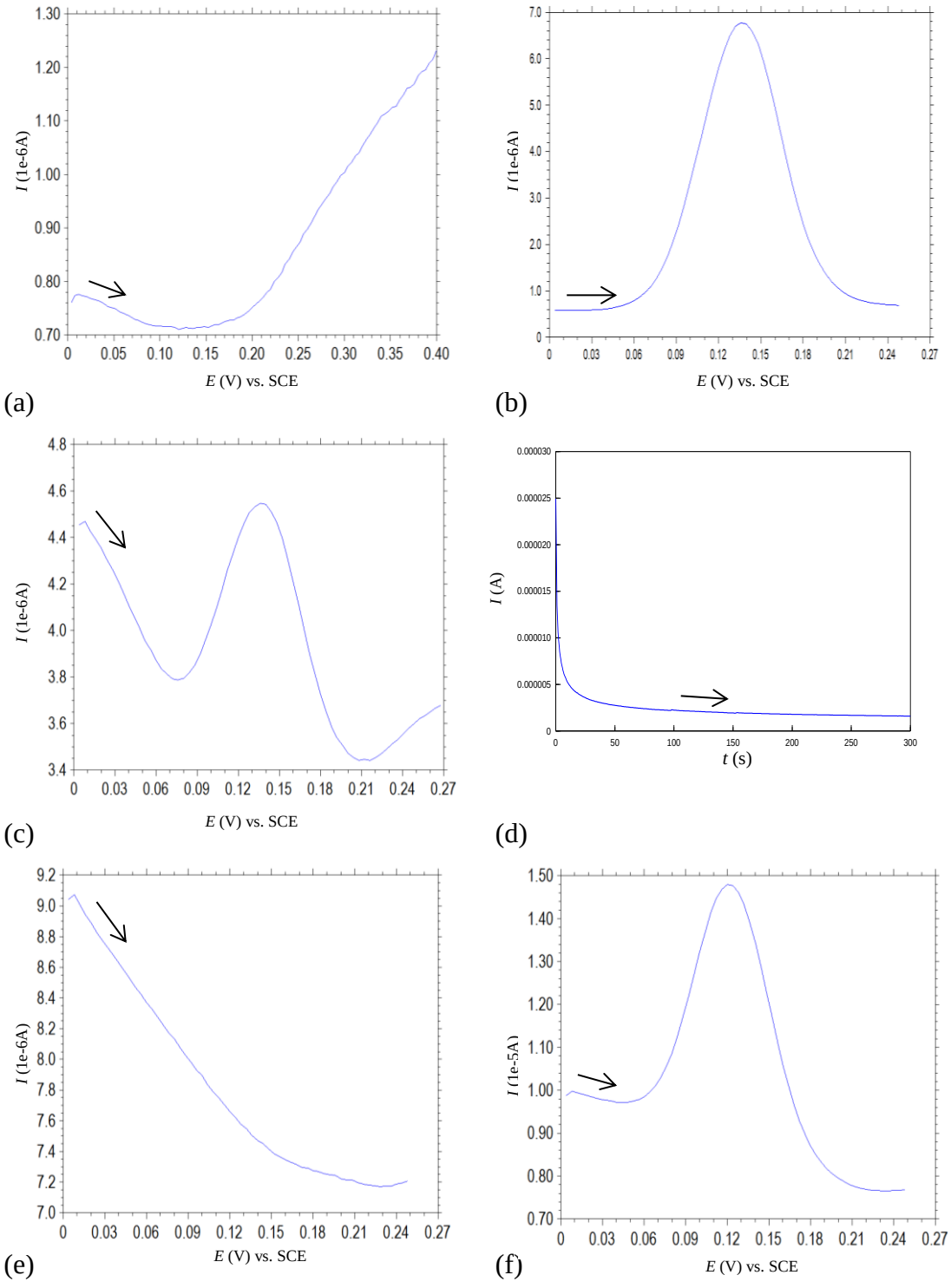

Figure 4.18: Differential pulse voltammograms recorded at S-β-CD modified CPE. Voltammograms recorded in 0.1 M PBS (a) and 5 × 10^{-5} M DA (b). Electrode rinsed and voltammogram obtained in 0.1 M PBS (c). Potentiostatic treatment of the modified electrode in 0.1 M PBS (d) and voltammogram obtained in 0.1 M PBS showing removal of oxidation peak (e) and subsequent detection of 5 × 10-5 M DA (f).

Table 4.3: potentiostatic treatment for removal of DA species from S-β-CD modified CPE surface

DA I_{pa} before potentiostaic treatment (A)	DA I_{pa} after potentiostaic treatment (A)	DA I_{pa} ratio	Mean value of DA I_{pa} ratio
6.12×10^{-6}	6.03×10^{-6}	1.015	
5.89×10^{-6}	5.97×10^{-6}	0.987	0.998
6.07×10^{-6}	6.11×10^{-6}	0.993	

4.2.5 Protonated S-β-CD Modified CPE

Sulfated cyclodextrin can be obtained as single isomers or as randomly sulfated mixtures. Most of the commercially available sulfated cyclodextrin are mixture of randomly sulfated species [51, 52]. For randomly substituted cyclodextrins in general, only the average degree of substitution is known with certainty while the actual isomeric heterogeneity and / or charge distribution are not conclusively determined. Commercially available sulfated cyclodextrin used in this thesis was obtained from Sigma-Aldrich. It has approximately 7 to 11 sulfated groups per cyclodextrin. Meaning between 7 and 11 negative charges associated with it, which are counterbalanced with sodium ions as illustrated in Figure 4.19. Sulfated ends are at position 2 and 6, with position 3 intact with OH group [51].

In general, H^+ ion conducts better than metal ion such as Na^+. In addition, H^+ ion has a smaller size compared to Na^+. Therefore H^+ has a higher mobility in water.

In an attempt to increase sensitivity, the H^+ form of S-β-CD was obtained by recrystallisation after adjusting the pH of commercially available S-β-CD (using 0.1 M HNO_3 solution).

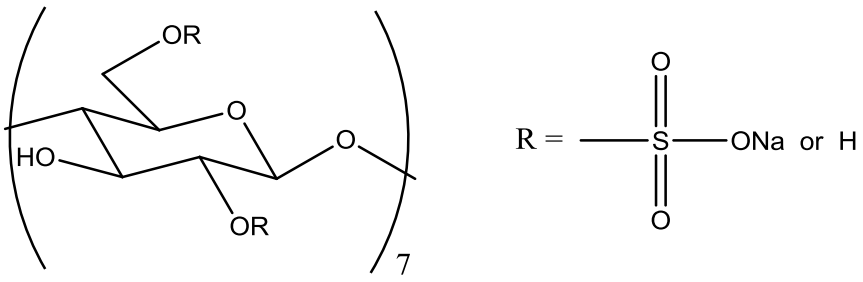

Figure 4.19: Chemical structure of β-Cyclodextrin, sulfated sodium salt (S-β-CD).

4.2.5.1 Conductivity measurements

Conductivity measurements were performed on both forms of sulfated cyclodextrin (commercially available S-β-CD and prepared H^+ form of S-β-CD). Typically, 0.211 g of each form was dissolved in 10 mL Milli Q water and conductivity recorded in triplicate. The average value of conductivity and corresponding pH and temperature are displayed in Table 4.4. Clearly, the prepared H^+ form of S-β-CD has conductivity two times higher than that of commercially available sulfated.

Table 4.4: Conductivity measurements of H-S-β-CD and Na-S-β-CD

CD compound	Conductivity (μS)	pH	Temperature (˚C)
H-S-β-CD	555	2.53	23.6
Na-S-β-CD	274	5.37	23.6

4.2.5.2 DA electrochemical redox process at protonated S-β-CD modified CPE

A modified CPE containing as-prepared H-S-β-CD (0.545 g) was fabricated using similar conditions and method utilised for S-β-CD modified CPE, which was described in Chapter 3. Cyclic voltammograms were obtained by placing H-S-β-CD modified CPE in 5×10^{-6} M DA at 50 mV / s. This relatively small concentration was chosen to test the sensitivity of the electrode. As shown in Figure 4.20, the voltammograms do not show distinct DA redox peaks. Under identical conditions, an oxidation peak current of 2.79×10^{-7} A was determined at commercially available sulfated cyclodextrin (Na-S-β-CD). H-S-β-CD was expected to have a better dissociation of sulfonic acid group at pH 6.8 to give corresponding sulfate anion, which would result in a strong electrostatic interaction with protonated DA. However this was not the case. The poor response at H-S-β-CD modified CPE requires further investigations.

(a)

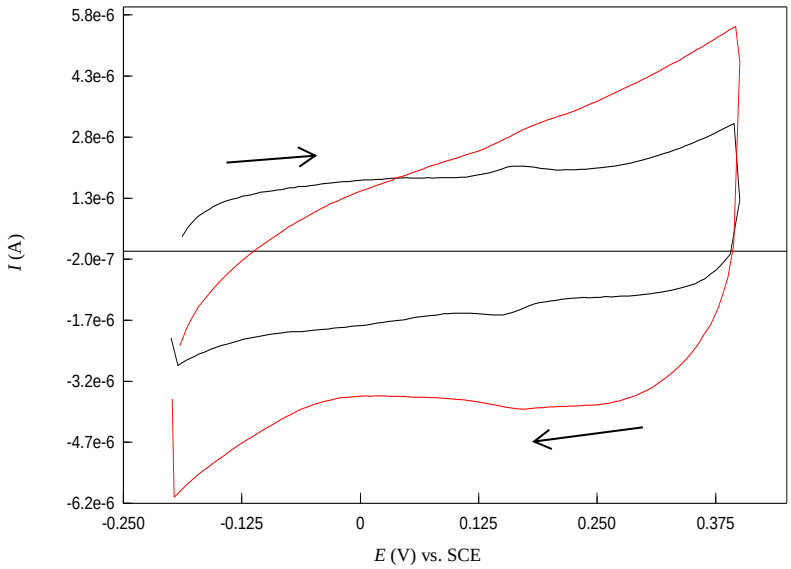

(b)

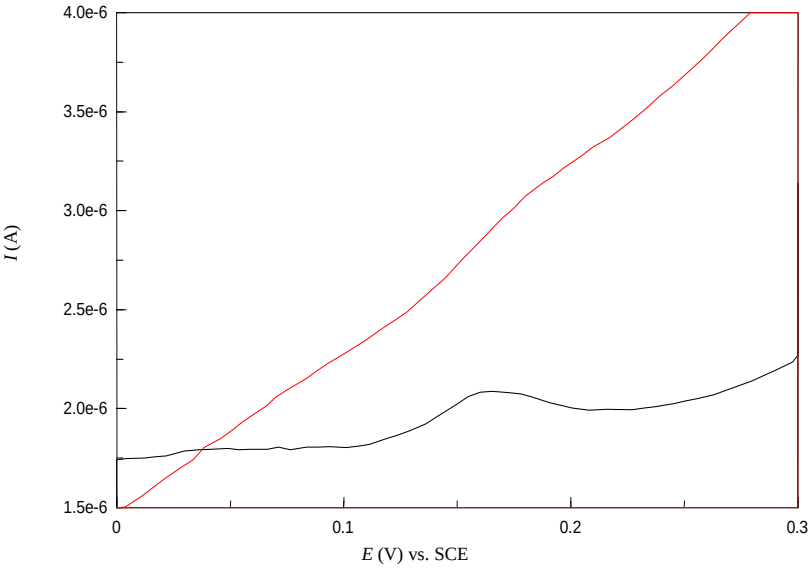

Figure 4.20: Cyclic voltammetry of DA (5 × 10^{-6} M) at H-S-β-CD modified CPE (—) and Na-S-β-CD modified CPE (—) (a) and their highlighted anodic peak (b). Supporting electrolyte PBS (0.1 M); scan rate 50 mV / s.

4.2.6 Carboxymethyl-β-CD Modified CPE

Carboxymethyl-β-CD (CM-β-CD) is another interesting anionic (and commercially available) cyclodextrin derivative. Compared to Neutral β-CD, improved molecular recognition with DA can be observed with CM-β-CD due to the binding properties of its cavity, combined with the charged carboxylic group at the primary or secondary site. CM-β-CD was employed as the second type of modifier for the detection of DA. The modified electrode was conveniently prepared by mixing CM-β-CD with carbon paste. The electrochemical sensor showed excellent response for determination of DA.

4.2.6.1 DA electrochemical redox process at CM-β-CD modified CPE

CM-β-CD modified CPE was prepared the same way as the S-β-CD modified CPE. Typically, 0.595 g CM-β-CD (corresponding to the optimal amount of S-β-CD) was inserted into the carbon paste. A redox peak of DA was observed when the modified electrode was placed into DA solution and analysed using cyclic voltammetry. It was observed that CM-β-CD modified CPE exhibited excellent electron transfer characteristics in the oxidation of DA. To demonstrate this, DA signal intensity at CM-β-CD modified CPE was compared to that at S-β-CD modified CPE. Figure 4.21 shows the cyclic voltammograms of 5×10^{-5} M DA in a pH 6.8 PBS at S-β-CD modified CPE and CM-β-CD modified CPE. The anodic peak current obtained at CM-β-CD modified CPE was 2.99×10^{-6} A, marginally higher than that of S-β-CD modified CPE (2.43×10^{-6} A). The anodic peak potential and corresponding cathodic peak appeared at 0.170 V and 0.140 V (vs. SCE). ΔE_p is 0.030 V, which suggests a reversible reaction process, is occurring at the CM-β-CD modified CPE. Yang *et al* [53] reported on similar reversibility for CM-β-CD in a polymer film composite. Moreover, the oxidation peak currents of DA at CM-β-CD modified CPE were far greater than those obtained at the bare CPE. The reason for the high peak current may originate from the structure of CM-β-CD and consequent interaction with DA. Commercially available CM-β-CD utilised in this study has an average degree of substitution of 3 carboxylic groups per molecule. It is in a sodium salt form as shown in Figure 4.22. At pH 6.8, the carboxylic group at the primary or secondary site of the cyclodextrin should be negatively charged (pK_a of COOH group being around 4.6 [54]). DA may be electrostatically attracted to CM-β-CD via carboxylate moiety and facilitate inclusion of DA into cyclodextrin cavity.

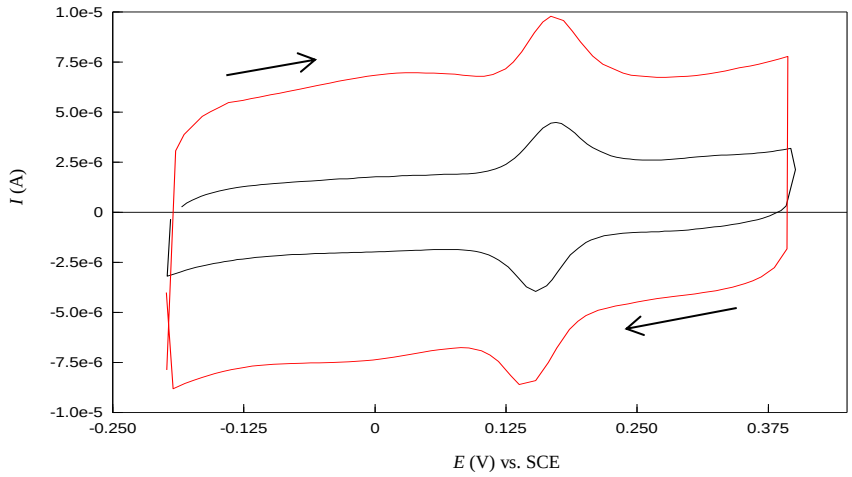

Figure 4.21: Cyclic voltammetry of DA (5×10^{-5} M) at CM-β-CD modified CPE (—) and S-β-CD modified CPE (—). Supporting electrolyte PBS (0.1 M); scan rate 50 mV / s.

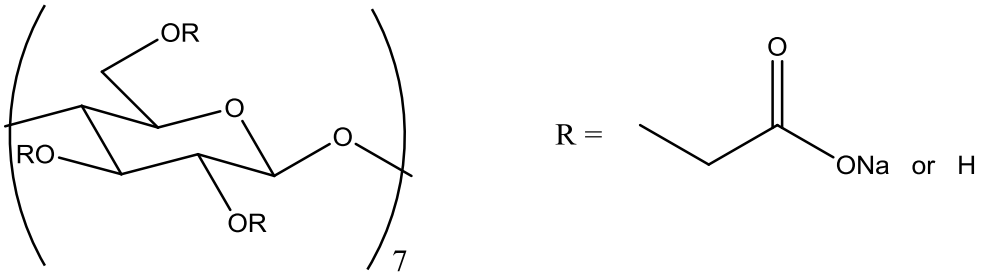

Figure 4.22: Chemical structure of Carboxymethyl β-Cyclodextrin sodium salt (CM-β-CD).

4.2.6.2 Effect of scan rate on peak current

The effect of scan rate on the peak current of DA was investigated, using cyclic voltammetry as shown in Figure 4.23(a). It showed that I_{pa} increased gradually with increasing the scan rates. The oxidation peak current of DA was directly proportional to the scan rates in the range of 10 to 80 mV / s, which suggested that an adsorption-controlled process of DA on the modified CM-β-CD modified CPE. The linear regression equation is such as I_{pa} (A) = 3.065×10^{-8} ν + 6.533×10^{-7} with a correlation coefficient, R^2, 0.9871 (Figure 4.23(b)).

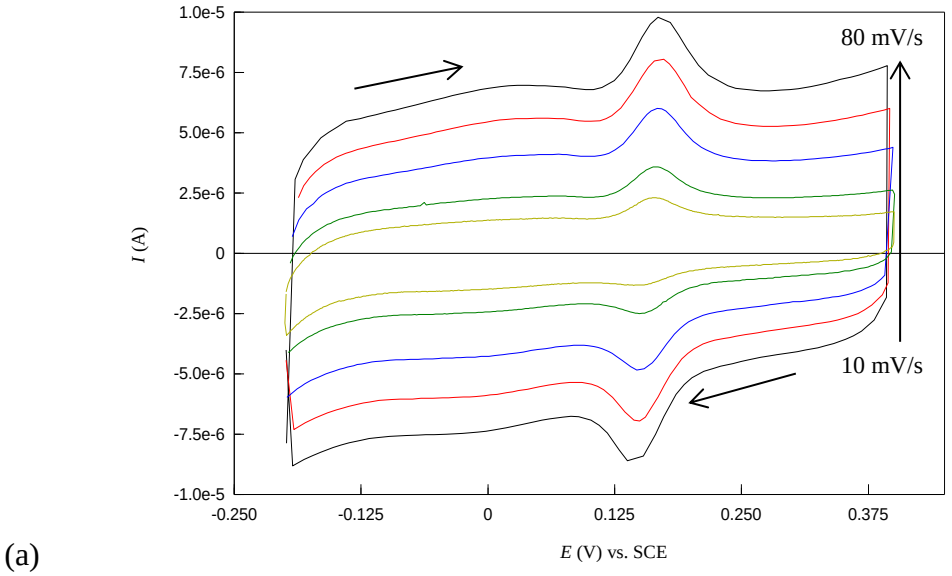

(a)

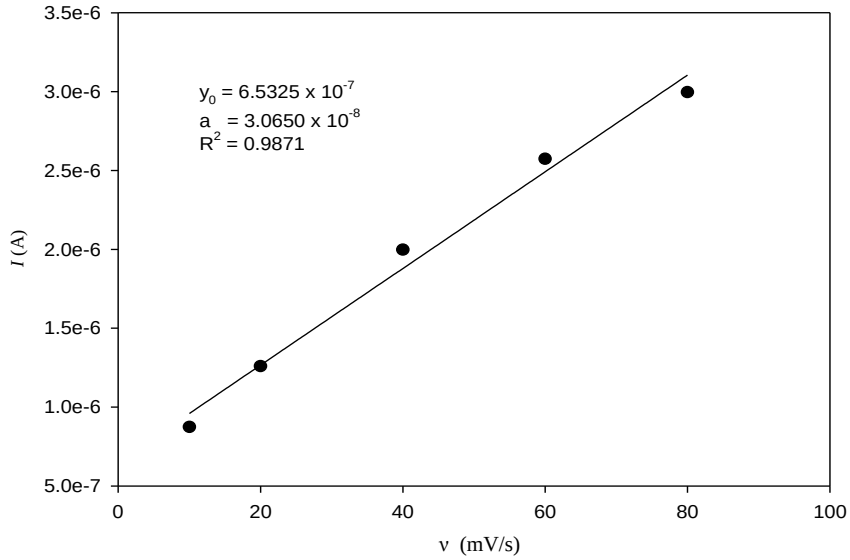

(b)

Figure 4.23: cyclic voltammograms for the effect of variation of scan rates of DA (5×10^{-5} M) at CM-β-CD modified CPE from 80 to 10 mV / s (a) and corresponding variation of oxidation peak current as a function of scan rate (b). Supporting electrolyte 0.1 M PBS (pH 6.8).

Because both types of cyclodextrin showed good electrochemical response towards detection of DA, a combination of both recognition elements on the DA signal was investigated. The electrode was prepared using an equal amount of S-β-CD and CM-β-CD. Typically, 0.2725 g of each cyclodextrin derivative was mixed with the carbon paste. The constructed electrode, containing a total of 0.545 g cyclodextrin was investigated under cyclic voltammetry at different scan rates, in 5×10^{-5} M DA solution and shown in Figure 4.24(a). Although, the oxidative peak current is proportional to scan rates with correlation coefficient of 0.9892 (Figure 4.25), the peak shape resembles to that obtained at CM-β-CD modified CPE. For clarity, the oxidation peaks at S-β-CD

modified CPE, CM-β-CD modified CPE and mixed (S-β-CD / CM-β-CD) modified CPE are highlighted and shown in Figure 4.24(b). The peak is perfectly symmetrical in the case of CM-β-CD modified CPE and mixed (S-β-CD / CM-β-CD) modified CPE. The shape of peak wave in this case suggests a stronger adsorption process for CM-β-CD modified CPE compared to the corresponding S-β-CD modified CPE. The effect of CM-β-CD modified CPE in the mixture seems to predominate in the sensing of DA (as reflected through its 'own' DA signal). Although, the background current of CM-β-CD modified CPE is higher than that of S-β-CD modified CPE, the oxidation peak potential remains the same (0.17 V vs. SCE). Additionally, the background current, recorded fall between that of S-β-CD modified and the S-β-CD / CM-β-CD mixture. Although, the results indicated that CM-β-CD modified CPE gives a higher oxidation peak current of DA compared to mixed (S-β-CD / CM-β-CD) modified CPE, the combination of both charged form of cyclodextrin may have a better application in interference studies, when DA is detected in presence of serotonin, as discussed in Chapter 5.

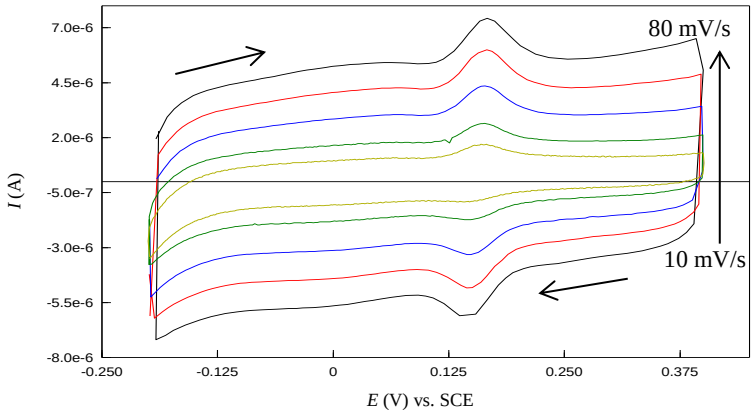

(a)

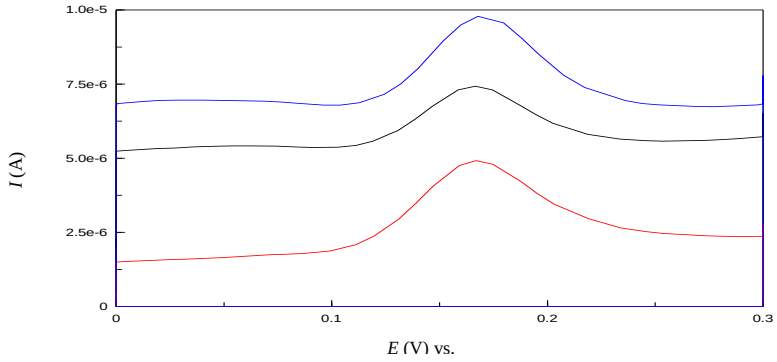

(b)

Figure 4.24: Cyclic voltammograms of DA (5×10^{-5} M) in PBS (0.1 M), pH 6.8 with different scan rates, from 10 to 80 mV / s at (a) S-β-CD / CM-β-CD modified CPE, (b) oxidation peak at CM-β-CD modified CPE (—), and S-β-CD / CM-β-CD modified CPE (—), S-β-CD modified CPE (—).

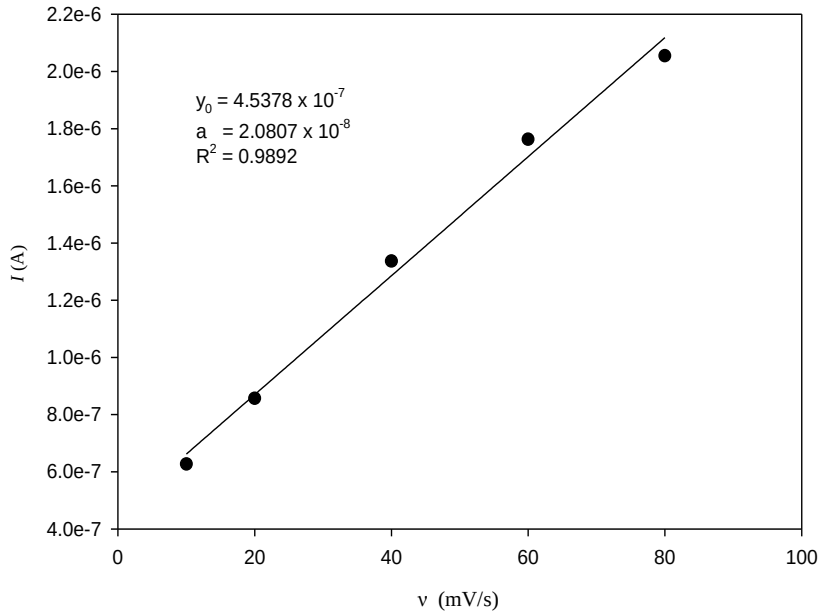

Figure 4.25: The variation of oxidation peak current for DA (5×10^{-5} M) at S-β-CD / CM-β-CD modified CPE as a function of scan rate. Supporting electrolyte 0.1 M PBS (pH 6.8).

4.2.7 Neutral β-CD Modified CPE

The electrochemical behaviour of cyclodextrin inclusion complexes with redox active guests has been well explored in the past 20 years [55]. The interaction of DA and neutral cyclodextrin was utilised to accelerate the diffusion of DA in cyclodextrin modified electrodes in previous reports [33].

In this section, a neutral β-CD modified CPE was prepared, mainly to compare its electrochemical performance characteristics in oxidation of DA with charged β-CD, namely S-β-CD modified CPE and CM-β-CD modified CPE.

4.2.7.1 DA electrochemical redox process at neutral β-CD modified CPE

As opposed to S-β-CD or CM-β-CD, neutral β-CD only possesses hydroxyl group at the primary and secondary rims, thus it is not charged at pH 6.8. Neutral β-CD behaves as a suitable host for a range of molecules for inclusion in its cavity including DA. Previous research suggests that neutral β-CD can certainly bind DA in solution and the dissociation constant of DA-β-CD inclusion complex is 3.56×10^{3} M^{-1} [56]. Therefore, it is necessary to compare the electrochemistry of DA at neutral β-CD modified CPE and relevant cyclodextrin analogue composites. In this study, the behaviour of neutral β-CD modified CPE in 5×10^{-5} M DA solution was investigated by cyclic voltammetry.

Figure 4.26 shows an oxidation peak located at 0.150 V and a corresponding reduction peak at 0.098 V vs. SCE. The peak potential separation was 0.052 V, indicative of a quasi-reversible system. The oxidation peak current, I_{pa}, was 1.50×10^{-6} A, higher than that of bare CPE (2.25×10^{-7} A). Thus, Neutral β-CD modified CPE exhibits an enhanced electrochemical response to DA oxidation. However, the oxidation peak value at Neutral β-CD modified CPE is much smaller than that obtained at S-β-CD modified CPE and CM-β-CD modified CPE, respectively. These results also indicate that the negative charge on cyclodextrin plays an important role in recognising DA. The charged cyclodextrin derivatives facilitate the insertion of DA into their cavity via electrostatic interaction between $-OSO_3^-$ and $-COO^-$ groups with protonated DA. The response mechanism of Neutral β-CD modified CPE for DA is only based on the inclusion interaction of Neutral β-CD for DA; the main driving force for complex formation being hydrophobic interaction. However, for both S-β-CD modified CPE and CM-β-CD modified CPE, it is a combination of electrostatic and inclusion interactions.

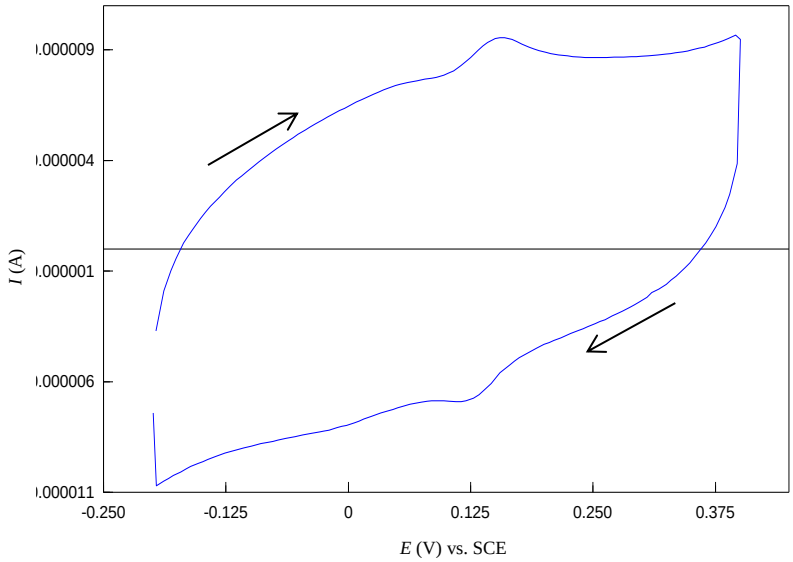

Figure 4.26: Cyclic voltammogram of DA (5×10^{-5} M) at Neutral β-CD modified CPE in PBS (0.1 M), pH 6.8; scan rate 50 mV / s.

4.2.7.2 Effect of scan rate on peak current

To investigate the mechanism of the electrochemical oxidation of DA at neutral β-CD modified CPE, the influence of scan rate on the voltammetric response of DA was studied. Figure 4.27(a) shows the cyclic voltammograms of DA at different scan rate ranging from 10 to 100 mV / s vs. SCE. It is clear that the oxidation peak currents are enhanced with increasing of the scan rate and linearly proportional to the scan rate (Figure 4.27(b)). The regression equation is I_{pa} (A) = 5.404×10^{-9} ν $+1.055 \times 10^{-7}$, with

a correlation coefficient of 0.9898. This suggests that the electrode reaction corresponds to an adsorption-controlled process in the studied scan rate range. The electron transfer process was identical to the one observed at both S-β-CD modified CPE and CM-β-CD modified CPE. Although, the peak currents are different in all three types of modified electrodes, it is clear that DA oxidation at the modified electrodes is enhanced by DA interaction with cyclodextrin recognition elements.

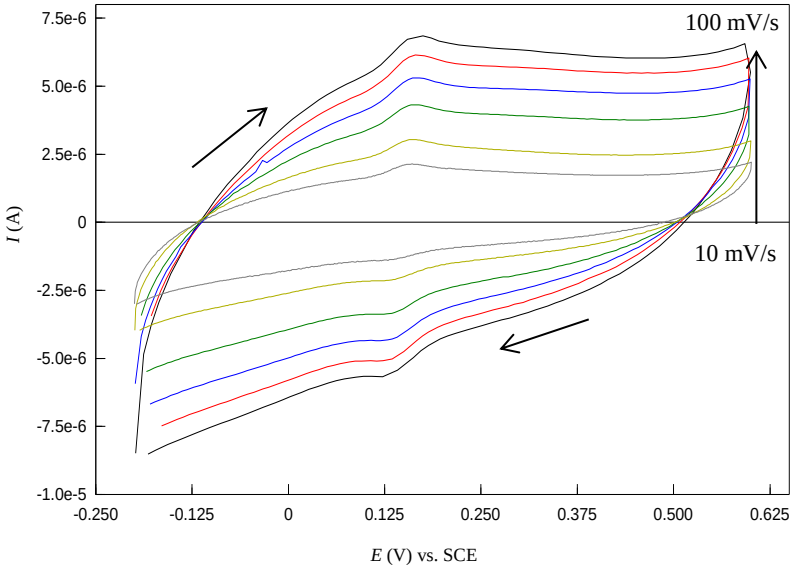

(a)

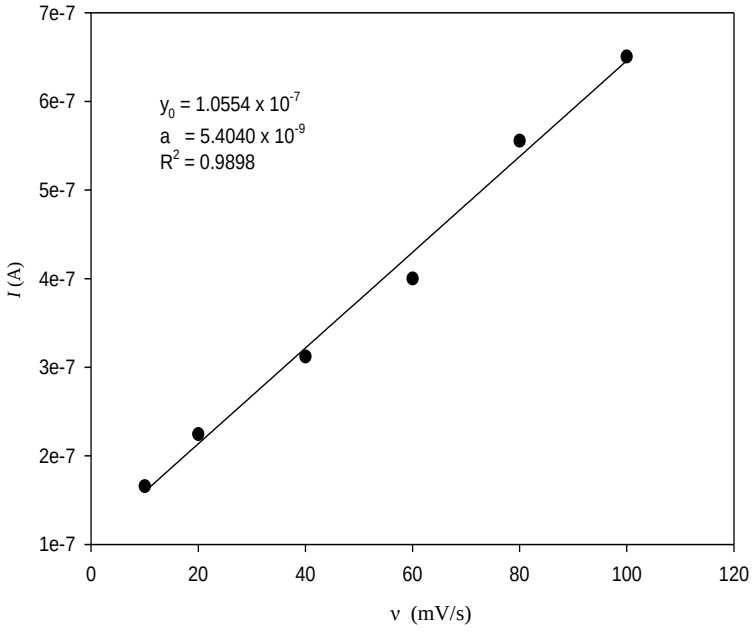

(b)

Figure 4.27: Cyclic voltammograms for the effect of variation of scan rates of DA (5×10^{-5} M) at Neutral β-CD modified CPE from 100 to 10 mV / s (a) and corresponding variation of oxidation peak current as a function of scan rate (b). Supporting electrolyte 0.1 M PBS (pH 6.8).

4.2.8 Fc-β-CD modified CPE

In order to verify the possibility of using the Fc-β-CD inclusion complex as an efficient electron-transfer mediator, studies in presence of DA were carried out. Ferrocene is widely used as effective mediator for electron transport in bioelectrocatalysis [57, 58], electro-oxidants in electrosynthesis [59], and electrochemical probes in electrochemical determination [60]. However, the use of Ferrocene as a electrochemical mediator in aqueous media is restricted due to sublimation and solubility of ferrocinium ion (Fc^+) [61], which may result in poor response to many electroactive substances. This problem can be solved by forming an inclusion complex of Ferrocene with β-CD.

In this study, an inclusion complex of Ferrocene with β-cyclodextrin (Fc-β-CD) was prepared and used to construct Fc-β-CD modified CPE. The results obtained and discussed in this section show that Ferrocene incorporated in β-CD cavity mediates electron transfer reaction of DA oxidation and can be used as an electrochemical sensor in aqueous solution.

4.2.9 Chemical Properties of Fc-β-CD complex

Ferrocene, namely bis-cyclopentadienyl iron (II), is a molecule with a sandwich-type structure in which the iron atom is sandwiched between two five-membered carbon rings. Ferrocene can form inclusion complex with β-CD in a 1:1 ratio. The structure of such complex formation is represented in Scheme 4.3. The complex has been shown to be stable, such that there are examples where the complex has been crystallised from water and is thermally stable up to the melting point of cyclodextrin ~200 °C [62]. The binding constant K_a has been reported to be in the range of $1 \times 10^{-3} – 1 \times 10^{-4}$ M^{-1} [63]. The main driving forces for the complex formation have been attributed to hydrophobic interactions, Van der Waals interactions, hydrogen bonding, and release of ring strain in the β-CD cavity [64-66].

In order to probe the possibility of using the Fc-β-CD inclusion complex as an efficient electron-transfer mediator, studies in presence of DA were carried out.

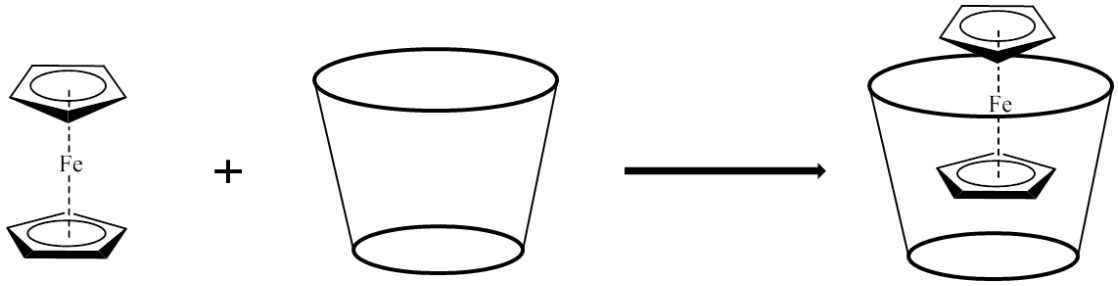

Scheme 4.3: Schematic representation of host-guest interaction between Ferrocene and Neutral β-CD.

4.2.9.1 Fc-β-CD modified CPE in phosphate buffer solution

The electrochemical behaviour of Fc-β-CD modified CPE was investigated in 0.1 M PBS (pH 6.8) by cyclic voltammetry at scan rate of 50 mV in the potential window ranging from +0.8 to −0.25 V vs. SCE. In the first part of this work, Fc-β-CD was drop-cast on bare CPE surface. A solution of nafion (0.05 % in ethanol) was added to Fc-β-CD (0.006g) and sonicated for one minute. 10 µL of the obtained mixture was loaded on the CPE surface, which was dried at room temperature for two hours before cyclic voltammetry was performed. The resulting voltammogram presented in Figure 4.28(a) shows clearly an oxidation and reduction peak occurring respectively at 0.230 V and 0.160 V vs. SCE. In the second part of the work, Fc-β-CD (0.006 g) was added to the bulk carbon paste. The voltammogram obtained when this modified electrode was run in 0.1 M PBS under similar conditions as the drop-cast method is shown in Figure 4.28(b). The oxidation and reduction peak potential (for bulk method) occur at 0.287 V and 0.220 V vs. SCE, respectively. In both cases, Ferrocene, from the complex, was oxidised to ferrocenium cation in a standard one electron process [67, 68] as illustrated in Equation 4.4. Ferrocene exhibits a reversible oxidation in PBS. The potential peak separation, ΔE_p, was found to be 0.063 V and 0.067 V vs. SCE respectively for drop-cast and bulk method.

$$Fc \leftrightharpoons Fc^{+} + e^{-} \qquad \text{Equation 4.4}$$

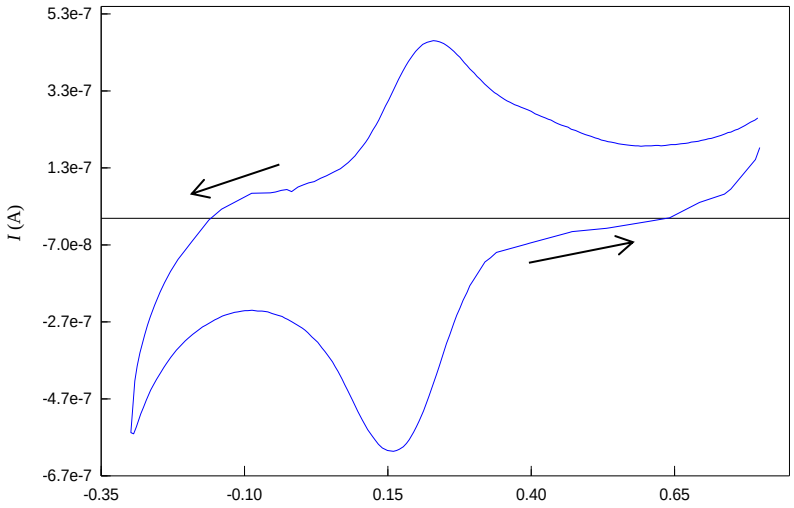

(a)

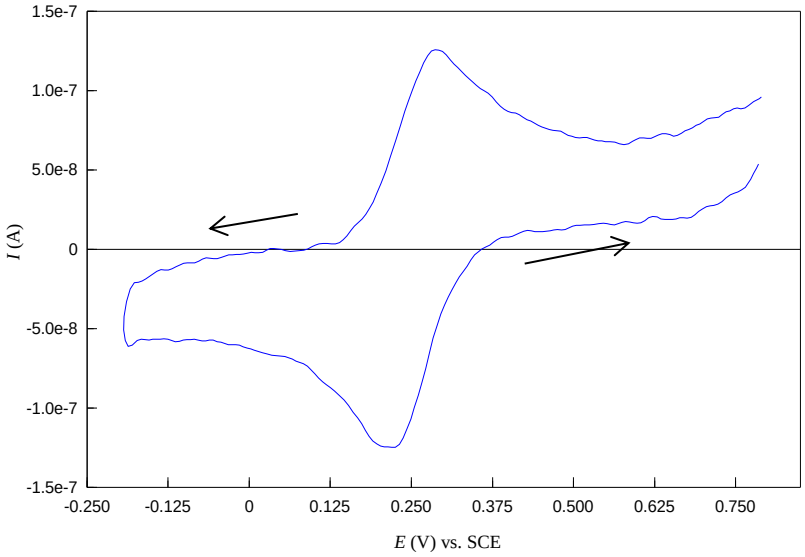

(b)

Figure 4.28: Cyclic voltammograms of PBS (0.1 M), pH 6.8 at Fc-β-CD modified CPE; (a) drop-cast method, (b) bulk composite method; scan rate 50 mV / s.

4.2.9.2 DA electrochemical redox process at Fc-β-CD modified CPE

The electrochemical behaviour of Fc-β-CD modified CPE (drop-cast method) in a DA solution was examined. In this experiment, the cyclic voltammograms of 7.1×10^{-5} M DA in 0.1 M PBS (pH 6.8) at Fc-β-CD modified CPE was obtained and compared to that of the bare CPE, under similar conditions. Figure 4.29 shows a higher peak current for the oxidation of DA at Fc-β-CD modified CPE (8.483×10^{-7} A) compared to the bare CPE (4.044×10^{-7} A). This current could be attributed to the catalytic activity of Ferrocene moiety from complex Fc-β-CD at the surface of the carbon paste. The resulting oxidative peak current relies on the reaction between ferrocenium ion and DA. A catalytic mechanism is given in Equation 4.2 and Equation 4.3.

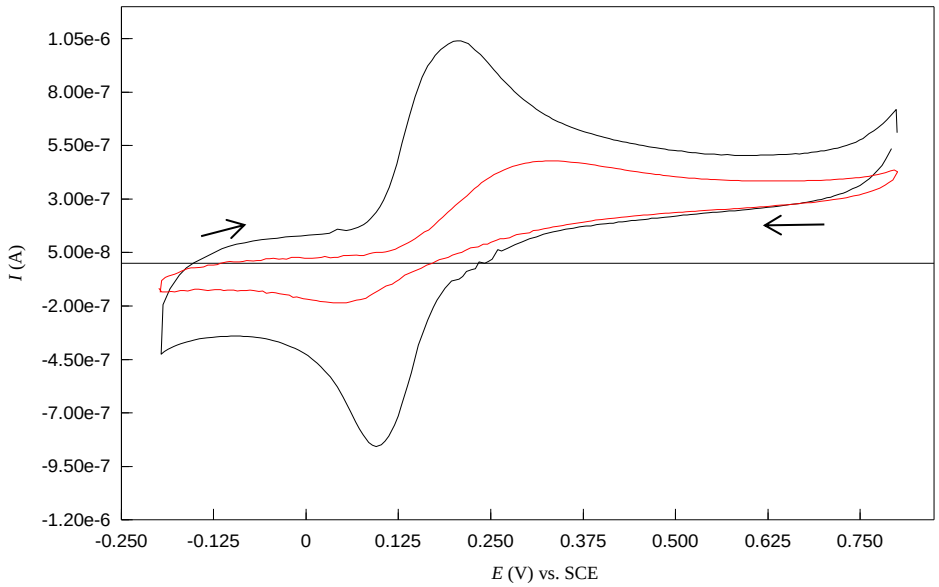

Figure 4.29: Cyclic voltammograms of DA (7.1×10^{-5} M) in PBS (0.1 M), pH 6.8 at Fc-β-CD modified CPE (─) and bare CPE (─). The modified electrode was prepared following the drop-cast method; scan rate 50 mV / s.

$$2Fc \leftrightharpoons 2Fc^{+} + 2e^{-} \qquad \text{Equation 4.5}$$

$$2Fc^{+} + DA \leftrightharpoons 2Fc + DOQ \qquad \text{Equation 4.6}$$

It is also important to mention that the oxidation and reduction peak potentials at bare CPE occurred at 0.332 V and 0.048 V vs. SCE, respectively. Under identical conditions, Fc-β-CD modified CPE gave well defined redox wave of DA, with the anodic peak potential at 0.205 V and the corresponding cathodic peak potential at 0.095 V vs. SCE. So, the peak separation for DA redox at Fc-β-CD modified CPE (ΔEp = 0.110 V) was smaller than that at the bare CPE (ΔEp = 0.280 V). Therefore, the role of the modifier is not only to enhance the peak current, but also to decrease the overpotential for oxidation of DA. Consequently, reversibility of DA is enhanced using Fc-β-CD.

The composite method, where Fc-β-CD (0.006g) impregnated with the carbon paste was also employed to examine electrocatalytic activity for DA. Figure 4.30 shows cyclic voltammograms for 5×10^{-5} M DA at both the modified CPE and bare CPE at 100 mV / s. The anodic peak potential and the cathodic peak potential at Fc-β-CD modified CPE were located at 0.273 V and 0.076 V vs. SCE. The potential difference, ΔE_p, was found to be 0.197 V. This value is higher than that obtained when Fc-β-CD was drop-cast on

CPE. However, the modified electrode still exhibits an enhanced electrochemical response towards DA detection. The enhancement is explained in terms of increasing in both I_{pa} and I_{pc} compared with bare CPE. For instance, I_{pa} for Fc-β-CD modified CPE and bare CPE at 100 mV / s are 6.16×10^{-7} A and 4.13×10^{-7} A respectively.

All these experimental results confirmed that Fc-β-CD modified CPE effectively enhances the oxidation of DA.

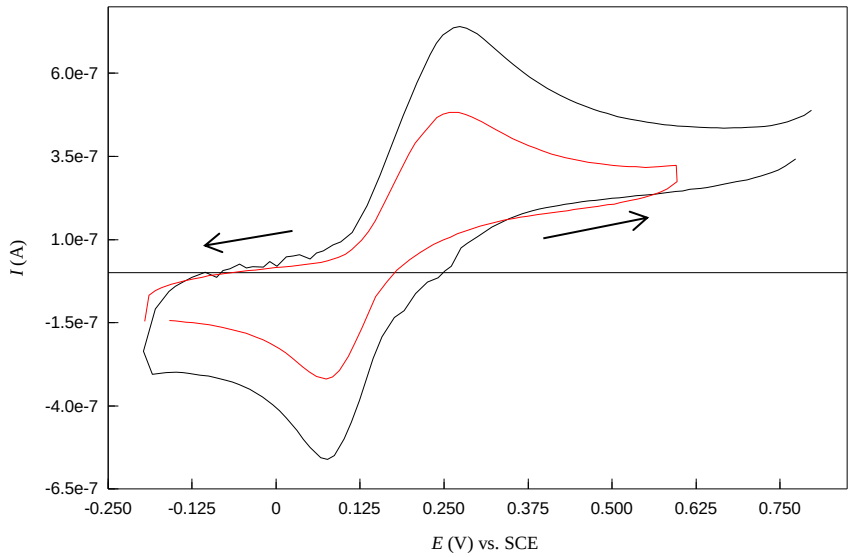

Figure 4.30: Cyclic voltammograms of DA (5×10^{-5} M) in PBS (0.1 M), pH 6.8 at Fc-β-CD modified CPE (─) and bare CPE (─). The modified electrode was prepared following the bulk composite method; scan rate 100 mV / s.

4.2.9.3 Effect of scan rate on peak current

To study the effect of scan rate, cyclic voltammograms were recorded at the Fc-β-CD modified CPE at different scan rates in 5×10^{-5} M DA (pH 6.8). The voltammograms of Fc-β-CD drop-cast at CPE surface was displayed in Figure 4.31(a). As can be seen, the increase in potential scan rate induced a corresponding increase in peak current, resulting in a shift to more cathodic values for the oxidation of DA. Furthermore, the peak current varies linearly with the square root of the scan rate (Figure 4.31(b)), indicating that the electron transfer process at the electrode surface is under diffusion-controlled. The linear equation between peak currents and the square root of the scan rate is presented as follows: I_{pa} (A) = 2.231×10^{-6} $\nu^{1/2}$ + 5.153×10^{-10} with a linear relative correlation coefficient of 0.9962, indicating that regression line is very well fitted with experimental data.

It is important to note that, in this type of electrode, Nafion was added to Fc-β-CD in order to obtain a good dispersion of Fc-β-CD and facilitate its stability at the surface of CPE. As will be seen in the next section, Nafion itself was used as a modifier. However, its role here in terms of enhancement the oxidation response of DA was negligible. As indicated in the following section the redox behaviour of DA at CPE modified with Nafion was under adsorption-controlled process. The fact that a diffusion process was observed at Fc-β-CD modified CPE, even with the presence of Nafion at the electrode surface strongly suggests that Nafion (an electrochemically inert polymer) facilitates Fc-β-CD stabilisation.

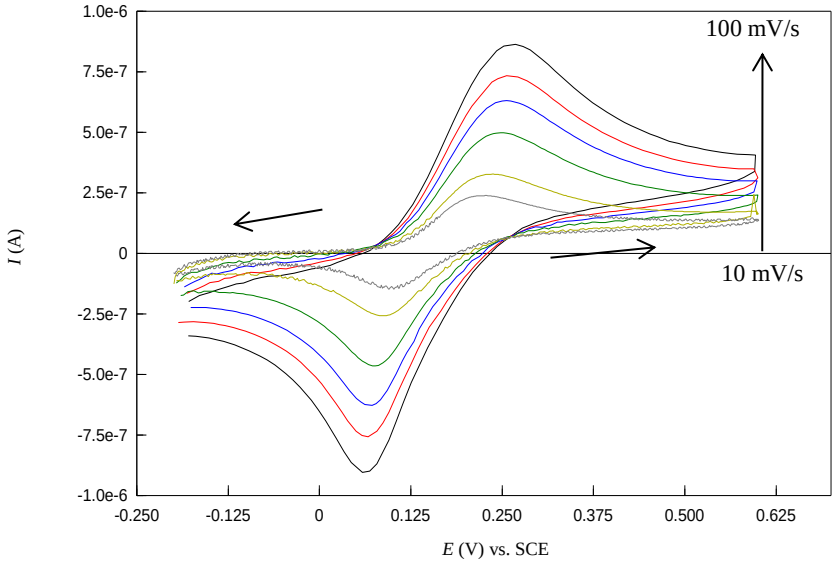

(a)

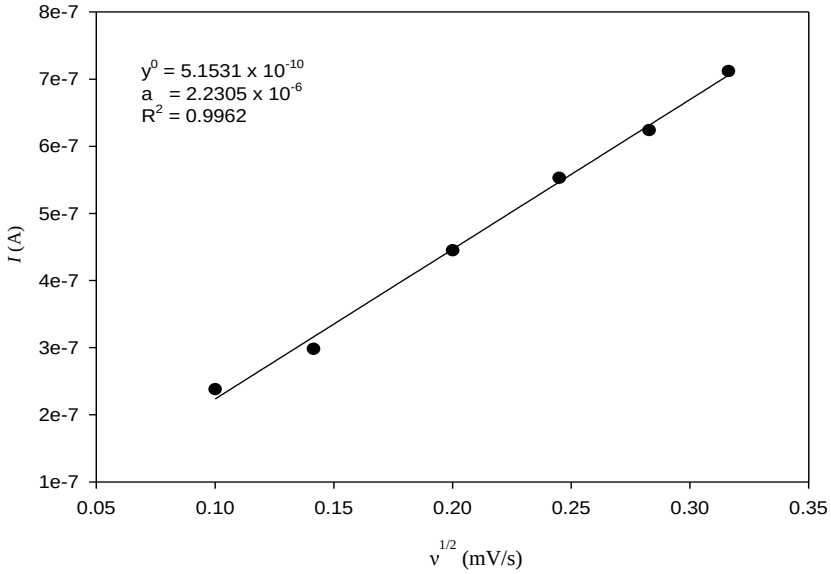

(b)

Figure 4.31: Cyclic voltammograms for the effect of variation of scan rates of DA (5×10^{-5} M) at Fc-β-CD modified CPE from 100 to 10 mV / s using a drop-cast method (a) and corresponding variation of oxidation peak current as a function of square root of scan rate (b). Supporting electrolyte 0.1 M PBS (pH 6.8).

The effect of potential scan rates was also examined at the modified electrode where Fc-β-CD was added to the bulk carbon paste. At a scan rates in the range from 120 mV to 20 mV / s, the oxidative peak current of DA increases with square root of scan rates as shown in Figure 4.32(a). However, there is a slight deviation from linearity compared to the drop-cast method, with correlation coefficient of 0.9804 (Figure 4.32(b)). Overall, these results demonstrated that the Fc-β-CD modified CPE can effectively be used for the determination of DA.

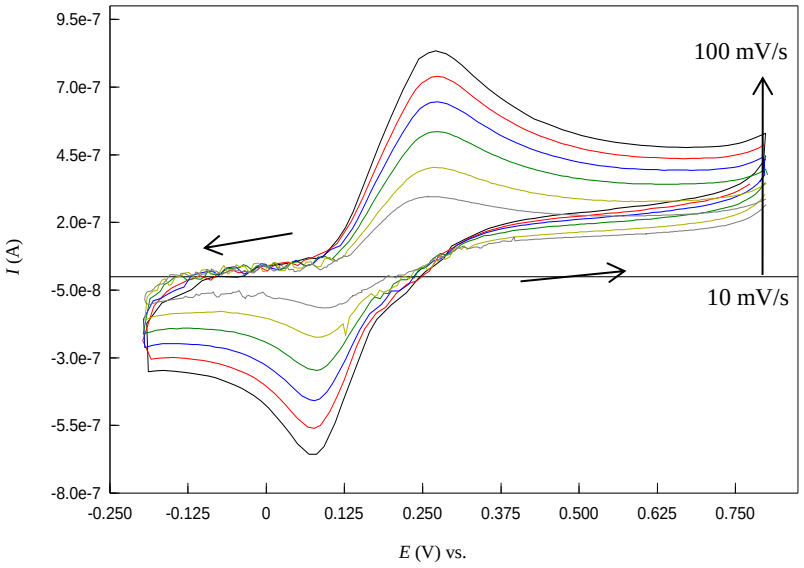

(a)

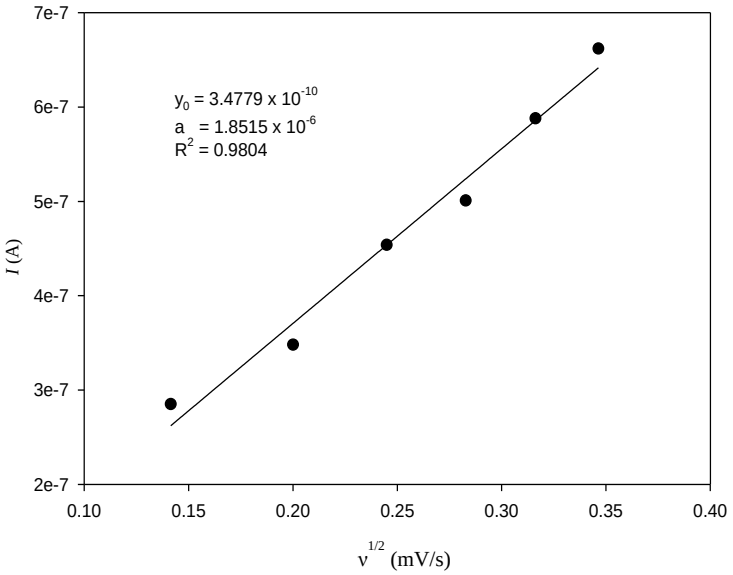

(b)

Figure 4.32: cyclic voltammograms for the effect of variation of scan rates of DA (5×10^{-5} M) at Fc-β-CD modified CPE from 100 to 10 mV / s using a bulk composite method (a) and corresponding plot of oxidation peak current as a function of square root of scan rate (b). Supporting electrolyte 0.1 M PBS (pH 6.8).

It is important to note that compared to neutral β-CD modified CPE, which shows adsorption-controlled process for oxidation of DA, Fc-β-CD modified CPE as shown earlier, follows a diffusion-controlled process. This change in electrochemical system demonstrates that Ferrocene blocks the access of DA to be included into the cyclodextrin cavity. Therefore, the oxidation of DA is only possible when DA molecules, approaching the surface of the modified electrode are oxidised through catalytic effect of Ferrocene moiety.

4.2.9.4 The amount of Fc-β-CD complex (Drop-cast method)

The amount of Fc-β-CD on the surface of bare CPE can have a significant influence on the voltammetric response of DA. This is shown more distinctly in Figure 4.33. As this figure illustrates, the oxidation peak current for 7.1×10^{-5} M DA results in a well-defined anodic and cathodic peaks when the concentration of Fc-β-CD, 2.66×10^{-4} g / mL, was cast at surface of bare CPE. However, using higher concentration (1.33×10^{-3} g / mL) leads to two distinct reduction waves at 0.118 V and 0.193 V vs. SCE, corresponding to reduction of DOQ to DA and Fc^{+} to Fc respectively. The anodic and cathodic peak at lower concentration Fc-β-CD is attributed to the redox activity of DA, so the oxidation and reduction peaks of Ferrocene (particularly the reduction peak) are masked by the redox activity of DA. Moreover, the reduction peak potential is shifted to a negative value at a lower concentration of Fc-β-CD.

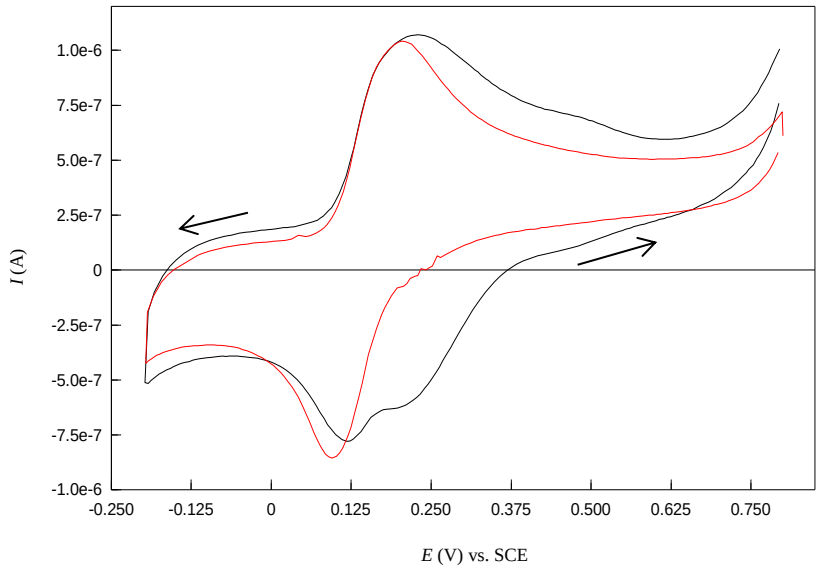

Figure 4.33: cyclic voltammograms of DA (7.1×10^{-5} M) in PBS (0.1 M), pH 6.8 at 2.66×10^{-4} g / mL Fc-β-CD modified CPE (—) and 1.33×10^{-3} g / mL Fc-β-CD modified CPE (—); scan rate 50 mV / s.

4.2.9.5 Stability of Fc-β-CD complex

One of the important requirements for application of sensor is its stability. It has been found that the oxidized forms of Ferrocene, Fc^{+}, and its derivatives are soluble in aqueous solution [69]. This presents a problem in that Fc^{+} tends to leach. Strategies to prevent Fc^{+} leaching from CPE have been reported by several groups. Ferrocene can be linked covalently with polymer or with high molecular weight compounds before immobilization on the surface of electrode [70, 71]. Gorton *et al* [72] studied ferrocene-containing siloxane polymer modified electrode surface with a poly (ester-sulphuric

acid) cation-exchanger to improve the stability of the mediator. Another alternative method is to synthesize a few Ferrocene derivatives with specific functional groups [73, 74], in a complicated preparation procedure. For instance, Jönsson *et al* [73] used hydroxymethyl Ferrocene and anthracene carboxylic acid to synthesize anthracene substituted ferrocene.

The other alternative method to increase the stability of Ferrocene is the formation of inclusion complex with cyclodextrin, which makes the solubility of ferrocenium ion decrease. For instance Zhang *et al* [75] used β-cyclodextrin-ferrocene inclusion complex modified CPE for amperometric determination of Ascorbic Acid. The approach used by those authors was followed in this study. The problem related to ferrocenium ion leaching (from the paste) improved, when Ferrocene was changed to Fc-β-CD inclusion complex. The guest molecule (Fc) was held in the hydrophobic cavity of β-CD (host molecule) by noncovalent interactions. This greatly decreased the water-solubility of the Fc^+ and correspondingly improved the stability of the modified electrode.

Figure 4.34(a) shows highlights of the anodic peak currents of Ferrocene. The anodic peak currents decrease continuously with repeated potential scans until a steady state was obtained after the 5^{th} cycle. This figure illustrates the behaviour of Fc-CPE in 0.1 M PBS at 50 mV / s. Although, ferricinium ion is soluble in aqueous solution, cyclic voltammetry experiments shows that Fc-CPE is stable enough in aqueous solution and it can be used as an electrochemical sensor. This unusual observation was also reported by Kamyabi *et al* [76].

Under similar conditions, Fc-β-CD inclusion complex shows that anodic peak currents almost overlap with increasing cycle numbers as shown in Figure 4.34(b).

It is demonstrated that the stability of Fc-β-CD modified CPE is slightly better than Fc-CPE.

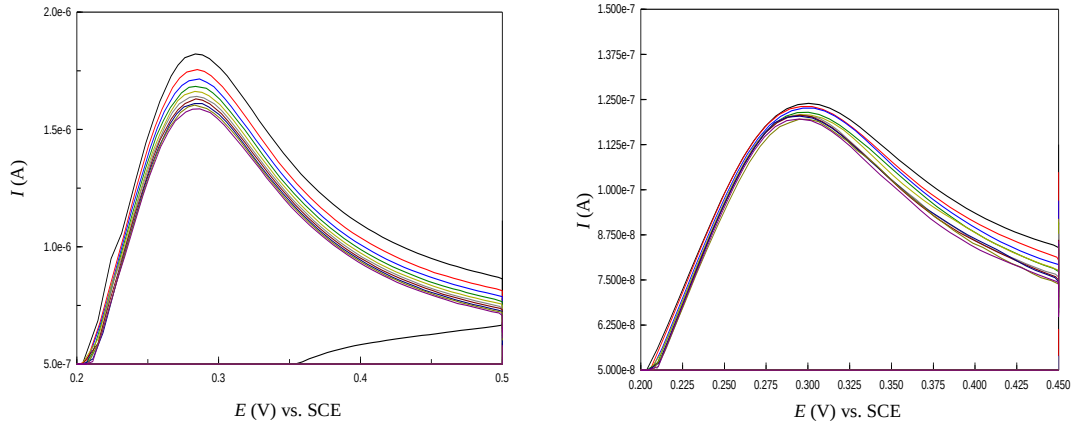

(a) (b)

Figure 4.34: Enlarged I_{pa} for cyclic voltammograms of (a) Fc modified CPE and (b) Fc-β-CD modified CPE in PBS (0.1 M), pH 6.8; scan rate 50 mV / s.

The electrochemical behaviour of Fc-β-CD remains similar compared to Fc itself in 0.1 M PBS. As seen in Figure 4.35. The peak potential separation for Fc-β-CD modified CPE and Fc-CPE are 0.072 and 0.073 V vs. SCE respectively, which is characteristic of a quasi-reversible system. Although, an amount of 0.006 g was utilised in both cases for the fabrication of the electrodes, the actual peak currents cannot be compared appropriately as the concentration of Fc in each electrode is not the same. However, the reversibility and remarkable symmetrical peak wave in Fc-CPE is probably related to the electron mediation action of Ferrocene. Therefore, Ferrocene 'non-included' may have an ability to mediate electron transfer much easier compared to Fc-β-CD inclusion complex.

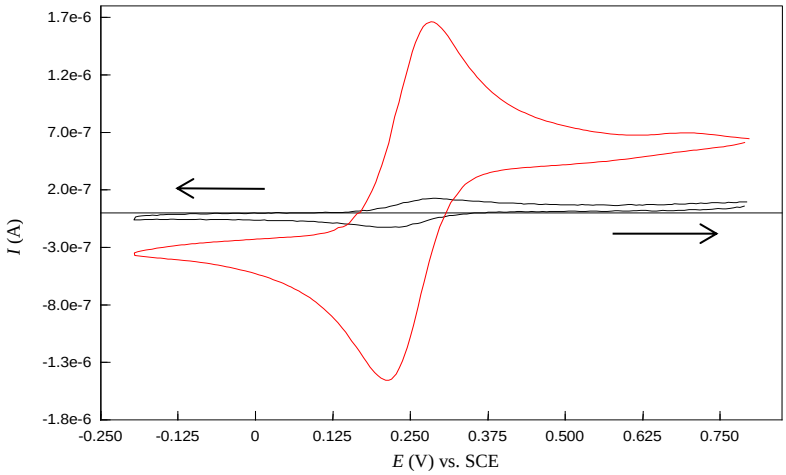

Figure 4.35: Cyclic voltammograms of Fc modified CPE (—) and Fc-β-CD modified CPE (—) in PBS (0.1 M), pH 6.8; scan rate 50 mV / s.

The stability of Fc-β-CD was further investigated at room temperature. Carbon pastes containing respectively Fc (0.006g) and a relatively higher amount of Fc-β-CD (0.695g) were stored separately into a vial. The vials were tightly closed over a period of 2 days. During this length of time, a yellow colour was formed (clearly visible) at the lid of the vial due to sublimation of Ferrocene (as shown from Figure 4.36). The yellow coloration is a result of gaseous Ferrocene which developed overtime. This phenomenon may result in a poor reproducibility and short lifetime of the modified electrode. Generally, Ferrocene can be purified by sublimation and gaseous Ferrocene are very pure compared to the bulk solid Ferrocene. It should be notice that commercial Ferrocene used in this work is 98 % pure; therefore, most of Ferrocene molecules may sublime if time is increased to more than 2 days. As already mentioned in chapter 3, the prepared carbon paste could be unused for at least 12 hours to allow 'self-homogenisation', which is required for consistent material composite. During this time frame, Ferrocene can sublime slowly at room temperature. It is also remarkable to observe sublimation of Ferrocene from carbon paste in the presence of a relatively high content of binder (200 μL silicon oil). In contrast, vial (B), composed of Fc-β-CD shows a stable paste as the lid retains its initial colour after 2 days. It is clear that the sublimation and release of complexed ferrocene molecules have been protected by the cyclodextrin cavity in which they were 'encapsulated'.

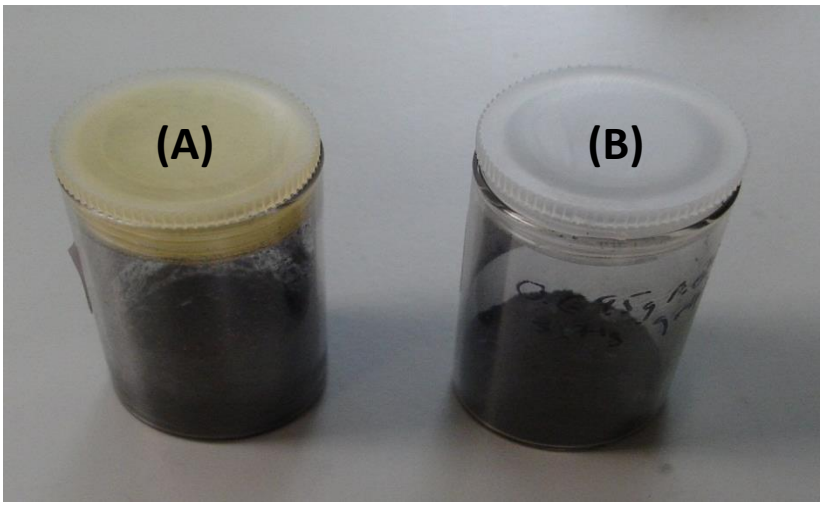

Figure 4.36: Photographic images of carbon paste composite containing (A) 0.006 g Ferrocene, (B) 0.695 g Fc-β-CD.

4.2.10 Nafion Modified CPE

Nafion, a perfluorosulfonated cation-exchange polymer, is a perm-selective polymer known for its ability to incorporate positively charged ions and reject anions [77-79] [80-82]. It is highly stable in aqueous solution [83] and electrochemically inert. Nafion contains two different regions: the hydrophobic polymer backbone and the ionized hydrophilic sulfonate groups outside the hydrophobic region as shown in Figure 4.37. The structure of Nafion unit illustrates the variability of the material; for example, the most basic monomer contains chain variation between the ether groups (z subscript). The special amphiphilic structure makes Nafion to be widely used in the field of electrochemistry.

In this study, Nafion was used as a modifier for DA sensing. Two methods for the preparation of the electrode were carried out. Nafion was incorporated into the carbon paste during the mixing of the graphite and silicone oil, and it was also drop-cast onto the surface of the CPE. These methods are simple and effective for the detection of DA.

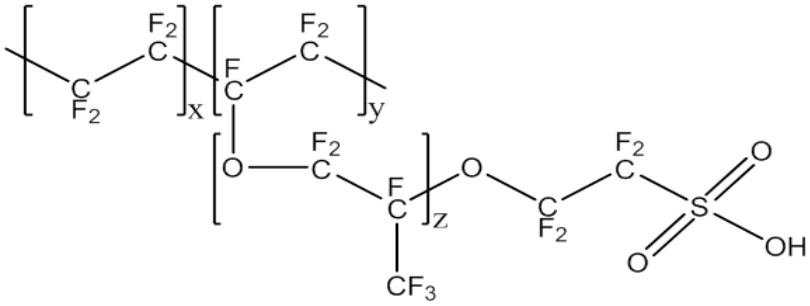

Figure 4.37: Chemical structure of Nafion unit.

4.2.10.1 DA electrochemical redox process at Nafion modified CPE

A portion of the composite mixture was then used to construct the modified electrode. In the second method, a concentration of nafion was dropped on the surface of CPE. In both cases, cyclic voltammetry were performed on 5×10^{-5} M DA in PBS (pH 6.8). Figure 4.38(a) shows the recorded voltammograms when Nafion (200 µL) was incorporated within CPE and dried at room temperature for three hours; no detection of DA was observed at all. The commercially available Nafion® 117 solution employed here is 5% concentrated in ethanol. Therefore, the high background current observed may result from insufficient time to dry fully the carbon paste composite. Experimental evidences have confirmed that alcohols penetrate into the non-polar regions of Nafion [84]. Although, three hours seems to be sufficient to allow evaporation of ethanol

contained into Nafion solution, this experiment demonstrates that higher amount of time was required to get a carbon paste composite free from ethanol. To improve the electrochemical response of DA, the carbon paste material composite was spread in a petri dish and allowed to dry overnight at room temperature. The fabricated electrode based on such material composite was tested in 5×10^{-5} M DA using cyclic voltammetry. As shown in Figure 4.38(b), a well-defined redox peak centred at 0.160 V was observed, indicating that ethanol was completely removed from the paste. Consequently, Nafion with its negatively charged sulfonic group was able to enhance the adsorption of DA. The resulting DA signal shows an anodic and a cathodic peak value of 1.94×10^{-6} A and 1.96×10^{-6} A, respectively. The ratio I_{pa} / I_{pc} was 0.99 and the peak potential separation 0.01 V vs. SCE. All these experimental results indicate a reversible electron transfer process at Nafion modified CPE. The presence of a pre-peak is also observed (midpoint 0.02 V vs. SCE), which describes the redox behaviour of oxide species.

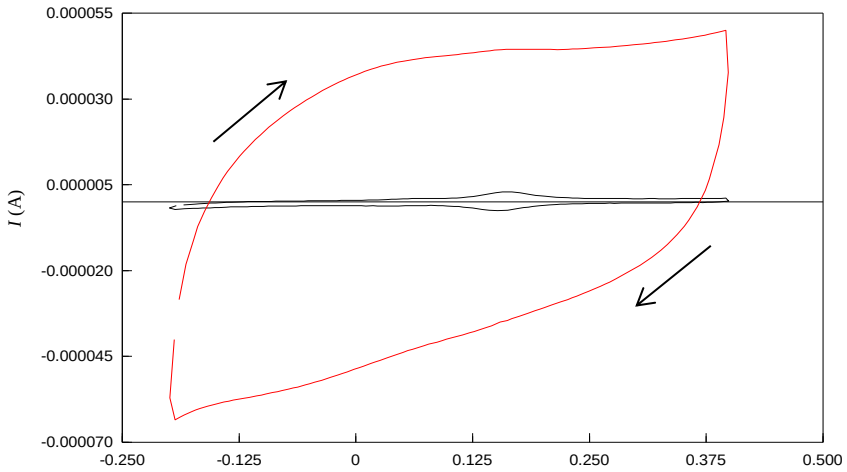

(a)

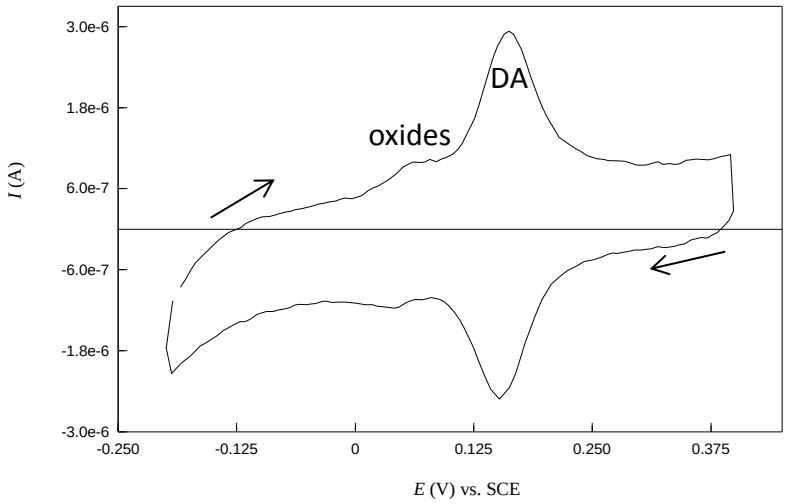

(b)

Figure 4.38: Cyclic voltammograms of DA (5×10^{-5} M) at (a) Nafion modified CPE with paste composite dried for 3 h (—) and Nafion modified CPE with paste composite dried for 24 h (—) in PBS (0.1 M), pH 6.8 (b) Enlarged cyclic voltammograms for Nafion modified CPE with paste composite dried for 24 h; scan rate 50 mV / s.

The second type of Nafion modified CPE was prepared by drop-casting of undiluted 10 µL of 5% Nafion® 117 on the surface of CPE. The electrode surface was then allowed to dry at room temperature until a visible film was observed. The cyclic voltammogram obtained when the modified electrode was placed in 5×10^{-5} M DA is displayed in Figure 4.39. As can be seen, no redox activity of DA was observed. A concentration of 0.05 % Nafion solution was then prepared from 5% Nafion® 117 solution, and 10 µL of it was drop-cast onto CPE surface, and allowed to dry at room temperature. Cyclic voltammetry was performed, which resulted in oxidation signal of DA, similar to that obtained previously at Nafion incorporated within the carbon paste. Here, the oxidation peak current was 2.43×10^{-6} A, higher than that obtained in the previous method.

However, the peak potential separation, ΔE_p (0.01 V vs. SCE) remained the same, characteristic of an adsorption controlled redox process. It is also noted that the oxidation peak potential were much the same. E_{pa} was found to be 0.150 V compared to 0.160 V in Nafion mixed with carbon paste.

It can be concluded that the effect of reducing Nafion concentration (from 5 % to 0.05 %) showed that 0.05% was favourable, as it resulted in a maximum peak current at a peak potential well separated from the non-faradaic current. A thicker Nafion coating (for instance 5 %) may result in Nafion molecules obstructing the mass transport of the analyte molecules and reducing considerably the electrode conductivity. This effect was also observed by White *et al* [85] and Hoyer *et al* [86].

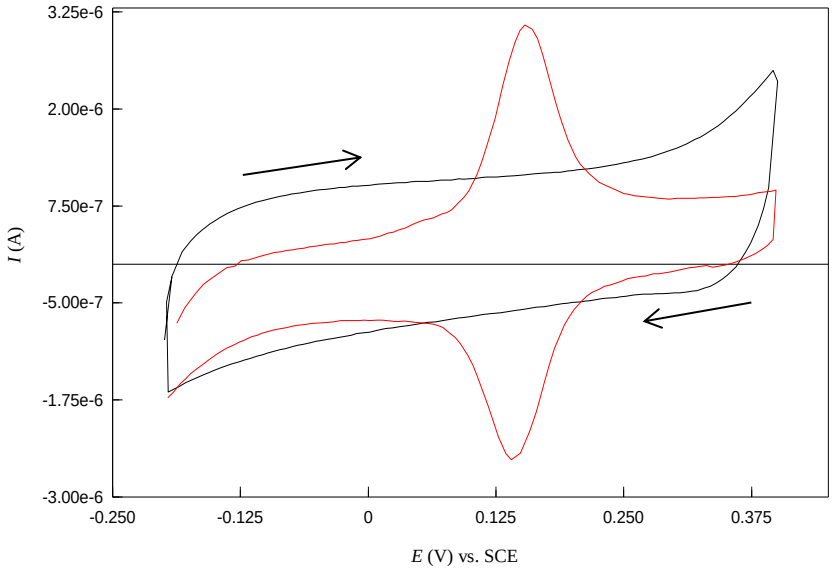

Figure 4.39: Cyclic voltammograms of DA (5×10^{-5} M) at Nafion modified CPE from 5 % Nafion solution (—) and Nafion modified CPE from 0.05 % Nafion solution (—), in PBS (0.1 M), pH 6.8; scan rate 50 mV / s.

4.2.10.2 Rate-controlling process within the Nafion membrane

A study of the effect of varying the scan rate allowed the determination of the rate controlling process within the Nafion layer. This study was carried out in DA (5×10^{-5} M) at Nafion incorporated in CPE. As seen in Figure 4.40(a), both the cathodic and anodic peak currents increased with increase in scan rate from 10 to 100 mV / s. A plot of DA oxidation peak current versus scan rate was linear (Figure 4.40(b)), indicating that the rate controlling process to be an adsorption of DA through the Nafion layer.

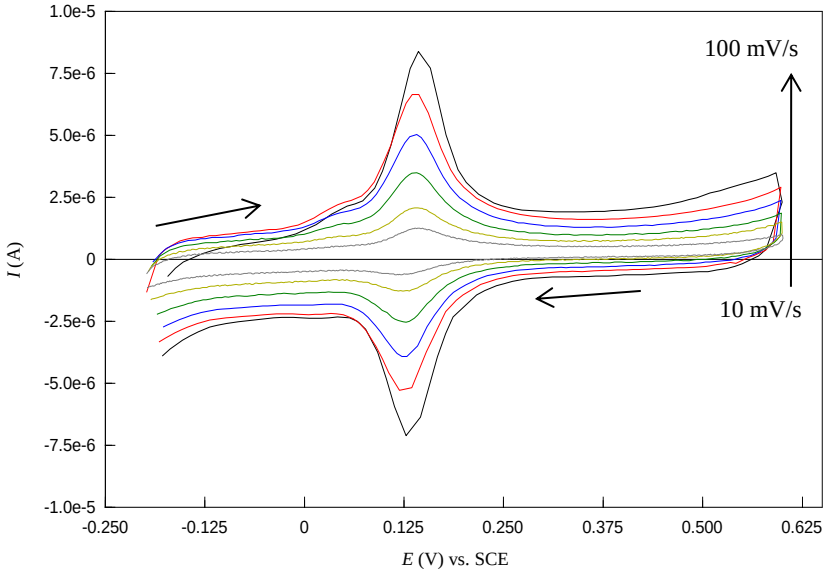

(a)

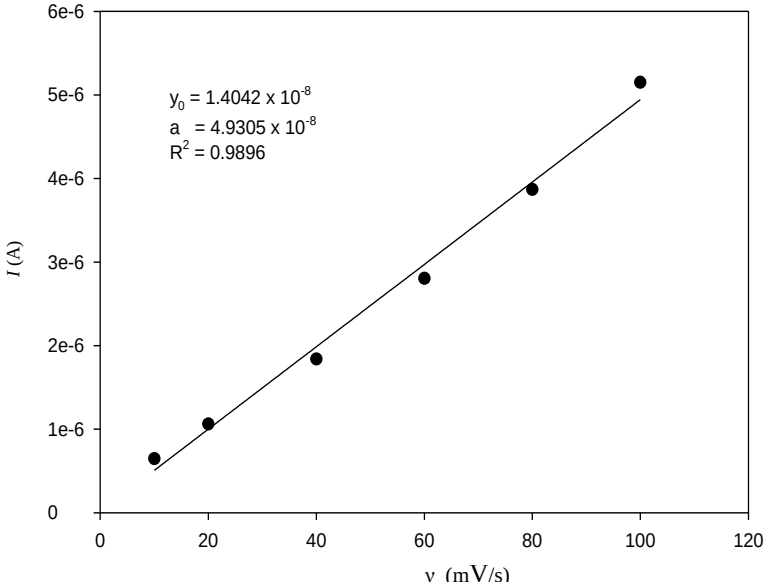

(b)

Figure 4.40: Cyclic voltammograms for the effect of variation of scan rates of DA (5×10^{-5} M) at Nafion modified CPE from 100 to 10 mV / s (a) and corresponding variation of oxidation peak current as a function of scan rate (b). Supporting electrolyte 0.1 M PBS (pH 6.8).

4.2.10.3 Mode of sensing

As already mentioned, Nafion is a member of perfluorosulfonate cation-exchange resins, which is highly stable in aqueous solution [83]. It is electrochemically inert and can be used as modifier. One important reason for the widespread application of Nafion modified electrodes in electroanalytical chemistry are their ability to preconcentrate positively charged molecules [80-82].

The accumulation mechanism of Nafion can be explained through an electrostatic interaction due to the negatively charged sulfonate groups in the polymer structure. In addition, Nafion ionic selectivity for hydrophobic organic cations is achieved through hydrophobic interactions with the hydrophobic fluorocarbons of the film [87].

At pH values below 7, DA exists predominantly in the cationic form. Because of this, the DA signal can be enhanced in the presence of Nafion. The adsorption of DA at Nafion modified CPE may be explained via the following Equation 4.7 [88].

$$\text{Nafion}\left(SO_3^-\right)\left(H^+\right)^{film} + \left(DA^+\right)^{solution} \leftrightharpoons \text{Nafion}\left(SO_3^-\right)\left(DA^+\right)^{film} + \left(H^+\right)^{solution} \qquad \text{Equation 4.7}$$

4.2.10.4 S-β-CD / Nafion modified CPE

A combination of S-β-CD and Nafion, two modifiers having separately an enhancing effect on DA signal was of interest as no reports have been previously released showing an electrochemical detection of DA using S-β-CD / Nafion modified CPE. Some authors such as Huong *et al* [89] used a conductive poly (3-methylthiophene) / Nafion modified glassy carbon electrode as a chemical sensor for the voltammetric analysis of DA. Lee *et al* [90] employed Nafion coated hybrid macroporous gold modified electrode with Platinum Nanoparticles for the selective detection of DA. The combination of Nafion and a chemical compound to form a complex material composite for the detection of DA appears a subject of interest. To achieve this goal; S-β-CD and Nafion were mixed in carbon paste. Typically, 0.545g S-β-CD and 200 µL Nafion (5 %) were mixed with graphite powder containing silicon oil (200 µL). The resulting composite material was dried overnight at room temperature. The cyclic voltammetry obtained from such material when used to detect 5×10^{-5} M DA at scan rate 50 mV / s was displayed in Figure 4.41 (red voltammogram). A pair of redox peaks is observed with anodic peak current equal to 1.29×10^{-6} A. Under the same conditions, the bare CPE only returned an anodic peak current of 2.25×10^{-7} A as demonstrated previously. Clearly, S-β-CD / Nafion modified CPE enhance the DA peak current and facilitate DA detection. This is also observed through the oxidative peak separation (ΔE_p = 0.020 V vs. SCE) compared to that of bare CPE (0.133 V vs. SCE). In order to increase furthermore the signal of DA using the modified electrode, the material composite was dried in the oven at 50° C for two days. The paste was mixed again to ensure homogeneity, before constructing the electrode. The cyclic voltammetry acquired at this type of modified electrode is given in Figure 4.41 (black voltammogram). As can be seen, the intensity of the oxidation peak current is greatly increased, with the anodic

peak current corresponding to 2.45 × 10^{-6} A. The ratio of the cathodic peak current over the anodic peak current is close to 1, suggesting a reversible redox process. The drying process may have enhanced the ability of Nafion to pre-concentrate DA molecules. Nagy *et al* [91] have shown that Nafion loaded at an electrode surface can be dried using a domestic hair-dryer; and such a heat-treatment step improves both the electrochemical performance and the stability of Nafion-coated electrode.

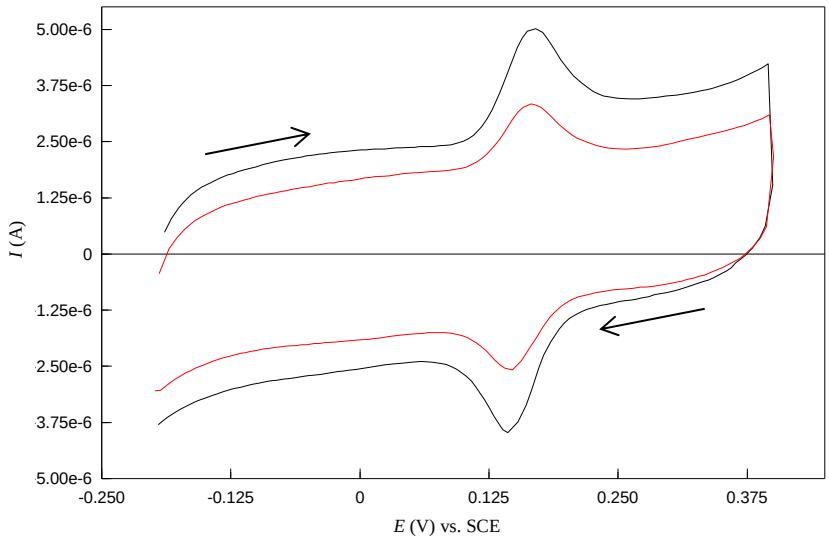

Figure 4.41: cyclic voltammograms of DA (5 × 10^{-5} M) S-β-CD / Nafion modified CPE (—) and S-β-CD / Nafion modified CPE with paste composite heated at 50˚C (—) in PBS (0.1 M), pH 6.8; scan rate 50 mV / s.

In the second part of this study, Nafion mainly served as a binder to improve dispersion of S-β-CD at the surface of CPE, and in addition with S-β-CD to enhance redox activity of DA. To prepare the modified electrode, 0.057 g of S-β-CD was dispersed in 1 mL Nafion (0.05 %) solution with the aid of sonication to form a viscous solution. Then, 10 µL was loaded on the surface of a previously prepared CPE. The modified electrode was allowed to dry at room temperature for three hours to dry. The cyclic voltammogram obtained with the modified electrode in 5 × 10^{-5} M DA is shown in Figure 4.42. The oxidation peak current (1.08 × 10^{-6} A) is also higher than that obtained at the bare CPE. However, this value is lower than the oxidation peak current at Nafion modified CPE (using identical drop-cast method). Perhaps a dispersion of S-β-CD and Nafion involved a much more important repulsive force between S-β-CD and Nafion, as they are both negatively charged at neutral pH. A possibility of electrostatic repulsion of sulfate group of the cyclodextrin against the sulfonate group of Nafion is likely to

hinder inclusion of DA into the cavity S-β-CD or reducing its accumulation into the Nafion film.

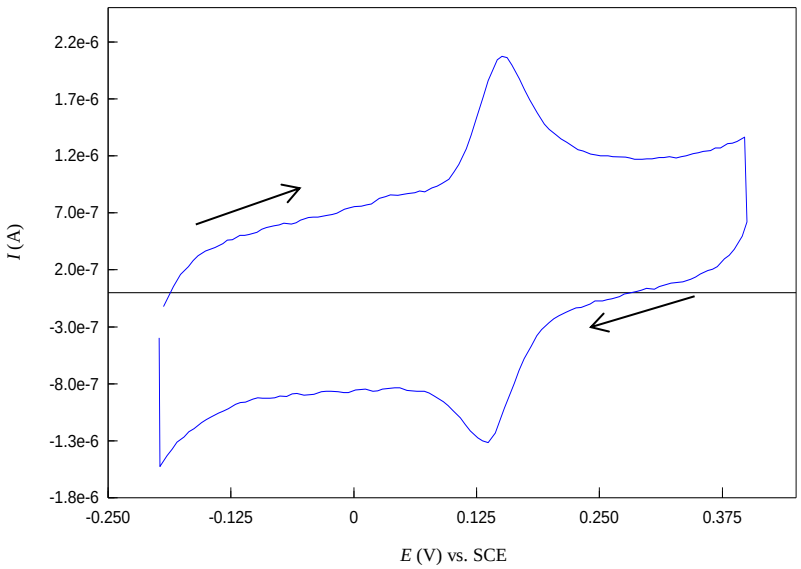

Figure 4.42: Cyclic voltammograms of DA (5×10^{-5} M) at S-β-CD / Nafion modified CPE, in PBS (0.1 M), pH 6.8 using a drop-cast method; scan rate 50 mV / s.

Alternatively, the modified electrode was dipped into the dispersive solution of S-β-CD and Nafion for 5 seconds and allowed to dry at room temperature. The cyclic voltammetry of DA at this type of modified electrode is shown in Figure 4.43. Although, a higher background current was observed, the redox pair was found to be similar to that obtained by drop-cast method. The intensity of the oxidation peak current, 1.07×10^{-6} A, remained the same. It can also be concluded that the bulk composite afforded a better DA response compared to the drop-cast method.

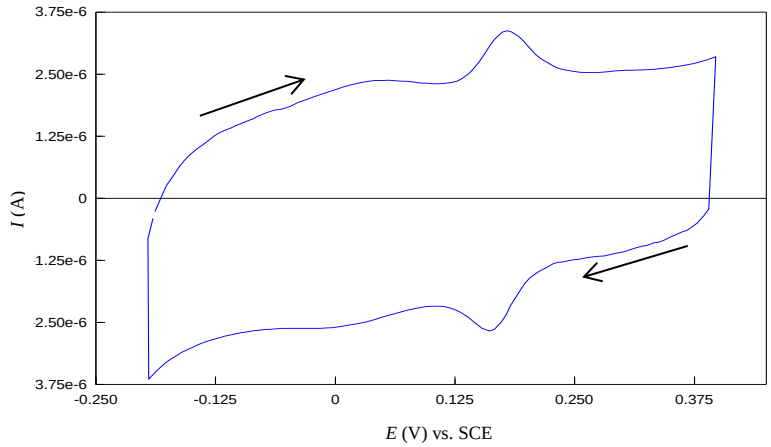

Figure 4.43: Cyclic voltammograms of DA (5×10^{-5} M) at S-β-CD / Nafion modified CPE in PBS (0.1 M), pH 6.8 using a dip drop method; scan rate 50 mV / s.

The stability of S-β-CD / Nafion modified CPE (dip-drop method) was checked by repetitive potential sweeps in 0.1 M PBS (pH 6.8) at 50 mV / s. Figure 4.44 shows that the voltammograms reach steady-state after the third cycle, indicating that S-β-CD / Nafion modified CPE is stable. S-β-CD is maintained at the surface of electrode by Nafion, which is insoluble in water. Therefore, S-β-CD / Nafion modified CPE by drop-cast method can be applied in aqueous system. Although, this type of modified electrode gives a fairly enhancement effect in the detection, it might have a better application for DA detection in aqueous media if an optimum ratio is developed.

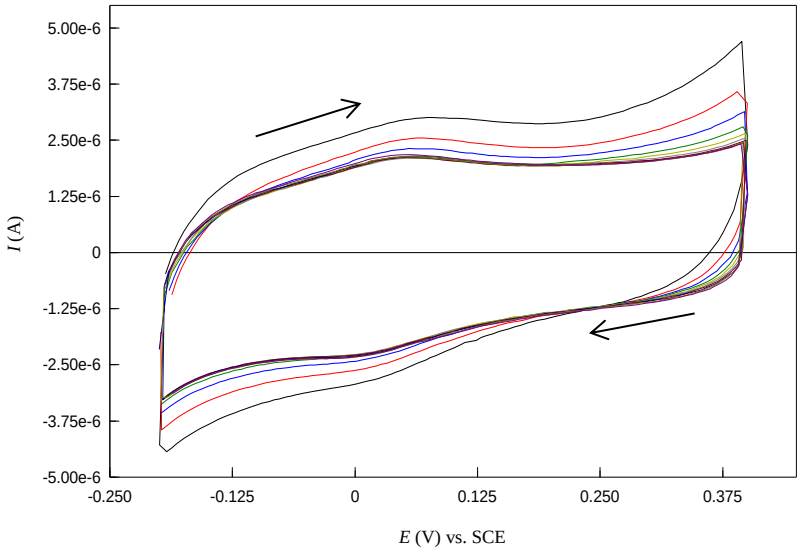

Figure 4.44: Cyclic voltammograms of S-β-CD / Nafion modified CPE in PBS (0.1 M), pH 6.8; scan rate 50 mV / s.

Based on a possible electrostatic interaction between the negatively charged group both from S-β-CD and Nafion, it was decided to lower the concentration of S-β-CD and compare the effect on DA to result obtained from the voltammogram in Figure 4.42. The concentration of S-β-CD was reduced to 1.04×10^{-2} g / mL (in 0.05 % Nafion). Again, 10 µL of the mixture was loaded on the surface of CPE. The resulting voltammogram displayed in Figure 4.45 gave a much lower DA signal (3.80×10^{-7} A). In addition, a more diffusion profile of redox peak was observed, suggesting that the ratio S-β-CD / Nafion at the surface of CPE was important. Therefore, the effect of increasing the concentration of S-β-CD (in the mixture S-β-CD / Nafion) on CPE surface was then studied. The mixture was prepared by dispersing S-β-CD in Nafion (0.05%) with aid of ultrasonic bath for 10 minutes. Different concentrations of S-β-CD in Nafion were made: 9.64×10^{-3} g / mL, 1.04×10^{-2} g / mL, 1.11×10^{-2} g / mL and

1.22×10^{-2} g / mL. Each homogeneous mixture was placed separately in different vials. Then, an aliquot of 10 μL from each solution was drop-cast on bare CPE and allowed to dry at room temperature. The electrochemical behaviour of the modified electrodes was recorded using cyclic voltammetry in 5×10^{-5} M DA. Figure 4.46 shows there is an inverse relationship between DA oxidation peak current and Nafion concentration at the electrode surface. Otherwise, DA oxidation peak current increase with increasing concentration of S-β-CD. As displayed in Table 4.5, I_{pa} increases as the amount of Nafion is lowered, indicating that Nafion membrane ratio directly controls the electrode performance. In fact, the higher the amount of S-β-CD, the lower the amount of Nafion at the CPE surface (and vice versa). In addition, oxidation peak potential shifts slightly to a more anodic value as Nafion concentration is lowered. These experimental results suggest that a relatively higher Nafion ratio may form a thicker film at the electrode surface, therefore, acting as a diffusion barrier to the uptake of DA from the analyte solution and also preventing effective interaction between S-β-CD and DA. As already mentioned, the electrochemical response could be the sum of contributions both from S-β-CD and Nafion. So, the effect of S-β-CD may be inhibited by such a high Nafion content. The effect of Nafion in the modified film is very significant for the voltammetric response of DA. From Table 4.5, 1.22 g / mL appeared to give the maximum value for peak current, but it cannot be considered as the optimal mixture. These experimental results simply describe the successful combination of S-β-CD and Nafion in order to provide S-β-CD / Nafion coated CPE. Further work needs to be done to develop an optimal mixture of S-β-CD / Nafion and consequently a maximum loading onto the CPE surface.

To conclude this section, there was a considerable increase in peak current using S-β-CD / Nafion-modified CPE over an unmodified CPE. A combination of S-β-CD and Nafion, particularly in bulk carbon paste, proved to exhibits excellent electrocatalytic activity towards the oxidation of DA.

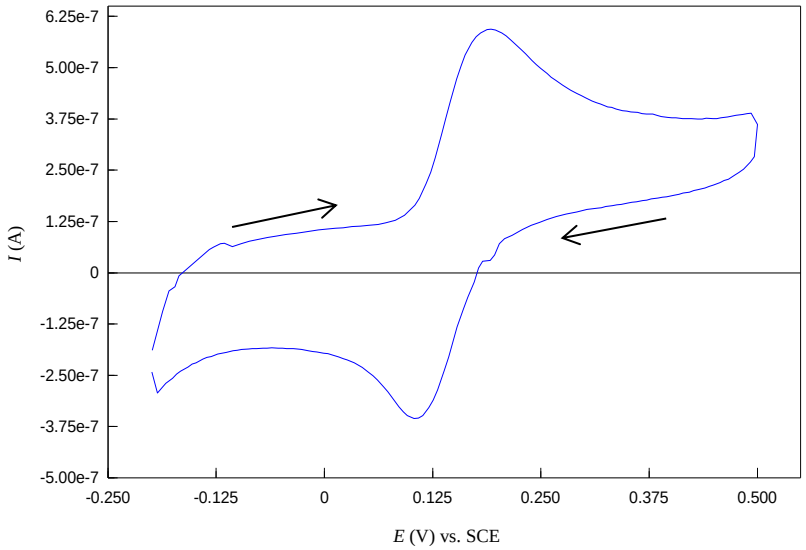

Figure 4.45: Cyclic voltammetry for DA (5×10^{-5} M) at S-β-CD / Nafion (1.04×10^{-2} g / mL) modified CPE in PBS (0.1 M), pH 6.8; scan rate 50 mV / s.

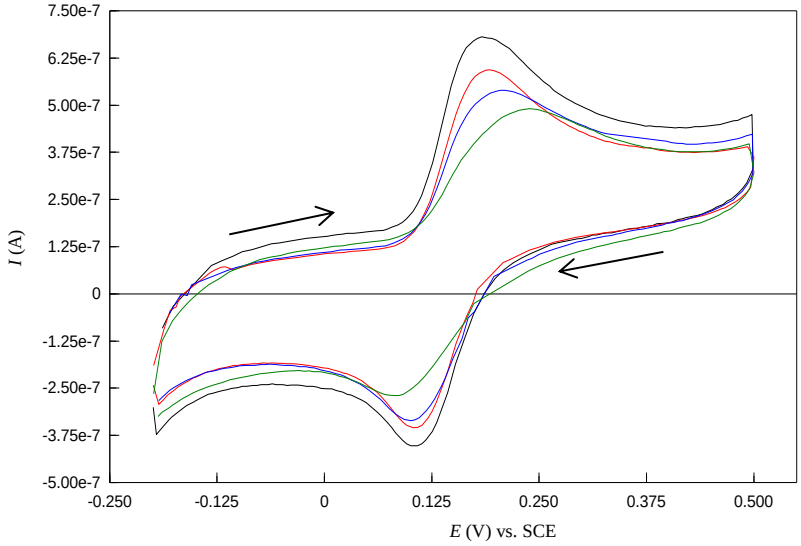

Figure 4.46: Cyclic voltammetry for DA (5×10^{-5} M) at (—) S-β-CD / Nafion (9.64×10^{-3} g / mL) modified CPE, (—) S-β-CD / Nafion (1.04×10^{-2} g / mL) modified CPE, (—) S-β-CD / Nafion (1.11×10^{-2} g / mL) modified CPE, (—) S-β-CD / Nafion (1.22×10^{-2} g / mL) modified CPE, in PBS (0.1 M), pH 6.8; scan rate 50 mV / s.

Table 4.5: Effect of S-β-CD / Nafion concentration on the redox DA.

S-β-CD concentration (g / mL)	**DA oxidation peak current (A)**	**DA oxidation peak potential (Volt)**
9.64×10^{-3}	2.99×10^{-7}	0.24
1.04×10^{-2}	3.80×10^{-7}	0.21
1.11×10^{-2}	4.29×10^{-7}	0.19
1.22×10^{-2}	4.82×10^{-7}	0.18

4.2.11 Bare Graphene Paste Electrode

Graphene is now considered as a 'rising star' material and has received much popularity because of its physical and chemical properties [92]. Based on its reported properties, it was hypothesized that graphene would have a significantly better performance as compared to common CPEs and glassy carbon electrodes. Therefore, the aim of this section was to replace graphite by graphene and assess its performance for detection of DA in comparison of graphite based CPE used throughout this thesis. Graphene was successfully prepared and it was found that it exhibits a superior sensing performance than graphite towards DA detection.

4.2.11.1 Preparation of Graphene paste electrode (GPE)

GPE was fabricated the same way as CPE. Typically, 0.71 g Graphene and 200 µL silicone oil were thoroughly hand-mixed in an agate mortar using a pestle to obtain a homogeneous paste. A portion of the resulting paste was packed into one end of a Teflon tube (internal diameter of 2 mm) and a copper rod was inserted through the opposite end to establish an electrical contact. The modified GPE was prepared similarly by addition of appropriate amount of the modifier. Prior to use the surface of the electrode was polished on a weighing paper.

4.2.11.2 DA electrochemical redox process at bare GPE

In order to evaluate the ability of bare GPE for DA determination, the electrochemical behaviour of DA was studied using Differential Pulse Voltammetry (DPV). DPV has higher current sensitivity and better resolution than cyclic voltammetry (CV). In the DPV mode, charging current contribution to background current is negligible leading to more accurate measurements. Therefore, this technique was employed to compare graphite and graphene based electrodes and later, in Chapter 5, for the trace level detection of DA. Figure 4.47 shows the DPV curves of 5×10^{-5} M DA at bare graphite

paste electrode (CPE) and bare graphene paste electrode (GPE). Clearly, the voltammogram obtained at bare GPE shows a higher oxidation peak current of DA compared with bare CPE. I_{pa} for GPE and CPE are 1.65×10^{-6} A and 6.53×10^{-7} A respectively. This means that GPE is up to three times more efficient than corresponding CPE towards the detection of DA. In addition, the oxidation of DA occurs at 0.132 V at CPE, whereas it is 0.116 V at GPE. This negative-shift of the overpotential at GPE confirms the eletrocatalytic effect of GPE on DA. This is also reflected in the sharper peak obtained at GPE. All these effects may be attributed to the larger surface area and the larger number of defects such as kinks, steps, and vacancies [93] that have great affinity toward DA. The defects in graphene result from its oxidation-reduction preparation process [94] and serve as highly active sites in the electrochemical reactions at GPE. Moreover, the interaction and electron communication between graphene and (benzene ring of) DA can be further strengthened via π-π stacking force [95]. The redox activity DA has been improved by replacing graphite for graphene.

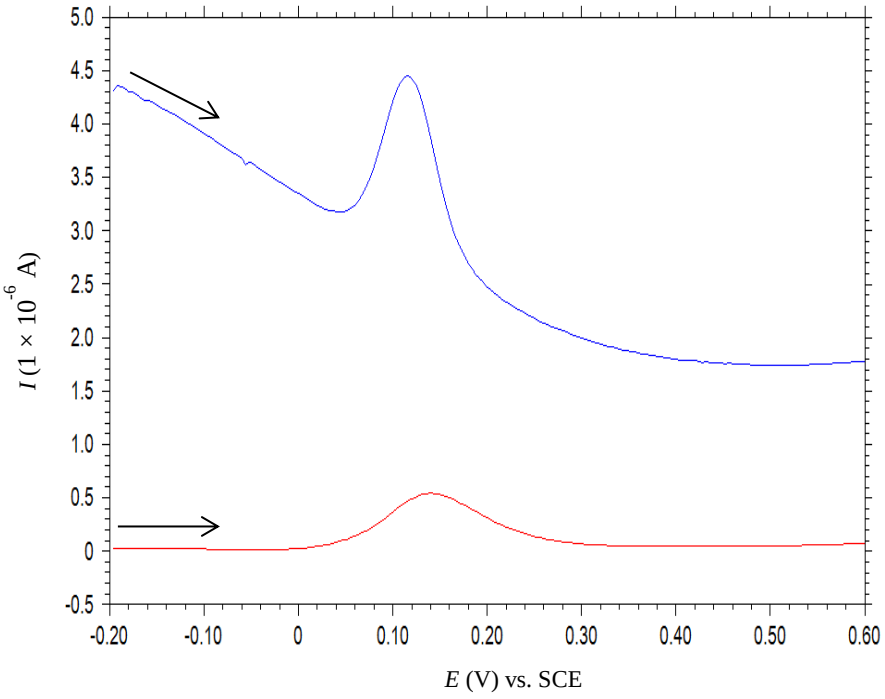

Figure 4.47: Differential pulse voltammograms of DA (5×10^{-5} M) at bare GPE (—) and bare CPE (—) in 0.1 M PBS, pH 6.8.

4.2.11.3 DA electrochemical redox process at S-β-CD modified GPE

The good electrochemical behaviour of DA at bare GPE has encouraged the study of DA determination at S-β-CD modified GPE. The electrode was made using optimum amount of S-β-CD (0.545 g) into the GPE. Under identical conditions described for bare GPE, DPV curve for S-β-CD modified GPE shows a higher oxidation peak current compare to bare GPE as shown in Figure 4.48. The value of oxidation peak current was 7.22×10^{-6} A. As already mentioned S-β-CD at the surface of the electrode can recognize protonated DA molecules and facilitate their insertion into the cyclodextrin cavity. This increased peak current was attributed to the combined effect of high conductivity of graphene and complexation ability of S-β-CD with DA. Graphene acts as a semi-metal or a zero-band semiconductor with remarkably high electron mobility at room temperature [93]. Therefore it could accelerate the electron transfer on the electrode surface to amplify the electrochemical signal due to its outstanding electric conductivity. It is also characterised by an abundance of surface defects which could enhance electron transfer process. On the other, S-β-CD can form an electrostatic interaction and an inclusion complex with DA molecule. Graphene paste modified with S-β-CD is a remarkable sensor toward the detection of DA. An illustration of S-β-CD modified GPE is displayed in Figure 4.49.

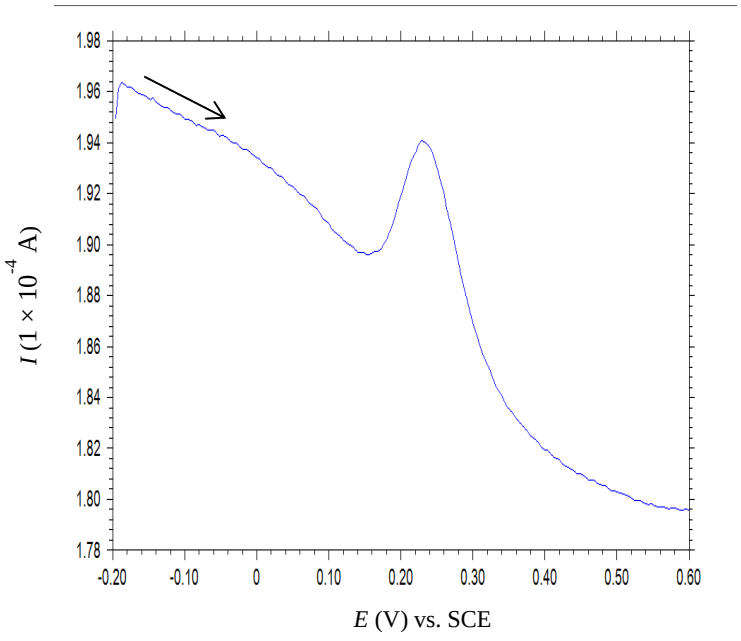

Figure 4.48: Differential pulse voltammogram of DA (5×10^{-5} M) at S-β-CD modified GPE in 0.1 M PBS, pH 6.8.

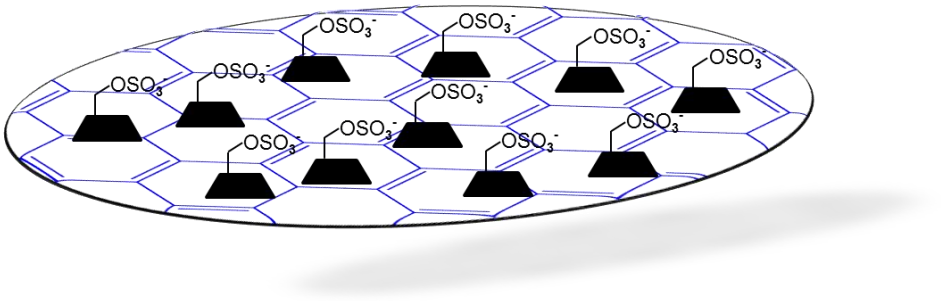

Figure 4.49: Simplified schematic representation of S-β-CD modified GPE

4.2.12 Rotating Disc Electrode Voltammetric studies

RDE voltammetry was used to elucidate the kinetics of S-β-CD modified CPE. The RDE voltammograms were recorded for 1×10^{-5} M DA solution in 0.1 M PBS (pH 6.8) at various rotation rates (from 500 to 2000 rpm). Typical current–potential curves are shown in Figure 4.50. As observed, the hydrodynamic voltammograms show that a steady-state condition is not attained fully. However, under similar experimental conditions, the bare CPE show defined limiting currents, which increase with an increase of the rotating rate (Figure 4.51). This unexpected results obtained at S-β-CD modified CPE may be related to the modifier − S-β-CD − which interact specifically with DA. In this case, the diffusion layer is more likely to be dependent on time and the species at the electrode surface. Even at a higher rotation speed such as 2000 rpm a peak shape wave was observed. When Nafion modified CPE was used a steady state was observed (Figure 4.52). This probably indicates that there is complexation event at the S-β-CD modified CPE/DA interface. DA is oxidised to DOQ, and DOQ is probably released from the cavity and diffused away from the electrode surface before another DA molecule interacts with CD. The space of time taken for DA to interact with CD and get oxidised is more likely responsible for the peak shape wave. Although, kinetic informations could not be obtained, it is worth mentioning that the RDE voltammetric studies are at a preliminary stage and further experiments are required to get a better understanding of the system.

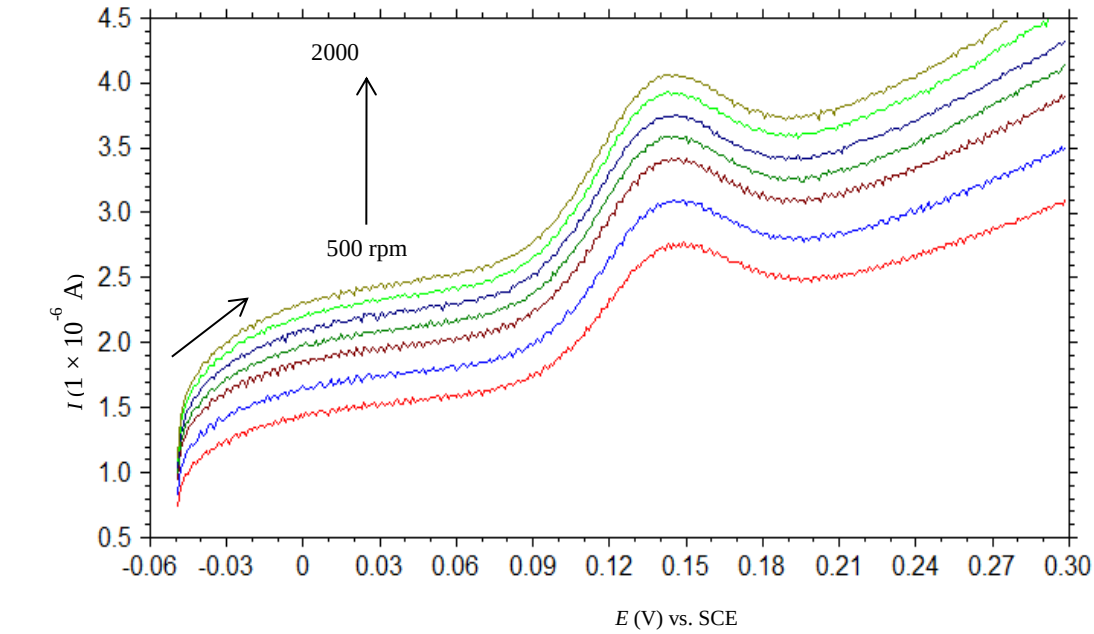

Figure 4.50: RDV of S-β-CD modified CPE in 1 × 10^{-5} M DA at various rotation rate from 500 to 2000 rpm.

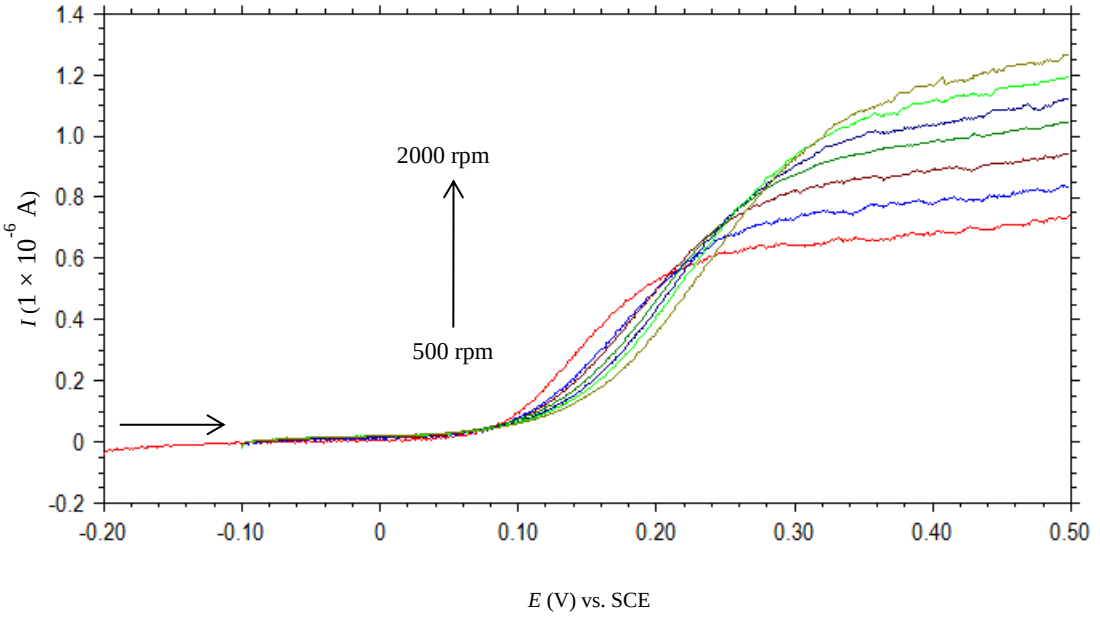

Figure 4.51: RDV of bare CPE in 1 × 10^{-5} M DA at various rotation rate from 500 to 2000 rpm.

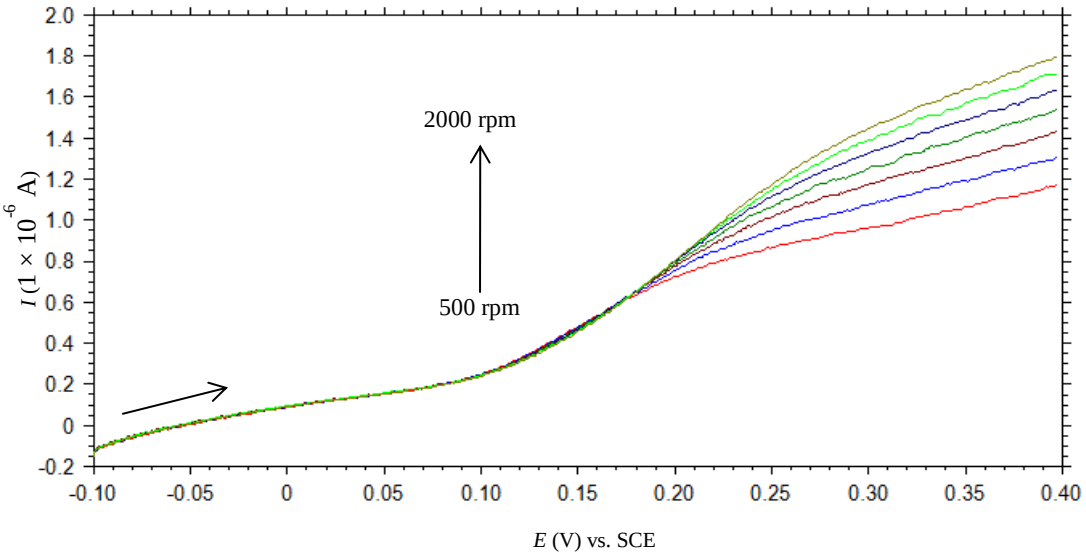

Figure 4.52: RDV of Nafion modified CPE in 1 × 10^{-5} M DA at various rotation rates from 500 to 2000 rpm.

All the modified electrodes employed until now (S-β-CDCPE, CM-β-CDCPE, Fc-β-CDCPE, β-CDCPE and NCPE) exhibit a remarkable enhancement in DA oxidation peak current compared to that obtained at the bare CPE. The presence of the modifiers at the electrode surface plays a key role in the attraction of DA molecules, resulting in an improved DA current response. The proposed sensors can effectively be employed to detect of DA using different electrochemical techniques such as CV, DPV or RDV. However, as already mentioned, DA coexists with compounds such as ascorbic acid and serotonin in biological samples. These three chemicals mutually influence their respective determination at bare electrodes. Therefore, it is important to analyse the behaviour of the modified CPE in a mixture solution containing DA, ascorbic acid and serotonin. This approach is dealt with in the next chapter.

4.3 References

1. Rice, M.E., Galus, Z., and Adams, R.N., *Graphite Paste Electrodes - Effects of Paste Composition and Surface-States on Electron-Transfer Rates.* Journal of Electroanalytical Chemistry, 1983. **143**(1-2): p. 89-102.

2. Kalcher, K., *Chemically Modified Carbon Paste Electrodes in Voltammetric Analysis.* Electroanalysis, 1990. **2**(6): p. 419-433.

3. Wang, J., et al., *Metal-Dispersed Carbon Paste Electrodes.* Analytical Chemistry, 1992. **64**(11): p. 1285-1288.

4. Lindquis.J, *Carbon Paste Electrode with a Wide Anodic Potential Range.* Analytical Chemistry, 1973. **45**(6): p. 1006-1008.

5. Olson, C. and Adams, R.N., *Carbon Paste Electrodes Application to Cathodic Reductions and Anodic Stripping Voltammetry.* Analytica Chimica Acta, 1963. **29**(4): p. 358-363.

6. Deng, Y., et al., *Fabrication of an Electrochemical Biosensor Array for Simultaneous Detection of L-Glutamate and Acetylcholine.* Journal of Biomedical Nanotechnology, 2013. **9**(8): p. 1378-1382.

7. Heli, H., et al., *Copper nanoparticles-modified carbon paste transducer as a biosensor for determination of acetylcholine.* Biosensors & Bioelectronics, 2009. **24**(8): p. 2328-2333.

8. Mahanthesha, K.R. and Swamy, B.E.K., *Pretreated/Carbon paste electrode based voltammetric sensors for the detection of dopamine in presence of ascorbic acid and uric acid.* Journal of Electroanalytical Chemistry, 2013. **703**: p. 1-8.

9. Gilbert, O., et al., *Poly (Alanine) Modified Carbon Paste Electrode for Simultaneous Detection of Dopamine and Ascorbic Acid.* International Journal of Electrochemical Science, 2008. **3**(10): p. 1186-1195.

10. Chowdappa, N., et al., *Cyclic Voltammetric Studies of Serotonin at Sodium Dodecyl Sulfate Modified Carbon Paste Electrode.* International Journal of Electrochemical Science, 2009. **4**(3): p. 425-434.

11. Apetrei, I.M. and Apetrei, C., *Amperometric Tyrosinase Based Biosensors for Serotonin Detection.* Romanian Biotechnological Letters, 2013. **18**(3): p. 8253-8262.

12. Chandrashekar, B.N. and Swamy, B.E.K., *Simultaneous cyclic voltammetric determination of norepinephrine, ascorbic acid and uric acid using TX-100 modified carbon paste electrode.* Analytical Methods, 2012. **4**(3): p. 849-854.

13. Mazloum-Ardakani, M., et al., *New strategy for simultaneous and selective voltammetric determination of norepinephrine, acetaminophen and folic acid using ZrO_2 nanoparticles-modified carbon paste electrode.* Sensors and Actuators B-Chemical, 2010. **151**(1): p. 243-249.

14. Xua, Y.X., Hu, C.G., and Hu, S.S., A *reagentless nitric oxide biosensor based on the direct electrochemistry of hemoglobin adsorbed on the gold colloids modified carbon paste electrode.* Sensors and Actuators B-Chemical, 2010. **148**(1): p. 253-258.

15. Ciolkowski, E.L., et al., *Disproportionation during Electrooxidation of Catecholamines at Carbon-Fiber Microelectrodes.* Analytical Chemistry, 1994. **66**(21): p. 3611-3617.

16. Mo, J.W. and Ogorevc, B., *Simultaneous measurement at dopamine and ascorbate at their physiological levels using voltammetric microprobe based on overoxidized poly(1,2-phenylenediamine)-coated carbon fiber.* Analytical Chemistry, 2001. **73**(6): p. 1196-1202.

17. Volkow, N.D., et al., *Dopamine in drug abuse and addiction: results from imaging studies and treatment implications.* Molecular Psychiatry, 2004. **9**(6): p. 557-569.

18. Scheller, C., et al., *Dopamine activates HIV in chronically infected T lymphoblasts.* Journal of Neural Transmission, 2000. **107**(12): p. 1483-1489.

19. Nohta, H., et al., A*romatic glycinonitriles and methylamines as pre-column fluorescence derivatization reagents for catecholamines.* Analytica Chimica Acta, 1997. **344**(3): p. 233-240.

20. Zhao, J.J., et al., *Development and application of an electrochemiluminescent flow-injection cell based on CdTe quantum dots modified electrode for high sensitive determination of dopamine.* Analyst, 2011. **136**(19): p. 4070-4074.

21. Jin, W., et al., *Determination of monoamine transmitters and their metabolites by capillary electrophoresis with electrochemical detection.* Analytica Chimica Acta, 1999. **382**(1-2): p. 33-37.

22. Tong, C.L., et al., *Determination of dopamine and epinephrine by ion chromatography with fluorescence detection.* Chinese Journal of Analytical Chemistry, 2001. **29**(10): p. 1237-1237.

23. Kawagoe, K.T. and Wightman, R.M., *Characterization of* A*mperometry for in-Vivo Measurement of Dopamine Dynamics in the Rat-Brain.* Talanta, 1994. **41**(6): p. 865-874.

24. Njagi, J., et al., A*mperometric Detection of Dopamine in Vivo with an Enzyme Based Carbon Fiber Microbiosensor.* Analytical Chemistry, 2010. **82**(3): p. 989-996.

25. Vickrey, T.L., Condron, B., and Venton, B.J., *Detection of Endogenous Dopamine Changes in Drosophila melanogaster Using Fast-Scan Cyclic Voltammetry.* Analytical Chemistry, 2009. **81**(22): p. 9306-9313.

26. Colin-Orozco, E., et al., *Electrochemical quantification of dopamine in the presence of ascorbic acid and uric acid using a simple carbon paste electrode modified with SDS micelles at pH 7.* Electrochimica Acta, 2012. **85**: p. 307-313.

27. Winter, E., Codognoto, L., and Rath, S., *Electrochemical behavior of dopamine in the presence of citrate: Reaction mechanism.* Electrochimica Acta, 2006. **51**(7): p. 1282-1288.

28. Svancara, I., et al., *Carbon Paste Electrodes in Facts, Numbers, and Notes:* A *Review on the Occasion of the 50-Years Jubilee of Carbon Paste in Electrochemistry and Electroanalysis.* Electroanalysis, 2009. **21**(1): p. 7-28.

29. Colin-Orozco, E., et al., *On the Electrochemical Oxidation of Dopamine,* A*scorbic* A*cid and Uric* A*cid onto a Bare Carbon Paste Electrode from a 0.1 M NaCl* A*queous Solution at pH 7.* International Journal of Electrochemical Science, 2012. **7**(7): p. 6097-6105.

30. Svancara, I. and Schachl, K., *Testing of unmodified carbon paste electrodes.* Chemicke Listy, 1999. **93**(8): p. 490-499.

31. Laviron, E., *General Expression of the Linear Potential Sweep Voltammogram in the Case of Diffusionless Electrochemical Systems.* Journal of Electroanalytical Chemistry, 1979. **101**(1): p. 19-28.

32. Corona-Avendano, S., et al., *On the electrochemistry of dopamine in aqueous solution. Part I: The role of [SDS] on the voltammetric behavior of dopamine on a carbon paste electrode.* Journal of Electroanalytical Chemistry, 2007. **609**(1): p. 17-26.

33. Majewska, U.E., et al., *Dopamine oxidation at per(6-deoxy-6-thio)-alpha-cyclodextrin monolayer modified gold electrodes.* Electroanalysis, 2006. **18**(15): p. 1463-1470.

34. Malem, F. and Mandler, D., *Self-*A*ssembled Monolayers in Electroanalytical Chemistry - A*pplication *of Omega-Mercapto Carboxylic-*A*cid Monolayers for the Electrochemical Detection of Dopamine in the Presence of a High-Concentration of* A*scorbic-*A*cid.* Analytical Chemistry, 1993. **65**(1): p. 37-41.

35. Aslanoglu, M., et al., *Electrochemical determination of dopamine in the presence of ascorbic acid using a poly(3-acetylthiophene) modified glassy carbon electrode.* Acta Chimica Slovenica, 2007. **54**(4): p. 834-839.

36. Hendy, G.M. and Breslin, C.B., A*n electrochemical study in aqueous solutions on the binding of dopamine to a sulfonated cyclodextrin host.* Electrochimica Acta, 2012. **59**: p. 290-295.

37. Hendy, G.M. and Breslin, C.B., A *spectrophotometric and NMR study on the formation of an inclusion complex between dopamine and a sulfonated cyclodextrin host.* Journal of Electroanalytical Chemistry, 2011. **661**(1): p. 179-185.

38. Harley, C.C., Rooney, A.D., and Breslin, C.B., *The selective detection of dopamine at a polypyrrole film doped with sulfonated beta-cyclodextrins.* Sensors and Actuators B-Chemical, 2010. **150**(2): p. 498-504.

39. Bordwell, F.G. and Algrim, D., *Nitrogen Acids .1. Carboxamides and Sulfonamides.* Journal of Organic Chemistry, 1976. **41**(14): p. 2507-2508.

40. Mccreery, R.L., et al., *Control of Reactivity at Carbon Electrode Surfaces.* Colloids and Surfaces a-Physicochemical and Engineering Aspects, 1994. **93**: p. 211-219.

41. Chen, P.H., Fryling, M.A., and Mccreery, R.L., *Electron-Transfer Kinetics at Modified Carbon Electrode Surfaces - the Role of Specific Surface Sites.* Analytical Chemistry, 1995. **67**(18): p. 3115-3122.

42. Hung, N.C. and Nagy, Z., *Kinetics of the Ferrous Ferric Electrode-Reaction in the Absence of Chloride Catalysis.* Journal of the Electrochemical Society, 1987. **134**(9): p. 2215-2220.

43. Forshey, P.A. and Kuwana, T., *Electrochemistry of Oxygen Reduction .4. Oxygen to Water Conversion by Iron(II) Tetrakis(N-Methyl-4-Pyridyl)Porphyrin Via Hydrogen-Peroxide.* Inorganic Chemistry, 1983. **22**(5): p. 699-707.

44. Hossain, M.S., Tryk, D., and Yeager, E., *The Electrochemistry of Graphite and Modified Graphite Surfaces - the Reduction of O_2.* Electrochimica Acta, 1989. **34**(12): p. 1733-1737.

45. Yeager, E., *Dioxygen Electrocatalysis - Mechanisms in Relation to Catalyst Structure.* Journal of Molecular Catalysis, 1986. **38**(1-2): p. 5-25.

46. Deakin, M.R., Stutts, K.J., and Wightman, R.M., *The Effect of Ph on Some Outer-Sphere Electrode-Reactions at Carbon Electrodes.* Journal of Electroanalytical Chemistry, 1985. **182**(1): p. 113-122.

47. Cabaniss, G.E., et al., *Electrocatalysis of Proton-Coupled Electron-Transfer Reactions at Glassy-Carbon Electrodes.* Journal of the American Chemical Society, 1985. **107**(7): p. 1845-1853.

48. Kekedy, L. and Makkay, F., *Experimental Approach to Characterization of Pretreated Platinum Electrode Surfaces .I. A Chronopotentiometric Study.* Revue Roumaine De Chimie, 1968. **13**(6): p. 739-740.

49. Panzer, R.E. and Elving, P.J., *Behavior of Carbon Electrodes in Aqueous and Non-Aqueous Systems.* Journal of the Electrochemical Society, 1972. **119**(7): p. 864-873.

50. Granger, M.C., et al., *Standard electrochemical behavior of high-quality, boron-doped polycrystalline diamond thin-film electrodes.* Analytical Chemistry, 2000. **72**(16): p. 3793-3804.

51. Chen, F.T.A., Shen, G., and Evangelista, R.A., *Characterization of highly sulfated cyclodextrins.* Journal of Chromatography A, 2001. **924**(1-2): p. 523-532.

52. Perrin, C., et al., *Robustness testing of chiral separations by capillary electrophoresis using highly-sulfated cyclodextrins.* Journal of Chromatography A, 2003. **1007**(1-2): p. 165-177.

53. Yang, Y., et al., *Highly selective dopamine determination by using carboxymethylated beta-cyclodextrin polymer film modified electrode.* Analytical Letters, 2004. **37**(11): p. 2267-2282.

54. Holmes, D.L. and Lightner, D.A., *Synthesis and* A*cidity Constants of (CO_2H)-C-13-Labeled Mono and Dipyrrole Carboxylic-*A*cids - Pk(a) from C-13-Nmr.* Tetrahedron, 1995. **51**(6): p. 1607-1622.

55. Gadde, S., Batchelor, E.K., and Kaifer, A.E., *Electrochemistry of Redox* A*ctive Centres Encapsulated by Non-Covalent Methods.* Australian Journal of Chemistry, 2010. **63**(2): p. 184-194.

56. Gao, Z.N., Wen, X.L., and Li, H.L., *Study of the inclusion complexes of catecholamines with beta-cyclodextrin by cyclic voltammetry.* Polish Journal of Chemistry, 2002. **76**(7): p. 1001-1007.

57. Cosnier, S., Shan, D., and Ding, S.N., A*n easy compartment-less biofuel cell construction based on the physical co-inclusion of enzyme and mediator redox within pressed graphite discs.* Electrochemistry Communications, 2010. **12**(2): p. 266-269.

58. Shan, D., Yao, W., and Xue, H., *Electrochemical study of ferrocenemethanol-modified layered double hydroxides composite matrix:* A*pplication to glucose amperometric biosensor.* Biosensors & Bioelectronics, 2007. **23**(3): p. 432-437.

59. Watkins, J.D., et al., *Liquid vertical bar liquid biphasic electrochemistry in ultra-turrax dispersed acetonitrile vertical bar aqueous electrolyte systems.* Electrochimica Acta, 2010. **55**(28): p. 8808-8814.

60. Zhao, N., et al., *Electrochemical assay of active prostate-specific antigen (PS*A*) using ferrocene-functionalized peptide probes.* Electrochemistry Communications, 2010. **12**(3): p. 471-474.

61. Kamyabi, M.A. and Aghajanloo, F., *Electrocatalytic Response of Dopamine at a Carbon Paste Electrode Modified with Ferrocene.* Croatica Chemica Acta, 2009. **82**(3): p. 599-606.

62. Harada, A. and Takahashi, S., *Preparation and Properties of Cyclodextrin-Ferrocene Inclusion Complexes.* Journal of the Chemical Society-Chemical Communications, 1984(10): p. 645-646.

63. Jeon, W.S., et al., *Complexation of ferrocene derivatives by the cucurbit[7]uril host:* A *comparative study of the cucurbituril and cyclodextrin host families.* Journal of the American Chemical Society, 2005. **127**(37): p. 12984-12989.

64. Rekharsky, M.V. and Inoue, Y., *Complexation thermodynamics of cyclodextrins.* Chemical Reviews, 1998. **98**(5): p. 1875-1917.

65. Komiyama, M. and Bender, M.L., *Thermodynamic Studies of Cyclodextrin-Accelerated Cleavage of Phenyl Esters.* Journal of the American Chemical Society, 1978. **100**(14): p. 4576-4579.

66. Reetz, M.T., *New supramolecular transition metal catalysts.* Journal of Heterocyclic Chemistry, 1998. **35**(5): p. 1065-1073.

67. Laoire, C.O., et al., *Electrochemical studies of ferrocene in a lithium ion conducting organic carbonate electrolyte.* Electrochimica Acta, 2009. **54**(26): p. 6560-6564.

68. Fernandez, L. and Carrero, H., *Electrochemical evaluation of ferrocene carboxylic acids confined on surfactant-clay modified glassy carbon electrodes: oxidation of ascorbic acid and uric acid.* Electrochimica Acta, 2005. **50**(5): p. 1233-1240.

69. Brooks, S.L., et al., *Development of an Online Glucose Sensor for Fermentation Monitoring.* Biosensors, 1987. **3**(1): p. 45-56.

70. Tsiafoulis, C.G., et al., *Electrochemical study of ferrocene intercalated vanadium pentoxide xerogel/polyvinyl alcohol composite films: Application in the development of amperometric biosensors.* Electrochemistry Communications, 2005. **7**(7): p. 781-788.

71. Kandimalla, V.B., Tripathi, V.S., and Ju, H.X., A *conductive ormosil encapsulated with ferrocene conjugate and multiwall carbon nanotubes for biosensing application.* Biomaterials, 2006. **27**(7): p. 1167-1174.

72. Gorton, L., et al., A *Glucose Electrode Based on Carbon Paste Chemically Modified with a Ferrocene-Containing Siloxane Polymer and Glucose-Oxidase, Coated with a Poly(Ester-Sulfonic Acid) Cation-Exchanger.* Analytica Chimica Acta, 1990. **228**(1): p. 23-30.

73. Jonsson, G., L. Gorton, and Pettersson, L., *Mediated Electron-Transfer from Glucose-Oxidase at a Ferrocene-Modified Graphite Electrode.* Electroanalysis, 1989. **1**(1): p. 49-55.

74. Foulds, N.C. and Lowe, C.R., *Immobilization of Glucose-Oxidase in Ferrocene-Modified Pyrrole Polymers.* Analytical Chemistry, 1988. **60**(22): p. 2473-2478.

75. Zhang, G.R., et al., *beta-Cyclodextrin-ferrocene inclusion complex modified carbon paste electrode for amperometric determination of ascorbic acid.* Talanta, 2000. **51**(5): p. 1019-1025.

76. Monfared, H.H., et al., *Synthesis, structural characterization and electrochemical studies of a nicotinamide-bridged dinuclear copper complex derived from a tridentate hydrazone Schiff base ligand.* Zeitschrift Fur Anorganische Und Allgemeine Chemie, 2007. **633**(11-12): p. 1945-1948.

77. Vining, W.J. and Meyer, T.J., *Direct Evidence for Chemically Distinct Regions within Nafion Films on Electrodes.* Journal of Electroanalytical Chemistry, 1987. **237**(2): p. 191-208.

78. Martin, C.R., Rubinstein, I., and Bard, A.J., *Polymer-Films on Electrodes .9. Electron and Mass-Transfer in Nafion Films Containing $[Ru(Bpy)_3]^{2+}$*. Journal of the American Chemical Society, 1982. **104**(18): p. 4817-4824.

79. Yeager, H.L. and Eisenberg, A., *Perfluorinated Ionomer Membranes - Introduction.* Acs Symposium Series, 1982. **180**: p. 1-6.

80. Martin, C.R. and Freiser, H., *Ion-Selective Electrodes Based on an Ionic Polymer.* Analytical Chemistry, 1981. **53**(6): p. 902-904.

81. Szentirmay, M.N. and Martin, C.R., *Ion-Exchange Selectivity of Nafion Films on Electrode Surfaces.* Analytical Chemistry, 1984. **56**(11): p. 1898-1902.

82. Rubinstein, I. and Bard, A.J., *Polymer-Films on Electrodes .5. Electrochemistry and Chemi-Luminescence at Nafion-Coated Electrodes.* Journal of the American Chemical Society, 1981. **103**(17): p. 5007-5013.

83. Buttry, D.A. and Anson, F.C., *Effects of Electron Exchange and Single-File Diffusion on Charge Propagation in Nafion Films Containing Redox Couples.* Journal of the American Chemical Society, 1983. **105**(4): p. 685-689.

84. Li, H.W. and Schlick, S., *Structure and Dynamics of Perfluorinated Ionomers Using Paramagnetic Cations - ESR of VO(2+) in Swollen Membranes and in Ionomer Solutions.* Abstracts of Papers of the American Chemical Society, 1993. **206**(34): p. 446-447.

85. White, H.S., Leddy, J., and Bard, A.J., *Polymer-Films on Electrodes .8. Investigation of Charge-Transport Mechanisms in Nafion Polymer Modified Electrodes.* Journal of the American Chemical Society, 1982. **104**(18): p. 4811-4817.

86. Hoyer, B., Florence, T.M., and Batley, G.E., A*pplication of Polymer-Coated Glassy-Carbon Electrodes in* A*nodic-Stripping Voltammetry*. Analytical Chemistry, 1987. **59**(13): p. 1608-1614.

87. Zhou, J.X. and Wang, E., *Ion-Exchange of Cationic Drugs at a Nafion-Coated Electrode in Flow-through* A*nalysis.* Analytica Chimica Acta, 1991. **249**(2): p. 489-494.

88. Rocha, L.S. and Carapuca, H.M., *Ion-exchange voltammetry of dopamine at Nafion-coated glassy carbon electrodes: Quantitative features of ion-exchange partition and reassessment on the oxidation mechanism of dopamine in the presence of excess ascorbic acid.* Bioelectrochemistry, 2006. **69**(2): p. 258-266.

89. Huong, V.T., et al., *Polymethylthiophene/Nafion-modified glassy carbon electrode for selective detection of dopamine in the presence of ascorbic acid.* Journal of Applied Electrochemistry, 2009. **39**(10): p. 2035-2042.

90. Lee, Y.J. and Park, J.Y., *Highly Selective and Sensitive Electrochemical Detection of Dopamine Using a Nafion Coated Hybrid Macroporous Gold Modified Electrode With Platinum Nanoparticles.* Ieee Transactions on Nanobioscience, 2011. **10**(4): p. 250-258.

91. Nagy, G., et al., *Ion-Exchange and Transport of Neurotransmitters in Nafion Films on Conventional and Microelectrode Surfaces.* Journal of Electroanalytical Chemistry, 1985. **188**(1-2): p. 85-94.

92. Davies, T.J., Hyde, M.E., and Compton, R.G., *Nanotrench arrays reveal insight into graphite electrochemistry.* Angewandte Chemie-International Edition, 2005. **44**(32): p. 5121-5126.

93. Shang, N.G., et al., *Catalyst-Free Efficient Growth, Orientation and Biosensing Properties of Multilayer Graphene Nanoflake Films with Sharp Edge Planes.* Advanced Functional Materials, 2008. **18**(21): p. 3506-3514.

94. Ma, X.Y., Chao, M.Y., and Wang, Z.X., *Electrochemical detection of dopamine in the presence of epinephrine, uric acid and ascorbic acid using a graphene-modified electrode.* Analytical Methods, 2012. **4**(6): p. 1687-1692.

95. Sheng, Z.H., et al., *Electrochemical sensor based on nitrogen doped graphene: Simultaneous determination of ascorbic acid, dopamine and uric acid.* Biosensors & Bioelectronics, 2012. **34**(1): p. 125-131.

5 Interference studies: Electrochemical Detection of DA in the Presence of AA and 5-HT

5.1 Introduction

Determination of DA levels in the cerebrospinal fluid is of paramount medical importance due to its significant role as a neurotransmitter [1]. Monitoring the changes in DA levels has proven to be a very effective route toward understanding brain function. DA is linked to learning and memory formation, and the physiological and pathological process of Parkinson's Disease, Alzheimer's Disease, schizophrenia, depression and numerous other neurological disorders [1, 2]. Therefore, there is a continued and pressing interest in the development of simple and sensitive methods for the quantification of DA in the CSF. Several methods can be employed for determination of DA, including electrochemical techniques. The problem with electrochemical determination of DA at common solid electrodes is the presence of a myriad of other redox active species that populate the cerebrospinal fluid. For example Ascorbic acid (AA) or vitamin C is the main electroactive interferent. AA is used in large scales as an antioxidant in food, animal feed, beverages, pharmaceutical formulations and cosmetic applications [3, 4]. It has been investigated for the prevention and treatment of the common cold, mental illness, infertility and cancer [5].

Serotonin (5-hydroxytryptamine, 5-HT) plays a vital role in the regulation of mood, sleep, sexuality, and appetite. Low levels of 5-HT are associated with several disorders, including depression, anxiety, and migraines [6, 7]. Extremely high levels of 5-HT can cause toxicity and fatal effects known as serotonin syndrome [8]. These three substances influence each other in their respective determination from biological systems [9].

In the extra-cellular fluid of the central nervous system, AA concentration is generally higher than that of DA. Usually, the concentration of DA is 10^{-8} to 10^{-6} M while AA is as high as 10^{-4} M in biological systems [10]. Moreover, AA oxidized at nearly same potential as DA at bare electrodes [11, 12]. The voltammetric response is generally characterised by an overlapping signal [13-15]. In addition, the oxidation products of DA can homogeneously catalyse the oxidation of AA, which may lead to the inaccurate detection of DA and AA [16]. AA is therefore a major interfering compound in the detection and analysis of DA. On the other hand, it is well known that 5-HT and DA influence each other in their respective brain functions, and determination, from biological systems [9]. The direct oxidation of these three species at the bare electrodes occurs at very similar potentials. Further redox products can cause a pronounced fouling of the electrode surface, which results in rather poor selectivity, sensitivity, and reproducibility. So, the ability to selectively detect DA, 5-HT and AA, has been a

matter of great interest in electrochemical research. Up to now, there are a few reports in the literature about the simultaneous electrochemical determination of DA, 5-HT and AA, particularly with the use of carbon materials.

Simultaneous electrochemical determination requires an electrode material capable of resolving these oxidation processes. The situation can be resolved by using chemically modified electrodes. As already mentioned, CPE is one of the convenient conductive matrixes to prepare chemically modified electrodes by simple mixing of graphite / binder paste and modifier [17]. These kinds of electrodes are inexpensive and possess many advantages such as low background current, wide range of used potential, easy fabrication, and rapid renewal [18, 19].

Carbon paste electrodes modified with TX-100 [20], carbon nanotubes dispersed in polyethylenimine [21] and non-ionic polymer films [22] have been employed for the voltammetric determination of DA and 5-HT in the presence of AA.

The main objective of this study encompasses the use of carbon paste modified electrodes, detailed in Chapter 4, for selective or simultaneous determination of DA, AA and 5-HT in 0.1 M PBS (pH 6.8). In Chapter 4, it was shown that modifiers such as S-β-CD, CM-β-CD and Nafion are charged and gave enhancement effect on the DA oxidation peak currents. Therefore, the major consideration of the present study is based on the difference in ionic forms of DA, AA and 5-HT at pH 6.8. AA exists in the anionic form (pK_a = 4.10), while DA and 5-HT are in the cationic form [23]. Consequently, the carbon paste electrode modified with S-β-CD, CM-β-CD or Nafion, may act as an ion exchanger to repel the negatively charged AA, thus enabling the selective sensing of DA and 5-HT. As a result, the discrimination between voltammetric response of DA and 5-HT in the presence of AA was achieved. Initially, data pertaining to the voltammetric responses of DA, AA and 5-HT, at the CPE with the different modifiers are presented. Calibration curves, the limits of detection, and comparative data tables, are presented in the latter part of this chapter.

5.2 Results and Discussion

5.2.1 Electrochemical Study of a Mixture of AA and DA

The successful route to overcome the problem of selectivity is to modify the electrode surface. Modified electrodes, when compared to unmodified electrodes, can decrease analyte overpotentials and improve mass transfer velocity profiles, which, effectively, enrich analyte concentrations at the electrode / solution interface [24, 25]. In this study, the electrochemical behaviour of a mixture of AA (1×10^{-3} M) and DA (5×10^{-5} M) was investigated on various type of electrodes, including, S-β-CD modified CPE, CPE with oxide layer (CPE/O), Nafion modified CPE, Fc-β-CD modified CPE, bare GPE and S-β-CD modified CPE using cyclic voltammetry and differential pulse voltammetry. The resulting voltammograms were compared to those obtained at bare CPE.

5.2.1.1 Electrochemical investigation of AA at bare CPE

The electrochemical behaviour of AA (1×10^{-3} M) in 0.1 M PBS (pH 6.8) at bare CPE was investigated by cyclic voltammetry and typical data are presented in Figure 5.1. From the voltammetric trace we observe an oxidation peak ($I_{pa} = 1.087 \times 10^{-6}$ A), which occurs at +0.150 V vs. SCE, and an absence of a reduction wave on the reverse sweep. Therefore, direct oxidation of AA at an unmodified CPE shows an irreversible oxidation wave at a positive potential. This experimental result is in agreement with those presented in the literature [26]. In fact, the oxidation of AA at bare electrodes is generally believed to be totally irreversible.

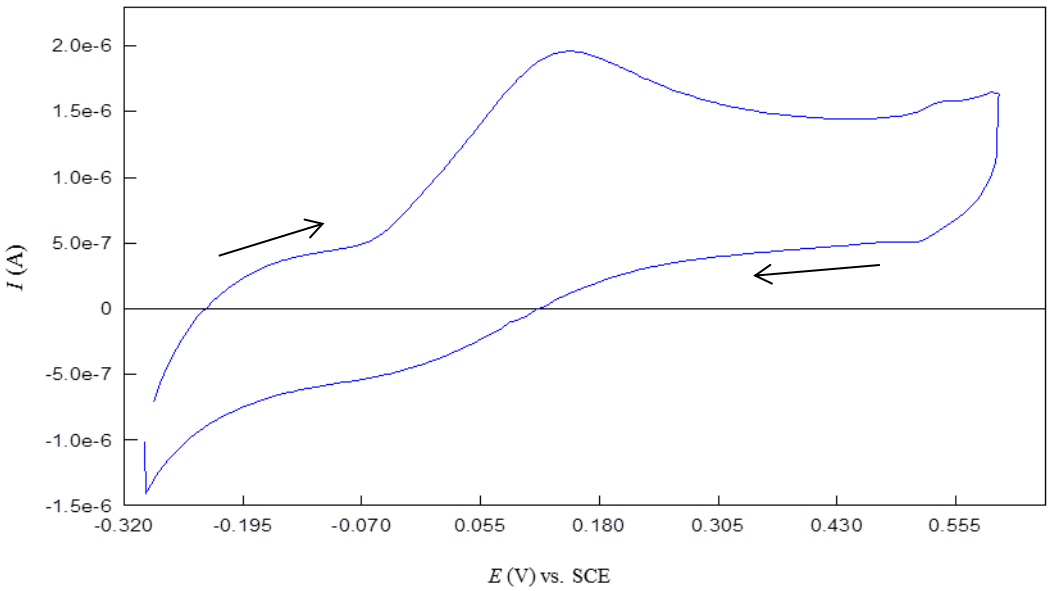

Figure 5.1: Cyclic voltammogram of AA (1×10^{-3} M) at bare CPE in 0.1 M PBS (pH 6.8); scan rate: 50 mV / s.

The electrochemical oxidation of AA has been extensively studied [12, 27, 28], and a mechanism proposed by Ruiz using a mercury electrode for the reaction below pH 8 is widely accepted [27]. According to this mechanism, two-electron oxidation from AA to dehydro-ascorbic acid (DHA) consists of two consecutive one-electron transfers, the second of which is the rate determining step. It is well known that the electrochemical oxidation of AA proceeds similarly on carbon electrodes without any metal catalyst [12]. Scheme 5.1 illustrates the reaction mechanism from AA to DHA. This mechanism involves a pre-dissociation of a proton to give the monoanionic species (Equation 5.1) followed by a 1 e^-, 1 H^+ oxidation of the monoanionic species to form a radical anion (Equation 5.2), which then undergoes a second irreversible 1 e^- oxidation to DHA (Equation 5.3). The latter species can be protonated and then dehydrated to yield the final product of 2,3-diketogulonic acid (Equation 5.4) [29]. This final product is readily adsorbed on the electrode surface and could cause electrode fouling [30]. A high overpotential for AA oxidation may then be required.

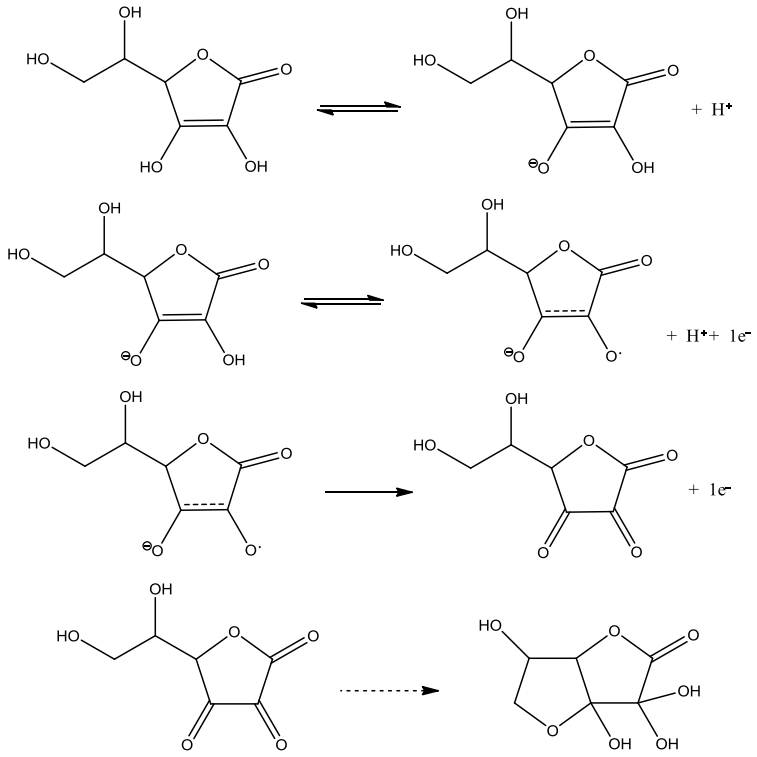

Equation 5.1

Equation 5.2

Equation 5.3

Equation 5.4

Scheme 5.1: Proposed AA reaction at bare CPE in 0.1 M PBS (pH 6.8).

5.2.1.2 Electrochemical investigation of a mixture of AA and DA at bare CPE

The investigation into the electrochemical behaviour of AA and DA at bare CPE was performed using cyclic voltammetry in AA / DA solution mixtures ([AA] = 1×10^{-3} M, [DA] = 5×10^{-5} M in 0.1 M PBS), and single analyte only solutions. As observed in Figure 5.2(a), the oxidation peak potential for AA at the bare CPE electrode surface occurs at +0.150 V, which is fairly close to that of DA (+0.225 V vs. SCE). Therefore, the oxidation of the two species results in an overlapping voltammetric response. A typical trace obtained in a solution mixture is shown in Figure 5.2(b). The voltammograms obtained exhibit only one anodic oxidation peak due to overlapping signal for DA and AA. In addition, a small reduction peak corresponding to the reduction of DOQ is observed. Through this interference, AA hinders the accurate detection of DA. In addition, the oxidised DA product, DOQ, can be catalytically reduced to DA by AA [1] that again becomes available for oxidation according to equation shown in Scheme 5.2. The mechanism for DA oxidation at bare CPE in the presence of AA, resulting in a homogeneous catalytic oxidation of AA, regenerating DA to the electrode has been reported by Dayton *et al* and Domenech *et al* [16, 31], and corresponds to the above observations. Furthermore, the products of AA oxidation foul the electrode surface, thus complicating the determination of both AA and DA. These

observations clearly indicate that the existence of AA detrimentally interferes with the determination of DA at bare CPE electrode. These experimental results are in agreement with those reported in literature [23, 30] and show that simultaneous electrochemical detection of DA and AA is not feasible at bare CPE.

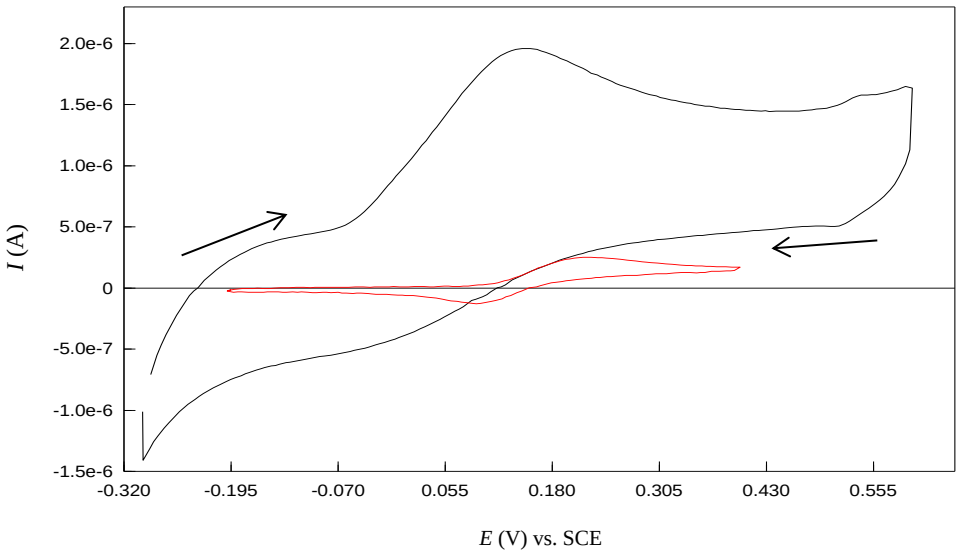

(a)

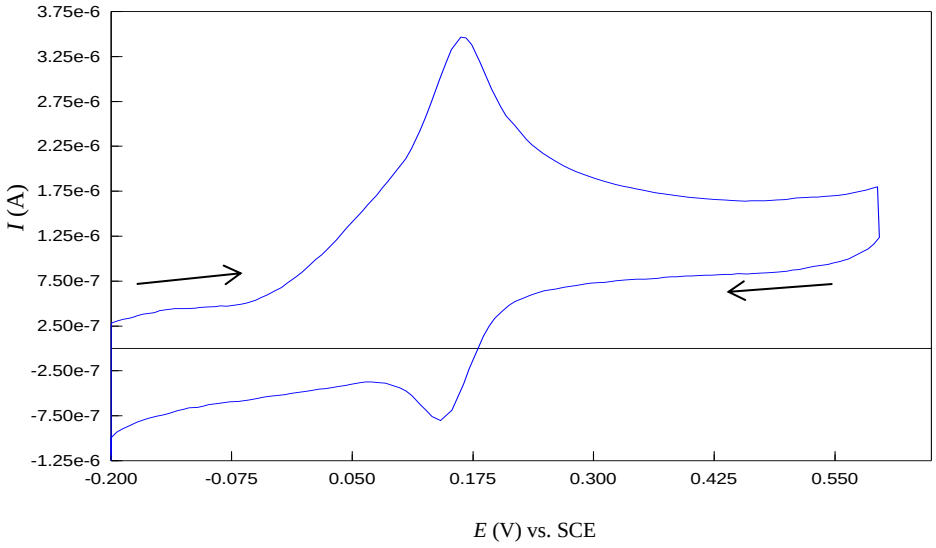

(b)

Figure 5.2: Typical cyclic voltammograms obtained in solutions of 1×10^{-3} M AA (–) and 5×10^{-5} M DA (–) (a), and the DA, AA mixture (b) at bare CPE in 0.1 M PBS (pH 6.8); scan rate: 50 mV / s.

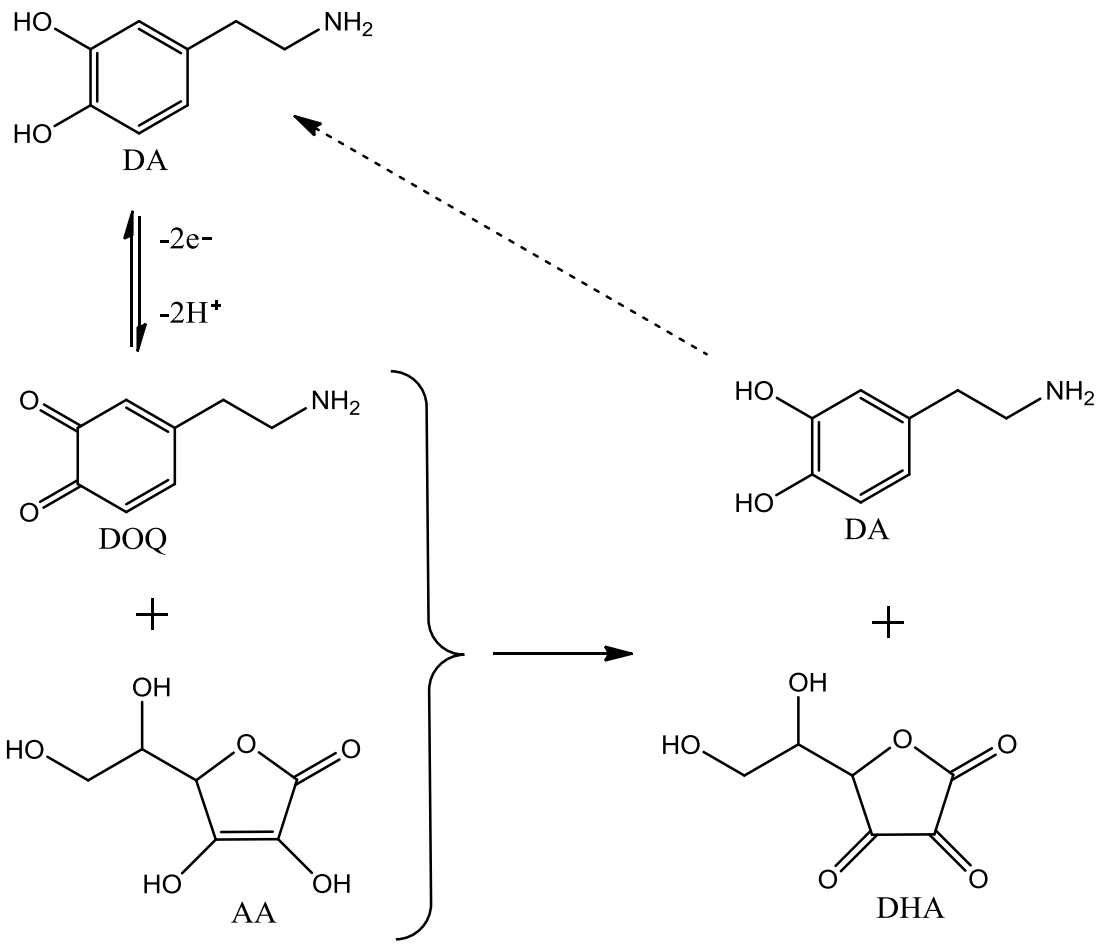

Scheme 5.2: Proposed mechanism for simultaneous oxidation of DA and AA at bare CPE.

5.2.1.3 Experimental Timescale in Simultaneous Detection of AA and DA at bare CPE

In order to observe whether or not experimental timescale has an effect on the behaviour of the mixture of DA and AA at bare CPE, a scan rate study was performed. Figure 5.3 shows the variation of scan rate (from 10 to 80 V vs. SCE) in a mixture of DA (5×10^{-5} M) and AA (1×10^{-3} M). As can be seen, the overlapping signal of DA and AA increased with increasing scan rate. However, the signals were not resolved by experimental timescale, thus, signal separation of the two species is not dependant on scan rate.

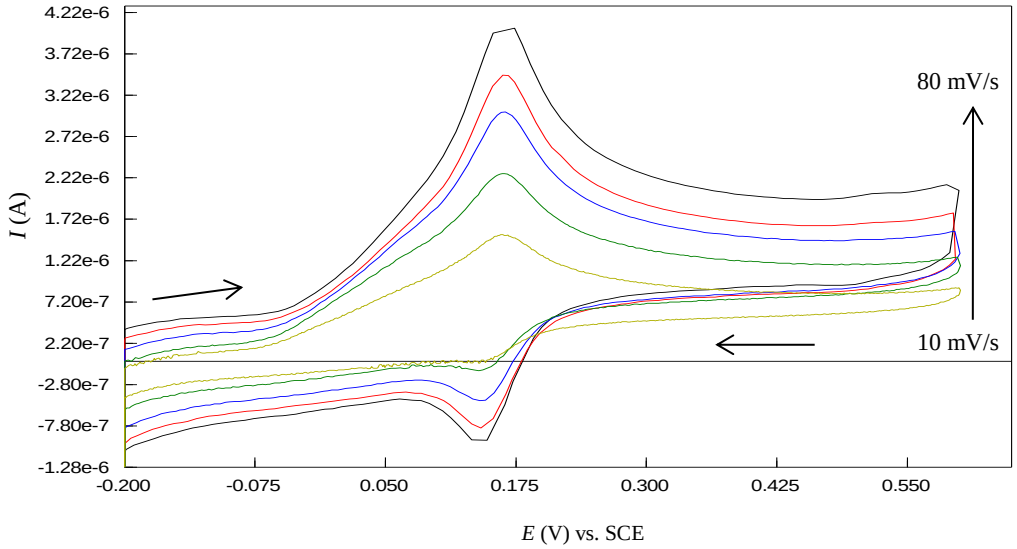

Figure 5.3: Cylic voltammetric responses obtained in a mixture of AA (1×10^{-3} M) and DA 5×10^{-5} M DA at bare CPE at scan rates ranging from 10 to 80 mV / s, in 0.1 M PBS (pH 6.8).

5.2.1.4 Electrochemical behaviour of AA at S-β-CD modified CPE

The electrochemical behaviour of S-β-CD modified CPE in AA (1×10^{-3} M) solution was studied by cyclic voltammetry and a typical voltammogram is displayed in Figure 5.4(a). A defined peak corresponding to the oxidation of AA to DHA was obtained at a peak potential of 0.018 V vs. SCE. This value indicates that the oxidation of AA shifted to less positive potential compared to that obtained at bare CPE. In addition, compared to CPE, an enhancement of peak current was observed ($I_{pa} = 3.515 \times 10^{-6}$ A).

Overall, the anodic potential shift and the improved value of peak current of AA at S-β-CD modified CPE indicate that an affinity exists between the modified electrode and AA. A probable explanation is related to charge carried by AA and S-β-CD at pH 6.8. The modified electrode is negatively charged due to dissociation of sulfonic acid groups present on the rims of cyclodextrin. Therefore, in theory, the sulfate groups should prevent the AA anions from approaching the electrode surface. However, some amount of AA should reach the electrode surface, overcoming the repulsion. At close proximity to the electrode AA is then oxidised easily, probably facilitated through hydrogen bonding at the surface. It is important to recall that S-β-CD modified CPE used in this study is a mixture of cyclodextrin with 7 to 11 sulfated groups per molecule. A repulsive force may occur between the negatively charged sulfates. Hence, allowing hydrogen bonding between AA and several hydroxyl groups at the primary and secondary rims of S-β-CD. This phenomenon was observed by T. Thomas *et al* [32].

The author showed that graphite oxide bulk modified CPE could be used for selective detection of DA in the presence of large excess of AA at physiological pH. The modifier, graphite oxide, contained some carboxylic acid and phenolic groups. Therefore, it was negatively charged at pH 7.4. However, AA was easily oxidised at the electrode surface by overcoming the repulsive force of negatively charged functional groups through hydrogen-bonding. The resulted peak potential of AA was lower than that observed at the bare CPE.

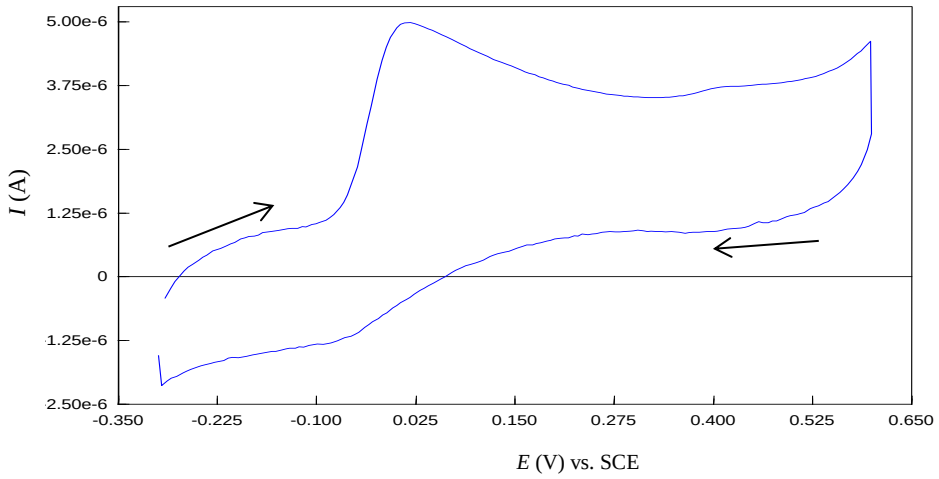

(a)

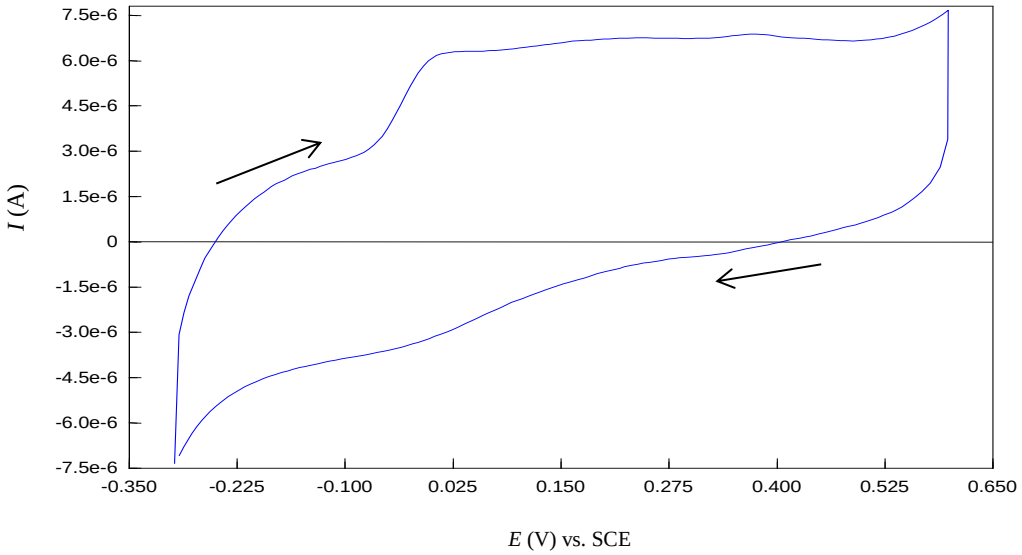

(b)

Figure 5.4: Cyclic voltammograms of AA(1×10^{-3} M) at S-β-CD (0.345 g) modified CPE (a) and at S-β-CD (0.545 g) modified CPE (b) in 0.1 M PBS (pH 6.8); scan rate: 50 mV / s.

It is worth mentioning that the modified electrode used from Figure 5.4 (a) contains a relatively low amount of 0.345 g S-β-CD. When 0.545 g S-β-CD (which the optimum

amount for detection of DA) was used, a different peak shape of AA was observed as shown in Figure 5.4 (b). Although, the oxidation peak potential remained nearly unchanged, the voltammogram shows a more steady-state type character with a limiting current plateau. Even though a limiting current behaviour would indicate that the surface is saturated with AA, it was also observed that the peak response (2.43×10^{-6} A) declined slightly when 0.545 g S-β-CD was employed. This can be justified in that a larger amount of S-β-CD, through the increased coulombic repulsion, restricts AA access to the electrode surface, but the bulk solution concentration ensures active site saturation. In effect the number of active sites, available to AA for oxidation, decreases with an increase in amount of S-β-CD. Since the oxidation of AA is shifted to a less positive potential at the S-β-CD modified CPE, the electrode should, in principle not interfere with the measurement of DA.

5.2.1.5 Electrochemical behaviour of a mixture of AA and DA at S-β-CD modified CPE

One of the main objectives of this study was to achieve the selective determination of AA and DA. This was investigated using S-β-CD modified CPE as working electrode. Figure 5.5 shows the cyclic voltammogram of a mixture AA (1×10^{-3} M) and DA (5×10^{-5} M) in 0.1 M PBS (at pH 6.8) at S-β-CD modified CPE. The voltammogram exhibits two clear oxidation peaks for both analytes, which corresponds to AA and DA oxidation, respectively. The (broad) oxidation peak for AA observed ~0.014 V and that for DA oxidation at 0.161 V vs. SCE. So, compared to bare CPE, S-β-CD modified CPE resolved the voltammetric response of AA and DA into two distinct signals. AA can form hydrogen bonds with the hydroxyl groups of cyclodextrin as the electrostatic repulsion between the AA anions and the negatively charged sulfate groups on the electrode surface is partial. AA is readily oxidised and consequently hydrogen-bonding diminishes, releasing DHA. The separation between the oxidative peak potential of DA and AA was approximately 0.147 V vs. SCE. This difference is large enough for the simultaneous determination of DA in the presence of AA at S-β-CD modified CPE. Interestingly, the redox activity of DA in the mixture was still reversible as demonstrated by a ΔE_p value of 0.016 V. A peak separation of this magnitude usually denotes an adsorption regime, indicating that DA molecules are electrostatically attracted to sulfate groups, and probably included in the cyclodextrin cavity.

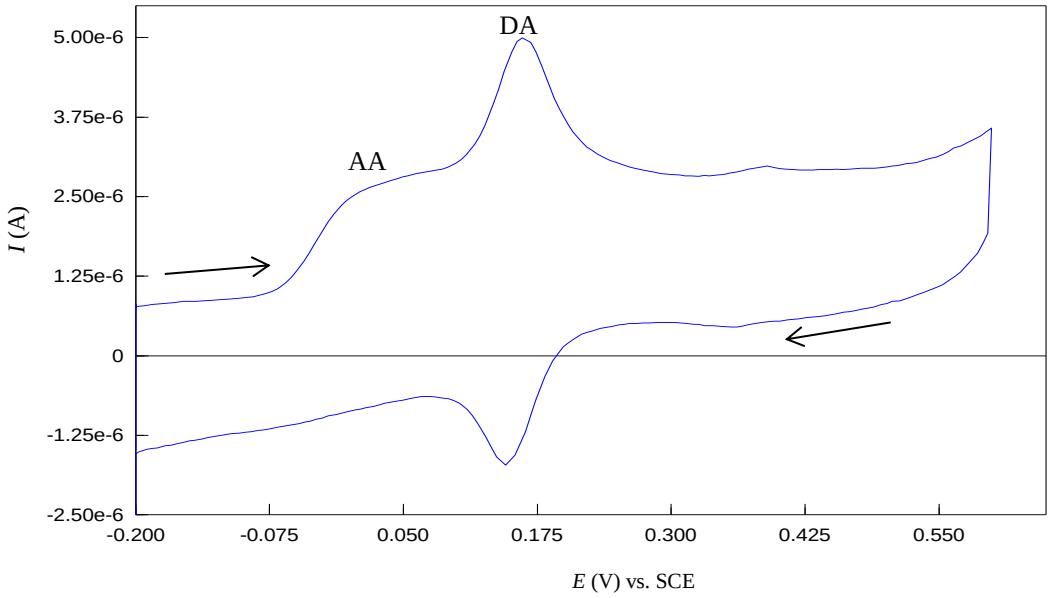

Figure 5.5: Cyclic voltammogram for a mixture of AA (1×10^{-3} M) and DA (5×10^{-5} M) at S-β-CD modified CPE in 0.1 M PBS (pH 6.8); scan rate: 50 mV / s.

The attraction and exclusion properties of S-β-CD modified CPE toward DA and AA is related to the charge carried by the S-β-CD at pH 6.8. Further supporting this evidence, the electrochemical behaviour of a mixture of AA (1×10^{-3} M) and DA (5×10^{-5} M) at neutral β-CD modified CPE was carried out and typical data are shown in Figure 5.6(a). It can be seen that a broad oxidation peak appeared at neutral β-CD modified CPE, rendering the oxidation peak potentials of AA and DA indistinguishable. In fact, the hydrophobic cavity of neutral β-CD can serve as perfect host cavity, not just for DA, but also for AA. Bratu *et al* has demonstrated a 1:1 molecular complex formation between AA and neutral β-CD, using several techniques included FTIR, X-ray powder diffraction, DSC, ^{1}H NMR and UV-Vis [6]. Hu *et al*, also has prepared β-CD : AA inclusion complex using a high hydrostatic pressure technique [33]. Thus it seems likely that a competitive adsorption regime between AA and DA exists at the electrode surface via inclusion with neutral β-CD, which might result in the overlapping peaks of these two analytes. For the sake of comparison, the voltammogram corresponding to oxidation of DA (5×10^{-5} M) only at neutral β-CD was presented in Figure 5.6(b). These results also show evidence that the presence of sulfate groups on the cyclodextrin rims is necessary for simultaneous detection of AA and DA.

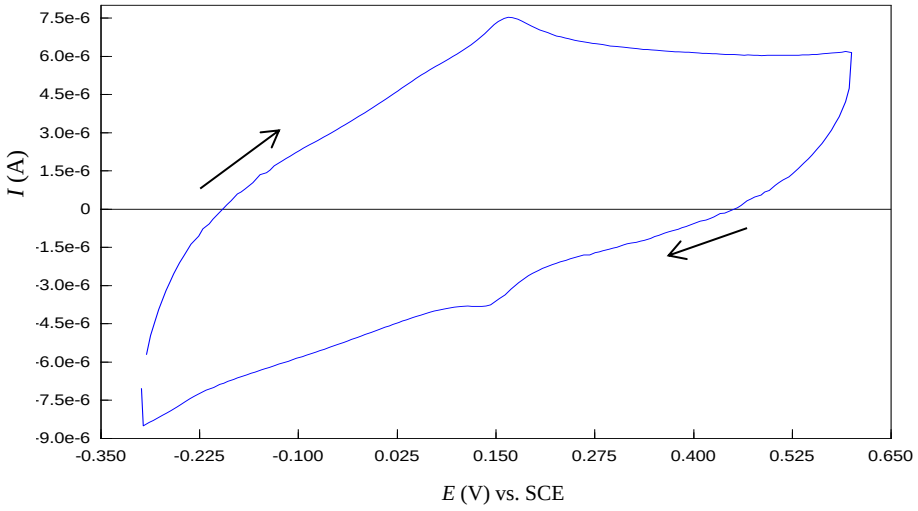

(a)

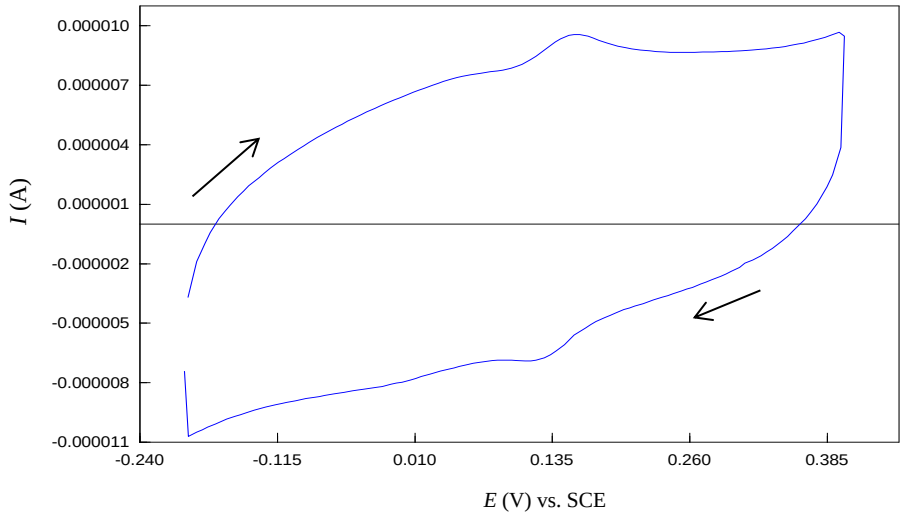

(b)

Figure 5.6: Cyclic voltammograms obtained at neutral β-CD modified CPE for a mixture of AA (1×10^{-3} M) and DA (5×10^{-5} M) (a) and DA (5×10^{-5} M) solution (b) in 0.1 M PBS (pH 6.8); scan rate: 50 mV / s.

5.2.1.6 Effect of scan rate for a mixture of AA and DA at S-β-CD modified CPE

The effect of scan rate on the oxidative peak potential and peak currents for a mixture of AA (1×10^{-3} M) and DA (5×10^{-5} M) at the surface of S-β-CD modified CPE was studied, with resultant typical cyclic voltammetric curves shown in Figure 5.7(a). When the scan rate is increased, the oxidation peak potentials for AA species shifts cathodically, while that of DA remains constant. The oxidation peak potentials are

given in Table 5.1. In addition, the oxidation peak current of AA was proportional to the scan rate over the range of 10 to 80 mV / s. The linear regression equation was I_{pa} (A) = 1.4332 × 10^{-8} v + 2.2468 × 10^{-8}, with a correlation coefficient of 0.9902. So, the electrode process for AA in the mixture at S-β-CD modified CPE was adsorption-controlled. On the other hand, the anodic peak current of DA at the modified electrode also increased linearly with the scan rate, confirming the direct electron transfer on the surface of S-β-CD modified CPE between it and DA. Therefore, the electrode reaction of DA (in the mixture) at S-β-CD modified CPE was under adsorption-control. Figure 5.7(b) presents the reasonable linearity of the plots, with a regression equation of I_{pa} (A) = 3.7128 × 10^{-8} v + 8.2880 × 10^{-7} and correlation coefficient of 0.9935. The results clearly demonstrate that S-β-CD has the ability to attract DA and partially reject AA in solution of coexisting DA and AA.

(a)

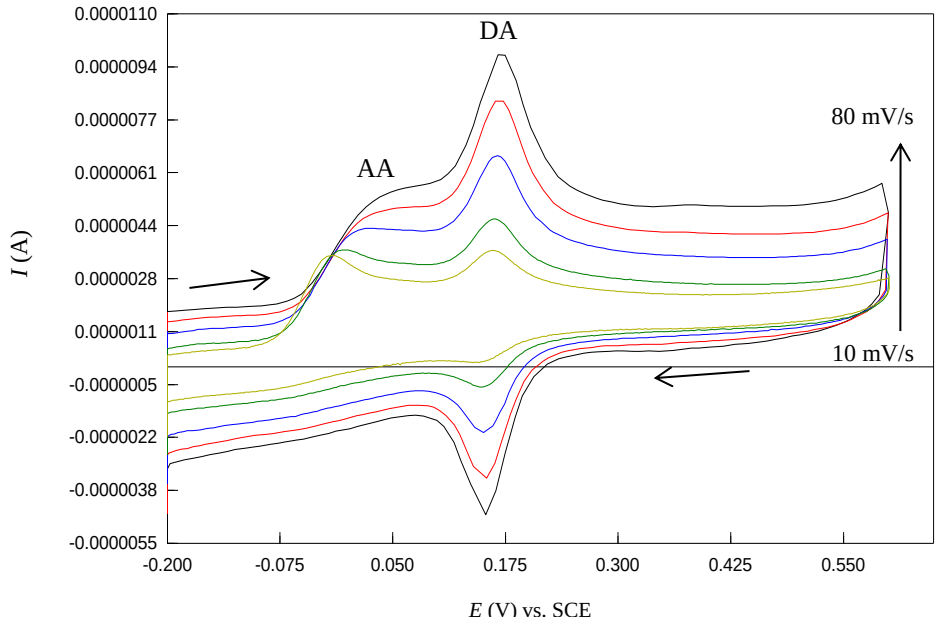

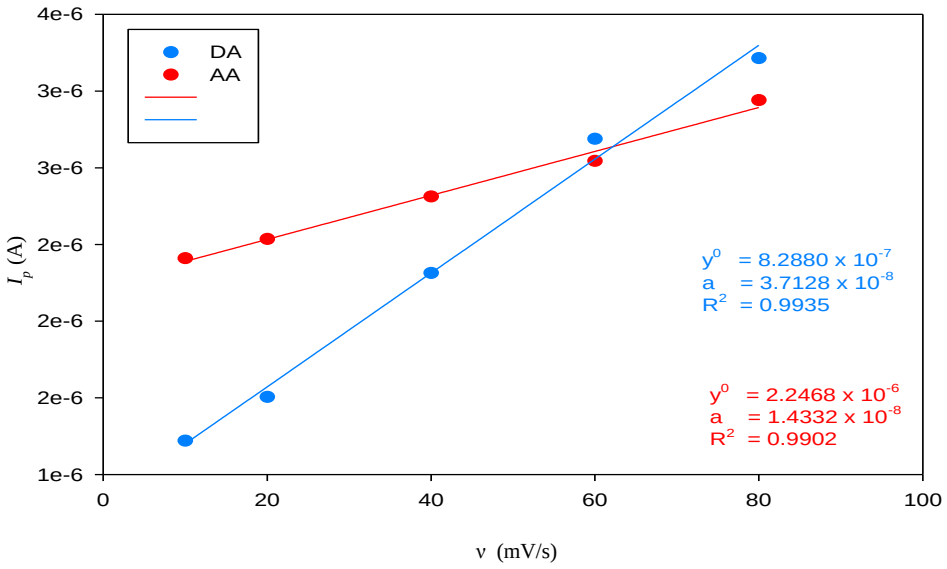

(b)

Figure 5.7: cyclic voltammograms showing the effect of scan rate variation for a mixture of DA (5×10^{-5} M) and AA (1×10^{-3} M) at S-β-CD modified CPE from 80 to 10 mV / s (a) and corresponding plot of oxidation peak current as a function of scan rate (b). Supporting electrolyte 0.1 M PBS (pH 6.8).

Table 5.1: Effect of scan rate on oxidation peak currents and peak potentials of AA and DA at S-β-CD modified CPE (using CV).

Scan rate (mV / s)	AA		DA	
	Oxidation Peak Potential (Volt)	Oxidation Peak Current (A)	Oxidation Peak Potential (Volt)	Oxidation Peak Current (A)
10	-0.020	2.411×10^{-6}	0.16	1.220×10^{-6}
20	-0.001	2.535×10^{-6}	0.16	1.505×10^{-6}
40	0.026	2.813×10^{-6}	0.16	2.313×10^{-6}
60	0.059	3.044×10^{-6}	0.16	3.189×10^{-6}
80	0.063	3.441×10^{-6}	0.16	3.715×10^{-6}

In order to elucidate the electrochemical properties of AA oxidation at the S-β-CD modified CPE electrode and clarify whether or not electron transfer process of AA in the mixture is dependent on coexisting DA species, cyclic voltammetry measurements of a solution of AA (1×10^{-3} M) only in 0.1 M PBS were carried out on S-β-CD modified CPE at different potential scan rates, as shown in Figure 5.8(a). Clearly, the peak potentials increase linearly with increasing scan rate. It can also be noted that the peak shape is more defined at lower scan rates, probably due to a relatively longer timescale, which allowed AA species to interact much more with electrode surface. Figure 5.8(b) shows that the anodic peak currents also increased linearly with scan rate. This suggests that the electrochemical oxidation of AA was not diffusion-controlled but surface controlled. The regression equation describing the electron transfer occurring at the surface of the electrode in the studied range of potential scan rates is as follow: I_{pa} (A) = 1.8755×10^{-8} v + 1.5099×10^{-6}, with the correlation coefficient of 0.9930. This result was consistent with the one obtained for AA in the mixture. Therefore, the kinetic process of AA electro-oxidation at the modified electrode surface was not related to the presence of DA species or DA adsorption process at the electrode surface.

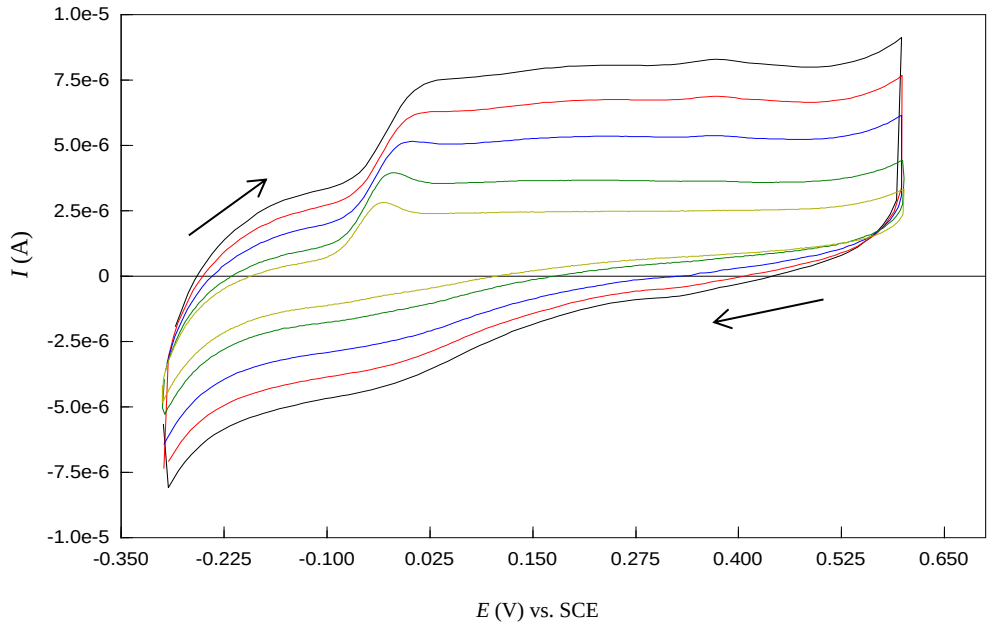

(a)

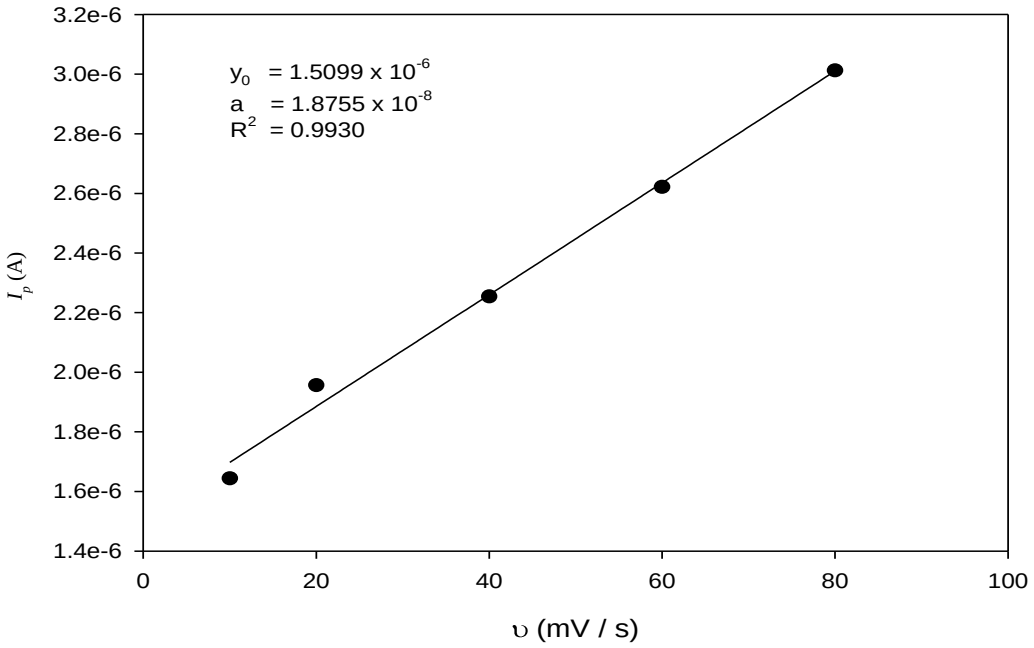

(b)

Figure 5.8: Cyclic voltammograms showing the effect of scan rate variation for AA (1 × 10^{-3} M) at S-β-CD modified CPE from 80 to 10 mV / s (a) and corresponding plot of oxidation peak current as a function of scan rate (b). Supporting electrolyte 0.1 M PBS (pH 6.8).

5.2.1.7 Electrochemical behaviour of a mixture of AA and DA at CPE with oxide layer

The electrochemical behaviour of a mixture of AA (1×10^{-3} M) and DA (5×10^{-5} M) in a pH 6.8 PBS was examined by cyclic voltammetry at CPE with oxide layer, and a typical resultant voltammogram is shown in Figure 5.9(a). It was observed that the (irreversible) oxidation peak of AA nearly overlapped with that of oxides. However, the peak due to DA oxidation is well-defined. The presence of oxide species at the electrode surface causes an anodic shift in AA peak potential. This indicates that the activation energy required for AA oxidation at CPE/O is slightly lower than that required at bare CPE. The oxidative peak potential of AA at CPE containing oxides shifted to −0.013 V vs. SCE. What is also remarkable in this study is the redox property of DA. DA can be clearly quantified (with oxidation peak current of 1.411×10^{-6} A) in the presence of AA. DA redox activity in the mixture at CPE with oxide layer is reversible based on its low ΔE_p of 0.016 V. Thus, DA oxidation at CPE/O is independent of AA. The oxidation peak current of oxide species occurring (at 0.064 V vs. SCE) between those of AA and DA reduced in magnitude. This may be a consequence of the interaction between oxide species at the electrode surface and protonated DA. For the sake of comparison, the cyclic voltammogram of the electrode in 0.1 M PBS, prior to immersion in the mixture was displayed in Figure 5.10.

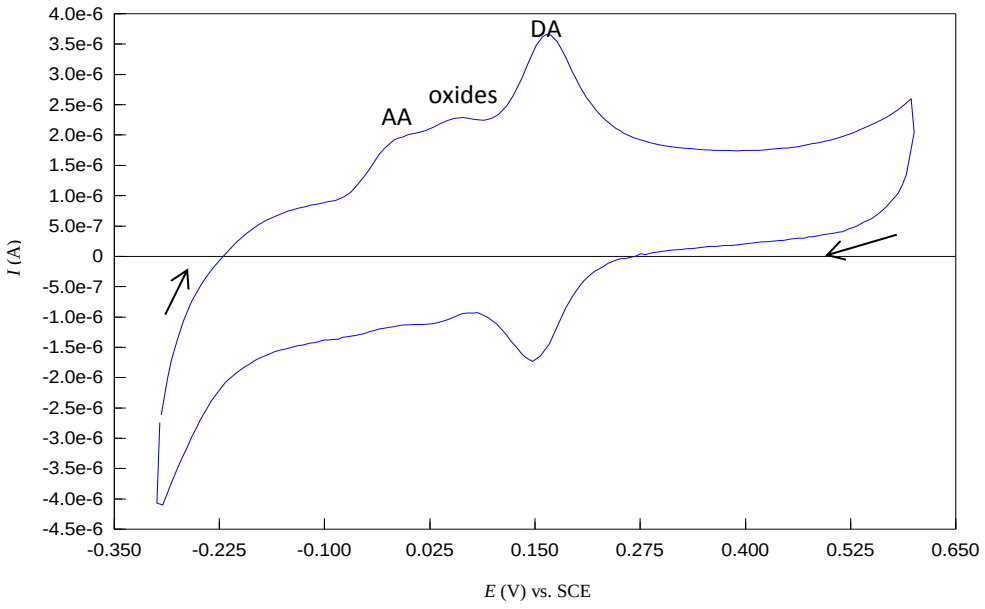

Figure 5.9: Cyclic voltammograms obtained at CPE with oxide layer for a mixture of AA (1×10^{-3} M) and DA (5×10^{-5} M) in 0.1 M PBS (pH 6.8); scan rate: 50 mV / s.

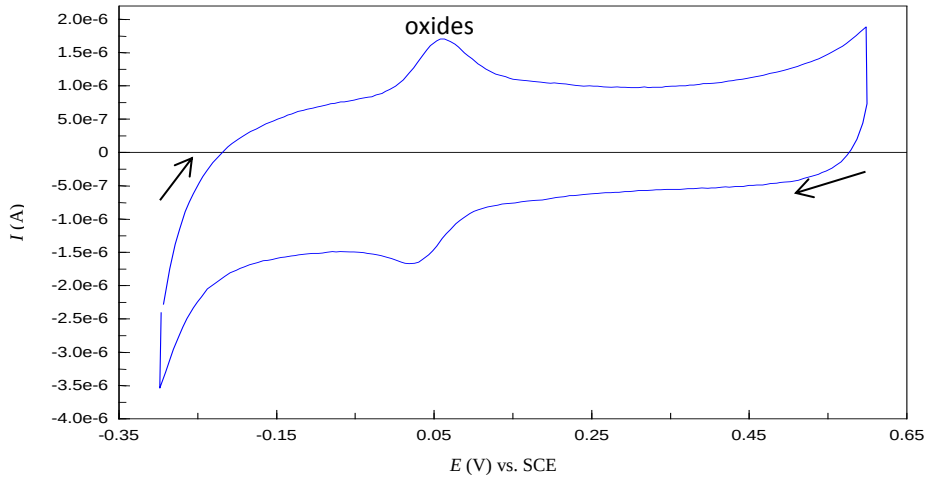

Figure 5.10: Cyclic voltammograms of 0.1 M PBS (pH 6.8) at CPE with oxide layer; scan rate: 50 mV / s.

The oxidation of surface oxides seems to be effective in repelling AA, which has four OH groups and one CO group on its periphery. Since AA is negatively charged at pH 6.8, a relatively strong repulsive force may exist with oxide species such as carboxylate group. Figure 5.11 shows repetitive cycles of CPE with oxide layer in the mixture of AA (1×10^{-3} M) and DA (5×10^{-5} M). As observed, the oxidation peak current of AA decreases until a steady state is reached in the 5th cycle, while the oxidation peak of DA remained constant over repetitive cycling.

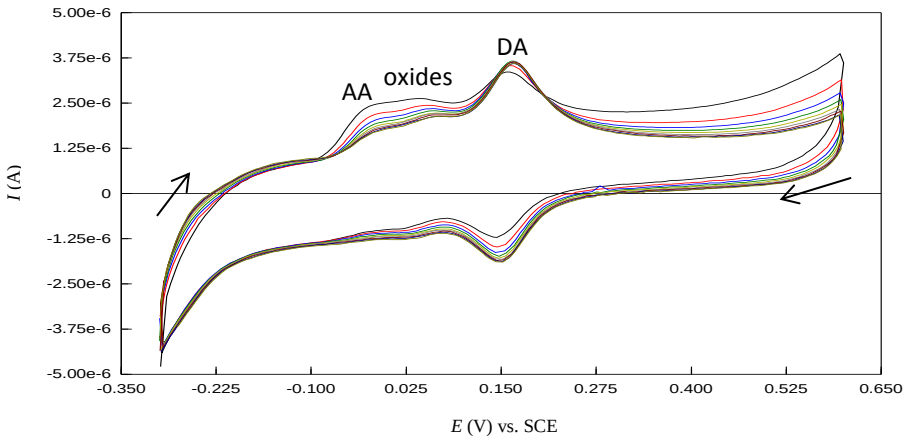

Figure 5.11: Repetitive cyclic voltammograms (10 cycles) obtained at CPE with oxide layer for a mixture of AA (1×10^{-3} M) and DA (5×10^{-5} M) in 0.1 M PBS (pH 6.8); scan rate: 50 mV / s.

5.2.1.8 Electrochemical behaviour of a mixture of AA and DA at Nafion modified CPE

It was demonstrated from Chapter 4 that a relatively low concentration of Nafion coated CPE resulted in an enhancement of the oxidation peak current of DA. A thick Nafion coating leads to a decrease in sensitivity, compared to bare CPE, due to hindered mass transport of DA throughout the thick layer. Good electrochemical detection of DA was obtained by using 10 µL of 0.05 % Nafion drop-cast onto CPE. Hence, 10 µL of 0.05 % Nafion was drop-cast onto CPE/O and employed to detect DA in the presence of an excess AA. At the pH of 6.8 used, AA is expected to exist as ascorbate anion which will not favour its approach onto a negatively charge surface. Figure 5.12 shows typical cyclic voltammograms of a mixture of DA (5×10^{-5} M) and AA (1×10^{-3} M) in 0.1 M PBS (performed at different scan rates) at Nafion-coated CPE. When AA was present in the voltammetric cell, major alterations of DA signal were observed. There is a pronounced decay of the reduction peak current of DOQ when compared those obtained in a DA only solution. This feature may indicate of the occurrence of a regenerative process, certainly induced by AA, where the catalytic reaction of AA with the DOQ results in a higher anodic peak and reduced cathodic peak of DA redox activity. In addition, a shoulder peak is observed at around −0.020 V vs. SCE, resulting from the oxidation of AA. Under the experimental conditions, Nafion did not successfully suppress completely the voltammetric signal of AA. The overall process depends on the mass transport / ionic exchange features of the species (DA and AA) within the Nafion layer.

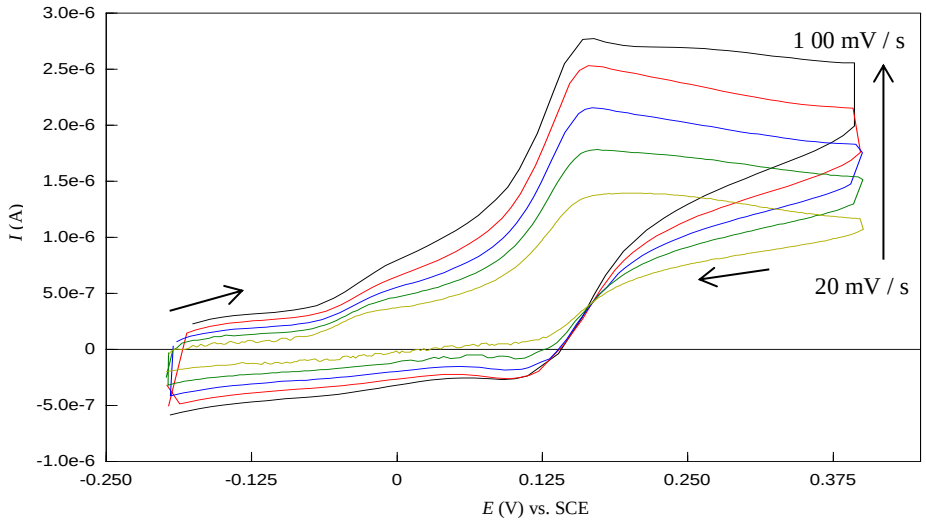

Figure 5.12: Cyclic voltammograms for a mixture of DA (5×10^{-5} M) and AA (1×10^{-3} M) in 0.1 M PBS (pH 6.8) at Nafion coated CPE; scan rate: 20, 40, 60, 80 and 100 mV / s.

It must be highlighted that Nafion is an ionomer with a rather low content of ion exchange groups [19, 21]. Therefore, it could be expected a higher content of sulfonate cation-exchange group would lead to an improvement of the incorporation of positively charged DA and complete repulsion of negatively charged AA. However, as already mentioned, a high concentration or a thick layer of Nafion at the electrode surface can reduce the sensitivity in the detection of DA. Taking into account the above result, the key question in the utilisation of Nafion coated CPE as an analytical tool for the determination of DA coexisting with an excess of AA, is how to obtain adequate Nafion concentration (for selectivity towards negatively charged AA, keeping a satisfactory sensitivity for DA).

5.2.1.9 Electrochemical behaviour of AA at Fc-β-CD modified CPE

One of the most important properties of Ferrocene, as demonstrated in Chapter 4, is its redox behaviour. Ferrocene was used as an agent to modify CPE. However, Ferrocene itself is not adsorbed strongly on CPE. The stability of Ferrocene at electrode surface was improved by formation of inclusion complex with β-CD. The prepared Fc-β-CD modified CPE was used to test its electrochemical behaviour in AA solution.

Fc-β-CD modified CPE was dipped in 0.1 M PBS (pH 6.8) and cyclic voltammetry was carried out at 50 mV / s in the potential range from 0.8 V to −0.3 V. The resulting voltammogram is shown in Figure 5.13 (black trace). A pair of reversible redox peaks was observed which corresponded to the electrochemical process Fc/Fc^{+}. Under identical conditions, Fc-β-CD modified CPE was then placed in AA (1×10^{-3} M) to test its activity toward AA oxidation. Typical data are given in Figure 5.13 (red trace). As can be seen, the oxidation of AA occurred irreversibly at a potential of 0.370 V vs. SCE. The anodic peak current (1.375×10^{-6} A) slightly increased over that observed at bare CPE (1.087×10^{-6} A, blue trace). The corresponding cathodic wave for reduction of ferrocenium ion (normally observed in PBS) is substantially depressed. Although, the peak current of AA was slightly enhanced at Fc-β-CD modified CPE, this could not be related to an electrocatalytic effect. An electrocatalytic oxidation of AA at Fc-β-CD modified CPE should result in a shift to the negative direction of the oxidation potential of AA and would correspond to Equation 5.5, as reported by Raoof *et al* [34]. In this equation $Fc^{+}\beta CD$, $Fc\beta CD$, H_2AA and DHA represent ferrocenium β-cyclodextrin, Ferrocene β-cyclodextrin, ascorbic acid and dehydro-ascorbic acid, respectively.

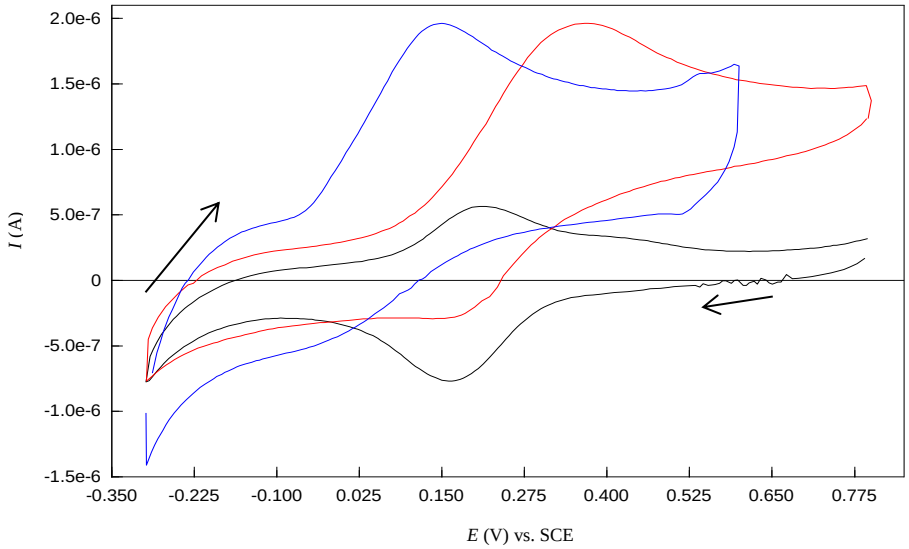

Figure 5.13: Cyclic voltammograms obtained at Fc-β-CD modified CPE in 1 × 10^{-3} M AA (–) and 0.1 M PBS (–) compared with cyclic voltammograms obtained at bare CPE in 1 × 10^{-3} M AA (–); scan rate: 50 mV / s.

$$2Fc^{+}\beta CD + H_2AA \rightarrow 2FcCD + DHA + 2H^{+} \qquad \text{Equation 5.5}$$

5.2.1.10 Electrochemical behaviour of a mixture of AA and DA at Fc-β-CD modified CPE

It was demonstrated in Chapter 4 that Fc-β-CD modified CPE shows an electrocatalytic effect on the oxidation of DA. On the other hand, the anodic current magnitude due to the oxidation of AA was (slightly) enhanced at Fc-β-CD modified CPE. These experimental results have encouraged investigation whether or not Fc-β-CD modified CPE was able to separate the voltammetric signals of DA and AA in a mixture.

To test the electrochemical behaviour of a mixture of AA (1× 10^{-3} M) and DA (5 × 10^{-5} M) at Fc-β-CD modified CPE, a cyclic voltammetric response was obtained in a 0.1 M PBS (pH 6.8). The data is given in Figure 5.14. As can be seen, the electrochemical oxidation results in single and sharp anodic peak corresponding to the oxidation of both AA and DA. This anodic peak shows a higher peak current compared with the individual oxidation peak current of AA and DA at Fc-β-CD modified CPE, due to homogeneous catalytic oxidation of AA by DOQ. Therefore, Fc-β-CD modified CPE cannot dissociate the voltammetric signal of AA and DA from a mixture. In addition, a broad cathodic wave was observed, which was attributed to the overlapping reduction of Fc^{+} and DOQ.

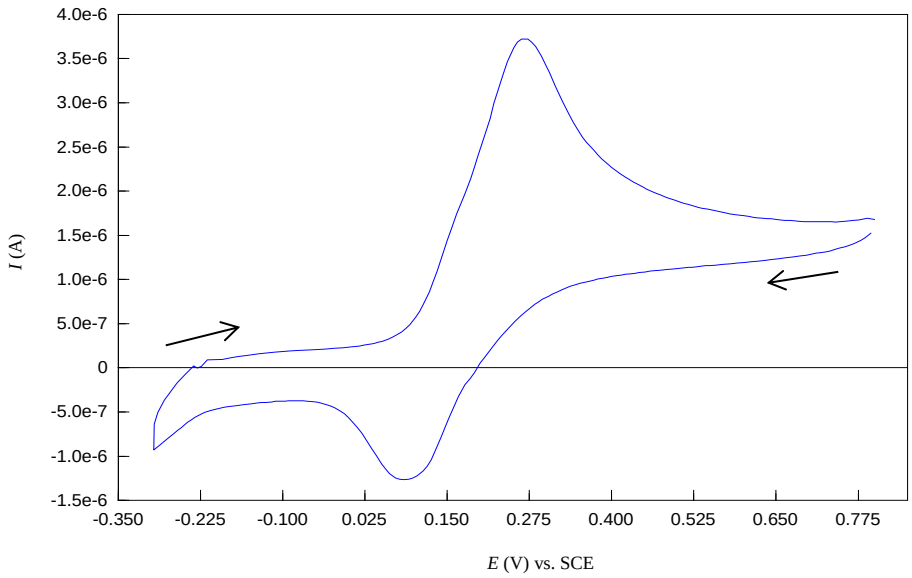

Figure 5.14: Cyclic voltammograms for a mixture of AA (1×10^{-3} M) and DA (5×10^{-5} M) in 0.1 M PBS (pH 6.8) at Fc-β-CD modified CPE; scan rate: 50 mV / s.

5.2.1.11 Electrochemical behaviour of a mixture of AA and DA at S-β-CD modified GPE

The aim of this section was to investigate if the impressive properties of graphene modified electrode (S-β-CD modified GPE) could enhance sensor sensitivity in the selective detection of DA. As differential pulse technique offers a much higher current sensitivity and better resolution than the cyclic voltammetry technique, it was used to determine DA in the presence of AA at S-β-CD modified GPE. Differential pulse voltammetry was performed on a mixture of AA (1×10^{-3} M) and DA (5×10^{-5} M) scanning in the potential range from −0.2 to +1.0 V (Figure 5.15, red trace). A single peak current was observed at the modified electrode. This well-defined peak signal occurring at 0.17 V vs. SCE with a peak magnitude of 8.988×10^{-7} A is characteristic of the oxidation of DA only. The oxidation of DA resulting from a solution containing DA (5×10^{-5} M) only, under similar experimental parameters was displayed in Figure 5.15 (blue trace). The peak potential was also observed around 0.17 V vs. SCE with corresponding peak current value 1.252×10^{-6} A. Although, the peak current for oxidation of DA from the mixture had slightly reduced this experimental result was quite encouraging and suggested selective detection of DA in the presence of AA.

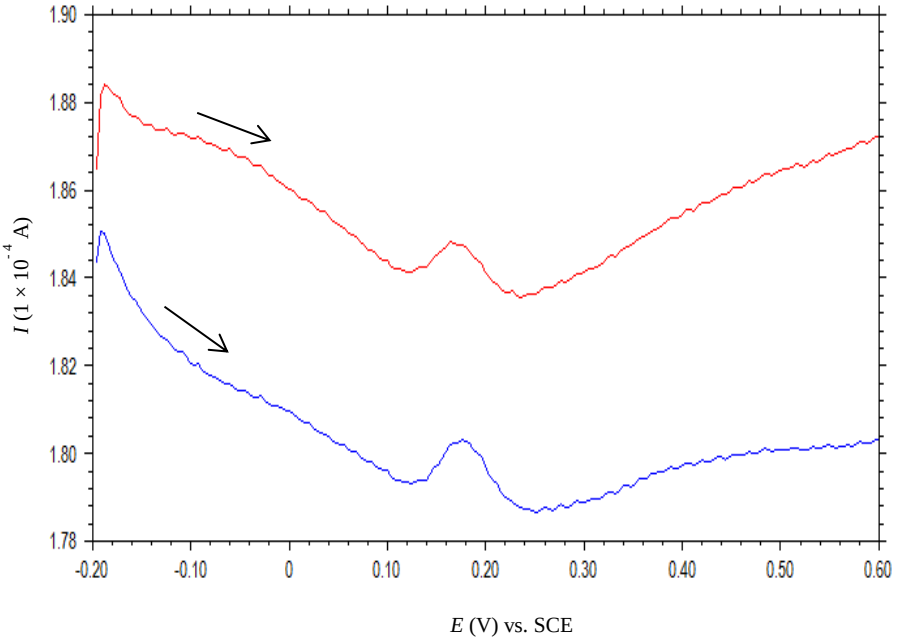

Figure 5.15: Differential pulse voltammograms for a mixture of AA (1 × 10^{-3} M) and DA (5 × 10^{-5} M) (–) and DA (5 × 10^{-5} M) solution (–) in 0.1 M PBS (pH 6.8) at S-β-CD modified GPE.

Further studies were then carried out to support the above result. The first one consisted of evaluating the electrochemical behaviour of the modified graphene electrode in an individual solution of AA (1 × 10^{-3} M). No peak related to oxidation of AA was found in the studied potential range as shown in Figure 5.16 (red trace), indicating that AA cannot be oxidised on the modified electrode. The shape of the voltammograms obtained was similar to the one observed when the modified electrode was run in 0.1 M PBS (Figure 5.16, blue trace), prior to detection AA.

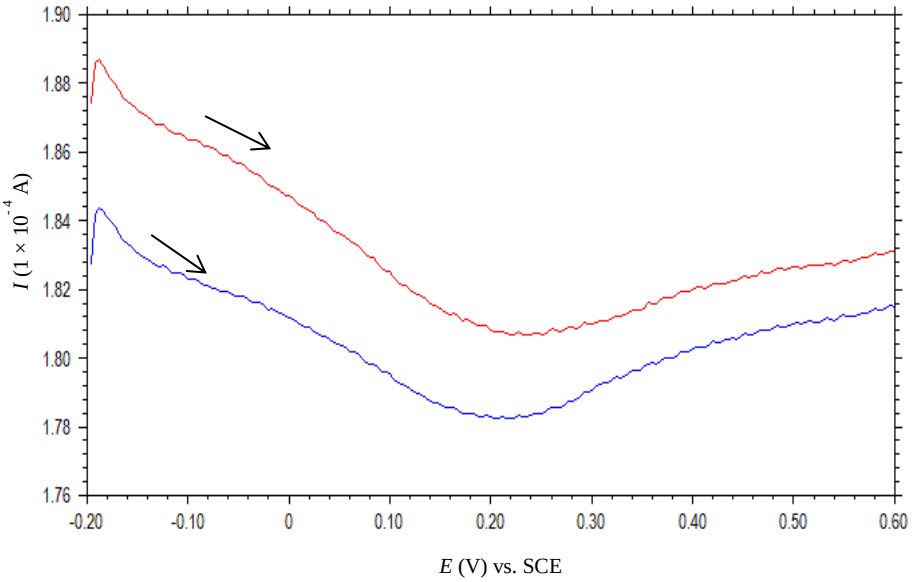

Figure 5.16: Differential pulse voltammograms of AA (1 × 10^{-3} M) (–) and 0.1 M PBS (–) at S-β-CD modified GPE.

Attention was next turned to exploring the differential pulse voltammetry of AA (1×10^{-3} M) at bare GPE. A broad peak signal was observed around 0.098 V vs. SCE, corresponding to oxidation of AA to DHA (Figure 5.17, red trace). In addition, to prove that the peak observed was a 'true' peak related to oxidation of AA, background subtraction was carried out and showed a defined peak signal, with a current intensity of 1.393×10^{-6} A (Figure 5.17 (b)). Unlike the modified graphene electrode, bare GPE was able to sense AA. However this peak current value is relatively low with respect to the concentration of AA, 1×10^{-3} M. So, bare GPE exhibits slow heterogeneous electron transfer kinetics towards electrochemical oxidation of AA.

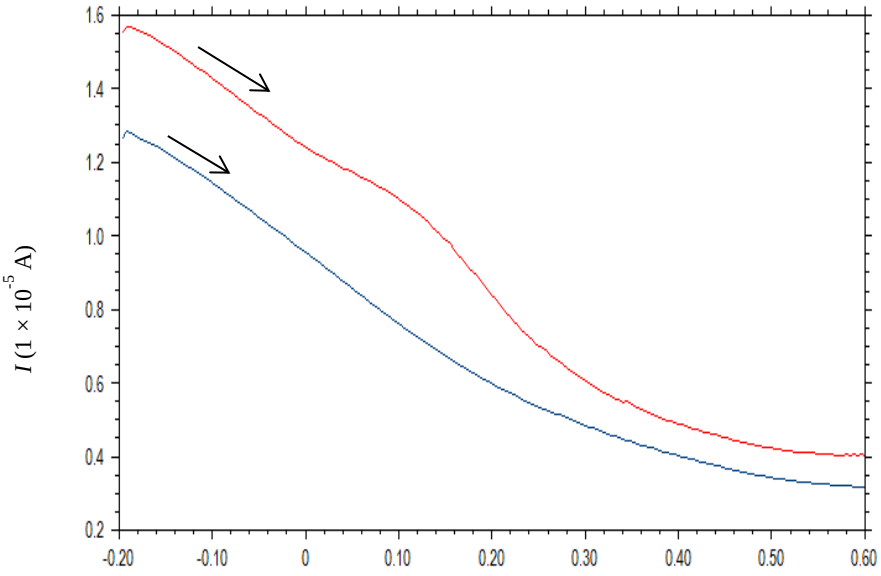

(a)

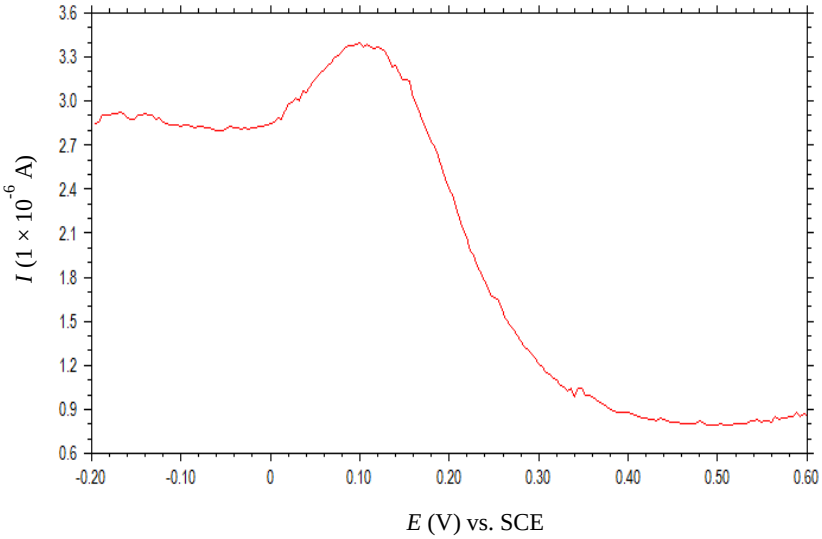

(b)

Figure 5.17: Differential pulse voltammograms obtained at bare GPE for AA (1×10^{-3} M) (–) and (0.1 M PBS) blank solution (–) (a) and corresponding background subtraction (b).

It is important to note that, compared to AA, the electron transfer between DA and graphene (at bare GPE) is more feasible through π-π interaction since DA has a phenyl moiety [35]. In addition, characterisation studies (carried out in Chapter 2) have shown that the synthesised graphene possesses a degree of oxygen content (more likely) in the form of carboxylic groups. Such functional groups within graphene material may not promote the electrochemical oxidation of AA, thus, reducing considerably its electrochemical activity. Modification of GPE using S-β-CD increases the content of charged functional groups at the electrode surface (at pH 6.8). COO^- covalently attached at the edge plane of graphene and OSO_3^- on the primary and secondary rims of cyclodextrin completely blocks the electrochemical activity of AA through electrostatic repulsion. Conversely, an improvement in DA electrochemical response is observed owing to an increased electrostactic attraction is observed. To confirm selective sensing of DA is dependent on contribution of both carboxylate and sulfate groups, differential pulse voltammogram of a mixture of AA (1×10^{-3} M) and DA (5×10^{-5} M) was recorded at bare GPE and shown in Figure 5.18. As can be seen, a broad peak signal was observed, corresponding to an overlapping signal response of both AA and DA. This voltammogram is totally different from the sharp DA peak observed at bare GPE, previously shown in Chapter 4.

It can be concluded that the presence of AA does not interfere with the determination of DA in a 20:1 ratio. These experimental results indicate that the selective and sensitive determination of DA can be achieved using S-β-CD modified GPE.

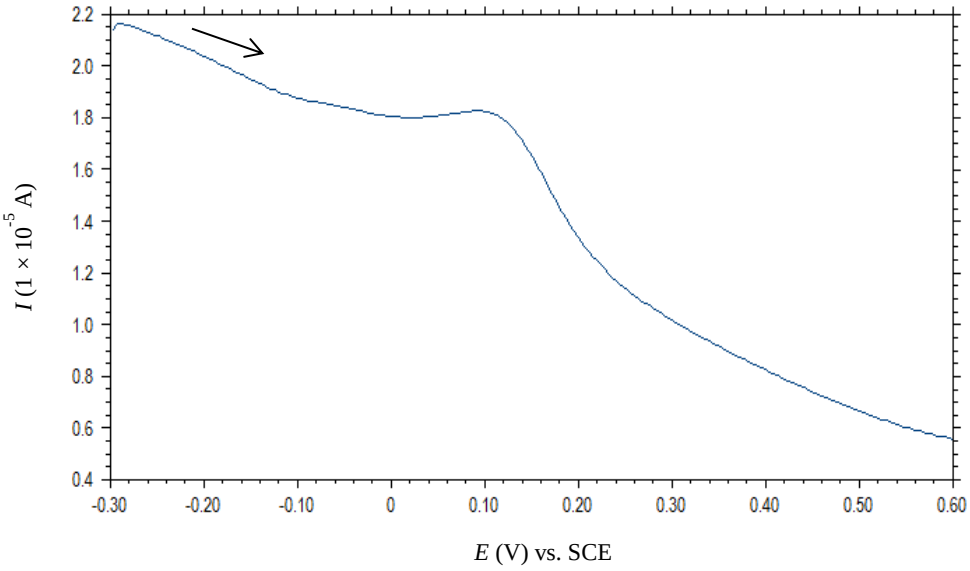

Figure 5.18: Differential pulse voltammogram for a mixture of AA (1×10^{-3} M) and DA (5×10^{-5} M) in 0.1 M PBS (pH 6.8) at bare GPE.

5.2.2 Electrochemical Study of a Mixture of DA and 5-HT

Simultaneous measurement of DA and 5-HT is particularly important since these molecules coexist in biological system and their relative levels have implications in many diseases. However, simultaneous measurement of these species has been mainly unsuccessful due to the inability of common solid electrodes to separate their respective potentials significantly enough to allow accurate discrimination.

In this study, modified of carbon based electrodes were fabricate to try to overcome these difficulties in the simultaneous determination of DA and 5-HT.

5.2.2.1 Electrochemical behaviour of 5-HT at S-β-CD modified CPE

The electroanalysis of 5-HT was performed at S-β-CD modified CPE using cyclic voltammetry. Figure 5.18(a) shows the voltammogram of 5-HT (5×10^{-5} M) in 0.1 M PBS at S-β-CD modified CPE (black trace) compared with that obtained at bare CPE (red trace). In both cases, an irreversible oxidation peak is observed at 0.499 V and 0.349 V (vs. SCE) for bare CPE and S-β-CD modified CPE, respectively. At bare CPE, the oxidation wave of 5-HT is broad with a peak current value of 1.237×10^{-7} A. In contrast, the peak current signal significantly increased (with a value of 6.263×10^{-7} A) at S-β-CD modified CPE. The larger peak current and the less positive peak potential observed at S-β-CD modified CPE indicates that the S-β-CD modified CPE has a strong affinity towards 5-HT. A possible electrocatalytic mechanism may be related to the adsorption of 5-HT on the surface of S-β-CD modified CPE firstly through electrostatic interaction with anionic cyclodextrin (as 5-HT is a cation at pH 6.8), followed possibly by host-guest interaction between 5-HT and S-β-CD. The electron transfer can then easily take place. This is characterised by higher peak signal compared to that at bare CPE. It also has to be noted that there is a broad redox peak centred at 0.026 V at S-β-CD modified CPE. The electrochemical oxidation of 5-HT is believed to take place at the phenol group of the molecule to form the corresponding ketone (a quinonimine [36]) as shown in scheme 5.3 (Equation 5.6). The absence of the corresponding reduction peak indicates the instability of this oxidation product, which can then undergo chemical reaction to form the easily oxidisable hydroquinone (Equation 5.7) [37]. Therefore, the redox couple centred at 0.026 V can be attributed to this quinone / hydroquinone couple (Equation 5.8). Wrona *et al* have speculated that the oxidation of 5-HT to corresponding ketone and the redox couple quinone / hydroquinone involved the removal of two electrons and two protons concomitantly [37-39] as shown in scheme 5.3.

(a)

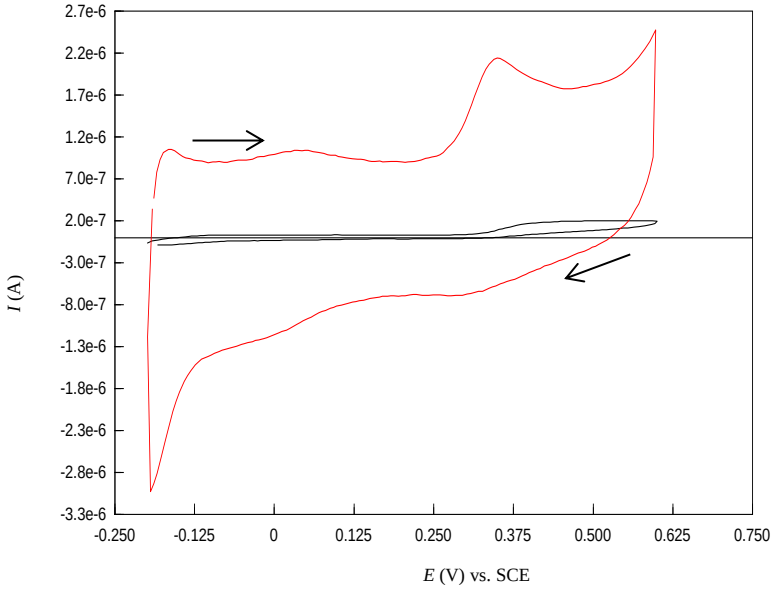

(b)

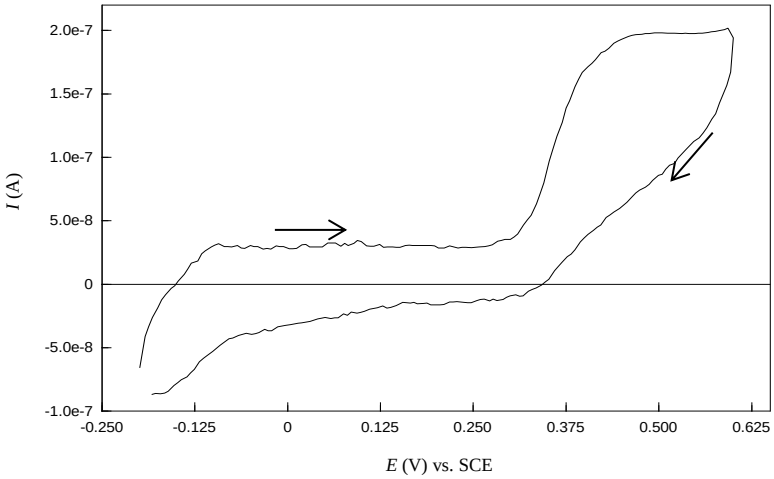

Figure 5.19: Cyclic voltammogram of 5-HT (5×10^{-5} M) 0.1 M PBS (pH 6.8) at bare CPE (–) and S-β-CD modified CPE (–) (a) and enlarged voltammogram for bare CPE (b); scan rate 50 mV / s.

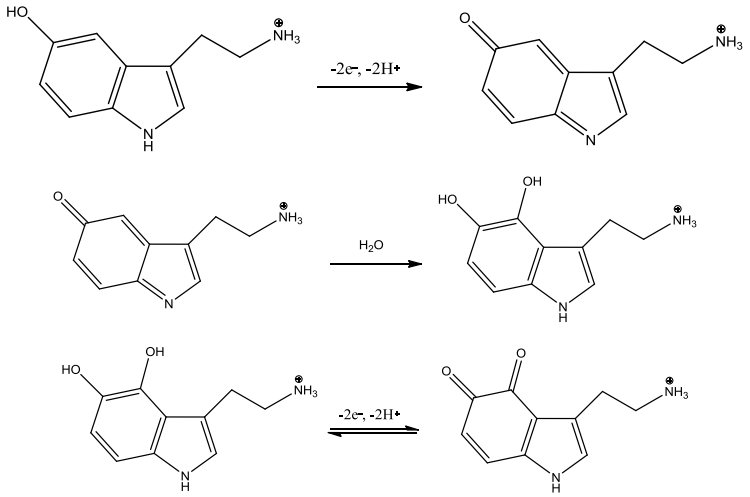

Equation 5.6

Equation 5.7

Equation 5.8

Scheme 5. 3: Proposed 5-HT reaction at S-β-CD modified CPE in 0.1 M PBS (pH 6.8).

5.2.2.2 Electrochemical behaviour of a mixture of AA and 5-HT at S-β-CD modified CPE

As already mentioned, in biological environments, the main interference in the electrochemical detection of the catecholamine is the presence of high concentration of AA. So, it is important to investigate the electrochemical response of 5-HT in the presence of AA. A study was performed to illustrate the voltammetric behaviour of 5-HT at bare CPE and S-β-CD modified CPE in the presence of AA using cyclic voltammetry with scan rate 50 mV / s. AA is usually present at a higher concentration than 5-HT. To try to mimic the conditions of species ratios present in the cerebrospinal fluid, the concentration of 5-HT was maintained at 20 times less than that of the AA. Figure 5.20 (a) shows the voltammogram obtained for the mixture solution of AA (1×10^{-3} M) and 5-HT (5×10^{-5} M) recorded at bare CPE and in 0.1 M PBS (pH 6.8). A single peak was observed at the bare CPE due to the overlapping current response of AA and 5-HT. The bare CPE does not resolve the detection of AA and 5-HT. Therefore, determination of the individual species concentrations, from the broad voltammetric peak at the bare CPE, was deemed futile. The same AA / 5-HT mixture was then used to examine the voltammetric behaviour of S-β-CD modified CPE. As expected, using S-β-CD modified CPE as a working electrode caused an effective separation of the anodic peaks of 5-HT and AA (Figure 5.20 (b). The anodic peak of 5-HT and AA occurred at 0.097 V and 0.348 V (vs. SCE), respectively. The oxidation peak current for 5-HT oxidation in the mixed solution was 3.655×10^{-7} A.

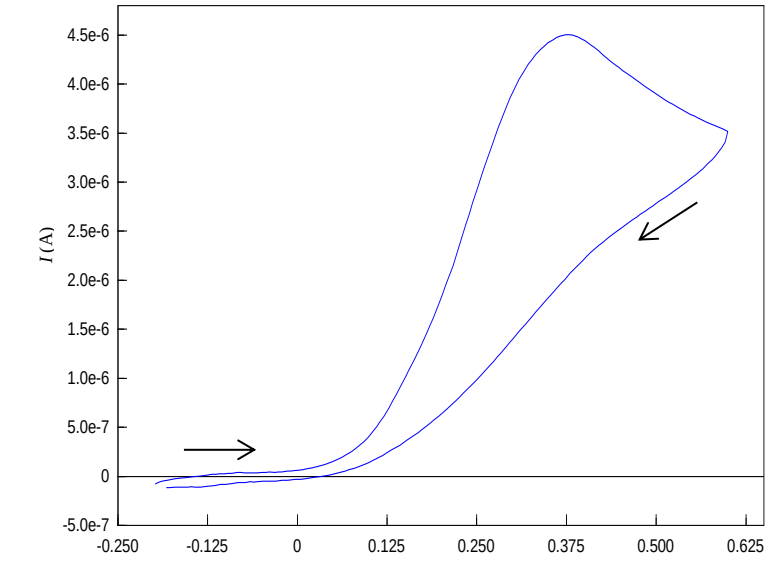

(a)

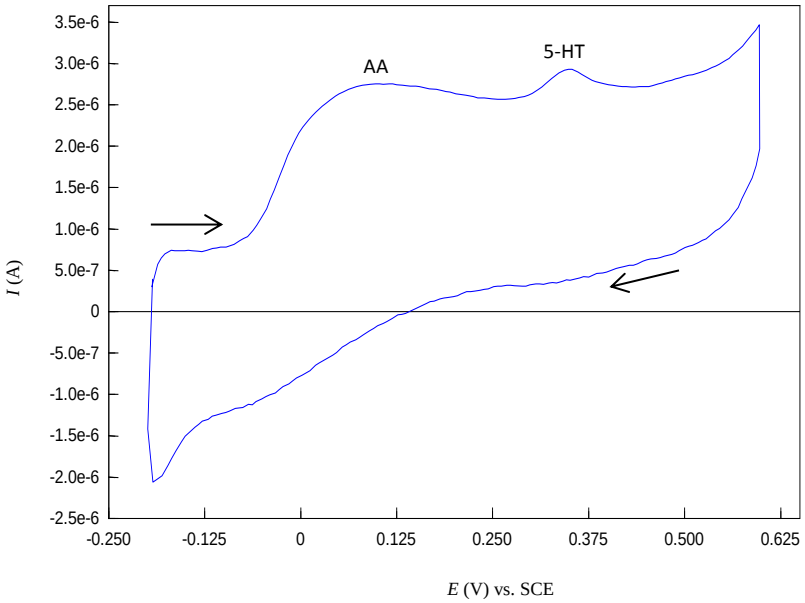

(b)

Figure 5.20: Cyclic voltammogram for a mixture of 5-HT (5×10^{-5} M) and AA (1×10^{-3} M) in 0.1 M PBS (pH 6.8) recorded at bare CPE (a) and S-β-CD modified CPE (b); scan rate 50 mV / s.

Within the diffusion layer, the negatively charged S-β-CD (at pH 6.8) accelerates protonated 5-HT interaction with the electrode surface, and as consequence, the reaction becomes easier. On the other hand, anionic AA oxidation process is partially blocked at the electrode surface, but can still interact through hydrogen bonding. The obtained results demonstrate that S-β-CD modified CPE is suitable for simultaneous detection of 5-HT and AA.

5.2.2.3 Electrochemical behaviour of a mixture of DA and 5-HT at S-β-CD modified CPE

Although simultaneous detection of DA or 5-HT and AA using S-β-CD modified CPE as working electrode was a success based primarily on charge difference, it appears more challenging to use the same modified electrode for simultaneous detection DA and 5-HT. Research shows that DA and 5-HT influence each other in their respective synaptic release [40], thus, simultaneous detection of both is highly desirable. Like DA, 5-HT is a monoamine neurotransmitter, which is also positively charged at pH 6.8. Their respective pK_a values, 8.9 for DA, and 9.8 for 5-HT, are very close, making any charge discrimination between 5-HT and DA difficult.

The electrochemical behaviour of DA and 5-HT mixture on bare CPE and S-β-CD modified CPE was investigated by cyclic voltammetry. Figure 5.21(a) shows the cyclic voltammograms of a mixture of equimolar concentration of 5-HT (5×10^{-5} M) and DA (5×10^{-5} M) in 0.1 M PBS (pH 6.8) on bare CPE and S-β-CD modified CPE. At bare CPE, 5-HT and DA show broad peak which correspond to overlapping oxidation peak currents due to DA and 5-HT oxidation. This result indicates that CPE cannot be used for any real application for the detection of 5-HT in presence of DA, or vice versa.

To explore whether modification of CPE give a different result, the voltammetric behaviour of DA (5×10^{-5} M) and 5-HT (5×10^{-5} M) mixture was investigated at S-β-CD modified CPE using cyclic voltammetry. As shown in Figure 5.21 (b), DA and 5-HT yielded two well-defined oxidation peaks at 0.170 and 0.349 V (vs. SCE). The reduction peak of DA was still observed at 0.153 V. The presence of S-β-CD results in significant increase in oxidation signal of DA and 5-HT from the mixture. The anodic peak value for DA and 5-HT are 1.283×10^{-6} A and 1.076×10^{-6} A, respectively. These peak current values are higher than their corresponding individual peak current at bare CPE. The enhanced oxidation signals may indicate different degree of electrostatic interaction between positively charged DA and 5-HT with sulfate groups of the cyclodextrin or a probable penetration of both species into the relatively less polar cavity of the cyclodextrin, resulting in the formation of DA:S-β-CD and 5-H:S-β-CD inclusion complexes. Moreover, it was demonstrated previously that S-β-CD has strong catalytic activity toward the oxidation of DA and 5-HT, through their individual response at S-β-CD modified CPE. Therefore, a probable competition in the adsorption of the species at the electrode surface can be considered for quantitative and qualitative determination of these neurotransmitters.

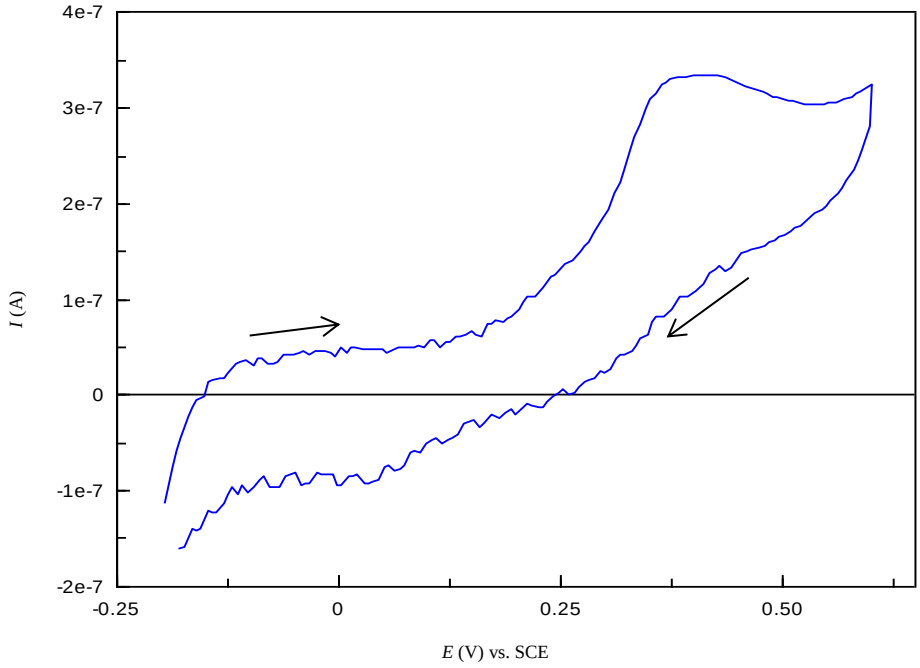

(a)

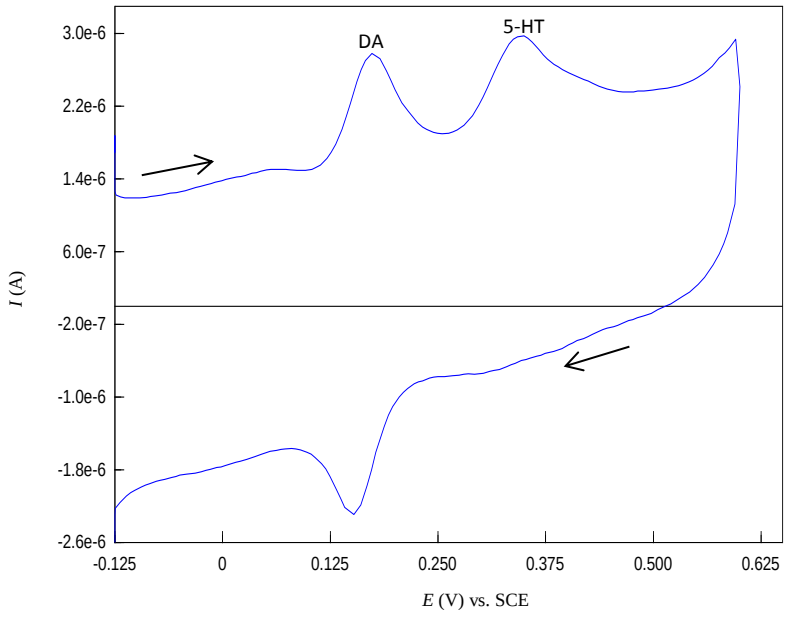

(b)

Figure 5.21: Cyclic voltammogram of a mixture of DA (5 × 10-5 M) and 5-HT (5 × 10-5 M) at bare CPE (a) and S-β-CD modified CPE in 0.1 M PBS (pH 6.8); scan rate 50 mV / s.

To further probe the electrochemical behaviour of a mixture of DA and 5-HT at CPE, DPV was employed. Figure 5.22(a) shows DPV responses of DA and 5-HT in mixtures at the S-β-CD modified CPE in comparison with that obtained at bare CPE. As shown in Figure 5.22(a), the voltammogram of a sample solution containing DA (5×10^{-5} M)

and 5-HT (5×10^{-5} M) at bare CPE shows a large peak occurring at 0.292 V, which corresponds to the oxidation of 5-HT, while a small and broad peak at 0.152 V represents oxidation of DA. From this experimental result, it appeared that 5-HT has a stronger affinity for bare CPE compared to DA. It is well-known that 5-HT adsorbs strongly on carbon materials, thus providing good sensitivity [37, 41]. The indole moiety may provide a relatively greater affinity with carbon (via π-π interaction) compared to benzene moiety. This observation is in agreement with the electrochemical response of these species (in their individual solution) at bare CPE, where the determined peak current of 5-HT was higher than that obtained at DA. Furthermore, much better resolved peaks were obtained at S-β-CD modified CPE (Figure 5.22 (b). The peaks occurring at 0.140 V and 0.272 V (vs. SCE) correspond to the oxidation of DA and 5-HT, respectively. The separation between peak potentials (ΔE_p) was 0.132 V. This value was large enough for simultaneous determination of DA and 5-HT. From the mixture, the peak current of DA was 1.55×10^{-6} A, while that of 5-HT was 1.15×10^{-6} A. So, DA had a slightly larger current response than 5-HT at S-β-CD modified CPE. Such a difference in peak current observed by DPV is in agreement with the results obtained using cyclic voltammetry, and may be related to different orientation of these two neurotransmitters in the cyclodextrin cavity.

(a)

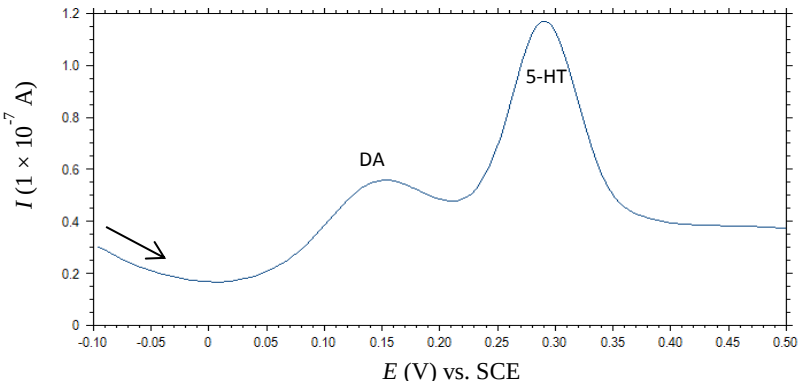

(b)

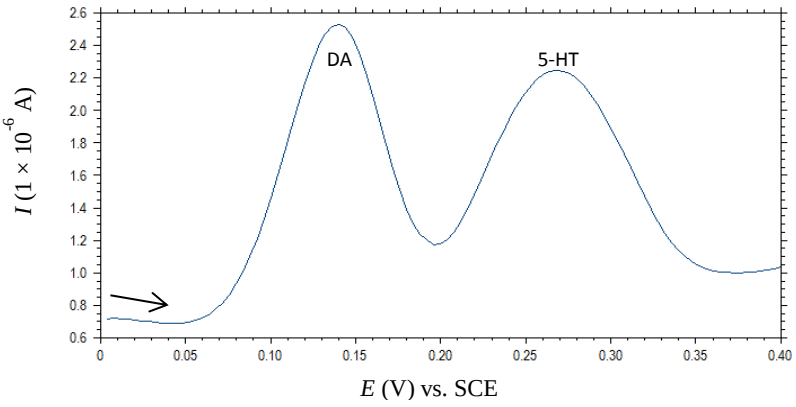

Figure 5.22: differential pulse voltammograms for a mixture of DA (5×10^{-5} M) and 5-HT (5×10^{-5} M) in 0.1 M PBS (pH 6.8) obtained at bare CPE (a) and S-β-CD modified CPE (b).

Docking studies performed by Sengupta *et al* [42] show that the indole moiety of serotonin is incorporated into the relatively less polar cavity of β-CD, while the aliphatic amine side chain protrudes through the primary rim of β-CD. Although complex formation through the inclusion of the aliphatic amine side chain of 5-HT within S-β-CD is possible, it is more likely that similar 5-HT orientation observed by Sengupta *et al* may happen using S-β-CD, with sulfate group facilitating diffusion of protonated 5-HT into the cyclodextrin cavity. In fact, the most stable conformation may correspond to the hydrophobic indole moiety of 5-HT dipped within the cavity of cyclodextrin, while the polar monoamine side is exposed to buffer and stabilised by electrostatic interaction with sulfate group.

Previous studies in our laboratory [43] have demonstrated that DA is included in S-β-CD cavity through its phenolic group, while cationic group is maintained outside the cavity and electrostatically attracted to anionic sulfate group on the rim of the cavity. Although both neurotransmitters show an enhanced signal at S-β-CD modified CPE, DA provides a quicker kinetic reaction than 5-HT which is characterised by its higher peak current.

However, it is more likely that S-β-CD greatly stabilizes 5-HT compared to DA. To support this hypothesis, the modified electrode was thoroughly rinsed with distilled water and a differential pulse voltammogram was recorded in a fresh buffer solution. As can be seen from Figure 5.23, the peaks corresponding to oxidation of DA and 5-HT were clearly observed at S-β-CD modified CPE, pointing that DA and 5-HT were significantly adsorbed onto the surface of the modified electrode. Interestingly, the oxidative peak current of 5-HT (4.781×10^{-7} A) was higher than that obtained for DA (3.462×10^{-7} A). These results show evidence of the stability of 5-HT over DA at S-β-CD modified CPE.

In summary, it was demonstrated that the S-β-CD modified CPE not only exhibited strong catalytic ability toward the oxidation of DA and 5-HT, but also resolved their voltammetric responses into two well-defined voltammetric peaks.

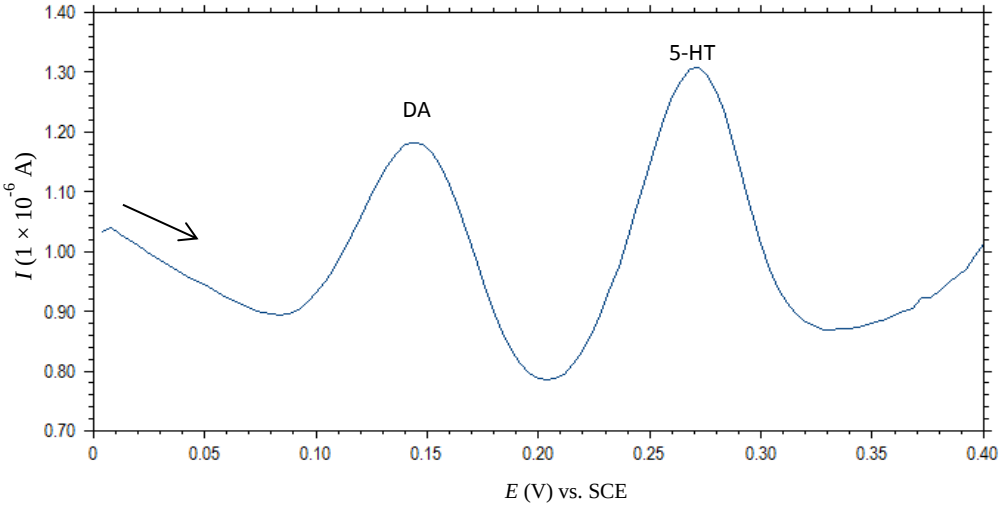

Figure 5.23: Differential pulse voltammogram obtained in 0.1 M PBS (pH 6.8) at S-β-CD modified CPE after a voltammogram was run in a mixture DA (5×10^{-5} M) and 5-HT (5×10^{-5} M).

5.2.2.4 Effect of electrochemical window for simultaneous detection of DA and 5-HT at S-β-CD modified CPE

Cyclic voltammetry was employed to observe if the electrochemical window has an effect on the determination of DA from a mixture of DA and 5-HT. In previous experiment carried out at S-β-CD modified CPE in the mixture of DA (5×10^{-5} M) and 5-HT (5×10^{-5} M), the upper potential limit was chosen to be 0.6 V. This potential was reduced to 0.27 V in order to detect DA only from the mixture. The corresponding voltammogram is shown in Figure 5.24 (black trace). For the sake of comparison, the same potential window was used for the detection of DA in the absence of 5-HT (Figure 5.24, red trace). The resulting DA peak currents are displayed in Table 5.2. As can been seen, the different oxidation peak currents obtained in DA solution and in the mixture are very close and the shape of the voltammograms are the same. This is evidence that DA detection is not affected by the applied electrochemical window, or more interestingly by the presence of 5-HT.

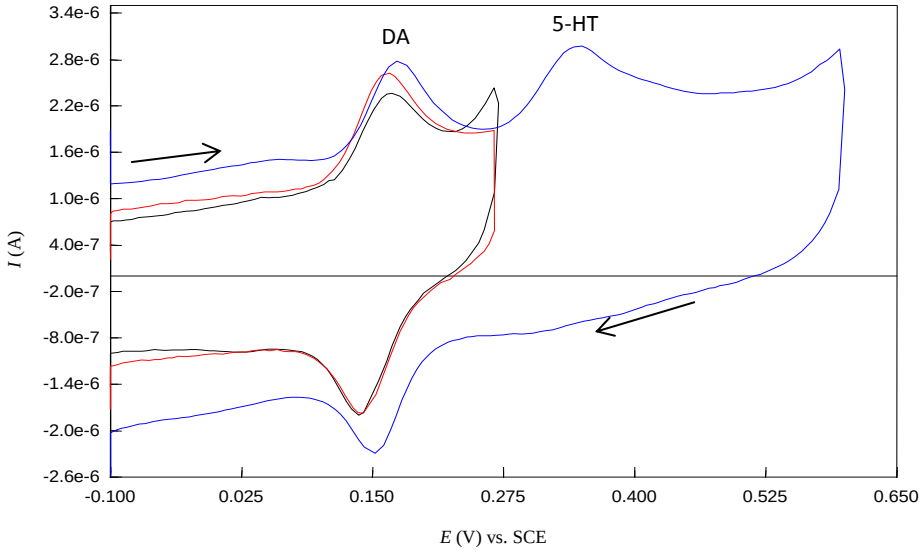

Figure 5.24: Cyclic voltammogram for a mixture of DA (5×10^{-5} M) and 5-HT (5×10^{-5} M) at S-β-CD modified CPE in 0.1 M PBS (pH 6.8) using upper potential limit +0.6 V (–) and +0.27 V (–), and cyclic voltammogram for DA (5×10^{-5} M) solution using upper potential limit +0.27 V (–). scan rate 50 mV / s.

Table 5.2: Effect of electrochemical window on DA oxidation peak currents

Sample analysed	Electrochemical window	DA oxidation peak current (A)
DA solution	[-0.2 V ; +0.27 V]	1.36×10^{-6}
Mixture DA / 5-HT	[-0.2 V ; +0.60 V]	1.28×10^{-6}
Mixture DA / 5-HT	[-0.2 V ; +0.27 V]	1.34×10^{-6}

5.2.2.5 Electrochemical behaviour of a mixture of DA and 5-HT at CM-β-CD modified CPE

CM-β-CD was employed as an alternative modifier (instead of S-β-CD) for simultaneous detection of DA and 5-HT. When a mixture of DA (5×10^{-6} M) and 5-HT (5×10^{-6} M) was investigated using DPV, it showed that the modified electrode had a better sensitivity for 5-HT compared to DA (Figure 5.25). The peak currents were 1.143×10^{-7} A and 4.430×10^{-7} A, corresponding to the oxidation of DA and 5-HT, respectively. The opposite effect was observed at S-β-CD modified CPE, where the peak current of DA was higher than that of 5-HT in the mixture. This is probably related to specific affinity the cyclodextrin derivatives have for DA and 5-HT. As mentioned in

Chapter 4, both forms of cyclodextrin derivatives used in this study are commercially available and randomly substituted mixtures. Charge distribution is not conclusively determined. Sulfated and carboxylated groups at the primary or secondary site of the cyclodextrin are different in their elemental composition and atom arrangement. Therefore, several factors such as geometry of molecule or acid dissociation of both modifiers and analytes may play a role in specific electrostatic interaction between host and guest prior to inclusion complex. Voltammetric sensing based on chemically modified electrodes depends largely on how sensitively electrode modifiers recognize target analytes and how rapidly they communicate the resulting electric signal to the underlying electrode [18]. So, kinetics has to be taken into account because the first molecule to interact with the cyclodextrin derivatives (or more specifically to enter cyclodextrin cavity), could in principle not be replaced by the other.

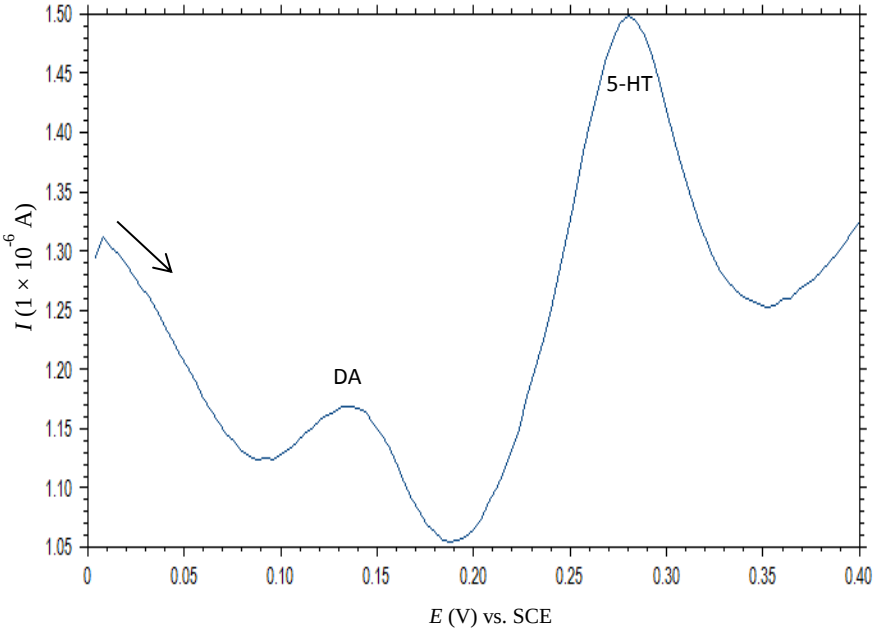

Figure 5.25: Differential pulse voltammograms for a mixture of DA (5×10^{-6} M) and 5-HT (5×10^{-6} M) in 0.1 M PBS (pH 6.8) obtained at CM-β-CD modified CPE.

As, it appeared that S-β-CD modified CPE showed a better oxidation response for DA, and, on the other hand CM-β-CD modified CPE gave a better peak signal for 5-HT, a combination of the modifiers was employed for simultaneous detection of DA and 5-HT. An equal amount (0.273 g) of each cyclodextrin derivative was mixed with the carbon paste. The prepared electrode was used to investigate the electrochemical behaviour of a mixture of DA (5×10^{-6} M) and 5-HT (5×10^{-6} M). The resulting voltammogram, displayed in Figure 5.26 shows that the oxidation of DA peak current was obtained as 1.483×10^{-7} A, whereas the oxidation of 5-HT was 4.095×10^{-7} A. Compared to CM-β-CD modified CPE, the peak intensity of DA has slightly increased, while that of 5-HT

decreased when a mixture of cyclodextrin derivatives was employed as working electrode. From this result, it is more likely that an adequate ratio of S-β-CD and CM-β-CD could provide an optimum sensing of these neurotransmitters from a mixture.

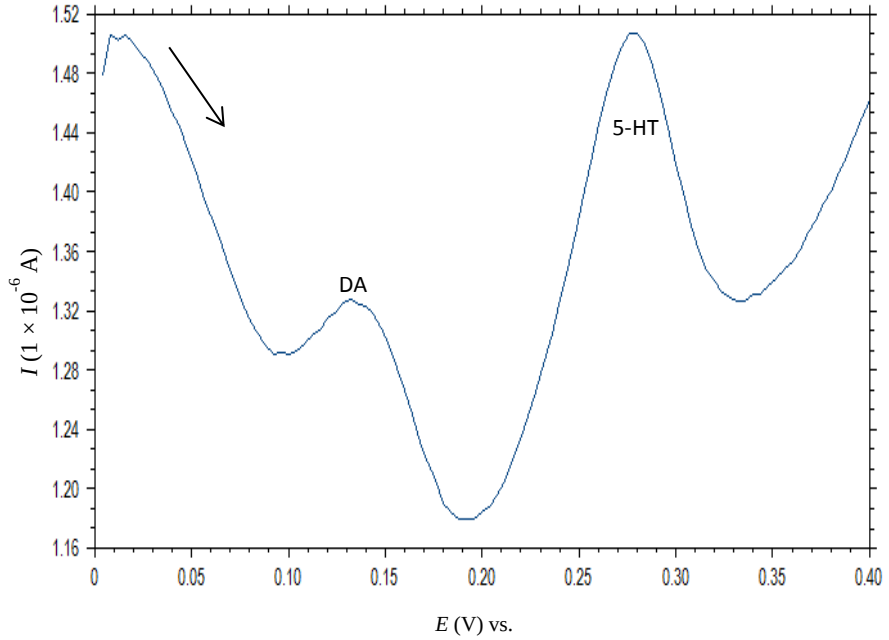

Figure 5.26: differential pulse voltammograms for a mixture of DA (5×10^{-6} M) and 5-HT (5×10^{-6} M) in 0.1 M PBS (pH 6.8) obtained at S-β-CD / CM-β-CD modified CPE.

5.2.2.6 Electrochemical behaviour of a mixture of DA and 5-HT at bare GPE

The voltammetric response at the bare GPE in a mixture of DA (5×10^{-5} M) and 5-HT (5×10^{-5} M) was obtained using DPV method. The data is illustrated in Figure 5.27. Two distinct peaks observed at 0.12 V and 0.27 V vs. SCE correspond to oxidation of DA and 5-HT respectively. The separation between the two peak potentials (0.15 V vs. SCE) was large enough, thus, the sensing of DA and 5-HT can be measured simultaneously in a mixture of equimolar concentration of DA and 5-HT. Unlikely, an efficient separation of the anodic peak signals of DA and 5-HT cannot be achieved at bare glassy carbon or bare CPE. Therefore, this performance obtained at bare GPE may be attributed to the structure of the graphene and the presence of many active sites such as defects and kinks. In addition, the presence of COOH groups on the bare GPE makes the surface highly electronegative, thereby contributing to electrostatic attraction of DA and 5-HT. The electrochemical oxidation of 5×10^{-5} M DA (from Chapter 4) and 5×10^{-5} M 5-HT (Figure 5.27) at bare CPE occurred at 0.13 V and 0.29 V (vs. SCE), respectively. The negative shift of peak potential of both neurotransmitters at bare GPE

(compared to bare CPE) provided evidence for the catalytic effects of graphene acting as a promoter to accelerate the electron transfer.

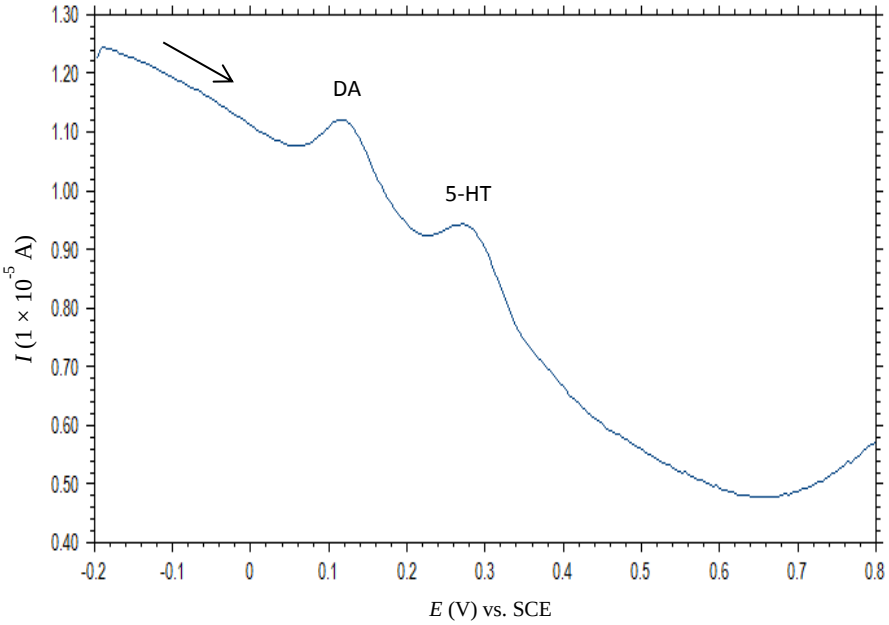

Figure 5.27: Differential pulse voltammogram for a mixture of DA (5×10^{-5} M) and 5-HT (5×10^{-5} M) in 0.1 M PBS (pH 6.8) obtained at bare GPE.

5.2.3 Electrochemical study of a mixture of AA, DA and 5-HT

Measurements of DA at bare CPE are complicated due to coexistence of high concentration of AA, which are oxidized at the same potential region. AA also attenuates the detection of 5-HT though 5-HT undergoes oxidation at more positive potential. It was demonstrated previously that simultaneous detection of AA and DA, and simultaneous measurement of AA and 5-HT was successful at S-β-CD modified CPE. Moreover, the overlapping voltammetric signal of DA and 5-HT was well separated using S-β-CD modified CPE. Therefore, it was assumed that satisfactory results could be obtain for analysing a mixture of AA, DA and 5-HT using S-β-CD. These three chemicals have been attracting great interest in bioelectroanalysis because they are extremely important analytes in clinical field. Many electrode modification strategies have been developed for improving their determination in terms of sensitivity and selectivity.

The purpose of this section is to investigate the ability of S-β-CD modified CPE for simultaneous detection of AA, DA and 5-HT. S-β-CD possesses high stability and good electron-mediating activity towards AA, DA and 5-HT. Therefore, one could exploit the electrostatic interaction of S-β-CD towards AA, DA and 5-HT to separate their overlapping anodic peaks.

5.2.3.1 Electrochemical behaviour of a mixture of AA, DA and 5-HT at S-β-CD modified CPE

The voltammetric behaviour for a mixture of AA (1×10^{-3} M), DA (5×10^{-5} M) and 5-HT (5×10^{-5} M) at S-β-CD modified CPE was examined using cyclic voltammetry. From Figure 5.28, S-β-CD modified CPE resolved the wave of AA and DA and 5-HT into a three well defined peaks. Hence, at the modified electrode three independent peaks could be observed at potentials around 0.08 V, 0.19 V and 0.34 V (vs. SCE) corresponding to the oxidation of AA, DA and 5-HT, respectively.

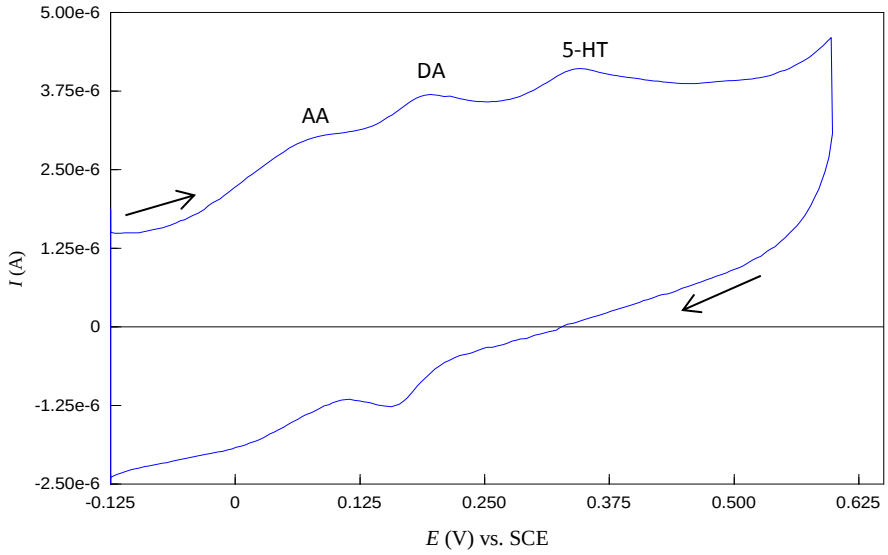

Figure 5.28: Cyclic voltammograms for a mixture of AA (1×10^{-3} M) DA (5×10^{-5} M) and 5-HT (5×10^{-5} M) in 0.1 M PBS (pH 6.8) obtained at S-β-CD modified CPE. Scan rate 50 mV / s.

As the charging current contribution to the background current is a limiting factor in the analytical determination of any electroactive species, the above experiment was carried out using DPV. When the DPV detection mode was applied instead of cyclic voltammetry for the mixture AA (1×10^{-3} M), DA (5×10^{-5} M) and 5-HT (5×10^{-5} M) at S-β-CD modified CPE, an improvement in the voltammetric peak heights corresponding to the oxidation of AA, DA and 5-HT, was observed. The presence of S-β-CD resolved the mixed voltammetric response into three well-defined voltammetric peaks at potentials 0.05, 0.15 and 0.28 V (vs. SCE), corresponding to the oxidations of AA, DA and 5-HT, respectively, as shown in Figure 5.29.

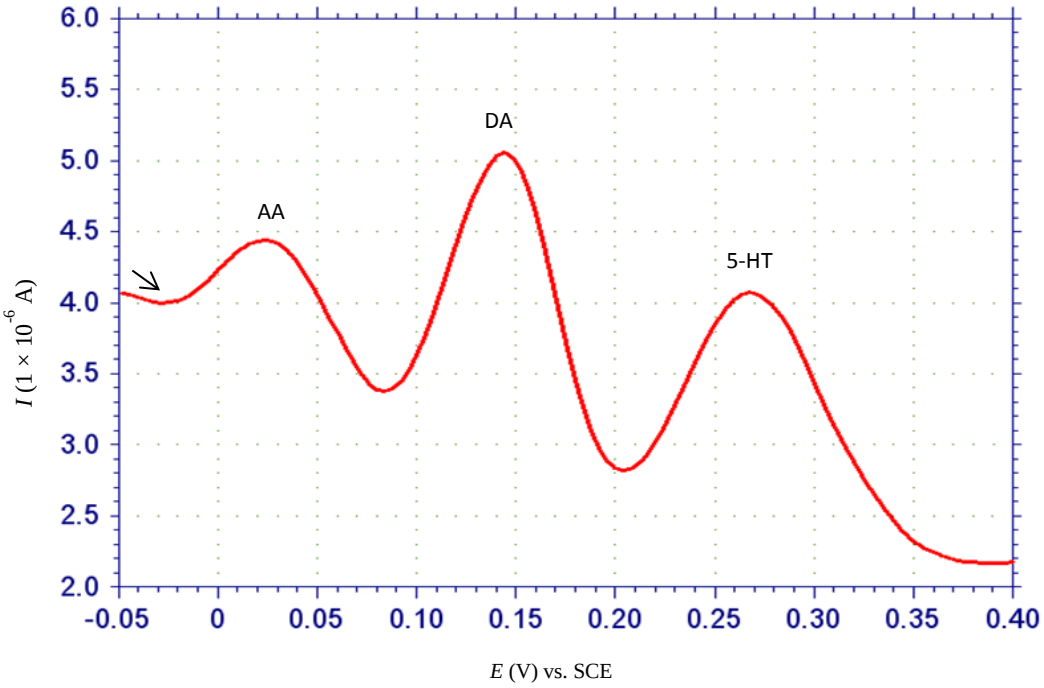

Figure 5.29: Differential pulse voltammogram obtained at S-β-CD modified CPE in a mixed solution containing AA (1×10^{-3} M), DA (5×10^{-5} M) and 5-HT (5×10^{-5} M). Supporting electrolyte 0.1 M PBS (pH 6.8).

5.2.4 Calibration Curves

A calibration curve is a method used in analytical chemistry to determine the concentration of an unknown sample solution. Most calibration curves are based on a linear relationship that can be expressed using the equation for a straight line, y = mx + b, where y is the instrument response, x is the concentration, m represents the slope of the line, and b is the y-intercept.

In this study, calibration curves were constructed for DA (AA and 5-HT) from electrochemical response obtained at the bare and most of modified electrodes employed in Chapter 4. The graph generated by experimental means, with the concentration of solution plotted on the x-axis and the peak currents on the y-axis show that in most cases a linear relationship was obtained between concentration and peak currents.

The theoretical limit of detection (LOD) was calculated in accordance with the $3S_b/m$ criteria [44], where S_b is the standard deviation of the blank response for n = 3 and m is the slope of the linear calibration plot. S_b, average mean value of background current

and relevant electrochemical technique employed for each of the studied modified electrode was given in Table 5.3.

Table 5.3: Average mean value of background current and corresponding standard deviation values obtained from each modified electrode. The standard deviation was used to calculate LOD

	S-β-CD modified CPE		**CM-β-CD modified CPE**	**Neutral β-CD modified CPE**	**Fc-β-CD modified CPE**
Electrochemical Techniques	CV	DPV	CV	CV	CV
Average mean value of background current (A)	9.520×10^{-7}	2.810×10^{-7}	1.415×10^{-6}	6.689×10^{-6}	2.685×10^{-7}
Standard Deviation, S_b	4.651×10^{-9}	1.966×10^{-9}	2.962×10^{-8}	4.673×10^{-8}	1.954×10^{-9}

Table 5.3 (continued): Average mean value of background current and corresponding standard deviation values obtained from each modified electrode. The standard deviation was used to calculate LOD

	CPE/O	**Bare GPE**	**S-β-CD modified GPE**
Electrochemical Techniques	CV	DPV	DPV
Average mean value of background current (A)	2.650×10^{-6}	6.481×10^{-6}	1.781×10^{-4}
Standard Deviation, S_b	6.027×10^{-6}	5.666×10^{-6}	9.000×10^{-6}

5.2.4.1 Detection of DA in DA only solutions

(i) At bare CPE

The electrocatalytic oxidation of DA was carried out at bare CPE by varying its concentration, using cyclic voltammetry method. Figure 5.30 (a) shows that by increasing the concentration of DA from 5×10^{-6} to 1×10^{-3} M the electrochemical anodic and cathodic peak currents increase with a shift of anodic peak potential toward the positive direction and cathodic peak potential toward the negative direction slightly.

Table 5.4 shows an increasing anodic peak potential with increasing DA concentration. The voltammograms corresponding to the two lowest concentrations of DA and the background current are displayed in Figure 5.30 (b). It is worth mentioning that the same electrode surface was used during this experiment. From Figure 5.31, it can be seen that the graph of anodic peak current versus concentration of DA shows a linear relationship in the range from 5×10^{-6} to 1×10^{-3} M DA. The regression equation was I_{pa} (A) = 0.0053 $_{[DA]}$ + 8.0727×10^{-8}, with a correlation coefficient of $R^2 = 0.9907$.

Table 5.4: Effect of DA concentration on oxidation peak currents and peak potential at bare CPE

Concentration of DA (M)	**Oxidation Peak Potential (V)**	**Oxidation peak current (A)**
5×10^{-6}	0.28	1.759×10^{-8}
1×10^{-5}	0.30	5.011×10^{-8}
5×10^{-5}	0.31	2.982×10^{-7}
1×10^{-4}	0.33	6.283×10^{-7}
5×10^{-4}	0.38	3.103×10^{-6}
1×10^{-3}	0.43	5.149×10^{-6}

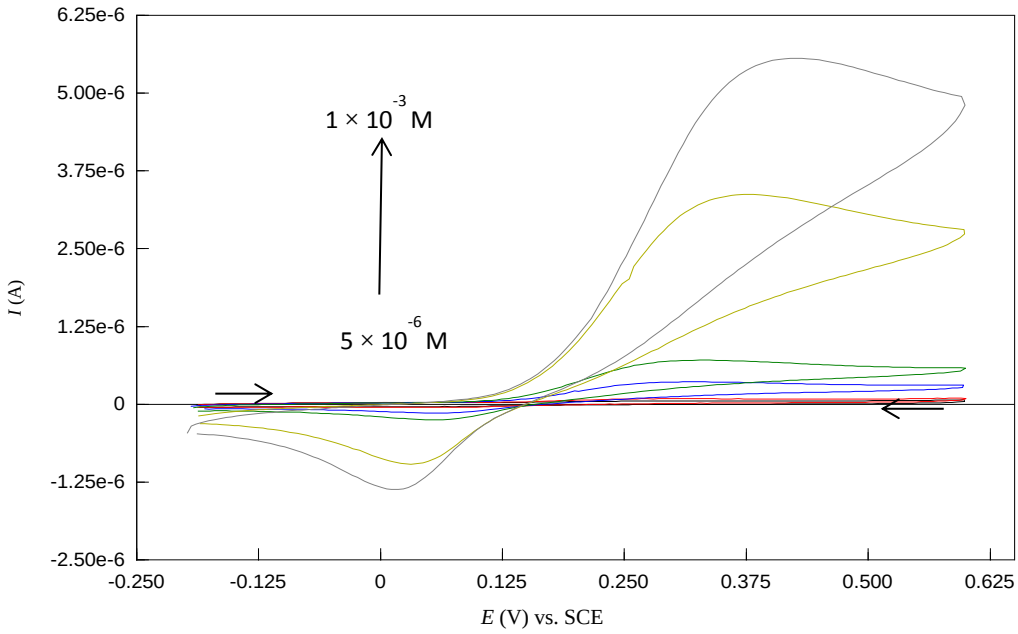

(a)

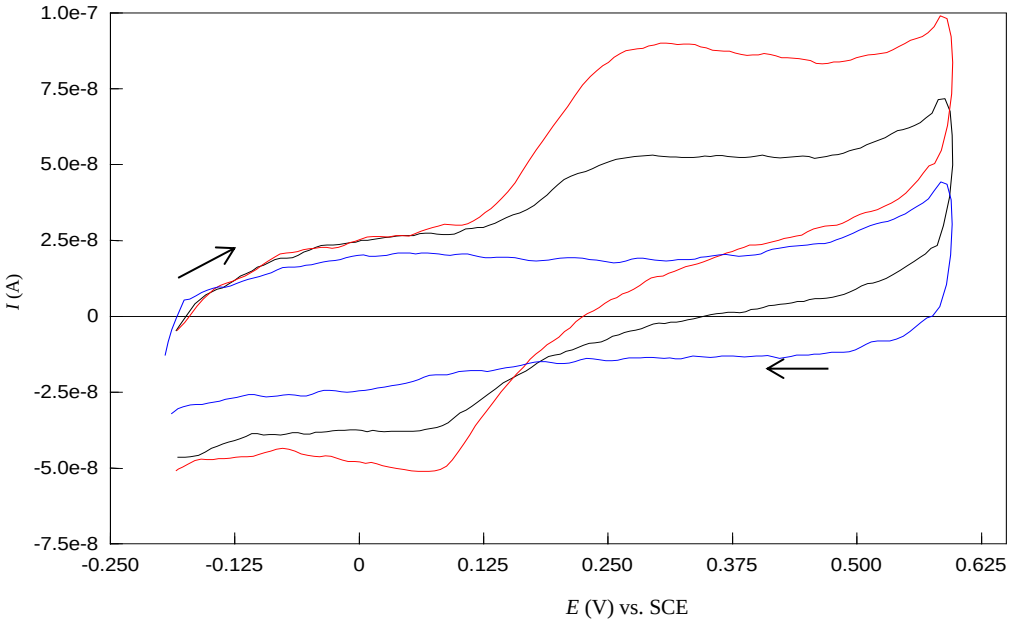

(b)

Figure 5.30: Cyclic voltammograms recorded at bare CPE in 0.1 M PBS containing different concentrations of DA (from 5 × 10^{-6} M to 1 × 10^{-3} M) (a) and enlarged voltammograms of 0.1 PBS (–), 5 × 10^{-6} M (–) and 1 × 10^{-5} M (–) DA (b); scan rate: 50 mV / s.

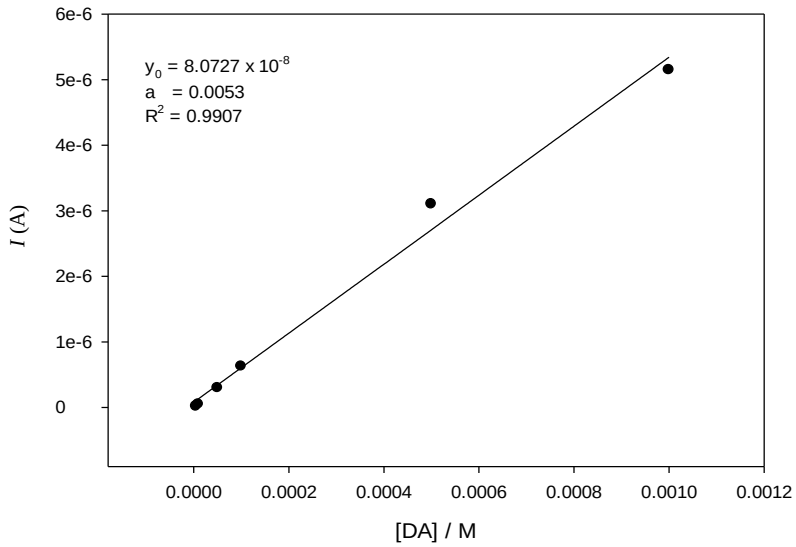

Figure 5.31: Calibration curve of oxidation current for the determination of DA using bare CPE.

(ii) At S-β-CD modified CPE

It was demonstrated previously that S-β-CD shows an electrocatalytic activity towards the detection of DA. Therefore, the response character of S-β-CD modified CPE to DA was undertaken for possible detection of different concentrations of DA. The concentration of DA was varied from 5×10^{-6} to 1×10^{-3} M, using the same electrode surface (Figure 5.32(a)) and a new electrode surface for each DA solution / concentration (Figure 5.33 (a)). It is clear that the relationship between anodic peak current and concentration of DA is linear between 5×10^{-6} M and 1×10^{-4} M, with the linear regression equation as I_{pa} (A) = 0.0382 $_{[DA]}$ + 6.834×10^{-8} (R^2 = 0.9959) and Ipa (A) = 0.0361 $_{[DA]}$ + 1.461×10^{-7} (R^2 = 0.9936) for 'polishing' and 'no polishing', respectively, as shown in Figure 5.34 (b). It has to be noted that 'polishing' refers to same electrode surface used for increasing concentration of DA. In 'no polishing', a new electrode surface was generated for each concentration of DA. The voltammograms corresponding to the two lowest DA concentrations was compared to the background in the case of 'polishing' and 'no polishing' as shown in Figure 5.32 (b) and Figure 5.33 (b), respectively.

As can be seen in Figure 5.34 (a), there is a slight deviation from linearity from 5×10^{-4} M to 1×10^{-3} M in both cases, probably due to electrode fouling effect at these relatively high concentrations of DA. Moreover, in the case of 'no polishing', the peak currents related to 5×10^{-4} M and 1×10^{-3} M are slightly lower than those obtained when using 'polishing' method.

(a)

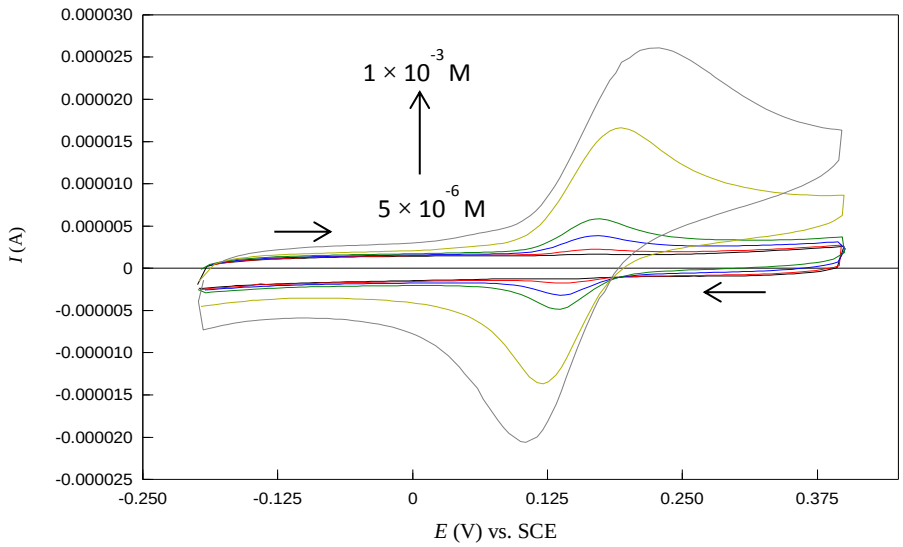

(b)

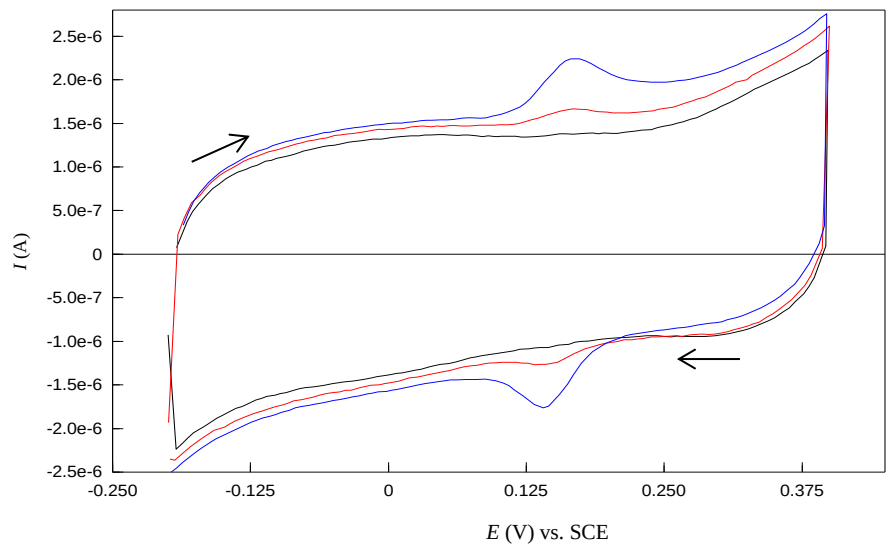

Figure 5.32: Cyclic voltammograms recorded at S-β-CD modified CPE (using 'no polishing' method) in 0.1 M PBS containing different concentrations of DA (from 5 × 10^{-6} M to 1 × 10^{-3} M) (a) and enlarged voltammograms of 0.1 PBS (–), 5 × 10^{-6} M (–) and 1 × 10^{-5} M (–) (b); scan rate: 50 mV / s.

(a)

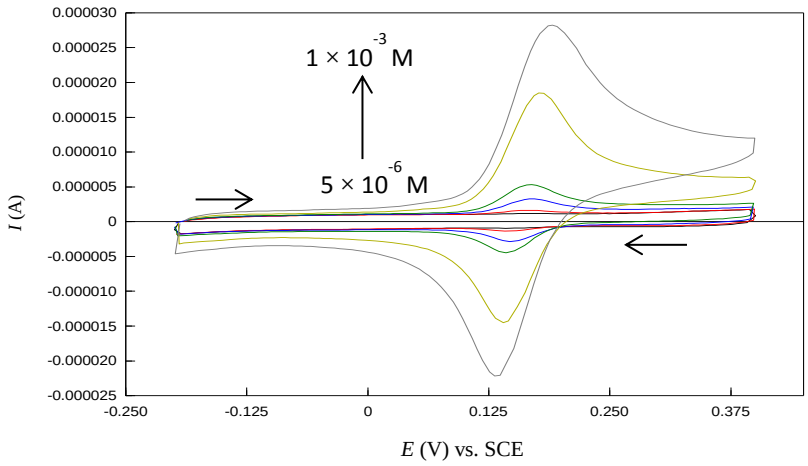

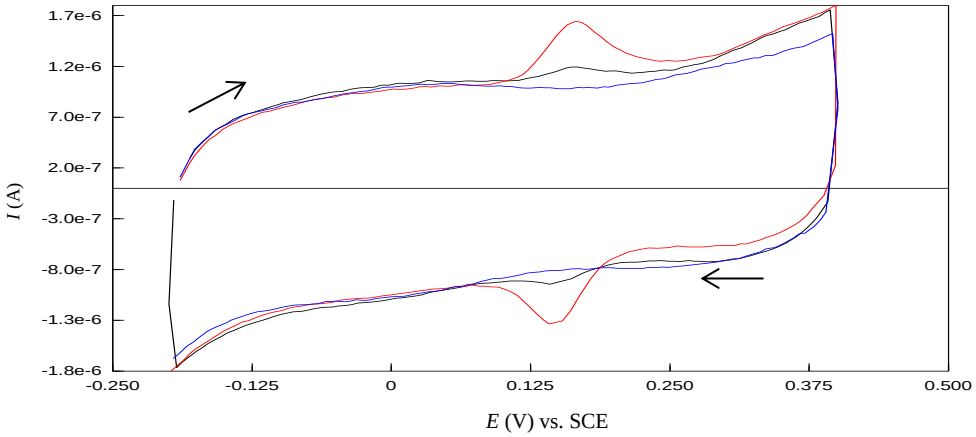

(b)

Figure 5.33: Cyclic voltammograms recorded at S-β-CD modified CPE (using 'polishing' method) in 0.1 M PBS containing different concentrations of DA (from 5 × 10^{-6} M to 1 × 10^{-3} M) (a) and enlarged voltammograms of 0.1 PBS (–), 5 × 10^{-6} M (–) and 1 × 10^{-5} M (–) (b); scan rate: 50 mV / s.

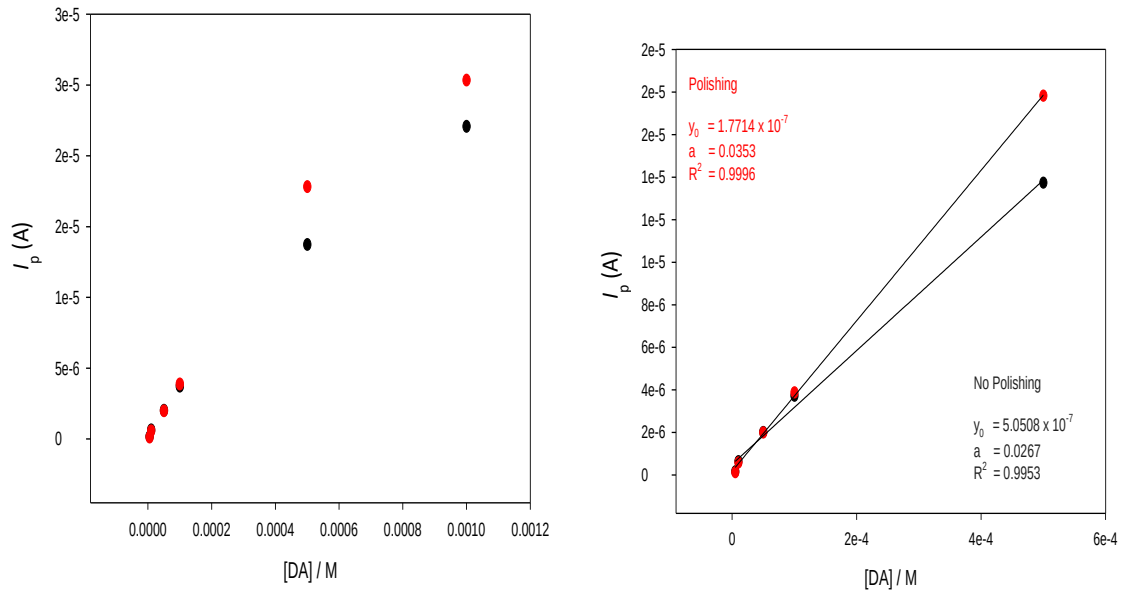

(a) (b)

Figure 5.34: Calibration curve of oxidation current for the determination of DA obtained at S-β-CD modified CPE using 'polishing' (·) and 'no polishing'(·) (a), and corresponding linear region (b).

In addition, the peak shape in the case of 'no polishing' at 1×10^{-3} M DA suggests a more diffusion profile compared to the 'polishing' method, with a resulting higher ΔE_p value, as shown in Figure 5.35. What is also remarkable in this study is that in the linear region, the peak currents obtained from 'polishing' and 'no polishing' clearly overlap. This may indicate that DA, or more importantly, the oxidation products of DA (i.e. DOQ) follow the same approach. As we know, DA is adsorbed at the modified electrode surface via electrostatic interaction and / or inclusion complex formation, where it is oxidised to DOQ. DOQ then moves away from the electrode surface allowing other DA molecules to be oxidised. Therefore, electrode fouling is considerably reduced at relatively low concentration of DA.

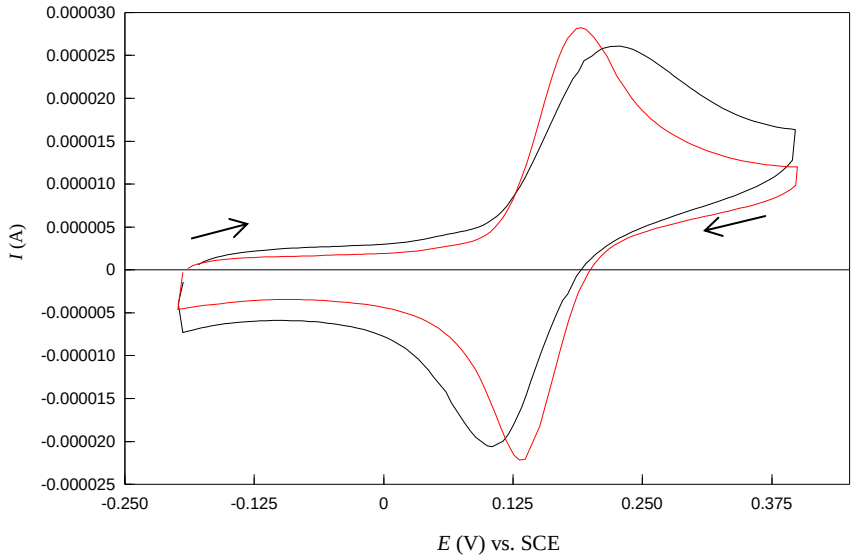

Figure 5.35: cyclic voltammograms recorded at S-β-CD modified CPE using 'no polishing' (–) and 'polishing' (–) method in DA (1 × 10^{-3} M) from different concentrations of DA; scan rate: 50 mV / s.

It is important to note that, as the concentration of DA increases, E_{pa} shifts towards more positive potentials with corresponding negative shift in E_{pc} as expected for a quasi-reversible process. From Table 5.5, the oxidation peak potentials of DA at S-β-CD modified CPE was constant enough and lower that those observed at bare CPE under similar conditions, indicating electrocatalytic effect of S-β-CD towards the detection of DA.

The experimental detection limit for DA at S-β-CD modified CPE using cyclic voltammetry was found to 5 × 10^{-6} M. The same detection limit was obtained at bare CPE with different signal intensity. The oxidation peak current corresponding to 5 × 10^{-6} M DA at bare CPE and S-β-CD modified CPE were 1.759 × 10^{-8} A and 1.669 × 10^{-7} A, respectively. Although, the peak current at S-β-CD modified CPE was about nine times higher than that obtained at bare CPE, a concentration lower than 5 × 10^{-6} M DA could not be detected. This may be due to the remarkable high background current observed at S-β-CD modified CPE compared to bare CPE. Charges associated with movement of electrolyte ions, adsorption / desorption at electrode-electrolyte interface were much more complex at the modified electrode. Therefore, this high charging capacitance may affect the detection of concentration lower than 5 × 10^{-6} M DA.

Table 5.5: Effect of DA concentration on oxidation peak currents and peak potential at S-β-CD modified CPE (using CV)

Concentration of DA (M)	Oxidation Peak Potential (V)	Oxidation peak current (A)
5×10^{-6}	0.17	1.669×10^{-7}
1×10^{-5}	0.17	6.390×10^{-7}
5×10^{-5}	0.17	2.020×10^{-6}
1×10^{-4}	0.17	3.721×10^{-6}
5×10^{-4}	0.19	1.374×10^{-5}
1×10^{-3}	0.23	2.207×10^{-5}

In an attempt to detect a concentration of DA lower than 5×10^{-6} M at S-β-CD modified CPE, DPV was employed. The electrochemical behaviour of 5×10^{-6} M DA at the modified electrode was studied in 0.1 M PBS in the potential range of -0.3 V to +0.6 V vs. SCE and the resulted voltammogram was displayed in Figure 5.26 (a). The peak occurring at around 0.00 V corresponds to oxidation of oxide species, which was previously discussed in Chapter 2. The small peak observed at 0.13 V is due to oxidation of DA. As already mentioned, oxidation peak potential of oxides and DA are very close and the DA signal is masked by the oxide peak when a relatively small concentration of DA is used. Therefore, it was decided to reduce the electrochemical window in order to improve the detection of 5×10^{-6} M DA. Successfully a distinct peak signal was obtained when a potential window ranging from 0 V to 0.25 V was used as shown in Figure 5.36 (b). Under similar conditions, the detection of 1×10^{-6} M and 5×10^{-7} M DA was achieved and the corresponding voltammograms are displayed in Figure 5.37 (a) and Figure 5.37 (b), respectively. As the peak current for 5×10^{-7} M DA was not clearly defined, background current was subtracted in order to determine the true peak current. The data was shown in Figure 5.38. Furthermore, differential pulse voltammetry response of DA at various concentration of DA was performed and shown in Figure 5.39 (a). As can be seen, the peak current increase as increasing the concentration of DA from 5×10^{-7} M to 1×10^{-3} M. The plot of I_{pa} against concentration of DA (Figure 5.39 (b)) showed a linear dynamic range of $5 \times 10^{-7} – 5 \times 10^{-4}$ M with a correlation coefficient value of 0.9955. The linear regression equation for this range is I_{pa} (A) = 0.0442 $_{[DA]}$ + 5.008×10^{-7}. Therefore LOD was found to be 1.33×10^{-7} M. The dependence of DA concentration on the peak potential and peak current is displayed in Table 5.6.

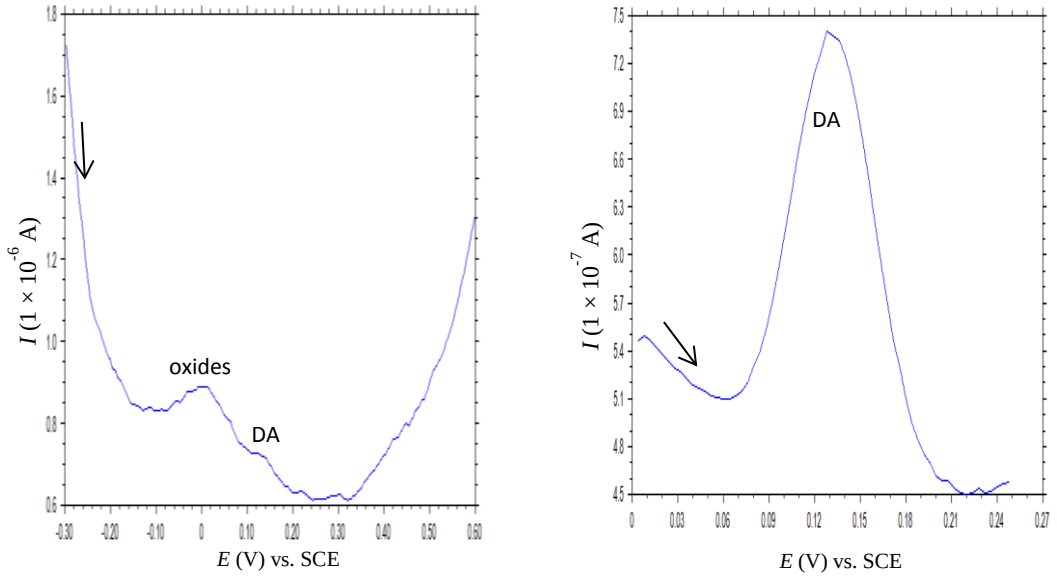

(a) (b)

Figure 5.36: Differential pulse voltammograms of DA (5 × 10^{-6} M) recorded at S-β-CD modified CPE using potential windows from -0.3 V to +0.6 V (a) and from 0.0 V to 0.25 V (b) vs. SCE. Supporting electrolyte 0.1 M PBS (pH 6.8).

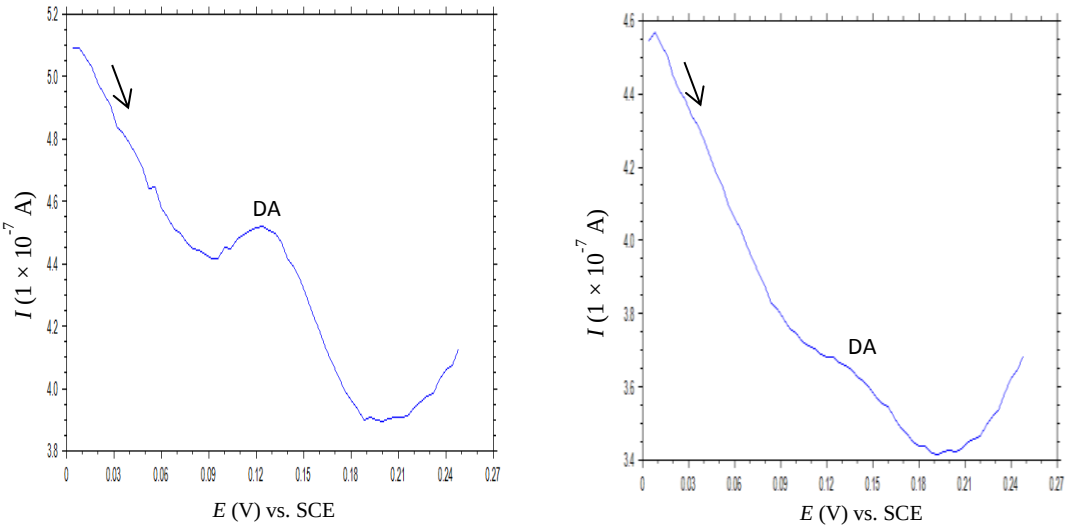

(a) (b)

Figure 5.37: Differential pulse voltammograms recorded at S-β-CD modified CPE in 1 × 10^{-6} M DA (a) and (5 × 10^{-7} M DA (b). Supporting electrolyte 0.1 M PBS (pH 6.8).

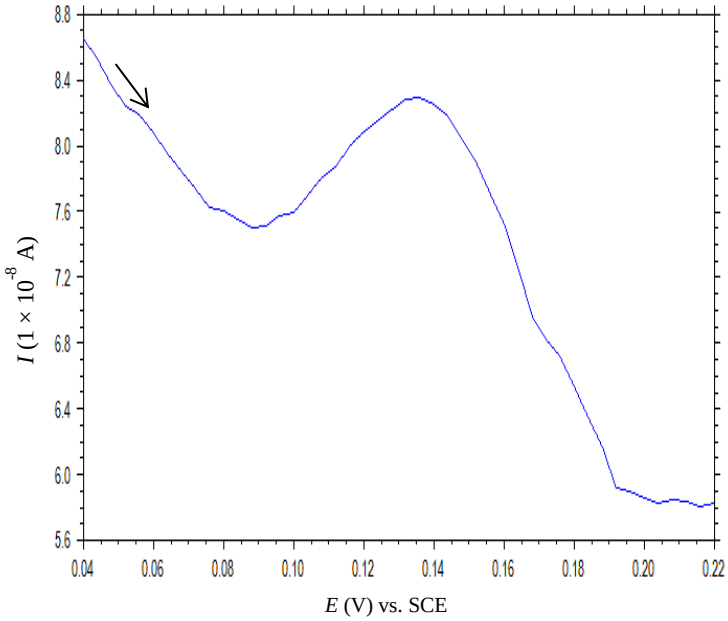

Figure 5.38: Differential pulse voltammograms recorded at S-β-CD modified CPE in 5×10^{-7} M DA afar background subtraction. Supporting electrolyte: 0.1 M PBS (pH 6.8).

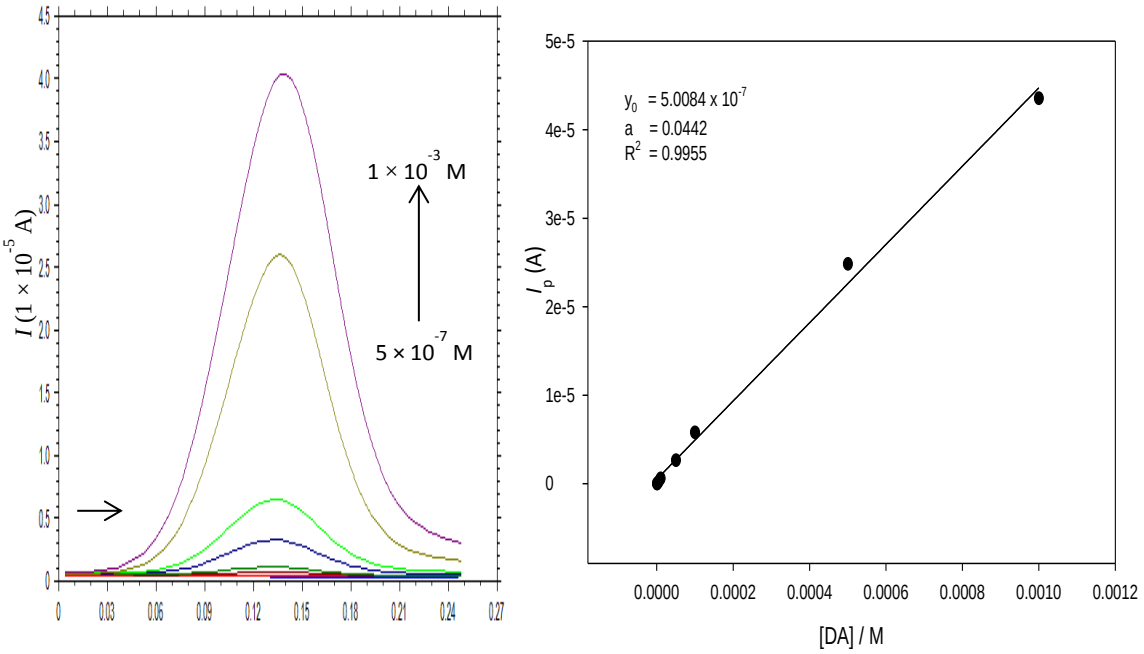

(a) (b)

Figure 5.39: Differential pulse voltammograms of various concentration of DA (from 5×10^{-7} M to 1×10^{-3} M) recorded at S-β-CD modified CPE (a) and corresponding calibration curve (b). Supporting electrolyte 0.1 M PBS (pH 6.8).

Table 5.6: Effect of DA concentration on oxidation peak currents and peak potential at S-β-CD modified CPE (using DPV)

Concentration of DA (M)	Oxidation Peak Potential (V)	Oxidation peak current (A)
5×10^{-7}	0.13	4.344×10^{-9}
1×10^{-6}	0.13	2.965×10^{-8}
5×10^{-6}	0.13	2.545×10^{-7}
1×10^{-5}	0.13	5.947×10^{-7}
5×10^{-5}	0.13	2.649×10^{-6}
1×10^{-4}	0.14	5.803×10^{-6}
5×10^{-4}	0.14	2.484×10^{-5}
1×10^{-3}	0.14	4.354×10^{-5}

(iii) At CM-β-CD modified CPE

A calibration plot was obtained at CM-β-CD modified CPE using similar conditions employed for S-β-CD modified CPE. The concentration of DA was varied from 5×10^{-6} M to 1×10^{-3} M and the electrochemical current was obtained at the modified electrode. The cyclic voltammogram (Figure 5.40 (a)) showed an oxidation peak at 0.16 V on the first concentration of DA. On further increasing the concentration of DA, the peak potential shifted slightly to the right with a rise in peak current (Table 5.7). This behaviour shows the analytical importance of the CM-β-CD modified CPE in the determination of DA. Figure 5.40 (b) shows the two lowest concentration of DA compared to background current. As the concentration of DA was varied from 5×10^{-6} M to 1×10^{-3} M, oxidation peak current holds linear relationship with concentration of DA, with a linear regression equation of I_{pa} (A) = 0.0289 $_{[DA]}$ - 1.4234×10^{-7}, as shown in Figure 5.41 (b). The coefficient of determination, $R^2 = 1$, indicating that the regression line is very well fitted with the experimental data. Thus, these results demonstrate that CM-β-CD modified CPE can be used for the determination of DA. The detection limit of DA at CM-β-CD modified CPE was calculated to be 3.09×10^{-6} M.

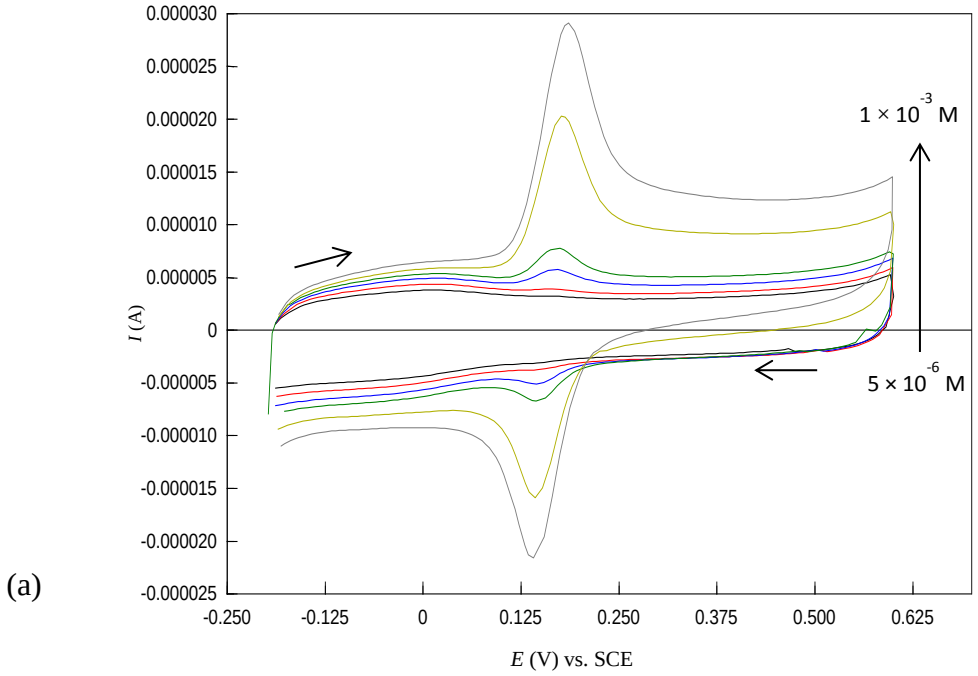

(a)

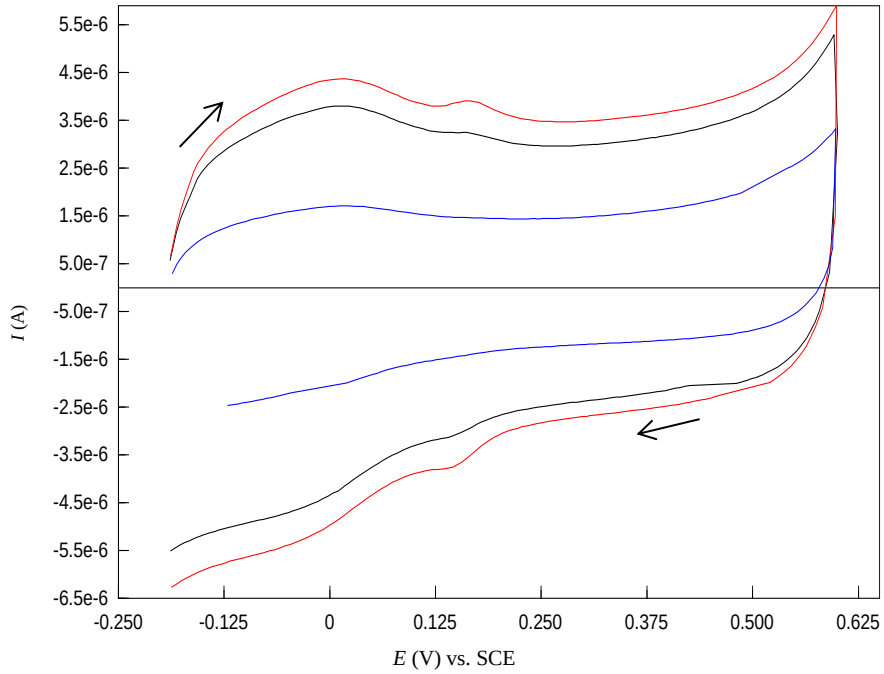

(b)

Figure 5.40: Cyclic voltammograms recorded at CM-β-CD modified CPE in 0.1 M PBS containing different concentrations of DA (from 5 × 10^{-6} M to 1 × 10^{-3} M) (a) and enlarged voltammograms of 0.1 PBS (–), 5 × 10^{-6} M (–) and 1 × 10^{-5} M (–) DA (b); scan rate: 50 mV / s.

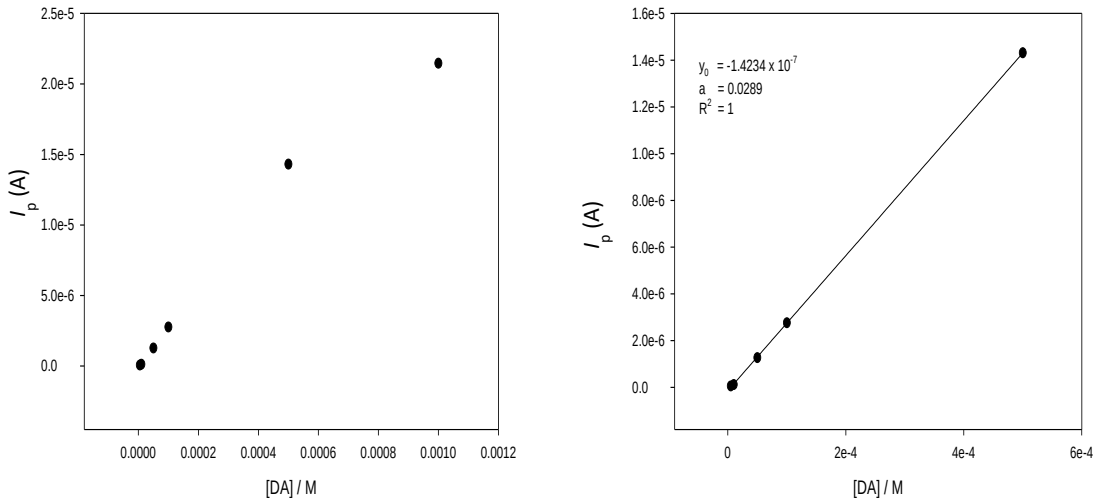

(a) (b)

Figure 5.41: Calibration curve of oxidation current for the determination of DA obtained at CM-β-CD modified CPE (a), and corresponding linear region (b).

Table 5.7: Effect of DA concentration on oxidation peak currents and peak potential at CM-β-CD modified CPE

Concentration of DA (M)	Oxidation Peak Potential (V)	Oxidation peak current (A)
5×10^{-6}	0.16	5.708×10^{-8}
1×10^{-5}	0.16	1.143×10^{-7}
5×10^{-5}	0.17	1.267×10^{-6}
1×10^{-4}	0.17	2.759×10^{-6}
5×10^{-4}	0.18	1.431×10^{-5}
1×10^{-3}	0.19	2.146×10^{-5}

(iv) At Neutral β-CD modified CPE

From Chapter 4, it was observed that the peak current for 5×10^{-5} M DA at Neutral β-CD modified CPE was higher than that of bare CPE. Therefore, determination of different concentrations of DA at Neutral β-CD modified CPE appeared important. However, the concentration range for the determination of DA was only 5×10^{-5} M – 1×10^{-3} M (Figure 5.42 (a)). The oxidation current of DA within this range was proportional to the concentration of DA (Figure 5.42 (b)), following the linear regression equation I_{pa} (A) = 0.0114 $_{[DA]}$ – 4.0891×10^{-8}. The plots showed good linearity, with a correlation coefficient of 0.9959 and the calculated detection limit was

1.23 × 10^{-5} M. It can be noted that the peak potential remained constant as the concentration of DA was increased (Table 5.8).

(a)

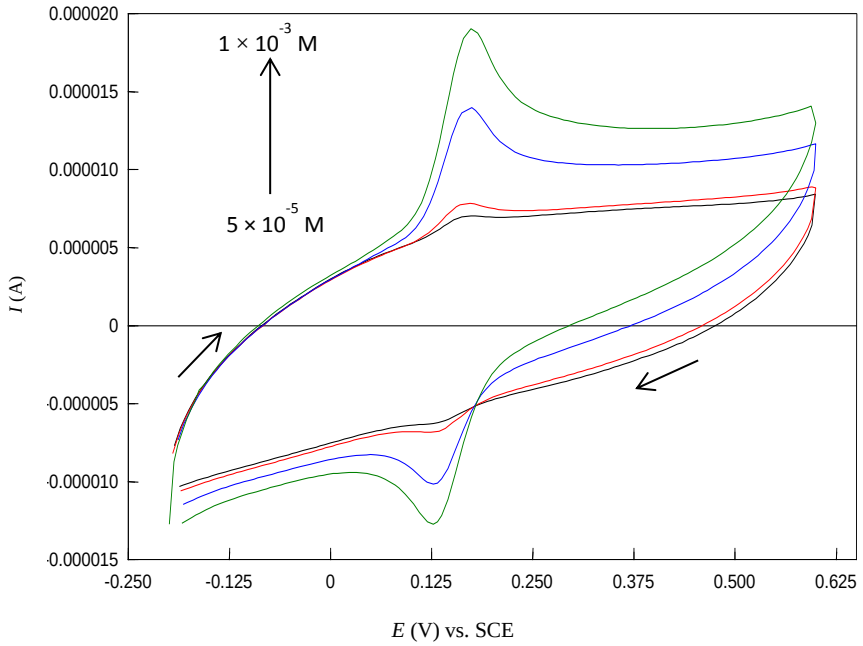

(b)

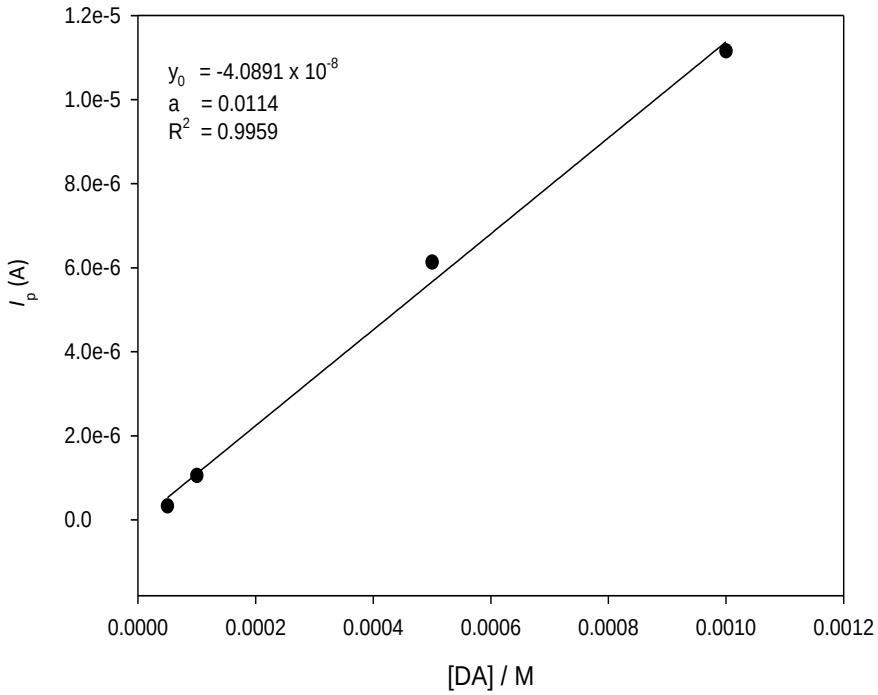

Figure 5.42: Cyclic voltammograms of the application of various concentration of DA (from 5 × 10^{-5} M to 1 × 10^{-3} M) recorded at neutral β-CD modified CPE (a) and corresponding calibration curve (b). Supporting electrolyte 0.1 M PBS (pH 6.8).

Table 5.8: Effect of DA concentration on oxidation peak currents and peak potential at neutral β-CD modified CPE

Concentration of DA (M)	Oxidation Peak Potential (V)	Oxidation peak current (A)
5×10^{-5}	0.17	3.284×10^{-7}
1×10^{-4}	0.17	1.054×10^{-6}
5×10^{-4}	0.17	6.134×10^{-6}
1×10^{-3}	0.17	1.116×10^{-5}

(v) At Fc-β-CD modified CPE

Fc-β-CD modified CPE is not charged and has different sensing mechanism for DA compared to S-β-CD modified CPE or CM-β-CD modified CPE. Using optimised conditions such as concentration of Fc-β-CD, scan rate, potential to be applied for analysis, the sensor was calibrated for determination of DA. As can be seen from Figure 5.43 (a), the oxidation peak current increased as the concentration of DA increased. The three lowest DA concentrations are displayed in Figure 5.43 (b). The calibration curve illustrated in Figure 5.44 shows linearity from 5×10^{-6} M to 1.01×10^{-4} M DA, with $R^2 = 0.9981$. The linear regression equation is I_{pa} (A) = $0.0105_{[DA]} + 9.3410 \times 10^{-8}$. The limit of detection was determined to be 1.70×10^{-6} M. It is worth noting that a far better sensitivity was obtained at Fc-β-CD modified CPE compared to neutral β-CD modified CPE, indicating that Fc is a good electron mediator for the determination of DA. The electrocatalytic oxidation of DA at Fc-β-CD modified CPE was described in Chapter 4. Fe (III) produced during anodic scanning oxidizes DA molecule when it is reduced to Fe (II). DA is oxidized at the electrode surface of Fc-β-CD modified CPE following an effective diffusional process. This mode of electron transfer was different from that obtained at neutral β-CD modified CPE or S-β-CD modified CPE. In addition, the oxidation of DA at Fc-β-CD modified CPE (from Table 5.9) occurs at a lower potential compared to that of obtained at bare CPE.

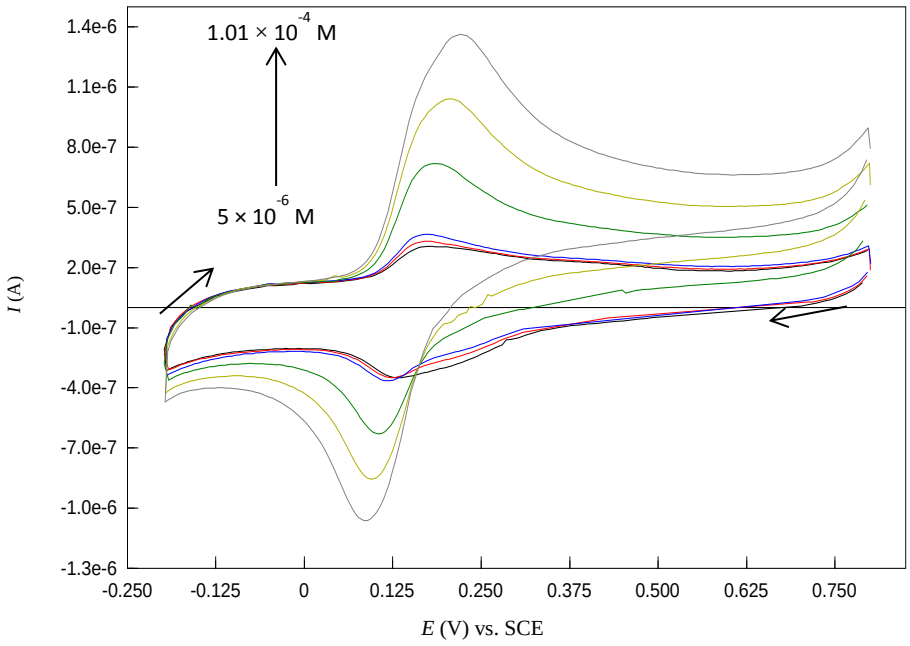

(a)

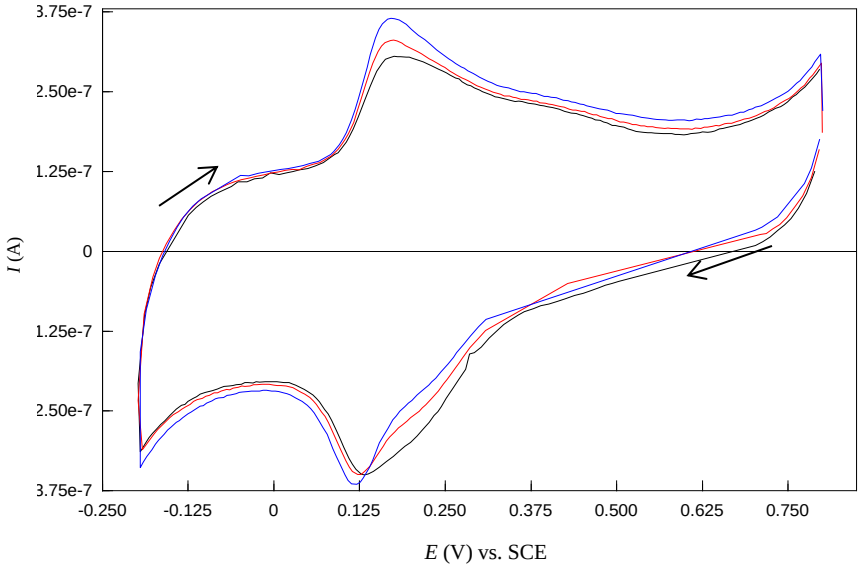

(b)

Figure 5.43: Cyclic voltammograms recorded at Fc-β-CD modified CPE in 0.1 M PBS containing different concentrations of DA (from 5 × 10^{-6} M to 1.01 × 10^{-4} M) (a) and enlarged voltammograms of 5 × 10^{-6} M (–), 8 × 10^{-6} M (–) and 1.1 × 10^{-5} M (–) DA (b); scan rate: 50 mV / s.

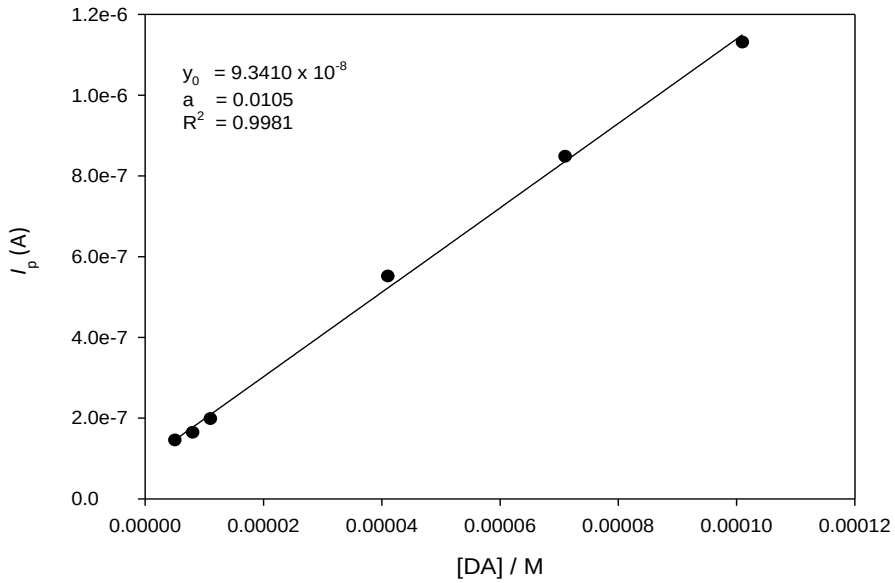

Figure 5.44: Calibration curve of oxidation current for the determination of DA obtained at Fc-β-CD modified CPE.

Table 5.9: Effect of DA concentration on oxidation peak currents and peak potential at Fc-β-CD modified CPE

Concentration of DA (M)	Oxidation Peak Potential (V)	Oxidation peak current (A)
5×10^{-6}	0.18	1.453×10^{-7}
8×10^{-6}	0.18	1.644×10^{-7}
1.1×10^{-5}	0.18	1.982×10^{-7}
4.1×10^{-5}	0.19	5.518×10^{-7}
7.1×10^{-5}	0.20	8.483×10^{-7}
1.01×10^{-4}	0.22	1.131×10^{-6}

(vi) At CPE with oxide layer

It was found that oxides have a positive effect on the redox properties of DA. However, this experimental result is only true when a relatively high concentration of DA was used. Figure 5.45 (a) presents the relationship between DA concentration and current signal recorded at CPE with oxide layer. It is clear that the oxidative peak current increases as increasing the concentration of DA. Based on oxidation peak potential (Table 5.10), less energy was needed to oxidise DA at CPE with oxide layer compared to the bare CPE. However, the lowest detected DA concentration at oxide containing electrode was only 1×10^{-5} M. This relatively poor sensitivity is due to the strong effect

the oxidation of oxide species has on that of DA. From the voltammogram presented in Figure 5.45 (b), the oxidation of oxide species and DA are very close. Therefore, the peak signal of DA is masked by the oxidation peak of oxides. It can also be noted that the oxide peak decrease as the concentration of DA increase. From Figure 5.46, the graph of anodic peak current versus concentration of DA shows two linear ranges with a transition point at 1×10^{-4} M. The sensor displays linear ranges of 1×10^{-5} M – 1×10^{-4} M and 1×10^{-4} M – 1×10^{-3} M with the linear regression equations as I_{pa} (A) = 0.0175 $_{[DA]}$ - 1.3932×10^{-7} and I_{pa} (A) = 0.0045 $_{[DA]}$ + 1.2262×10^{-6}, respectively. The correlation coefficient for the first linearity was 0.9993 and for the second it was 0.9955. The decrease of sensitivity (slope) in the second linear range is likely due to kinetic limitation. The detection limit of DA in the lower range was found to be 1.81×10^{-5} M.

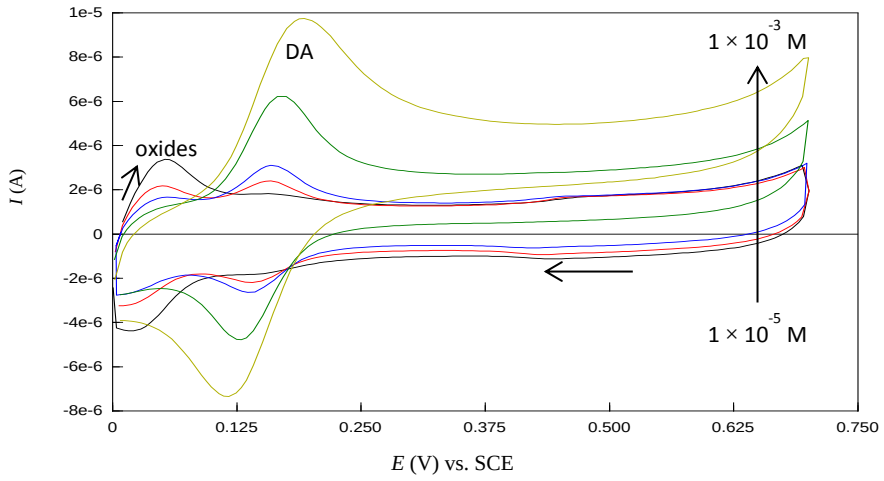

(a)

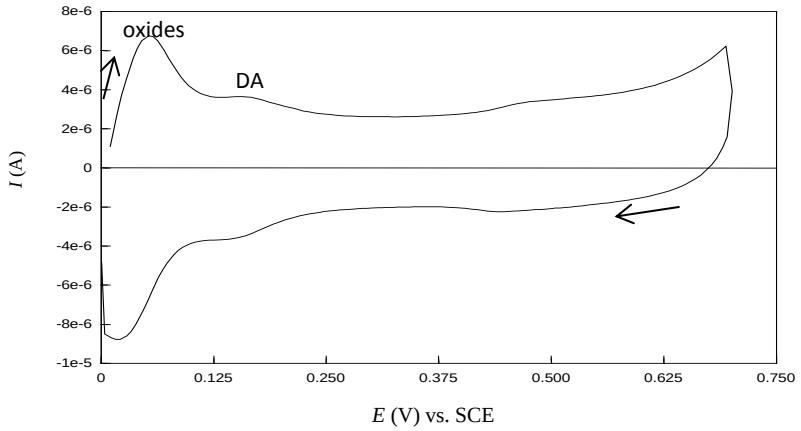

(b)

Figure 5.45: Cyclic voltammograms recorded at CPE with oxide layer in 0.1 M PBS containing different concentrations of DA (from 1×10^{-5} M to 1×10^{-3} M) (a) and enlarged voltammograms of 1×10^{-5} M DA (b); scan rate: 50 mV / s.

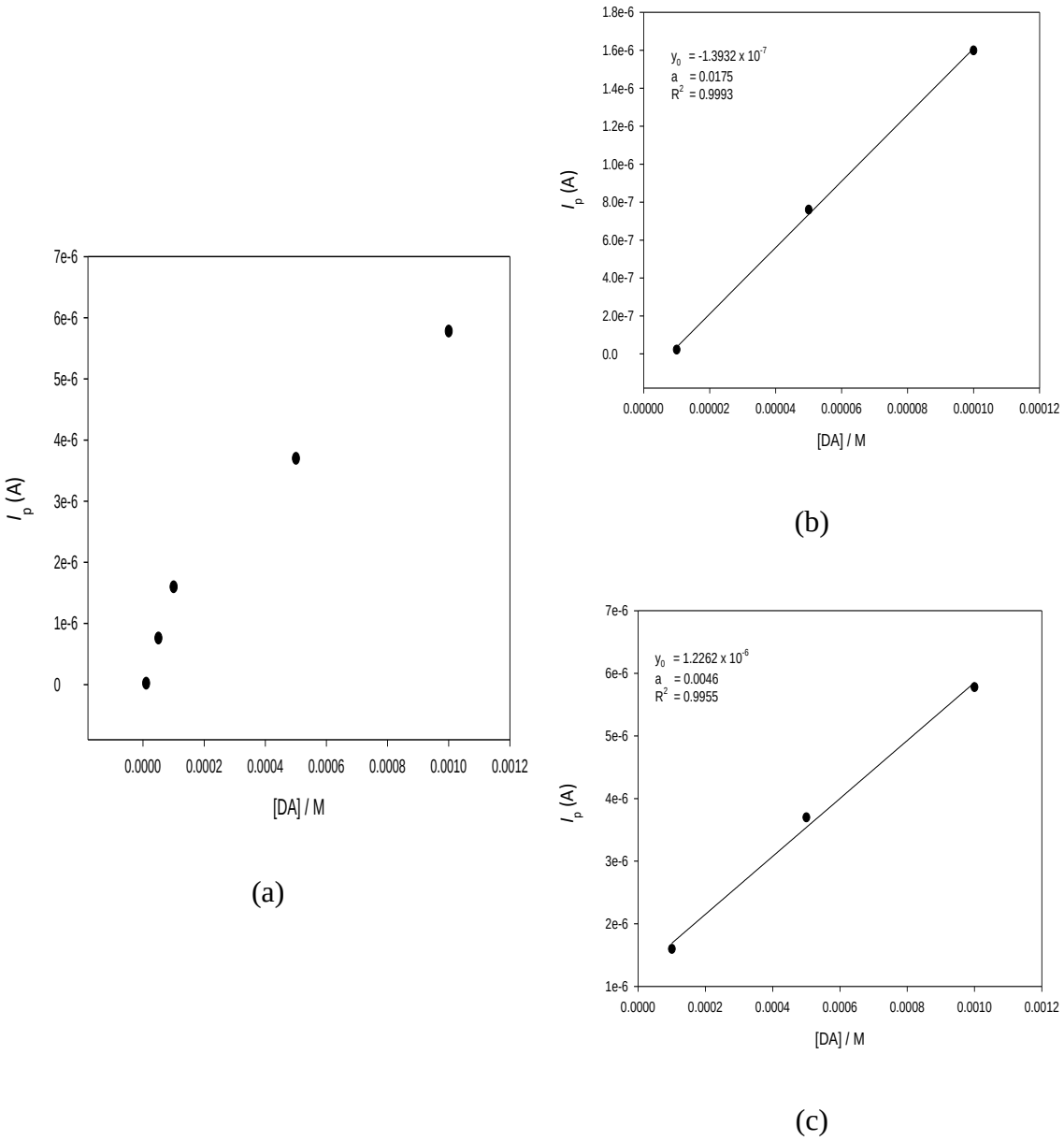

Figure 5.46: calibration curve of oxidation current for the determination of DA obtained at CPE with oxide layer (a), and corresponding linear region for the lower oxidation range (b) and linear region for the higher oxidation range (c).

Table 5.10: Effect of DA concentration on oxidation peak currents and peak potential at CPE with oxide layer

Concentration of DA (M)	Oxidation Peak Potential (V)	Oxidation peak current (A)
1×10^{-5}	0.16	2.190×10^{-8}
5×10^{-5}	0.16	7.600×10^{-7}
1×10^{-4}	0.16	1.550×10^{-6}
5×10^{-4}	0.17	3.701×10^{-6}
1×10^{-3}	0.19	5.780×10^{-6}

(vii) At bare GPE

Differential pulse voltammetry technique was applied for the quantitative detection of DA at bare GPE. The corresponding results are showed in Figure 5.47 (a). As seen, the peak currents enhance gradually with the increase of DA concentration. The oxidation peak currents show a good linear relationship with the concentrations of DA ranging from 5×10^{-5} M to 1×10^{-3} M (Figure 5.48). The voltammograms corresponding to the first two lowest DA concentrations are highlighted in Figure 5.47 (b). The linear equation was I_{pa} (A) = 0.0325 $_{[DA]}$ + 3.2904×10^{-7} (R^2 = 0.9978). The limit of detection for this electrode was estimated to be 1.70×10^{-5} M. From Table 5.11, it is observed that GPE give the lowest peak potential values compared to all studied electrodes. This remarkable shift in peak potential is more likely due to the unique properties of graphene such as large surface-to-volume ratio and high electrical conductivity.

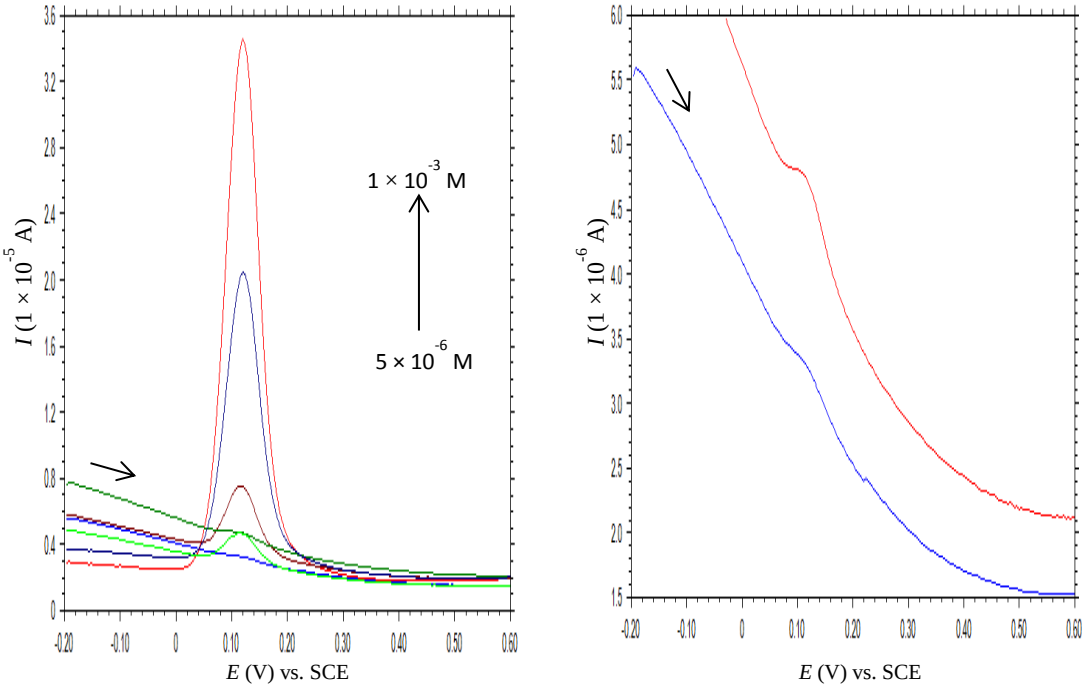

(a) (b)

Figure 5.47: Differential pulse voltammograms recorded at bare GPE in 0.1 M PBS containing different concentrations of DA (from 5 × 10^{-6} M to 1 × 10^{-3} M) (a) and enlarged voltammograms of 5 × 10^{-6} M DA (–) and 1 × 10^{-5} M DA (–).

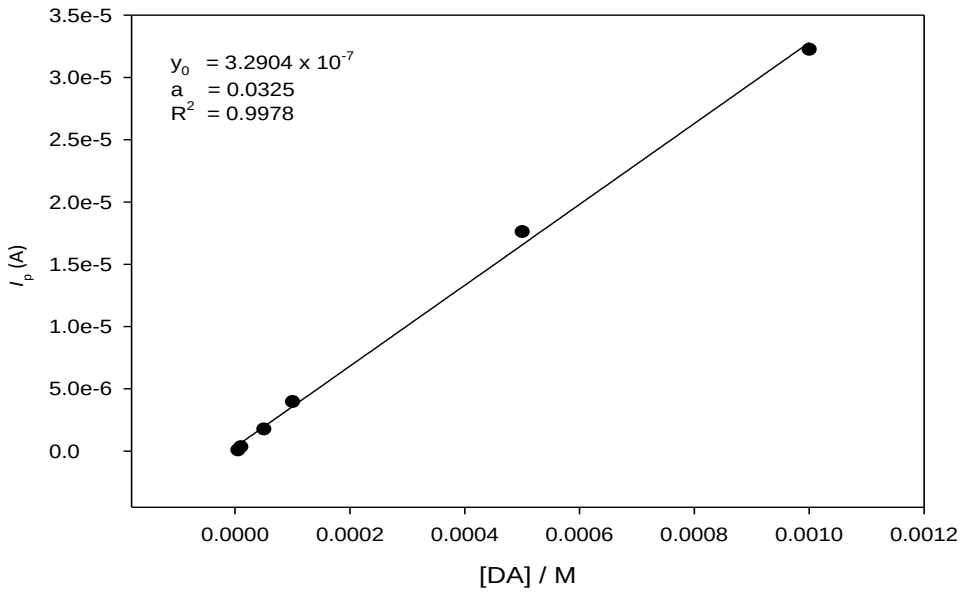

Figure 5.48: Calibration curve of oxidation current for the determination of DA obtained at bare GPE.

Table 5.11: Effect of DA concentration on oxidation peak currents and peak potential at bare GPE

Concentration of DA (M)	Oxidation Peak Potential (V)	Oxidation peak current (A)
5×10^{-6}	0.11	9.213×10^{-8}
1×10^{-5}	0.11	3.389×10^{-7}
5×10^{-5}	0.12	1.774×10^{-6}
1×10^{-4}	0.12	3.967×10^{-6}
5×10^{-4}	0.12	1.762×10^{-5}
1×10^{-3}	0.12	3.225×10^{-5}

(viii) At S-β-CD modified GPE

The calibration curve of DA at S-β-CD modified graphene electrode was obtained by increasing the concentration of DA from 5×10^{-6} M to 1×10^{-3} M. Prior to determination, the modified electrode was conditioned by repeated potential scanning in a blank 0.1 M PBS solution, pH 6.8, with the purpose of obtaining a steady background current.

Figure 5.49 depicts the voltammograms at various concentrations of DA using S-β-CD modified GPE. The plot of oxidation peak current versus the concentration of DA shows a fair relationship in the concentration range 5×10^{-6} M – 1×10^{-4} M (Figure 5.50) with a correlation coefficient $R^2 = 0.9805$. The linear regression equation was expressed as I_{pa} (A) = $0.1108_{[DA]} + 7.2589 \times 10^{-7}$. The detection limit was obtained to be 2.44×10^{-4} M. Although, S-β-CD modified GPE shows a better electrochemical response (using 5×10^{-5} M DA) as compared to bare GPE, the detection limit was poor. The synthesised graphene utilised in this study already contained some degree of functional groups such as carboxylate (Chapter 2). Therefore, the addition of 0.545 g S-β-CD to the paste may cause some kinetic limitation, particularly for detection of successive concentrations of DA. This 'difficult' reactivity is characterised by the higher peak potentials (Table 5.12) compared to those obtained at bare CPE.

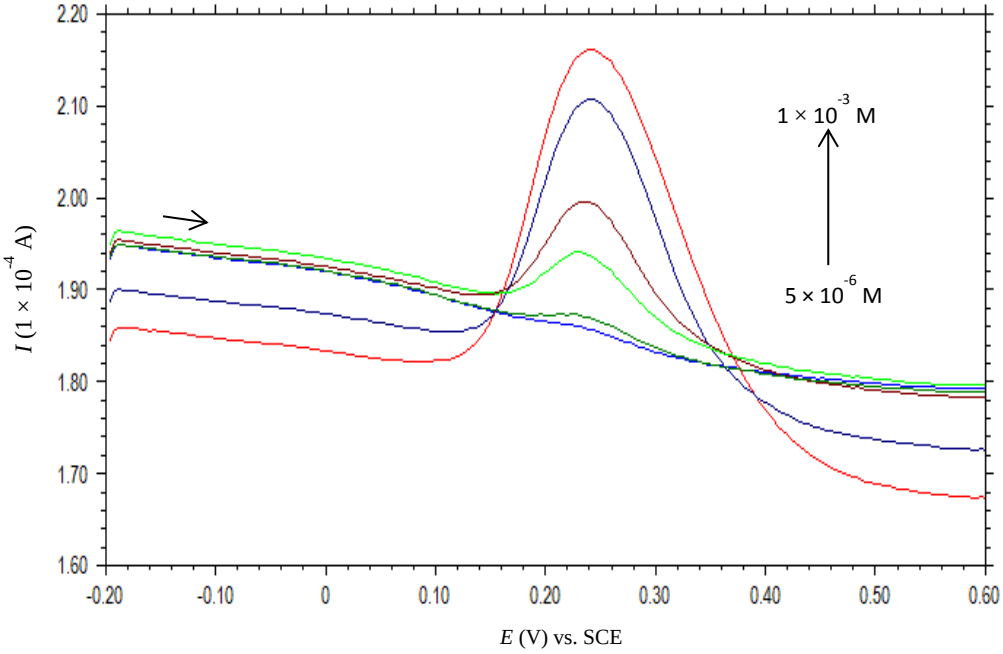

Figure 5.49: Differential pulse voltammograms recorded at S-β-CD modified GPE in 0.1 M PBS containing different concentrations of DA (from 5 × 10^{-6} M to 1 × 10^{-3} M).

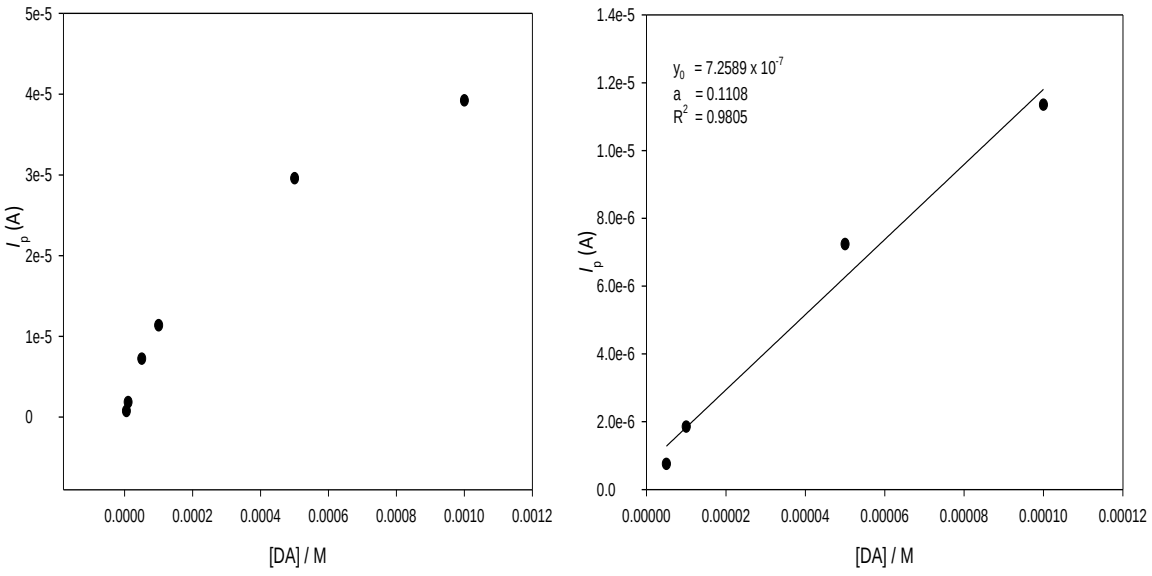

(a) (b)

Figure 5.50: Calibration curve of oxidation current for the determination of DA obtained at S-β-CD modified GPE (a) and corresponding linear region (b).

Table 5.12: Effect of DA concentration on oxidation peak currents and peak potential at S-β-CD modified GPE

Concentration of DA (M)	Oxidation Peak Potential (V)	Oxidation peak current (A)
5×10^{-6}	0.23	7.542×10^{-7}
1×10^{-5}	0.23	1.853×10^{-6}
5×10^{-5}	0.23	7.232×10^{-6}
1×10^{-4}	0.24	1.350×10^{-5}
5×10^{-4}	0.24	2.960×10^{-5}
1×10^{-3}	0.24	3.924×10^{-5}

5.2.4.2 Detection of DA from solution mixtures of AA and DA at S-β-CD modified CPE

As already mentioned, the analysis of DA is normally affected by the presence of other electroactive species especially AA. Therefore, DA sensing in the presence of AA was investigated. Figures 5.51 and 5.52 show typical cyclic voltammograms obtained at S-β-CD modified CPE, in solution mixtures of 1 mM AA and different concentrations of DA (from 5×10^{-6} to 1×10^{-3} M) in pH 6.8, at a scan rate 50 mV / s, using 'polishing' and 'no polishing' methods, respectively. As can be seen, the cathodic and anodic peak current of DA increases with increase in concentration. The voltammograms corresponding to the three lowest concentrations for 'polishing' and 'no polishing' are displayed in Figure 5.51 (b) and Figure 5.52 (b), respectively. It is worth mentioning that the signal corresponding to AA decreases as the concentration of DA increase (Figure 5.53 (a) and Figure 5.53 (b)).

The current response shows that DA oxidation peak current (in both cases) was directly proportional to concentration within the range 5×10^{-6} M – 5×10^{-4} M (Figure 5.54). The linear regression equation describing the behaviour was I_{pa} (A) = 0.0292 $_{[DA]}$ + 3.5290×10^{-8} A ($R^2 = 0.9996$) and I_{pa} (A) = 0.0252 $_{[DA]}$ + 1.5205×10^{-7} A ($R^2 = 0.9993$). The detection limit of DA in the presence of AA using 'no polishing' method was calculated as 5.55×10^{-7} M. Moreover, the calibration plots of DA in the absence and presence of 1 mM AA using both 'polishing' and 'no polishing' methods are compared in Figure 5.55 (a) and Figure 5.55(b), respectively. The current response of DA in the mixture remains the same as when it was studied independently, indicating that the

electrochemical reaction of DA at the electrode surface is not affected by the presence of AA.

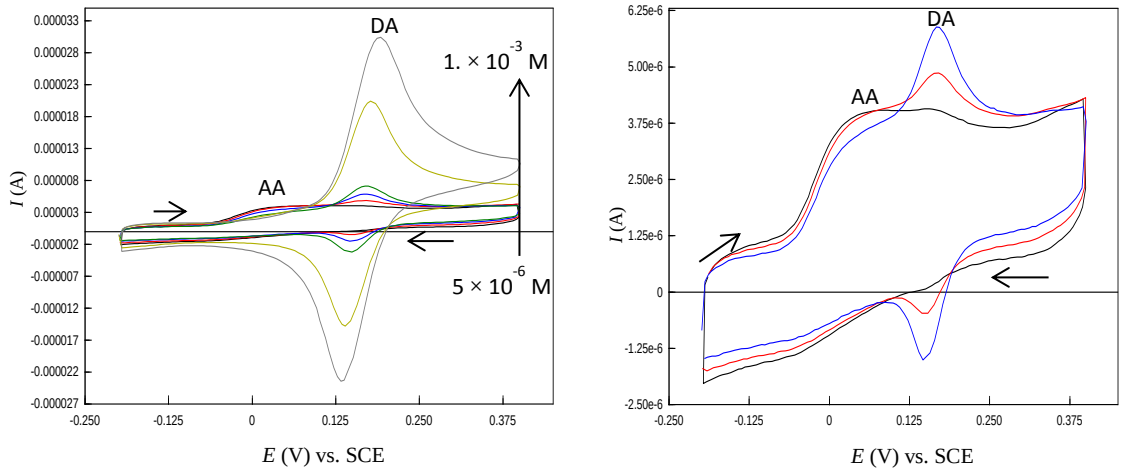

(a) (b)

Figure 5.51: Cyclic voltammograms recorded at S-β-CD modified CPE (using 'no polishing' method) in 1mM AA containing different concentrations of DA (from 5 × 10^{-6} M to 1 × 10^{-3} M) (a) and enlarged voltammograms of a mixture of AA (1 × 10^{-3} M) and DA (5 × 10^{-6} M) (–), AA (1 × 10^{-3} M) and DA (1 × 10^{-5} M) (–) and AA (1 × 10^{-3} M) and DA (5 × 10^{-5} M) (–) (b); scan rate: 50 mV / s.

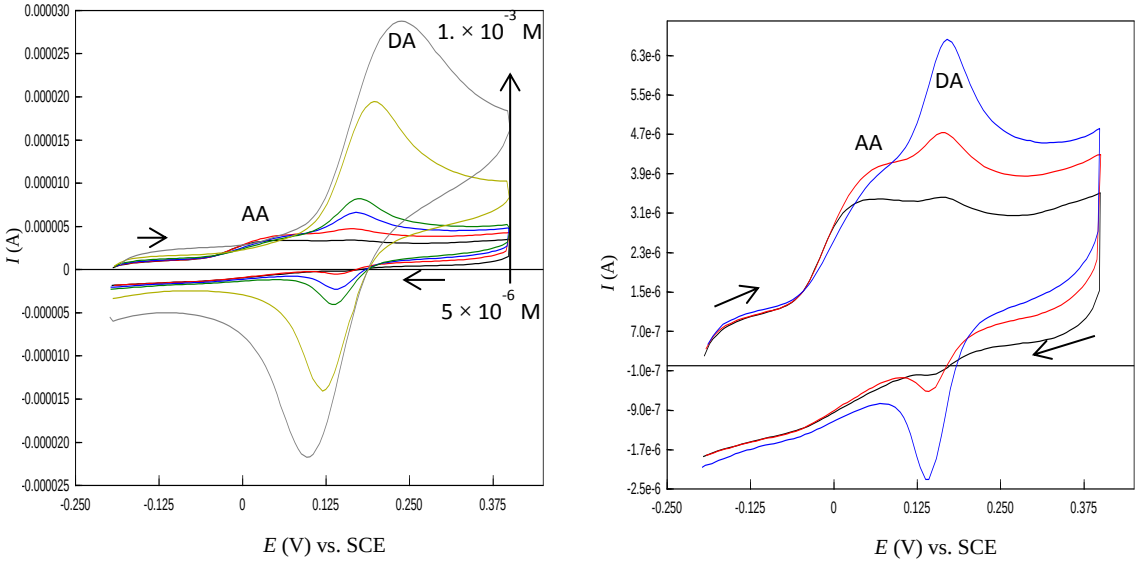

(a) (b)

Figure 5.52: Cyclic voltammograms recorded at S-β-CD modified CPE (using 'polishing' method) in 1mM AA containing different concentrations of DA (from 5 × 10^{-6} M to 1 × 10^{-3} M) (a) and enlarged voltammograms of a mixture of AA (1 × 10^{-3} M) and DA (5 × 10^{-6} M) (–), AA (1 × 10^{-3} M) and DA (1 × 10^{-5} M) (–) and AA (1 × 10^{-3} M) and DA (5 × 10^{-5} M) (–) (b); scan rate: 50 mV / s.

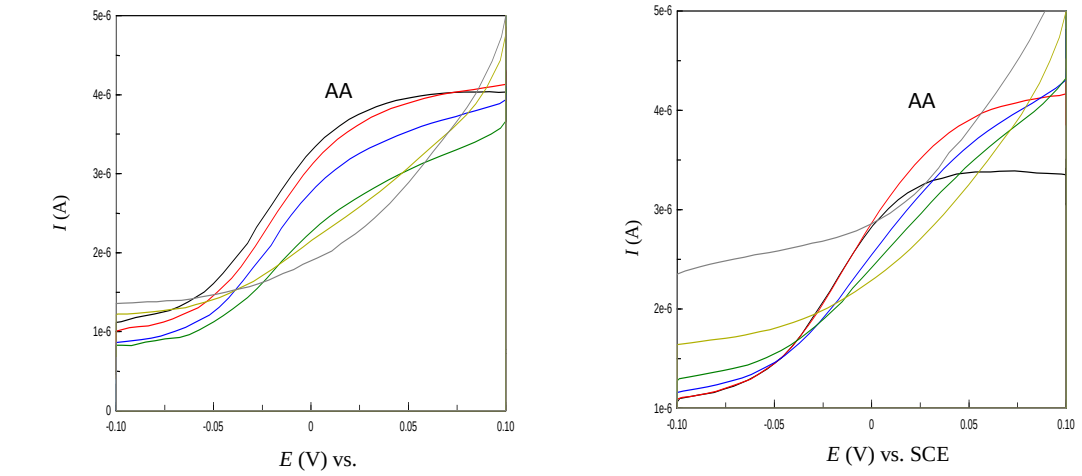

(a) (b)

Figure 5.53: Cyclic voltammograms showing oxidation peak of AA (1×10^{-3} M) in presence of increasing concentration of DA at S-β-CD modified CPE using 'no polishing' method (a) and 'polishing' method (b); scan rate: 50 mV / s.

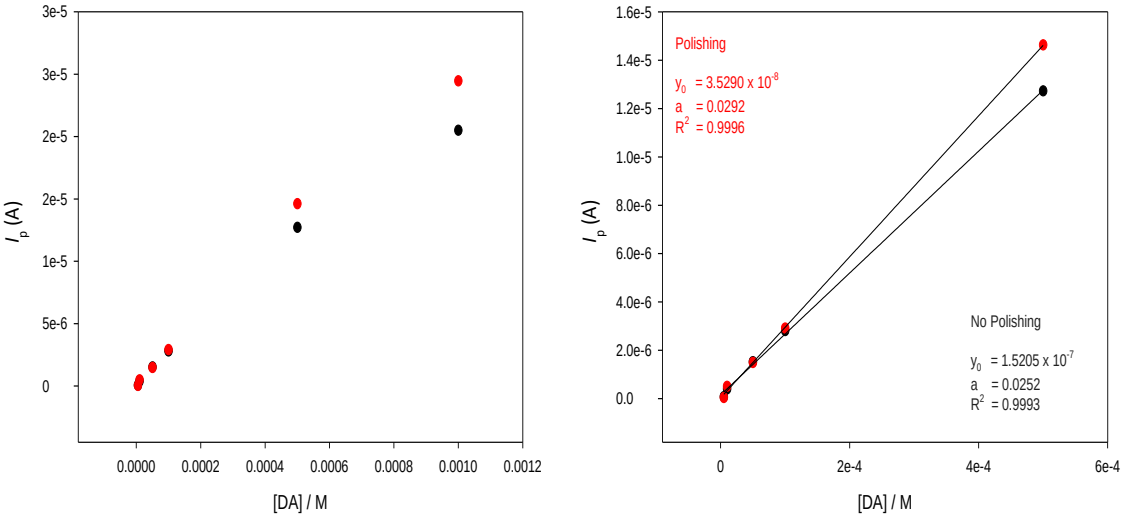

(a) (b)

Figure 5.54: Calibration curve of oxidation current for the determination of DA from a mixed solution of 1 mM AA and increasing concentration of DA obtained at S-β-CD modified CPE using 'polishing' (·) and 'no polishing'(·) (a), and corresponding linear region (b).

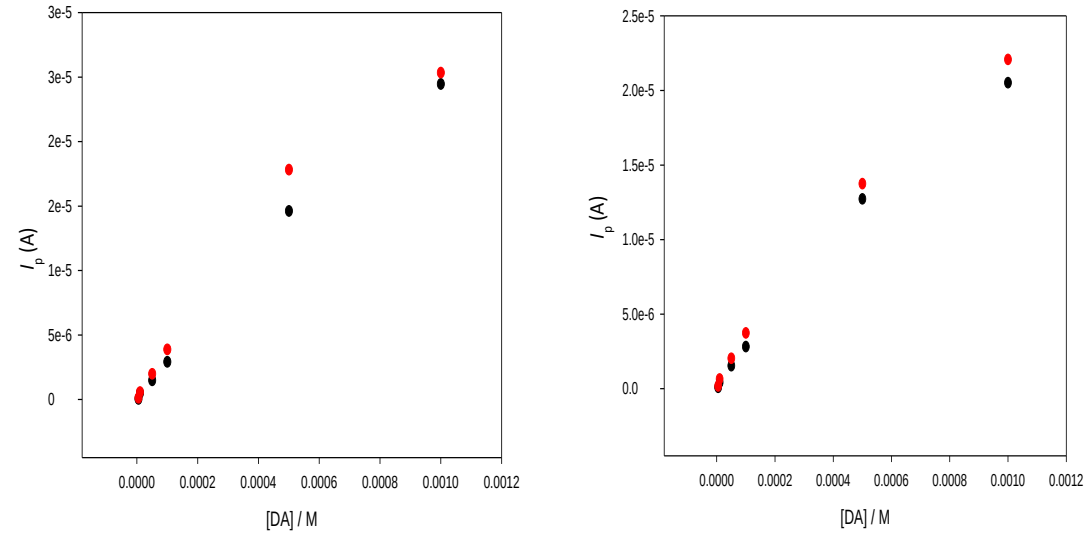

(a) (b)

Figure 5.55: Calibration curve of oxidation current for the determination of DA in the presence (·) and absence (·) of 1 mM AA recorded at S-β-CD modified CPE using 'polishing' method (a) and 'no polishing' (b) method.

5.2.4.3 Detection of 5-HT in 5-HT only solutions

(i) At bare CPE

The dependence of oxidation peak current of 5-HT at bare CPE was investigated by cyclic voltammetry. It was observed that with increasing the concentration of 5-HT, the peak current was gradually increased as shown in Figure 5.56(a). A calibration plot could not be described adequately for the determination of 5-HT within the range studied (Figure 5.57). It is well-known that 5-HT adsorbs strongly on graphite [37], thus providing good sensitivity. A peak response for 5×10^{-6} M 5-HT was clearly obtained at bare CPE with peak intensity of 1.525×10^{-6} A (Table 5.13), while the detection of such concentration for DA at bare CPE under the same conditions gave a peak current of 1.759×10^{-8} A.

The oxidation products of 5-HT are known to form insulating layers on the electrode surface, causing electrode fouling [45]. As shown in Figure 5.56 (b), a concentration higher than 5×10^{-5} M resulted in voltammograms where the peak current could not be measured accurately. This confirmed that bare CPE cannot effectively be used for determination of DA.

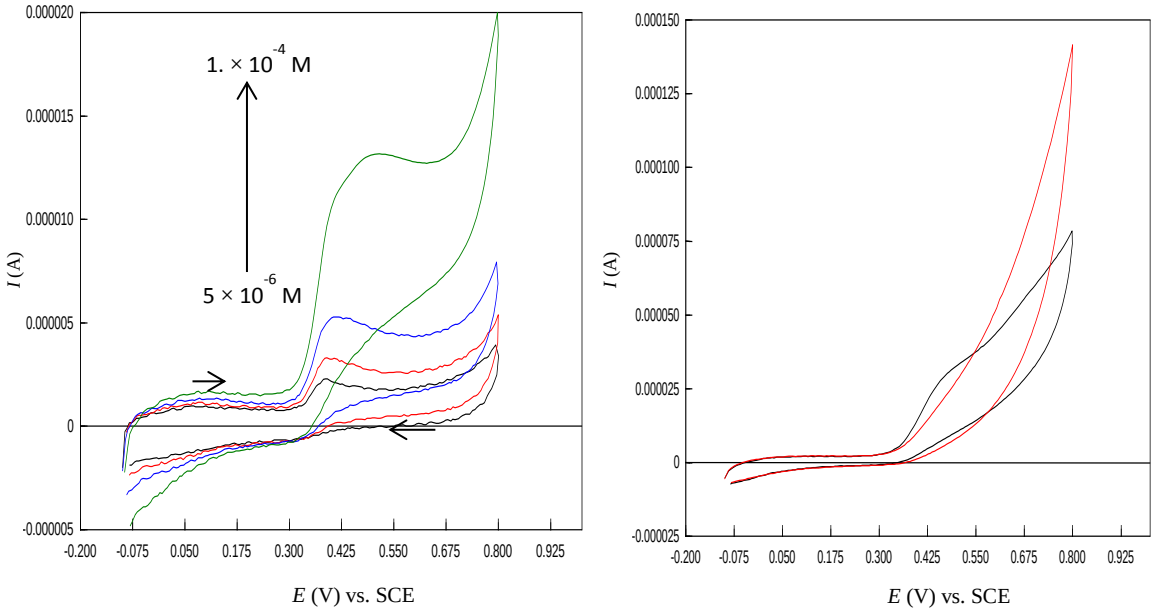

(a) (b)

Figure 5.56: Cyclic voltammograms recorded at bare CPE in 0.1 M PBS containing different concentrations of 5-HT (from 5 × 10^{-6} M to 1 × 10^{-4} M) (a) and voltammograms of 5 × 10^{-4} M (–) and 1 × 10^{-3} M (–) (b); scan rate: 50 mV / s.

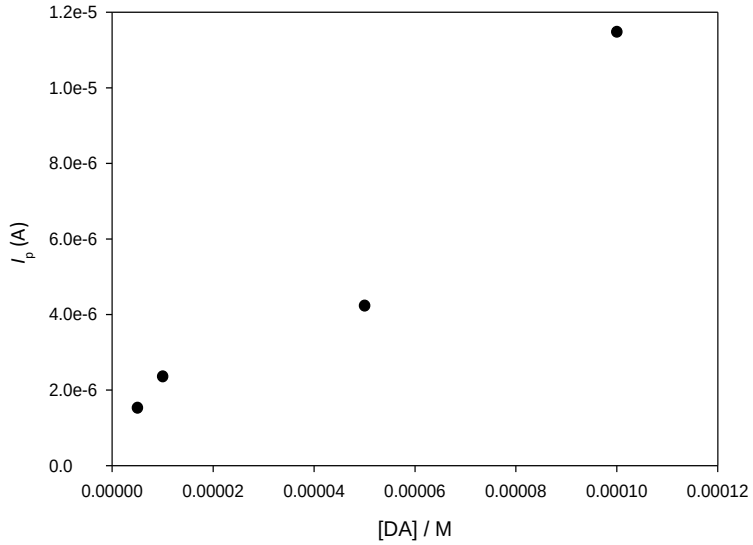

Figure 5.57: Calibration curve of oxidation current for the determination of 5-HT obtained at bare CPE.

Table 5.13: Effect of 5-HT concentration on oxidation peak currents and peak potential at bare CPE

Concentration of 5-HT (M)	Oxidation Peak Potential (V)	Oxidation peak current (A)
5×10^{-6}	0.39	1.525×10^{-6}
1×10^{-5}	0.39	2.354×10^{-6}
5×10^{-5}	0.41	4.230×10^{-6}
1×10^{-4}	0.50	1.148×10^{-5}

(ii) At S-β-CD modified CPE

The calibration curve for the oxidation of 5-HT at the S-β-CD modified CPE was generated using cyclic voltammetry. The peak current was found to increase as the concentration of 5-HT increase in both cases of 'polishing' and 'no polishing' (Figure 5.58 (a) and Figure 5.59 (a)). The plot of peak current versus concentration was linear in the ranges 5×10^{-6} M – 5×10^{-4} M and 5×10^{-6} M – 1×10^{-4} M, for 'polishing' and 'no polishing', respectively (Figure 5.60). The corresponding regression equations were obtained as I_{pa} (A) = 0.0150 $_{[5\text{-HT}]}$ + 7.5966×10^{-7} A (R^2 = 0.9902) and I_{pa} (A) = 0.0211 $_{[5\text{-HT}]}$ + 6.6767×10^{-7} A (R^2 = 0.9984). This reasonable linearity and remarkable enhancement in peak current indicate clearly that S-β-CD modified CPE could effectively be used for determination of 5-HT. In addition, it was observed from Table 5.14 that the oxidation overpotential was considerably lowered. Therefore, 5-HT was oxidised under catalytic effect at S-β-CD modified CPE. The detection limit was estimated as 6.60×10^{-7} M.

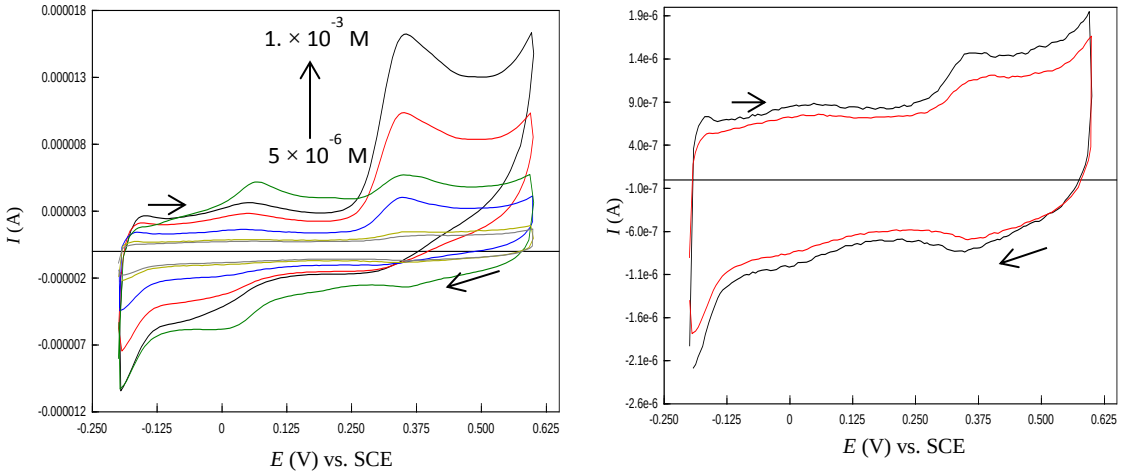

Figure 5.58: Cyclic voltammograms recorded at S-β-CD modified CPE in 0.1 M PBS containing different concentrations of 5-HT (from 5 × 10^{-6} M to 1 × 10^{-3} M) (a) and enlarged voltammograms of 5 × 10^{-6} M (–) and 1 × 10^{-5} M (–) (b); scan rate: 50 mV / s.

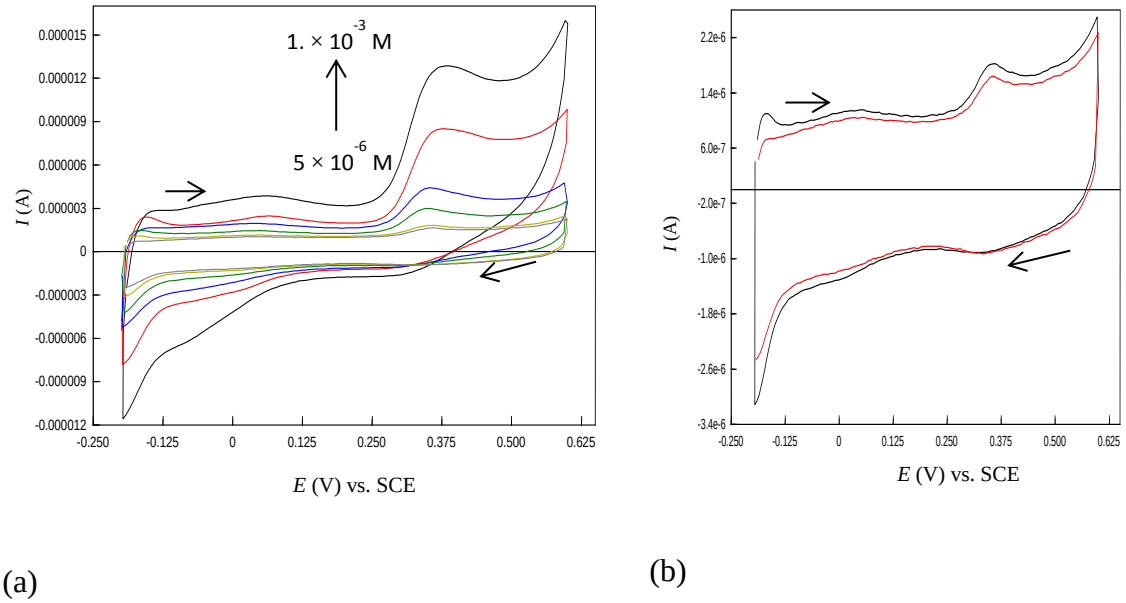

Figure 5.59: Cyclic voltammograms recorded at S-β-CD modified CPE in 0.1 M PBS containing different concentrations of 5-HT (from 5 × 10^{-6} M to 1 × 10^{-3} M) (a) and enlarged voltammograms of 5 × 10^{-6} M (–) and 1 × 10^{-5} M (–) (b); scan rate: 50 mV / s.

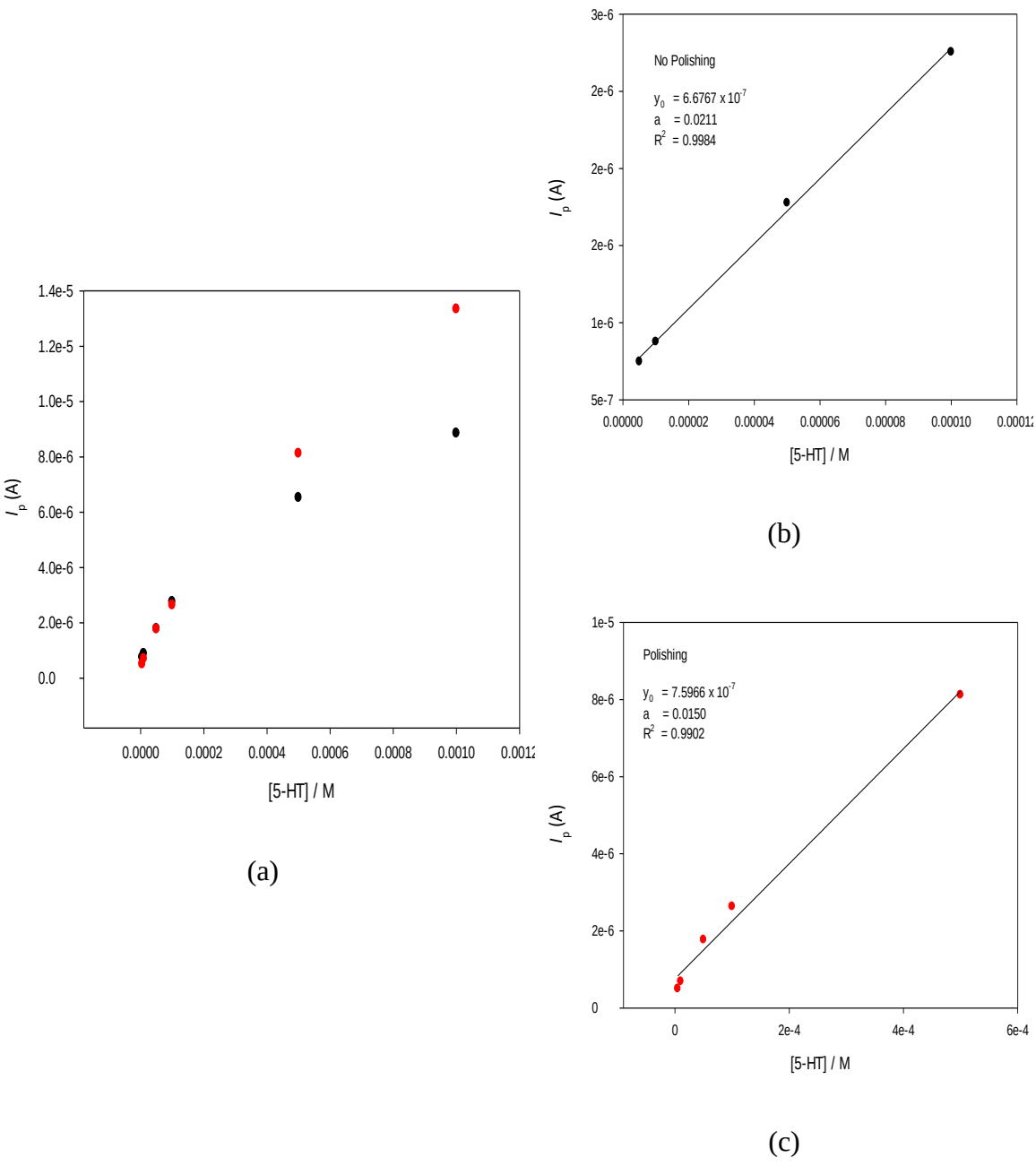

Figure 5.60: Calibration curve of oxidation current for the determination of 5-HT recorded at S-β-CD modified CPE using 'no polishing' (·) method and 'polishing' (·) method (a), and corresponding linear region for 'no polishing' method (b) and 'polishing' method (c).

Table 5.14: Effect of 5-HT concentration on oxidation peak currents and peak potential at S-β-CD modified CPE

Concentration of 5-HT (M)	Oxidation Peak Potential (V)	Oxidation peak current (A)
5×10^{-6}	0.35	7.473×10^{-7}
1×10^{-5}	0.35	8.767×10^{-7}
5×10^{-5}	0.35	1.777×10^{-6}
1×10^{-4}	0.35	2.755×10^{-6}
5×10^{-4}	0.38	6.524×10^{-6}
1×10^{-3}	0.38	8.851×10^{-6}

(iii) At CM-β-CD modified CPE

CM-β-CD modified CPE has been proven to be an effective sensor in the detection of 5-HT. Therefore, using the optimum conditions utilised for S-β-CD modified CPE, the calibration curve of 5-HT was constructed using cyclic voltammetry. As shown in Figure 5.61 (a), the oxidative current increased with increasing concentrations of DA. The first three lowest 5-HT concentrations are displayed in Figure 5.61 (b). A linear relationship between oxidation peak current and concentration was observed in the range from 3×10^{-6} M to 1×10^{-3} M, with a correlation coefficient of 0.9981 (Figure 5.62). The detection limit was estimated to be 2.89×10^{-7} M. These experimental results indicated that CM-β-CD modified CPE can effectively be used as a chemical sensor for the determination of 5-HT.

(a)

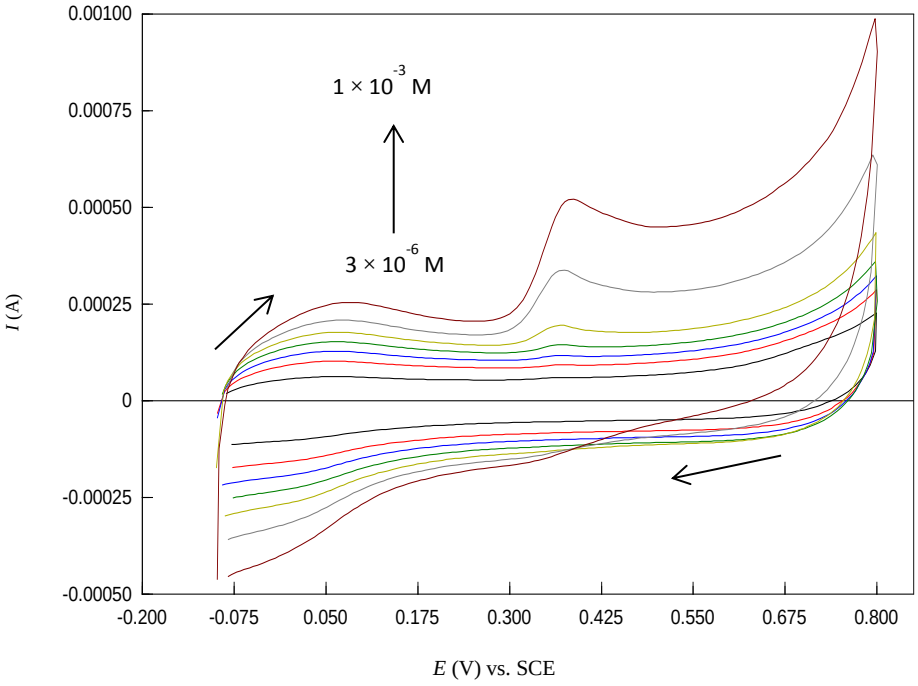

(b)

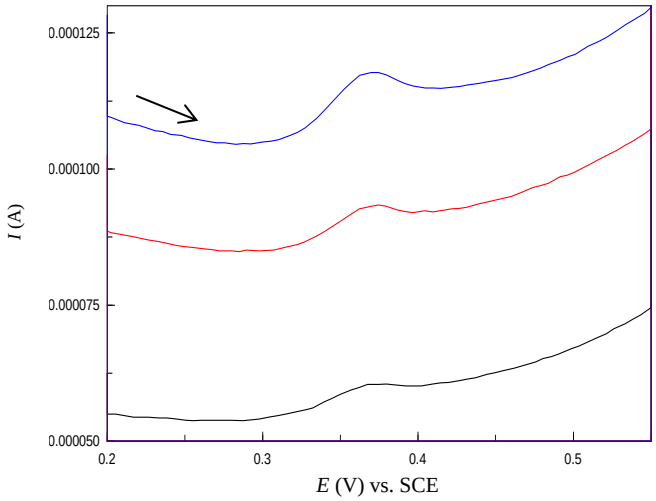

Figure 5.61: Cyclic voltammograms recorded at CM-β-CD modified CPE in 0.1 M PBS containing different concentrations of 5-HT (from 3×10^{-6} M to 1×10^{-3} M) (a) and enlarged voltammograms of 3×10^{-6} M (–) and 5×10^{-6} M (–) (b) and 1×10^{-5} M (–); scan rate: 50 mV / s.

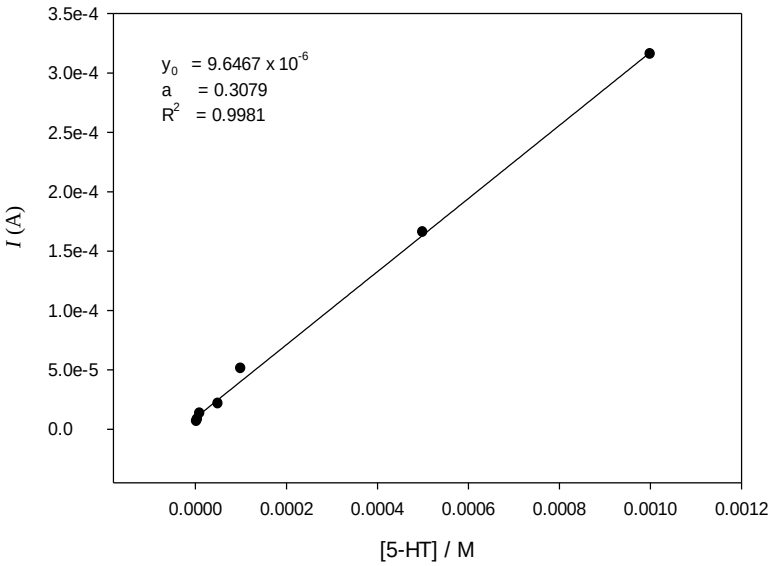

Figure 5.62: Calibration curve of oxidation current for the determination of 5-HT recorded at CM-β-CD modified CPE.

5. 15: Effect of 5-HT concentration on oxidation peak currents and peak potential at CM-β-CD modified CPE

Concentration of 5-HT (M)	Oxidation Peak Potential (V)	Oxidation peak current (A)
3×10^{-6}	0.37	6.372×10^{-6}
5×10^{-6}	0.37	8.075×10^{-6}
1×10^{-5}	0.37	1.306×10^{-5}
5×10^{-5}	0.37	2.130×10^{-5}
1×10^{-4}	0.37	5.095×10^{-5}
5×10^{-4}	0.37	1.657×10^{-5}
1×10^{-3}	0.39	3.156×10^{-5}

5.2.4.4 Simultaneous Detection of DA and 5-HT from solution mixtures of DA and 5-HT

The detection of DA and 5-HT from solution mixtures of DA and 5-HT, in 0.1 M PBS (pH 6.8), was performed using both S-β-CD and CM-β-CD modified CPE under differential pulse voltammetry. Typical voltammograms obtained from a mixture of increasing DA concentrations in a presence of 5×10^{-6} M 5-HT are shown in Figure 5.63 (a). A linear response was obtained for DA detection in the range 5×10^{-6} M – 1.5×10^{-5} M. The linear regression equation was I_{pa} (A) = 0.0490 $_{[DA]}$ - 8.0336×10^{-7} A, with a correlation coefficient of R^2 = 0.9970 (Figure 5.63 (b)). The detection limit for

DA from the mixture was calculated as 3.52×10^{-7} M. It has to be noted that while the concentration of DA was varied from 5×10^{-6} M to 1.5×10^{-5} M, no remarkable change in the oxidation peak current of 5-HT was detected.

Figure 5.64 (a) shows differential pulse voltammograms of 5×10^{-6} M DA with coexisting 5-HT concentrations ranging from 5×10^{-6} M to 1.5×10^{-5} M. It was observed that with increasing 5-HT concentration, the oxidation peak current increases linearly within the studied concentration range. The regression equation was I_{pa} (A) = $0.0460\ _{[5\text{-HT}]} + 3.2900 \times 10^{-8}$ A, with a correlation coefficient of $R^2 = 0.9949$ (Figure 5.64 (b)). The detection limit was estimated as 1.13×10^{-6} M. The oxidation peak current for 5×10^{-6} M DA remained relatively constant over the 5-HT concentration range.

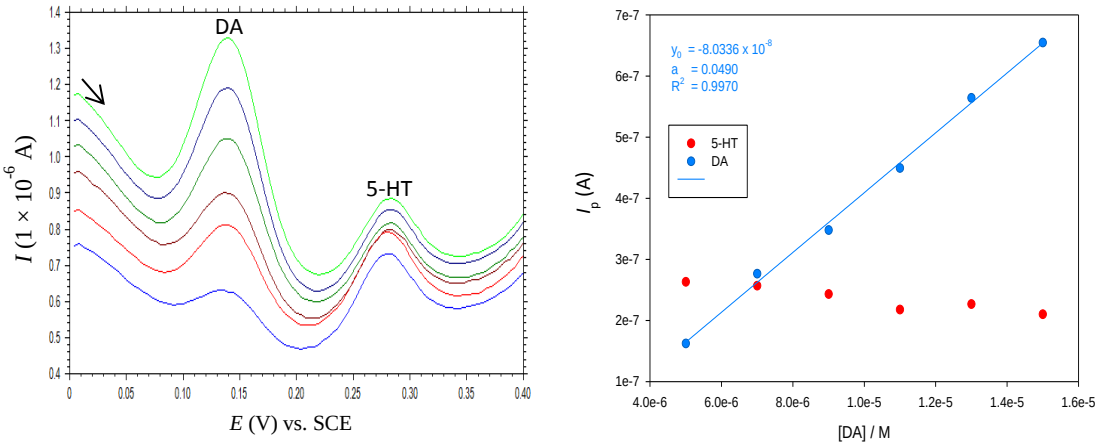

(a) (b)

Figure 5.63: Differential pulse voltammograms of the application of various concentration of DA (from 5×10^{-5} M to 1×10^{-3} M) in the presence of 5-HT (5×10^{-5} M) recorded at S-β-CD modified CPE (a) and corresponding calibration curve of DA (·) and plot of oxidation peak current of 5-HT as a function of DA concentration (·) (b). Supporting electrolyte 0.1 M PBS (pH 6.8).

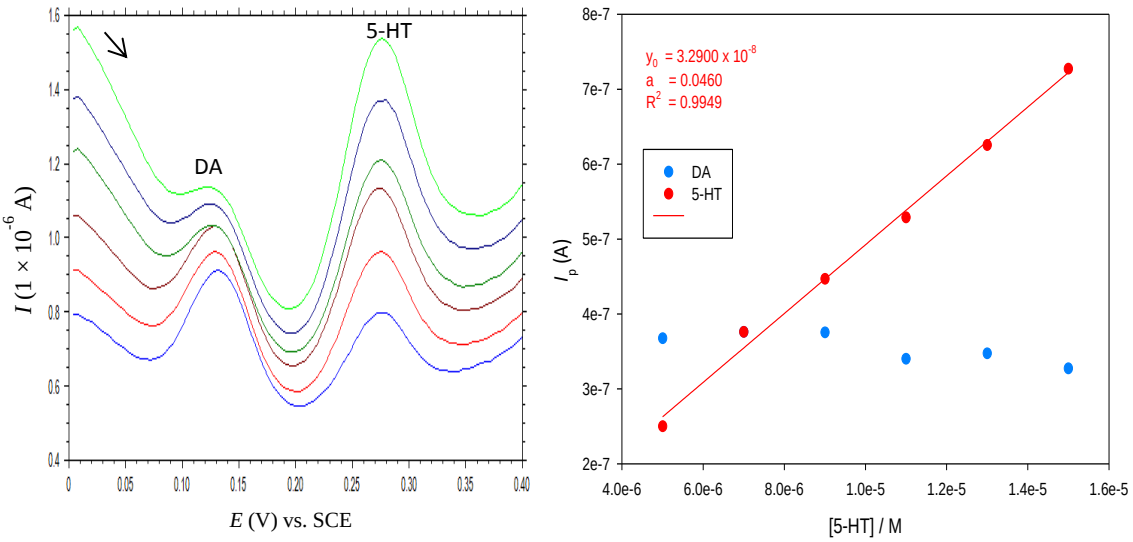

(a) (b)

Figure 5.64: Differential pulse voltammograms of the application of various concentration of 5-HT (from 5 × 10^{-5} M to 1 × 10^{-3} M) in the presence of DA (5 × 10^{-5} M) recorded at S-β-CD modified CPE (a) and corresponding calibration curve of 5-HT (·) and plot of oxidation peak current of DA as a function of 5-HT concentration (·) (b). Supporting electrolyte 0.1 M PBS (pH 6.8).

As CM-β-CD modified CPE showed strong catalytic activity towards the detection of 5-HT, it was also employed for analysis of the mixture sample DA and 5-HT, where the concentration of DA (5 × 10^{-6} M) was constant while the concentration of 5-HT was varied from 5 × 10^{-6} M to 1.5 × 10^{-5} M. From Figure 5.65 (a), it is clear that with increase in the concentration of 5-HT the peak current increases. The plot of oxidative peak current versus concentration of 5-HT shows a linear relation with regression equation of I_{pa} (A) = 0.0767 $_{[DA]}$ + 3.8460 × 10^{-8} and R^2 = 0.9949 (Figure 5.65 (b)). The limit of detection was estimated as 3.06 × 10^{-7} M.

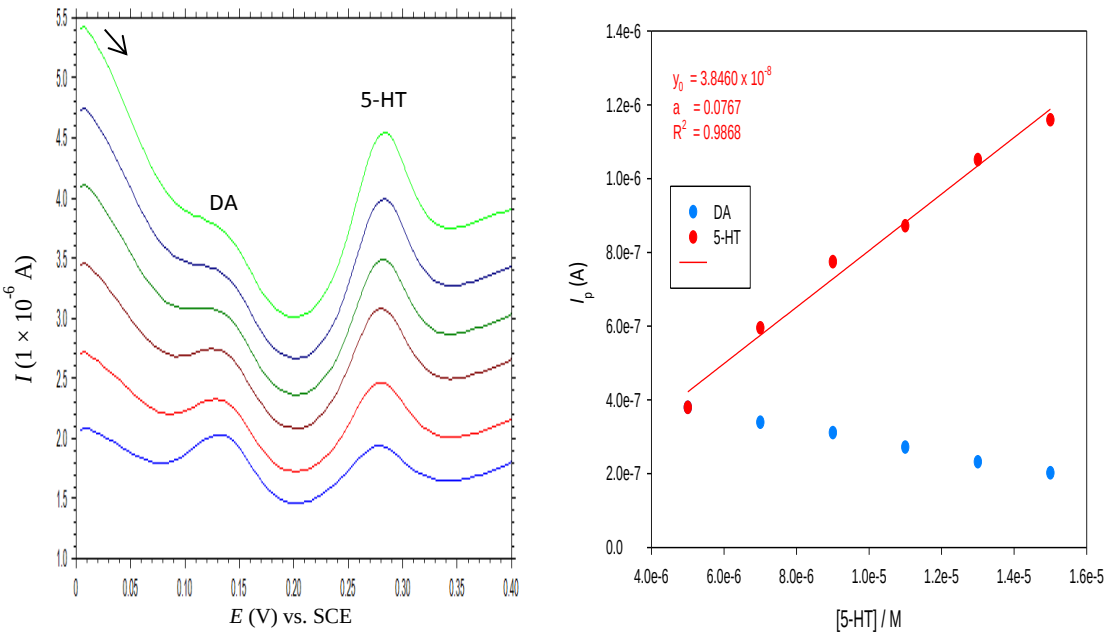

(a) (b)

Figure 5.65: Differential pulse voltammograms of the application of various concentration of 5-HT (from 5 × 10^{-5} M to 1 × 10^{-3} M) in the presence of DA (5 × 10^{-5} M) recorded at CM-β-CD modified CPE (a) and corresponding calibration curve of 5-HT (·) and plot of oxidation peak current of DA as a function of 5-HT concentration (·) (b). Supporting electrolyte 0.1 M PBS (pH 6.8).

In the case of DA, a linear decrease in oxidation peak currents is observed as the 5-HT concentration increases. This decrease can be, at least partially attributable to the significant increase in background current. An increase in background currents may result from a build-up of analytes and ions at the electrode surface, or possibly physisorbed species.

5.2.4.5 Detection of 5-HT from solution mixtures of AA, DA and 5-HT

The potential use of the S-β-CD modified CPE as a viable sensor for the simultaneous determination of AA, DA and 5-HT, was probed. Figure 5.66 (a) shows voltammograms obtained at S-β-CD modified CPE after increasing concentration of 5-HT (5 × 10^{-6} M – 1 × 10^{-3} M) to the electrochemical cell containing fixed concentration of DA (5 × 10^{-5} M) and AA (1 × 10^{-3} M). As can be seen, the oxidation peak current of 5-HT increased with concentration, generating a linear relationship in the range 5 × 10^{-6} M – 5 × 10^{-4} M 5-HT. The regression equation was I_{pa} (A) = 0.0142 $_{[5\text{-HT}]}$ + 2.9282 × 10^{-7} A with corresponding correlation coefficient 0.9948 (Figure 5.67). The limit of detection was found to be 3.28 × 10^{-7} M 5-HT. Although, linearity between peak

current and concentration was obtained for 5-HT from the tertiary mixture (AA, DA and 5-HT), the peak currents of DA and AA were considerably altered. It was observed that the peak current responses for of DA and AA decreased when the concentration of 5-HT was increased from 5×10^{-6} M to 5×10^{-5} M (Figure 5.66 (b)) and disappeared at 5-HT concentrations higher than 1×10^{-4} M (Figure 5.66 (c)).

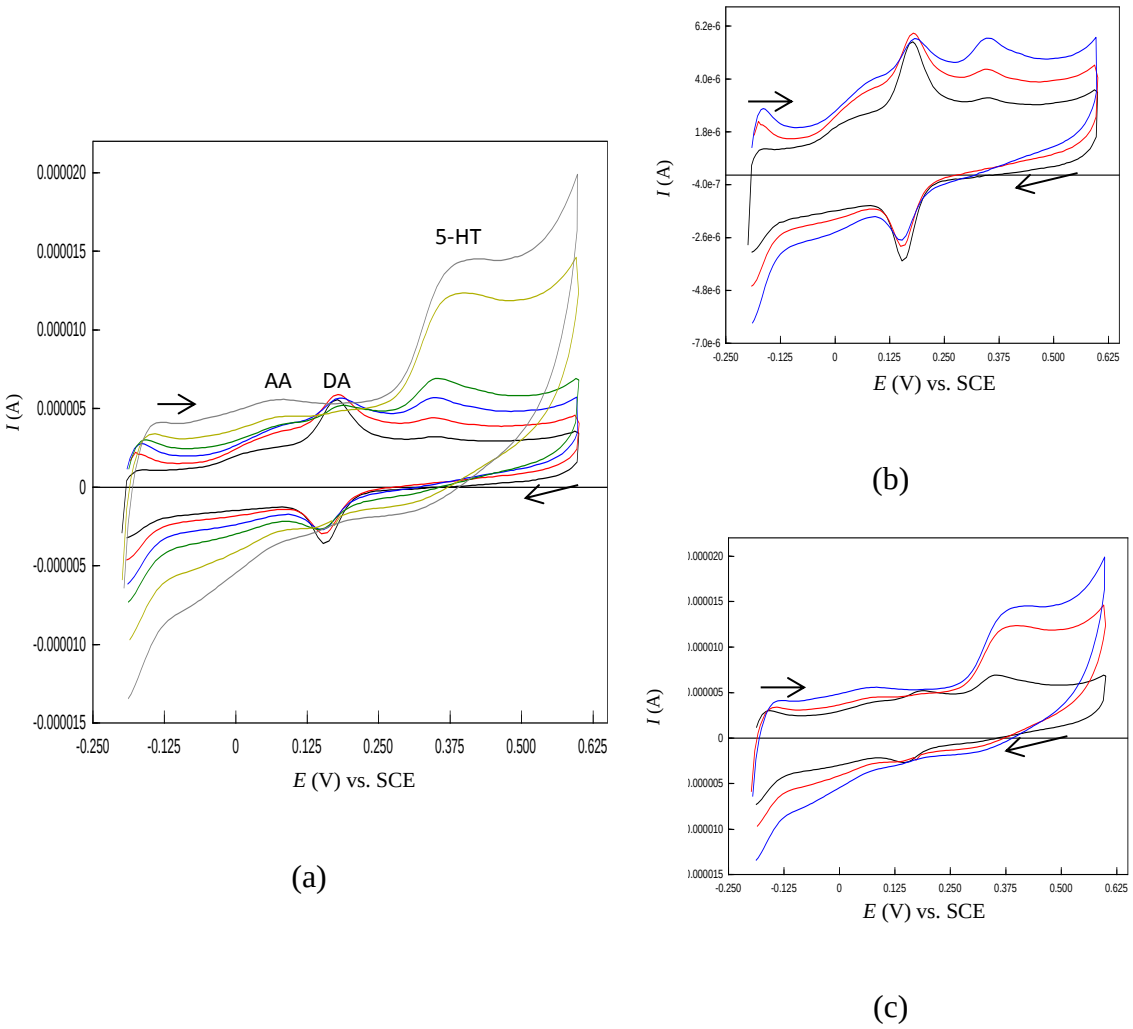

Figure 5.66: Cyclic voltammograms recorded at S-β-CD modified CPE in 0.1 M PBS containing different concentrations of 5-HT (from 5×10^{-6} M to 1×10^{-3} M) in the presence of AA (1×10^{-3} M) and DA (5×10^{-5} M) (a) and highlighted voltammograms showing the variation of 5-HT concentration: 5×10^{-6} M (–), 1×10^{-5} M (–) and 5×10^{-5} M 5-HT (–) (b) ; 1×10^{-4} M (–), 5×10^{-4} M (–) and 1×10^{-3} M 5-HT (–) (c); scan rate: 50 mV / s.

Table 5.16: Effect of 5-HT concentration on oxidation peak currents and peak potential at S-β-CD modified CPE

Concentration of 5-HT (M)	Oxidation Peak Potential (V)	Oxidation peak current (A)
5×10^{-6}	0.35	1.599×10^{-7}
1×10^{-5}	0.35	3.441×10^{-7}
5×10^{-5}	0.35	1.005×10^{-6}
1×10^{-4}	0.35	2.074×10^{-6}
5×10^{-4}	0.40	7.323×10^{-6}
1×10^{-3}	0.43	9.142×10^{-6}

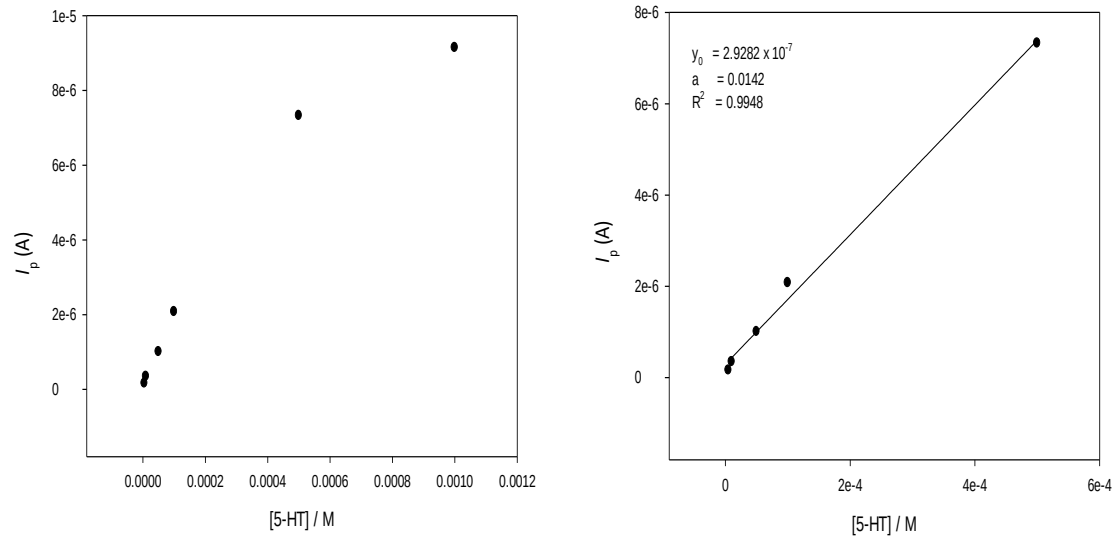

(a) (b)

Figure 5.67: Calibration curve of oxidation current for the determination of 5-HT in the presence of AA (1×10^{-3} M) and DA (5×10^{-5} M) obtained at S-β-CD modified CPE (a) and corresponding linear region (b).

In Table 5.17, a summary of the LOD is given. In general, LOD for DA varied from 2.44×10^{-4} to 1.33×10^{-7} with respect to electrode employed as well as the technique and sample solution.

Table 5.17: LOD with corresponding electrode and electrochemical technique

Compound analysed	Electrode	LOD (M)	Electrochemical technique
DA (from a solution of DA)	S-β-CD modified CPE	1.33×10^{-7}	DPV
	CM-β-CD modified CPE	3.09×10^{-6}	CV
	Fc-β-CD modified CPE	1.70×10^{-7}	CV
	Neutral β-CD modified CPE	1.23×10^{-5}	CV
	Oxide containing CPE	1.81×10^{-5}	CV
	Bare GPE	1.70×10^{-5}	DPV
	S-β-CD modified GPE	2.44×10^{-4}	DPV
DA (from a mixture of AA and DA)	S-β-CD modified CPE	5.55×10^{-7}	CV
DA (from a mixture of DA and 5-HT)	S-β-CD modified CPE	1.06×10^{-6}	DPV
5-HT (from a mixture of AA, DA and 5-HT)	S-β-CD modified CPE	9.81×10^{-7}	CV
5-HT (from a solution of 5-HT)	S-β-CD modified CPE	6.60×10^{-7}	CV
	CM-β-CD modified CPE	2.89×10^{-7}	CV
5-HT (from a mixture of DA and 5-HT)	S-β-CD modified CPE	1.13×10^{-6}	DPV
	CM-β-CD modified CPE	3.06×10^{-7}	DPV

5.3 References

1. Wightman, R.M., May, L.J., and Michael, A.C., *Detection of Dopamine Dynamics in the Brain.* Analytical Chemistry, 1988. **60**(13): p. A769-A779.

2. Cao, X.M., et al., *Electrochemical methods for simultaneous determination of dopamine and ascorbic acid using cetylpyridine bromide/chitosan composite film-modified glassy carbon electrode.* Sensors and Actuators B-Chemical, 2008. **129**(2): p. 941-946.

3. Ragupathy, D., et al., *Electro-assisted fabrication of layer-by-layer assembled poly(2,5-dimethoxyaniline)/phosphotungstic acid modified electrode and electrocatalytic oxidation of ascorbic acid.* Electrochemistry Communications, 2008. **10**(4): p. 527-530.

4. Toth, J.E. and Anson, F.C., *Electrocatalytic Reduction of Nitrite and Nitric-Oxide to Ammonia with Iron-Substituted Polyoxotungstates.* Journal of the American Chemical Society, 1989. **111**(7): p. 2444-2451.

5. Drisko, J.A., Chapman, J., and Hunter, V.J., *The use of antioxidants with first-line chemotherapy in two cases of ovarian cancer.* Journal of the American College of Nutrition, 2003. **22**(2): p. 118-123.

6. Lin, M.T., et al., *Changes in extracellular serotonin in rat hypothalamus affect thermoregulatory function.* American Journal of Physiology-Regulatory Integrative and Comparative Physiology, 1998. **274**(5): p. R1260-R1267.

7. Imeri, L., et al., *5-hydroxytryptophan, but not L-tryptophan, alters sleep and brain temperature in rats.* Neuroscience, 2000. **95**(2): p. 445-452.

8. Isbister, G.K., et al., *Relative toxicity of selective serotonin reuptake inhibitors (SSRIs) in overdose.* Journal of Toxicology-Clinical Toxicology, 2004. **42**(3): p. 277-285.

9. Dremencov, E., et al., *The serotonin-dopamine interaction is critical for fast-onset action of antidepressant treatment: in vivo studies in an animal model of depression.* Progress in Neuro-Psychopharmacology & Biological Psychiatry, 2004. **28**(1): p. 141-147.

10. Ghita, M. and Arrigan, D.W.M., *Dopamine voltammetry at overoxidised polyindole electrodes.* Electrochimica Acta, 2004. **49**(26): p. 4743-4751.

11. Zhang, L. and Lin, X.Q., *Electrochemical behavior of a covalently modified glassy carbon electrode with aspartic acid and its use for voltammetric differentiation of dopamine and ascorbic acid.* Analytical and Bioanalytical Chemistry, 2005. **382**(7): p. 1669-1677.

12. Deakin, M.R., et al., *Heterogeneous Mechanisms of the Oxidation of Catechols and Ascorbic-Acid at Carbon Electrodes.* Analytical Chemistry, 1986. **58**(7): p. 1474-1480.

13. Gonon, F., et al., *Invivo Electrochemical Detection of Catechols in the Neostriatum of Anesthetized Rats - Dopamine or Dopac.* Nature, 1980. **286**(5776): p. 902-904.

14. Salimi, A., MamKhezri, H., and Hallaj, R., *Simultaneous determination of ascorbic acid, uric acid and neurotransmitters with a carbon ceramic electrode prepared by sol-gel technique.* Talanta, 2006. **70**(4): p. 823-832.

15. Lane, R.F. and Hubbard, A.T., *Differential Double Pulse Voltammetry at Chemically Modified Platinum-Electrodes for Invivo Determination of Catecholamines.* Analytical Chemistry, 1976. **48**(9): p. 1287-1293.

16. Dayton, M.A., Ewing, A.G., and Wightman, R.M., *Response of Microvoltammetric Electrodes to Homogeneous Catalytic and Slow Heterogeneous Charge-Transfer Reactions.* Analytical Chemistry, 1980. **52**(14): p. 2392-2396.

17. Zen, J.M., Kumar, A.S., and Tsai, D.M., *Recent updates of chemically modified electrodes in analytical chemistry.* Electroanalysis, 2003. **15**(13): p. 1073-1087.

18. Degefa, T.H., Chandravanshi, B.S., and Alemu, H., *Differential pulse anodic stripping voltammetric determination of lead(II) with N-p-chlorophenylcinnamohydroxamic acid modified carbon paste electrode.* Electroanalysis, 1999. **11**(17): p. 1305-1311.

19. Valentini, F., et al., *Carbon nanotube purification: Preparation and characterization of carbon nanotube paste electrodes.* Analytical Chemistry, 2003. **75**(20): p. 5413-5421.

20. Shankar, S.S., Swamy, B.E.K., and Chandrashekar, B.N., *Electrochemical selective determination of dopamine at TX-100 modified carbon paste electrode: A voltammetric study.* Journal of Molecular Liquids, 2012. **168**: p. 80-86.

21. Rodriguez, M.C., Rubianes, M.D., and Rivas, G.A., *Highly Selective Determination of Dopamine in the Presence of Ascorbic Acid and Serotonin at Glassy Carbon Electrodes Modified with Carbon Nanotubes Dispersed in Polyethylenimine.* Journal of Nanoscience and Nanotechnology, 2008. **8**(11): p. 6003-6009.

22. Wei, J.A., et al., *Enhanced sensing of ascorbic acid, dopamine and serotonin at solid carbon paste electrode with a nonionic polymer film.* Talanta, 2010. **83**(1): p. 190-196.

23. Malem, F. and Mandler, D., *Self-Assembled Monolayers in Electroanalytical Chemistry - Application of Omega-Mercapto Carboxylic-Acid Monolayers for the Electrochemical Detection of Dopamine in the Presence of a High-Concentration of Ascorbic-Acid.* Analytical Chemistry, 1993. **65**(1): p. 37-41.

24. Price, J.F. and Baldwin, R.P., *Preconcentration and Determination of Ferrocenecarboxaldehyde at a Chemically Modified Platinum-Electrode.* Analytical Chemistry, 1980. **52**(12): p. 1940-1944.

25. Guadalupe, A.R. and Abruna, H.D., *Electroanalysis with Chemically Modified Electrodes.* Analytical Chemistry, 1985. **57**(1): p. 142-149.

26. Roy, P.R., Okajima, T., and Ohsaka, T., *Simultaneous electroanalysis of dopamine and ascorbic acid using poly (N,N-dimethylaniline)-modified electrodes.* Bioelectrochemistry, 2003. **59**(1-2): p. 11-19.

27. Ruiz, J.J., Aldaz, A., and Dominguez, M., *Mechanism of L-Ascorbic-Acid Oxidation and Dehydro-L-Ascorbic Acid Reduction on a Mercury-Electrode .1. Acid-Medium.* Canadian Journal of Chemistry-Revue Canadienne De Chimie, 1977. **55**(15): p. 2799-2806.

28. Hu, I.F. and Kuwana, T., *Oxidative Mechanism of Ascorbic-Acid at Glassy-Carbon Electrodes.* Analytical Chemistry, 1986. **58**(14): p. 3235-3239.

29. Perone, S.P. and Kretlow, W.J., *Application of Controlled Potential Techniques to Study of Rapid Succeeding Chemical Reaction Coupled to Electro-Oxidation of Ascorbic Acid.* Analytical Chemistry, 1966. **38**(12): p. 1760-1763.

30. Raj, C.R., Tokuda, K., and Ohsaka, T., *Electroanalytical applications of cationic self-assembled monolayers, square-wave voltammetric determination of dopamine and ascorbate.* Bioelectrochemistry, 2001. **53**(2): p. 183-191.

31. Domenech, A., et al., *2,4,6-triphenylpyrylium ion encapsulated into zeolite Y as a selective electrode for the electrochemical determination of dopamine in the presence of ascorbic acid.* Analytical Chemistry, 2002. **74**(3): p. 562-569.

32. Thomas, T., et al., *Graphite oxide bulk modified carbon paste electrode for the selective detection of dopamine: A voltammetric study.* Journal of Electroanalytical Chemistry, 2011. **659**(1): p. 113-119.

33. Hu, X.T., et al., *Preparation of the beta-cyclodextrin-vitamin C (beta-CD-Vc) inclusion complex under high hydrostatic pressure (HHP).* Carbohydrate Polymers, 2012. **90**(2): p. 1193-1196.

34. Raoof, J.B., Ojani, R., and Kiani, A., *Carbon paste electrode spiked with ferrocene carboxylic acid and its application to the electrocatalytic determination of ascorbic acid.* Journal of Electroanalytical Chemistry, 2001. **515**(1-2): p. 45-51.

35. Wang, Y., et al., *Application of graphene-modified electrode for selective detection of dopamine.* Electrochemistry Communications, 2009. **11**(4): p. 889-892.

36. Wu, Z., Shen, X.M., and Dryhurst, G., *Oxidation Chemistry of 5-[[3-(2-Amino-2-Carboxyethyl)-5-Hydroxy-1h-Indol-4-Yl]Oxy]-[3-(2-Amino-2-Carboxyethyl)]-1h-Indole - a Putative Aberrant Metabolite of 5-Hydroxytryptophan.* Bioorganic Chemistry, 1995. **23**(3): p. 227-255.

37. Wrona, M.Z. and Dryhurst, G., *Oxidation Chemistry of 5-Hydroxytryptamine .1. Mechanism and Products Formed at Micromolar Concentrations.* Journal of Organic Chemistry, 1987. **52**(13): p. 2817-2825.

38. Wrona, M.Z. and Dryhurst, G., *Electrochemical Oxidation of 5-Hydroxytryptamine in Aqueous-Solution at Physiological pH.* Bioorganic Chemistry, 1990. **18**(3): p. 291-317.

39. Wrona, M.Z. and G. Dryhurst, G., *Electrochemical Oxidation of 5-Hydroxytryptamine in Acidic Aqueous-Solution.* Journal of Organic Chemistry, 1989. **54**(11): p. 2718-2721.

40. Shirane, M. and Nakamura, K., *Aniracetam enhances cortical dopamine and serotonin release via cholinergic and glutamatergic mechanisms in SHRSP.* Brain Research, 2001. **916**(1-2): p. 211-221.

41. Pihel, K., et al., *Electrochemical Detection of Histamine and 5-Hydroxytryptamine at Isolated Mast-Cells.* Analytical Chemistry, 1995. **67**(24): p. 4514-4521.

42. Chaudhuri, S., Chakraborty, S., and Sengupta, P.K., *Encapsulation of serotonin in beta-cyclodextrin nano-cavities: Fluorescence spectroscopic and molecular modeling studies.* Journal of Molecular Structure, 2010. **975**(1-3): p. 160-165.

43. Hendy, G.M. and Breslin, C.B., *A spectrophotometric and NMR study on the formation of an inclusion complex between dopamine and a sulfated cyclodextrin host.* Journal of Electroanalytical Chemistry, 2011. **661**(1): p. 179-185.

44. Hegde, R.N., et al., *Electro-oxidation and determination of gabapentin at gold electrode.* Journal of Electroanalytical Chemistry, 2009. **635**(1): p. 51-57.

45. Jackson, B.P., Dietz, S.M., and Wightman, R.M., *Fast-Scan Cyclic Voltammetry of 5-Hydroxytryptamine.* Analytical Chemistry, 1995. **67**(6): p. 1115-1120.

6 The synthesis of Cyclodextrin Derivatives - Optimisation of Sensitivity for Dopamine Detection

6.1 Introduction

Molecular host–guest systems have captured much attention in recent years. By carefully selecting the host molecule, an effective inclusion complex with DA could be achieved. Among a wide range of host molecules, examples of well-known hosts are calixarenes. These are macrocyclic compounds with typical cavity that can selectively bind certain ligands. They can act as receptors for cations [1], anions [2] or neutral molecules [3] when they were appropriately functionalized. Calixcrown ether is one of the important derivatives of calixarene. As a novel class of host molecules which combine calixarene and crown ether in a single molecule, calixcrowns have attracted more attention during the last few decades because of their increased ability for selective binding to guest molecules as compared with crown ethers or calixarenes. They have been proved to be useful vehicles for the study of hydrogen bonding and electrostatic interactions as well as cation-π interactions that occur when ions are complexed [4, 5]. Lai *et al* [6] have analysed the voltammetric determination of DA at calix[4]arene crown-4 ether [6] (Figure 6.1) film modified glassy carbon electrode [7]. The author demonstrated that the CACE solution drop-cast on a GCE displayed a significant electrocatalytic response of DA. The detection limit was estimated to be 3.4 x 10^{-6} M. An alternative calix modified electrode was developed by Doyle *et al* [8]. The author used a platinum electrode modified with polypyrrole doped with *p*-sulphonatocalix[6]arene for electrochemical detection of DA. Studies on the mode of sensing indicated that DA forms a partial *endo*-inclusion complex with the calixarene. However, the sensor was only able to detect DA at concentrations of 2 x 10^{-5} M.

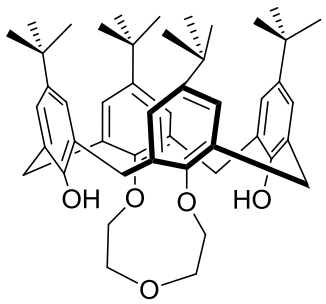

Figure 6.1: General structure for calix[4]arene crown-4 ether [6].

Cyclodextrins [9] are another class of DA receptors. CDs can bind a variety of guest molecules inside their torus-shaped cavities and serve as a model of host site [10]. As discussed throughout this thesis, the literature, reports show that CDs based sensors were used with good results for the determination of DA. Alarcon-Angeles *et al* [11]

developed a sensor based on modification of glassy carbon electrode with MWCNT/β-CD for the electrochemical detection of DA. The response mechanism of the MWCNT/β-CD modified electrode for DA is based on the combination of electrostatic and inclusion interaction of β-CD with DA which is distinguished from the response mechanism of non-modified electrode. The proposed integrated sensor showed improved analytical performance characteristics in catalytic oxidation of DA compared with bare glassy carbon electrode. However, the detection limit for the MWCNT/β-CD modified electrode was only 3.7 x 10^{-5} M DA.

Although, the electrochemical behaviour of DA at the macrocycles modified electrodes (mentioned above) showed improved analytical performance characteristics in oxidation of DA compared with non-modified electrode, their respective LOD for DA are relatively poor.

6.1.1 Aim of Chapter

Earlier in Chapter 5 it was demonstrated that the sensitive detection of DA was improved when S-β-CD or CM-β-CD was employed as modifiers. S-β-CD showed a LOD of 1.33 x 10^{-7} M for DA by using DPV technique. This remarkable enhancement in sensitivity could be due to the formation of a molecular complex between S-β-CD and DA. It is worth mentioning that the S-β-CD used in this thesis is a commercially available CD derivative. Its main structural features consist of a hydrophobic cavity and the randomly sulfated group on the CD rims, it is estimated by the commercial supplier that the degree of sulfation per molecule of cyclodextrin ranges between 7 and 11 sulfate groups. It is expected that all seven primary hydroxyl groups in the β-CD are sulfated, as they would be the most reactive ones (Figure 6.2). However, it would be extremely difficult to predict or identify the precise chemical structure of β-CD with further degree of sulfation.

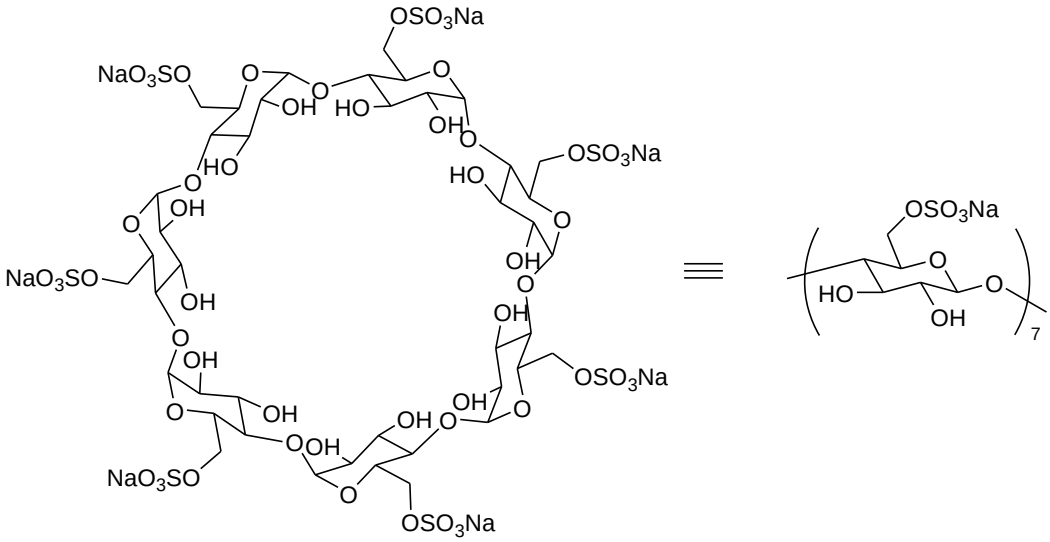

Figure 6.2: Structure of Heptakis-S-β-CD (7 sulfated groups are present).

The aim of this chapter is the synthesis of some cyclodextrin derivatives that could be used to further improve sensitivity in DA detection. The challenges in the modification of CD lie on the presence of the hydrophobic cavity and a large number of hydroxyl groups. Since each hydroxyl group present at the 2-, 3-, and 6-positions could be able to compete for the reagent, selective modification is extremely difficult. Moreover, the hydrophobic cavity often has the tendency to complex the reagent to direct the reaction to unexpected place [12].

In this Chapter, the synthesis of Heptakis 6-deoxy-6-(1-(4,5-dicarboxyl)-1,2,3-triazolyl)-β-CD **6.6** (Figure 6.3) was completed following reported literature procedures [13].

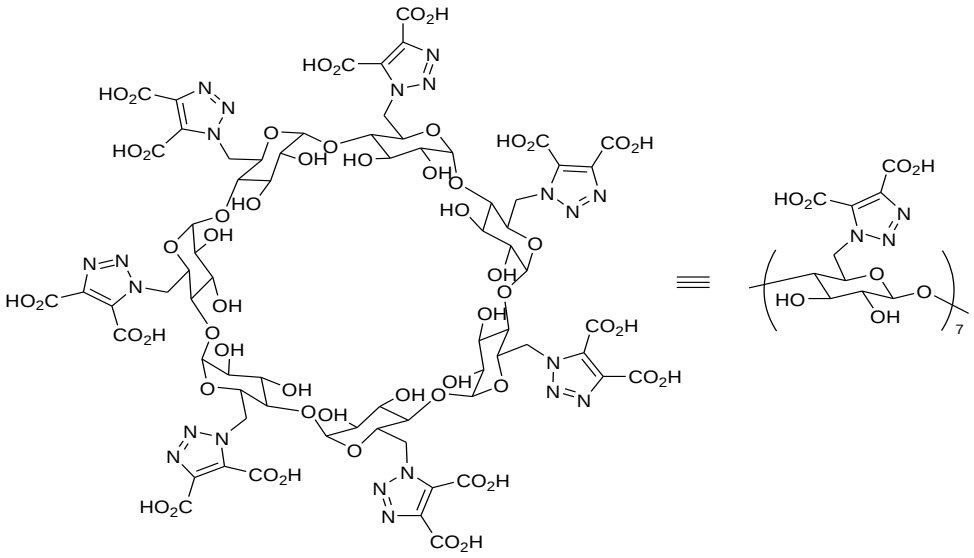

Figure 6.3: Structure of Heptakis 6-deoxy-6-(1-(4,5-dicarboxyl)-1,2,3-triazolyl)-β-CD 6.6 [13].

As already mentioned, the synthesis of this macrocycle is based on modification of neutral β-CD. However, the size of the cavity was not altered, which is sufficient for encapsulating DA molecule. Similarly to S-β-CD, the modified β-CD **6.6** has the possibility to display numerous negative charges, as the carboxylate groups can form an electrostatic interaction with protonated DA. In addition, the triazole moieties in the modified CD may enhance its affinity for DA due to attractive aromatic stacking interactions with the aromatic core of DA (Figure 6.4).

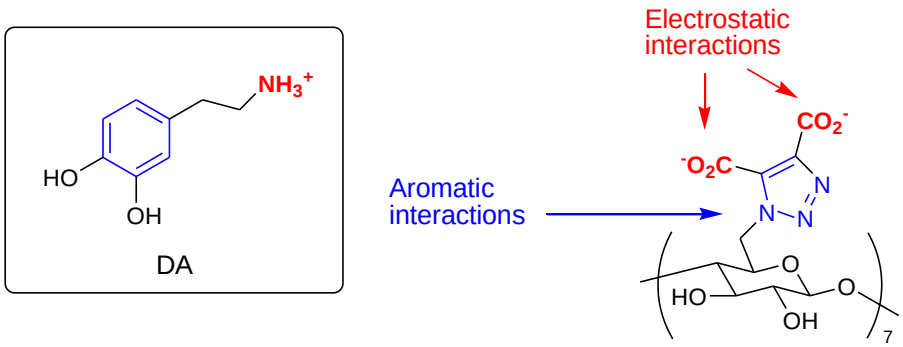

Figure 6.4: Possible stabilizing interactions of Heptakis 6-deoxy-6-(1-(4,5-dicarboxyl)-1,2,3-triazolyl)-β-CD 6.6 with DA.

The synthesised cyclodextrin derivative **6.6** was mixed with carbon paste, and its electrochemical performance for the determination of DA was investigated. It was shown that the combined effect of the carboxylate arms, the triazole moiety and the non-polar cavity improve molecular recognition towards DA.

A second cyclodextrin derivative, Heptakis (6-(4-hydroxymethyl-1*H*-[1, 2, 3] triazol-1-yl)-6-deoxy)-β-cyclodextrin **6.7** (Figure 6.5) was also synthesised following literature procedures [14].

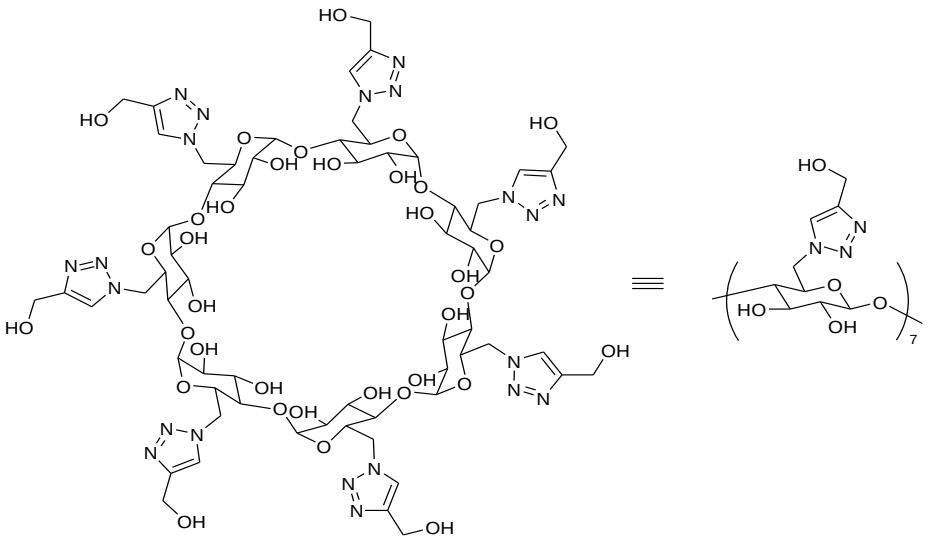

Figure 6.5: Structure of Heptakis (6-(4-hydroxymethyl-1*H*-[1, 2, 3] triazol-1-yl)-6-deoxy)-β-cyclodextrin 6.7 [14].

In this case, the modified cyclodextrin did not have acid groups that could become ionized to give negative charges, but it still features the triazole moieties that could provide aromatic interactions. This derivative has primary hydroxyl groups, similarly to non-modified β-CD, which could act as H-bond donors and acceptors (Figure 6.6).

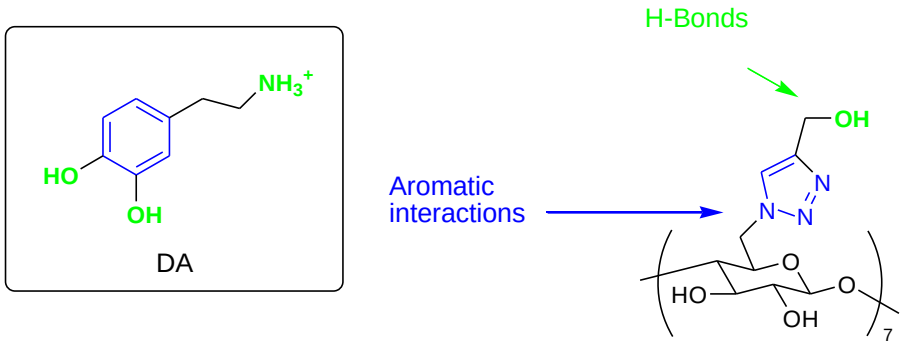

Figure 6.6: Possible stabilizing interactions of Heptakis (6-(4-hydroxymethyl-1*H*-[1, 2, 3] triazol-1-yl)-6-deoxy)-β-cyclodextrin 6.7 with DA.

Synthetic CD **6.7** was used as a modifier for the electrochemical detection of DA. It is worth noting that although the preparation of the modified CD was previously described, their ability to bind DA has never been investigated.

6.2 Results and discussion

6.2.1 Synthesis of Heptakis 6-deoxy-6-(1-(4,5-dicarboxyl)-1,2,3-triazolyl)-β-CD 6.6

The synthesis of compound **6.6** (Scheme 6.1) [13] reported in this study starts from the conversion of native β-CD into β-CD-I_7 **6.1**, which was prepared via selective replacement of all primary hydroxyl groups of β-CD by iodine atoms.

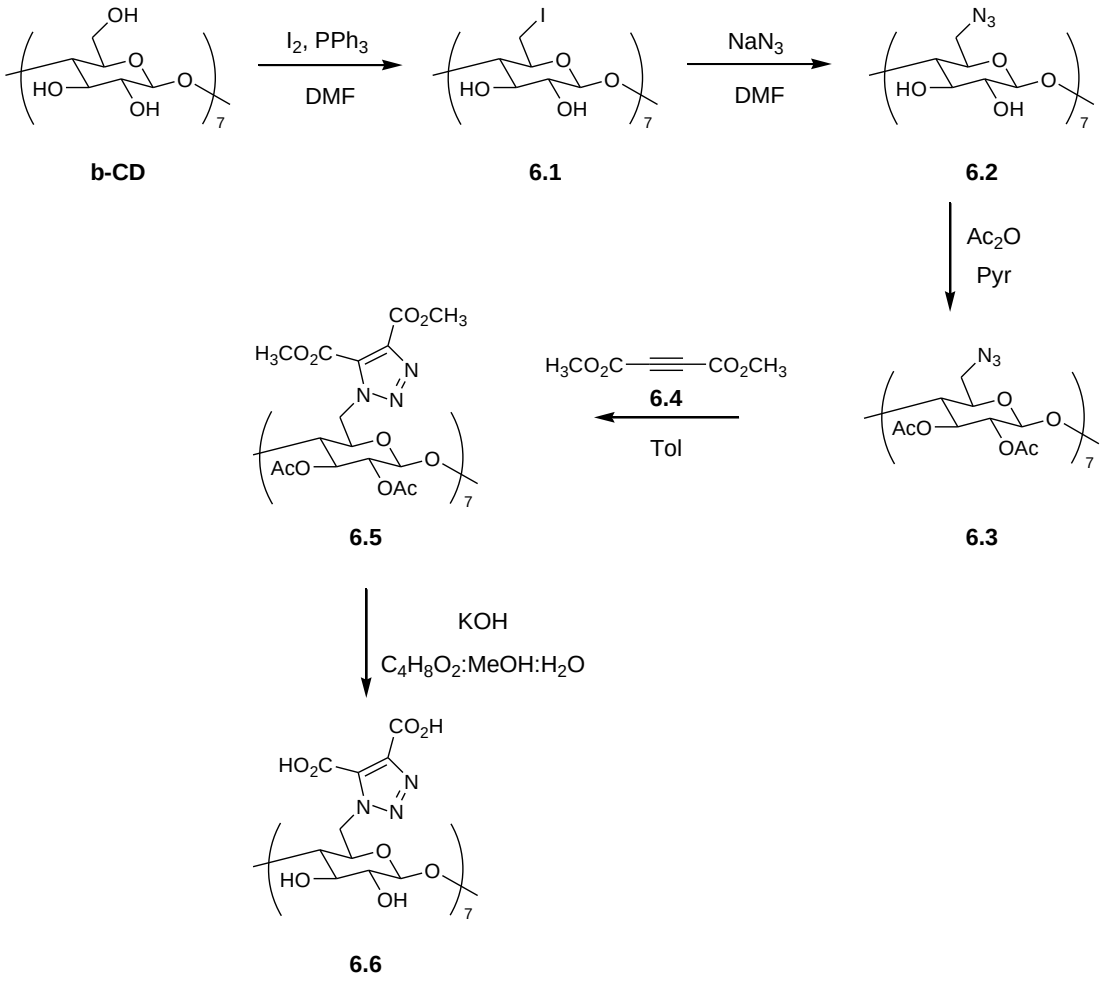

Scheme 6.1: Synthesis of cyclodextrin derivatives β-CD 6.6 [13].

The subsequent reaction of **6.1** with NaN_3 in DMF led to the formation of β-CD-$(N_3)_7$ **6.2**. ^{1}H NMR analysis of **6.2** in DMSO-d_6 (Figure 6.7) revealed the complete disappearance of the hydroxyl proton (6-CH2O***H***) signal at 4.47 ppm, which is present in β-CD. The chemical structure of **6.2** was further examined by IR spectroscopy. The spectrum of **6.2** (Figure 6.8) exhibits an absorption band at 2107 cm^{-1} which is characteristic of N_3 azido group. In addition, the mass spectrometry of **6.3** confirmed the introduction of seven azide groups on the small rim of β-CD.

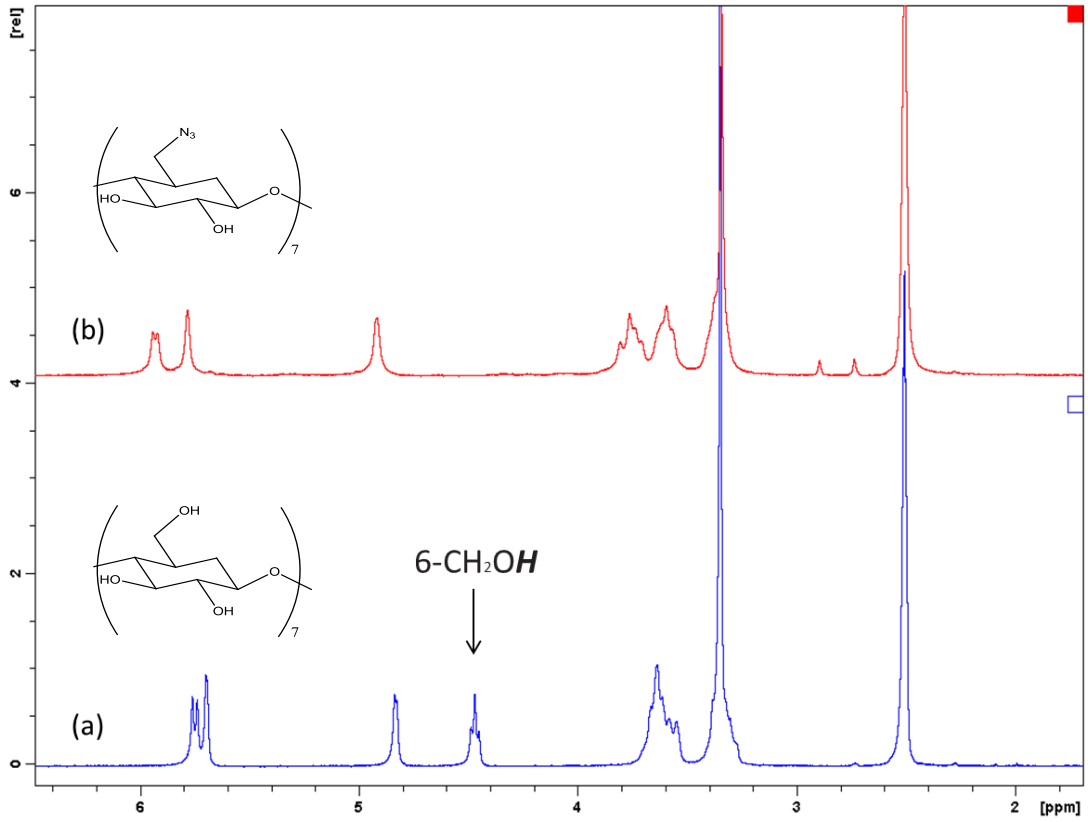

Figure 6.7: ^{1}H-NMR spectra of β-CD (a) and β-CD-$(N_3)_7$ 6.2 (b) recorded in DMSO-d_6.

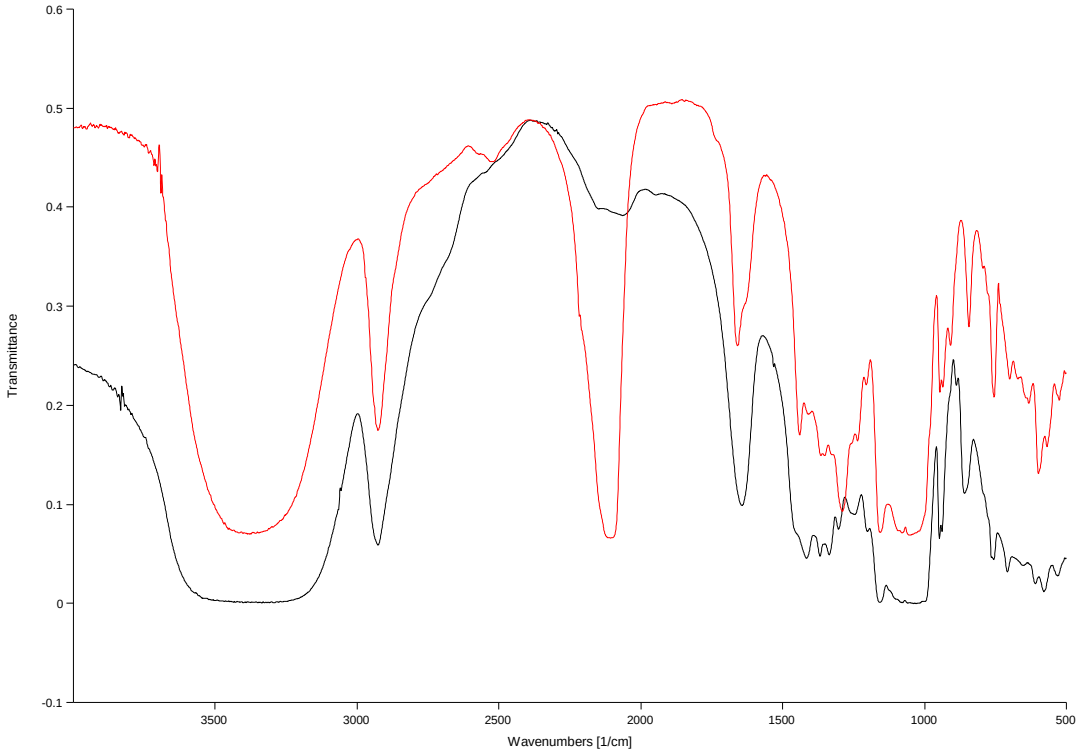

Figure 6.8: IR spectra of β-CD (—) and β-CD-$(N_3)_7$ 6.2 (—).

To facilitate the isolation of pure compound by column chromatography and to assure that the product obtained was symmetrically substituted, β-CD-$(N_3)_7$ **6.2** was acetylated using Ac_2O and pyridine to give the acetylated product **6.3** in 70 % yield. The structure and symmetrical substitution have been confirmed by mass spectrometry and NMR spectroscopy as described in the experimental procedure in Chapter 2. The appearance of absorption band in the IR spectrum of cyclodextrin **6.3** at 1742 cm^{-1}, characteristic of carbonyl groups strongly indicates the effective acetylation of azide derivative **6.2**.

The formation of the triazole moieties in cyclodextrin **6.5** was accomplished by the thermal Huisgen cycloaddition of alkyne dimethyl acetylenedicarboxylate **6.4** and the azide cyclodextrin **6.3**. A solution of both compounds in toluene was refluxed for 17 hours at 110 °C to afford acetylated compound **6.5** with a yield of 85 % after purification by column chromatography. In this case, the cycloaddition reaction can take place in the absence of a catalyst due to the fact that alkyne **6.4** is symmetrically substituted. The thermal Huisgen cycloaddtion between an azide and a non-symmetrical alkyne gives poor regiospecificity, leading to a mixture of regioisomers 1,2,3-triazole products. Figure 6.9 shows the IR spectrum of the triazole cyclodextrin **6.5**, where the disappearance of N_3 absorbance band at 2107 cm^{-1} present in cyclodextrin **6.4** can be clearly observed. Although ^{1}H-NMR spectrum for cyclodextrin **6.5** recorded in DMSO-d_6 presents a relatively poor definition of the signal multiplicity (as shown in Figure 6.10), the integration of the different ^{1}H-NMR resonance shows clearly that the ratio of the protons from the acetyl group (COCH_3) and the overlapping peaks representing anomeric *H* and *H*-3 protons (occurring approximately at 5.49 ppm) is 3:1. These results allow concluding that all azide groups have been converted into dimethylester substituted 1,2,3-triazole.

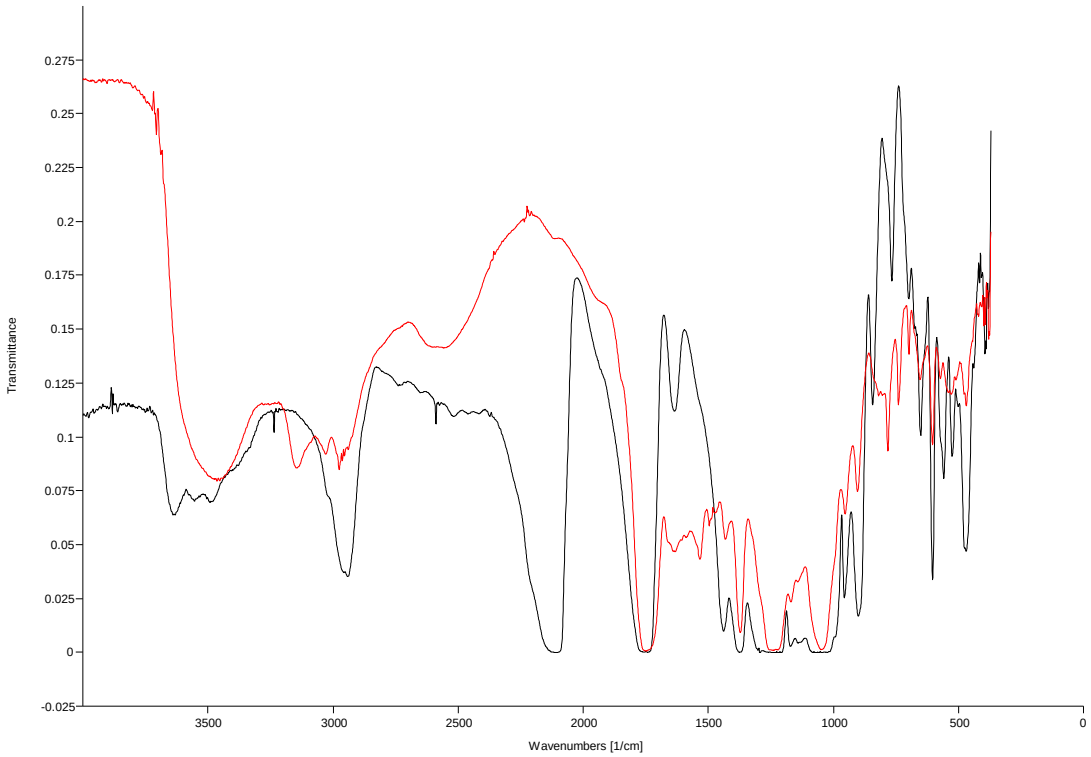

Figure 6.9: IR spectra of Acetylated β-CD-$(N_3)_7$ 6.3 (—) and triazole compound 6.5 (—).

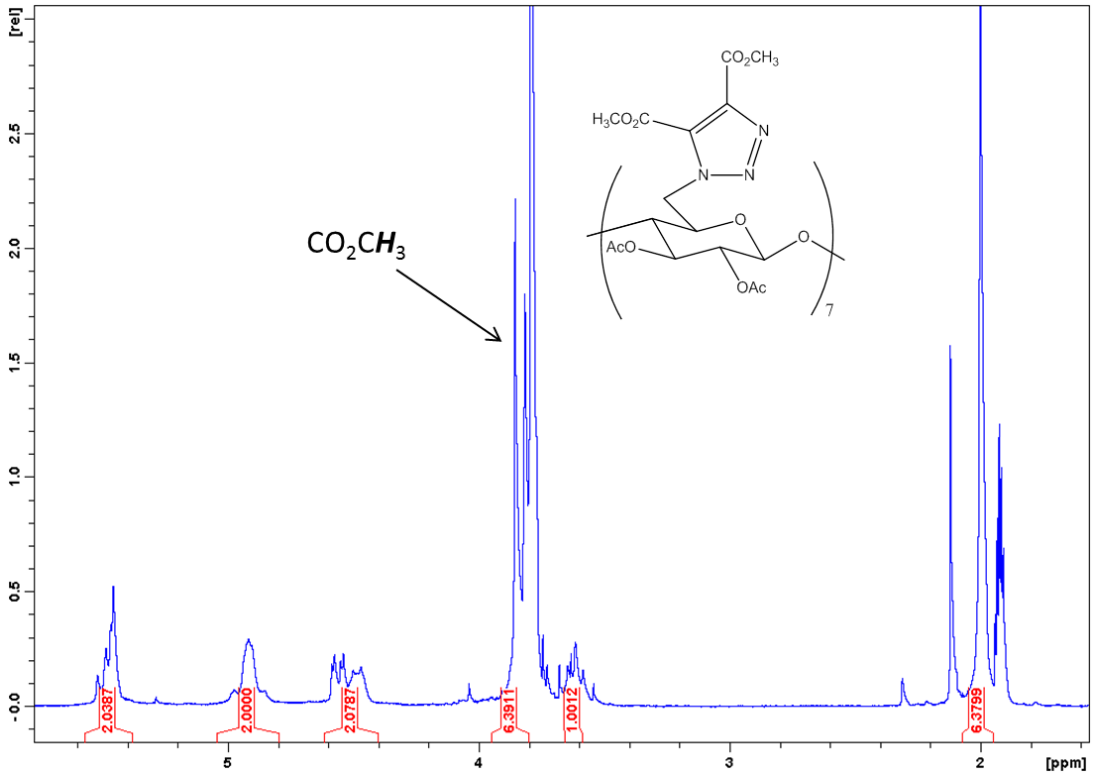

Figure 6.10: The ^{1}H-NMR spectrum of acetylated Heptakis 6-deoxy-6-(1-(4,5-dicarboxyl)-1,2,3-triazolyl)-β-CD 6.5 recorded in CD_3CN.

The treatment of cyclodextrin **6.5** with KOH in an aqueous mixture of dioxane and methanol at room temperature yielded complete hydrolysis of both acetyl and methyl esters. The NMR data of the final compound **6.6** (described in detail in Chapter 2) is in agreement with the reported literature values [13]. In addition, its ^{1}H-NMR spectrum, displayed in Figure 6.11 reveals the disappearance of peaks from the methyl esters of protected cyclodextrin **6.5**, which were occurring as singlet at 3.82 and 3.86 ppm.

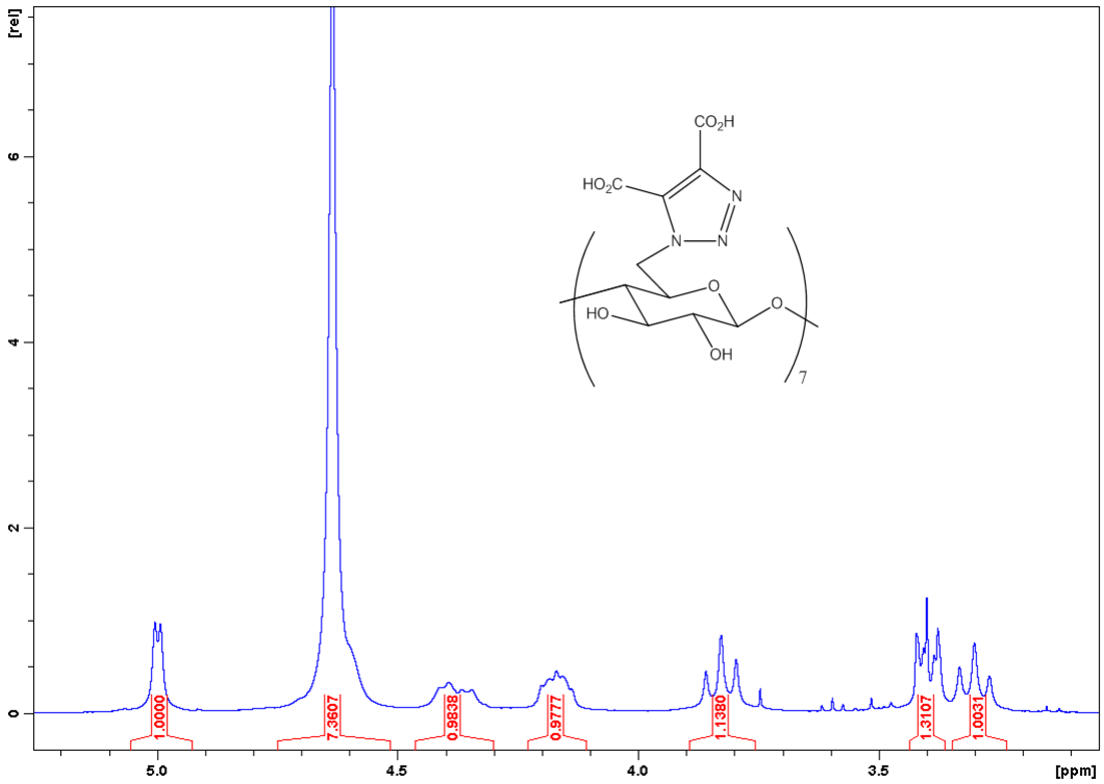

Figure 6.11: The ^{1}H-NMR spectrum of Heptakis 6-deoxy-6-(1-(4,5-dicarboxyl)-1,2,3-triazolyl)-β-CD 6.6 recorded in D_2O.

6.2.2 Synthesis of Heptakis (6-(4-hydroxymethyl-1H-[1, 2, 3] triazol-1-yl)-6-deoxy)-β-cyclodextrin 6.7

The synthetic approach for the second target cyclodextrin **6.7** involved the use of copper (I)-catalysed azide-alkyne cycloaddition (CuAAC). The CuAAC process has emerged as the first example of click chemistry, a term developed by Sharpless to describe a set of 'near-perfect' bond-forming reactions, useful for rapid assembly of molecules [15]. In this work, the CuAAC was performed following literature procedures by treatment of β-CD-$(N_3)_7$ **6.2** with propargyl alcohol in the presence of CuI and DIEA for 24 hrs to afford the desired product **6.7** (Scheme 6.2) [16]. The use of the copper catalyst leads to the formation of exclusively the corresponding 1,4-disubstituted triazole. An excess alkynyl reactant with respect to the cyclodextrin was used to ensure conversion of all

the β-CD-$(N_3)_7$ **6.2**. After 24 hours reaction time, the reaction was found to be clean as TLC analysis of the crude product only revealed two spots (desired product and excess alkyne), and a third small spot corresponding to copper salt. The bright green colour of the crude product in solution indicated the formation of copper (II) complexes. The copper was removed by addition of the chelating resin Chelex 100 sodium form. Excess alkyne was easily removed by washing the crude product with ethanol.

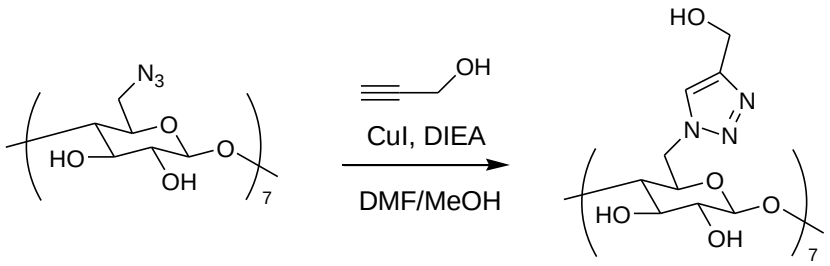

6.2 **6.7**

Scheme 6.2: Synthesis of cyclodextrin derivatives β-CD 6.7.

^{1}H-NMR spectrum, of β-CD **6.7** recorded in DMSO-d_6 revealed a characteristic peak at 7.84 ppm, which was assigned to be the triazole proton. On the other hand, as generally observed for substituted cyclodextrins, other signals were hardly possible to assign due to overlapping. By contrast, the ^{13}C-NMR was much more informative. As can be seen from Figure 6.12, all peaks were clearly distinguishable. In particular, the presence of the carbon peaks at 124.11 and 147.58 ppm (from triazole) shows evidence of the formation of the desired cyclodextrin **6.7**.

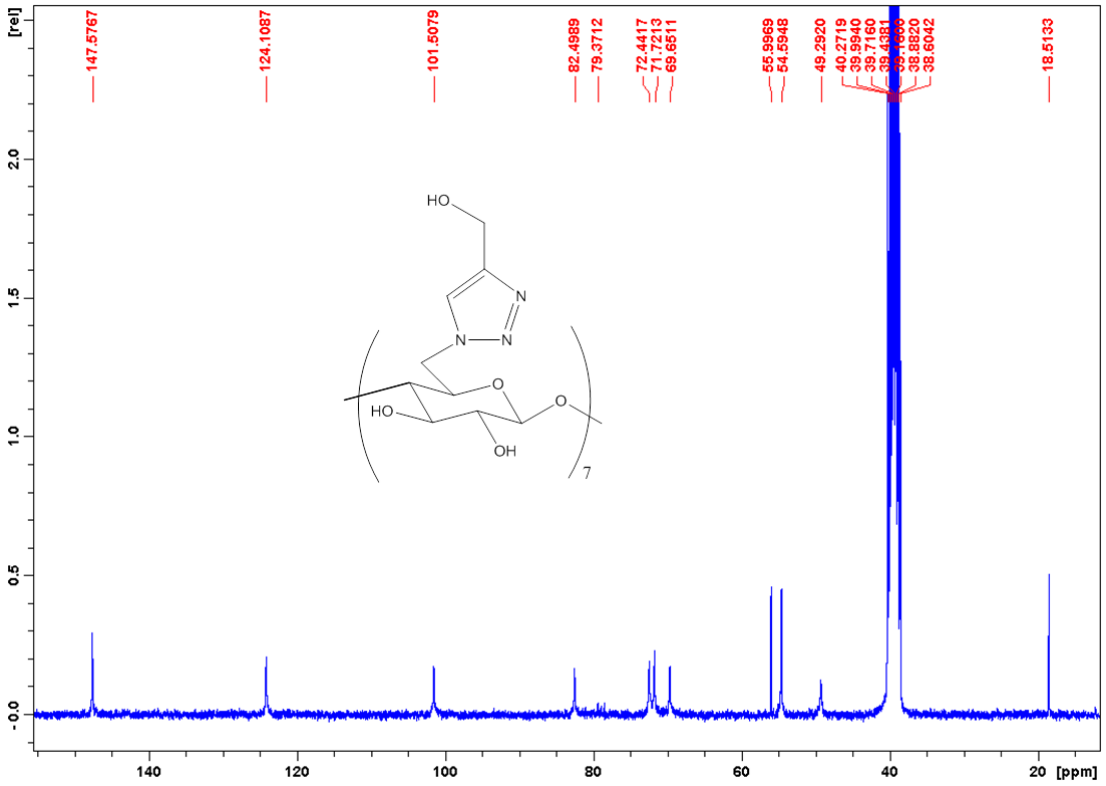

Figure 6.12: The ^{13}C-NMR spectrum of Heptakis(6-(4-hydroxymethyl-1*H*-[1, 2, 3] triazol-1-yl)-6-deoxy)-β-cyclodextrin 6.8 recorded in DMSO-d_6.

The target compound was further characterised by mass spectrometry (Chapter 2). It is worth noting that, unlike the thermal Huisgen cycloaddition to prepare compound **6.6**, the CuAAC reaction was performed at room temperature and allowed the synthesis of one regioisomer specifically regardless the symmetry of alkyne. A possible mechanistic pathway of the CuAAC process [17, 18] is displayed in Scheme 6.3. In brief, copper coordinates to the acetylene π-electrons. The resulting copper-acetylide binds to the azide, followed by rearrangement of complex to an unusual six-membered copper-metallocycle and further into a copper-metallated triazole complex. Ring contraction to copper-triazole is followed by protonolysis that delivers the triazole product.

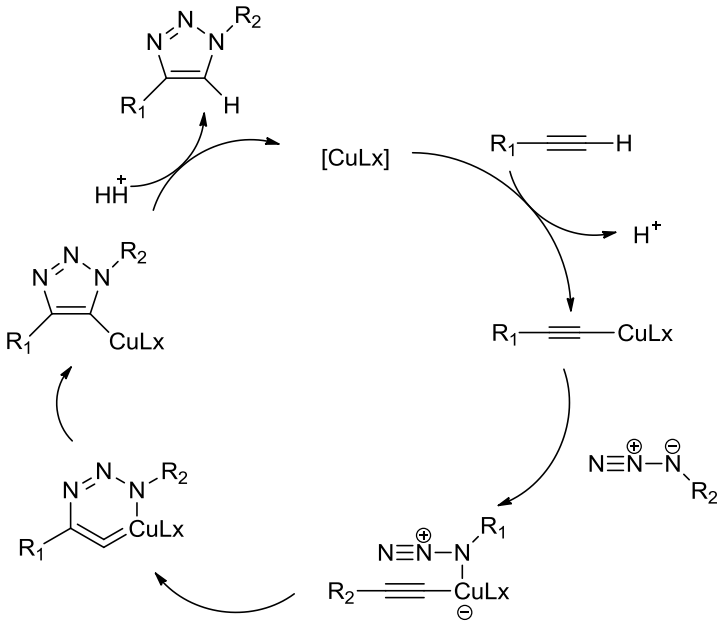

Scheme 6.3: Proposed mechanism of the CuAAC reaction [17].

6.2.3 Attempted Synthesis of Cyclodextrin Derivative 6.9

The preparation of a third target cyclodextrin was investigated preliminary. The aromatic triazole groups, present in both cyclodextrins 6.6 and 6.7, were substituted by the trihydroxyphenyl moiety, as shown in Scheme 6.4. It was envisaged that this aromatic moiety could have good stacking interactions with the catechol moiety present in DA. The attempted synthesis of compound **6.9** (Scheme 6.4) was based on the procedure analogue to that reported by Ashton *et al* [19], which consisted of coupling amino-cyclodextrin **6.8** with gallic acid.

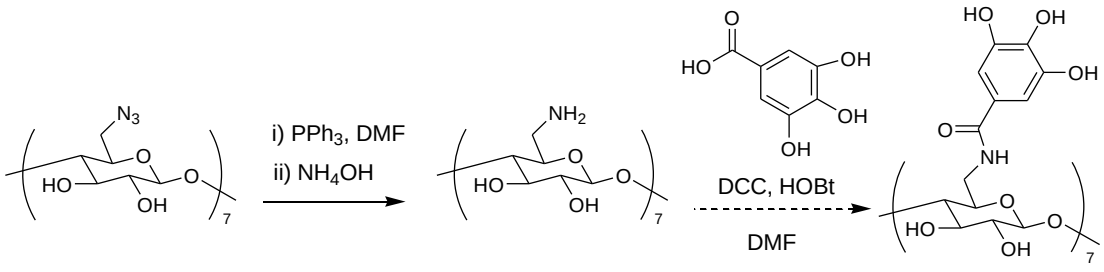

6.2 **6.8** **6.9**

Scheme 6.4: Attempted synthesis of cyclodextrin derivatives β-CD 6.9.

The starting material **6.8** was obtained by reduction of azido-cyclodextrin **6.2**. This reaction was carried out via the Staudinger method, using Ph_3P in DMF followed by subsequent treatment with aqueous ammonia. A proposed mechanism for the reaction [20] is displayed in Scheme 6.5. Ph_3P reacts with the azide to generate a phosphazide,

which loses N_2 to form an iminophosphorane. Hydrolysis by aqueous work-up leads to the amine and the very stable phosphine oxide.

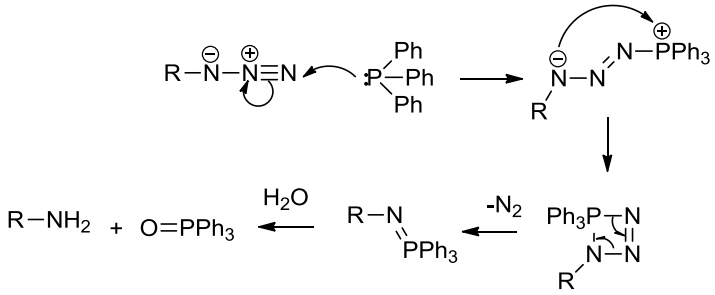

Scheme 6.5: Proposed mechanism of the Staudinger reaction [20].

The amino-cyclodextrin **6.8** was obtained in good yield (89 %) and its chemical structure was confirmed by mass spectrometry. In addition, IR spectroscopy revealed disappearance of N_3 group. Surprisingly, amino-cyclodextrin **6.8** was extremely insoluble in H_2O. However, as the pH of an aqueous suspension of **6.8** was lowered to neutrality or slightly acidic conditions, the compound was dissolved rapidly. Indeed, to carry out characterization using NMR spectroscopy, compound **6.8** had to be converted into its HCl salt, which was highly soluble in D_2O. The amino-cyclodextrin **6.8** was then reacted with gallic acid using the HOBt / DCC system. However, these amide coupling conditions were not successful, as none of the desired product **6.9** was isolated. The ^{1}H-NMR spectrum showed very broad signals and the amide characteristic peak (RN*H*COR') could not be identified. Instead, the spectrum indicated the presence of dichlorohexylurea with traces of unreacted gallic acid. In the future, alternative amide coupling conditions should be explored to carry out the formation of gallic acid derivative cyclodextrin **6.9.**

6.2.4 Host-guest Complexation Studies

As mentioned earlier in this thesis, cyclodextrins belong to the family of cyclic oligosaccharides, and have been studied extensively as hosts in supramolecular chemistry. They can encapsulate organic, inorganic and biomolecules and intensive studies of their inclusion complexes have been reported previously [21-23]. In the pharmaceutical field for instance, bioavailability and stability of commonly used drugs have been enhanced as a result of their complexation with CDs [24].

CDs have a torus-like macro-rings made of glucose units, in particular β-CD has seven glucose units. The number of glucose units directly influences CD physical properties such as water solubility and cavity size. The non-bonding electron pairs of the

glycosidic oxygens point toward the inside of the cavity, providing a high electron density and a Lewis base character. The CD cavity is relatively hydrophobic compared to the exterior faces which are hydrophilic [25-27]. A great variety of guest molecules of suitable size and shape may be entirely or partially included in this hydrophobic cavity, resulting in a stable association without formation of covalent bonds. The complexation driving force have been attributed to hydrophobic interactions, Van der Waals-London dispersion forces, and hydrogen bonds [25, 28, 29].

Among various techniques, NMR spectroscopy is the most reliable method for the study of inclusion phenomenon in solution [25, 28]. NMR titration measure chemical shift changes of the signals for host and guest protons, affected by the formation of a complex, as a function of host/guest concentration and can be used to determine the binding constant K_a. The observed shift changes can offer an insight into the conformation of the formed supramolecular complexes, which is difficult to extract from other analysis such as UV-visible titrations [25]. In general, the informations provided by the NMR titration method include: (i) confirmation of complex formation, (ii) calculation of stoichiometry of the complex, and (iii) establishment of the geometry of the complex [28-31].

The simplest NMR experiment that can give indication of complexation is the observation of the difference in the proton chemical shifts between the free guest or host species and a mixture of both, which would be a result of the formation of the suggested complex.

β-CD and some of their derivatives are known to bind to DA [32, 33]. However there is no published report on the interaction of DA and cyclodextrin derivatives **6.6** ($CD_{6.6}$) and **6.7** ($CD_{6.7}$).

In this section, the complexation between DA and both $CD_{6.6}$ and $CD_{6.7}$ was investigated in aqueous solution using ^{1}H-NMR spectroscopy. The binding stoichiometry was determined by a continuous variation method (Job's plot) and the binding constants (K_a) was evaluated following NMR titration.

6.2.4.1 Sample preparation and NMR measurements

Before considering analysis of the interaction between DA and the cyclodextrin derivatives, DA molecule was characterised by ^{1}H-NMR spectroscopy. Figure 6.13 illustrates the ^{1}H-NMR spectrum of protonated DA in 0.1 KCl / D_2O. As can be seen, clear and well resolved signals are observed. Two doublets and a doublet of doublets

(from the aromatic ring) correspond to H-b, H-a and H-c, as illustrated. Two triplets (from the aliphatic ethylene amine chain) correspond to H-e and H-d.

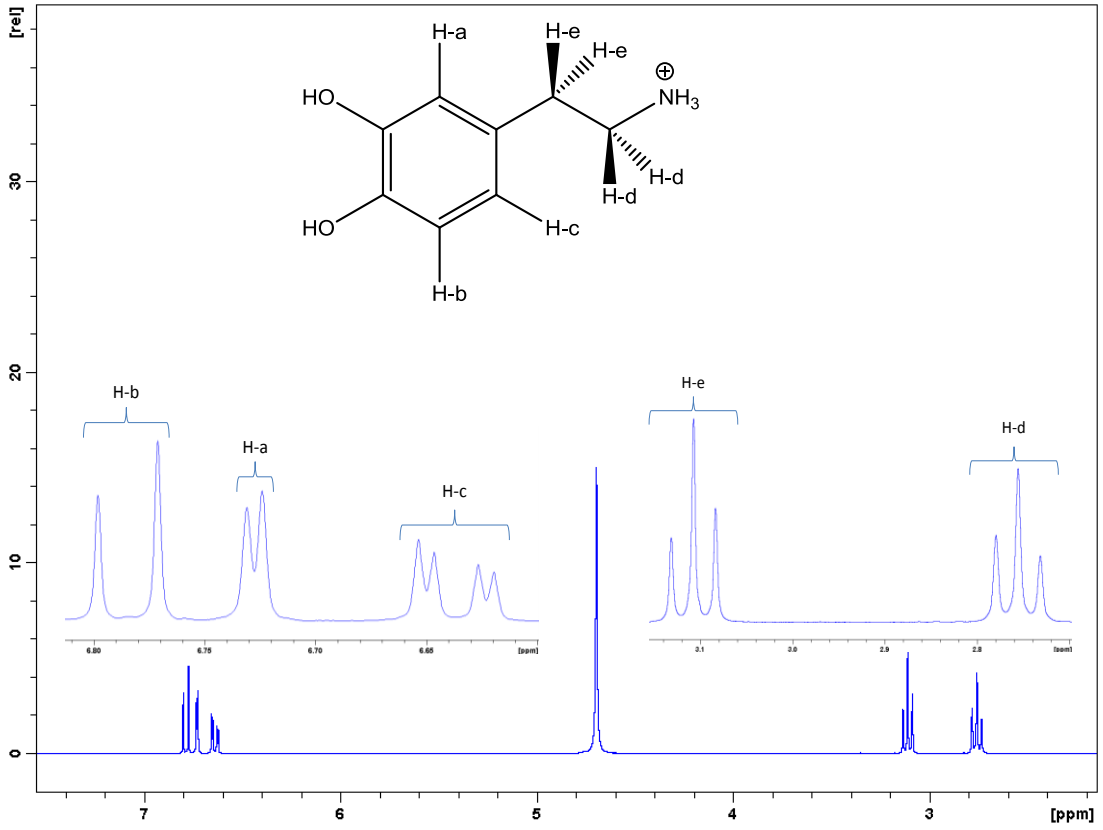

Figure 6.13: The ^{1}H-NMR spectrum of protonated DA recorded in 0.1 M KCl / D_2O.

In order to investigate the interaction between DA and the cyclodextrin derivatives, a stock solution for the hosts ($CD_{6.6}$ and $CD_{6.7}$) and the guest (DA) were obtained by dissolving appropriate amount of each compound in a solution of 0.1 M KCl / D_2O to achieve a concentration of 7.4×10^{-2} M. A series of solutions were prepared by mixing variable volumes of (host and guest) stock solutions in varying proportions so that a complete range of molar ratios was sampled ($0 \leq r \leq 1$), keeping the total concentration of DA and CD as 2×10^{-2} M ([DA] + [CD] = 2×10^{-2} M) and the total volume (0.27 mL) constant for each solution. The different mixtures were filled up to 1 mL with 0.1 M KCl / D_2O and shaken thoroughly before NMR measurement. The volumes taken from each stock solution to give the required molar fraction are shown in Table 6.1.

Table 6.1: The solution composition for the Job's plot measurement and corresponding mole fraction of DA.

Solutions	Volume of CDs (mL)	Volume of DA (mL)	Molar fraction of DA (*r*)
1	0.2700	0.0000	0.00
2	0.2250	0.0450	0.17
3	0.2159	0.0541	0.20
4	0.2024	0.0676	0.25
5	0.1799	0.0901	0.33
6	0.1350	0.1350	0.50
7	0.0901	0.1799	0.67
8	0.0676	0.2024	0.75
9	0.0541	0.2159	0.80
10	0.0450	0.2250	0.83
11	0.0000	0.2700	1.00

In this study, the aromatic region of DA spectrum was used to monitor chemical shift variations. All ^{1}H-NMR measurements were performed at ambient temperature in D_2O containing 0.1 M KCl in order to maintain a constant pD and ionic strength.

It is well-known that the chemical shift (δ) of a given nucleus depends on its shielding constant and in turn is sensitive to medium effects. Therefore, changes in δ (ppm) values of the DA nuclei can provide a measure of the degree of complex formation. As the chemical environment of some protons changes upon complexation, there is a consequent variation in the chemical shift (Δδ) of the ^{1}H-NMR (shielding or deshielding effect). Figure 6.14 shows clearly that all protons from DA aromatic ring shift downfield in the presence of $CD_{6.6}$. This significant change in the chemical shifts strongly suggests an interaction event between DA and $CD_{6.6}$. Although, there is a general tendency for chemical shift displacement (downfield), it cannot be inferred from these data that an inclusion complex has been formed. The chemical shift displacement of the DA protons may be regarded as a combination of interactions with $CD_{6.6}$. It has to be noted that the macrocycle $CD_{6.6}$ contains seven triazole units bearing two carboxylic acid groups each. Electrostatic interactions and other types of non-covalent attractive interactions are likely taking place between DA and the different functionalities of $CD_{6.6}$.

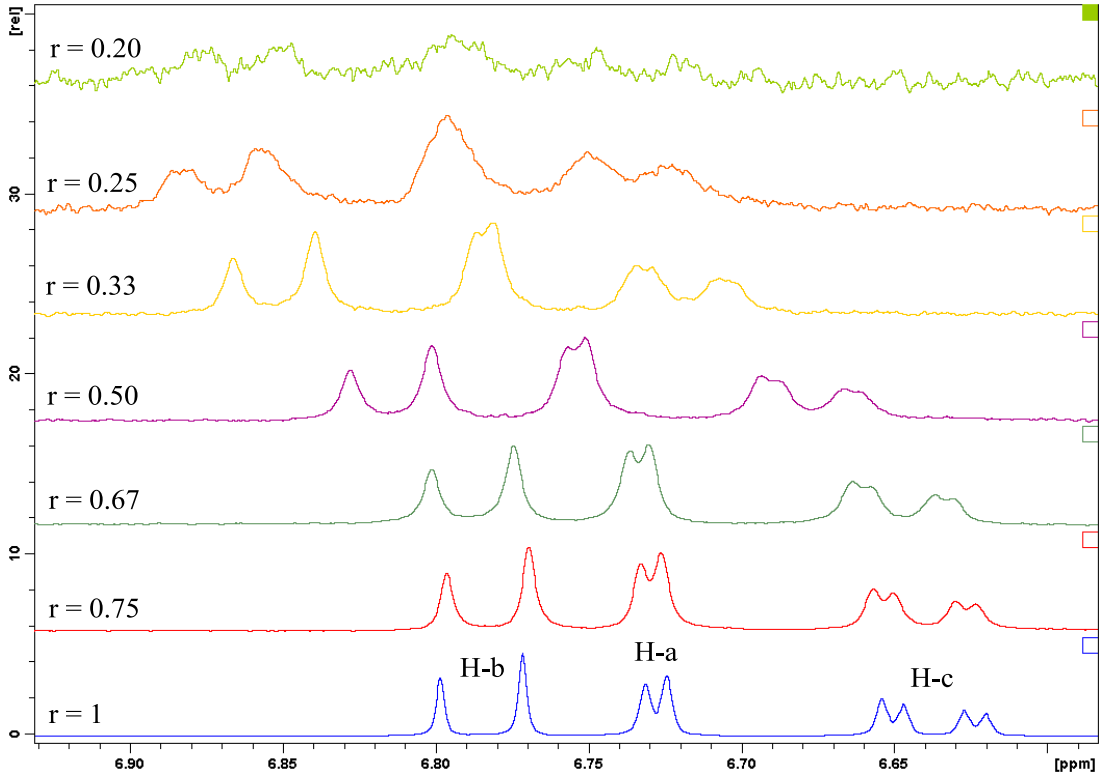

Figure 6.14: ^{1}H-NMR spectra recorded in 0.1 M KCl / D_2O for the Job's method showing the different chemical shift changes for DA (aromatic region) upon addition of $CD_{6.6}$. The molar fraction of DA was varied from 0.2 to 1, as shown on each spectrum.

The ^{1}H-NMR spectra reporting the changes in the chemical shifts for the protons of DA in the presence of $CD_{6.7}$ was also analysed as presented in Figure 6.15. The most significant change of DA chemical shifts was observable for H-b, where a more noticeable downfield displacement occurred upon reducing the molar fraction of DA. A slight upfield shift for H-c was observed. However, there was no consistent shift of H-a. The chemical shift change in DA aromatic protons (in particular H-b and H-c) once again could be interpreted as an evidence for the formation of an interaction between DA and $CD_{6.7}$.

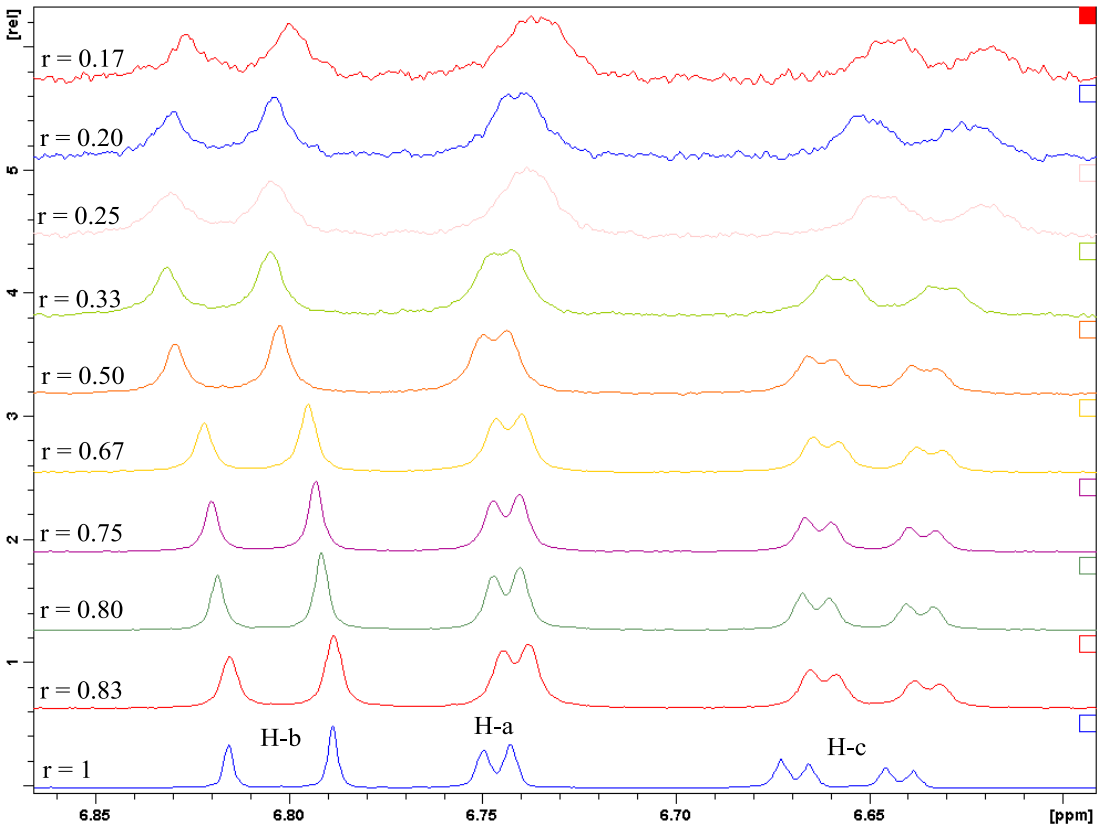

Figure 6.15: ^{1}H-NMR spectra recorded in 0.1 M KCl / D_2O for the Job's method showing the different chemical shift changes for DA (aromatic region) upon addition of $CD_{6.7}$. The molar fraction of DA was varied from 0.17 to 1, as shown on each spectrum.

The observed changes in chemical shift for the aromatic protons of DA (H-a, H-b and H-c) upon interaction with $CD_{6.6}$ and $CD_{6.7}$ are given in Table 6.2 and Table 6.3, respectively. The dimensionless quantity *r* is defined as $r = m / (m + n)$, where *m* and *n* represent the stoichiometric ratios of DA and cyclodextrin derivatives, respectively. The chemical shift change of DA protons was calculated according to formula: $\Delta\delta = \delta_{(complex)} - \delta_{(free)}$. In other words, $\Delta\delta$ is defined as the difference in chemical shifts in the presence and absence of the cyclodextrin derivatives for each NMR measurement. By convention, a positive sign of $\Delta\delta$ (ppm) shows a downfield displacement and a negative sign shows an upfield one.

Table 6.2: Chemical shift change of DA (aromatic protons) upon addition to $CD_{6.6}$

	r = **1.00**	*r* = **0.75**	*r* = **0.67**	*r* = **0. 50**	*r* = **0.33**	*r* = **0.25**	*r* = **0.20**
H-a (ppm)	6.7849	6.7829	6.7877	6.8145	6.8525	6.8706	6.8628
H-b (ppm)	6.7278	6.7295	6.7333	6.7536	6.7838	6.7971	6.7949
H-c (ppm)	6.6368	6.6398	6.6465	6.6773	6.7191	6.7372	6.7363
$\Delta\delta_{(H\text{-}a)}$ (ppm)	-0.0020	0.0028	0.0296	0.0676	0.0857	0.0779	0.1310
$\Delta\delta_{(H\text{-}b)}$ (ppm)	0.0017	0.0055	0.0258	0.0560	0.0693	0.0671	0.1118
$\Delta\delta_{(H\text{-}c)}$ (ppm)	0.0030	0.0097	0.0405	0.0823	0.1004	0.0995	0.1490

Table 6.3: Chemical shift change of DA (aromatic protons) upon addition to $CD_{6.7}$

	r = **1.00**	*r* = **0.83**	*r* = **0.80**	*r* = **0. 75**	*r* = **0.67**	*r* = **0.50**	*r* = **0.33**	*r* = **0.25**	*r* = **0.20**	*r* = **0.17**
H-a (ppm)	6.8025	6.8022	6.8054	6.8069	6.8088	6.8163	6.8183	6.8186	6.8172	6.8140
H-b (ppm)	6.7466	6.7416	6.7440	6.7441	6.7435	6.7471	6.7448	6.7399	6.7413	6.7367
H-c (ppm)	6.6560	6.6487	6.6506	6.6500	6.6494	6.6449	6.6449	6.6334	6.6388	6.6315
$\Delta\delta_{(H\text{-}a)}$ (ppm)	0.0000	-0.0003	0.0029	0.0044	0.0063	0.0138	0.0158	0.0161	0.0147	0.0115
$\Delta\delta_{(H\text{-}b)}$ (ppm)	0.0000	-0.0050	-0.0026	-0.0025	-0.0031	0.0005	-0.0018	-0.0067	-0.0053	-0.0099
$\Delta\delta_{(H\text{-}c)}$ (ppm)	0.0000	-0.0073	-0.0054	-0.0060	-0.0078	-0.0066	-0.0111	-0.0226	-0.0172	-0.0245

6.2.4.2 Stoichiometry of the inclusion complexes

There is abundant reports on ordinary stoichiometric 1:1, 2:1, and 1:2 complexes between host CD and guests [26, 35-37]. Job's plot, which depicts the dependence of chemical shift on substrate / CD ratio, has been widely used to determine complex stoichiometry [38]. Therefore, the first focus in this study was to derive a Job's plot using the continuous variation method that would correctly describe the stoichiometric nature of the possible complexes formed between DA in cyclodextrin derivatives $CD_{6.6}$ and $CD_{6.7}$. Important assumptions of the method of continuous variation are: (i) neither host nor guest self-associate, (ii) the law of mass action is obeyed, and (iii) only one

complex is formed [39]. In NMR spectroscopy, two situations may occur when using the continuous variation method in experiments with CD inclusion complexes: (i) the slow exchange condition and (ii) the fast exchange condition [40]. In slow exchange, the free and complexed forms of one component produce separated signals, and the ratio of the free and complexed forms can be measured directly by digital integration of the relevant signals on the NMR spectrum. In fast exchange, only shifts of the spectral lines are observed due to fast averaging by the exchange between free and included states. As no free, as well as complexed signals for DA protons could be observed in the ^{1}H-NMR, it was presumed that a rapid exchange between free and bound state on the NMR time scale was obtained. Therefore, the chemical shift differences were multiplied by the mole fraction of DA in order to create a Job's plot. Tables 6.4 and Table 6.5 indicate the calculated quantity $|\Delta\delta| \times r$, which was plotted as a function of the mole fraction of DA, r, in the case of interaction form $CD_{6.6}$:DA and $CD_{6.7}$:DA, respectively.

Table 6.4: Chemical shift change of DA (aromatic protons) multiplied by the corresponding mole fraction upon addition to $CD_{6.6}$

	r = **1.00**	r = **0.75**	r = **0.67**	r = **0. 50**	r = **0.33**	r = **0.25**	r = **0.20**	r = **0.00**
$\|\Delta\delta_{(H\text{-}a)}\| \times r$ (ppm)	0.0000	0.00150	0.00188	0.01480	0.02231	0.02143	0.01558	0.0000
$\|\Delta\delta_{(H\text{-}b)}\| \times r$ (ppm)	0.0000	0.00128	0.00369	0.01290	0.01848	0.01733	0.01342	0.0000
$\|\Delta\delta_{(H\text{-}c)}\| \times r$ (ppm)	0.0000	0.00225	0.00650	0.02025	0.02716	0.02510	0.01990	0.0000

Table 6.5: Chemical shift change of DA (aromatic protons) multiplied by the corresponding mole fraction upon addition to $CD_{6.7}$

	r = **1.00**	r = **0.83**	r = **0.80**	r = **0.75**	r = **0.67**	r = **0. 50**	r = **0.33**	r = **0.25**	r = **0.20**	r = **0.17**	r = **0.00**
$\|\Delta\delta_{(H\text{-}a)}\| \times r$ (ppm)	0.00000	0.00025	0.00232	0.00330	0.00422	0.00690	0.00521	0.00403	0.00294	0.00196	0.00000
$\|\Delta\delta_{(H\text{-}b)}\| \times r$ (ppm)	0.00000	0.00415	0.00208	0.00200	0.00208	0.00025	0.00059	0.00168	0.00106	0.00168	0.00000
$\|\Delta\delta_{(H\text{-}c)}\| \times r$ (ppm)	0.00000	0.00606	0.00432	0.00450	0.00523	0.00330	0.00366	0.00565	0.00344	0.00417	0.00000

Figure 6.16 shows the generated Job's plot when DA interacts with $CD_{6.6}$. This plot is characterised by possessing a maximum centred at r = 0.33 for all aromatic protons of DA which strongly suggests that the complex formed between $CD_{6.6}$ and DA favoured a 2:1 stoichiometry.

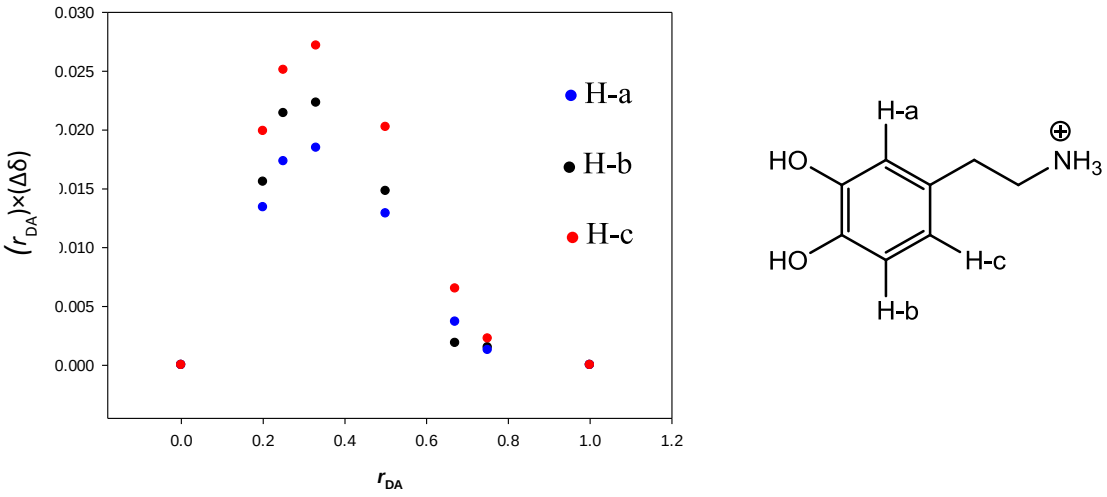

Figure 6.16: ^{1}H-NMR Job plots for the binding of DA to $CD_{6.6}$. The plot is generated for each DA aromatic proton.

In the case of $CD_{6.7}$, the continuous variation analysis (Job's plot) was applied to H-b as this aromatic proton showed the most obvious chemical shift variation. As presented in Figure 6.17, the plot shows a maximum value at r = 0.50 and a fairly symmetrical shape, which indicates the existence of a $CD_{6.7}$:DA complex with a 1:1 stoichiometry.

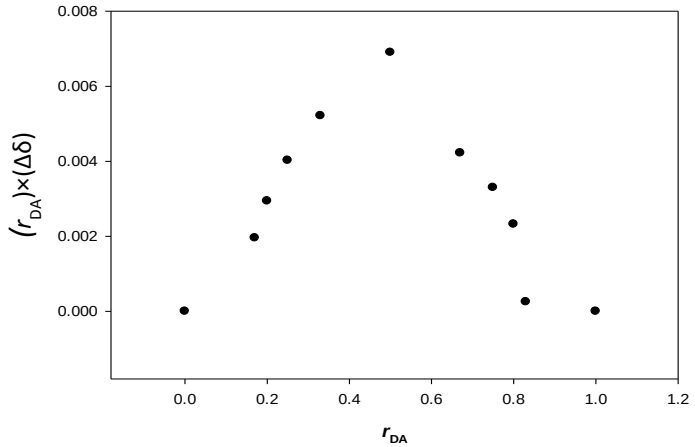

Figure 6.17: ^{1}H-NMR Job's plot for the binding of DA to $CD_{6.7}$. The plot is generated for H-b from DA aromatic region.

6.2.4.3 Insights into the mode of interaction

(i) $CD_{6.6}$:DA interaction

It has been demonstrated from the stoichiometry studies that $CD_{6.6}$ forms a 2:1 complex with DA. In other words, two molecules of $CD_{6.6}$ interact with one molecule of DA. The interaction of DA with $CD_{6.6}$ is related to the structure (and chemical features) of the macrocycle. The narrow rim of $CD_{6.6}$ cavity is linked to triazole moieties which provide additional hydrophobic regions and consequently an expansion of the hydrophobic CD cavity. The protonated amine group of the DA molecule could form an ion-pair with the charged carboxylate groups of one $CD_{6.6}$ molecule, while the hydroxyl groups may be included in the cavity of the other $CD_{6.6}$ which could result in the formation of hydrogen bonding. Hydrogen bonds could also be formed between the hydroxyls and the carboxylate groups. It was shown from the continuous variation analysis that all DA aromatic protons followed a downfield shift; therefore, it appears likely that some of the above interactions may be taking place. It was reported in the literature [38, 39] that a downfield displacement of a drug proton indicates that it is close to an electronegative atom, like oxygen, whereas, an upfield shift displacement is probably due to a variation in the local polarity when the protons are inside the CD cavity. This indicates shielding effect due to Van der Waals forces between the drug and carbohydrate C-H framework.

The methylene protons of DA (H-e and H-d) are also significantly deshielded as presented in Figure 6.18. The DA molecule has to arrange its conformation in the additional hydrophobic environment provided by the triazole moieties and to allow for the different interactions with $CD_{6.6}$. Thus, the chemical shift displacement of H-e and H-d may indicate their proximity to electronegative atoms.

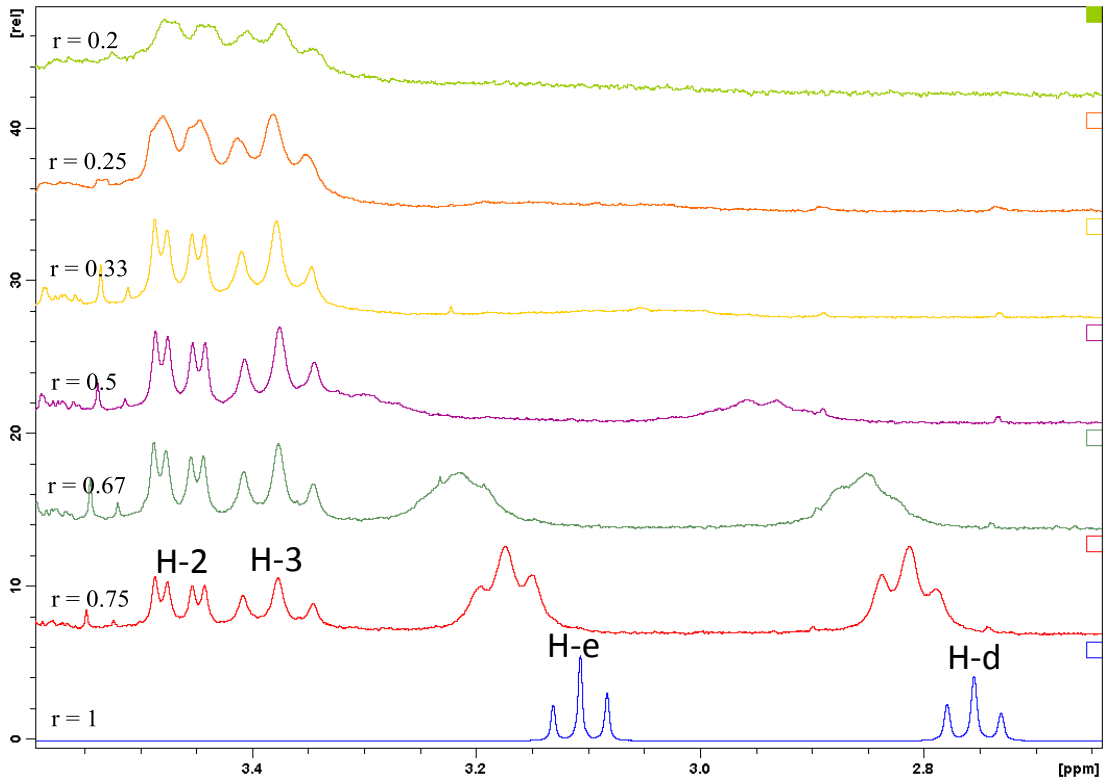

Figure 6.18: ^{1}H-NMR spectra recorded in 0.1 M KCl / D_2O showing the chemical shift changes for DA (aliphatic chain protons H-e and H-d) upon addition of $CD_{6.6}$. The molar fraction of DA was varied from 0.17 to 1, as shown on the diagram.

The variations undergone by some $CD_{6.6}$ protons (H-3 and H-5) as a consequence of the presence of DA were also analysed. H-3 and H-5 from each sugar unit face the internal cavity and they are located near the wide and the narrow ring, respectively. They can be used to probe the internal cavity of $CD_{6.6}$ for the presence of a guest molecule and to understand the nature the interaction.

If a DA molecule is completely included into the $CD_{6.6}$ cavity, H-3 or H-5 will be considerably shielded by benzene ring of DA and show a significant upfield shift. However, it was noticed in this work (continuous variation analysis) that H-3 was unaffected whereas a slight downfield shift of H-5 signal was observed. Although an exact value of the shift from H-5 was hard to determine, as it splits as a multiplet (Figure 6.19), it was suggested that this proton could be close to some of the hydroxyl groups of $CD_{6.6}$. The fact that H-3 does not experience a chemical shift variation (as shown in Figure 6.18 above) strongly suggests that the interaction between $CD_{6.6}$ does not occur at the larger rim. In addition, the signal of H-1 and H-2 are unaffected by the presence of DA, demonstrating that these protons do not participate in $CD_{6.6}$:DA interactions. Interestingly, one of the H-6 protons (diastereotopic H-6a proton) followed

an upfield shift as shown in Figure 6.19. Such a shift suggests that H-6a could be in proximity of the benzene ring. The local circulation of the electrons (from benzene ring) around H-6a causes a shielding effect (or magnetic anisotropic effect [38]). Thus, H-6a resonates at a relatively lower chemical shift in the presence of DA. Since the exterior proton H-4 closer to the narrow rim is also influenced (follows a slight downfield shift similar to that of H-5), it cannot be excluded the existence of interactions with external surface of the macrocycle.

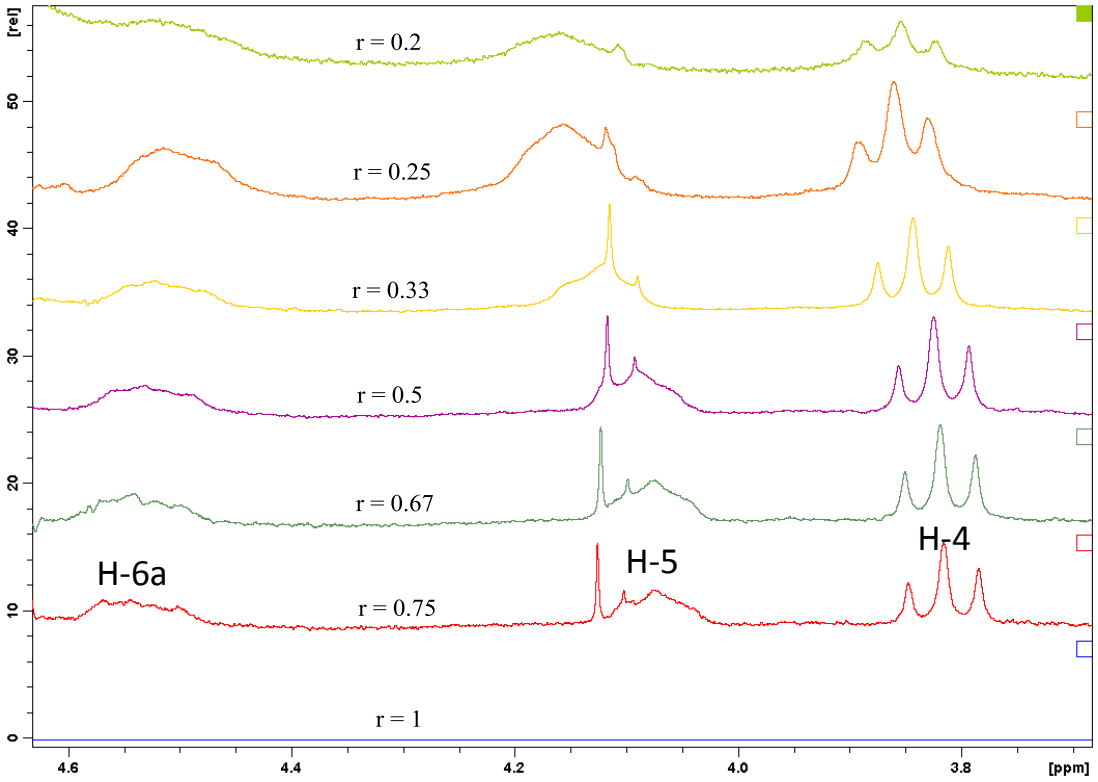

Figure 6.19: Expanded region of the part of ^{1}H-NMR spectra displaying $CD_{6.6}$ protons H-6a, H-5 and H-4 with respect to DA molar ratio.

In view of these data, it seems possible that the complexation between DA and $CD_{6.6}$ seems not to be governed by hydrophobic effect via the CD cavity but through interactions taking place closer to the triazole moiety at the narrow rim of the cavity, which offers an alternative hydrophobic environment to the guest DA and possibility for electrostatic and hydrogen bonding interactions.

As previously reported by Zia *et al* [42], chemical modification of β-CD with sulfobutylether substituents may provide supplementary binding sites for molecules capable of forming ionic interactions with the charged sulfate moieties. The author also mentioned that the charged sulfate groups on each β-CD are likely to repel one another

by extending out and away from each other, providing a hydrophobic region near the cavity. This additional hydrophobic region participates in the stabilisation of the complex. The same phenomenon is likely to happen in this study, where seven triazole moieties associated with fourteen carboxylate groups on each $CD_{6.6}$ allow stabilisation of the protonated DA molecule and seem to prevent somehow its (complete) penetration into the cavity. Therefore, the formation of several non-covalent weak forces, including electrostatic, hydrogen-bonding, Van der Waals and π-π interactions cooperatively contributes to the formation of the complex. The latter has been described by Karimov [43], where aromatic π-π stacking interactions between benzene and triazole rings are possible, as shown in Figure 6.20. In addition, the electronegative and sp^2 hybridized nitrogen atoms on each triazole unit could participate in hydrogen-bonding, further stabilising the complex.

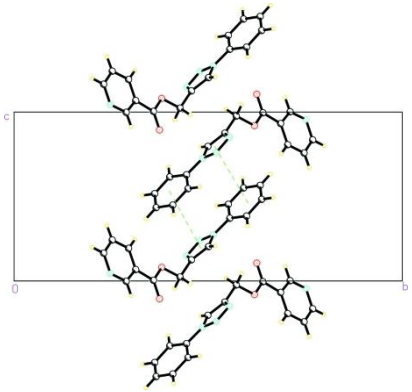

Figure 6.20: Part of the crystal structure showing a π-π stacking interactions observed between triazole and benzene ring [41].

Based on the above explanation, a plausible representation of the interaction between DA and $CD_{6.6}$ is shown in Scheme 6.6. More detailed NMR studies, alongside with crystallography and molecular modelling would be required for the determination of the precise structure of the complex.

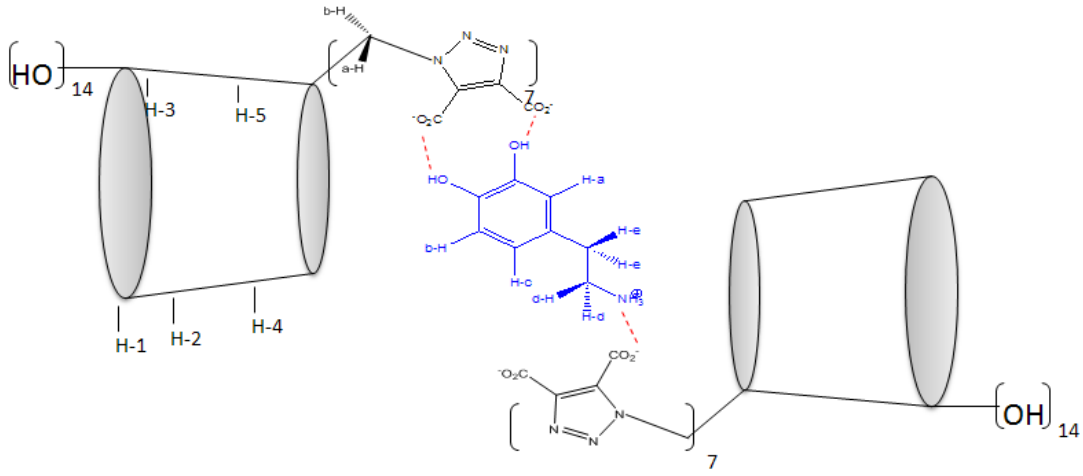

Scheme 6.6: Possible representation of the interaction between DA and $CD_{6.6}$.

(ii) $CD_{6.7}$:DA interaction

As already mentioned, the continuous variation method applied to proton H-b of DA showed a maximum at r = 0.5, indicating a complexation of 1:1 stoichiometry between $CD_{6.7}$ and DA. Therefore, one molecule of $CD_{6.7}$ interacts with another molecule of DA in solution. Although, $CD_{6.7}$ contains seven triazole moieties, this macrocycle is not charged. Unlike $CD_{6.6}$, an ion-ion interaction does not occur between the protonated DA and $CD_{6.7}$.

Analysis of chemical shift changes of H-a, H-b and H-c (as shown in Figure 6.15) revealed that these aromatic protons experienced different type of interactions to the ones described above. In the presence of $CD_{6.7}$, H-b is shifted to a high frequency, whereas H-c is shifted to a lower frequency. No significant shift is observed for H-a. The probable explanation for this observation is based on the fact that DA may adopt a conformation so that H-c is inserted into the cavity of $CD_{6.7}$. Thus, the chemical shift variation of H-c could be attributed to the shielding effect, due to the electron density inside the cavity. On the other side, H-b is probably positioned outside the cavity and may be deshielded by the effect of nitrogen atoms from the triazole moieties. The fact that H-a is practically unaffected remains unclear.

In the presence of $CD_{6.7}$, the DA aliphatic ethylene amine protons, H-e and H-d, are shifted slightly downfield (Figure 6.21). Therefore, it is more likely that these protons are outside the $CD_{6.7}$ cavity and exposed to the environment provided by the triazole moieties. It is worth mentioning that there is a fair degree of flexibility of the aliphatic

ethylene amine chain. The complex may be further stabilised by formation of hydrogen-bonding of the DA hydroxyl protons the free electron pairs on nitrogen atoms of the triazole group or with the hydroxymethilene on its side chain.

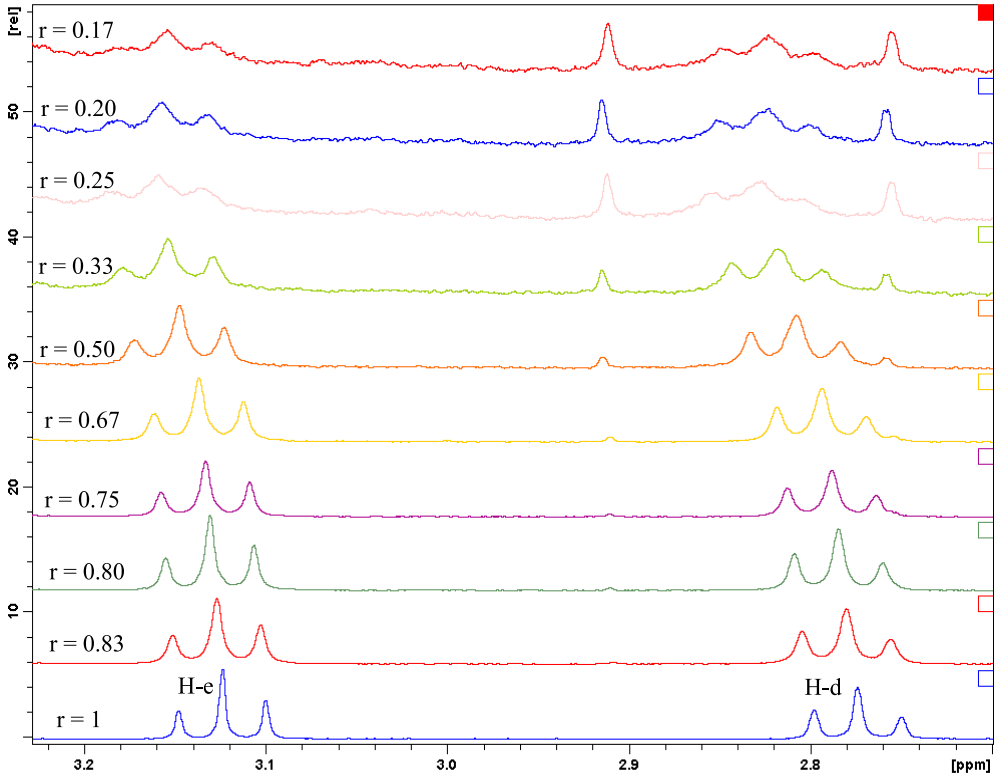

Figure 6.21: Expanded region of the ^{1}H-NMR spectra displaying DA aliphatic amine protons upon addition to $CD_{6.7}$.

The molecular interactions taking place between $CD_{6.7}$ and DA were further investigated by monitoring the chemical shifts of $CD_{6.7}$ protons. Because of the higher shielding effect on H-5 with respect to H-3, it could be assumed that H-c penetrates the $CD_{6.7}$ cavity from the lower rim. In addition, the external $CD_{6.7}$ protons (H-1, H-2 and H-4) remained essentially unchanged. However, the proton belonging to the triazole moiety experienced slight downfield shift variation as displayed in Figure 6.22. The magnitude of the shift difference for this proton is probably dependent on aromatic stacking interactions with the benzene ring in DA.

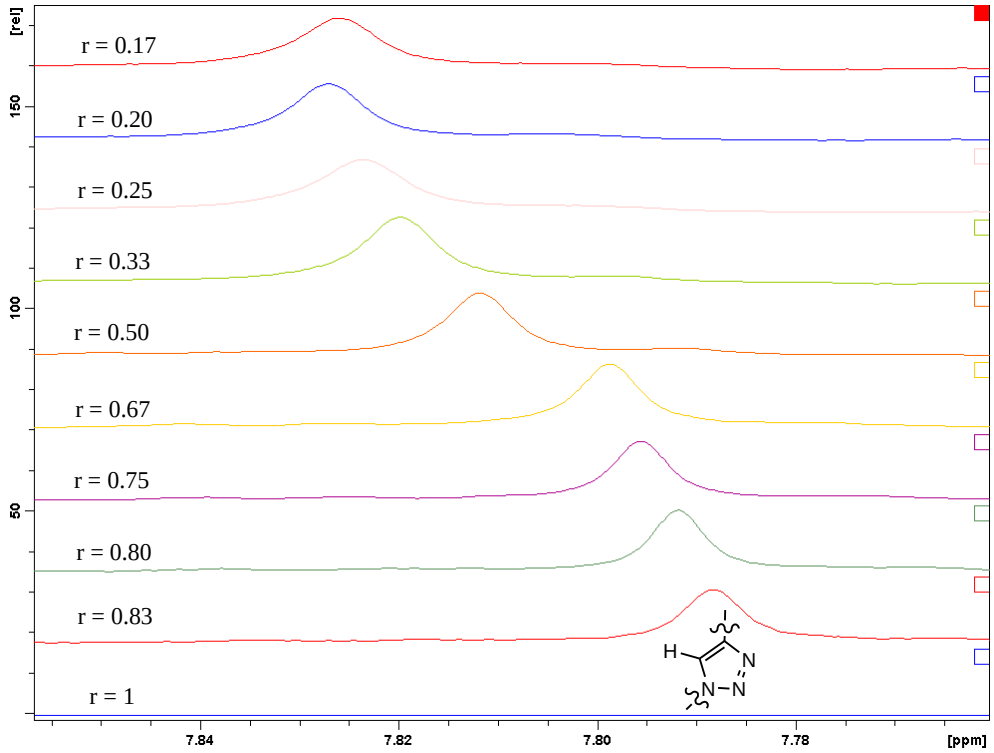

Figure 6.22: Expanded region of the part of ^{1}H-NMR spectra displaying triazole proton of $CD_{6.7}$ with respect to DA mole ratio.

Considering all above, it could be concluded that DA could be partially included into the $CD_{6.7}$ cavity. However, this complexation event seems to occur mostly through the triazole moiety. A series of interactions (hydrogen-bonding, π-π stacking, Van der Waals forces) may contribute to stabilise the complex. A plausible representation of the complexation is displayed in Scheme 6.7. As before, more detailed NMR studies, alongside with crystallography and molecular modelling would be required for the determination of the precise structure of the complex.

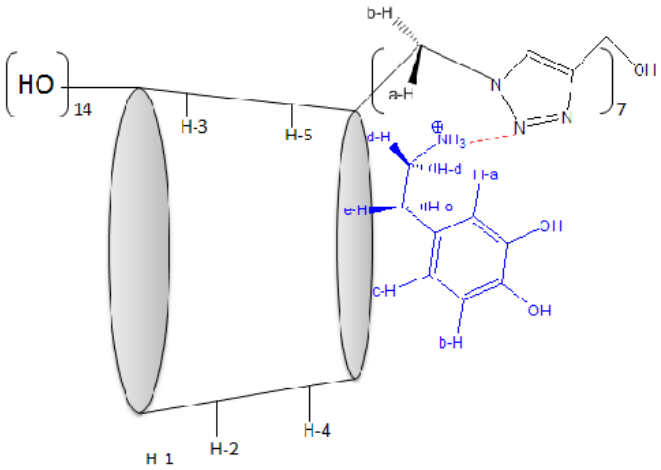

Scheme 6.7: Possible representation of the interaction between DA and $CD_{6.7}$.

There are abundant reports describing complexes between CDs and guests, showing an aromatic or hydrophobic moieties of a guest included into the CD cavity [33, 44, 45]. However, this study clearly presents a different mode of interaction. The aromatic group of DA interacts with $CD_{6.6}$ and $CD_{6.7}$ essentially via the triazole moieties. The involvement in the coordination of triazole (and / or carboxylate groups) to the cyclodextrin derivatives plays a crucial role in the complexation event; therefore, it appears important to evaluate the strength of the complex by calculation of the binding constant K_a.

6.2.4.4 Determination of binding constant, K_a

NMR spectroscopy is very well suited to study molecular complexes of weak and moderate strength. In particular, NMR titration has found tremendous success in the determination of binding constants for inclusion complexes formed between a variety of organic molecules and CDs [46-48]. NMR titrations were performed at a constant DA concentration (1×10^{-2} M) while increasing progressively the amount of cyclodextrin derivatives from 2.38×10^{-3} to 2.4×10^{-2} M and from 2.38×10^{-3} to 3.1×10^{-2} M for $CD_{6.7}$ and $CD_{6.6}$, respectively. Aliquots (20 µL) from a stock solution of the CDs (5×10^{-2} M) were titrated with 0.4 mL DA (1×10^{-2} M) in the NMR tube with aid of a microsyringe. The sample tube was shaken carefully after each addition and the ^{1}H-NMR spectra were recorded at ambient temperature. The spectra were recorded at a (relatively) constant time within 5 minutes after the addition of each CD aliquot and the chemical shifts were checked considering D_2O / H_2O (4.7 ppm) as reference sample.

Macomber's model [49] was used to evaluate the binding constants supposing that an equilibrium was reached between the DA and CD. Under "fast-exchange" conditions, the observed chemical shift change, Δδ, for a DA proton was expected to vary as a function of the CD molar ratio, R = [CD] / [DA], according to equation 6.1.

$$\boldsymbol{\delta = \delta_h - \left(\frac{\Delta\delta}{2}\right)\left(b - \sqrt{b^2 - 4R}\right)} \qquad \text{Equation 6.1}$$

where,

$$\boldsymbol{b = 1 + R + \frac{1}{K_a\,[DA]}} \qquad \text{Equation 6.2}$$

and, δ is the observed chemical shift in absence of CD and δ_h is the chemical shift observed in the presence of CD. Δδ is the chemical shift change, and R the molar ratio of CD.

Considering Equations 6.1 and 6.2, a value for K_a could be obtained from a non-linear curve fitting by plotting Δδ as a function of CD molar ratio, R. Sigmaplot 12.0 was used to generate the plot and determine a value for K_a.

(i) Binding constant (K_a) for $CD_{6.6}$:DA complex

In order to determine the $CD_{6.6}$:DA binding constant, the chemical shift of the proton H-b from DA was taken into account as this showed the highest chemical shift changes. In general, the chemical shift observed for H-b ($\Delta\delta_{(H\text{-}b)}$) is quite significant, which might indicate a moderate association constant. Table 6.6 displays $\Delta\delta_{(H\text{-}b)}$ and corresponding molar ratio of $CD_{6.6}$. $|\Delta\delta_{(H\text{-}b)}|$ was plotted as a function of the molar ratio of $CD_{6.6}$, R (Figure 6.23), and the value $K_a = 1.563 \times 10^7\ M^{-2}$ was extracted from the fitting procedure. Hemmateenejad *et al* [50] studied the inclusion complex formed between DA and neutral β-CD using a chronoamperometric technique. The authors found that DA formed a 1:1 complex, with K_a value of $2.1 \times 10^3\ M^{-1}$. Goa *et al* [51] reported an inclusion complex between DA and neutral β-CD using cyclic voltammetry technique. They found that the inclusion complex has a 1:1 stoichiometry, with a corresponding K_a value of $0.28 \times 10^3\ M^{-1}$. Although normally different K_a values for the same complexation event can be observed depending on the techniques used to measure it, the binding constant values obtained for complexation of DA by $CD_{6.6}$ seems too high and probably indicates that NMR is not the ideal technique to accurately measure the K_a value of this particular host-guest system at the described concentrations, The reason for this very high binding constant in this study is not certain. Ayling *et al* [52] reported that the dilution factor of host and guest species may be a key parameter for the accurate

determination of K_a, particularly for a powerful receptor. In fact, a significant concentration of unbound receptor must remain after one equivalent of substrate has been added, thus, the complex formation must not be essentially quantitative. This also implies that the sensitivity of the spectroscopic method employed determines the upper limit of K_a which can be measured. Therefore, the results obtained constitute a preliminary work on the binding constant studies and further experiments need to be performed in order to determine an accurate K_a value for complex formation between CD6.6 and DA.

Table 6.6: 1H-NMR chemical shift change of DA proton H-b in the presence of increasing concentration of $CD_{6.6}$

Aliquot No	$CD_{6.6}$ added (µL)	[DA] (M)	[$CD_{6.6}$] (M)	Molar ratio of $CD_{6.6}$ (equivalent)	$\lvert\Delta\delta_{(H\text{-}b)}\rvert$ from DA (ppm)
1	20	0.01	0.00238	0.238	0.0015
2	40	0.01	0.00455	0.455	0.0056
3	60	0.01	0.00652	0.652	0.00055
4	80	0.01	0.0083	0.83	0.00055
5	100	0.01	0.01	1	0.0025
6	120	0.01	0.012	1.2	0.0085
7	140	0.01	0.013	1.3	0.0147
8	160	0.01	0.014	1.4	0.0217
9	180	0.01	0.016	1.6	0.0256
10	200	0.01	0.017	1.7	0.0303
11	220	0.01	0.018	1.8	0.0354
12	240	0.01	0.019	1.9	0.0387
13	260	0.01	0.02	2.0	0.0437
14	280	0.01	0.021	2.1	0.0464
15	300	0.01	0.0214	2.14	0.0515
16	320	0.01	0.022	2.2	0.0547
17	340	0.01	0.023	2.3	0.0557
18	360	0.01	0.024	2.4	0.0596
19	380	0.01	0.0244	2.44	0.0621
20	400	0.01	0.025	2.5	0.0622
21	420	0.01	0.026	2.6	0.0623
22	440	0.01	0.0262	2.62	0.0623
23	460	0.01	0.027	2.7	0.0624
24	480	0.01	0.0272	2.72	0.0624
25	500	0.01	0.028	2.8	0.0624
26	520	0.01	0.029	2.9	0.0625
27	540	0.01	0.03	3	0.0626
28	560	0.01	0.03	3	0.0626
29	580	0.01	0.031	3.1	0.0627

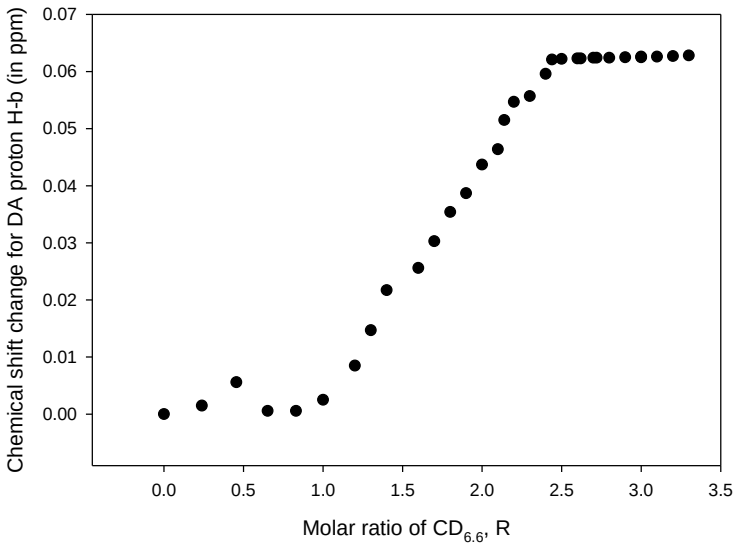

Figure 6.23: Non-linear regression fitting of experimental data for chemical shift changes of DA proton H-b as a function of $CD_{6.6}$ molar ratio.

(ii) Binding constant (K_a) for $CD_{6.7}$:DA complex

In the same manner as described above, the chemical shift changes of DA nuclei were monitored in the presence of added $CD_{6.7}$ while DA concentration was kept constant. The proton signals of H-b underwent the most prominent shifts. Table 6.7 displays $\Delta\delta_{(H\text{-}b)}$ and corresponding molar ratio of $CD_{6.7}$. The chemical shift change of H-b versus the molar ratio of $CD_{6.7}$ was plotted (Figure 6.24) and used for the determination of the binding constant, K_a. Non-linear analysis of the data points using Sigmaplot yields K_a = 2.538 M^{-1}. As opposed to what was observed for $CD_{6.6}$, this indicates a very weak complex formation between DA and of $CD_{6.7}$.

Table 6.7: 1H-NMR chemical shift change of DA proton H-b in the presence of increasing concentration of $CD_{6.7}$

Aliquot No	$CD_{6.7}$ added (μL)	[DA]	[$CD_{6.7}$]	Molar ratio of $CD_{6.7}$ (equivalent)	$\|\Delta\delta_{(H\text{-}b)}\|$ from DA (ppm)
1	20	0.01	0.00238	0.238	0.0037
2	40	0.01	0.00455	0.455	0.00775
3	60	0.01	0.00652	0.652	0.01155
4	80	0.01	0.0083	0.830	0.01485
5	100	0.01	0.0100	1.000	0.01725
6	120	0.01	0.012	1.2	0.0205
7	140	0.01	0.013	1.3	0.0225
8	160	0.01	0.014	1.4	0.0234
9	180	0.01	0.016	1.6	0.0261
10	200	0.01	0.017	1.7	0.0261
11	220	0.01	0.018	1.8	0.0265
12	240	0.01	0.019	1.9	0.0268
13	260	0.01	0.02	2.0	0.0276
14	280	0.01	0.021	2.1	0.0277
16	320	0.01	0.022	2.2	0.0281
18	360	0.01	0.024	2.4	0.0282

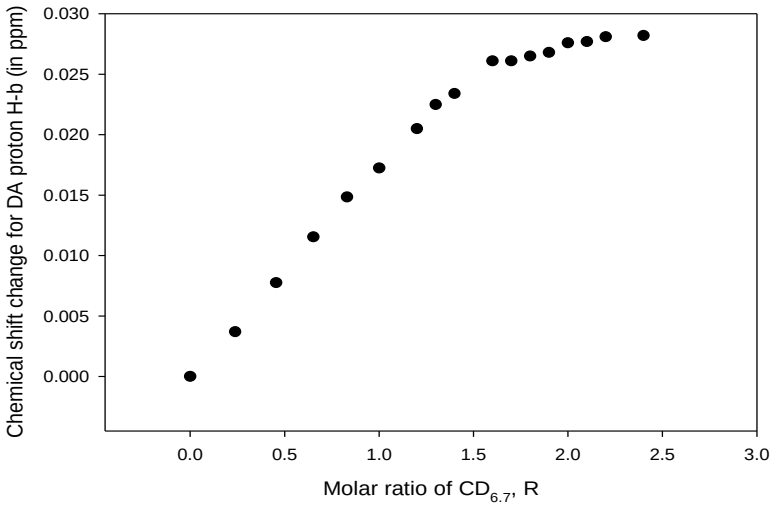

Figure 6.24: Non-linear regression fitting of experimental data for chemical shift changes of DA proton H-b as a function of $CD_{6.7}$ molar ratio..

The difference in the K_a values obtained from the analysis of the titrations of $CD_{6.6}$ and $CD_{6.7}$ are striking. Both modified CDs investigated in this study feature a relatively similar chemical structure, the main difference being the absence of anionic groups in

$CD_{6.7}$ capable of forming electrostatic interactions with protonated dopamine. These results highlight the importance of an appropriate design in the chemical structure of the host in order to achieve the molecular recognition necessary to form stable host-guest complexes.

6.3 DA Electrochemical Redox Process at Carbon Paste Modified with the Synthesised CD Derivatives

In Chapter 4, electrochemical performances of various types of carbon paste composite electrodes towards the detection of DA were examined. Overall, these modified CPEs showed a better DA detection compared to bare CPE. To further increase the analytic determination of DA, modified CPEs were prepared with cyclodextrin derivatives $CD_{6.6}$ and $CD_{6.7}$. As described in the previous sections, these cyclodextrins can form a complex with DA. Therefore, it was envisaged that a great electrochemical response of DA could be achieved by using $CD_{6.6}$ in particular, as this host seemed to form very stable complexes.

The $CD_{6.6}$ and $CD_{6.7}$ modified carbon paste electrode were prepared according to previously used procedure: 0.095 g of the cyclodextrin derivatives ($CD_{6.6}$ or $CD_{6.7}$), 200 µL of silicone oil and 0.71 g of graphite (or graphene) powder were hand-mixed in a mortar and ground carefully. The prepared homogeneous mixed paste was packed firmly into a Teflon holder (internal diameter = 2 mm), with a copper wire as the electrical contact. Prior to use, the modified electrode was polished on a piece of weighing paper.

The electrochemical behaviour of DA (5×10^{-5} M) at $CD_{6.7}$ modified CPE using cyclic voltammetry showed the detection of DA could not be obtained as illustrated in Figure 6.25. The cyclodextrin sample used for the construction of the working electrode may contain some impurities which hindered the access of DA at the electrode surface. It is worth mentioning that the synthesis of $CD_{6.7}$ was performed using copper iodide (CuI) as a catalyst. Although, the copper was removed by addition of the chelating resin Chelex 100 sodium form, $CD_{6.7}$ may still contain traces of copper, which complicate the detection of DA. Further investigations have to be carried out to determine how $CD_{6.7}$ could be used as an efficient modifier for the electrochemical detection of DA. Meanwhile, $CD_{6.6}$ show promising results and was subject to more attention.

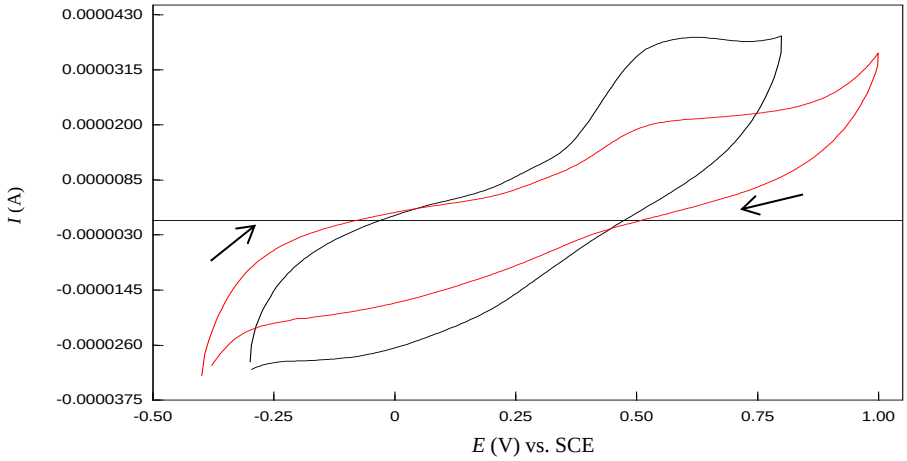

Figure 6.25: Cyclic voltammograms recorded at $CD_{6.7}$ in DA (5×10^{-5} M) (–) and in 0.1 M PBS (–); scan rate: 50 mV / s.

6.3.1 Electrochemical response of DA at $CD_{6.6}$

The voltammetric responses of bare CPE and $CD_{6.6}$ modified CPE towards the detection of DA were compared by cyclic voltammetry as illustrated in Figure 6.26, which shows typical cyclic voltammograms of 5×10^{-5} M DA solution in 0.1 M PBS (pH 6.8) using the potential range [−0.2 V; +0.6 V].

The oxidation peak potential (E_{pa} = 0.165 V vs. SCE) of DA at $CD_{6.6}$ modified CPE is a more negative than the oxidation peak potential observed at bare CPE (E_{pa} = 0.220 V vs. SCE). This peak potential shift may be attributed to $CD_{6.6}$ molecules on the surface of the electrode with high supramolecular recognition capability which can form complexes with DA. The complexation action may further enhance the accumulation effect of $CD_{6.6}$ modified CPE and consequently increase the concentration of DA on the interface of the modified electrode. As a result, DA oxidation peak current is greatly enhanced (about 1.7 times). This phenomenon based on recognition capability of cyclodextrin was also reported by Alarcon-Angeles *et al* [11]. The DA sensor developed by the authors was a glassy carbon electrode modified with β-CD and multiwall carbon nanotubes (MWCNT). β-CD was used as molecular receptor to immobilised DA into its cavity. Thus, an enhancement in DA oxidation peak current was observed at the modified electrode.

Moreover, the cyclic voltammogram of DA (5×10^{-5} M) at $CD_{6.6}$ modified CPE revealed that the peak potential separation, $\Delta E_p = E_{pa} - E_{pc}$, was 31 mV. Therefore, ΔE_p is close to $2.3RT/nF$ (or $59/n$ mV at 25 °C) [53], which is in accordance with a Nernst

reversible behaviour. Thus, the number of electrons, *n*, involved in the reaction was about 2.

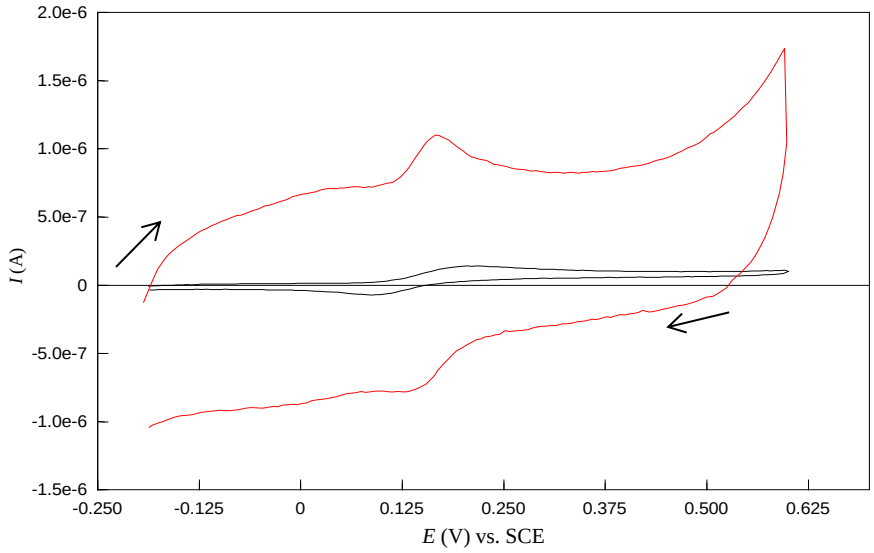

Figure 6.26: Cyclic voltammograms recorded at $CD_{6.7}$ in DA (5×10^{-5} M) (–) and in 0.1 M PBS (–); scan rate: 50 mV / s.

A charged cyclodextrin could also interact with DA via ion pairing interaction. For example, Colleran *et al* [54] used PEDOT/S-β-CD modified gold electrodes for electrochemical detection of DA, in which the mode of sensing at this electrode was based on the ability of S-β-CD to form electrostatic or ion-pairing interaction between randomly sulfated groups on the cyclodextrin and protonated DA.

Although in solution $CD_{6.6}$ forms a 2:1 inclusion complex with DA (as previously demonstrated), it is difficult to determine the exact mode of sensing at the modified electrode surface. $CD_{6.6}$ molecules are immobilised at the surface of the electrode. Therefore, the ability of 2 $CD_{6.6}$ molecules to interact with one DA is not obvious. The most possible interactions are the occurrence of ion-pairing between the anionic carboxylate groups on $CD_{6.6}$ and the cationic protonated DA, and π-π stacking interaction between triazole moieties on $CD_{6.6}$ and aromatic benzene moiety of DA.

To support the evidence of DA accumulation at the surface of the modified electrode through ion-pairing and π-π stacking interaction it is important to study the reaction kinetics.

6.3.1.1 Effect of scan rate of DA at $CD_{6.6}$ modified CPE

The influence of scan rate on DA oxidation at the $CD_{6.6}$ modified CPE was investigated by cyclic voltammetry. It can be observed (from Figure 6.27) that the oxidation peak currents of DA (5×10^{-5} M) were linearly proportional to the scan rate. The linear

regression equation is such as I_{pa} (A) = 3.7988 × 10^{-9} ν + 1.7956 × 10^{-7} with a correlation coefficient, R^2, 0.9934. The equations indicate that the electro-oxidative reaction of DA on the surface of the electrode is adsorption-controlled process. This behaviour points out that electron transfer occurred differently at the modified electrode with respect to the bare CPE. Therefore, this electrochemical evidence strongly suggests a complexation event between the DA and the $CD_{6.6}$ immobilized at the surface of the CPE.

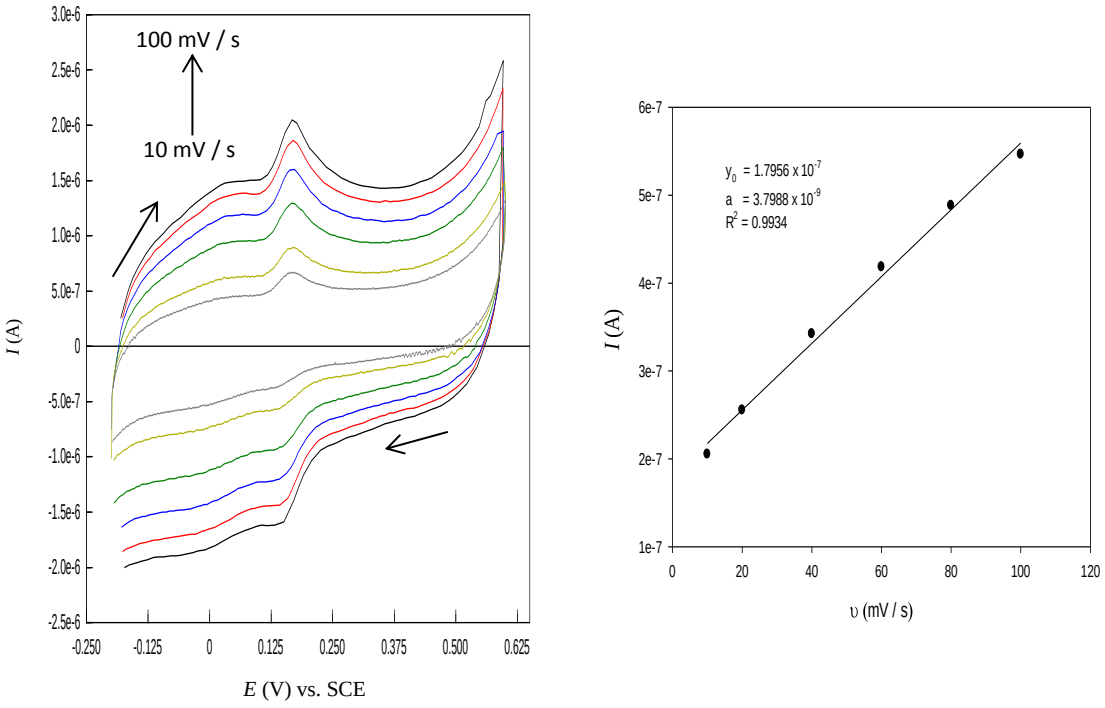

(a) (b)

Figure 6.27: Cyclic voltammograms for the effect of variation of scan rates of DA (5 × 10^{-5} M) at $CD_{6.6}$ modified CPE from 10 to 100 mV / s (a) and corresponding variation of oxidation peak current as a function of scan rate (b). Supporting electrolyte 0.1 M PBS (pH 6.8).

6.3.1.2 Electrochemical quantification of DA at $CD_{6.6}$ modified CPE

Cyclic voltammetry was used to determine the relationship between the oxidation peak current and concentration of DA on $CD_{6.6}$ modified CPE. As shown in Figure 6.28, under optimal conditions, the oxidation peak current of DA increased with its concentration in the range from 5 × 10^{-6} M to 1 × 10^{-3} M. Therefore, $CD_{6.6}$ modified CPE can be used to determine DA in this concentration range.

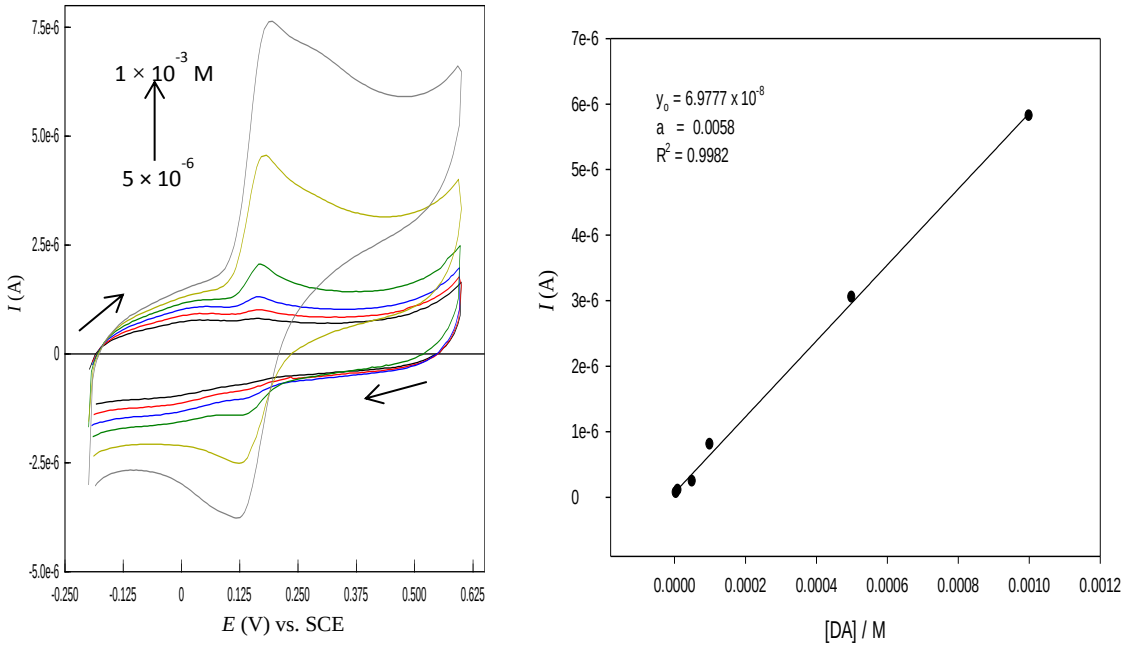

(a) (b)

Figure 6.28: Cyclic voltammograms of the application of various concentration of DA (from 5 × 10^{-5} M to 1 × 10^{-3} M) recorded at $CD_{6.6}$ modified CPE (a) and corresponding calibration curve (b). Supporting electrolyte 0.1 M PBS (pH 6.8).

Because differential pulse voltammetry (DPV) exhibits higher sensitivity compared with cyclic voltammetry, it was used to detect micro-molar concentration of DA on $CD_{6.6}$ modified CPE. The voltammograms presented in Figure 6.29 show that it is possible to detect DA concentrations low as 5 × 10^{-6}, 1 × 10^{-6} and more importantly 5 × 10^{-7} M.

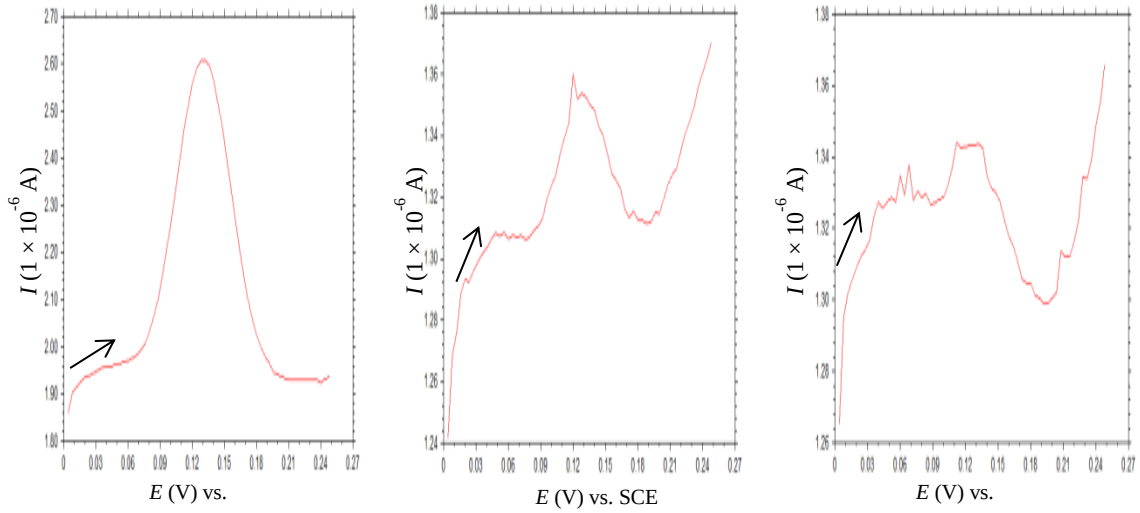

(a) (b) (c)

Figure 6.29: Differential pulse voltammograms recorded at CD6.6 modified CPE in 0.1 M PBS containing DA concentration of 5 × 10^{-6} M (a), 1 × 10^{-6} M (b) and 5 × 10^{-7} M.

6.3.1.3 Electrochemical detection of DA at carbon paste microelectrodes

Since the early work of Adams *et al* [123, 124] which introduced electrochemistry to neuroscience, numerous electrochemical techniques and electrode materials have been used to determine catecholamines including DA.

So far, CPEs of conventional macro-size dimension modified with S-β-CD, CM-β-CD or nafion have been used for electroanalysis of DA. However, in this section, carbon paste microelectrode is employed in order to improve the detection limit of DA. The small area of carbon paste microelectrodes means that the background or capacitive current is low in comparison to the faradaic current so that the signal to noise (S/N) could be enhanced. This feature allows measurements of analytes at lower concentrations.

In many literature reports, the measurement of DA with microelectrodes is made using cyclic voltammetry technique on a 3-electrodes potentiostat. As already stated, DPV gives better sensitivity; therefore, this method was performed to investigate the relationship between the peak current and the concentrations of DA. The general procedure for the construction of chemically modified carbon paste microelectrode was described in Chapter 2. In the case $CD_{6.6}$, 0.095 g was mixed with graphene (0.71 g) and silicone oil (200 µL). Figure 6.30(a) shows the differential pulse voltammograms of increasing DA concentrations on a carbon paste microelectrode modified with $CD_{6.6}$. One important observation is that well-defined oxidation peaks are obtained. Moreover, the oxidation peak currents increase as increasing the concentration of DA. Remarkably, the detection of 3×10^{-7} M DA was achieved, which is highlighted in Figure 6.30(b). This confirms that $CD_{6.6}$ modified carbon paste microelectrode has promising results concerning the electrochemical behaviour of DA. The oxidation peak current of DA is linear to its concentration in the range from 3×10^{-7} to 5×10^{-4} M. The regression equation can be demonstrated as: I_{pa} (A) = 0.0028 $_{[DA]}$ + 3.1575×10^{-8} (R^2 = 0.9934) (Figure 6.30(c)). The detection limit was calculated as 3.76×10^{-5} M. As already stated, the detection limit was calculated by using the formula LOD = $3S_b/m$ criteria [55], where S_b is the standard deviation of the blank response for n = 3 and m is the slope obtained from the calibration plot.

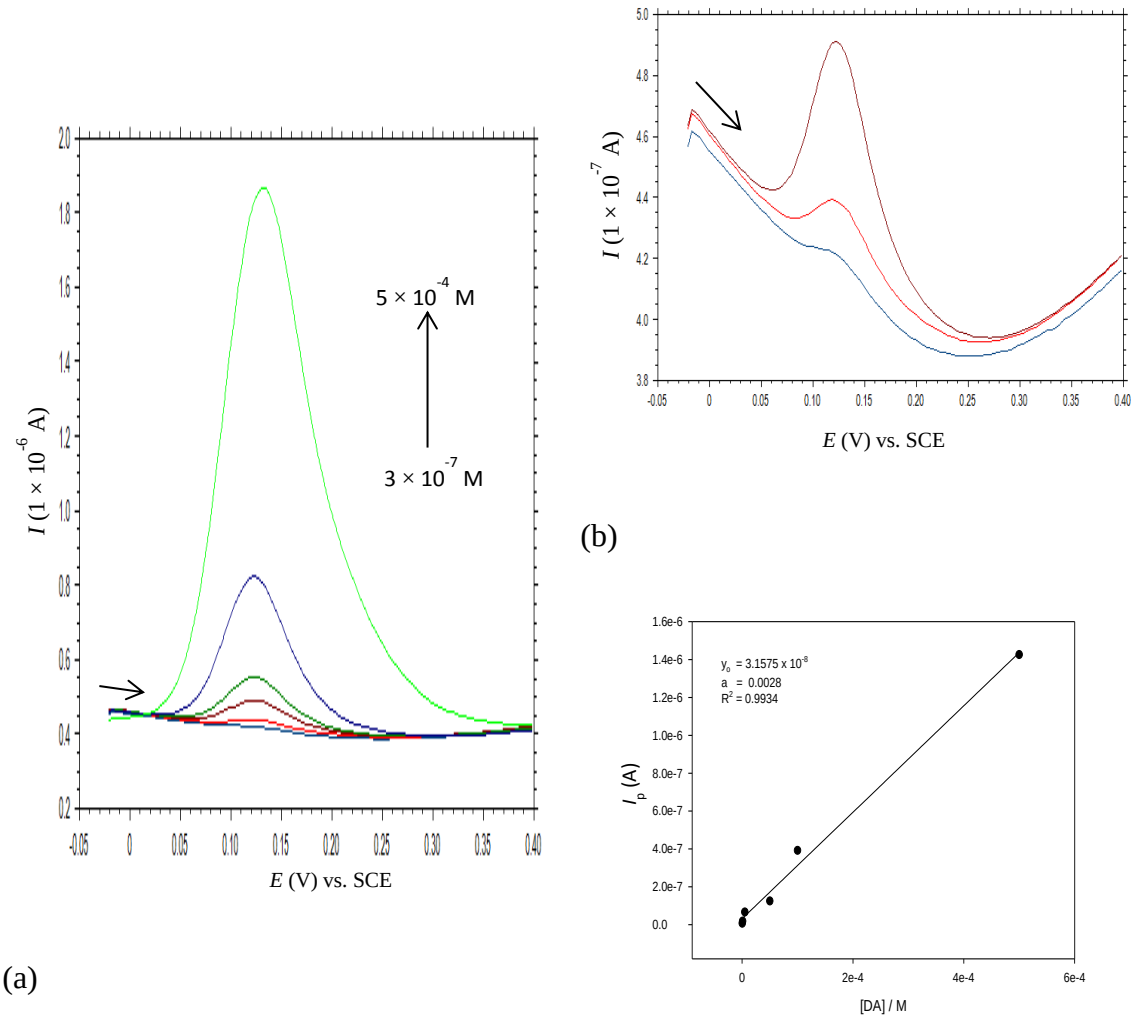

Figure 6.30: Differential pulse voltammograms recorded at $CD_{6.6}$ modified carbon paste microelectrode in 0.1 M PBS containing different concentrations of DA (from 3×10^{-7} M to 3×10^{-4} M) (a) and enlarged voltammograms of 3×10^{-7} M (–), 5×10^{-7} M (–) and 1×10^{-6} M (–) DA (b). The corresponding calibration curve of oxidation current (c); scan rate: 50 mV / s.

Based on the above results, it is more likely that the use of carbon paste microelectrode (modified with $CD_{6.6}$) can be advantageous to macroelectrode for DA measurement. This is probably related to the size of microelectrodes. In fact, when the diameter of an electrode is decreased from the millimetre scale down to micron scale, radial diffusion of the electroactive species towards the electrode surface becomes more dominant rather than linear diffusion. The microelectrode produces a greater signal-to-background ratio due to radial diffusion [56-58]. Therefore, reducing the size of the electrode increases the mass flux and hence there is more analyte at the interface. This difference in behaviour is illustrated in Figure 6.31.

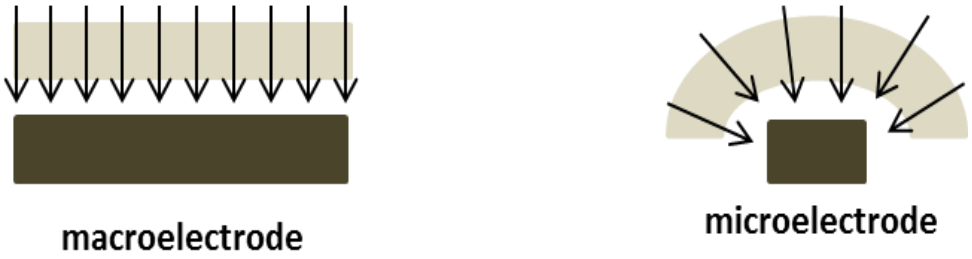

Figure 6.31: Schematic illustration of linear diffusion at a macroelectrode and radial diffusion at a microelectrode.

A number of microelectrodes were then constructed in order to compare their DA oxidative response with $CD_{6.6}$ modified carbon paste microelectrode. Figure 6.32 shows the determination of DA and corresponding calibration curves obtained at bare GPE, S-β-CD (0.545 g) modified GPE and Nafion modified CPE. Their limit of detection and linear range are presented in Table 6.8. It can be noted from Table 6.8 that the sensitivity and detection limit obtained using these modified carbon paste microelectrode are inferior than the corresponding sensitivity and detection limit obtained at $CD_{6.6}$ modified carbon paste microelectrode. The wide linear range and the good sensitivity might be attributed to the properties of $CD_{6.6}$ modified GPE, such as the excellent recognition effect and ion-pairing capacity due to $CD_{6.6}$, and acceleration of electron transfer provided by graphene. Thus, the combination of $CD_{6.6}$ and graphene as a composite material can greatly improve the sensitivity because electrochemical detection of DA is inner sphere, surface dependent, and kinetically dominated by adsorption processes at the electrode surface [59, 60].

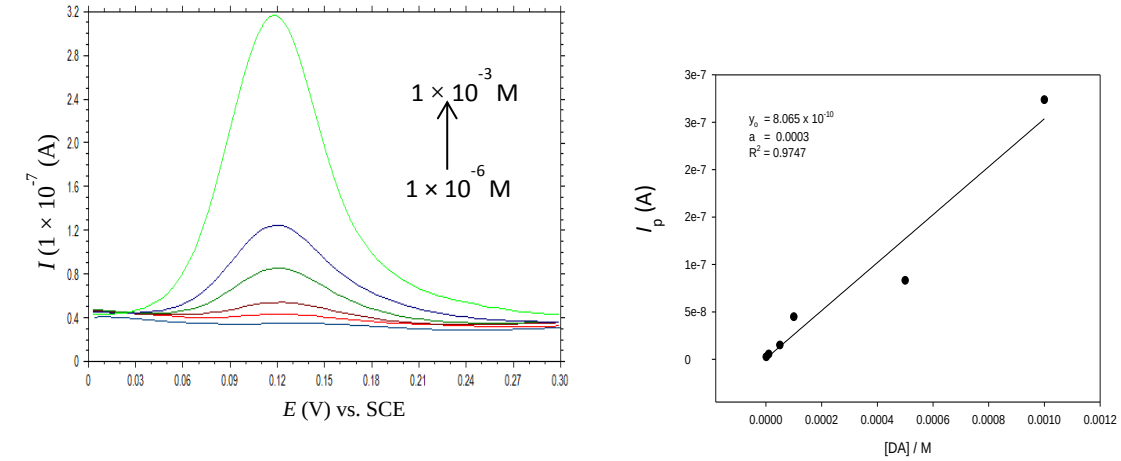

(a)

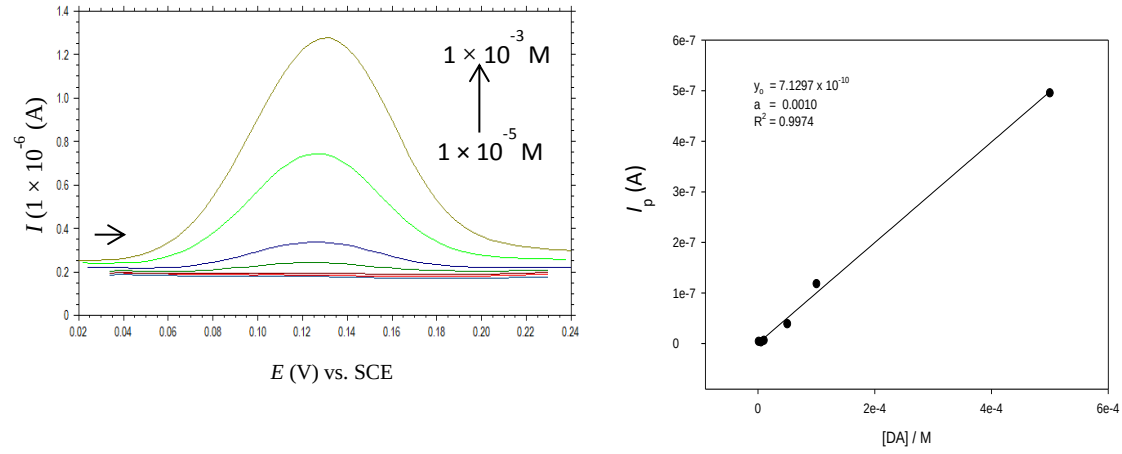

(b)

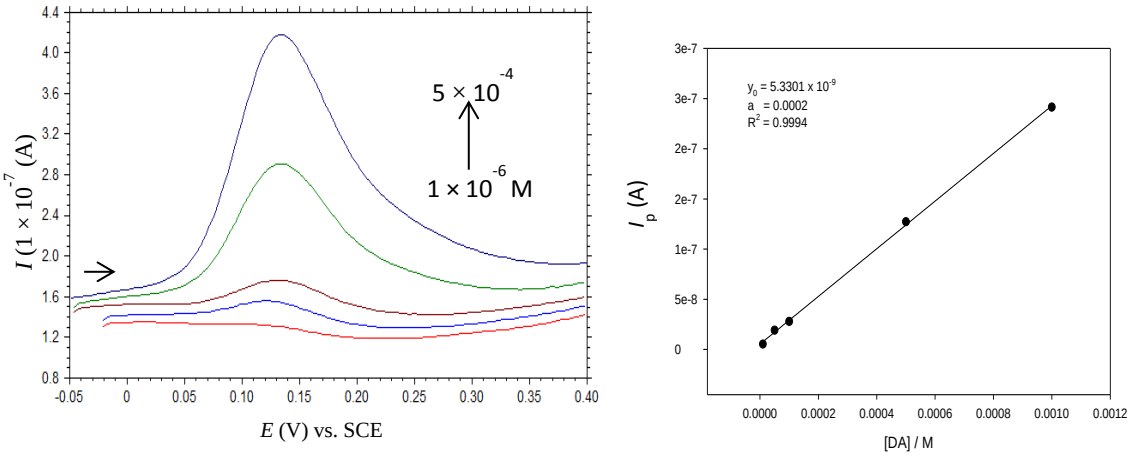

(c)

Figure 6.32: Differential pulse voltammograms recorded at three microelectrodes modified CPE in 0.1 M PBS containing different concentrations of DA: Bare GPE with corresponding calibration curve (a), S-β-CD (0.545 g) modified GPE with corresponding calibration curve and Nafion modified CPE with corresponding calibration curve (c); scan rate: 50 mV / s.

Table 6.8: Limit of detection and linear dynamic range for the microelectrodes studied

Microelectrode	LOD (M)	Linear range (M)
Bare GPE	6.78×10^{-6}	$[1 \times 10^{-6} - 1 \times 10^{-3}]$
S-β-CD (0.545 g) modified GPE	3.61×10^{-5}	$[1 \times 10^{-5} - 1 \times 10^{-3}]$
Nafion modified CPE	3.22×10^{-4}	$[1 \times 10^{-6} - 5 \times 10^{-4}]$

6.3.1.4 Electrochemical investigation of a mixture of AA and DA at $CD_{6.6}$ modified CPE

As already mentioned, the selective determination of DA in the presence of AA is still a major challenge in biological analysis. This goal has been achieved using S-β-CD modified CPE with an internal diameter of 2 mm (Chapter 5). The electrochemical behaviour of $CD_{6.6}$ modified CPE in a mixture of AA and DA was carried out. The aim of this section is to separate the overlapping signals of AA and DA normally observed at bare CPE and eventually use the microelectrode modified with $CD_{6.6}$ to obtain the same result.

Like $CD_{6.6}$, S-β-CD is negatively charged and may be able to discriminate the signal of AA and DA. Figure 6.33 indicates the cyclic voltammogram of $CD_{6.6}$ modified CPE in a mixed solution of AA (1×10^{-3} M) and DA (5×10^{-5} M). Although, the oxidation and reduction peaks of DA are relatively small, they can be identified as they appeared at 0.182 and 0.160 V vs. SCE respectively. The irreversible peak of AA seems not to be present, leading to the assumption that AA was partially rejected at the electrode surface. Unexpectedly, a broad signal was observed at about 0.282 V vs. SCE. Although further studies need to be done to clarify the origin of this peak, it has to be noted that the electrode contains only 0.095 g of $CD_{6.6}$. An optimisation of $CD_{6.6}$ concentration within the paste can lead to an effective discrimination of DA signal in the presence of an excess AA.

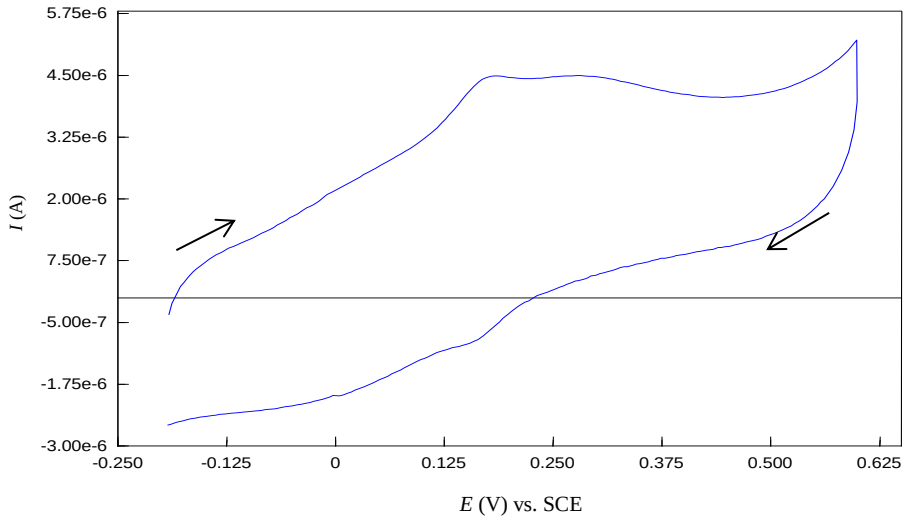

Figure 6.33: Schematic illustration of linear diffusion at a macroelectrode and radial diffusion at a microelectrode.

As discussed in Chapter 5, S-β-CD modified CPE is able to differential the electrochemical signal of AA and DA. Therefore, this electrode was miniaturised to investigate a solution of DA coexisting with AA.

6.3.1.5 Electrochemical investigation of a mixture of AA and DA at S-β-CD (0.545 g) modified carbon paste microelectrode

The development of selective method for simultaneous detection of DA and AA in brain fluid is highly desirable for analytical applications and for diagnostic research [61, 62]. To mimic the extracellular space of the brain, artificial cerebrospinal fluid (aCSF) was used instead of PBS as supporting electrolytes solution. The cyclic voltammetric response of aCSF containing a mixture of AA (1×10^{-3} M) and DA (5×10^{-5} M) was recorded at S-β-CD modified carbon paste microelectrode as illustrated in Figure 6.34. As can be seen, two well-defined oxidation peaks occurred at 0.141 V and 0.378 V vs. SCE which correspond to the oxidation of AA and DA, respectively. It is also important to note that the oxidation and reduction peak for DA occurred almost at the same potential (ΔE_p = 0.019 vs. SCE) indicating a high reversibility.

The mechanism behind the oxidation of DA and AA might be resulted from the nature of the electrode as discussed previously in Chapter 5. However, the potential separation between AA and DA (0.237 V vs. SCE) is larger than that of the same electrode at a macro-scale. Again, the radial diffusion of both analytes at the electrode surface may be an advantage using size microelectrode.

The large separation of the peak potential allows simultaneous detection of AA and DA in their mixture. This impressing result could be exploited for *in vivo* measurement of DA using S-β-CD carbon paste microelectrode.

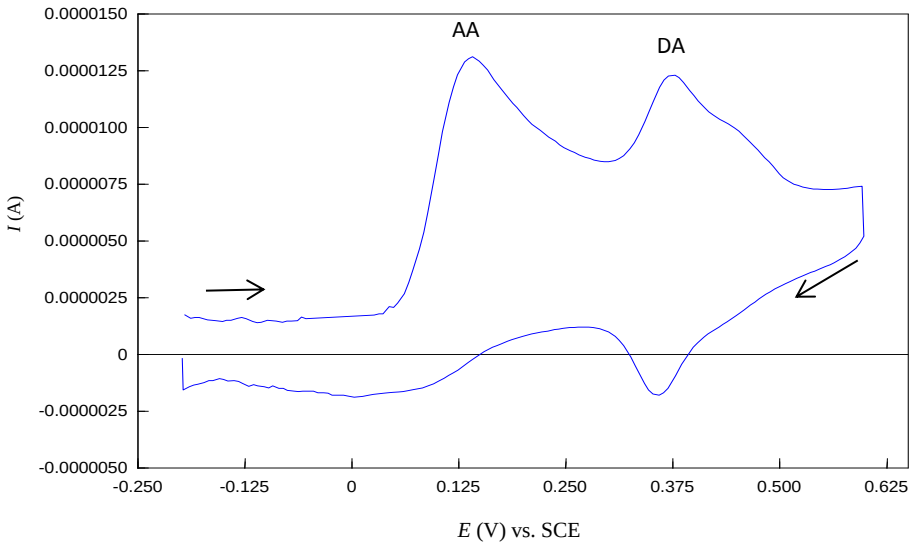

Figure 6.34: Cyclic voltammogram recorded at S-β-CD modified CPE in aCSF containing a mixture of DA (5×10^{-5} M) and AA (1×10^{-3} M). Scan rate: 50 mV / s.

6.4 References

1. Cunningham, K., et al., *Sodium-Selective Membrane-Electrode Based on P-Tert-Butylcalix[4]Arene Methoxyethylester.* Analyst, 1993. **118**(4): p. 341-345.

2. Miyaji, H., et al., *Anthracene-linked calix[4]pyrroles: fluorescent chemosensors for anions.* Chemical Communications, 1999(17): p. 1723-1724.

3. Gutsche, C.D., et al., *Calixarenes .4. The Synthesis, Characterization, and Properties of the Calixarenes from Para-Tert-Butylphenol.* Journal of the American Chemical Society, 1981. **103**(13): p. 3782-3792.

4. Gokel, G.W., Leevy, W.M., and Weber, M.E., *Crown ethers: Sensors for ions and molecular scaffolds for materials and biological models.* Chemical Reviews, 2004. **104**(5): p. 2723-2750.

5. Geraci, C., et al., *Cation encapsulation within a ten-oxygen spheroidal cavity of conformationally preorganized 1,5-3,7-calix[8]bis-crown-3 derivatives.* Chemical Communications, 1997(10): p. 921-922.

6. Lai, G.S., Zhang, H.L., and Jin, C.M., *Electrocatalysis and voltammetric determination of dopamine at a calix[4]arene crown-4 ether modified glassy carbon electrode.* Electroanalysis, 2007. **19**(4): p. 496-501.

7. Aslanoglu, M., et al., *Electrochemical determination of dopamine in the presence of ascorbic acid using a poly(3-acetylthiophene) modified glassy carbon electrode.* Acta Chimica Slovenica, 2007. **54**(4): p. 834-839.

8. Doyle, R., Breslin, C.B., and A.D. Rooney, A.D., *A Simple But Highly Selective Electrochemical Sensor for Dopamine.* Chemical and Biochemical Engineering Quarterly, 2009. **23**(1): p. 93-98.

9. Astray, G., et al., *A review on the use of cyclodextrins in foods.* Food Hydrocolloids, 2009. **23**(7): p. 1631-1640.

10. Chawla, H.M., Srinivas, K., and Meena, *Calix(N)Arene-Quinone Interactions - Molecular Recognition of 2,6-Naphthoquinone by 5,11,17,23,29,35-Hexa-Tert-Butyl-37,38,39,40,41,42-Hexahydroxycalix(6)Arene.* Tetrahedron, 1995. **51**(9): p. 2709-2718.

11. Alarcon-Angeles, G., et al., *Enhanced host-guest electrochemical recognition of dopamine using cyclodextrin in the presence of carbon nanotubes.* Carbon, 2008. **46**(6): p. 898-906.

12. Ueno, A. and Breslow, R., *Selective Sulfonation of a Secondary Hydroxyl Group of Beta-Cyclodextrin.* Tetrahedron Letters, 1982. **23**(34): p. 3451-3454.

13. Roehri Stoeckel, C., Dangles, O., and Brouillard, R., *A simple synthesis of a highly water soluble symmetrical beta-cyclodextrin derivative.* Tetrahedron Letters, 1997. **38**(9): p. 1551-1554.

14. Kim, H.Y., et al., *Click synthesis of estradiol-cyclodextrin conjugates as cell compartment selective estrogens.* Bioorganic & Medicinal Chemistry, 2010. **18**(2): p. 809-821.

15. Kolb, H.C., Finn, M.G., and Sharpless, K.B., *Click chemistry: Diverse chemical function from a few good reactions.* Angewandte Chemie-International Edition, 2001. **40**(11): p. 2004-2021.

16. Chen, L., et al., *Synthesis and chromatographic properties of a novel chiral stationary phase derived from heptakis(6-azido-6-deoxy-2,3-di-O-phenylcarbamoylated)-beta-cyclodextrin immobilized onto amino-functionalized silica gel via multiple urea linkages.* Journal of Chromatography A, 2002. **950**(1-2): p. 65-74.

17. Himo, F., et al., *Copper(I)-catalyzed synthesis of azoles. DFT study predicts unprecedented reactivity and intermediates.* Journal of the American Chemical Society, 2005. **127**(1): p. 210-216.

18. Ahlquist, M. and Fokin, V.V., *Enhanced reactivity of dinuclear Copper(I) acetylides in dipolar cycloadditions.* Organometallics, 2007. **26**(18): p. 4389-4391.

19. Ashton, P.R., et al., *Amino acid derivatives of beta-cyclodextrin.* Journal of Organic Chemistry, 1996. **61**(3): p. 903-908.

20. Tian, W.Q. and Wang, Y.A., *Mechanisms of Staudinger reactions within density functional theory.* Journal of Organic Chemistry, 2004. **69**(13): p. 4299-4308.

21. Douhal, A., *Ultrafast guest dynamics in cyclodextrin nanocavities.* Chemical Reviews, 2004. **104**(4): p. 1955-1976.

22. Szejtli, J., *Introduction and general overview of cyclodextrin chemistry.* Chemical Reviews, 1998. **98**(5): p. 1743-1753.

23. Messner, M., et al., *Self-assembled cyclodextrin aggregates and nanoparticles.* International Journal of Pharmaceutics, 2010. **387**(1-2): p. 199-208.

24. Davis, M.E. and Brewster, M.E., *Cyclodextrin-based pharmaceutics: Past, present and future.* Nature Reviews Drug Discovery, 2004. **3**(12): p. 1023-1035.

25. Schneider, H.J., et al., *NMR studies of cyclodextrins and cyclodextrin complexes.* Chemical Reviews, 1998. **98**(5): p. 1755-1785.

26. Alexander, J.M., et al., *Chiral discrimination in cyclodextrin complexes of amino acid derivatives: beta-cyclodextrin/N-acetyl-L-phenylalanine and N-acetyl-D-phenylalanine complexes.* Proceedings of the National Academy of Sciences of the United States of America, 2002. **99**(8): p. 5115-5120.

27. Li, S. and Purdy, W.C., *Cyclodextrins and Their Applications in Analytical-Chemistry.* Chemical Reviews, 1992. **92**(6): p. 1457-1470.

28. Dondon, W. and Fery-Forgues, S., *Inclusion complex of fluorescent 4-hydroxycoumarin derivatives with native beta-cyclodextrin: Enhanced stabilization induced by the appended substituent.* Journal of Physical Chemistry B, 2001. **105**(43): p. 10715-10722.

29. Abdel-Shafi, A.A., *Effect of beta-cyclodextrin on the excited state proton transfer in 1-naphthol-2-sulfonate.* Spectrochimica Acta Part a-Molecular and Biomolecular Spectroscopy, 2001. **57**(9): p. 1819-1828.

30. Mucci, A., et al., *One- and two-dimensional NMR study of complexation of ursodeoxycholic acid with beta-cyclodextrin.* Journal of the Chemical Society-Perkin Transactions 2, 1996(11): p. 2347-2349.

31. Yamamoto, Y. and Y. Inoue, Y., *Nmr-Studies of Cyclodextrin Inclusion Complex.* Journal of Carbohydrate Chemistry, 1989. **8**(1): p. 29-46.

32. Zhou, Y.Y., et al., *A preliminary investigation of the complexation of dopamine by p-sulfonated calix[4,6] arene and beta-cyclodextrin using fluorescence spectrometry.* Spectroscopy Letters, 2006. **39**(5): p. 409-420.

33. Hendy, G.M. and Breslin, C.B., *A spectrophotometric and NMR study on the formation of an inclusion complex between dopamine and a sulfonated cyclodextrin host.* Journal of Electroanalytical Chemistry, 2011. **661**(1): p. 179-185.

34. Domenech, A., et al., *2,4,6-triphenylpyrylium ion encapsulated into zeolite Y as a selective electrode for the electrochemical determination of dopamine in the presence of ascorbic acid.* Analytical Chemistry, 2002. **74**(3): p. 562-569.

35. Clark, J.L., Booth, B.R., and Stezowski, J.J., *Molecular recognition in cyclodextrin complexes of amino acid derivatives. 2. A new perturbation: The room-temperature crystallographic structure determination for the N-acetyl-p-methoxy-L-phenylalanine methyl ester/beta-cyclodextrin complex.* Journal of the American Chemical Society, 2001. **123**(40): p. 9889-9895.

36. Makedonopoulou, S., et al., *Organisation of long aliphatic monocarboxylic acids in beta-cyclodextrin channels: crystal structures of the inclusion complexes of tridecanoic acid and (Z)-tetradec-7-enoic acid in beta-cyclodextrin.* Chemical Communications, 1998(19): p. 2133-2134.

37. Braga, S.S., et al., *Solid state inclusion compound of S-ibuprofen in beta-cyclodextrin: structure and characterisation.* New Journal of Chemistry, 2003. **27**(3): p. 597-601.

38. Greatbanks, D. and Pickford, R., *Cyclodextrins as Chiral Complexing Agents in Water, and Their Application to Optical Purity Measurements.* Magnetic Resonance in Chemistry, 1987. **25**(3): p. 208-215.

39. Ingham, K.C., *Application of Jobs Method of Continuous Variation to Stoichiometry of Protein-Ligand Complexes.* Analytical Biochemistry, 1975. **68**(2): p. 660-663.

40. Djedaini, F., et al., *High-Field Nuclear-Magnetic-Resonance Techniques for the Investigation of a Beta-Cyclodextrin-Indomethacin Inclusion Complex.* Journal of Pharmaceutical Sciences, 1990. **79**(7): p. 643-646.

41. Zornoza, A., et al., *Inclusion complexation of glisentide with alpha-, beta- and gamma-cyclodextrins.* International Journal of Pharmaceutics, 1998. **169**(2): p. 239-244.

42. Zia, V., Rajewski, R.A., and Stella, V.J., *Effect of cyclodextrin charge on complexation of neutral and charged substrates: Comparison of (SBE)(7M)-beta-CD to HP-beta-CD.* Pharmaceutical Research, 2001. **18**(5): p. 667-673.

43. Karimov, Z., et al., *(1-Phenyl-1H-1,2,3-triazol-4-yl)methyl pyridine-3-carboxylate.* Acta Crystallographica Section E-Structure Reports Online, 2010. **66**: p. O1674-U311.

44. Liu, Y., et al., *Interaction between beta-cyclodextrin and 1,10-phenanthroline: uncommon 2 : 3 inclusion complex in the solid state.* Carbohydrate Research, 2004. **339**(9): p. 1649-1654.

45. Terekhova, I., et al., *Complex formation of native and hydroxypropylated cyclodextrins with benzoic acid in aqueous solution: Volumetric and H-1 NMR study.* Chemical Physics Letters, 2011. **514**(4-6): p. 341-346.

46. Ishizu, T., Kintsu, K., and H. Yamamoto, H., *NMR study of the solution structures of the inclusion complexes of beta-cyclodextrin with (+)-catechin and (-)-epicatechin.* Journal of Physical Chemistry B, 1999. **103**(42): p. 8992-8997.

47. Dupuy, N., et al., *H-1 NMR study of inclusion compounds of phenylurea derivatives in beta-cyclodextrin.* Spectrochimica Acta Part a-Molecular and Biomolecular Spectroscopy, 2005. **61**(6): p. 1051-1057.

48. Polyakov, N.E., et al., *beta-ionone cyclodextrins inclusion complexes H-1 NMR study and photolysis.* Journal of Photochemistry and Photobiology a-Chemistry, 2004. **161**(2-3): p. 261-267.

49. Macomber, R.S., *An Introduction to Nmr Titration for Studying Rapid Reversible Complexation.* Journal of Chemical Education, 1992. **69**(5): p. 375-378.

50. Hemmateenejad, B., Safavi, A., and Honarasa, F., *Electrochemical study of weak inclusion complex interactions by simultaneous MCR-ALS analyses of potential step-chronoamperometric data matrices.* Analytical Methods, 2012. **4**(6): p. 1776-1782.

51. Gao, Z.N., Wen, X.L., and Li, H.L., *Study of the inclusion complexes of catecholamines with beta-cyclodextrin by cyclic voltammetry.* Polish Journal of Chemistry, 2002. **76**(7): p. 1001-1007.

52. Ayling, A.J., et al., *An extraction-based assay for neutral anionophores: The measurement of high binding constants to steroidal receptors in a nonpolar solvent.* Chemistry-a European Journal, 2002. **8**(9): p. 2197-2203.

53. Bard, A.J. and L.R. Faulkner, L.R., *Electrochemical Methods: Fundamentals and Applications*. 2 ed ed2001, Hoboken NJ: John Wiley & Sons.

54. Colleran, J.J. and Breslin, C.B., *Simultaneous electrochemical detection of the catecholamines and ascorbic acid at PEDOT/S-beta-CD modified gold electrodes.* Journal of Electroanalytical Chemistry, 2012. **667**: p. 30-37.

55. Hegde, R.N., et al., *Electro-oxidation and determination of gabapentin at gold electrode.* Journal of Electroanalytical Chemistry, 2009. **635**(1): p. 51-57.

56. Wightman, R.M., *Microvoltammetric Electrodes.* Analytical Chemistry, 1981. **53**(9): p. 1125-1134.

57. Ewing, A.G., Dayton, M.A., and Wightman, R.M., *Pulse Voltammetry with Microvoltammetric Electrodes.* Analytical Chemistry, 1981. **53**(12): p. 1842-1847.

58. Weisshaar, D.E. and Tallman, D.E., *Chronoamperometric Response at Carbon-Based Composite Electrodes.* Analytical Chemistry, 1983. **55**(7): p. 1146-1151.

59. Bath, B.D., et al., *Dopamine adsorption at surface modified carbon-fiber electrodes.* Langmuir, 2001. **17**(22): p. 7032-7039.

60. Bath, B.D., et al., *Subsecond adsorption and desorption of dopamine at carbon-fiber microelectrodes.* Analytical Chemistry, 2000. **72**(24): p. 5994-6002.

61. Gonon, F., et al., *In vivo Electrochemical Detection of Catechols in the Neostriatum of Anesthetized Rats - Dopamine or Dopac.* Nature, 1980. **286**(5776): p. 902-904.

62. Crespi, F. and C. Mobius, C., *In-vivo Selective Monitoring of Basal Levels of Cerebral Dopamine Using Voltammetry with Nafion Modified (Na-Cro) Carbon-Fiber Microelectrodes.* Journal of Neuroscience Methods, 1992. **42**(3): p. 149-161.

7 General Conclusions and Future Recommendations

7.1 General Conclusions

In this thesis, a number of modified CPEs were examined, aimed at enhancing the sensitive and selective detection of DA. CPEs were chosen as opposed to common solid electrodes because they offer several interesting possibilities when studying compounds that are soluble in aqueous media. In some cases, CPEs offer a better sensitivity. In addition, the surface of the CPE can be renewed by squeezing a small amount of carbon paste out the holder and a fresh surface is exposed whenever needed. Thus, CPE offer a simple method for the modification of the electrode and fast analysis of analytes.

Initially, the preparation and characterisation of modified CPE sensors was examined. The modification of CPEs was performed on the surface or in the bulk paste and characterised using a number of techniques such as optical microscopy, scanning electron microscopy, energy disperse X-ray spectroscopy and electrochemical impedance spectroscopy. In the process, a great understanding of surface or bulk modifications examined was sought.

The first DA sensors developed in this study are based on the modification of CPE with a variety of compounds including Nafion, Sulfated β-cyclodextrin, Carboxymethyl β-cyclodextrin and Ferrocene β-cyclodextrin complex. In general, the results have demonstrated that modified CPEs exhibit an increase in current response, and thus sensitivity, for DA over the bare electrode. The mechanism of sensing at the modified electrodes has been determined to be a combination of complexation and electrostatic interactions. The increase of the current intensity can be attributed to the preconcentration of the analyte at the electrode surface due to the interaction with the modifiers which retains more molecules at the surface of the electrode. The negative shift of peak potential, compared to the bare CPE, can also be explained by the mediator effect.

The kinetic parameters of the electrochemical oxidation process of DA in 0.1 M PBS was determined for each of the modified electrodes. In the case of Nafion, Sulfated β-CD and Carboxymethyl β-cyclodextrin modified CPE; the electron transfer was under adsorption-control. However, Ferrocene β-cyclodextrin complex modified CPE presented a system corresponding to a diffusion-controlled process. The blocked β-cyclodextrin cavity (by Ferrocene) indicates the mode of interaction DA / β-cyclodextrin. The electron transfer process goes from adsorption at β-cyclodextrin

modified CPE to a diffusion-controlled process at Ferrocene β-cyclodextrin complex modified CPE.

Compared with graphite, graphene possesses a much larger surface area and an excellent electrical conductivity [1]. Therefore, graphene was chemically synthesised and the performance of the bare graphene paste electrode (GPE) towards the detection of DA showed a dramatic enhancement of the oxidation peak current. The composite of graphene with Sulfated β-cyclodextrin was also prepared for the achievement of effective electrochemical communication between DA and the electrode surface. The modified graphene electrode exhibited a higher electrocatalytic activity and good selectivity towards the oxidation of DA.

One of the aims outlined in the introduction of this thesis is the detection of DA in the presence of high concentration AA. This goal was achieved in two distinctive ways: simultaneous and selective detection of DA in the presence of AA. S-β-CD modified CPE has the ability to separate the anodic oxidation peak potentials of AA and DA with a well-defined peak separation and a strong current response. On another hand, AA had no effect (as its voltammetric response was suppressed) when detecting DA with S-β-CD modified GPE, which indicated that the selective and sensitive determination of DA in the presence of AA was feasible. Moreover, the chemical reactions accompanying the electrode process of DA, which interfere in the electrochemical DA determination, were described.

Perhaps one of the most interesting results of this thesis is the ability of the S-β-CD modified CPE to discriminate between the oxidation AA, DA and 5-HT. The highly electrocatalytic activity of the sensor to the three analytes was demonstrated from the sensitive, well-separated voltammetric signals and potential shift. By using cyclic voltammetry or differential pulse voltammetry, a good resolution of the oxidation peak potential for the three species was obtained. In addition, electrochemical behaviour of a solution mixture containing DA and 5-HT was extensively studied. The results indicated that S-β-CD modified CPE and CM-β-CD modified CPE can promote DA and 5-HT oxidation, and could be simultaneously detected. In order to check the intermolecular effect s between DA and 5-HT, the concentration of one analyte was varied while keeping constant the concentration of the other. The results obtained show that the peak currents for DA or 5-HT increased linearly with increasing their respective concentration without considerable effects on the other peak current.

Starting from neutral β-CD, the cyclodextrin analogue $CD_{6.6}$ was obtained from a suitable synthetic route. It was demonstrated that DA forms a significantly strong complex with $CD_{6.6}$ in aqueous solution. Clear evidence for the formation of this complex was obtained using NMR spectroscopy measurements. The complex was formed as a 2:1 stoichiometry of $CD_{6.6}$ to the DA; while NMR analyses indicated that the protonated DA molecule was binding $CD_{6.6}$ through a combination of interactions between the triazole moieties and the carboxylate groups of $CD_{6.6}$. The discussed $CD_{6.6}$ modified CPE enhanced the oxidation peak current of DA, which is corroborated by the detection of 5×10^{-7} M using differential pulse voltammetry. This great result had inspired the fabrication of $CD_{6.6}$ modified graphene paste microelectrode. The developed sensor used a combination of features allowing a more rational design of analytical strategies for the detection of DA. For example, $CD_{6.6}$ was used as a molecular receptor, graphene as enhancer of electron transfer and the micro-size of the electrode for radial diffusion of DA species. This novel sensor possesses properties such as high sensitivity and wide linear dynamic range. Along with S-β-CD modified CPE, $CD_{6.6}$ modified graphene paste microelectrode was compared to other modified carbon based electrodes reported in the literature for electrochemical detection of DA (Table 7.1).

Table 7.1: comparison of the performance of different DA sensors

Electrode	Linear dynamic range (M)	LOD (M)	Technique used	Refs.
TiO_2–grapheme/GCE	$[5 \times 10^{-6} - 2 \times 10^{-4}]$	2.00×10^{-6}	DPV	[2]
L-arginine/CPE	$[5 \times 10^{-5} - 1 \times 10^{-4}]$	5.00×10^{-7}	LSV	[3]
Graphene/GCE	$[2.5 \times 10^{-6} - 1 \times 10^{-4}]$	5.00×10^{-7}	CV	[4]
cucurbit[8]uril (CB[8])/Nafion/GCE	$[2.99 \times 10^{-7} - 2.99 \times 10^{-5}]$	9.90×10^{-8}	CV	[5]
S-β-CDCPE	$[5 \times 10^{-7} - 5 \times 10^{-4}]$	1.33×10^{-7}	DPV	This work
$CD_{6.6}$ modified graphene paste microelectrode	$[3 \times 10^{-7} - 5 \times 10^{-4}]$	3.76×10^{-5}	DPV	This work

Another significant result obtained in this study is the simultaneous detection of AA and DA in aCSF using S-β-CD modified carbon paste microelectrode. A comparison of the resolution for AA and DA with reported literature is shown in Table 7.2.

Table 7.2: The comparison of S-β-CD modified carbon paste microelectrode with other electrodes for simultaneous determination of AA and DA.

Electrode	Reference electrode	$\Delta E_{p(AA/DA)}$ (V)	Concentration of species in mixture (M)	Technique used	Refs.
Poly(Alanine)/CPE	SCE	0.054	[AA] = 1×10^{-3} [DA] = 1×10^{-4}	CV	[6]
Poly(p-aminobenzene sulfonic acid)/GCE	SCE	0.158	[AA] = 1×10^{-3} [DA] = 1×10^{-5}	CV	[7]
Polyglycine/CPE	SCE	0.197	[AA] = 1×10^{-3} [DA] = 1×10^{-4}	CV	[8]
CuZEA/RGO/GCE	SCE	0.200	[AA] = 5×10^{-4} [DA] = 5×10^{-5}	CV	[9]
Polyethylene oxide/GCE	SCE	0.216	[AA] = 1×10^{-3} [DA] = 1×10^{-4}	DPV	[10]
DDAB/GCE	Ag/AgCl	0.300	[AA] = 5×10^{-4} [DA] = 5×10^{-4}	CV	[11]
S-β-CD modified carbon paste microelectrode	SCE	0.240	[AA] = 1×10^{-3} [DA] = 5×10^{-5}	CV	This work

7.2 Future Recommendations

This study has demonstrated that the developed carbon based sensors are promising electrode materials for DA detection. Taking the results into consideration, many innovative ideas could be applied on the biosensing systems regarding working electrode

The S-β-CD modified GPE was effective in the elimination of AA during the selective determination of DA, and the S-β-CD modified CPE was capable of simultaneously detecting AA, DA and 5-HT. However, there are a number of electrochemical interferents present during the detection of DA in biological fluids. These include uric acid [12], histamine [13], acetylcholine [14] and some amino acids such as aspartic acid and glutamic acid [15]. The detection and analysis of these compounds in the presence of DA offers many advantages in the medical field due to their biological significance. Therefore, it would be of interest to determine the effect that the developed sensors have on DA in the presence of these compounds. Moreover, the detection of DA in complex biological samples, such as blood serum and urine, should be conducted. This would be

carried out in order to assess the feasibility of the developed sensors for real samples and potential commercial application. Finally the developed sensors, particularly the $CD_{6.6}$ modified graphene paste microelectrode can be tested for real time detection of DA *in-vivo*. The modified electrode could be able to measure DA in awake rats – thus correlate neurochemistry with behaviour [16].

7.3 References

1. Pumera, M., et al., *Graphene for electrochemical sensing and biosensing.* Trac-Trends in Analytical Chemistry, 2010. **29**(9): p. 954-965.

2. Fan, Y., et al., *Hydrothermal preparation and electrochemical sensing properties of TiO2-graphene nanocomposite.* Colloids and Surfaces B-Biointerfaces, 2011. **83**(1): p. 78-82.

3. Chandrashekar, B.N., et al., *Electropolymerisation of L-arginine at carbon paste electrode and its application to the detection of dopamine, ascorbic and uric acid.* Colloids and Surfaces B-Biointerfaces, 2011. **88**(1): p. 413-418.

4. Ma, X.Y., Chao, M.Y., and Wang, Z.X., *Electrochemical detection of dopamine in the presence of epinephrine, uric acid and ascorbic acid using a graphene-modified electrode.* Analytical Methods, 2012. **4**(6): p. 1687-1692.

5. del Pozo, M., et al., *Cucurbit[8]uril-based electrochemical sensors as detectors in flow injection analysis. Application to dopamine determination in serum samples.* Sensors and Actuators B-Chemical, 2014. **193**: p. 62-69.

6. Gilbert, O., et al., *Poly (Alanine) Modified Carbon Paste Electrode for Simultaneous Detection of Dopamine and Ascorbic Acid.* International Journal of Electrochemical Science, 2008. **3**(10): p. 1186-1195.

7. Jin, G.Y., Zhang, Y.H., and Cheng, W.X., *Poly(p-aminobenzene sulfonic acid)-modified glassy carbon electrode for simultaneous detection of dopamine and ascorbic acid.* Sensors and Actuators B-Chemical, 2005. **107**(2): p. 528-534.

8. Gilbert, O., et al., *Simultaneous detection of dopamine and ascorbic acid using polyglycine modified carbon paste electrode: A cyclic voltammetric study.* Journal of Electroanalytical Chemistry, 2009. **636**(1-2): p. 80-85.

9. He, P., et al., *Zeolite A functionalized with copper nanoparticles and graphene oxide for simultaneous electrochemical determination of dopamine and ascorbic acid.* Analytica Chimica Acta, 2012. **739**: p. 25-30.

10. Gong, W., et al., *Simultaneous determination of dopamine, ascorbic acid by polyethylene oxide (PEO) covalently modified glassy carbon electrode.* Journal of Electroanalytical Chemistry, 2012. **666**: p. 62-66.

11. Chen, S.M. and W.Y. Chzo, *Simultaneous voltammetric detection of dopamine and ascorbic acid using didodecyldimethylammonium bromide (DDAB) film-modified electrodes.* Journal of Electroanalytical Chemistry, 2006. **587**(2): p. 226-234.

12. Huang, J.S., et al., *Simultaneous electrochemical determination of dopamine, uric acid and ascorbic acid using palladium nanoparticle-loaded carbon nanofibers modified electrode.* Biosensors & Bioelectronics, 2008. **24**(4): p. 632-637.

13. Oguri, S. and Yoneya, Y., *Assay and biological relevance of endogenous histamine and its metabolites: application of microseparation techniques.* Journal of Chromatography B-Analytical Technologies in the Biomedical and Life Sciences, 2002. **781**(1-2): p. 165-179.

14. Lin, S., Liu, C.C., and Chou, T.C., *Amperometric acetylcholine sensor catalyzed by nickel anode electrode.* Biosensors & Bioelectronics, 2004. **20**(1): p. 9-14.

15. Gifford, R., et al., *Protein interactions with subcutaneously implanted biosensors.* Biomaterials, 2006. **27**(12): p. 2587-2598.

16. Robinson, D.L., et al., *Detecting subsecond dopamine release with fast-scan cyclic voltammetry in vivo.* Clinical Chemistry, 2003. **49**(10): p. 1763-1773.